

# ABSTRACTS

(690-853)

GENITOURINARY PATHOLOGY  
(INCLUDING RENAL TUMORS)

2024



# ABSTRACTS | GENITOURINARY PATHOLOGY (INCLUDING RENAL TUMORS)

## 690 HLA Class I Loss in Primary Prostate Cancer and Association with Immune Tumor Microenvironment

Adrianna A Mendes<sup>1</sup>, Tamara Lotan<sup>2</sup>

<sup>1</sup>Johns Hopkins Medical Institutions, Baltimore, MD, <sup>2</sup>Johns Hopkins University School of Medicine, Baltimore, MD

**Disclosures:** Adrianna A Mendes: None; Tamara Lotan: None

**Background:** HLA Class I molecules are involved in antigen presentation and cytotoxic CD8+ T cell activation and their downregulation in cancer cells may contribute to tumor immune evasion and dissemination. Prostate cancer (PCa) is poorly immunogenic and elucidating the mechanisms preventing immunologic activity against the tumor will improve our understanding of tumor biology and development of target therapies. We examined HLA class I protein expression in untreated PCa and its association with tumor infiltrating immune cell subsets and clinicopathological features.

**Design:** A cohort of 339 grade-matched, self-identified White or Black men with surgically-treated PCa (Race cohort, RC) and a cohort of 323 surgically-treated patients with intermediate/high risk PCa (Natural History cohort, NHC) were assessed for HLA Class I protein expression via immunohistochemistry (IHC) on a tissue microarray. Tumors were semi-quantitatively scored for HLA Class I intensity (0/1+/2+/3+) and dichotomously grouped by absent/low (0/1+) and high (2+/3+) expression for analysis. Cases with heterogenous loss of HLA Class I expression were included in the absent/low expression group. The results were compared with previously published clinicopathological data, immune cell subset densities, and B7-H3 expression.

**Results:** Absent/low expression of HLA Class I was observed in 8% and 11% of cases in the RC and NHC, respectively, with only 2% of cases in both cohorts having complete loss. Absent/low HLA expression was associated with higher grade group in the NHC ( $p=0.002$ ) and higher stage ( $p=0.0008$ ) or non-organ confined disease ( $p=0.034$ ) in the RC. Absent/low HLA expression was significantly associated with lower T-cell ( $p=0.002$ ) and T-cell subsets densities ( $p=0.0009$  for CD8 cells and  $p=0.007$  for FOXP3 cells) in the RC, and with lower T-( $p=0.01$ ) and B-cell ( $p=0.02$ ) densities in the NHC. Interestingly, expression of the immunomodulatory B7-H3 (CD276) protein was inversely correlated with HLA expression in both cohorts ( $p=0.005$  and  $p=0.001$ ).

**Conclusions:** To our knowledge, this is the first study to show the correlation between HLA Class I protein expression and immune cell density in primary PCa, corroborating with its role in immune cell activation. The inverse correlation of HLA Class I expression with B7-H3 is a novel finding and may be relevant in future clinical trials of enoblituzumab, a monoclonal antibody targeting B7-H3, in PCa. Future work will focus on digital quantification of HLA Class I expression.

## 691 Molecular Characterization of Large Cell Calcifying Sertoli Cell Tumors: A Multi-institutional Study of 6 Benign and 2 Malignant Tumors

Eman Abdulfatah<sup>1</sup>, Khaleel Al-Obaidy<sup>2</sup>, Dan Robinson<sup>1</sup>, Yi-MI Wu<sup>1</sup>, Amer Heider<sup>3</sup>, Muhammad Idrees<sup>4</sup>, Thomas Ulbright<sup>4</sup>, Angela Wu<sup>1</sup>, Lakshmi Kunju<sup>3</sup>

<sup>1</sup>Michigan Medicine, University of Michigan, Ann Arbor, MI, <sup>2</sup>Henry Ford Health System, Detroit, MI, <sup>3</sup>University of Michigan, Ann Arbor, MI, <sup>4</sup>Indiana University School of Medicine, Indianapolis, IN

**Disclosures:** Eman Abdulfatah: None; Khaleel Al-Obaidy: None; Dan Robinson: None; Yi-MI Wu: None; Amer Heider: None; Muhammad Idrees: None; Thomas Ulbright: None; Angela Wu: None; Lakshmi Kunju: None

**Background:** Large cell calcifying Sertoli cell tumors (LCCSCTs) are rare testicular tumors and approximately 40% of patients present in the context of an inherited tumor predisposition syndrome, such as Carney complex or Peutz-Jeghers. While the immunomorphologic features of these tumors has been characterized, the genetic profile of sporadic LCCSCTs is largely unknown.

**Design:** The aim of our study was to evaluate clinico-morphologic features and molecular characterization of LCCSCTs including PRKAR1A gene mutations and other novel alterations and gene expression. LCCSCTs diagnosed at 2 institutions were identified. H&E slides were reviewed to evaluate morphologic features. Clinical charts and outcome data were reviewed. Targeted next-generation sequencing (NGS) was performed.

**Results:** Eight LCCSCTs were included (median 17, range 5-37 years). Two patients (25%) had Carney complex diagnosis on subsequent germline genetic testing. Grossly, 6 (75%) tumors were well-circumscribed and 2 (25%) showed extratesticular extension. Microscopically, the tumor consisted of nests, cords and tubules of pale to deeply eosinophilic cells within a myxohyaline, often calcified stroma. In 2 cases, several adverse pathological features were identified: significant cytologic atypia, necrosis, mitoses, LVI and extratesticular extension. Targeted NGS detected PRKAR1A mutations in all (100 %) cases with heterozygous PRKAR1A mutation in 6 (75%) tumors and germline Carney complex- associated PRKAR1A in 2 (25%) patients. Additionally, CDKN1B and TERT mutations were identified in 1 of the 2 malignant cases. All tumors showed low tumor mutational burden and unremarkable copy number alterations except for frequent LOH of 17q24 including PRKAR1A locus. RNA expression analysis showed increased expression of several markers including novel PRUNE2, and usual markers like beta-catenin, calretinin, inhibin and S100. Median follow-up period was 26 months. One patient presented with metastatic disease involving lymph nodes.

# ABSTRACTS | GENITOURINARY PATHOLOGY (INCLUDING RENAL TUMORS)

and developed lung metastasis 20 months later. This tumor showed adverse pathological features and had an additional driver mutation.

**Conclusions:** While LCCSCTs have been reported in the setting of cancer predisposition syndromes, the majority of these tumors occur sporadically. *PRKAR1A* mutations are present in all cases and appear to be the major driver and can serve as a genetic marker for diagnosis of LCCSCTs. It remains to be determined whether malignant progression may be caused by additional driver mutations.

## 692 Identification of Radiomics Features of High Grade Renal Cell Carcinoma by Precise Radiologic-Pathologic Correlation in ex vivo Radical Nephrectomy Specimens

Tarek Abi-Saab<sup>1</sup>, Huihua Li<sup>2</sup>, Madhu Gowda<sup>1</sup>, E Jason Abel<sup>3</sup>, Ruben Ngnitewe Massa'a<sup>1</sup>, Daniel Shapiro<sup>3</sup>, Andrew Wentland<sup>3</sup>, Israa Laklouk<sup>3</sup>, Rong Hu<sup>4</sup>, Meghan Lubner<sup>3</sup>

<sup>1</sup>University of Wisconsin-Madison Hospital and Clinics, Madison, WI, <sup>2</sup>University of Chicago, Chicago, IL, <sup>3</sup>University of Wisconsin-Madison, Madison, WI, <sup>4</sup>University of Wisconsin School of Medicine and Public Health, Madison, WI

**Disclosures:** Tarek Abi-Saab: None; Huihua Li: None; Madhu Gowda: None; E Jason Abel: None; Ruben Ngnitewe Massa'a: None; Daniel Shapiro: None; Andrew Wentland: None; Israa Laklouk: None; Rong Hu: None; Meghan Lubner: None

**Background:** Tumor heterogeneity of renal cell carcinoma (RCC) is well known. There is an increasing need to identify high grade RCC via percutaneous needle core biopsy. This study investigates whether precise radiologic-pathologic correlation can be used to delineate the imaging signatures of aggressive features of RCC in ex vivo radical nephrectomy specimens.

**Design:** Twenty patients with large renal cell masses were prospectively enrolled. Following radical nephrectomy, the kidney was placed in a 3D mold created based on the presurgery imaging. Three tissue localization clips were placed in the tumor and imaged by noncontrast MRI and CT. The specimen was grossed following routine protocol and three additional consecutive sections were obtained around each localization clip. Each section was assessed for tumor subtype, tumor grade, sarcomatoid transformation or rhabdoid features, the amount of hyalinized stroma and blood clot on H&E slides. These features were precisely correlated with ex vivo CT and MRI imaging data using the clips as landmarks and radiomics features were extracted from each clip site.

**Results:** The 20 RCC cases included 15 clear cell, 3 papillary, and 2 chromophobe. 147 sections obtained around the clip sites were eligible for analysis and contained the following features: 84 sections showed high-grade tumor, with nuclear grades 3-4; 28 had sarcomatoid transformation and/or rhabdoid features; 17 had tumor necrosis; 31 had hyalinized stroma, 11 of which were without viable tumor cells. Ten different machine learning algorithms were trained using the radiomics data from MRI and CT imaging to distinguish high versus low grade tumor and to identify tumor necrosis. Support vector machine algorithm of MRI showed a sensitivity of 83% and specificity of 92% for identifying high grade tumors using T1 non-contrast images. The k-nearest neighbor algorithm of CT imaging showed a sensitivity of 88% and specificity of 85% in identifying high grade tumors. Logistic regression of CT imaging identified areas of tumor necrosis with a sensitivity and specificity of 86% and 86% respectively.

**Conclusions:** Preliminary data from this precise ex vivo radiological-pathologic correlation model suggests that high grade areas of heterogeneous RCC may be identifiable using unenhanced CT and MRI radiomics features. Features learned from this ex vivo model may be used to guide high yield renal mass biopsies in the future.

## 693 Large Cribriform Pattern 4 is a Codependent Variable with Tumor Volume, Percent of Pattern 4, and Margin Status and Does Not Independently Influence Biochemical Recurrence After Radical Prostatectomy

Amr Abulaban<sup>1</sup>, Guannan Zhang<sup>2</sup>, Ivan Nemov<sup>3</sup>, Sheida Khosravaniardakani<sup>4</sup>, Felipe Ruiz Casas<sup>1</sup>, Oleksii Iakymenko<sup>5</sup>, Jamie Thomas<sup>6</sup>, Jasmine Kannikal<sup>6</sup>, Merce Jorda<sup>3</sup>, Oleksandr Kryvenko<sup>3</sup>

<sup>1</sup>University of Miami Miller School of Medicine/Jackson Health System, Miami, FL, <sup>2</sup>Jackson Memorial Hospital/ University of Miami Hospital, Miami, FL, <sup>3</sup>University of Miami Miller School of Medicine, Miami, FL, <sup>4</sup>Florida International University, Miami, FL, <sup>5</sup>Albert Einstein College of Medicine, Montefiore Medical Center, Bronx, NY, <sup>6</sup>University of Miami, Miami, FL

**Disclosures:** Amr Abulaban: None; Guannan Zhang: None; Ivan Nemov: None; Sheida Khosravaniardakani: None; Felipe Ruiz Casas: None; Oleksii Iakymenko: None; Jamie Thomas: None; Jasmine Kannikal: None; Merce Jorda: None; Oleksandr Kryvenko: None

**Background:** The presence of large cribriform growth pattern 4 in Grade Group (GG) 2 and GG3 prostate cancers has been associated with a worse pathological outcome at radical prostatectomy (RP) and a higher risk of biochemical recurrence (BCR). However, it has not yet been truly proven whether this pattern has independent prognostic value, or whether it is confounded by other coexisting variables. We have recently demonstrated that large cribriform pattern 4 is a co-dependent variable with the percent of Gleason pattern 4 (GP4%) and tumor volume (TV) in GG2 and GG3 cancers and does not independently affect

# ABSTRACTS | GENITOURINARY PATHOLOGY (INCLUDING RENAL TUMORS)

pathological RP outcomes when the latter two variables are accounted for. In this study, we assess whether large cribriform pattern 4 influences BCR after RP when other established risk factors are accounted for.

**Design:** 496 RP's with GG2 and GG3 prostate cancers were reviewed in a retrospective cohort analysis. Using a multivariate COX regression model, the individual predictive value of large cribriform pattern 4 for BCR was analyzed and controlled for tumor stage, surgical margin status, GP4%, and TV.

**Results:** 107 (21.6%) patients experienced BCR. Large cribriform pattern 4 was seen in larger tumors with higher GP4%, more frequent positive margin, and more advanced stage. In univariable analysis all of these measures correlated with BCR (all  $P < 0.05$ ). In multivariable analysis, tumor stage pT3b (32/496; OR=2.7;  $p=0.01$ ), positive surgical margins (175/496; OR=2.7;  $p < 0.001$ ), higher GP4% (OR=1.02;  $p < 0.001$ ), and higher tumor volume (OR=1.37;  $p=0.001$ ) were found to be individual independent predictors for BCR after RP, while large cribriform growth pattern (273/496;  $P=0.37$ ), stage pT3a (239/496;  $p=0.47$ ) and stage pT2+ (44/496;  $p=0.45$ ) were not.

**Conclusions:** Large cribriform pattern 4 is a co-dependent variable with other established risk factors for BCR. After controlling for tumor stage, surgical margin status, GP4%, and TV, all of which were individual independent predictors of BCR, large cribriform pattern 4 lost its independent influence on BCR after RP in GG2 and GG3 cancers. While other studies have previously hypothesized that large cribriform growth pattern 4 is an individual predictor for recurrence, it appears to us that not all variables were considered. The currently described finding has significant implications on management and counseling of patients with a diagnosis of large cribriform pattern 4 at radical prostatectomy.

## 694 Expanding the Family of EWSR1-rearranged Primary Renal Sarcomas: Ewing and Beyond

Abbas Agaimy<sup>1</sup>, Robert Stoehr<sup>2</sup>, Arndt Hartmann<sup>3</sup>, Nasir Ud Din<sup>4</sup>

<sup>1</sup>Universitätsklinikum, Erlangen, Germany, <sup>2</sup>Institute of Pathology, University Hospital, Erlangen, Erlangen, Germany, <sup>3</sup>Institut für Pathologie, Erlangen, Germany, <sup>4</sup>Aga Khan University Hospital, Karachi, Pakistan

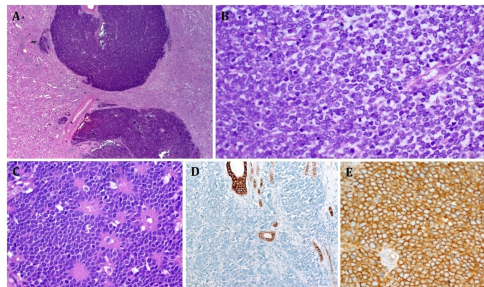
**Disclosures:** Abbas Agaimy: None; Robert Stoehr: None; Arndt Hartmann: None; Nasir Ud Din: None

**Background:** Primary renal Ewing sarcoma family tumors (ESFT) are rare, representing <1% of all kidney tumors and <4% of all ESFTs. Diagnosis is based on characteristic morphology supplemented by immunohistochemistry (IHC) for CD99 and NKX2.2 and demonstration of *EWSR1* rearrangements. Recent studies however have pointed to rare occurrence of other *EWSR1*-rearranged non-ESFTs in the kidney, thus questioning the reliability of *EWSR1* FISH testing.

**Design:** We retrieved and reviewed all renal ESFTs including any *EWSR1*-rearranged mesenchymal neoplasm to illustrate the spectrum and differential of these rare entities. Molecular testing was performed via targeted RNA sequencing and/ or *EWSR1* FISH.

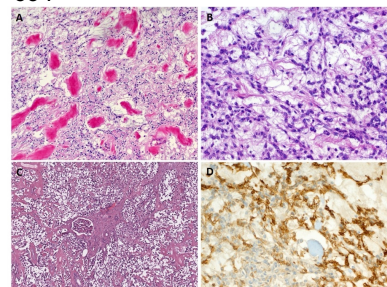
**Results:** Overall, 30 tumors were identified (22 ESFTs and 8 others). The ESFTs affected 12 males and 10 females aged 7 to 66 y (median, 25). Median size was 12.5 cm (3.5 – 17). *EWSR1* rearrangements was confirmed by either NGS or FISH in 16/22 cases; all 14 sequenced cases revealed the canonical *EWSR1*::*FLI1* fusion. Age range for non-ESFTs was 23 – 76 (median, 46). Affected were 5 females and 3 males. The size rang was 3 – 22 cm (median, 7.1). The histology of the non-ESFT corresponded to sclerosing epithelioid fibrosarcoma/ low-grade fibromyxoid sarcoma (3; two with confirmed *EWSR1*::*CREB3L1* and all three were MUC4+), two unclassified sarcomas with epithelioid features and *EWSR1*::*CREM* fusions, and one case each of desmoplastic small round cell tumor (*EWSR1*::*WT1*), unclassified round/ spindle cell sarcoma (*EWSR1*::*PATZ1*), and myoepithelial carcinoma (*EWSR1*::*POU5F1P3*). Only a single epithelial malignancy with an *EWSR1* rearrangement was encountered (follicular thyroid-like carcinoma with an *EWSR1*::*LOC284889* fusion). No *EWSR1*::*TFE3*-fusion MiTF carcinoma was found during study period.

Figure 1 - 694



Primary renal Ewing family tumors with multinodular invasive growth (A), monotonous small round cells (B) and (in this case) prominent rosetting (C). D: negative pankeratin. E: membranous homogeneous CD99.

Figure 2 - 694



Non-ESFT renal sarcomas. A+B: *EWSR1*::*CREM* sarcoma with bland fibromyxoid features and variable amianthoid-like deposits. C: sclerosing epithelioid fibrosarcoma. D: both entities expressed MUC4.

# ABSTRACTS | GENITOURINARY PATHOLOGY (INCLUDING RENAL TUMORS)

**Conclusions:** This series expands the histogenetic, phenotypic and genotypic spectrum of *EWSR1*-rearranged primary mesenchymal renal neoplasms showing that ESFT is the most frequent entity (73% of all cases) occurring at lower age (25 y), mainly in males while non-ESFTs represent a heterogeneous category encompassing a variety of rare but either well defined (LGFMS/SEF) or emerging (CREM-rearranged sarcoma and myoepithelial carcinoma) entities occurring at relatively higher age (46 y), mainly in females. Inclusion of these newer entities in the differential diagnosis is mandatory, given the heterogeneous tumor behavior and the varying responsiveness to chemotherapy. Finally, identification of the exact fusion variants and not the simple *EWSR1* FISH has diagnostic impact as the genotypic landscape of these rare cancers is still emerging.

## 695 The Prognostic Significance of Stem Cell-Like Marker PLCG2 and Novel Neuroendocrine Markers in Bladder Neuroendocrine Carcinomas

Dilara Akbulut<sup>1</sup>, Gamze Gokturk Ozcan<sup>2</sup>, Merve Basar Yerebakan<sup>2</sup>, Karissa Whiting<sup>2</sup>, Jie-Fu Chen<sup>2</sup>, Judy Sarungbam<sup>2</sup>, Ying-Bei Chen<sup>2</sup>, Anuradha Gopalan<sup>2</sup>, S. Joseph Sirintrapun<sup>2</sup>, Samson Fine<sup>2</sup>, Natasha Rekhtman<sup>2</sup>, Marina Baine<sup>2</sup>, David Solit<sup>2</sup>, Gopa Iyer<sup>2</sup>, Hikmat Al-Ahmadie<sup>2</sup>

<sup>1</sup>National Cancer Institute, National Institutes of Health, Bethesda, MD, <sup>2</sup>Memorial Sloan Kettering Cancer Center, New York, NY

**Disclosures:** Dilara Akbulut: None; Gamze Gokturk Ozcan: None; Merve Basar Yerebakan: None; Karissa Whiting: None; Jie-Fu Chen: None; Judy Sarungbam: None; Ying-Bei Chen: None; Anuradha Gopalan: None; S. Joseph Sirintrapun: None; Samson Fine: None; Natasha Rekhtman: None; Marina Baine: None; David Solit: None; Gopa Iyer: None; Hikmat Al-Ahmadie: None

**Background:** Bladder small cell carcinoma (SmCC) can be classified into distinct subtypes based on the expression of the novel neuroendocrine (NE) markers ASCL1, NEUROD1 and POU2F3. Single cell RNA sequencing of lung SmCC showed a distinct PLCG2-high subpopulation with stem cell-like and pro-metastasis features and poor prognosis. We evaluated PLCG2 expression in bladder NE carcinoma and correlated the expression with that of novel NE markers and clinical outcomes.

**Design:** We identified 102 SmCC and 20 large cell NE carcinomas (LCNEC), 32 of which co-existed with a non-NE component. Cases were assembled in tissue microarray blocks. IHC for PLCG2 and NE markers CD56, SYP, CHR, INSM1, NEUROD1, ASCL1, POU2F3, DLL3 was performed. Co-expression patterns were assessed between markers, and associations with progression-free survival (PFS), overall survival (OS) and pathological response to neoadjuvant/adjuvant chemotherapy were analyzed.

**Results:** Interpretable results were available from 116 cases (98 SmCC and 18 LCNEC), of which 40 (34%) were positive for PLCG2. PLCG2 was expressed more frequently in LCNEC than SmCC (54% vs 29%) and H-score was higher in LCNEC (median 30, IQR: 0-82 vs. SmCC median 0, IQR: 0-15), although differences were not significant. PLCG2 was expressed in only 4 of non-NE components in mixed tumors. Expression of PLCG2 was positively correlated with that of POU2F3 (spearman corr 0.76, p < 0.001) and negatively correlated with other tested NE markers (p<0.05 for ASCL1, NEUROD1, SYP and DLL3). In a subset of 72 patients with M0 disease who underwent RC, tumors expressing PLCG2 or POU2F3 were associated with worse PFS and OS (p<0.05) but their expression was not associated with metastasis status or pathologic response to neoadjuvant/adjuvant chemotherapy. There were no significant differences in OS or PFS between any other marker +/- groups.

Figure 1 - 695

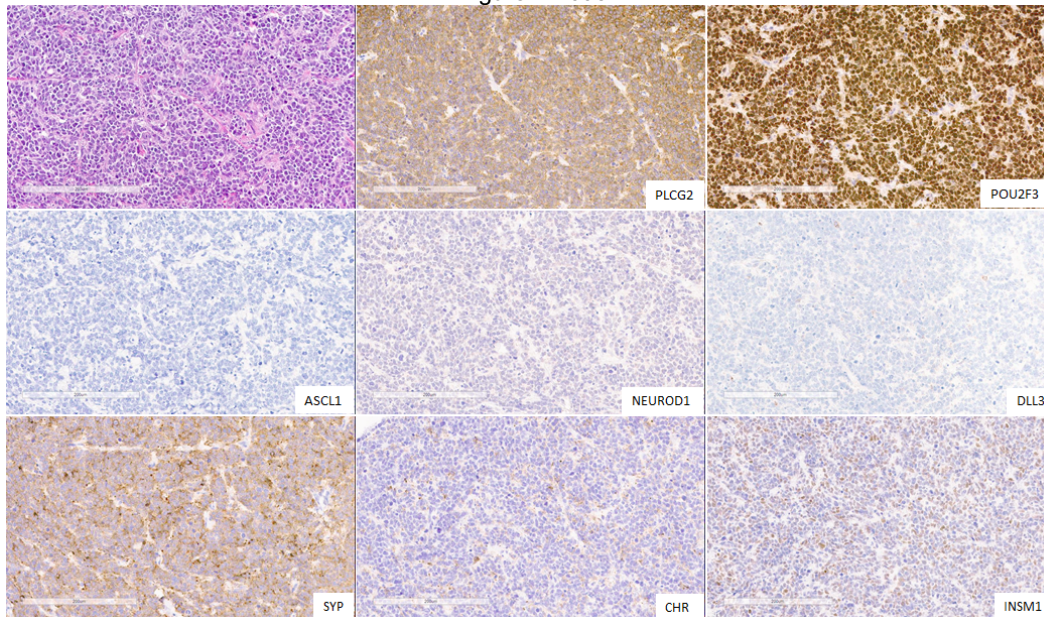
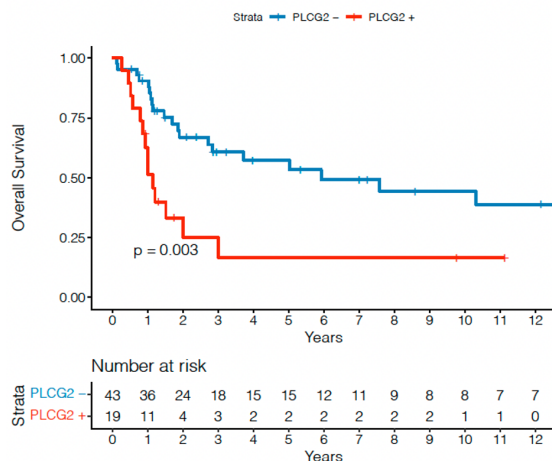


Figure 2 - 695



**Conclusions:** In neuroendocrine carcinoma of the bladder, PLCG2 and POU2F3 are expressed in approximately 34% and 24% of tumors, respectively, and their expression is associated with shorter progression-free and overall survival. PLCG2 positive NE carcinoma of bladder shows infrequent expression of both traditional and novel NE markers. There is a strong correlation between PLCG2 and POU2F3 expression, and the biologic significance of such an association is not yet fully elucidated. In sum, our data suggest that PLCG2+ and POU2F3+ NE carcinomas define a new molecular subset of potential prognostic significance.

## 696 Renal Cell Carcinoma with Fibromyxomatous Stroma: A Clinicopathologic and Molecular Study of 15 Cases

Khaleel Al-Obaidy<sup>1</sup>, Ahmad Alkashash<sup>2</sup>, Liang Cheng<sup>3</sup>, Oudai Hassan<sup>1</sup>, Nilesh Gupta<sup>1</sup>, Sean Williamson<sup>4</sup>, Muhammad Idrees<sup>5</sup>

<sup>1</sup>Henry Ford Health System, Detroit, MI, <sup>2</sup>Indiana University, Indianapolis, IN, <sup>3</sup>Alpert Medical School of Brown University, Providence, RI, <sup>4</sup>Cleveland Clinic, Cleveland, OH, <sup>5</sup>Indiana University School of Medicine, Indianapolis, IN

**Disclosures:** Khaleel Al-Obaidy: None; Ahmad Alkashash: None; Liang Cheng: None; Oudai Hassan: None; Nilesh Gupta: None; Sean Williamson: None; Muhammad Idrees: None

**Background:** Renal cell carcinoma with fibromyxomatous stroma (RCC-FMS) is a rare renal tumor that was included in the 2016 World Health Organization classification of renal tumors as an emerging/provisional entity. Recent studies documented the presence of *TSC1*, *TSC2*, and *MTOR* mutations in subset of these tumors. Most importantly, these have no molecular alterations in the *VHL* gene. These tumors were separated from the RCC with mutation of ELOC (formerly *TCEB1*) which now represents a distinct molecularly defined entity in the current 2022 WHO classification system. We herein studied the clinicopathologic and molecular characteristics of RCC-FMS

**Design:** Fifteen RCC-FMS were included in this study. The H&E stained slides were reviewed, and 5 tumors underwent next-generation sequencing. Follow-up information was obtained from patients' electronic records

**Results:** Ten were men, and 5 were women, with an age range of 32-76 years (median 62 years) and tumor size range of 1.7-11 cm (median 2.2 cm). None had significant medical history. One patient had ipsilateral chromophobe RCC and developed recurrence of the chromophobe RCC. Histologically, tumors were circumscribed and composed of nodules and nests of cells with clear cytoplasm and were embedded in a cellular stroma formed of bundles of smooth muscle fibers. Two-thirds were of WHO/ISUP nucleolar grade 2. No tumor necrosis or mitotic figures in the epithelial or spindle cell components was noted. Immunohistochemically, tumors were consistently positive for keratin 7 (12/12), carbonic anhydrase-9 (11/11) and CD10 (11/11), whereas they were negative for AMACR (8/8) and translocation carcinoma markers [TFE3, cathepsin K, HMB45 or Melan A (5/5)]. Additionally, the smooth muscle stroma was highlighted by desmin, caldesmon and/or smooth muscle actin (7/7). Using next-generation sequencing, one tumor had mutation in *TSC1* and one had mutation in *TSC2* genes. No pathogenic mutations were identified in *ELOC* (*TCEB1*) gene. Follow up data were available for 10 patients, showing no evidence of recurrence or metastasis at a median follow up of 12 months (range, 4-130 months).

**Conclusions:** RCC-FMS has a distinct morphology with characteristic immunohistochemical and molecular features, including alterations in the *TSC* genes. Further studies are necessary to determine whether these should be considered a distinct tumor type, or part of other tumor entities such as clear cell renal cell tumor.

## 697 A Contemporary Clinicopathological Analysis of Renal Cell Carcinoma with Vena Cava Involvement

Omar Al-Rusan<sup>1</sup>, Viraj Master<sup>1</sup>, Adeboye Osunkoya<sup>1</sup>

<sup>1</sup>Emory University School of Medicine, Atlanta, GA

**Disclosures:** Omar Al-Rusan: None; Viraj Master: None; Adeboye Osunkoya: None

**Background:** Renal cell carcinoma (RCC) is occasionally associated with vena cava (VC) involvement. Despite recent advances in chemotherapeutic and immunotherapeutic modalities, the 5-year survival in this population continues to be poor. Therefore, further studies are required to better characterize this patient population, especially from the clinicopathologic standpoint.

**Design:** A comprehensive review of patients with RCC and VC involvement managed at our institution from 2014-2022 was performed. Multiple clinicopathologic parameters including follow-up were obtained.

**Results:** A total of 114 patients with RCC and VC involvement were included in the study. The mean patient age was 63 years (range: 30-84 years). The cohort consisted of 78/114 (68%) males and 36/114 (32%) females. The mean primary tumor size (excluding tumor thrombus) was 11 cm. The majority of tumors (104/114, 91.2%) were unifocal. Tumor stages were categorized as follows: pT3b (51/114, 44%), pT3c (52/114, 46%), and pT4 (11/114, 10%). Most of the tumors were clear cell RCC 89/114 (78.0%), although other more aggressive RCC subtypes were also present. Most tumors were WHO/ISUP grade 3 (44/114, 38.5%) or 4 (67/114, 58.7%) with sarcomatoid differentiation present in 39/67 (58.2%). Necrosis was present in 94/114 (82.4%) tumors. Twenty three of 114 (20.1%) tumors were categorized as pM1 and the ipsilateral adrenal gland was the most common site of metastasis. Of the 91 patients categorized as pMX at nephrectomy, 42/91 (46.1%) subsequently developed metastasis, most frequently to the lung. Of all patients, only 16/114 (14%) had positive vascular margins and 7/114 (6.1%) had positive soft tissue margins despite having very advanced disease.

**Conclusions:** This is one of the largest contemporary institutional studies on the detailed clinicopathologic findings of RCC with VC involvement. Our study demonstrates that a significant number of patients with VC involvement still benefit from radical nephrectomy/tumor debulking performed by an experienced urologic oncologist. This could conceivably play a critical role in counseling, management, and second opinions for patients with RCC and VC involvement detected on imaging.

## 698 An Independent Prospective Validation of a Deep Learning Algorithm for Prostate Cancer Detection and Gleason Grading

Daniel Albertson<sup>1</sup>, In Hye Suh<sup>2</sup>, Sheila Mota<sup>3</sup>, Marc Barry<sup>4</sup>, Jonathon Mahlow<sup>4</sup>, Beatrice Knudsen<sup>4</sup>, Deepika Sirohi<sup>4</sup>, Tae-Yeong Kwak<sup>5</sup>, Yoon Lee<sup>2</sup>, Sun Woo Kim<sup>2</sup>, Hyeyoon Chang<sup>2</sup>

<sup>1</sup>The University of Utah, Salt Lake City, UT, <sup>2</sup>Deep Bio Inc., Seoul, South Korea, <sup>3</sup>ARUP Laboratories, University of Utah, Salt Lake City, UT, <sup>4</sup>The University of Utah/ARUP Laboratories, Salt Lake City, UT, <sup>5</sup>Deep Bio Inc., Guro-gu, South Korea

**Disclosures:** Daniel Albertson: None; In Hye Suh: None; Sheila Mota: None; Marc Barry: None; Jonathon Mahlow: None; Beatrice Knudsen: None; Deepika Sirohi: None; Tae-Yeong Kwak: None; Yoon Lee: None; Sun Woo Kim: None; Hyeyoon Chang: None

**Background:** The Gleason grade is an important prognostic factor in prostate cancer but suffers from high discordance among pathologists (up to 30-50%). To this end, we developed a deep learning algorithm for the detection and grading of cancer in prostate needle biopsy tissues. Here, we evaluate the performance of the AI algorithm on independent, consecutively accrued real-world cases that the algorithm had not previously seen.

**Design:** A pilot study confirmed the workflow of the project. Hematoxylin-and-eosin (H&E) stained diagnostic prostate core needle biopsies processed at an independent hospital were prospectively enrolled from November 2021 to March 2022. Four board-certified and subspecialty-trained GU pathologists rendered standard-of-care clinical diagnoses after review of all H&E-stained levels using microscopes, using ancillary studies as needed. Slides were scanned using a 3DHISTECH scanner at 40x magnification and provided to the AI model for analysis without site-specific tuning. Analysis was performed to assess the diagnostic concordance of the algorithm compared to the original hospital diagnoses, with the primary endpoint of cancer detection and secondary endpoint of Gleason grading. The reference standard diagnosis was derived from the three pathologists not involved in the original diagnosis.

**Results:** A total of 1701 prostate biopsy slides from 851 biopsy sites of 141 consecutive patients were included. A reference standard was constructed for 599 biopsy sites of 101 patients. A review of false-positive results given by the algorithm showed that the model tends to misclassify atrophic glands and seminal vesicles as suspicious for cancer. Compared to the reference standard, the AI model showed a sensitivity of 0.992 and a specificity of 0.844 for cancer detection while the sensitivity and specificity of original diagnoses (pathologists compared to reference standard) were 0.979 and 0.994, respectively. The results showed substantial diagnostic concordance between the AI model's grade group classification and the reference standard (0.820 quadratic-weighted Cohen's kappa coefficient).

# ABSTRACTS | GENITOURINARY PATHOLOGY (INCLUDING RENAL TUMORS)

Figure 1 - 698

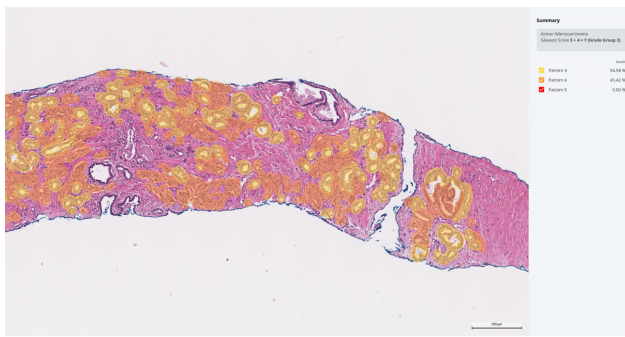


Figure 1. Screenshot of AI Analysis Results

Figure 2 - 698

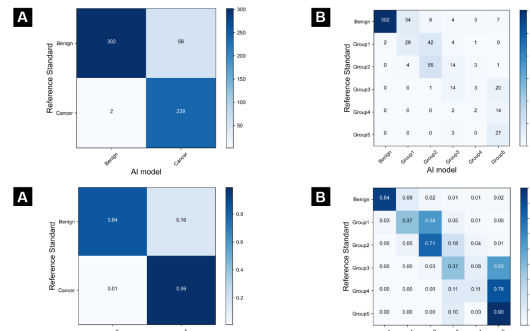


Figure 2. Confusion matrices between the AI model and the reference standard diagnosis for  
(A) Cancer detection performance B) Gleason Group grading performance

**Conclusions:** This study validates the AI algorithm in an independent set of cases that the algorithm had not previously seen and also highlights its potential benefit as a high-sensitivity tool in anatomic pathology practice. Overall, the AI model shows the potential to be a versatile tool with varied use-cases in real-world settings.

## 699 Genotype Phenotype Correlation of Renal Tumor in The Cancer Genome Atlas Database

Daniel Albertson<sup>1</sup>, Jonathon Mahlow<sup>2</sup>, Ting Liu<sup>2</sup>, Marc Barry<sup>2</sup>, Deepika Sirohi<sup>2</sup>

<sup>1</sup>The University of Utah, Salt Lake City, UT, <sup>2</sup>The University of Utah/ARUP Laboratories, Salt Lake City, UT

**Disclosures:** Daniel Albertson: None; Jonathon Mahlow: None; Ting Liu: None; Marc Barry: None; Deepika Sirohi: None

**Background:** Classification of renal tumors has expanded significantly in the past decade with identification of renal tumors with defining molecular alterations. The World Health Organization's 2022 classification now includes a new class of Molecularly Defined Renal Carcinomas (RCCs), a first step in the molecular classification of renal tumors. Recognition of morphological features is the first step in evaluation of renal tumors and directing molecular workup. The objective of the study was to review and characterize histomorphological features of renal tumors with known molecular alterations.

**Design:** Renal tumors in the Cancer Genome Atlas (TCGA) database were reviewed to identify tumors with known pathogenic molecular alterations previously reported. Single representative digital slides and pathology reports for each case available through the database were consensus reviewed by 5 genitourinary pathologists and morphologic features recorded.

**Results:** There were 52 cases of RCCs identified with a previously known molecular abnormality within the papillary (KIRP), clear cell (KIRC), and chromophobe (KICH) data sets. Morphological features of these are listed in Table-1. Salient findings included presence of both low- and high-grade histology in *TFE3* rearranged RCCs, *TFEB* amplified RCCs, Succinate dehydrogenase (*SDH*) mutated RCCs and RCCs with mutations in mismatch repair genes. One of three cases of *ELOC* mutated RCC demonstrated infiltrative features. Significant morphologic overlap was noted across most molecularly defined tumors. *SDH* mutations included *SDHA* (2), *SDHC* (1), *SDHD* (1) and *SDHB* (1) and were all present in the KIRP database with none identified in the KICH database. Pseudostratification of nuclei in *FH* mutated RCCs (2/3) and nuclear grooves in *SDH* mutated RCCs (2/5) were intriguing findings that we have not previously encountered. Mucin was noted in *NF2*, *KRAS* and *SDH* mutated and *ALK* rearranged tumors.

# ABSTRACTS | GENITOURINARY PATHOLOGY (INCLUDING RENAL TUMORS)

RCC Subtypes and Database	Architecture	Cytoplasmic features	Nuclear features	Other
<i>TFE3</i> rearranged RCC (N=12) KIRC (4), KIRP (8)	Papillary (7), nests (4), multinodular (3), tubulopapillary (2), intracystic (2), desmoplasia (2), trabecular (2), infiltrative (1), encapsulated (1), hyalinized blood vessels (1), stellate lumen (3), solid (1), cystic (1), zonation of cells with dark and pale cells (1), thick loose cores (1), central scarring (1)	Eosinophilic (9), vacuolated (3), clear (3), voluminous (3), oncocytic (2), amphophilic (1), tall cells (1), prominent cell borders (1)	Low grade (6), high grade (6)	Calcifications (3), necrosis (2), lymphocyte aggregates (2), psammoma bodies (1), pigment (1)
<i>TFEB</i> amplified RCCs (N=3) KIRC (1), KIRP (2)	Biphasic (1), tubular (1), nested (1), alveolar (1), oncocyotoma-like (1), micropapillary (1)	Eosinophilic (2), oncocytic (1), granular cytoplasm (1), basal vacuoles (1), melanin-like cytoplasmic pigment (1)	High grade (2), low grade (1), grade 3 in larger nuclei in biphasic pattern	Lymphocyte aggregates (1)
<i>ELOC</i> mutated RCCs (N=3) KIRC (2), KIRP (1)	Cystic (2), fibromuscular stroma (2), nests (1), papillary (1), solid (1), tubular (1), tubulopapillary (1), infiltrative (1)	Clear (3), luminal vacuolization (1)	Low grade (3).	Necrosis (1), sarcomatoid differentiation per report (1), macrophages (1), calcification (1)
<i>NF2</i> mutated RCC (N=9) KIRC (2), KIRP (7)	Type 2 papillary (4), tubulopapillary (4), hierachial papillary branching (3), basement membrane like material with pseudorosetting (2), mucin (1), sarcomatoid (1), rhabdoid, solid (1), hyalinized cores (1), tubules with abortive papillae (1), focal abluminal arrangement of nuclei (1)	Eosinophilic (8), vacuolated (4), clear (2), oncocytic (2), distinct cell borders (1), cytoplasmic mucin (1)	High grade (8), low grade (1), HLRCC-like nucleoli (1), nuclear variability (1)	Lymphocytic aggregates (3), calcifications (2), desmoplastic response (1)
<i>TSC</i> mutated RCC (N=3) KIRC (1), KICH (2)	Encapsulated (2), nests (2), tubules (2), well circumscribed (1), sheets (1)	Eosinophilic, vacuolated and flocculated cytoplasm (3)	Low grade (1) to chromophobe-like (2)	Calcifications (1)
<i>ALK</i> rearranged RCCs (N=2) KIRP (2)	Nests separated by thick stromal septae (1), solid pseudopapillary (1), solid (1), papillary with hierachial branching (1), mucinous secretions (1)	Eosinophilic and clear (1), fat-like intracytoplasmic vacuoles (1), supranuclear vacuoles (1)	Low grade (2)	Macrophages (1)
<i>KRAS</i> mutated RCCs (N=5) KIRP (5)	Tubulopapillary (3), luminal mucin (2), encapsulated (1), well circumscribed (1), papillary (1), compact nests (1), edematous cores with colloid-like secretions (1), nephrogenic adenoma-like (1)	Oncocytic (2), eosinophilic (2), clear (1), supranuclear vacuoles (1)	Low grade (5), Abluminal nuclei (3)	Macrophages (2)
<i>BRAF</i> rearranged/mutated RCCs (N=3) KIRP (3)	Papillary (3), encapsulated (2), type 1 (1), intracystic (1), edematous cores with proteinaceous secretions (1). Characteristic metanephric adenoma (1)	Cytoplasmic clearing (2), distinct cell borders (1)	High grade (1), low grade (2)	Macrophages (2), cholesterol cleft (1)
<i>FH</i> mutated RCCs (N=3) KIRP (3)	Papillary (3), infiltrative (2), tubular (1), cystic (1), pattern heterogeneity (1)	Eosinophilic (3), pseudostratification of nuclei (2), hobnailing (1)	High grade (3), HLRCC-like nucleoli (1), focal abluminal nuclear arrangement (1)	Macrophages (1)
<i>SDH</i> mutated RCCs (N=5) KIRP (5)	Papillary (3), intracystic (2), extracellular mucin (2), well circumscribed (1), hierachial branching (1), tubulopapillary (1), ramifying large tubules (1), sieve-like (1), hyalinized cores (1), hyaline material with pseudorosetting (1), perivascular hyalinization (1), myxoid stroma (1)	Eosinophilic (5), focally clear (1), irregular luminal borders (1), pseudostratification (1), high NC ratio (1)	High grade (3), low grade (2), nuclear grooves (2), coarse chromatin (1), polygonal (1), reverse polarity (1)	Necrosis (2), macrophages (2), calcification (2), psammoma bodies (1)
MMR gene mutated RCCs (N=3) KIRP (3)	Tubulopapillary (2), papillary (1)	Eosinophilic (3), clear (1), pale (1)	Low grade (2), high grade (1)	Macrophages (1)
RCCs with more than 1 mutation (N=1): <i>FH</i> , <i>NF2</i> mutations, <i>TFEB</i> amplification KIRP (1)	CDC-like, solid, tubular, infiltrative, desmoplastic myxoid stroma (1)	Eosinophilic (1)	Focal HLRCC like nucleoli (1)	

**Conclusions:** There exists significant morphologic heterogeneity and phenotypic overlap across RCCs with defined molecular alterations and morphologic features provide limited clues to subclassification of RCCs. While the number of diagnostic entities for kidney tumors continues to increase, we must recognize that many of these entities have overlapping/subtle features that makes

# ABSTRACTS | GENITOURINARY PATHOLOGY (INCLUDING RENAL TUMORS)

histologic classification challenging/impossible, thereby highlighting the significant role molecular typing currently plays in renal pathology and will continue to play in the future.

## 700 Histopathologic and Molecular Characterization of Primary Bladder Intra-Diverticular Carcinomas

Mohamed Alhamar<sup>1</sup>, Lara Harik<sup>2</sup>, Jie-Fu Chen<sup>1</sup>, Judy Sarungbam<sup>1</sup>, Ying-Bei Chen<sup>1</sup>, Anuradha Gopalan<sup>1</sup>, S. Joseph Sirintrapun<sup>1</sup>, Samson Fine<sup>1</sup>, Victor Reuter<sup>1</sup>, Hikmat Al-Ahmadi<sup>1</sup>

<sup>1</sup>Memorial Sloan Kettering Cancer Center, New York, NY, <sup>2</sup>Emory University School of Medicine, Atlanta, GA

**Disclosures:** Mohamed Alhamar: None; Lara Harik: None; Jie-Fu Chen: None; Judy Sarungbam: None; Ying-Bei Chen: None; Anuradha Gopalan: None; S. Joseph Sirintrapun: None; Samson Fine: None; Victor Reuter: None; Hikmat Al-Ahmadi: None

**Background:** Bladder diverticula are outpouchings of urothelial mucosa through weaknesses in the muscular wall. The clinicopathologic and molecular profiles of bladder intra-diverticular carcinomas (BIDC) are not fully established. In addition, staging BIDC is complicated by altered anatomy, primarily due to absence of a muscularis propria in the wall.

**Design:** A retrospective review of all bladder diverticula with neoplasia was performed from 2005-2022, and identified 95 primary BIDC with complete resections. Tumor type, grade, stage and diverticular wall constituents were evaluated. Targeted next-generation sequencing was performed on 28 tumors, including additional 4 BIDC biopsies without resection.

**Results:** BIDC was primarily seen in men (n=93, 98%), with median age of 70y (49-95y). Diverticulectomy or partial cystectomy was performed in 66 cases (69%) & radical cystectomy in 29 (31%). Non-invasive carcinoma was noted in 23 cases (24%, 8=flat, 13=high-grade papillary, 2=low-grade papillary). Invasion was present in 72 cases (76%), 43 of which invaded the perivesical fat (45%). Urothelial carcinoma NOS was the most common in invasive tumors, 35 cases (37%). Divergent differentiation was present in 28 cases (30%), most commonly as squamous (n=17, 61%). Micropapillary features were noted in 4 cases (4%). Pure squamous cell carcinoma was seen in 2 cases and adenocarcinoma was noted in one case. Muscularis mucosa was identified in 77/84 cases (92%) with median thickness of 0.4 mm (ranging from wisps/0.1 mm to 1.0 mm) and 45 cases (58%) showed hypertrophic features (defined as ≥ 0.4 mm). Muscularis propria was identified in 78/84 cases (93%); located mainly at the edge of the os (n=67) or surrounding the diverticula (n=11). Seven patients had lymph node metastases and 9 patients developed distant metastasis. In 28 tumors profiled, oncogenic/likely oncogenic mutations were detected in *TERT* promoter (75%) *TP53* (50%), *ERBB2* (29%), *KMT2D* (29%), *RB1* (25%), *CDKN1A* (25%), *KDM6A* (21%) and *PIK3CA* (21%). Notable copy number alterations include *CDKN2A* deletion (29%) and *MDM2* amplification (14%). Oncogenic *FGFR3* mutations were rare (7%).

**Conclusions:** Primary BIDC arise mainly in adult males and span the entire spectrum of tumors arising within the bladder proper. BIDC shows a higher percentage of invasive tumors, but comparable rate of divergent differentiation to bladder proper tumors. The molecular profiles of BIDC are overall comparable to usual bladder urothelial carcinoma.

## 701 Best Practices for Grossing and Reporting of Post-immunotherapy Nephrectomy Specimens: A Single Institution Experience of 70 Cases

Bassam Alkamachi<sup>1</sup>, Michael Hwang<sup>2</sup>, Kanishka Sircar<sup>1</sup>, Mekenzie Peshoff<sup>1</sup>, Pheroze Tamboli<sup>1</sup>, Priya Rao<sup>1</sup>

<sup>1</sup>The University of Texas MD Anderson Cancer Center, Houston, TX, <sup>2</sup>Indiana University Health, Indianapolis, IN

**Disclosures:** Bassam Alkamachi: None; Michael Hwang: None; Kanishka Sircar: None; Mekenzie Peshoff: None; Pheroze Tamboli: None; Priya Rao: None

**Background:** Immunotherapy is being increasingly used as a neoadjuvant treatment in the management of advanced stage renal cell carcinoma. We present the largest cohort of such cases & outline guidelines for the pathologic examination & reporting of these cases.

**Design:** 70 cases of RCC s/p immunotherapy & nephrectomy collected from 2015-2022 were evaluated. A grossing protocol was developed to assess percent viable tumor. A complete cross section of the largest diameter of tumor was submitted along with sections from areas of gross extrarenal involvement. Percentage of necrosis was reported as an average by assessing gross & microscopic necrosis. Follow up (FU) was calculated in months from the date of surgery to the last known event.

**Results:** We found a discrepancy between the gross & the microscopic stages in 15 cases; 12 cases were grossly pT3 (including 8 with a renal vein thrombus), 2 were pT4; all with no viable extrarenal tumor. Of these, 1 pT1 tumor & 3 pT3 tumors showed complete pathologic response. We divided groups based on % viable tumor in the post treatment nephrectomy. Group A (n=21, mean FU 37.5 mths) showed <20% viable tumor. Group B: (n=48, mean FU 37.6 mths) showed ≥ 20% viable tumor. 1 case did not have % viable tumor available. Kaplan Meir curve showed statistically significant differences in survival within the 2 groups p=0.261

# ABSTRACTS | GENITOURINARY PATHOLOGY (INCLUDING RENAL TUMORS)

(Fig 2). Common histologic findings included hypocellularity, hyalinization, chronic inflammation & myxoid change. Pseudoprogression (an increase in T size of 2 or more cm post therapy) was noted in 8 cases, predominantly due to dense inflammatory infiltrate mimicking a mass lesion grossly; 1 such case showed a pathologic CR and a gross tumor size of 11.5 cm.

Figure 1 - 701

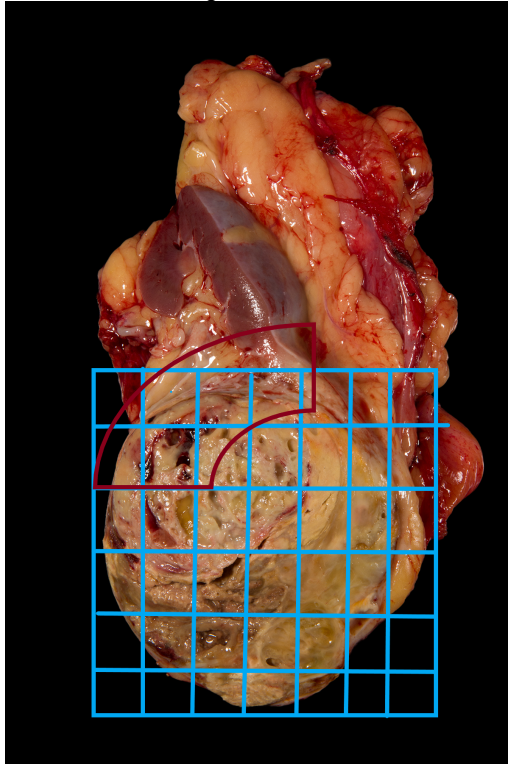
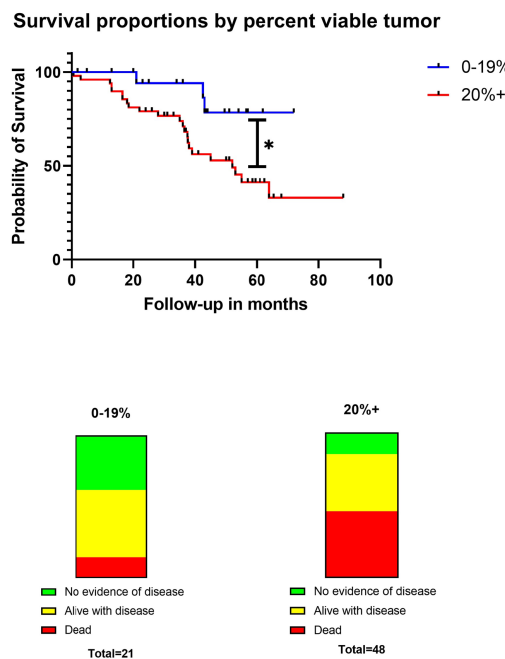


Figure 2 - 701



**Conclusions:** There is a distinct survival difference in patients with <20% viable tumor vs those with ≥ 20% viable tumor. pT stage should be based on the extent of the microscopically viable tumor, as there may be a disconnect between extent of the microscopically viable tumor vs the grossly visible tumor. Conventional staging guidelines may not apply to such cases due to discrepancy between the gross estimate of tumor burden and microscopic extent of viable tumor. Extensive sampling of grossly visible tumor outside the kidney is essential to exclude microscopic tumor involvement, to avoid inaccurate downstaging of the tumor. Although long term FU data is limited in our cohort, there may be some benefit to routinely reporting percent viable tumor in post treatment resection specimens.

## 702 Diagnosis of Oncocytic Renal Neoplasms at Renal Tumour Biopsy and Correlation with Final Classification at Nephrectomy

Shifaa Alqaqa<sup>1</sup>, Carol Cheung<sup>1</sup>, Susan Prendeville<sup>2</sup>

<sup>1</sup>Laboratory Medicine Program, Departments of Anatomical Pathology, University Health Network and University of Toronto, Toronto, ON, <sup>2</sup>University Health Network, University of Toronto, Toronto, ON

**Disclosures:** Shifaa Alqaqa: None; Carol Cheung: None; Susan Prendeville: None

**Background:** Renal tumor biopsy (RTB) is increasingly used to guide the clinical management of patients with small renal masses. Renal tumours with oncocytic morphology are among the most difficult to classify at RTB since the distinction between oncocytoma and chromophobe renal cell carcinoma (ChRCC) has significant implications for patient management and can be challenging in limited specimens. In addition, a number of emerging entities with low-grade oncocytic morphology have been recently described. In this study we evaluated the spectrum of oncocytic tumours diagnosed in a series of RTB and correlated with final diagnosis in patients undergoing nephrectomy.

**Design:** Cases were identified from a consecutive institutional RTB series. All RTB with a diagnosis or differential diagnosis including oncocytoma, ChRCC or low-grade oncocytic neoplasm that could not be classified (incorporating new and emerging entities and tumours with intermediate or hybrid features) were included. High grade and papillary tumours with eosinophilic morphology were not part of this study. RTB findings were correlated with final diagnosis in cases undergoing nephrectomy. Diagnosis was based on the original classification at the time of reporting with review of discordant cases.

# ABSTRACTS | GENITOURINARY PATHOLOGY (INCLUDING RENAL TUMORS)

**Results:** Of 425 RTB, the biopsy diagnosis was oncocytoma/favor oncocytoma in 69% (291/425); ChRCC/favor ChRCC in 27% (116/425) and oncocytic neoplasm NOS (indeterminate) in 18/425 (4%). The latter included tumors with features of emerging entities including 7 low-grade oncocytic tumor (LOT) and 2 eosinophilic vacuolated tumor (EVT). 85 patients had subsequent nephrectomy (table 1). The RTB and final diagnosis was discordant in 3 cases (4%). In 1 discordant case, there was very minimal lesional tissue (<1mm) in the biopsy which limited interpretation. On review, the remaining 2 discordant cases showed features consistent with newly described emerging entities (LOT x 1; EVT x 1).

Cases with RTB and subsequent nephrectomy (n=85)			
RTB Diagnosis	Nephrectomy Diagnosis	Number of cases	Comment
Oncocytoma/favour oncocytoma	Oncocytoma	n=19	-
ChRCC/favour ChRCC	ChRCC	n=57	-
Oncocytic neoplasm unclassified (indeterminate/hybrid features)	ChRCC	n=2	-
Oncocytic neoplasm unclassified (indeterminate/hybrid features)	Oncocytic neoplasm unclassified (indeterminate/hybrid features)	n=4	-
Favour ChRCC	Oncocytoma *	n=1	Features consistent with EVT on review
Favour oncocytoma	ChRCC *	n=1	Features consistent with LOT on review
Favour ChRCC	Oncocytoma *	n=1	<1mm tumour on biopsy

\* discordant cases

**Conclusions:** Despite known challenges, there was overall good concordance between RTB and nephrectomy for the diagnosis of oncocytic tumours. Discordance occurred primarily in tumours with hybrid or intermediate features and some of these cases could be reclassified based on recently described emerging entities. Additional evaluation of the series and correlation with clinical outcome is underway. Further defining reproducible criteria for clinically relevant categories of oncocytic neoplasms may aid risk stratification at RTB to optimise patient management.

## 703 High-Grade Serous Carcinoma of the Testis and Paratestis: A case series of 29 cases

Isabel Alvarado-Cabrero<sup>1</sup>, Raquel Valencia-Cedillo<sup>2</sup>, Rafael Estevez-Castro<sup>3</sup>, Ana Elena Martin-Aguilar<sup>4</sup>, Maria Delia Perez Montiel<sup>5</sup>

<sup>1</sup>Mexican Oncology Hospital SXXI, IMSS, Mexico City, Mexico, <sup>2</sup>Mexican Oncology Hospital IMSS, Mexico City, Mexico, <sup>3</sup>Santiago, Dominican Republic, <sup>4</sup>Hospital de Oncología, CMN Siglo XXI IMSS, <sup>5</sup>Instituto Nacional de Cancerología, Mexico City, Mexico

**Disclosures:** Isabel Alvarado-Cabrero: None; Raquel Valencia-Cedillo: None; Rafael Estevez-Castro: None; Ana Elena Martin-Aguilar: None; Maria Delia Perez Montiel: None

**Background:** Rarely müllerian epithelial tumors (also referred to as ovarian-type epithelial tumors) arise in the testis and paratesticular region. They may arise from müllerian metaplasia of the peritoneal surface of the tunica vaginalis in a process similar to that of primary peritoneal serous tumors in women or from embryonic remnants such as the appendix testis. Most of these tumors are borderline serous tumors but low and high-grade serous carcinomas have also been reported in this location.

**Design:** We therefore investigated the clinical, morphologic, and immunohistochemical features of 29 cases of high-grade serous carcinomas of the testis and paratesticular region diagnosed at two Tertiary Cancer Centers from 1999 to 2021 to better characterize and understand these lesions. Clinical information was obtained from the Institutional clinical files

**Results:** The patients were from 49 to 76 years of age (mean 59 years) and all underwent radical orchietomy. Presenting symptoms included, palpable masses (58%) and scrotal enlargement (42%); 14 were left-sided. Tumors were located in the tunica vaginalis (41.3%), spermatic cord (27.5%), testis (17.2%) and epididymis (13.7%). None of the patients had elevated serum markers. The tumors measured 1.8 to 9.0 cm (mean 3.5 cm) in size. All cases (100%) had infiltrative borders. Histologically they showed the various typical patterns of high-grade serous carcinoma of the ovary. The predominant morphology was papillary, glandular and solid. On immunohistochemical study, the tumor cells were positive for AE1/AE-3 cytokeratin (29/29), CK7(29/29), PAX 8 (29/29), WT-1 (29/29), Calretinin (14/29) and Estrogen Receptor (18/29). Ber.EP4, CK20, OCT3 and SALL4 were negative. At presentation, 11 patients had retroperitoneal lymph node metastasis and 3 patients had lung metastasis. Follow-up available in 27 cases (range 14-82 months, median 52 months), showed 12 (44.4%) dead of disease, 9 (33.3%) alive with disease and 6 (22.2%) alive without disease

**Conclusions:** This series, the largest to date, confirmed the aggressive behavior for high-grade serous carcinoma of the testis and paratestis. Also, our findings indicate that morphological and immunophenotypic features are similar to that of ovarian high-grade serous carcinoma.

## 704 Clinicopathological and Molecular Characterization of Large Nested and Nested Subtypes of Urothelial Carcinoma of the Upper Urinary Tract: An International Multi-Institutional Study

Manju Aron<sup>1</sup>, Darshan Chandrashekhar<sup>2</sup>, Sofia Canete-Portillo<sup>2</sup>, Fadi Brimo<sup>3</sup>, Sean Williamson<sup>4</sup>, Adeboye Osunkoya<sup>5</sup>, Maria Rosaria Raspolli<sup>6</sup>, Lakshmi Kunju<sup>7</sup>, George Netto<sup>2</sup>

<sup>1</sup>Keck School of Medicine of USC, Los Angeles, CA, <sup>2</sup>The University of Alabama at Birmingham, Birmingham, AL, <sup>3</sup>McGill University, Montréal, QC, <sup>4</sup>Cleveland Clinic, Cleveland, OH, <sup>5</sup>Emory University School of Medicine, Atlanta, GA, <sup>6</sup>University Hospital Careggi, Firenze, Italy, <sup>7</sup>University of Michigan, Ann Arbor, MI

**Disclosures:** Manju Aron: None; Darshan Chandrashekhar: None; Sofia Canete-Portillo: None; Fadi Brimo: None; Sean Williamson: None; Adeboye Osunkoya: None; Maria Rosaria Raspolli: None; Lakshmi Kunju: None; George Netto: None

**Background:** Nested (NUC) and large nested (LNUC) subtypes of urothelial carcinoma of the upper urinary tract (UUT) are exceedingly rare. This study describes the clinical and pathological features of the largest cohort to date of these rare tumors and sheds new light on their molecular underpinnings.

**Design:** Resection specimens of LNUC and NUC of UUT were retrospectively collected from 7 institutions. Clinicopathologic data was obtained. DNA was extracted from formalin-fixed paraffin embedded tissue sections. Whole exome sequencing (WES) was performed by trimming raw sequencing reads using Trim\_galore, mapping reads to human primary reference assembly (hg38) using bwa-mem followed by somatic variant calling using Genome Analysis Toolkit (GATK4) 'maftools' R package. Microsatellite instability assay was performed using Idylla™ MSI assay

**Results:** 10 patients with LNUC and 7 patients with NUC were included in this study. The clinicopathologic features of these patients are listed in Table 1. 85.7% of NUC presented as high stage tumors (pT3 and pT4) compared to 40% of LNUC. 60% of LNUC had no evidence of disease on follow up compared to 14.2% of NUC. On WES a total of 26,707 genetic alterations (range: 407- 4168) in 11,451 genes (range: 374-3031) were identified. The 10 most frequently mutated genes were *MT-CYB*, *GOLGA6L6*, *MUC16* (16/17, 94%); and *CCDC187*, *FCGBP*, *FOXD4L4*, *MUC12*, *NBPF26*, *OR4E1*, *TYW1* (15/17, 88%). Pathogenic mutations most commonly involved *MT-CYB* (16/17; 94%), followed by *FGFR3* (8/17; 47%) and *PIK3CA* (5/17; 29.4%) (Fig.1). The latter two were seen only in LNUC. *HOXD9*, *FAM25C*, *DSCAML1*, *MT-CO3* & *PIK3CA* & *CNTNAP 3* showed significant differential mutation among the two subtypes (Fig.2). *KDM6A*, *STAG2*, *TERT* and *FGFR3* showed a trend, with increased mutations in LNUC. Analysis of differential mutational profiles based on pathologic stage (low stage vs high stage) showed statistical significance for *USPY9*, *PARP4* and *FGFR3* in low stage tumors. All tumors were microsatellite stable (MSS) (MSI score of 0).

Table 1. Clinicopathologic Characteristics of Large Nested and Nested subtypes of Urothelial Carcinoma of the Upper Urinary Tract

	Large Nested Subtype (n=10)	Nested Subtype (n=7)
Age (years)	45-83 (mean: 74; median: 78)	55-76 (mean: 68.1; median: 70)
Sex Distribution	Male: 8; Female: 2	Male: 6; Female: 1
Location	Ureter: 6 Renal Pelvis: 4	Ureter: 4 Renal Pelvis: 2 Both: 1
Focality	Unifocal: 7 Multifocal: 3	Unifocal: 6 Multifocal: 1
Size (cm)	1.5-11 (mean: 5.2; median: 3.3)	1.5-8.5 (mean: 3.1; median: 2)
Pathologic Tumor Stage (pT)	pT1: 3 pT2: 3 pT3: 3 pT4: 1	pT1: 0 pT2: 1 pT3: 4 pT4: 2
Lymph Node Metastasis at Presentation (pN)	pNX: 5 pN0: 3 pN1: 1 pN2: 1	pNX: 1 pN0: 3 pN1: 1 pN2: 2
Histologic Type	Pure: 4 Mixed: 6	Pure: 3 Mixed: 4
Urothelial Carcinoma in Situ	5/10 (50%)	4/10 (40%)
Surface Papillary Component	8/10 (80%)	2/7 (28.6%)
Clinical Follow Up	3-84 months (median 10 months) NED: 6 AWD: 1 DOD: 3	2-48 months (median 9 months) NED: 1 AWD: 5 DOD: 1

NED: No evidence of disease, AWD: Alive with disease, DOD: Dead of disease, Mixed: indicates presence of invasive conventional urothelial carcinoma

Figure 1 - 704

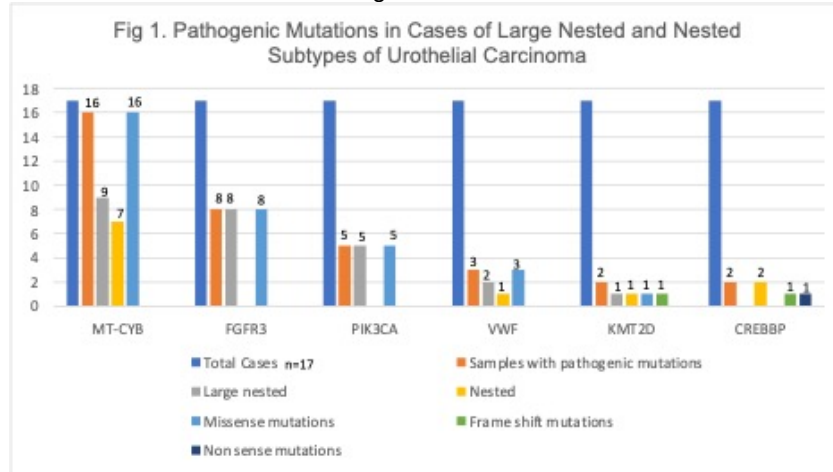
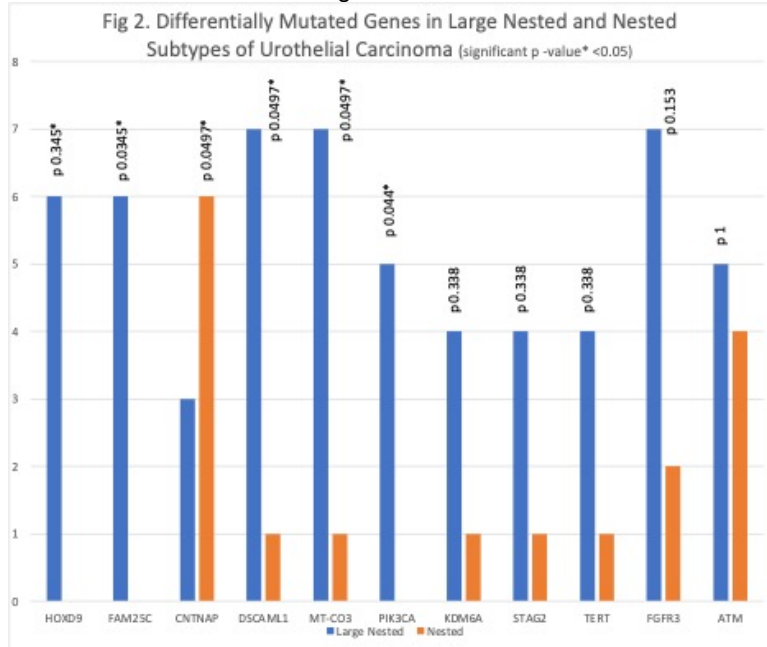


Figure 2 - 704



**Conclusions:** NUC involving the UUT appears to be more aggressive than LNUC. The most frequent pathogenic mutation in both subtypes involve *MT-CYB*, which has not been previously reported. *PIK3CA* is significantly mutated in LNUC while *FGFR3* mutations are more common in LNUC and is significantly associated with low stage tumors. This study expands the clinicopathologic spectrum and molecular profile of these tumors, highlighting genetic alterations of potential therapeutic and prognostic value.

## 705 TRPS1 Expression in Primary and Metastatic Prostatic Adenocarcinoma: Is TRPS1 Truly Specific and Sensitive for a Breast Primary?

Sara Bachert<sup>1</sup>, Jing Di<sup>2</sup>, Zin Myint<sup>1</sup>, Dava Piecoro<sup>3</sup>, Robert McDonald<sup>1</sup>, Derek Allison<sup>1</sup>

<sup>1</sup>University of Kentucky College of Medicine, Lexington, KY, <sup>2</sup>University of Kentucky College of Medicine Dept. of Pathology and Laboratory Medicine, Lexington, KY, <sup>3</sup>University of Kentucky, Lexington, KY

**Disclosures:** Sara Bachert: None; Jing Di: None; Zin Myint: None; Dava Piecoro: None; Robert McDonald: None; Derek Allison: None

**Background:** Trichorhinophalangeal syndrome type 1 (TRPS1) has recently been reported as a highly sensitive and specific immunohistochemical (IHC) marker for breast carcinomas, especially when determining the primary site of origin. Interestingly, to date, there is no data on TRPS1 expression in prostate cancer, which is important because a subset of breast carcinomas, particularly hormone receptor positive cases of the type that occur in men, can be positive for NKX3.1 and show overlapping

# ABSTRACTS | GENITOURINARY PATHOLOGY (INCLUDING RENAL TUMORS)

morphologic features. As a result, this study was performed to evaluate TRPS1 and GATA3 staining in primary and metastatic prostatic adenocarcinoma.

**Design:** A cohort of primary and metastatic prostatic adenocarcinomas was identified at our institution and selected for TRPS1 and GATA3 IHC staining. TRPS1 was optimized based on previously published protocols with appropriate positive and negative controls, and GATA3 was performed per clinical protocol. Stains were scored utilizing a modified quick score method in the same manner as previously published: expression score= percent of tumor staining (0, <1%; 1, 1–10%; 2, 11–50%; 3, 51–100%) multiplied by the average staining intensity (0, negative; 1, weak; 2, moderate; 3, strong). Expression scores of 0-1, 2, 3-4, or 6-9 were considered negative, low, intermediate, and high, respectively.

**Results:** Sixty-nine cases were stained with both markers, including 35 primary tumors and 34 metastases (local and distant); 26 cases were matched primaries and metastases. TRPS1 expression was seen in 22 cases overall (31.9%), including 10 primaries (28.6%) and 12 (35.3%) metastases. Intermediate or high expression was seen in 17 cases (24.6%). For the 26 matched cases, 9 primaries and 7 metastases were positive for TRPS1. There was no statistically significant difference in primary versus metastasis in TRPS1 expression ( $p=0.13$ ). All cases were negative for GATA3.

**Conclusions:** In this study, a significant number of prostatic adenocarcinomas were positive for TRPS1 (31.9% in our cohort), including a quarter of cases showing intermediate or high expression. This finding is significant and suggests TRPS1 may not be as specific for a breast primary as the current literature states. Importantly, all cases were negative for GATA3, which underscores its usefulness in ruling out a prostatic primary in a scenario where TRPS1 or NKX3.1 could be positive. In summary, more work is needed to evaluate TRPS1 expression in a variety of primary and metastatic tumors before accurate claims of specificity and sensitivity can be made.

## 706 Large Cribriform Pattern 4 in Grade Group 2 and Grade Group 3 Prostate Cancer May Not Have an Independent Influence on Pathological Radical Prostatectomy Outcomes

Hisham Bahmad<sup>1</sup>, Oleksii Iakymenko<sup>2</sup>, Ivan Nemov<sup>3</sup>, Sheida Khosravaniardakani<sup>4</sup>, Alisia Gilleard<sup>5</sup>, Laurence Briski<sup>6</sup>, Robert Poppiti<sup>1</sup>, Merce Jorda<sup>3</sup>, Oleksandr Kryvenko<sup>3</sup>

<sup>1</sup>Mount Sinai Medical Center of Florida, Miami Beach, FL, <sup>2</sup>Albert Einstein College of Medicine, Montefiore Medical Center, Bronx, NY, <sup>3</sup>University of Miami Miller School of Medicine, Miami, FL, <sup>4</sup>Florida International University, Miami, FL, <sup>5</sup>University of Miami, Miami, FL, <sup>6</sup>University of Miami Health System, Miami, FL

**Disclosures:** Hisham Bahmad: None; Oleksii Iakymenko: None; Ivan Nemov: None; Sheida Khosravaniardakani: None; Alisia Gilleard: None; Laurence Briski: None; Robert Poppiti: None; Merce Jorda: None; Oleksandr Kryvenko: None

**Background:** Several studies have found that the presence of large cribriform pattern 4 (LCP4) correlates with worse pathological outcomes at radical prostatectomy (RP). We assessed if LCP4, controlled for percent of Gleason pattern 4 (GP4%) and tumor volume (TV), is an independent predictor of adverse pathological RP outcomes.

**Design:** A single-center retrospective cohort analysis was performed. All cases were re-reviewed and only Grade Group (GG) 2 and 3 tumors were included in the analysis. Tumor grade, GP4%, stage, TV and margin status of each tumor were measured individually. We assessed statistical differences between the presence or absence of LCP4 groups based on patient age, prostate specific antigen density (PSAD), TV, GP4%, pathologic stage (pT2, pT2+, pT3a, and pT3b), positive surgical margin (SM+), and lymph node metastasis (LN+). We conducted univariable analysis (UVA) and multivariable analysis (MVA) where in each tumor we assessed the association of the presence of LCP4 with pathological RP outcomes accounting for the effect of TV and GP4%.  $P$  values were obtained by Chi-square test and Student's  $t$ -test. Statistical analysis was conducted using SAS v9.4.

**Results:** Patients with LCP4 cancer (487/1108) had higher PSAD ( $P < 0.001$ ), larger TV (1078.56 cm<sup>3</sup> vs. 564.48 cm<sup>3</sup>;  $P < 0.001$ ), and higher GP4% (70% vs. 20%;  $P < 0.001$ ). In UVA, LCP4 predicted higher GG, stage (all  $P < 0.001$ ), SM+ ( $P = 0.002$ ), and LN+ ( $P = 0.034$ ). In a MVA based on a multiple-effects generalized linear model, when TV and GP4% were accounted for, LCP4 lost its independent statistically significant impact on RP outcomes: pT2+, pT3a, pT3b, SM+, and LN+, all  $P > 0.05$  but TV and GP4% retain it (Table 1).

# ABSTRACTS | GENITOURINARY PATHOLOGY (INCLUDING RENAL TUMORS)

**Table 1. Effect of presence of large cribriform pattern 4 (LCP4) on tumor stage (pT2+, pT3a and pT3b), LN+, and SM+.**

Outcome	Variable	Category	Multivariate analysis 1	P-value	Multivariate analysis 2	P-value
			OR (95% CI)		OR (95% CI)	
pT2+	<b>LCP4</b>	NO	Reference		Reference	
		YES	1.104 (0.572-2.131)	0.769	1.127 (0.581-2.186)	0.723
	<b>LOC(POST)</b>	NO	N/A		Reference	
		YES	N/A		0.859 (0.493-1.498)	0.593
pT3a	<b>Log of TV</b>	Every one unit increased	2.118 (1.647-2.723)	<0.001	2.071 (1.607-2.670)	<0.001
		Every one unit increased	0.991 (0.978-1.004)	0.158	0.991 (0.979-1.004)	0.184
	<b>Log of GP4%</b>	NO	Reference		Reference	
		YES	1.12 (0.631-1.989)	0.699	1.076 (0.603-1.920)	0.805
pT3b	<b>LOC(POST)</b>	NO	N/A		Reference	
		YES	N/A		6.832 (2.840-16.434)	<0.001
	<b>Log of TV</b>	Every one unit increased	2.449 (1.938-3.095)	<0.001	2.726 (2.129-3.489)	<0.001
		Every one unit increased	1.012 (1.002-1.021)	0.021	1.010 (1.000-1.020)	0.056
SM+	<b>LCP4</b>	NO	Reference		Reference	
		YES	0.947 (0.615-1.458)	0.805	0.928 (0.599-1.437)	0.737
	<b>Log of TV</b>	Every one unit increased	2.473 (2.132-2.894)	<0.001	N/A	
		Every one unit increased	0.997 (0.990-1.003)	0.351	N/A	
LN+	<b>LCP4</b>	NO	Reference		N/A	
		YES	1.899 (0.368-14.932)	0.482	N/A	
	<b>Log of TV</b>	Every one unit increased	2.175 (1.309-3.701)	0.003	N/A	
		Every one unit increased	1.015 (0.991-1.043)	0.239	N/A	

**Abbreviations:** GP4%: percentage Gleason pattern 4; LCP4: large cribriform pattern 4; LN+: lymph node metastasis; N/A: not applicable; SM+: positive surgical margin; TV: tumor volume.

**Conclusions:** LCP4, TV, and GP4% are codependent variable in GG2 and GG3 cancer. Similar to previous studies, we demonstrated a significant association of LCP4 with PSAD, TV, GP4%, GG, pathologic stage, SM+, and LN+ when TV and GP4% of corresponding TNs were not taken into consideration. After controlling for the effect of GP4% and TV on adverse pathological RP outcomes, LCP4 alone was no longer an independent predictor. Therefore, higher GP4% and TV of tumors in which LCP4 is present are likely to explain the more adverse cancer found at RP rather than the presence of LCP4 alone. Our findings are clinically pertinent to patients with LCP4 diagnosed on needle biopsy for their preoperative risk stratification management planning.

## 707 Molecular Features of High Grade, Non-Sarcomatoid Chromophobe Renal Cell Carcinoma

Ezra Baraban<sup>1</sup>, Pedram Argani<sup>1</sup>, Jonathan Epstein<sup>2</sup>

<sup>1</sup>Johns Hopkins Hospital, Baltimore, MD, <sup>2</sup>Johns Hopkins Medical Institutions, Baltimore, MD

**Disclosures:** Ezra Baraban: None; Pedram Argani: None; Jonathan Epstein: None

**Background:** Chromophobe Renal Cell Carcinoma (ChRCC) is a common subtype of renal cell carcinoma which typically behaves indolently. However a rare subset of ChRCC cases shows high-grade morphologic features and is more likely to demonstrate aggressive clinical behavior. While the molecular features of histologically classic ChRCC have been well characterized, there is limited data available regarding the molecular features of histologically high-grade ChRCC. We therefore assembled a cohort of high-grade ChRCC cases and investigated their molecular features using next-generation sequencing (NGS).

**Design:** Kidney resections were collected and examined histologically for cases showing areas of classic ChRCC as well as morphologically distinct areas of high-grade ChRCC, which were defined by: increased cellularity, high mitotic rate, atypical mitotic

# ABSTRACTS | GENITOURINARY PATHOLOGY (INCLUDING RENAL TUMORS)

figures, necrosis, and loss of typical ChRCC morphologic features. For six cases, separate areas of low and high grade ChRCC were independently dissected and analyzed by NGS using a panel analyzing 800 cancer related genes.

**Results:** Compared to adjacent classic ChRCC areas (Figure 1A, 2A), high grade ChRCC showed tumor necrosis (1B), vascular invasion within renal sinus fat (2B), increased cellularity with atypical mitotic figures (1C, 2C) and tumor cells with prominent central nucleoli (1D, 2D). High grade ChRCC areas harbored additional oncogenic mutations not seen in adjacent areas of classic ChRCC. Five of six high grade ChRCC cases harbored damaging *TP53* alterations, four of which were not seen in the adjacent classic ChRCC areas. Two high grade ChRCC cases harbored damaging *PTEN* alterations not seen in the adjacent classic ChRCC areas. Five of the high grade ChRCC cases harbored damaging *RB* alterations, none of which were seen in the adjacent classic ChRCC areas. Figures 1 and 2 demonstrate morphologic features of classic and high-grade ChRCC areas from two representative cases along with molecular alterations detected only in areas of high-grade ChRCC. Additional studies are in progress to spatially map the molecular alterations using immunohistochemical surrogates for the observed mutations.

Figure 1 - 707

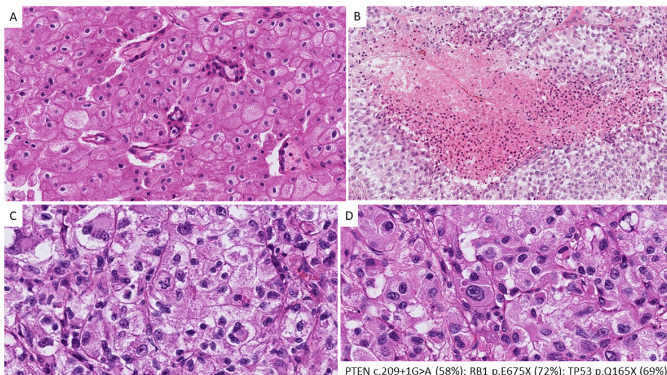
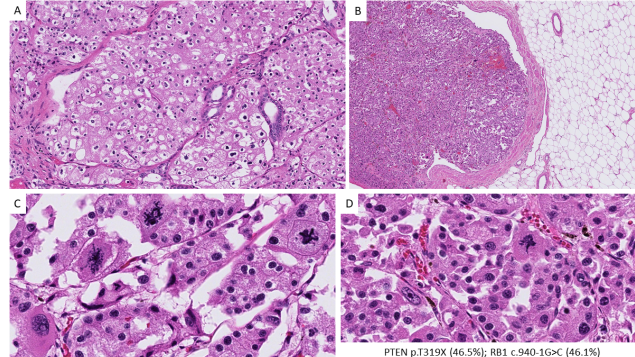


Figure 2 - 707



**Conclusions:** High Grade ChRCC shows aggressive behavior and harbors molecular alterations not seen in adjacent classic ChRCC. This study provides insight into the molecular pathogenesis of high grade ChRCC, implicating *TP53*, *PTEN*, and *RB* in the progression from classic to high-grade ChRCC.

## 708 Morphologic and Molecular Features of Mismatch Repair Deficient (MMR-d) Prostate Cancer: Insights from a Series of Radical Prostatectomies

Ezra Baraban<sup>1</sup>, Eric Erak<sup>2</sup>, Tamara Lotan<sup>2</sup>

<sup>1</sup>Johns Hopkins Hospital, Baltimore, MD, <sup>2</sup>Johns Hopkins University School of Medicine, Baltimore, MD

**Disclosures:** Ezra Baraban: None; Eric Erak: None; Tamara Lotan: None

**Background:** Although uncommon in primary prostate cancer, mismatch repair protein deficiency (MMR-d) is enriched in Grade Group 4-5 tumors and has clinical implications, raising consideration for genetic counseling as well as eligibility for immunotherapy. Thus far limited data regarding MMR-d prostate cancer is available based on a small number of described cases. We assembled a large cohort of MMR-d primary prostate cancers to investigate their clinical, morphologic, immunohistochemical, and genetic features.

**Design:** MMR-d prostate cancers were identified by IHC or germline/somatic sequencing. For 20 radical prostatectomies, the following parameters were evaluated: Grade Group (GG), stage, intraductal carcinoma, intratumoral stromal tumor infiltrating lymphocytes (TIL) (assessed visually according to International TILS Working Group guidelines on a representative tumor block with maximal inflammation), intratumoral germinal centers.

**Results:** MMR-d prostate cancers (Table 1) were frequently of high grade and stage (85% GG5, 90%  $\geq$ pT3), and often harbored intraductal carcinoma (65%). Large cribriform glands were common (80%), with the diameter of the largest cribriform glands exceeding 1 mm in 60% of cases. Tumors frequently harbored striking inflammatory infiltrates, with an average stromal tumor infiltrating lymphocyte (TIL) content of 30%, and germinal centers noted in 40% of cases. Distinctive morphologies were noted in a subset of cases, including foci reminiscent of lymphoepithelial-like carcinoma (LELC) seen in other organs (30%) as well as Crohn's-like lymphoid aggregates noted in MMR-d colorectal cancer (55%). The distribution of MMR protein loss by IHC was: 90% MSH2/6, 5% MSH6, 5% MLH1/PMS2, 0% PMS2. Germline testing was performed in 65% of cases and 38% of these had confirmed pathogenic germline mutations. 75% of cases had available somatic sequencing and all had confirmed pathogenic MMR gene alterations. The average tumor mutational burden (TMB) was 31/Mb (range: 3-104), but only 43% of cases had microsatellite instability (MSI) by sequencing.

# ABSTRACTS | GENITOURINARY PATHOLOGY (INCLUDING RENAL TUMORS)

Figure 1 - 708

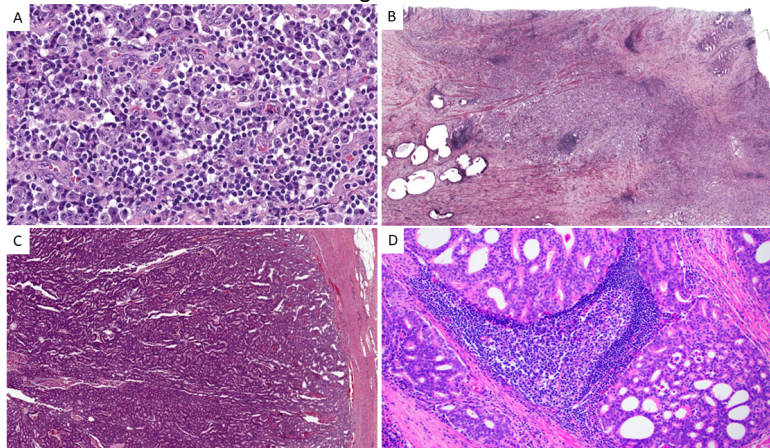


Figure 1. Morphologic Features of MMR-d Prostate Cancer. A. Focus of high grade carcinoma dispersed within a dense lymphoid infiltrate, resulting in a lymphoepithelial-like morphology (Case 8, 40x magnification). B. Dense "Crohn's-like" lymphoid aggregates at the periphery of the tumor nodule (Case 20, 2x magnification). C. Expansile cribriform gland which approaches 1 cm in diameter (Case 17, 2x magnification). D. Intratumoral germinat center directly adjacent to a focus of infiltrating cribriform carcinoma (Case 11, 20x magnification).

Figure 2 - 708

Case #	Age at Diagnosis	RP stage	Gleason Score	MMR IHC Loss	Germline MMR Status	Somatic MMR Alteration	NGS MSI Status	Tumor Mutation Burden	Intraductal Carcinoma	Large Cribriform Glands	Largest Cribriform Gland (mm)	Crohn-like Aggregates	Stromal TIL	LELC-like foci	Germlinal Centers
1	60	pT3bN0	4+5=9	MSH2/6	N/A	N/A	N/A	N/A	0	1	<1	1	50	0	1
2	56	pT3aN0	4+5=7	MSH6	MSH6	N/A	N/A	N/A	1	1	2	1	50	0	0
3	66	pT2N0	5+4=9	MSH2/6	none	MSH2	MSI-H	24	1	1	4	0	30	1	1
4	48	pT3bN1	5+4=9	MSH2/6	none	MSH2	MSI-H	27	1	1	5	1	40	0	1
5	68	pT3aN1	4+5=9	MSH2/6	none	MSH2	Indeterminate	14	1	1	10	1	20	0	0
6	69	pT3aN0	5+4=9	MSH2/6	MSH2	MSH2	MSI-H	104	0	1	<1	1	30	1	1
7	58	pT3bN0	5+4=9	MSH2/6	N/A	MSH2	MSI-H	76	1	1	<1	0	60	1	1
8	56	pT3bN0	5+4=9	MSH2/6	MSH2	MSH2	MSI-H	9	0	0	N/A	1	30	0	0
9	65	pT3bN0	5+4=9	MSH2/6	N/A	N/A	N/A	N/A	1	1	4	0	10	0	0
10	63	pT3bN0	4+5=9	MSH2/6	N/A	N/A	N/A	N/A	1	1	4	0	50	1	1
11	71	pT3bN0	4+5=9	MSH2/6	N/A	N/A	N/A	N/A	1	1	7	0	20	0	0
12	48	pT3aN0	3+4=7	MSH2/6	MSH2	MSH2	Indeterminate	10	0	0	N/A	1	10	0	0
13	63	pT2N0	4+5=9	MSH2/6	none	MSH2	MSS	28	0	0	N/A	0	20	0	0
14	64	pT3aN0	4+5=9	MSH2/6	none	MSH2	MSS	3	0	1	3	0	10	0	0
15	66	pT3aN0	5+4=9	MSH2/6	none	MSH2	Indeterminate	24	1	1	<1	1	10	0	0
16	63	pT3bN0	5+4=9	MSH2/6	none	MSH2	Indeterminate	34	1	1	10	0	30	0	1
17	63	pT3bN1	5+4=9	MSH2/6	MSH2	MSH2	MSI-H	45	1	1	2	1	60	1	1
18	61	pT3aN0	4+5=9	MSH2/6	N/A	MSH2	MSS	N/A	1	1	10	1	50	0	0
19	70	pT3aN0	4+5=9	MLH1/PMS2	none	MLH1	MSS	10	1	0	N/A	1	50	1	0
20	56	pT3bN0	3+4=7	MSH2/6	N/A	MSH2	N/A	N/A	0	1	5	0	0	0	0

Figure 2. Clinicopathologic Features of A Series of 20 Radical Prostatectomies with MMR-d Prostatic Adenocarcinoma.

**Conclusions:** Several morphologic features (cribriform glands >1mm, germinal centers, lymphoepithelial-like foci) may suggest MMR-d, but these are insensitive and systematic IHC screening for GG4-5 cancers is warranted. Cases with MMR-d by IHC and somatic mutations may lack MSI as assessed by sequencing and have variable TMB. Further studies to characterize the tumor microenvironment in this series of MMR-d prostate cancers are ongoing.

## 709 Are Histological Patterns of Prostate Carcinoma Predictive of Homologous Recombination Deficiency Gene Mutations?

Marc Barry<sup>1</sup>, Jonathon Mahlow<sup>1</sup>, Daniel Albertson<sup>2</sup>, Yeonjung Jo<sup>3</sup>, Michael Balatico<sup>2</sup>, Tori Seasor<sup>2</sup>, Georges Gebrael<sup>3</sup>, Shruti Kumar<sup>3</sup>, Nicolas Sayegh<sup>3</sup>, Nishita Tripathi<sup>3</sup>, Umang Swami<sup>3</sup>, Neeraj Agarwal<sup>3</sup>, Deepika Sirohi<sup>1</sup>

<sup>1</sup>The University of Utah/ARUP Laboratories, Salt Lake City, UT, <sup>2</sup>The University of Utah, Salt Lake City, UT, <sup>3</sup>Huntsman Cancer Institute, Salt Lake City, UT

**Disclosures:** Marc Barry: None; Jonathon Mahlow: None; Daniel Albertson: None; Yeonjung Jo: None; Michael Balatico: None; Tori Seasor: None; Georges Gebrael: None; Shruti Kumar: None; Nicolas Sayegh: None; Nishita Tripathi: None; Umang Swami: None; Neeraj Agarwal: None; Deepika Sirohi: None

**Background:** Somatic or germline Homologous Recombination Deficiency (HRD) gene mutations are seen in up to 20% of prostate carcinomas and are predictive of response to poly (ADP-ribose) polymerase (PARP) inhibitors. In this study we hypothesize that histological patterns of prostate carcinoma are predictive of HRD gene mutations.

# ABSTRACTS | GENITOURINARY PATHOLOGY (INCLUDING RENAL TUMORS)

**Design:** 130 cases of prostate carcinoma with somatic or germline mutations (38 with *BRCA1/2*, 36 with non-*BRCA1/2* HRD gene mutations) and 56 cases negative for HRD gene mutations (*ATM*, *BARD1*, *BRIP1*, *CHEK2*, *MRE11A*, *NBN*, *PALB2*, *RAD51C*, *RAD51D*, *EMSY*, *PTEN*, *ATR*, *CHEK1*, *FAM175A*) were included. Comprehensive genomic profiling was performed at a CLIA-certified laboratory. Cases were evaluated for presence or absence of histological patterns of prostate carcinoma and quantified by 4 genitourinary pathologists. Discordances were resolved by consensus review. Presence of prostate carcinoma histological patterns were analyzed for any correlation with mutations in HRD genes, *BRCA1/2* or non-*BRCA1/2* HRD genes compared to the negative control group using Chi-square test. Patterns at greater than 20 and 30% of tumor volume were additionally evaluated for any correlation.

**Results:** Cribriform pattern, intraductal carcinoma (IDC), ductal carcinoma, neuroendocrine carcinoma, signet ring-like pattern and lobular carcinoma-like patterns were not predictive of *BRCA1/2*, non-*BRCA1/2* HRD gene or HRD gene mutations (Table-1). Analyzing for tumors with greater than 20 or 30% patterns also did not show any correlation. Neuroendocrine carcinoma showed a marginal increase in cases with *BRCA1/2* mutations compared to the negative group ( $p=0.07$ ), although the number of neuroendocrine carcinomas in the entire cohort was small ( $n=6$ ). The non-*BRCA1/2* HRD group showed a marginally greater increase in volume of cribriform pattern (greater than 30%) compared to the negative group.

Histological Pattern	<i>BRCA1/2</i> mutated N=38	Non- <i>BRCA1/2</i> HRD mutated N=36	Negative Control N=56
Cribriform pattern	29 (73.6%)	29 (80.6%)	38 (71.7%)
Intraductal carcinoma	13 (34.2%)	7 (19.4%)	20 (37%)
Ductal carcinoma	6 (15.8%)	2 (5.6%)	7 (12.5%)
Neuroendocrine carcinoma	4 (10.5%)	1 (2.8%)	1 (1.8%)
Signet ring-like pattern	17 (44.7%)	19 (52.8%)	27 (78.2%)
Lobular carcinoma-like pattern	16 (42.1%)	16 (44.4%)	17 (30.4%)
Grade group 5	26 ((68.4%)	18 (50%)	31 (55.3%)
Grade group 4	5 (13.2%)	12 (33.3%)	13 (23.2%)
Grade group 3	3 (7.9%)	3 (8.3%)	6 (10.7%)
Grade group 2	2 (5.3%)	3 (8.3%)	5 (8.9%)

**Conclusions:** In this study histological patterns were not predictive of HRD gene mutations. A marginal increase of neuroendocrine morphology and high-volume cribriform patterns were seen in *BRCA1/2* and non-*BRCA1/2* HRD mutated prostate carcinomas respectively. This data suggests that histopathologic examination alone is insufficient to distinguish *BRCA1/2* and HRD gene mutated prostate cancers, further highlighting the importance of ancillary molecular diagnostics in therapy selection for those who may benefit from PARP inhibitors.

## 710 Clinical, Molecular and Immunohistochemical Profiles Of Nested Subtype Of Urothelial Carcinoma

Merve Basar Yerebakan<sup>1</sup>, Timothy Clinton<sup>2</sup>, Karissa Whiting<sup>1</sup>, Carissa Chu<sup>3</sup>, Gamze Gokturk Ozcan<sup>1</sup>, Dilara Akbulut<sup>3</sup>, Jie-Fu Chen<sup>1</sup>, Judy Sarungbam<sup>1</sup>, Ying-Bei Chen<sup>1</sup>, Anuradha Gopalan<sup>1</sup>, S. Joseph Sirintrapun<sup>1</sup>, Samson Fine<sup>1</sup>, Gopa Iyer<sup>1</sup>, Bernard Bochner<sup>1</sup>, David Solit<sup>1</sup>, Hikmat Al-Ahmadie<sup>1</sup>

<sup>1</sup>Memorial Sloan Kettering Cancer Center, New York, NY, <sup>2</sup>Brigham and Women's Hospital, Dana-Farber Cancer Institute, Harvard Medical School, Boston, MA, <sup>3</sup>National Cancer Institute, National Institutes of Health, Bethesda, MD

**Disclosures:** Merve Basar Yerebakan: None; Timothy Clinton: None; Karissa Whiting: None; Carissa Chu: None; Gamze Gokturk Ozcan: None; Dilara Akbulut: None; Jie-Fu Chen: None; Judy Sarungbam: None; Ying-Bei Chen: None; Anuradha Gopalan: None; S. Joseph Sirintrapun: None; Samson Fine: None; Gopa Iyer: None; Bernard Bochner: None; David Solit: None; Hikmat Al-Ahmadie: None

**Background:** Nested urothelial carcinoma (NUC) is a rare but aggressive subtype of bladder cancer despite its deceptively bland histopathologic features. Therefore, identifying pathogenic and potentially targetable genomic alterations could inform novel treatment approaches. Herein, we analyzed clinical and genomic data and expression of basal and luminal immunohistochemical (IHC) markers in a cohort of NUC.

**Design:** Targeted next generation sequencing was performed on 51 NUC tumors and 26 high-grade urothelial carcinomas with nested features (HGUC-N). In addition, IHC for luminal (FOXA1, GATA3, PPARG) and basal (CK5/6, CK14) markers was performed on 34 NUC and 23 HGUC-N tumors, assembled in a tissue microarray. Clinical and molecular data were compared between the NUC and HGUC-N tumors and a prospectively annotated cohort of 600 clinically localized urothelial carcinomas, not otherwise specified (UC-NOS).

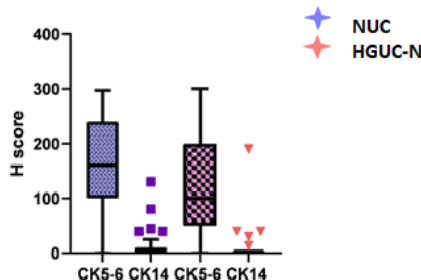
**Results:** In NUC cohort, there was 19 male and 15 female patients. The age ranged from 55 to 87 (69.7). With a median following-up of 4.3 years, classic NUC was significantly associated with higher risk of cancer death compared to UC NOS (HR 2.06,  $p=0.004$ ). Tumor mutational burden was lower in NUC tumors compared to HGUC-N and UC NOS ( $p<0.001$ ). Evaluation of 136

# ABSTRACTS | GENITOURINARY PATHOLOGY (INCLUDING RENAL TUMORS)

altered cancer-associated genes detected differences in the frequency of commonly mutated genes among the 3 cohorts (Table 1). Mutations in *TP53*, *FGFR3*, *ARID1A* and *KDM6A* were less frequent in NUC than in UC-NOS. A subset of NUC was enriched with recurrent *RhoA* mutations and *FOXA1* amplification. All NUC cases expressed luminal markers including GATA3, *FOXA1* and *PPARG* (range from 94.2% to 100%). NUC also expressed the basal markers CK5/6 and CK14 in 30 (88%) and 7 (21%) of cases, respectively. Although the mean H-score of CK5/6 expression was higher in NUC compared to HGUC-N (152>123), this difference not significant ( $p=0.15$ ). *PAX8* was expressed in 8 (24%) NUC compared to 5 (21.7%) HGUC-N.

Alteration	Nested variant of UC (N=51)	High-grade UC with nested features (N=26)	UC NOS (N=611)	p-value	q-value
<b>TERT</b>	34 (67)	17 (65)	433 (71)	0.70	0.70
<b>FGFR3</b>	6 (12)	4 (15)	188 (31)	<0.01	0.06
<b>RhoA</b>	8 (16)	8 (31)	24 (4)	<0.01	<0.01
<b>CCND1 amp</b>	12 (24)	7 (27)	78 (13)	0.02	0.20
<b>TP53</b>	10 (20)	14 (54)	239 (39)	<0.01	0.06
<b>KDM6A</b>	13 (25)	15 (58)	212 (35)	0.02	0.20
<b>ARID1A</b>	8 (16)	12 (46)	184 (30)	0.01	0.20
<b>FOXA1</b>	6 (12)	6 (23)	29 (5)	<0.01	0.02

Figure 1 - 710



**Conclusions:** Despite its bland histomorphology, the NUC subtype of bladder cancer is associated with worse outcome than UC NOS. Despite the overlapping genomic landscape of NUC and UC-NOS, NUC is enriched for recurrent *RhoA* mutations and *FOXA1* amplification, with less frequent mutations in *TP53*, the *TERT* promoter, *KDM6A* and *ARID1A*. HGUC with nested features is molecularly more comparable to UC NOS than to NUC. A subset of NUC tumors express both luminal and basal markers, the significance of which will require further study.

## 711 Clinicopathologic Differences in Unilateral Versus Bilateral Seminal Vesicle Invasion of Prostate Cancer in Radical Prostatectomies

Yekaterina Belogrivtseva<sup>1</sup>, Mohamad Mazen Gafeer<sup>2</sup>, Aileen Grace Arriola<sup>1</sup>

<sup>1</sup>Temple University Hospital, Philadelphia, PA, <sup>2</sup>Hospital of the University of Pennsylvania, Philadelphia, PA

**Disclosures:** Yekaterina Belogrivtseva: None; Mohamad Mazen Gafeer: None; Aileen Grace Arriola: None

**Background:** Reporting seminal vesicle invasion (SVI) following radical prostatectomy (RP) has historically been associated with a poor prognosis. The extent of SVI has also been included in some previous studies, but results regarding its influence on prognosis were contradictory. Our aim is to provide more data on whether bilateral SVI is associated with worse oncological outcomes by analyzing a large RP cohort from our institution, potentially helping to further define the prostate cancer protocol for future prognostic applications.

**Design:** We reviewed clinicopathological data of men who underwent RP during the period from 1/1/12-06/28/19. The following data were collected from pathology reports and patient charts: age, race, grade group, margin status, lymph node (LN) status, type of LN dissection, extraprostatic extension (EPE), SVI, bladder neck involvement, tumor volume, and follow-up such as recurrence and progression of the disease. Differences between categorical values were assessed by chi-square/Fisher exact test and continuous values by student T-test.

**Results:** 769 RP cases were identified. Among them, 114/769 (14.8%) had SVI, out of which 56 (7.2%) had bilateral and 54 (7%) had unilateral SVI. Table 1 shows the clinical and pathological characteristics of the series stratified by unilateral and bilateral SVI. Our study shows that bilateral SVI was present more frequently in patients with higher tumor volumes ( $p\text{-value}=0.0006$ ), positive margins ( $p\text{-value}=0.0064$ ), EPE other than SVI ( $p\text{-value}<0.0001$ ), and LN affection ( $p\text{-value}=0.0013$ ). These features are considered adverse pathological factors and represent more aggressive tumors. In our study, there was a shorter time interval for the development of biochemical recurrence (BCR) with higher PSA values in the bilateral SVI group compared to unilateral SVI, although did not reach statistical significance. There was also no difference in the progression of disease between the two groups. Limitations of the present study include its retrospective nature and the fact that it was a single-center study.

# ABSTRACTS | GENITOURINARY PATHOLOGY (INCLUDING RENAL TUMORS)

Clinicopathologic feature	Bilateral SVI (N=56)	Unilateral (N=58)	p-value
<b>Age</b> in years, mean (range)	62.6 (46-73)	63.9 (40-76)	0.2630
<b>Race</b>	2 (3.6%) Asian Black Caucasian Hispanic Unknown/Other	0 (0%) 19 (33.9%) 29 (51.7%) 3 (5.4%) 3 (5.4%)	0.2476
<b>Pathologic LN Stage</b>	21 (37.5%) 0 1	41 (70.7%) 17 (29.3%)	<b>0.0004</b>
<b>Number Positive LN</b> , mean (range)	2 (0-17)	0.6 (0-7)	<b>0.0013</b>
<b>Total Number LN in PLND</b> , mean (range)	16.7 (3-43)	15.6 (2-68)	0.5444
<b>PLND Type</b>	21 (38.2%) Standard Extended Unknown	27 (46.6%) 31 (53.5%) 0 (0%)	0.4472
<b>LN Present in Periprostatic Fat</b>	38 (67.9%) No Yes	43 (74.1%) 15 (25.9%)	0.4598
<b>Grade Group</b>	1 (1.8%) 12 (21.4%) 2 3 4 5	0 (0%) 19 (33.3%) 14 (24.6%) 8 (14.0%) 13 (28.1%)	0.5612
<b>RP Margin Status</b>	10 (17.9%) Negative Positive	24 (41.4%) 34 (58.6%)	<b>0.0061</b>
<b>EPE, other than SVI</b>	1 (1.8%) No Yes	19 (32.8%) 39 (67.2%)	<0.0001
<b>Bladder Neck Invasion</b>	39 (73.6%) No Yes	48 (84.2%) 9 (15.8%)	0.1709
<b>Tumor Volume %</b> , mean (range)	56.2 (10-95)	40.2 (10-90)	<b>0.0006</b>
<b>Biochemical Recurrence (BCR)</b>	30 (55.6%) Yes No	29 (53.7%) 25 (46.3%)	0.8467
<b>Time to BCR (months)</b> , mean (range)	16.4 (2-56)	23.4 (2-89)	0.1710
<b>BCR PSA value</b> , mean (range)	1.9 (0.3-11.4)	0.9 (0.35-4.3)	0.1046
<b>Progression of Disease</b>	9 (16.4%) Yes No	9 (16.7%) 45 (83.3%)	0.9660
SVI-seminal vesicle invasion, LN-lymph node, PLND-pelvic lymph node dissection, RP-radical prostatectomy, EPE-extraprostatic extension			

**Conclusions:** Bilateral SVI did not influence future BCR or progression, despite being associated with worse pathological features. Although not statistically significant, our study showed a shorter interval to BCR and a higher PSA value at BCR for bilateral SVI. Further studies with a larger sample size would be worthwhile to pursue in order to understand the clinical implications of pathologic reporting of bilateral versus unilateral SVI.

## 712 Fumarate Hydratase Deficient Renal Cell Carcinoma Involving the Peritoneum with a Pseudomesotheliomatous Pattern: A Diagnostic Pitfall

Anna Calio<sup>1</sup>, Stefano Marletta<sup>1</sup>, Elena Bariani<sup>1</sup>, Lavinia Stefanizzi<sup>2</sup>, Lisa Marcolini<sup>2</sup>, Matteo Brunelli<sup>1</sup>, Guido Martignoni<sup>3</sup>

<sup>1</sup>University of Verona, Verona, Italy, <sup>2</sup>Ospedale Pederzoli, Peschiera del Garda, Italy, <sup>3</sup>University of Verona, Ospedale Pederzoli, Peschiera del Garda, Italy

**Disclosures:** Anna Calio: None; Stefano Marletta: None; Elena Bariani: None; Lavinia Stefanizzi: None; Lisa Marcolini: None; Matteo Brunelli: None; Guido Martignoni: None

**Background:** Fumarate Hydratase (FH) deficient renal cell carcinoma is a rare neoplasm characterized by mutations in the FH gene, often associated with cutaneous and uterine leiomyomas. Neoplastic cells may be arranged in a great variety of architectural patterns, including papillary, solid, and tubulocystic. These tumors often show an aggressive behavior with rapid metastatic spread to many distant organs, like the liver, the lungs, the bones, and the peritoneum. Involvement of this latter one is not such an infrequent finding and could cause difficulties in differentiating between primary mesothelial reactive or neoplastic diseases and metastatic localizations. This is of particular concern when peritoneum involvement firstly shows up.

**Design:** Among a series of eleven FH deficient renal cell carcinomas, eight of them with aggressive behaviour, we retrieved three tumors with peritoneal metastasis resembling mesothelial proliferations. In one case the peritoneal involvement was the first finding of the disease and in two cases previous diagnosis of renal cell carcinoma was on record.

**Results:** One patient was female, two were males. Peritoneal involvement was represented by papillary to microcystic proliferation made up of cells characterized by eosinophilic cytoplasm, roundish nuclei and prominent nucleoli, initially suspicious for a benign reactive mesothelial process or a primary peritoneal mesothelioma. The neoplastic cells were positive for CK8-18 and CKAE1/AE3 but did not express mesothelial markers (podoplanin, calretinin, and WT1). Nuclear staining for PAX8 suggested to consider the possibility of a localization from a renal cell tumor. Loss of immunohistochemical expression of FH led to the diagnosis of metastatic FH deficient renal cell carcinoma. The revision of the primary renal tumors confirmed this histotype.

**Conclusions:** FH deficient renal cell carcinomas are aggressive neoplasms with early metastatic spread. In our series of aggressive FH deficient renal cell carcinoma, a significant percentage of the cases (3/8, 37%) displayed the peritoneum involvement mimicking a mesothelial disease due to either cytological or architectural features. Therefore, in patients with renal mass and peritoneal involvement with controversial histopathological features, an immunohistochemical panel should include PAX8 and FH in order to avoid misdiagnoses of such a morphological pitfall.

## 713 Papillary Renal Neoplasm with Reverse Polarity Versus Eosinophilic Papillary Renal Cell Carcinoma: Clinicopathological and Biological Comparison

Vincent Francis Castillo<sup>1</sup>, Kiril Trpkov<sup>2</sup>, Theodorus Van Der Kwast<sup>3</sup>, Fabio Rotondo<sup>4</sup>, Malek Hamdani<sup>5</sup>, Rola Saleeb<sup>1</sup>

<sup>1</sup>St. Michael's Hospital/University of Toronto, Toronto, ON, <sup>2</sup>University of Calgary, Calgary, AB, <sup>3</sup>University Health Network, Toronto, ON, <sup>4</sup>Unity Health Toronto, Toronto, ON, <sup>5</sup>Dynacare, Brampton, ON

**Disclosures:** Vincent Francis Castillo: None; Kiril Trpkov: None; Theodorus Van Der Kwast: None; Fabio Rotondo: None; Malek Hamdani: None; Rola Saleeb: None

**Background:** Papillary renal neoplasm with reverse polarity (PRNRP) is a renal entity with distinct oncocytic morphology, immunoprofile and frequent KRAS mutations (Raspollini, 2022). Although it is considered a subset of papillary renal cell carcinoma (PRCC), it has a very indolent clinical course (Al-Obaidy, 2019). Thus, the distinction of this renal tumor from other oncocytic/eosinophilic PRCCs (ePRCC) has important prognostic implications. ABCC2 is an active transporter protein that localizes to the apical cell membranes. It is overexpressed in more aggressive PRCCs on transcriptomic and proteomic levels and it shows prognostic utility in PRCC (Saleeb, 2022). In this study, we compare the PRNRP and ePRCC clinicopathological parameters and the ABCC2 expression.

**Design:** PRNRP (n=8) and ePRCC (n=21) cases were selected from resection specimens and corresponding clinicopathological data were collected. Immunohistochemical (IHC) staining for ABCC2 and GATA3 was performed. ABCC2 staining patterns were classified as negative, cytoplasmic, and cell "brush border". RNA in-situ hybridization (ISH) was used to assess ABCC2 transcript levels in-situ. A semi-quantitative scoring system (0-4) was adapted to assess the RNA ISH. Statistical analysis for T test, Fisher's exact, Chi-square and log-rank were performed using GraphPad Prism 9 software.

**Results:** All 8 PRNRPs had diffuse, moderate to strong IHC staining for GATA3 and very weak cytoplasmic staining for ABCC2. PRNRP had no detectable ABCC2 transcripts on RNA ISH (score 0). In contrast, none of the ePRCCs had GATA3 expression, while 16/21 (76%) showed ABCC2 IHC brush border expression. ePRCCs also had a significantly higher transcript level of ABCC2 by RNA ISH ( $p=0.001$ ). All PRNRPs had low grade (WHO/ISUP 1-2) and low-stage disease ( $pT1a$ ). ePRCCs were also characterized by significantly larger tumor size ( $p=0.0039$ ), higher WHO/ISUP grade ( $p<0.0001$ ), and higher stage ( $p=0.0374$ ) (Table 1). None of the PRNRP cases showed disease progression, while 2 ePRCCs (~10%) had disease progression.

**Table 1: Comparison of the Clinicopathologic Characteristics of PRNRP with ePRCC**

	PRNRP (n = 8)	ePRCC (n= 21)	P value
Age [mean (range), years]	64 (51-79)	62 (35-83)	
Sex (M:F ratio)	1:1	3:1	
Tumor laterality (R:L ratio)	0.6:1	1.1:1	
Tumor size [mean (range), cm]	1.3 (0.5-3.1)	5.9 (2.3-14)	P=0.0039 (T test)
WHO/ISUP grade			
1-2 (low)	8	4	P < 0.0001 (Fisher's exact)
3-4 (high)	0	17	
Pathologic stage			
pT1	8	12	P=0.0374 (Chi-square for trend)
pT2	0	4	
pT3	0	5	
pT4	0	0	
Clinical stage			
I	8	12	P=0.0436 (Chi-square for trend)
II	0	3	
III	0	4	
IV	0	2	
Follow-up [median (range), mos]	24 (5-124)	47 (1-209)	
Disease Status			
No evidence of disease	6*	16	P=0.5685 (Log-rank test)
Alive with disease	0	1	
Dead of disease	0	1	
Dead of other cause	0	3	

\*no follow-up data on two PRNRP cases

**Figure 1 - 713**

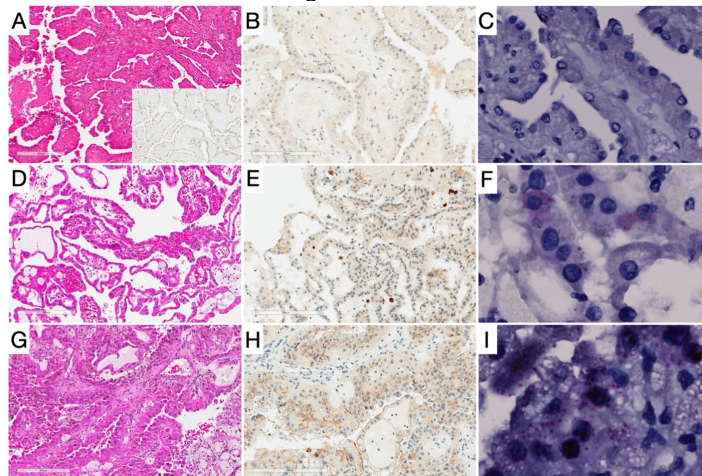


Figure 1: A) Representative H&E of PRNRP with strong, diffuse GATA3 (inset); B-C) PRNRP shows ABCC2 weak cytoplasmic staining (RNA-ISH score 0); D-F) ePRCC has ABCC2 brush border <50% reactivity (RNA-ISH score 2); G-I) ePRCC with ABCC2 brush border ≥50% staining (RNA-ISH score 4)

**Conclusions:** PRNRP is clinically and biologically distinct from ePRCC. ePRCCs show a significantly more aggressive tumour behaviour and have higher proteomic and transcriptomic ABCC2 expression highlighted by the IHC BB pattern and the RNA ISH analysis respectively. Hence, it is crucial to differentiate between these two entities with careful morphological and immunohistochemical analysis.

#### **714 Next Generation Sequencing Testing of Renal Mass Biopsies in an Academic Center Subspecialty Clinical Setting**

Tushar Chakravarty<sup>1</sup>, Jeffry Simko<sup>1</sup>, Bradley Stohr<sup>1</sup>, Emily Chan<sup>1</sup>

<sup>1</sup>University of California, San Francisco, San Francisco, CA

**Disclosures:** Tushar Chakravarty: None; Jeffry Simko: None; Bradley Stohr: None; Emily Chan: None

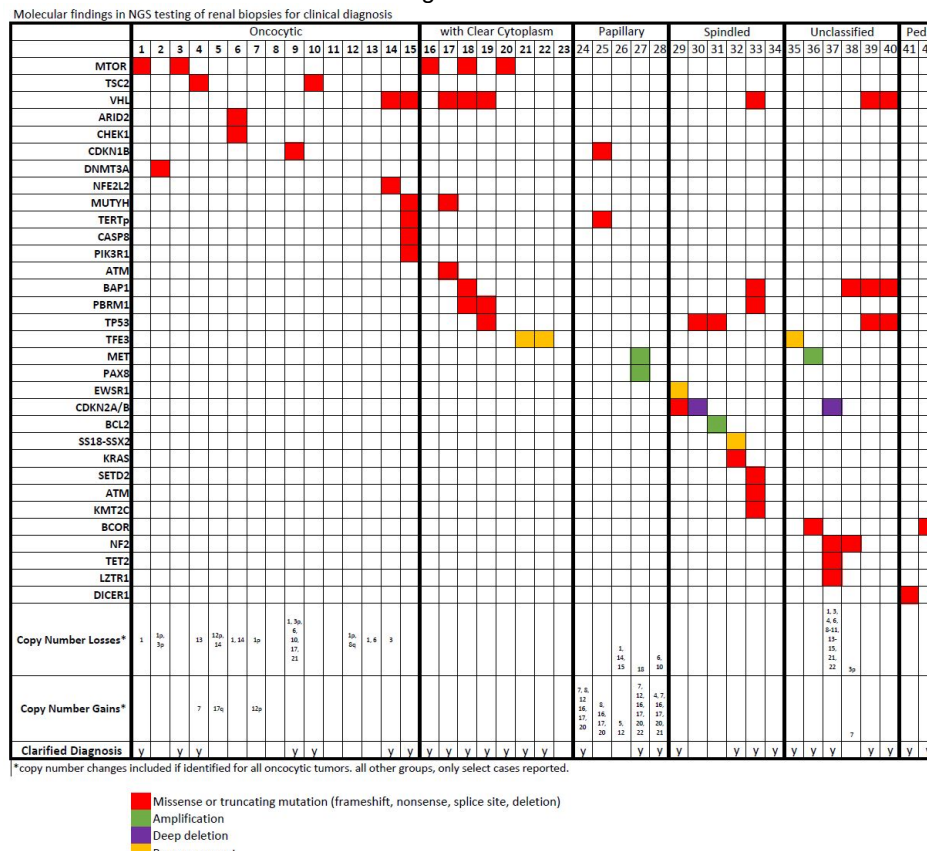
**Background:** Increasing number of kidney tumors are now molecularly defined, though next generation sequencing (NGS) testing is not routinely used in clinical practice, largely due to limited availability, cost and uncertain utility. In this study we present our institutional experience with NGS testing on renal mass biopsies in an academic center subspecialty clinical setting.

## ABSTRACTS | GENITOURINARY PATHOLOGY (INCLUDING RENAL TUMORS)

**Design:** Our pathology clinical database was searched for renal mass biopsies (2017-2022) in which our institution's NGS assay was ordered. The NGS assay uses capture-based NGS sequencing to target and analyze the coding regions of 479-520 cancer genes and select introns of 41-47 genes (dependent on iteration if test used). Clinical and pathologic information was extracted from the electronic medical record. The test was recorded as clarifying the diagnosis if a specific mutation, translocation or copy number profile previously reported for a known histologic subtype of renal tumor was identified without any other confounding molecular features.

**Results:** We identified 52/300 (17%) renal biopsies in which sequencing was ordered. 11 cases were ordered by the treating physician: 4 oncocytic renal neoplasms, 4 urothelial carcinomas, 2 clear cell renal cell carcinomas and one leukemia/lymphoma. 41 cases were ordered by the pathologist and divided into the following categories: oncocytic (12), with clear cytoplasm (9), papillary (5), spindled (6), unclassified (7) and pediatric (2). Indication for sequencing by the pathologist ranged from confirmation of expected diagnosis (due to an unusual morphology, immunochemical result, or clinical presentation) to complete diagnostic uncertainty. Of these 41 pathologist ordered cases plus the 4 oncocytic renal neoplasm ordered by the treating physician, the molecular findings clarified the diagnosis in 28 (62%): oncocytic 7/16 (44%), with clear cytoplasm 7/9 (78%), papillary 3/5 (60%), spindled 4/6 (67%), unclassified 5/7 (71%), and pediatric 2/2 (100%). Detailed molecular findings Fig 1. In 3 cases, sequencing was not performed due to tumor quantity not sufficient; in these cases, an extensive immunohistochemical workup had been performed, largely exhausting the specimen.

Figure 1 - 714



**Conclusions:** Molecular testing on renal biopsies was helpful to provide a more definitive diagnosis in the majority of our pathologist ordered cases, across multiple morphologic settings. Dividing renal biopsies into two cassettes can help preserve adequate tissue for molecular testing.

**715 Positive NKX3.1 as a Diagnostic Pitfall for Prostate Cancer in Extramammary Paget's Disease of Genitourinary Sites**

Constance Chen<sup>1</sup>, Rony Francois<sup>1</sup>, Thaddeus Mully<sup>1</sup>, Ankur Sangoi<sup>2</sup>, Jeffry Simko<sup>1</sup>, Philip LeBoit<sup>1</sup>, Emily Chan<sup>1</sup>  
<sup>1</sup>University of California, San Francisco, San Francisco, CA, <sup>2</sup>El Camino Hospital, Mountain View, CA

**Disclosures:** Constance Chen: None; Rony Francois: None; Thaddeus Mully: None; Ankur Sanghi: None; Jeffry Simko: None; Philip LeBoit: None; Emily Chan: None

**Background:** Extramammary Paget's disease (EMPD) is an uncommon condition that can affect genitourinary sites. In our experience, we have noted variable nuclear positivity with the prostatic marker NKX3.1 in some cases of EMPD, a potential

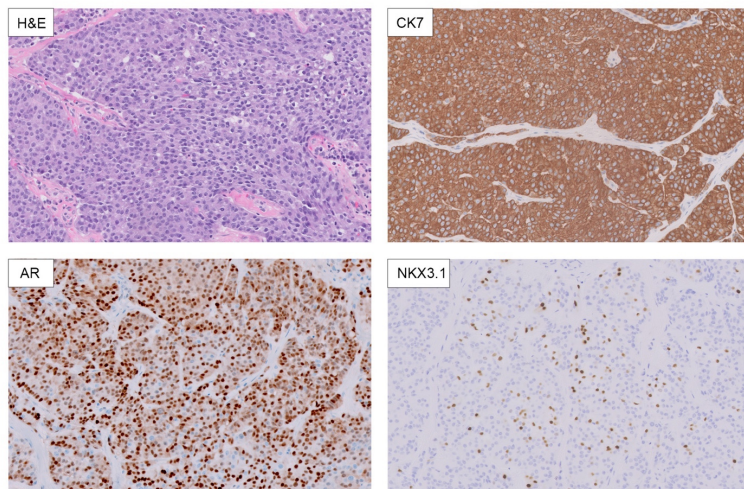
# ABSTRACTS | GENITOURINARY PATHOLOGY (INCLUDING RENAL TUMORS)

diagnostic pitfall for prostate cancer. A recent study on 20 cases of EMPD by *Shabikhani et al 2020* showed 1 case with positive PSA, but positive NKX3.1 in EMPD has not been reported. In this study, we sought to characterize the incidence of NKX3.1 staining in EMPD of genitourinary sites.

**Design:** A retrospective multi-center study was conducted. We obtained cases of EMPD involving genitourinary sites from our pathology databases and collaborators (2000-2020). H&E slides were reviewed, and IHC was performed and evaluated on available material (CK7, CK20, NKX3.1, AR, GATA3, and PSA). Demographics information and cancer history were obtained from the electronic medical record.

**Results:** We identified 19 cases of EMPD involving genitourinary sites (scrotum, penis, groin, suprapubic region, and inguinal crease) from male patients. The mean age at diagnosis was 72 years old. IHC showed: CK7 positive in 19/19, CK20 negative in 16/18, GATA3 positive in 18/18, androgen receptor (AR) positive in 16/18, PSA negative in 18/18, and NKX3.1 showed variable nuclear positivity in 4/19. One of the 4 cases with positive NKX3.1 had a reported history of prostate cancer with metastatic tumor to pelvic lymph nodes that were initially called metastatic prostatic cancer, but subsequently revised to metastatic EMPD following evaluation of their groin lesion and expert consultation. We also evaluated 3 cases of EMPD involving female vulvar sites. Mean age was 72 years old. NKX3.1 was positive in 1/3, CK7 was positive in 3/3, CK20 was negative in 2/3, and AR and PSA were negative in 3/3.

Figure 1 - 715



**Conclusions:** EMPD commonly shows diffuse AR+ IHC and occasional NKX3.1+ IHC, potentially leading to concern for metastatic cutaneous prostate cancer, especially in male patients with a history of prostate cancer in which EMPD may not be considered. However, a solid growth pattern and characteristic IHC pattern of CK7+, CK20-, and GATA3+ can be helpful in avoiding this diagnostic pitfall.

## 716 NOS-1: A Tumor-Specific Diagnostic Biomarker for Metanephric Adenoma

Anya Chinnaiyan<sup>1</sup>, Xiaoming (Mindy) Wang<sup>1</sup>, Rahul Mannan<sup>2</sup>, Yuping Zhang<sup>3</sup>, Christine Caldwell-Smith<sup>1</sup>, Amanda Miller<sup>1</sup>, Xuhong Cao<sup>1</sup>, Arul Chinnaiyan<sup>1</sup>, Saravana Dhanasekaran<sup>1</sup>, Rohit Mehra<sup>1</sup>

<sup>1</sup>University of Michigan, Ann Arbor, MI, <sup>2</sup>Michigan Medicine, University of Michigan, Ann Arbor, MI, <sup>3</sup>Michigan Center for Translational Pathology, Ann Arbor, MI

**Disclosures:** Anya Chinnaiyan: None; Xiaoming (Mindy) Wang: None; Rahul Mannan: None; Yuping Zhang: None; Christine Caldwell-Smith: None; Amanda Miller: None; Xuhong Cao: None; Arul Chinnaiyan: None; Saravana Dhanasekaran: None; Rohit Mehra: None

**Background:** Metanephric adenoma (MA), which arises from the undifferentiated metanephric mesenchyme, is a rare benign neoplasm that generally localizes to the renal cortex and comprises 0.2% of all adult renal neoplasms. It has overlapping morphological features with epithelial predominant Wilms' tumor (WT) and papillary renal cell carcinoma type (PRCC), which can cause diagnostic dilemmas. Current clinical practice includes immunohistochemical (IHC) based combination markers for MA which is generally CK7-, AMACR-, BRAF V600E+, WT1+, and CD57+. However, these biomarkers cannot accurately differentiate MA from its histopathological mimickers. Hence, we set our goal to identify MA-specific markers that can reinforce the current clinical IHC panel and validate them using an independent methodology.

**Design:** With the goal described above, we interrogated in-house and publicly available major and rare renal tumor subtypes' RNAseq data and nominated Trinucleotide Repeat Containing Gene 6C Protein (*TNRC6C*), Superoxide Dismutase 3 (*SOD3*), and Nitric Oxide Synthase 1 (*NOS1*) as three differentially expressed genes between MA and the remaining RCC subtypes including

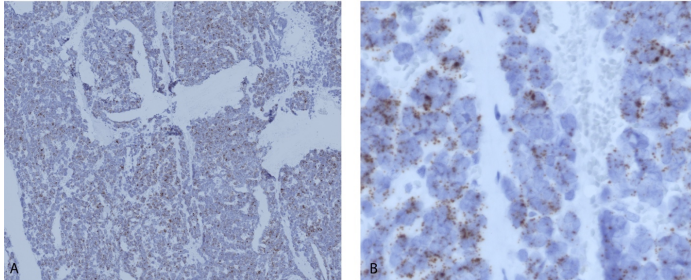
# ABSTRACTS | GENITOURINARY PATHOLOGY (INCLUDING RENAL TUMORS)

WT. We assembled a focused cohort containing 6 MA, 8 WT, and 8 PRCC cases for validation studies. We utilized a chromogenic RNA in-situ hybridization (RNA-ISH) assay on formalin-fixed paraffin-embedded (FFPE) sections for validating the nominated biomarkers. For RNA-ISH-based biomarker assessment, individual chromogenic mRNA transcripts were recorded in the neoplastic cells and final H-scores (out of 400) were calculated.

**Results:** *TNRC6C* expression was noted in all samples for both MA (6/6; 100%) and WT (8/8; 100%) and detected in a subset of PRCC (3/8; 37.5%) cases. *SOD3* was expressed in all (6/6; 100%) MA but also detected in 3/8 (37.5%) cases for both PRCC and WT. In contrast, *NOS1* expression was seen to be positive in all (6/6; 100%) MA samples and negative in all PRCC (0/8; 0%) and WT (0/8; 0%) samples. The expression of *NOS1* was variable with H-scores ranging from 90-252.

Figure 1 - 716

Figure-1A. *NOS1* RNA-ISH expression in a representative case of metanephric adenoma  
B. Higher magnification showing the m-RNA transcripts.



**Conclusions:** All nominated markers had positive expression in MA cases, however, *TNRC6C* and *SOD3* showed positive expression in a subset of WT and PRCC in the study cohort. On the other hand, robust *NOS1* expression was detected exclusively in MA and not in either WT or PRCC cases included in our validation cohort. Our analysis suggests that of the three nominated markers, *NOS1* staining can reliably distinguish between MA and WT or PRCC.

## 717 Genomic Landscape of Urothelial Carcinoma with Divergent Differentiation and Histologic Subtypes

Carissa Chu<sup>1</sup>, Ziyu Chen<sup>1</sup>, Karissa Whiting<sup>1</sup>, Rayan Rammal<sup>2</sup>, Andrew Lenis<sup>3</sup>, Gamze Gokturk Ozcan<sup>1</sup>, Dilara Akbulut<sup>4</sup>, Merve Basar Yerebakan<sup>1</sup>, Jie-Fu Chen<sup>1</sup>, S. Joseph Sirintrapun<sup>1</sup>, Ying-Bei Chen<sup>1</sup>, Anuradha Gopalan<sup>1</sup>, Samson Fine<sup>1</sup>, Bernard Bochner<sup>1</sup>, Gopa Iyer<sup>1</sup>, Judy Sarungbam<sup>1</sup>, David Solit<sup>1</sup>, Hikmat Al-Ahmadie<sup>1</sup>

<sup>1</sup>Memorial Sloan Kettering Cancer Center, New York, NY, <sup>2</sup>University of Pittsburgh Medical Center, Pittsburgh, PA, <sup>3</sup>Columbia Presbyterian Medical Center, New York, NY, <sup>4</sup>National Cancer Institute, National Institutes of Health, Bethesda, MD

**Disclosures:** Carissa Chu: None; Ziyu Chen: None; Karissa Whiting: None; Rayan Rammal: None; Andrew Lenis: None; Gamze Gokturk Ozcan: None; Dilara Akbulut: None; Merve Basar Yerebakan: None; Jie-Fu Chen: None; S. Joseph Sirintrapun: None; Ying-Bei Chen: None; Anuradha Gopalan: None; Samson Fine: None; Bernard Bochner: None; Gopa Iyer: None; Judy Sarungbam: None; David Solit: None; Hikmat Al-Ahmadie: None

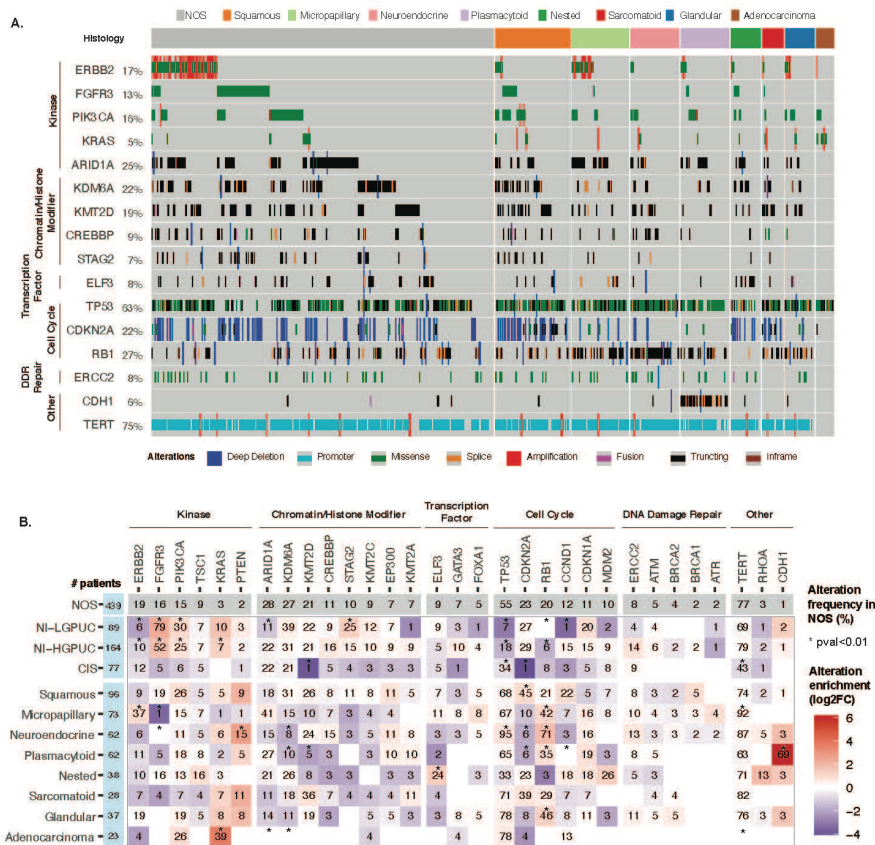
**Background:** Urothelial carcinoma (UC) displays a wide spectrum of morphologic subtypes that often co-exist within individual tumors resulting in a heterogeneous histomorphologic appearance. Although up to 40% of bladder cancers exhibit divergent differentiation and/or histopathologic subtypes, little is known about the differences in oncogenic drivers and clinical outcomes across these distinct entities.

**Design:** Molecular profiling by a next generation sequencing assay was performed on 1,188 primary bladder tumors, including invasive UC NOS (n=439), UC with squamous (n=96) and glandular and differentiation (n=37), micropapillary (n=73), high grade neuroendocrine (n=62), plasmacytoid (n=62), nested (n=38) and sarcomatoid (n=28) subtypes, and primary bladder adenocarcinoma (n=23). Also included was non-invasive (NI) low grade papillary UC (n= 89), NI high grade papillary UC (n=164) and urothelial carcinoma in situ (n=77). Associations between genetic alterations and morphologic features were assessed.

**Results:** The results are depicted in Figure 1. *FGFR3* mutations were enriched in non-invasive papillary UC (52% HG, 78% LG), and were less frequent in invasive UC NOS (15%), squamous (19%) and nested (15%) tumors. *ERBB2* mutations/amplification were identified in all histologic subtypes in a mutually exclusive pattern with *FGFR3* mutations/fusions with the highest prevalence noted in micropapillary (37%), glandular (19%) and UC NOS (19%) tumors. Plasmacytoid carcinoma was associated with *CDH1* mutations and small cell/neuroendocrine carcinoma was notable for frequent *TP53*, *RB1* and *TERT* promoter mutations. Patterns of gene mutations in adenocarcinoma were most distinct from other subtypes, with frequent mutations in *KRAS* and infrequent *TERT* promoter and chromatin modifying gene mutations.

# ABSTRACTS | GENITOURINARY PATHOLOGY (INCLUDING RENAL TUMORS)

Figure 1 - 717



**Conclusions:** This analysis highlights the genomic diversity and phenotypic plasticity of urothelial carcinoma and its subtypes. *CDH1* alterations are associated with plasmacytoid carcinoma and *ERBB2* alterations are enriched in micropapillary carcinoma. Targetable alterations in *FGFR3* and *ERBB2* are present across UC and its histologic subtypes and may be an attractive therapeutic approach in these settings. Genomic profiles of primary bladder adenocarcinoma are most distinct from other UC subtypes and suggests a distinct pathogenesis.

## 718 Detection of Extraprostatic Extension by Transperineal Multiparametric Magnetic Resonance Imaging-Utrasound Fusion-Targeted Combined with Systemic Template Prostate Biopsy

Hao-Wen Chuang<sup>1</sup>, Shulin Wu<sup>2</sup>, Sharron Lin<sup>2</sup>, Ting Zhao<sup>2</sup>, Chin-Lee Wu<sup>2</sup>

<sup>1</sup>Kaohsiung Veterans General Hospital, Kaohsiung, Taiwan, <sup>2</sup>Massachusetts General Hospital, Boston, MA

**Disclosures:** Hao-Wen Chuang: None; Shulin Wu: None; Sharron Lin: None; Ting Zhao: None; Chin-Lee Wu: None

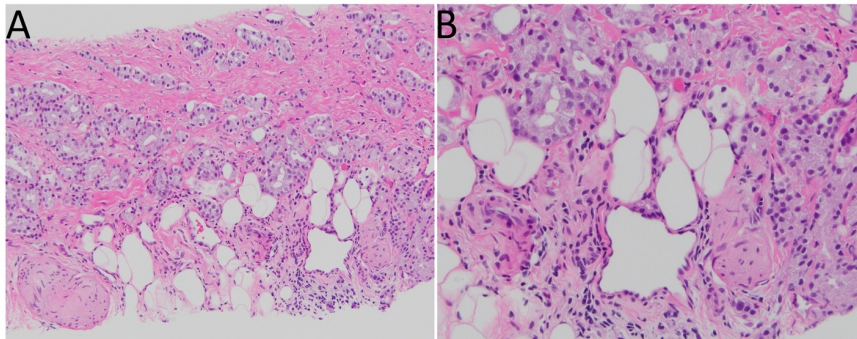
**Background:** Extraprostatic extension (EPE) of prostate cancer (PCa) on transrectal (TR) needle core biopsy (Bx) is a rare histopathological finding which will help clinical decision-making. The detection efficiency through transperineal (TP) approach has yet been explored.

**Design:** We retrospectively reviewed 2622 PCa cases having concomitant systemic template biopsy (SBx) and multiparametric magnetic resonance imaging (MRI)-ultrasound fusion-targeted biopsy (TBx) using TR (n = 1877) or TP (n = 745) approach in our institution between 01/2015 and 03/2022. We assessed and compared biopsy detection of EPE, defined as the presence of cancer cells within or immediately adjacent to periprostatic adipose tissue (Fig. A&B), by approaches (TP and TR) and methods (SBx and TBx).

**Results:** Thirty-six cases with EPE were identified (36/2622, 1.4%). TP showed a significantly higher EPE detection rate than TR in the combined methods (2.1% vs 1.1%,  $p = 0.032$ ), SBx (1.6% vs 0.7%,  $p = 0.044$ ) or TBx (1.2% vs 0.5%,  $p = 0.042$ ). SBx showed a higher EPE detection rate than TBx with no statistical significance. More EPEs were found at non-base sites of TP than TR (84% vs 50%,  $p = 0.028$ ).

<b>Extraprostatic extension detection rate in patients undergone both systematic template and MRI-US fusion-targeted prostate biopsy through transrectal or transperineal approach: comparison between transrectal and transperineal approach</b>			
<b>Methods</b>	<b>TR (n=1877)</b>	<b>TP (n=745)</b>	<b>p value</b>
EPE-detection rate, n (%)			
Combined	20 (1.1)	16 (2.1)	<b>0.032</b>
SBx	14 (0.7)	12 (1.6)	<b>0.044</b>
TBx	9 (0.5)	9 (1.2)	<b>0.042</b>
<b>Comparison of extraprostatic extension between systematic template biopsy and fusion-targeted prostate biopsy</b>			
<b>Biopsy approaches</b>	<b>EPE detected in SBx</b>	<b>EPE detected in TBx</b>	<b>p value</b>
EPE-detection rate, n (%)			
TR (n=1877)	14 (0.7)	9 (0.5)	0.296
TP (n=745)	12 (1.6)	9 (1.2)	0.510
<b>Comparison of total extraprostatic extension lesions and locations between transrectal and transperineal fusion-targeted prostate biopsy in 36 prostate cancer cases with identifiable extraprostatic extension</b>			
<b>Variables</b>	<b>TR (n=20)</b>	<b>TP (n=16)</b>	<b>p value</b>
Total EPE#, n	26	25	
Mean EPE#/case	1.3	1.6	
EPE location, n (%)			<b>0.010</b>
Base	13 (50.0)	4 (16.0)	
Non-base	13 (50.0)	21 (84.0)	
Laterality, n (%)			<b>1.000</b>
Right	10 (38.5)	11 (44.0)	
Left	15 (57.7)	14 (56.0)	
Midline	1 (3.8)	0 (0)	
EPE in Bx type, n (%)			<b>0.645</b>
SBx	15 (57.7)	16 (64.0)	
TBx	11 (42.3)	9 (36.0)	

Figure 1 - 718



**Conclusions:** TP may improve the EPE detection than TR and should be applied to patients with adverse pre-biopsy features.

## 719 Clinicopathologic Features of Clear Cell Renal Cell Carcinomas with Loss of Nuclear BAP1 Expression: A Multi-Institutional Study

Rebecca Czaja<sup>1</sup>, Anusmita Tripathy<sup>2</sup>, Nicole Zalles<sup>3</sup>, Sean Williamson<sup>3</sup>, Tatjana Antic<sup>2</sup>, Alexander Gallan<sup>4</sup>

<sup>1</sup>Indiana University Health, Indianapolis, IN, <sup>2</sup>University of Chicago, Chicago, IL, <sup>3</sup>Cleveland Clinic, Cleveland, OH, <sup>4</sup>Medical College of Wisconsin, Milwaukee, WI

**Disclosures:** Rebecca Czaja: None; Anusmita Tripathy: None; Nicole Zalles: None; Sean Williamson: None; Tatjana Antic: None; Alexander Gallan: None

**Background:** BRCA1-associated protein 1 (BAP1) is mutated in a subset of clear cell renal cell carcinoma (CCRCC) and is known to confer aggressive clinical behavior. The histologic features of tumors with previously known BAP1 mutations has been reported and BAP1 immunohistochemistry has shown effectiveness in identifying BAP1-mutated tumors. However, the clinicopathologic comparison of tumors with and without nuclear BAP1 loss has not been evaluated.

# ABSTRACTS | GENITOURINARY PATHOLOGY (INCLUDING RENAL TUMORS)

**Design:** Nuclear BAP1 expression was assessed in 295 unselected CCRCCs from nephrectomy specimens at three institutions. We evaluated the clinicopathologic features of tumors with and without BAP1 loss as a surrogate for BAP1 mutations. Data were analyzed using Fisher exact test and Wilcoxon rank sum test.

**Results:** A total of 61 of 295 (21%) of CCRCC showed nuclear BAP1 loss. In comparison to BAP1-retained tumors, tumors with BAP1 loss were larger in size (7.0 vs 5.0 cm, p<0.01), showed more necrosis (11% vs 4%, p=0.02), had more frequently positive margins (17% vs 5%, p<0.01), and had higher pathologic stage (63% vs 14% pT3a or above, p<0.01). In particular, tumors with BAP1 loss showed frequent sinus adipose invasion (49% vs 17%, p<0.01) and renal vein invasion (40% vs 23%, p=0.01). Previously reported histologic features of BAP1-mutated CCRCC were also more common including high nuclear grade (100% vs 24% G3/G4, p<0.01), rhabdoid/sarcomatoid differentiation (37% vs 5%, p=0.01), the degree of cytoplasmic eosinophilia (2.03 vs 0.78 on scale of 0-3+, p<0.01), voluminous cytoplasm (50% vs 18%, p<0.01), cytoplasmic granules (52% vs 22%, p<0.01, and cytoplasmic globules (38% vs 3%, p<0.01).

Figure 1 - 719

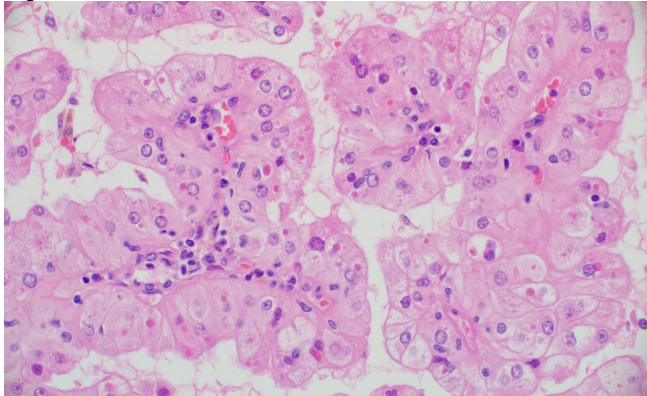
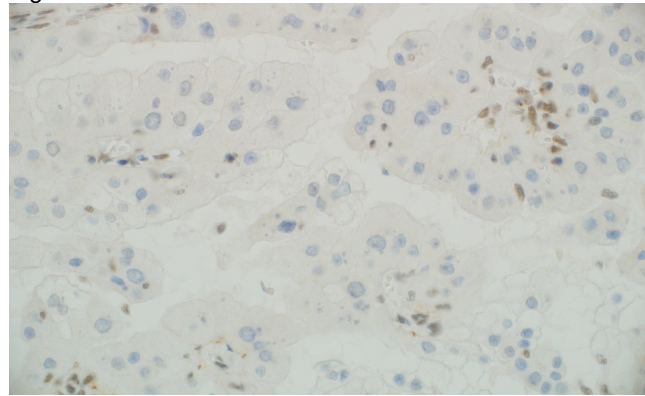


Figure 2 - 719



**Conclusions:** BAP1 loss was observed at a higher rate in our CCRCC cohort than has previously been reported. These tumors showed a higher pathologic stage including high rates of renal vein and sinus adipose invasion. The spectrum of histologic findings in tumors with BAP1 loss was wider than previously reported, but these do demonstrate characteristic yet non-specific high grade histologic features which could allow for prediction of BAP1 mutation during case review.

## 720 Modeling of Bladder Cancer Evolution from Whole-Organ Mutational and Proteomic Profiles

Bogdan Czerniak<sup>1</sup>, Sangkyou Lee<sup>1</sup>, Sung Jung<sup>2</sup>, Paweł Kus<sup>3</sup>, Roman Jaksik<sup>3</sup>, June-Goo Lee<sup>1</sup>, Huiqin Chen<sup>1</sup>, Neema Navai<sup>1</sup>, Charles Guo<sup>1</sup>, Peng Wei<sup>1</sup>, Marek Kimmel<sup>4</sup>

<sup>1</sup>The University of Texas MD Anderson Cancer Center, Houston, TX, <sup>2</sup>Baylor College of Medicine, Houston, TX, <sup>3</sup>Silesian University of Technology, Gliwice, Poland, <sup>4</sup>Rice University, Houston, TX

**Disclosures:** Bogdan Czerniak: None; Sangkyou Lee: None; Sung Jung: None; Paweł Kus: None; Roman Jaksik: None; June-Goo Lee: None; Huiqin Chen: None; Neema Navai: None; Charles Guo: None; Peng Wei: None; Marek Kimmel: None

**Background:** Bladder cancer is a useful model for the whole-organ studies as its simple anatomy permits mapping of microscopically identifiable *in situ* preneoplastic conditions and adjacent field effects in the entire organ. We used whole-organ histologic mapping combined with exome mutational and mass spectrometry-based protein profiling to model the evolution of bladder cancer from mucosal field effects.

**Design:** We performed a proof of principle analysis of whole-exome mutational landscape and mass spectrometry proteomic profiling on the whole-organ scale of a single cystectomy specimen with invasive bladder cancer. The 38 samples were microscopically classified into normal urothelium, low grade intraurothelial neoplasia, high-grade intraurothelial neoplasia, and invasive cancer. Exome sequencing with an average depth of approximately 300X was performed on Illumina NovaSeq 6000 sequencer and protein sequencing was performed with Orbitrap Fusion mass spectrometer (Thermo Fisher Scientific).

**Results:** We identified 12,764 nonsynonymous mutations and 8,475 proteins. Analysis of mutational patterns identified three types of mutations based on their geographic distribution and variant allele frequencies. The most common were mutations restricted to individual mucosal samples referred to as  $\alpha$  mutations. The two additional types of mutations were associated with clonal expansion. The mutations referred to as  $\beta$  occurred at low frequencies and  $\Delta$  mutations increased in frequency with progression. The analysis of proteomic profiles identified dysregulations of multiple pathways including neutrophil regulation, Hippo, cAMP, Hedgehog, and IL-17 signaling complemented by dysregulation of cellular adhesion, antigen processing, autophagy, and PD-1/PD-L1 checkpoint. Modeling of bladder cancer evolution revealed that it develops through multiple mutational waves spanning

# ABSTRACTS | GENITOURINARY PATHOLOGY (INCLUDING RENAL TUMORS)

approximately 10-15 years, which can be divided into dormant and progressive phases. The progressive phase lasted approximately two years and was driven by  $\Delta$  mutations.

**Conclusions:** This is the first proof of principle report of detailed combined mutational and proteomic characterization of mucosal field effects initiating bladder carcinogenesis on the whole-organ scale. It provides unique insights into bladder cancer initiation and will pave the way for future studies of early events in human carcinogenesis using bladder cancer as a model.

## 721 Comparative Evaluation of Microsatellite Instability, PDL-1 Expression and Molecular Subtypes of Upper and Lower Tract Urothelial Carcinoma

Shivangi Dagar<sup>1</sup>, Seema Kaushal<sup>1</sup>, Saumyaranjan Mallick<sup>1</sup>, Amlesh Seth<sup>1</sup>, Ranjit Sahoo<sup>1</sup>, Amit Dinda<sup>1</sup>  
<sup>1</sup>All India Institute of Medical Sciences, New Delhi, India

**Disclosures:** Shivangi Dagar: None; Seema Kaushal: None; Saumyaranjan Mallick: None; Amlesh Seth: None; Ranjit Sahoo: None; Amit Dinda: None

**Background:** Predictive biomarkers such as PDL1 expression and mismatch repair (MMR) status are advocated for immunotherapy in advanced urothelial cancer. The reported frequencies of microsatellite instability (MSI) in bladder carcinoma (MIBC) range between 1 to 3%, while for upper tract urothelial carcinoma (UTUC), it is 3% to 46%.

**Design:** This was an ambispective study of 60 cases including UTUC (n=30) and muscle invasive bladder cancer (MIBC, n=30). MSI was detected using fluorescent PCR-based assay by comparing allelic profiles of microsatellite markers generated by amplification of DNA from matching normal and test samples ,using the MSI Analysis System, Version 1.2 from Promega. Immunohistochemistry (IHC) for four MMR proteins (MSH2, MSH6, MLH1 and PMS2) was also done. CK5/6 and GATA3 IHC were performed for molecular subtyping and PDL1 expression was evaluated in molecular subtypes. Findings were correlated with clinical parameters and outcomes.

**Results:** Distal ureter (50%) was the most common site for UTUC. The most common molecular subtype was basal (60%) for MIBC and luminal (60%) for UTUC. MSI was seen in 20% (5/30) cases of UTUC, while in only 6.6% (2/30) cases of MIBC. Three of the six MSI cases of UTUC showed basal/squamous subtype, two were luminal (urothelial-like) subtype, while one was of double negative subtype. In UTUC, three out of six MSI cases (50%) showed PD-L1 positivity in tumor cells, while four cases (75%) showed PD-L1 immunoexpression in immune cells. Out of the two MSI cases of MIBC, one was of luminal subtype (urothelial-like), while other was basal/squamous subtype. One out of the two MSI cases of MIBC was positive for PD-L1 expression in tumor cells, while both MSI cases showed PD-L1 positivity in immune cells. PD-L1 positivity rates in tumor cells (TPS $\geq$ 1%) in MIBC cohort was 46%, while it was 50% in UTUC cohort, being 83.3% in MIBC basal subtype cases ( $p=0.003$ ) and 77.8% in UTUC basal subtype cases. PD-L1 positivity in immune cells (ICS $\geq$ 5%) was seen in 36.6% cases in both cohorts. Overall survival was least in basal subtype and worse in MSI tumors. Tumors expressing PD-L1 expression in tumor or immune cells had better survival.

Molecular subtype	MIBC: PD-L1 TPS $>$ 1%	UTUC: PD-L1 TPS $>$ 1%
Urothelial-like	2/7 (28.6%)	5/14 (35.7%)
Genomically unstable	0/3(0%)	0/1 (0%)
Basal/squamous	15/18 (83.3%)	7/9 (77.8%)
Double negative/ Non-specified	1/2 (50%)	1/1 (100%)

Table 1. Distribution of PD-L1 expression in tumor cells of molecular subtypes of MIBC and UTUC

Figure 1 - 721

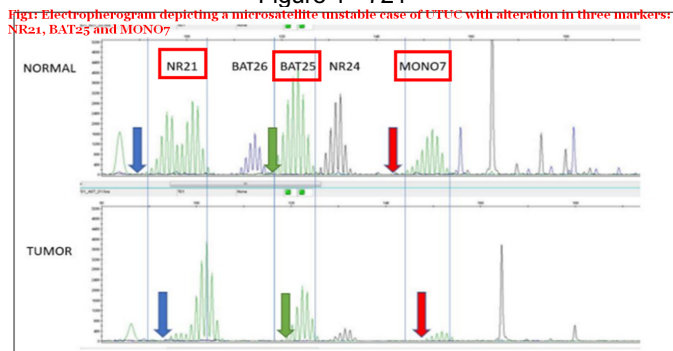
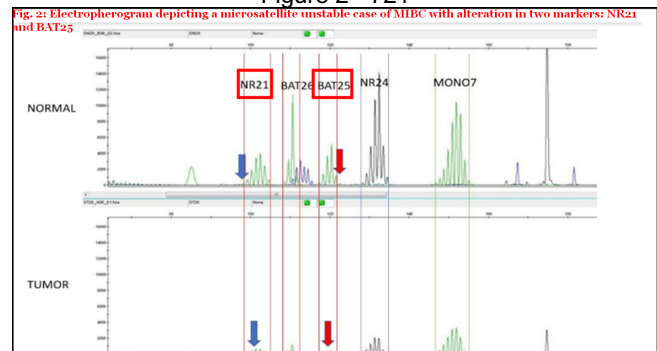


Figure 2 - 721



**Conclusions:** MSI is more prevalent in UTUC than MIBC and PD-L1 is differentially expressed in molecular subtypes at both sites. Our results indicate that upper and lower tract urothelial cancers have different molecular landscape and can be differentially stratified for prognostic and optimal therapeutic benefits of immune checkpoint therapy.

**722 Assessment of Pattern of Invasion and Depth of Invasion as Predictors of Lymph Node Metastasis in Penile Squamous Cell Carcinoma**

Debasmita Das<sup>1</sup>, Shreeya Indulkar<sup>1</sup>, Mohan Krishna<sup>1</sup>, B Vishal Rao<sup>1</sup>, Suseela Kodandapani<sup>1</sup>, Rakesh Sharma<sup>1</sup>, T Rao<sup>1</sup>

<sup>1</sup>Basavataram Indo-American Cancer Hospital and Research Institute, Hyderabad, India

**Disclosures:** Debasmita Das: None; Shreeya Indulkar: None; Mohan Krishna: None; B Vishal Rao: None; Suseela Kodandapani: None; Rakesh Sharma: None; T Rao: None

**Background:** Lymph-nodal metastasis is one of the most important factors in determining the outcome of penile squamous cell carcinoma (PC). Many patients with PC may present with inguinal lymph node enlargement which may be either reactive or due to metastases. But the rate of complication following radical inguinal lymphadenectomy can be quite high. Therefore, it is necessary to identify the factors on histopathology that indicate better risk stratification. Hence, we attempt to study the association of pattern of invasion (POI) and depth of invasion (DOI) in predicting the likelihood of positive inguinal nodal metastases.

**Design:** This was a retrospective observational study. 90 patients with PC who underwent inguinal lymph node dissection during the period January 2020 to April 2022 were included. The POI was classified as pushing or infiltrative. When both the patterns were noted in the same sample, it was classified as infiltrative pattern. The DOI was measured in mm from epidermal-dermal junction to deepest point of invasion and was classified as superficial ( $\leq 5$  mm) or deep ( $> 5$  mm). Statistical analysis was done in SPSS version 20. Categorical data was analyzed by Chi-square test along with Fisher's exact test. Odds ratio was calculated where required. Prediction model was done by binary regression. A p value of  $<0.05$  was considered statistically significant.

**Results:** The age ranged from 24 to 90 (median 56) years. Majority of the patients were aged between 51-60 years. Lymph node metastasis was identified in 40%. Infiltrative pattern was observed in 52.22% and pushing pattern in 47.78%. Infiltrative POI was identified in 36/48 (75%) of nodal metastases and pushing POI was not identified in any of the nodal metastases. Infiltrative POI showed association with nodal positivity which was statistically significant in different tumor stages (T1b, T2 and T3; p value= 0.005,  $<0.001$ , 0.006 respectively) and higher in combined (T3+T4) group (p value= 0.005). In T1b and T2 stages, both the positive (PPV) and negative predictive value (NPV) of POI were 100% and 77.8%, respectively with accuracy of 86.7%. A significant odds ratio showed that the infiltrative POI had 3.777 times chances of being node positive than the pushing POI. DOI  $> 5$ mm was seen in 66 (73.3%) and  $\leq 5$ mm in 24 (26.7%). Among 66, lymph nodal metastasis was noted in 46.97%. There was a significant association of DOI with lymph node metastasis (p value= 0.025). Regression analysis model of POI was not significant for nodal involvement (p >0.05), however, 75% of PC with nodal involvement could be attributed to POI.

ASSOCIATION OF PATTERN OF INVASION WITH LYMPH NODE METASTASIS IN DIFFERENT TUMOUR STAGES								
T stage	POI	Lymph node metastasis		Total	Chi-square			
		Absent	Present		X <sup>2</sup>	p value		
T1b	Infiltrative	0	6	6	8.000	$<0.001$		
	Pushing	2	0	2				
	Total	2	6	8				
T2	Infiltrative	5	9	14	14.69	<0.001		
	Pushing	16	0	16				
	Total	21	9	30				
T3	Infiltrative	6	20	26	7.436	0.006		
	Pushing	3	0	3				
	Total	9	20	29				
T4	Infiltrative	0	1	1	NA	NA		
	Total	0	1	1				
Total	Infiltrative	12	36	48	52.50	<0.001		
	Pushing	42	0	42				
	Total	54	36	90				
COMBINED STAGING								
	POI	Lymph node metastasis		Total	Chi-square			
		A	P		X <sup>2</sup>	p value		
T3+T4	Infiltrative	6	21	27	7.778	0.005		
	Pushing	3	0	3				
	Total	9	21	30				
ODDS RATIO								
POI	Lymph node metastasis		Total	Odds ratio				
	Absent	Present		Ratio	z value	95% C		
Infiltrative	12	36	48	248.2	3.777	14.1978-4338.9292		
	42	0	42					
	54	36	90					
REGRESSION ANALYSIS MODEL FIT								
POI	Regression co-ef (B)/ OR	R <sup>2</sup>	PPV %	NPV %	Accuracy %	p value		
Infiltrative pattern	-22.302	0.711	100	77.8	86.7	0.997		
Pushing pattern	22.302	0.711	100	77.8	86.7	0.997		
ASSOCIATION OF DEPTH OF INVASION WITH LYMPH NODE METASTASIS								
DOI	Lymph node metastasis		Total	Chi square				
	Absent	Present		X <sup>2</sup>	p value			
≤ 5mm	19	5	24	5.009	0.025			
	35	31	66					
	54	36	90					

# ABSTRACTS | GENITOURINARY PATHOLOGY (INCLUDING RENAL TUMORS)

**Conclusions:** A significant association of POI and DOI with increased lymph node metastasis is noted. In early stages, POI showed high PPV and NPV with good accuracy for predicting nodal invasion. We, hence, recommend the reporting of POI along with DOI on a routine basis in PC.

## 723 Expression of Programmed Cell-Death Ligand 1 (PD-L1) and Analysis of Microsatellite Instability/ DNA Mismatch Repair (MSI/MMR) Status in Penile Squamous Cell Carcinoma (PC)

Debasmita Das<sup>1</sup>, Shreeya Indulkar<sup>1</sup>, Mohan Krishna<sup>1</sup>, B Vishal Rao<sup>1</sup>, Suseela Kodandapani<sup>1</sup>, Rakesh Sharma<sup>1</sup>, T Rao<sup>1</sup>  
<sup>1</sup>Basavataramakam Indo-American Cancer Hospital and Research Institute, Hyderabad, India

**Disclosures:** Debasmita Das: None; Shreeya Indulkar: None; Mohan Krishna: None; B Vishal Rao: None; Suseela Kodandapani: None; Rakesh Sharma: None; T Rao: None

**Background:** PC is considered a rare malignancy in the West. The rates in Indian subcontinent is high, up to 3.32 per 10<sup>5</sup> men. Due to the social stigma, patients present at advanced stage with limited treatment options and poor outcomes. Immune checkpoint inhibitors (ICI) like anti PD-L1 are currently used in treatment of other tumours especially in colorectal cancer where it is well established. The strong immunogenicity and the widespread expression of immune-checkpoint ligands make MSI subtype more vulnerable to immunotherapy. Very few studies have been done related to PD-L1 and MSI expression in PC. This study attempts to evaluate the expression of PD-L1 in tumour cells (TCs) and tumour-infiltrating lymphocytes (TILs) along with the analysis of MSI/MMR status in PC.

**Design:** A retrospective observational study was done on 50 cases of PC from January 2020 to April 2022. The IHC was performed with anti-PD-L1 antibody (clone SP263 Ventana) to access PD-L1 expression and anti-MLH1 (clone M1), anti-PMS2 (clone A16-4), anti-MSH2 (clone G219-1129) and anti-MSH6 (clone SP93) antibodies to access MMR expression on tissue microarray. Both IHCs were performed on Ventana Benchmark ULTRA platform. The membranous expression of PD-L1 was evaluated with combined positive score (CPS) in TC and TILs. Values <1% was considered negative; ≥1% was considered positive, further divided into 2 subgroups: 1-50%: low positivity and >50%: high positivity. The nuclear staining of MMR was considered positive. It was divided into 3 subgroups: 1) pMMR cases with all four positive MMR staining; 2) lo-pa MMR cases with either loss of/ patchy positivity expression for one of the MMRs; 3) dMMR cases with loss of one of two heterodimers. Statistical analysis was done in SPSS version 20. Categorical data was analysed by Chi-square test along with Fisher's exact test. A p value of <0.05 was considered statistically significant.

**Results:** 42/50 cases (84%) showed positive PD-L1 expression. 30/42 cases showed low positive followed by 12/42 showing high PD-L1 expression. 8 cases showed <1% PD-L1 expression. There was significant association of PD-L1 with grading (p value= 0.042), lymph node metastasis (p value= 0.015), lymphovascular invasion (LVI) (p value= 0.015) and nodal stage (p value=0.007). The PD-L1 expression didn't correlate with tumour stage and perineural invasion (PNI) with p value >0.05. 42/50 cases (84%) showed pMMR, 7 cases (14%) showed lo-pa MMR and only 1 case (2%) showed loss of MMR expression/ dMMR. There was no significant association of expression of MMR with grading, tumour staging, nodal staging, LVI and PNI (p >0.05). However, only 2% with dMMR showed high PD-L1 expression.

# ABSTRACTS | GENITOURINARY PATHOLOGY (INCLUDING RENAL TUMORS)

ASSOCIATION OF PD-L1 EXPRESSION WITH TUMOR GRADING				Total	Chi Square			
Grading	PD-L1 expression		X2 6.349	p value 0.042	X2 8.467	p value 0.015		
	Negative							
	I	08	22	30				
	II	00	19	19				
Total	III	00	01	1				
	Total	08	42	50				
<b>ASSOCIATION OF PD-L1 EXPRESSION WITH LYMPH NODE METASTASIS</b>								
Lymph node metastasis	PD-L1 expression			Total	Chi Square			
	<1%				X2 8.467			
	Present	2	12	10	24	p value 0.015		
	Absent	6	18	2	26			
Total	8	30	12	50				
<b>ASSOCIATION OF PD-L1 EXPRESSION WITH LYMPHOVASCULAR INVASION (LVI)</b>								
LVI	PD-L1 expression			Total	Chi Square			
	<1%				X2 8.467			
	Present	2	12	10	24	p value 0.015		
	Absent	6	18	2	26			
Total	8	30	12	50				
<b>ASSOCIATION OF PD-L1 EXPRESSION WITH NODE STAGE (N STAGE)</b>								
N stage	PD-L1 expression			Total	Chi Square			
	<1%				p value			
	N0	6	18	2	26	0.007		
	N1	1	0	4	5			
N2	0	3	0	3				
N3	1	9	6	16				
Total	8	30	12	50				
<b>ASSOCIATION OF PD-L1 EXPRESSION WITH TUMOR STAGE (T STAGE)</b>								
T Stage	PDL1 expression			Total	Chi Square			
	<1%				p value			
	T1a	3	7	1	11	0.41		
	T1b	1	2	2	5			
T2	3	13	3	19				
T3	1	8	6	15				
Total	8	30	12	50				
<b>ASSOCIATION OF PD-L1 EXPRESSION WITH PERINEURAL INVASION (PNI)</b>								
PNI	PDL1 expression			Total	Chi Square			
	<1%				p value			
	Present	1	9	4	14	0.554		
	Absent	7	21	8	36			
Total	8	30	12	50				
<b>ASSOCIATION OF MMR EXPRESSION WITH TUMOR GRADING</b>								
Grading	MMR expression			Total	Chi Square			
	pMMR + low positive MMR				X2 0.680			
	I	29	1	30	0.712			
	II	19	0	19				
Total	49	1	1	50				
<b>ASSOCIATION OF MMR EXPRESSION WITH LYMPH NODE METASTASIS</b>								
Lymph node metastasis	MMR expression			Total		Chi square		
	pMMR					X2 1.160		
	Present	20	1	3	24	0.560		
	Absent	22	0	4	26			
Total	42	1	7	50				
<b>ASSOCIATION OF MMR EXPRESSION WITH LYMPHOVASCULAR INVASION (LVI)</b>								
LVI	MMR expression			Total	Chi square			
	pMMR				p value			
	Present	20	1	3	24	0.56		
	Absent	22	0	4	26			
Total	42	1	7	50				
<b>ASSOCIATION OF MMR EXPRESSION WITH PERINEURAL INVASION (PNI)</b>								
PNI	MMR expression			Total	Chi square			
	pMMR				p value			
	Present	12	0	2	14	0.82		
	Absent	30	1	5	36			
Total	42	1	7	50				
<b>ASSOCIATION OF MMR EXPRESSION WITH TUMOR STAGE (T STAGE)</b>								
T Stage	MMR expression			Total	Chi Square			
	pMMR				X2 0.911			
	T1a	9	0	2	11			
	T1b	4	0	1	5			
T2	16	1	2	19				
T3	13	0	2	15				
Total	42	1	7	50				
<b>ASSOCIATION OF MMR EXPRESSION WITH NODE STAGE (N STAGE)</b>								
N Stage	MMR expression			Total	Chi square			
	pMMR				p value			
	N0	22	0	4	26	0.122		
	N1	3	1	1	5			
N2	3	0	0	3				
N3	14	0	2	16				
Total	42	1	7	50				

**Conclusions:** The expression of PD-L1 was associated with high grade tumour, lymph nodal metastasis, LVI and nodal stage, hence propends for creating targeted therapy with ICI. dMMR, however was noted only in 2% of cases which showed high PDL1 expression.

## 724 CDH1 Mutated Plasmacytoid Urothelial Carcinoma of the Bladder: A Genomic Alteration Landscape Study

Elizabeth Davaro<sup>1</sup>, Facundo Davaro<sup>1</sup>, Taylor Peak<sup>1</sup>, Li Roger<sup>1</sup>, Philippe Spiess<sup>1</sup>, Dean Pavlick<sup>2</sup>, Natalie Danziger<sup>2</sup>, Jeffrey Ross<sup>3</sup>

<sup>1</sup>H. Lee Moffitt Cancer Center & Research Institute, Tampa, FL, <sup>2</sup>Foundation Medicine, Inc., Cambridge, MA, <sup>3</sup>SUNY Upstate Medical University, Syracuse, NY

**Disclosures:** Elizabeth Davaro: None; Facundo Davaro: None; Taylor Peak: None; Li Roger: None; Philippe Spiess: None; Dean Pavlick: None; Natalie Danziger: None; Jeffrey Ross: None

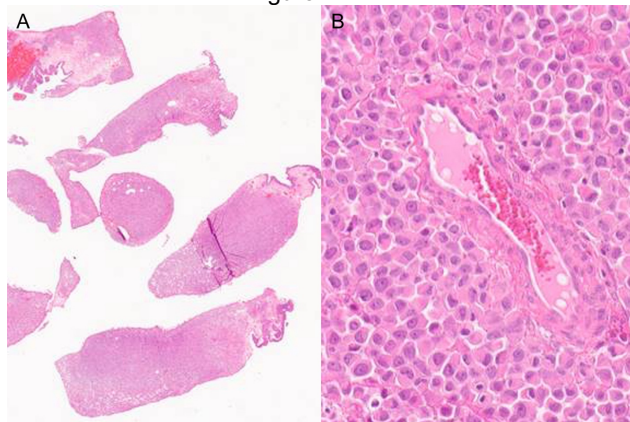
**Background:** Plasmacytoid (PLC) variant histology of urothelial bladder cancer (UCB) exhibits unique histological features. Genomic characterization has revealed *CDH1* mutation as a potential defining molecular event in PLC differentiation. Phenotypic characteristics of *CDH1* mutated UCB without PLC histology has not yet been elucidated. Herein we describe the genomic alteration landscape of *CDH1* mutated UCB in the setting of differing histological expression.

**Design:** 7,903 clinically advanced UBC underwent hybrid capture based comprehensive genomic profiling (CGP) to evaluate all classes of genomic alterations (GA). Selected cases featured *CDH1* short variant mutation. H&E stained digital pathology images were subjected to review by a single expert genitourinary pathologist. Minimum of 10% PLC histology on digital images was required for categorization into PLC cohort (PLC vs non-PLC). Tumor mutational burden (TMB) was determined on up to 1.1 Mb of sequenced DNA and microsatellite instability (MSI) was determined on 114 loci. Tumor cell PD-L1 expression was determined by IHC (Dako 22C3) and defined as tumor proportion score (TPS)  $\geq 1$ . Chi-Square test was used to compare differences between cohorts.

**Results:** 7,641 samples were *CDH1* wild-type while 158 patients were *CDH1* mutated with pathology available for central review. Of these samples, 103 (65.2%) had a minimum of 10% PLC histology. The PLC cohort was slightly younger than the non-PLC group. The non-PLC population featured a higher preponderance of MSI-High status (5.7% vs 1.9%, p=0.21). Cell-Cycle regulatory GA were significantly higher in the non-PLC cohort, specifically *CDKN2A* (25.5% vs 9.7%, p=0.01) and *CDKN2B* (23.6% vs 5.8%, p<0.01) homozygous deletions. *FGFR3* GA was similar between the *CDH1* wild-type UCB and non-PLC (ranging from 16.4%-18.7%) groups; however, significantly higher than the 4.9% *FGFR3* GA frequency seen in the PLC cases (p=0.02). *ERBB2* were similar in “total GA” in all groups but were an even mix of amplifications and mutations in the *CDH1* mutation negative UBC (p>0.05). *RB1* GA were more common in both PLC and non-PLC than in the *CDH1* mutation negative cases.

	CDH1 Mutation Negative	CDH1 Mutation Positive (All Cases)	CDH1 Mutation Positive (PLC)	CDH1 Mutation Positive (Non-PLC)	P-value
Number of Cases	7,641	262	103	55	
<b>Cell Cycle Regulatory GA</b>					
<i>TP53</i>	59.40%	63.40%	64.10%	60.00%	0.61
<i>CDKN2A</i>	37.80%	13.40%	9.70%	25.50%	0.01
<i>CDKN2B</i>	30.00%	10.30%	5.80%	23.60%	<0.01
<i>CCND1</i>	13.70%	3.40%	2.90%	5.50%	0.43
<i>RB1</i>	20.10%	52.70%	57.30%	45.50%	0.16
<b>Chromosomal and Chromatin Related GA</b>					
<i>TERT</i>	73.90%	87.10%	94.20%	78.20%	<0.01
<i>ARID1A</i>	24.00%	33.20%	35.90%	34.50%	0.86
<b>PI Kinase and MTOR Pathway GA</b>					
<i>PTEN</i>	4.30%	8.80%	9.70%	12.70%	0.56
<i>PIK3CA</i>	21.90%	30.50%	33.00%	29.10%	0.61
<i>TSC1</i>	9.00%	4.60%	4.90%	5.50%	0.87
<i>NF1</i>	3.10%	1.50%	0.00%	3.60%	0.05
<b>Receptor Tyrosine Kinase Targetable GA</b>					
<i>ERBB2</i> amp.	7.40%	2.70%	1.90%	3.60%	0.52
<i>ERBB2</i> all GA	16.60%	14.90%	16.50%	14.50%	0.75
<i>EGFR</i>	4.10%	4.60%	4.90%	1.80%	0.34
<i>FGFR1</i>	4.00%	1.10%	1.90%	1.80%	0.96
<i>FGFR2</i>	1.00%	0.40%	0.00%	1.80%	0.17
<i>FGFR3</i>	18.70%	8.40%	4.90%	16.40%	0.02
<i>MET</i>	1.00%	0.80%	1.00%	1.80%	0.65
<i>KIT</i>	0.80%	0.00%	0.00%	0.00%	-
<b>Emerging Potentially Genomic Alterations</b>					
<i>NOTCH1</i>	1.70%	1.50%	0.00%	3.60%	0.05
<i>NOTCH2</i>	1.30%	0.80%	0.00%	0.00%	-
<i>MTAP</i>	25.00%				

Figure 1 - 724



**Conclusions:** *CDH1* mutation positive UBC exhibits differential GA depending on histological appearance. *MTAP*, *CDKN2A*, and *CDKN2B*, genes located on chromosome 9p21, were increasingly mutated in non-PLC *CDH1* mutation positive UCB. The clinical implications of this mutational pattern require further exploration.

## 725 Identification of NNMT as a Novel Tumor Suppressor in Prostate Cancer

Qu Deng<sup>1</sup>, Rahul Mannan<sup>2</sup>, Erick Mitchell<sup>1</sup>, Mohammed Alhusayan<sup>1</sup>, Priti Lal<sup>3</sup>, Irfan Asangani<sup>1</sup>

<sup>1</sup>Perelman School of Medicine at the University of Pennsylvania, Philadelphia, PA, <sup>2</sup>Michigan Medicine, University of Michigan, Ann Arbor, MI, <sup>3</sup>University of Pennsylvania, Philadelphia, PA

**Disclosures:** Qu Deng: None; Rahul Mannan: None; Erick Mitchell: None; Mohammed Alhusayan: None; Priti Lal: None; Irfan Asangani: None

**Background:** Prostate cancer (PCa) is the top diagnosed cancer in men of North America, with 20% of the cases being lethal. In 2022, 268,490 new PCa diagnosis and 34,500 related deaths are projected to occur in the US. Although surgical, radiation, and androgen-ablation therapies are effective for localized PCa, progression to metastatic castration-resistant prostate cancer (CRPC) is essentially inevitable. However, the epigenetic and metabolic reprogramming involved in PCa progression is largely unknown. Recently, Nicotinamide N Methyltransferase (NNMT) is reported to modulate cancer cell epigenome by acting as a S-adenosyl-methionine (SAM) sink. Therefore, understanding its expression pattern and function in PCa development is of great potential for prognosis prediction and personalized therapies.

**Design:** To study the genetic profile of NNMT in PCa, we first explored publicly available Next Generation Sequencing datasets, which contains 753 of primary PCa, 203 treatment resistant PCa and 147 metastasis CRPC patient samples. Secondly, we studied NNMT expression pattern by immunohistochemistry (IHC) staining on human PCa tissue microarrays including 469 benign tissue, 473 primary and 305 metastases cores followed by pathological grading. Lastly, we generated a prostate specific *Nnmt* and *Pten* knockout (KO) mouse model and traced its cancer progression longitudinally.

**Results:** In the public PCa clinical datasets, we identified 5-8% of genetic deletions of NNMT in primary (TCGA), treatment resistant and metastases (SU2C, MET500, Michigan mCRPC) PCa patient samples. In the NNMT IHC staining of the PCa tissue microarrays, a statistically significant decrease of the IHC staining scores in the primary tumors ( $p<0.01$ ) and metastatic samples ( $p<0.03$ ) were observed when compared to the benign tissue. Of note, PCa metastases showed no NNMT expression while the hosting organs were highly NNMT positive. It suggests that NNMT negative prostate cells potentially gained growth advantage in different microenvironment. Finally, by analyzing 12-month-old *Nnmt* and *Pten* double KO ( $n=40$ ) and *Pten* KO prostate ( $n=26$ ), we observed that the double KO prostate displayed more severe florid atypical intraductal proliferation and/or infiltrating ductal carcinoma. It further supports that loss of NNMT being an early driver in PCa.

**Conclusions:** We identified NNMT as a *bona fide* tumor suppressor in PCa. NNMT IHC staining is a feasible way to detect its expression, the expression loss is an indicator for advanced PCa.

## 726 Atypical Intraductal Proliferation of the Prostate

James Denney<sup>1</sup>, Andres Acosta<sup>2</sup>, Ezra Baraban<sup>3</sup>, Jason Van Roo<sup>4</sup>, Jianping Zhao<sup>5</sup>, Jennifer Gordetsky<sup>1</sup>

<sup>1</sup>Vanderbilt University Medical Center, Nashville, TN <sup>2</sup>Brigham and Women's Hospital, Harvard Medical School, Boston, MA, <sup>3</sup>Johns Hopkins Hospital, Baltimore, MD, <sup>4</sup>Johns Hopkins University, MD, <sup>5</sup>The University of Texas MD Anderson Cancer Center, Houston, TX,

**Disclosures:** James Denney: None; Andres Acosta: None; Ezra Baraban: None; Jason Van Roo: None; Jianping Zhao: None; Jennifer Gordetsky: None

**Background:** It is recognized that there can be morphologic overlap between high grade prostatic intraepithelial neoplasia (HGPIN) and intraductal carcinoma of the prostate (IDCP). In cases with a small number of glands with atypical cribriform morphology, a definitive diagnosis may be difficult to achieve. Given that HGPIN is managed conservatively while IDCP is recommended to be treated with definitive therapy, the distinction is clinically significant. Cases with indeterminant features between the two entities are diagnosed as "Atypical Intraductal Proliferation" (AIP). We explored the pathologic findings of patients diagnosed with AIP.

**Design:** The surgical pathology databases from three institutions were searched from 2003-2022 for cases of AIP. Pathologic findings were evaluated in the initial biopsy specimen with AIP as well as any follow-up biopsies or resection specimens.

**Results:** We identified 102 patients with a diagnosis of AIP, which consisted of 100 biopsies and 2 transurethral resection specimens. Concurrent cancer was identified in 81/102 (79%) initial specimens. Of the cases with cancer on initial biopsy, 39/81 (48%) had grade group (GG) 1 tumor, 28/81 (35%) had GG2 tumor, 10/81 (12%) had GG3 tumor, 1/81 (1%) had GG4 tumor, and 3/81 (4%) had GG5 tumor. Subsequent management included radical prostatectomy (RP) (n=41), active surveillance (n=29), radiation therapy (n=15), androgen deprivation therapy (n=4), and no follow-up (n=6). Repeat biopsy results were available in 21 patients on active surveillance. Seven patients had no cancer on repeat biopsy, of which 3 had only AIP on initial biopsy. The remainder (14/21, 67%) had cancer on repeat biopsy (GG1=4, GG2=7, GG3=3). Five patients with only AIP on initial biopsy were found to have cancer on repeat biopsy (GG1=2, GG2=1, GG3=2). Cribriform morphology was present in 2 cases on repeat biopsy, both of which had only AIP on initial biopsy. Of the 81 patients with cancer on initial biopsy, 41 (51%) underwent RP. Of these, 15/41 (37%) had IDCP present and 22/41 (54%) had cribriform morphology on RP. Final GG on RP included GG1=3, GG2=29, and >GG2=9. Extraprostatic extension was found in 19/41 (46%) of cases. No lymph node metastases were identified.

Total Patients Identified with AIP	102
Concurrent Cancer on Initial Biopsy	81 (79%)
GG1	39 (48%)
GG2	28 (35%)
GG3	10 (12%)
GG4	1 (1%)
GG5	3 (4%)
AIP Only on Initial Biopsy	21 (21%)
Active Surveillance Patients Repeat Biopsy	21
Cancer on Repeat Biopsy	14 (67%)
GG1	4
GG2	7
GG3	3
AIP Only that had Repeat Biopsy	8
No Cancer	3
GG1	2
GG2	1
GG3	2
Cribriform Morphology	2
Underwent RP	41 (51%)
IDCP	22 (54%)
Extraprostatic Extension	19 (46%)
Cribriform Morphology	15 (37%)

**Conclusions:** AIP is often found concurrently with prostatic adenocarcinoma on biopsy. Most cases of AIP alone are found to have cancer on repeat biopsy. Many patients with AIP who subsequently undergo RP are found to have poor pathologic findings, including IDCP, EPE, and cribriform morphology.

## 727 Assessing Risk of Prostate Cancer Metastasis by Deep Learning in Surgically-Treated Patients

Lia DePaula Oliveira<sup>1</sup>, Eric Erak<sup>1</sup>, Adrianna A Mendes<sup>2</sup>, Carolina Gomes-Alexandre<sup>1</sup>, Daniela Salles<sup>3</sup>, Onur Ertunc<sup>4</sup>, Ibrahim Kulac<sup>5</sup>, Javier Baena-Del Valle<sup>6</sup>, Tracy Jones<sup>7</sup>, Jessica Hicks<sup>7</sup>, Stephanie Glavaris<sup>7</sup>, Gunes Guner<sup>8</sup>, Igor Damasceno Vidal<sup>9</sup>, Misop Han<sup>1</sup>, Bruce Trock<sup>2</sup>, Uttara Joshi<sup>10</sup>, Chaith Kondragunta<sup>10</sup>, Nilanjan Chattopadhyay<sup>11</sup>, Saikiran Bonthu<sup>11</sup>, Nitin Singhal<sup>10</sup>, Angelo De Marzo<sup>4</sup>, Tamara Lotan<sup>7</sup>

<sup>1</sup>Johns Hopkins Hospital School of Medicine, Baltimore, MD, <sup>2</sup>Johns Hopkins Medical Institutions, Baltimore, MD, <sup>3</sup>Baltimore, MD, <sup>4</sup>Johns Hopkins University, Baltimore, MD, <sup>5</sup>Koç University School of Medicine, Istanbul, Turkey, <sup>6</sup>Fundacion Santa Fe de Bogota University Hospital, Bogota, Colombia, <sup>7</sup>Johns Hopkins University School of Medicine, Baltimore, MD, <sup>8</sup>Hacettepe University, Ankara, Turkey, <sup>9</sup>UAB Hospital, Birmingham, AL, <sup>10</sup>AIRA Matrix Private Limited, Thane, India, <sup>11</sup>Thane, India

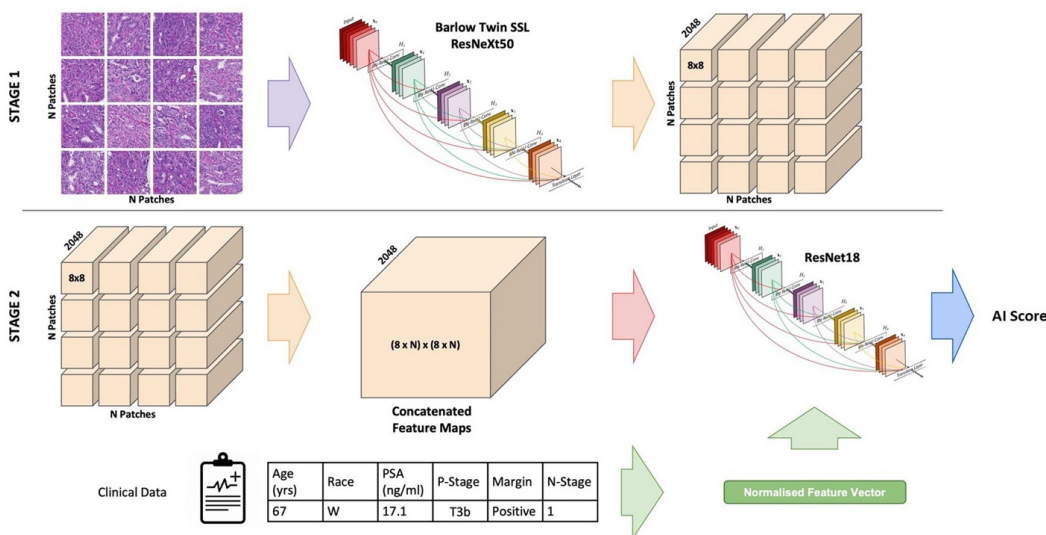
**Disclosures:** Lia DePaula Oliveira: None; Eric Erak: None; Adrianna A Mendes: None; Carolina Gomes-Alexandre: None; Daniela Salles: None; Onur Ertunc: None; Ibrahim Kulac: None; Javier Baena-Del Valle: None; Tracy Jones: None; Jessica Hicks: None; Stephanie Glavaris: None; Gunes Guner: None; Igor Damasceno Vidal: None; Misop Han: None; Bruce Trock: None; Uttara Joshi: None; Chaith Kondragunta: None; Nilanjan Chattopadhyay: None; Saikiran Bonthu: None; Nitin Singhal: None; Angelo De Marzo: None; Tamara Lotan: None

**Background:** Pathologic grade remains one of the most potent predictors of prostate cancer metastasis after radical prostatectomy (RP). Here, we tested whether deep learning algorithms applied to hematoxylin and eosin (H&E)-stained whole slide images (WSI) of prostate tumors and paired clinical-pathologic data can improve on standard metastasis prediction scores such as CAPRA-S.

**Design:** We developed a Concatenated Feature Based Classification (CFBC) system that integrates multi-modality data from histopathology images and clinical parameters (including age, race, pre-operative PSA, pathologic T- and N-stage and margin status). The system includes four stages: A) tumor identification in H&E-stained WSI or tissue microarray (TMA) samples from the dominant tumor nodule at RP; B) patch generation; C) pre-training; D) classification. A SegFormer transformer model was used for the tumor identification task. For the pre-training task, we apply self-supervised learning using the Barlow Twin SSL ResNeXt50 architecture, and for the classification task, we employ supervised learning using the ResNet18 architecture. The algorithm was trained on 241 patients from a previously published Johns Hopkins RP cohort and validated on 65 additional patients from this cohort, as well as tested in an independent Johns Hopkins RP cohort comprised of 242 patients. Model performance for metastasis prediction was assessed using area under the receiver-operator characteristic curve (AUC), and compared to the C-index obtained from Cox regression modeling for CAPRA-S alone.

**Results:** The baseline C-index for CAPRA-S was 0.780 in the 65 patient validation cohort, compared to an AUC of 0.874 using an algorithm incorporating WSI and clinical-pathologic parameters. In the 242 patient test cohort, the baseline C-index for CAPRA-S was 0.850 versus an AUC of 0.911 with using WSI and clinical-pathologic parameters. Similar algorithms using images of 4 tumor punches on TMA from the dominant nodule and clinical-pathologic parameters were also tested, with an AUC of 0.873 in the 65 patient validation cohort, and 0.834 in the 242 patient test cohort.

Figure 1 - 727



# ABSTRACTS | GENITOURINARY PATHOLOGY (INCLUDING RENAL TUMORS)

**Conclusions:** Deep learning algorithms incorporating WSI or TMA images from the dominant tumor nodule as well as clinical-pathologic parameters outperform current clinically-utilized prognostic nomograms such as CAPRA-S for prediction of metastasis. Validation in additional multi-institutional as well as racially diverse cohorts is underway.

## 728 Association of FASN Expression with Self-Identified Race and Immunogenomic Features of Primary Prostate Cancer

Lia DePaula Oliveira<sup>1</sup>, Oluwademilade Dairo<sup>1</sup>, Ethan Schaffer<sup>2</sup>, Adrianna A Mendes<sup>3</sup>, Thiago Vidotto<sup>3</sup>, Jiayun Lu<sup>4</sup>, Corinne Joshu<sup>4</sup>, Tamara Lotan<sup>5</sup>

<sup>1</sup>Johns Hopkins Hospital School of Medicine, Baltimore, MD, <sup>2</sup>Johns Hopkins School of Medicine, Baltimore, MD, <sup>3</sup>Johns Hopkins Medical Institutions, Baltimore, MD, <sup>4</sup>Johns Hopkins Bloomberg School of Public Health, Baltimore, MD, <sup>5</sup>Johns Hopkins University School of Medicine, Baltimore, MD

**Disclosures:** Lia DePaula Oliveira: None; Oluwademilade Dairo: None; Ethan Schaffer: None; Adrianna A Mendes: None; Thiago Vidotto: None; Jiayun Lu: None; Corinne Joshu: None; Tamara Lotan: None

**Background:** Fatty acid synthase (FASN) catalyzes the synthesis of long chain saturated fatty acids and is upregulated in prostate cancer. Recent studies have demonstrated that *FASN* gene expression may be higher among prostate tumors from self-identified Black (BL) compared to White (WH) patients, potentially due to increased frequency of *FASN* gene amplification or an altered androgen receptor (AR) cistrome. However, *FASN* expression also increases in cases with *ERG* gene rearrangement, which is less common in tumors from BL men. Here, we quantified *FASN* expression in a racially diverse cohort of primary prostate tumors and examined its association with clinical, genomic and immune tumor microenvironment (TME) characteristics.

**Design:** We genetically validated *FASN* immunohistochemistry using cell lines and analyzed its expression in a previously described tissue microarray constructed from radical prostatectomy (RP) specimens of 371 grade-matched, self-identified BL and WH men with clinical follow-up and genomic copy number analysis. Digital image analysis was performed using QuPath to quantify average *FASN* H-score in tumor glands identified by lack of p63 immunostaining.

**Results:** *FASN* expression was not significantly associated with tumor grade or pathologic stage, but was significantly higher among WH compared to BL patients ( $p=0.02$ ). *ERG*-positive tumors had significantly higher *FASN* expression in the overall cohort compared to *ERG*-negative tumors ( $p<0.0001$ ). In a generalized linear regression model including race and *ERG* status and adjusted by clinical-pathologic factors, *ERG* ( $p=0.02$ ) but not race ( $p=0.1$ ) remained significantly associated with *FASN* expression and there was no interaction between *FASN* and race ( $p=0.9$ ). *FASN* expression was weakly correlated with *FASN* gene copy number ( $r=0.14$ ,  $p=0.02$ ) and with percent genome altered by somatic copy number alterations ( $r=0.15$ ,  $p=0.01$ ). *FASN* expression was significantly correlated with density of FOXP3+ T-regulatory cells ( $r=0.21$ ,  $p=0.0002$ ) in both races, but not with cytotoxic T-cell, B-cell, macrophage, mast cell or neutrophil densities.

**Conclusions:** Consistent with prior studies, *ERG* positivity is associated with higher *FASN* expression, but there is not an independent association of *FASN* expression with self-identified race. The association of *FASN* expression with increased immunosuppressive T-regulatory cells suggests a potential interaction between prostate cancer lipid metabolism and the immune TME.

## 729 Mesothelioma of Uncertain Malignant Potential of Tunica Vaginalis (MUMP) – Novel Morphologies & Additional Follow-up Supporting Indolent Behavior

Chien-Kuang Cornelia Ding<sup>1</sup>, Oleksandr Kryvenko<sup>2</sup>, Huihui Ye<sup>3</sup>, Jonathan Epstein<sup>4</sup>

<sup>1</sup>Johns Hopkins University, Baltimore, MD, <sup>2</sup>University of Miami Miller School of Medicine, Miami, FL, <sup>3</sup>University of California, Los Angeles, Los Angeles, CA, <sup>4</sup>Johns Hopkins Medical Institutions, Baltimore, MD

**Disclosures:** Chien-Kuang Cornelia Ding: None; Oleksandr Kryvenko: None; Huihui Ye: None; Jonathan Epstein: None

**Background:** Arising from the testis tunica vaginalis, well-differentiated papillary mesothelial tumor (WDPMT) with pure papillary architecture lined by a single layer of bland cuboidal cells and malignant mesothelioma (MM) are well-recognized entities. With 8 cases first reported by one of the current authors in 2010, MUMP is rare with only 5 cases subsequently reported. MUMP has areas typical of WDPMT but predominantly consists of more complex cribriform architecture (Fig. 1A), and is not seen in other mesothelial sites.

**Design:** 12 cases of MUMP were identified (2010-2022) from the consultation files of the authors.

**Results:** Clinical features are summarized in Table 1. Patients' age at presentation averaged 56 years (range: 24 to 81). Only one patient self-identified with asbestos exposure. In addition to classic findings of MUMP, newly described histologies seen in the current series include: solid foci (Fig. 1B) (n=1); cystic areas (Fig. 1C) (n=1); cellular spindle cells lacking hyperchromasia, atypia,

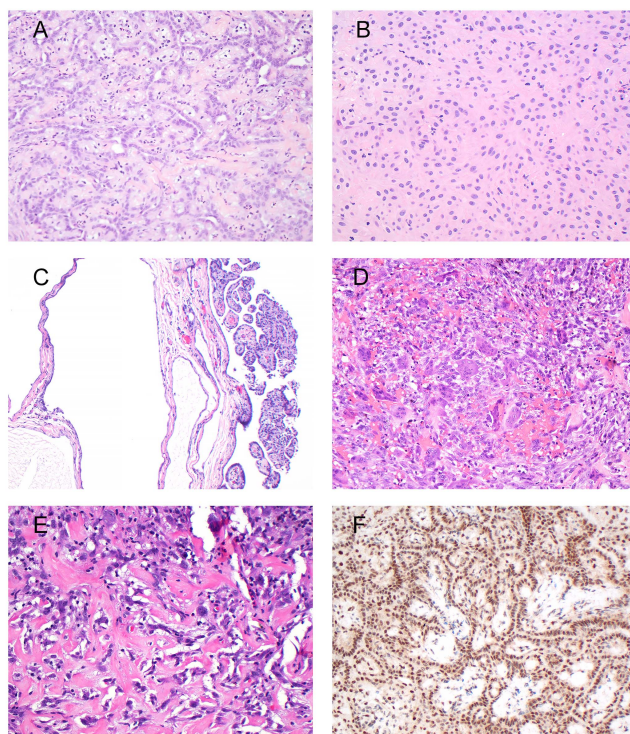
# ABSTRACTS | GENITOURINARY PATHOLOGY (INCLUDING RENAL TUMORS)

or increased mitotic activity (n=5) with osteoclast-like giant cells in 1 of these cases (Fig. 1D); and prominent collagen deposition in 2 of these cases (Fig. 1E). Despite architectural complexity, MUMP's cytology was identical to the WDPM-like area. No case showed cytological features of MM and none were associated with invasion. 9 cases were multifocal. All 5 analyzable cases showed retained MTAP and BAP1 immunohistochemically (Fig. 1F), with low Ki-67 labeling index (most <5%, up to 10%). No patient received adjuvant chemoradiation after surgery. Follow-up information was available in 8 patients, 6 patients for more than 1 year (1.5 - 11 years, median 2 years). None showed evidence of disease recurrence or metastases post-surgery.

Case No.	Age (yrs)	Clinical presentation	Treatment	Focality	Follow-up
1	76	Hydrocele	Orchiectomy	Multifocal	2 yrs NED
2	24	Hydrocele	Hydrocelectomy	Multifocal	Recent
3	36	Hydrocele	Hydrocelectomy	Multifocal	2 yrs NED
4	68	Hydrocele	Hydrocelectomy	Unifocal	11 yrs NED
5	56	Hydrocele	Hydrocelectomy	Unifocal	3 mos, NED Unknown
6	73	Hydrocele	Orchiectomy	Multifocal	4.5 yrs, NED
7	53	Hydrocele	Hydrocelectomy	Multifocal	Unknown
8	68	Testicular mass*	Orchiectomy	Multifocal	5 yrs, NED
9	81	Inguinal nodule	Excision	Multifocal	Unknown
10	46	Hydrocele	Hydrocelectomy	Unifocal	4 mos, NED Unknown
11	32	Hydrocele and soft mass	Hydrocelectomy and excision	Multifocal	1.5 yrs, NED
12	56	Scrotal mass	Orchiectomy	Multifocal	Recent

\*: self-reported asbestos exposure. NED: No evidence of disease. Unknown: loss of follow-up.

Figure 1 - 729



**Conclusions:** The current series expands the morphology that may be seen in MUMP with additional cases followed with no recurrence/metastases. Despite greater architectural complexity, evidence supporting MUMP is a variant of WDPMT includes: 1) bland cytology; 2) merging in with WDPMT areas; 3) low mitotic/Ki-67 rate; 4) retention of MTAP/BAP1; and 5) benign clinical follow-up. If these cases were MM, one would have expected at least some of the patients to demonstrate disease recurrence/progression without adjuvant therapy within the available follow-up time, particularly with limited resection in most patients. Nevertheless, MUMP is currently a reasonable term, given the limited number of these lesions that have been studied and followed.

## 730 Challenges of Using Deep Learning for Classification of Oncocytic Renal Tumors

Kingsley Ebare<sup>1</sup>, Katrina Collins<sup>2</sup>, Taryme Lopez Diaz<sup>3</sup>, Ahmed Naglah<sup>3</sup>, Ayman El-Baz<sup>3</sup>, Stephanie Siegmund<sup>4</sup>, Sean Williamson<sup>5</sup>, Michelle Hirsch<sup>4</sup>, Dibson Gondim<sup>3</sup>, Muhammad Idrees<sup>2</sup>

<sup>1</sup>Indiana University, Indianapolis, IN, <sup>2</sup>Indiana University School of Medicine, Indianapolis, IN, <sup>3</sup>University of Louisville, Louisville, KY, <sup>4</sup>Brigham and Women's Hospital, Boston, MA, <sup>5</sup>Cleveland Clinic, Cleveland, OH

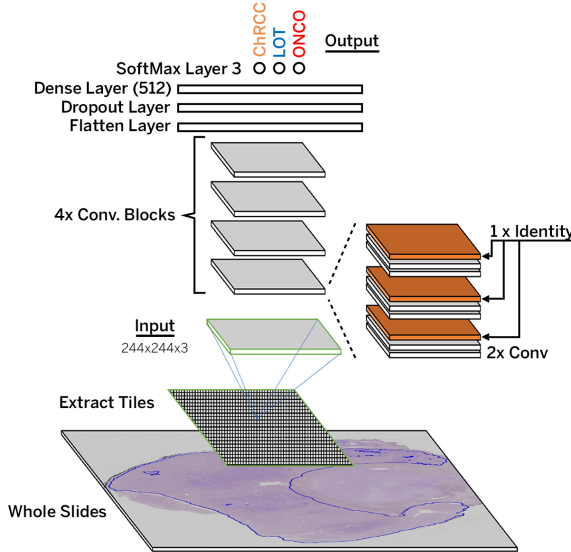
**Disclosures:** Kingsley Ebare: None; Katrina Collins: None; Taryme Lopez Diaz: None; Ahmed Naglah: None; Ayman El-Baz: None; Stephanie Siegmund: None; Sean Williamson: None; Michelle Hirsch: None; Dibson Gondim: None; Muhammad Idrees: None

**Background:** Low-grade oncocytic renal tumor of the kidney (LOT) has been proposed as a new entity. LOTs and oncocytomas cannot be differentiated from each other morphologically except by immunostains. Renal oncocytic neoplasms with low-grade features that characteristically demonstrate CK7-positivity and CD117-negativity are classified as LOTs while the converse is true for oncocytomas. Our study aims to use a deep learning artificial intelligence (AI) approach on hematoxylin and eosin-stained (H&E) whole-slide images (WSI) to classify these tumors as LOTs, oncocytomas, or chromophobe renal cell carcinomas (ChRCC).

**Design:** We retrospectively identified and retrieved (77) oncocytic tumors, including 29 cases of LOT, 25 cases of oncocytoma and 23 ChRCC. Clinicopathologic parameters including age, gender, tumor size, and location of tumor on radiology (exophytic vs endophytic) were recorded. H&E-stained slides and immunohistochemical slides were reviewed and digitized. Digitized images were annotated with labels of the three histologic classes by 3 GU pathologists. Extracted patch images were pre-processed and split into a 7:2:1 ratio and fed into a convolutional neural network.

**Results:** Patients with LOT ranged in age from 23 to 84 years (mean, 67.3 years). The tumors ranged in size from 1.0 cm to 11.5cm (mean, 4.38 cm). Patients with oncocytomas ranged in age from 38 to 77 (mean, 63.5 years). The tumors ranged in size from 1.7 cm to 10.4 cm (mean, 4.29 cm). The male: female ratio was 1:1.7 for LOT and 4:1 for oncocytoma. This difference was statistically significant ( $p=0.005$ ). Patients with oncocytomas were more likely described as having exophytic tumors (9/11 cases, 81.8%). We developed a residual learning-based deep learning framework for oncocytoma and LOT prediction on the patch level (Figure 1). The AI model was able to achieve 3-class predictions with accuracy of 61.7%, precision of 62.1%, and recall 60.2%.

Figure 1 - 730



**Conclusions:** Although this study shows promising results for the use of deep learning AI to differentiate LOTs from other renal oncocytic tumors, it also highlights the challenges that need to be overcome. Based on the limited dataset, a deep learning approach to distinguish between LOTs, oncocytomas and ChRCC using H&E WSI is not currently feasible and IHC use remains the gold standard. Creation of public large-scale curated datasets of oncocytic tumors is needed to allow investigation of multiple deep-learning approaches.

# ABSTRACTS | GENITOURINARY PATHOLOGY (INCLUDING RENAL TUMORS)

## 731 Clinical and Pathologic Features of Small Sized ( $\leq 4$ cm) Renal Cell Carcinomas Presenting at High Stage (pT3)

Sarah Edminster<sup>1</sup>, Ryan Xiao<sup>2</sup>, Brian Ma<sup>1</sup>, Guang-Qian Xiao<sup>3</sup>

<sup>1</sup>LAC+USC Medical Center, Los Angeles, CA, <sup>2</sup>Pasadena, CA, <sup>3</sup>Keck School of Medicine of USC, Los Angeles, CA

**Disclosures:** Sarah Edminster: None; Ryan Xiao: None; Brian Ma: None; Guang-Qian Xiao: None

**Background:** Renal cell carcinoma (RCC) is one of the most common malignancies. Like other types of cancer, the stage at presentation is one of the major prognostic parameters. Based on the size alone, RCC  $\leq 4$  cm is staged as pT1a. RCC  $\leq 3$  cm in size has also recently become recommended for surveillance. The aim of this study is to elucidate the prevalence of small RCC ( $\leq 4$  cm) that present at high stage (pT3) and their association with RCC variants as well as their clinicopathologic features.

**Design:** All RCC cases that were  $\leq 4$  cm, including clear cell RCC (cRCC), papillary RCC (pRCC), chromophobe RCC (chrRCC) and unclassified RCC (uRCC), accessioned from 2017 to 2021 at our institution were retrieved from the archives. There was a total of 496 RCC cases that met the size criteria, of which 408 were cRCCs, 46 pRCCs, 40 chrRCCs, and 2 uRCCs. Among the 496 RCCs  $\leq 4$  cm, 51 (10%) were staged pT3. For each of these small size and high stage RCC cases, patient demographic, pathologic, and any available follow-up information was collected.

**Results:** In our cohort of 51 RCC cases of small size and high stage, the tumor size ranged from 1 to 4 cm, patients' age from 39 to 89 (68 $\pm$ 11) and male: female ratio at 2.6:1. Based on the available follow up data, 29% (12/51) of patients presented with distant metastasis (liver, lung, bone, etc), 6% (3/51) with local recurrence, 23% (12/51) cases with no disease progression at follow up  $\geq 6$  months, and 41% (21/51) only had short follow up (<6 months) and /or were lost to follow up. In addition, of the 51 cases, 37% (19/51) of tumors were  $\leq 3$  cm in maximum dimension. The results are summarized in Table 1.

**Table 1. Prevalence and clinical and pathologic features of RCC with size  $\leq 4$  cm and stage pT3 (n=51)**

		Clear cell RCC	Papillary RCC	Chromophobe RCC	Unclassified	
# and % of RCC variants (n=51)		37/51 (72%)	10/51 (20%)	2/51 (4%)	2/51 (4%)	
# and % of RCC variant with distant metastasis (n=12)		7/37 (19%)	3/10 (30%)	0	2/2 (100%)	
# and % of RCC variant ( $\leq 4$ cm+pT3) among total respective RCC variant with size $\leq 4$ cm regardless of stage (408 cRCCs, 46 pRCCs, 40 ChRCCs, 2 uRCCs)		37/408 (9%)	10/46 (22%)	2/40 (5%)	2/2 (100%)	
Tumor site		Upper pole	Middle pole	Lower pole	Not specified	
	Primary tumor	18/51 (35%)	21/51 (41%)	7/51 (14%)	5/51 (10%)	
	Primary tumor with distant metastasis (n=12)	4/18 (22%)	6/21 (29%)	1/7 (14%)	1/5 (20%)	
Site of tumor extension for pT3		Renal vein invasion	Sinus fat invasion	Perinephric fat invasion	Pelvicalyceal extension	Combined ( $\geq 2$ )
	Total primary tumor	19/51 (37%)	9/51 (18%)	17/51 (33%)	1/51 (2%)	5/51 (10%)
	Primary tumor with distant metastasis (n=12)	5/19 (26%)	1/9 (11%)	3/17 (18%)	0/1 (0%)	3/5 (60%) (Vein+ Sinus)
Nuclear grade		Grade 1	Grade 2	Grade 3	Grade 4	N/A (not specified)
	Primary tumor	0	34/51 (67%)	10/51 (19%)	3/51 (6%)	4/51 (8%)
	Primary tumor with distant metastasis (n=12)	0	5/34 (15%)	5/10 (50%)	2/3 (67%)	0/4 (0%)

**Conclusions:** Although uncommon, small RCCs ( $\leq 4$  cm) may present at high stages, even tumors  $\leq 3$  cm that are often recommended for active surveillance. These tumors were found to be most often located in the upper to mid poles. Renal vein and perinephric invasion contributed to the high stage in most cases. Although the most common variants were cRCC and pRCC, PRCC and uRCC tumors seemed to be more likely to present at stage pT3 than the former. About 29% cases reviewed presented with distant metastasis. Metastasis appeared to be more strongly associated with middle lobe location, renal vein invasion, nuclear grades 3 and 4, and PRCC and uRCC subtypes. Like RCC in the general population, age and gender had no significant impact. Though further validation is warranted, the findings are of significant clinical implications in patient management.

## 732 Differences of MSH2/MSH6 Expression in Localized Prostate Cancer Between African and European Ancestries

Ahmed Elsaeed<sup>1</sup>, Jones Nauseef<sup>2</sup>, Yajas Shah<sup>3</sup>, Majd Al Assaad<sup>2</sup>, Zaheer Bukhari<sup>4</sup>, David Wilkes<sup>1</sup>, Malhaar Agrawal<sup>4</sup>, Michael Sigouros<sup>1</sup>, Jyothi Manohar<sup>1</sup>, Brian Robinson<sup>1</sup>, Olivier Elemento<sup>1</sup>, David Nanus<sup>2</sup>, Raavi Gupta<sup>4</sup>, Marcin Imielinski<sup>1</sup>, Juan Miguel Mosquera<sup>1</sup>

<sup>1</sup>Weill Cornell Medicine, New York, NY, <sup>2</sup>New York-Presbyterian/Weill Cornell Medicine, New York, NY, <sup>3</sup>Englander Institute for Precision Medicine, New York, NY, <sup>4</sup>SUNY Downstate Medical Center, New York, NY

**Disclosures:** Ahmed Elsaeed: None; Jones Nauseef: None; Yajas Shah: None; Majd Al Assaad: None; Zaheer Bukhari: None; David Wilkes: None; Malhaar Agrawal: None; Michael Sigouros: None; Jyothi Manohar: None; Brian Robinson: None; Olivier Elemento: None; David Nanus: None; Raavi Gupta: None; Marcin Imielinski: None; Juan Miguel Mosquera: None

**Background:** American men of African ancestry (AA) develop prostate cancer (PC) at twice the rate of their European ancestry (EA) counterparts, present at higher stages and tend to be more aggressive. Preliminary evidence from our whole-genome sequencing cohort of localized AA PC demonstrates differences in mutational signatures that implicate genomic stability. Interestingly, improved responses in AA men to Sipuleucel-T (an immune-based therapy) and radiotherapies have been observed in advanced disease. In this study we aim to investigate the correlation between the expression of MMR proteins in localized PC and their variation between AA and EA men.

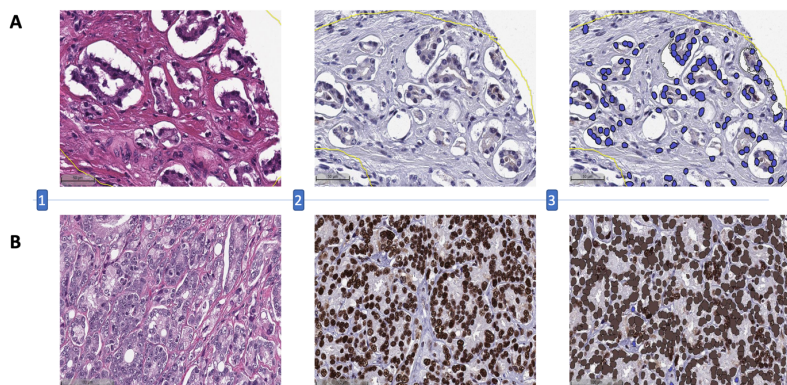
**Design:** Radical prostatectomies from self-reported ancestries of 156 AA and 41 EA specimens represented in tissue microarrays were interrogated by IHC for MSH2 and MSH6. Digital analysis was run by using HALO® software through annotating the Regions of Interest (ROIs), classifying tumor nuclei, and measuring the stain expression via an automated cytonuclear algorithm (Figure 1). A numerical score (0-4) was set to match the percentage of stain preservation within tumor nuclei and a threshold of 0.2 score to consider a case as MMR-deficient (MMR-d).

**Results:** Quantitative image analysis shows a significant loss of MSH6 stain in AA (mean score=1.56) compared to EA tumors (mean score=2.74) ( $P<0.0001$ ), observed in 27 (17%) and 3 (7%) cases, respectively (Figure 2A). There was not a statistical difference in MSH2 expression; 23 of AA PC (14.7%) were found to be MSH2 deficient compared to 5 EA cases (12%) with mean scores of 1.78 and 1.95, respectively ( $P=0.4$ ) (Figure 2B). Grade group 4 showed slightly lower expression than other groups, not significant. No correlation was identified between MSH2/MSH6 scores and age, Grade group or pathological stage (Table 1).

A.						
		African Ancestry Prostate Cancer			European Ancestry Prostate Cancer	
<b>No. of Cases</b>		156			41	
<b>Age at Prostatectomy</b>		Average 59.6 Range 40 to 78			Average 63.2 Range 41 to 75	
<b>Gleason Grade Group (GGG)</b>		No.	MSH2	MSH6	<b>No.</b>	<b>MSH2</b>
		<b>Mean Score</b>				
GGG1	42	1.7	0.8	3	2.2	
GGG2	75	1.8	1.8	20	2.3	
GGG3	27	1.4	1.8	12	1.6	
GGG4	2	2.45	0.55	3	0.4	
GGG5	9	1.7	2.3	3	2.2	
B.						
<b>Qualitative Score</b>		<b>Negative</b>	<b>Low</b>	<b>Moderate</b>	<b>High</b>	
<b>Stain Preservation</b>		0% - %5	5% - 25%	25% - 50%	50% - 100%	
<b>Numerical Score</b>		0 - 0.2	0.2 - 1	1 - 2	2 - 3	3 - 4
MSH2	AA%	EA%	14.7	12.2	25	9.7
MSH6	AA%	EA%	17.3	7.3	26.3	7.3
					20.5	9.7
					16	14.7
						19.9
						60

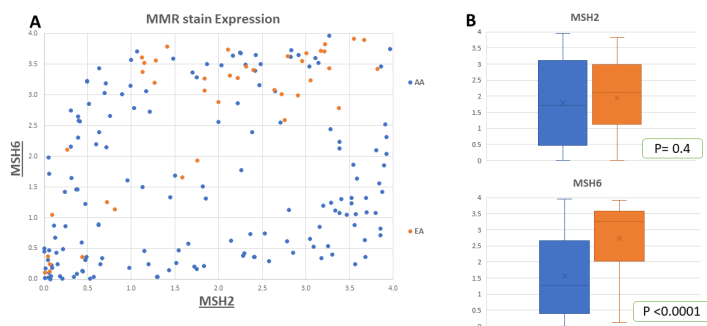
**Table 1. Image analysis of MSH2 and MSH6 immunohistochemistry in localized prostate cancer affecting men of African and European Ancestry:** A. Mean score values in different Gleason Grade Groups. B- Correlation of numerical scores with semiquantitative assessment of immunohistochemistry.

Figure 1 - 732



**Figure 1.** HALO® digital analysis of IHC stained tumor cores for MSH6 in localized prostate cancer. **A.** African Ancestry and **B.** European Ancestry prostate cancer. ROIs of tumor areas are digitally annotated on H&E (1) as a reference to evaluate corresponding MSH6 stained area (2). HALO® annotation and classifier modules with an automated cytonuclear algorithm were used to detect IHC stain within tumor nuclei (3). The algorithm quantitates the loss of MSH6 stain in AA compared to total preservation in EA case.

Figure 2 - 732



**Figure 2.** HALO® digital analysis of MSH 6 and MSH2 IHC in localized prostate cancer of African (n=156) and European (n=41) Ancestry. **A.** Scatter plot shows tendency of lower expression in AA cases (blue dots). Outliers of both populations are shown at the left lower corner. **B.** Box plots show lower average scores of stain preservation in AA, statistically significant for MSH6. Mean/Median for AA vs EA: MSH2= 1.78/1.71 and 1.95/2.1 compared to MSH6: 1.56/1.3 and 2.74/3.27 respectively. T-test was used to assess statistical significance.

**Conclusions:** We identified significant loss of MSH6 expression in localized PC of AA compared to EA. This may be relevant given the higher response proportions in AA men to immune- and radiotherapies. Further validation and expansion to metastatic tumors is ongoing.

## 733 Integrative Whole Genome and Transcriptome Sequencing Analysis of Advanced Prostate Cancer Unearths Genomic Signatures and Novel Events of Potential Significance

Ahmed Elsaeed<sup>1</sup>, Jones Nauseef<sup>2</sup>, Majd Al Assaad<sup>2</sup>, Gunes Gundem<sup>3</sup>, Max Levine<sup>3</sup>, Jyothi Manohar<sup>1</sup>, Michael Sigouros<sup>1</sup>, Brian Robinson<sup>1</sup>, Andrea Sboner<sup>1</sup>, Juan Medina-Martinez<sup>3</sup>, Olivier Elemento<sup>1</sup>, Juan Miguel Mosquera<sup>1</sup>

<sup>1</sup>Weill Cornell Medicine, New York, NY, <sup>2</sup>New York-Presbyterian/Weill Cornell Medicine, New York, NY, <sup>3</sup>New York, NY

**Disclosures:** Ahmed Elsaeed: None; Jones Nauseef: None; Majd Al Assaad: None; Gunes Gundem: Consultant: Isabl Technologies; Max Levine: Employee: Isabl Inc.; Jyothi Manohar: None; Michael Sigouros: None; Brian Robinson: None; Andrea Sboner: None; Juan Medina-Martinez: Employee: Isabl Inc.; Stock Ownership: Isabl Inc.; Olivier Elemento: None; Juan Miguel Mosquera: None

**Background:** Death from prostate cancer (PC) is most commonly due to the development of metastatic, castration-resistant prostate cancer (mCRPC). Among these, androgen-independent tumors with variant histology, often referred to as neuroendocrine prostate cancer (NEPC), represent the most aggressive variants. The aim of this study was to identify new targets – an unmet clinical need – via integrative whole genome (WGS) and transcriptome sequencing (RNAseq) analysis of metastatic PC.

**Design:** WGS was performed on 55 tumor/normal pairs (CRPC\_Adenocarcinoma n= 32, CRPC\_NEPC n=13, *de novo* NEPC n=7, metastatic hormone naive PC n=3) from 48 patients. RNAseq data was available in a subset of 21 samples. We employed the Isabl GxT analytic platform and manually curated single base substitution (SBS) molecular signatures and structural variants (SV) that involved tumor suppressor genes and oncogenes.

# ABSTRACTS | GENITOURINARY PATHOLOGY (INCLUDING RENAL TUMORS)

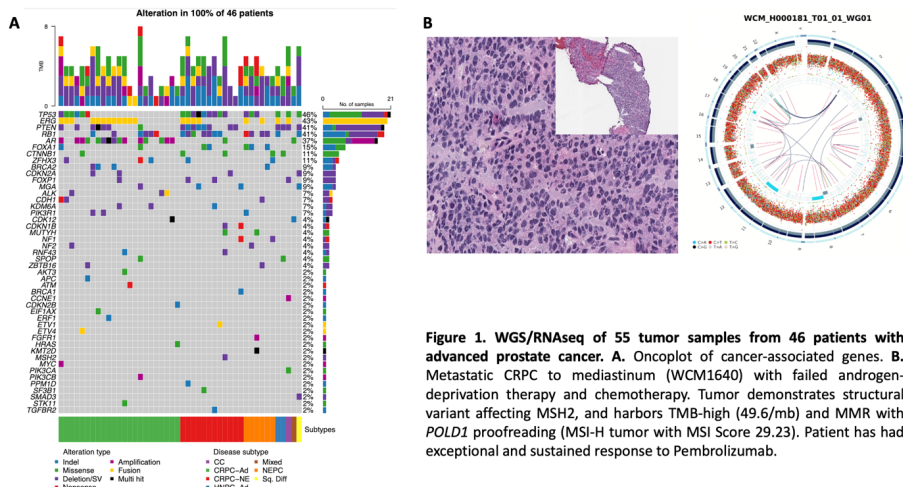
**Results:** We observed 184 events in cancer-associated genes and targets in 38 cases. Rare ETS fusions were identified in 2 patients (*MSMB-ERG* and *YWHAE-ETV4*). Other rare events included SVs affecting *ALK* (*SLC45A3-ALK*) and *FGFR1* amplification in 1 patient each. Relevant pathogenic germline alterations were identified in 15% of cases affecting genes such as *BRCA1*, *BRCA2*, and *ATM*, and other genes of uncertain relevance for prostate cancer (e.g., *PPM1D* and *MUTYH*). SBS genomic signatures associated with homologous recombination deficiency (HRD) were observed in 15% of the patients (7 cases): 3 harbored germline *BRCA1/2* mutations, 2 with somatic *BRCA2* mutations, and 2 without alteration in *BRCA1/2* (1 of these had a complex SV affecting *RAD51B*). Further, molecular signatures of potential clinical relevance were detected at varying contributions and included *CDK12*-type genomic instability (2 cases) (4%) and MMR deficiency with *POLD1* proofreading (1 case). See Table 1 and Figure 1 and Figure 2.

Mutated Genes / Fusions	Alteration	Treatment	N. of Cases	Tumor Type
CDKN2A	Oncogenic mutation	CDK inhibitors	2	1 Adenocarcinoma 1 NEPC
HRAS	Oncogenic mutation	Tipifarnib	1	Adenocarcinoma
PTEN	Oncogenic mutation	AZD8186 and GSK2636771	12	7 Adenocarcinoma 4 NEPC 1 Carcinosarcoma
MET	Amplification	Tepotinib, Capmatinib and Crizotinib	1	Adenocarcinoma
TMB	Tumor Mutational Burden-High	Check Point Inhibitors	2	1 Adenocarcinoma 1 NEPC
MSI	Microsatellite Instability-High	Check Point Inhibitors	1	NEPC
CDK12	Truncating and Oncogenic mutation	Check Point Inhibitors  Olaparib	2	1 Adenocarcinoma 1 NEPC
FGFR1/ FGFR2	Amplification/ Oncogenic mutation	FGFR inhibitors	2	NEPC
mTOR	Oncogenic mutation	Temsirolimus and Everolimus	1	NEPC
NF1	Oncogenic mutation	Cobimetinib and Trametinib	1	NEPC
ALK	SLC45A3-ALK	ALK inhibitors	1	Adenocarcinoma
PIK3CA	Oncogenic mutation	Alpelisib and Fulvestrant	1	Carcinosarcoma
PALB2	Oncogenic mutation	PARP inhibitors	1	Adenocarcinoma
BRCA2	Deletion	PARP inhibitors	1	Adenocarcinoma
CDK12	MED1-CDK12	Check Point Inhibitors	1	NEPC
ETS fusions	TPRSS2-ERG, MSMB-ERG and YWHAE-ETV4	N/A	5	Adenocarcinoma
Biomarker	SBS Molecular Signatures and Mutated Genes	N. of Cases	Tumor type	
HRD	SBS3  BRCA1/2 and RAD51B	8	5	Adenocarcinoma 2 NEPC 1 Squamous
MMR	SBS6, 15, 21, 26 and 44	34	20	Adenocarcinoma 13 NEPC 1 Squamous
MMR deficiency + POLD1 mutation	SBS20	6	4	Adenocarcinoma 2 NEPC

**Table 1: Molecular alterations and biomarker-driven treatments elucidated by WGS in 55 tumor samples from 48 patients with metastatic prostate cancer.** Median age at diagnosis was 62 years (range 44-86 years). For the entire cohort, average values were as follows: coverage 90.5x, coding tumor mutational burden (TMB) = 2.67 mut/Mb, Microsatellite instability (MSI) score = 1.21, Structural variants = 187.

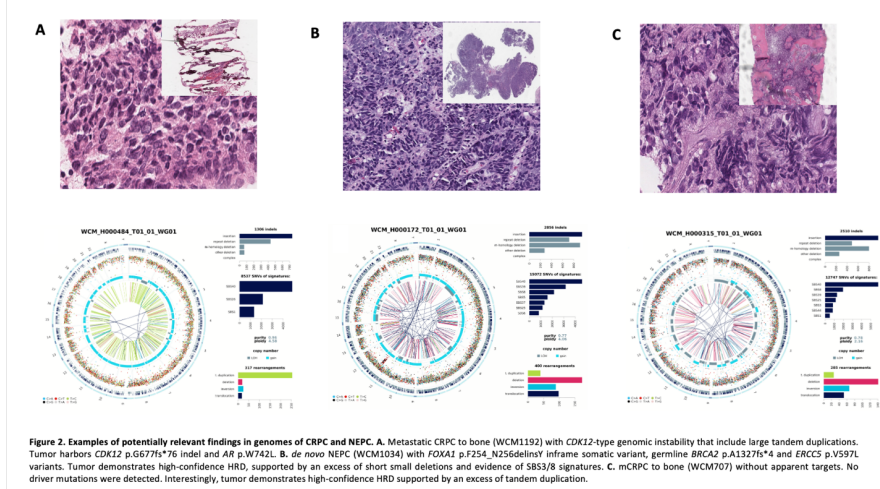
**MMR** = mismatch repair; **HRD** = homologous recombination deficiency; **SBS** = single base substitution.

Figure 1 - 733



**Figure 1.** WGS/RNAseq of 55 tumor samples from 46 patients with advanced prostate cancer. **A.** Oncplot of cancer-associated genes. **B.** Metastatic CRPC to mediastinum (WCM1640) with failed androgen-deprivation therapy and chemotherapy. Tumor demonstrates structural variant affecting MSH2, and harbors TMB-high (49.6/mb) and MMR with *POLD1* proofreading (MSI-H tumor with MSI Score 29.23). Patient has had exceptional and sustained response to Pembrolizumab.

Figure 2 - 733



**Figure 2.** Examples of potentially relevant findings in genomes of CRPC and NEPC. **A.** Metastatic CRPC to bone (WCM1192) with *CDK12*-type genomic instability that include large tandem duplications. Tumor harbors *CDK12* p.G677fs\*76 indel and AR p.W742L. **B.** *de novo* NEPC (WCM1034) with *FOXA1* p.F254\_N256delinsY frameshift somatic variant, germline *BRCA2* p.A132Tfs\*4 and *ERCC5* p.S597L variants. Tumor demonstrates high-confidence HRD, supported by an excess of short small deletions and evidence of SBS3/8 signatures. **C.** mCRPC to bone (WCM707) without apparent targets. No driver mutations were detected. Interestingly, tumor demonstrates high-confidence HRD supported by an excess of tandem duplication.

**Conclusions:** WGS/RNAseq in CRPC and NEPC elucidates genomic signatures associated with HRD and MMR, complex events affecting oncogenes, and rare ETS fusions. Our findings warrant further validation and clinical correlation.

## 734 Reconstruction of the Metastatic Castration-Resistant Prostate Tumor Microenvironment with Comprehensive Profiling Reveals Unique Subtypes

Ahmed Elsaeed<sup>1</sup>, Andrey Kravets<sup>2</sup>, Jones Nauseef<sup>3</sup>, Majd Al Assaad<sup>3</sup>, Erik Tadevosyan<sup>2</sup>, Emir Radkevich<sup>2</sup>, Olga Kudryashova<sup>2</sup>, Jyothi Manohar<sup>1</sup>, Michael Sigouros<sup>1</sup>, Vladimir Kushnarev<sup>2</sup>, Alexander Bagaev<sup>2</sup>, Nara Shin<sup>2</sup>, Anna Love<sup>4</sup>, Brian Robinson<sup>1</sup>, Andrea Sboner<sup>1</sup>, Olivier Elemento<sup>1</sup>, Cora Sternberg<sup>1</sup>, Juan Miguel Mosquera<sup>1</sup>

<sup>1</sup>Weill Cornell Medicine, New York, NY, <sup>2</sup>BostonGene Corporation, Waltham, MA, <sup>3</sup>New York-Presbyterian/Weill Cornell Medicine, New York, NY, <sup>4</sup>BostonGene Corporation, Boston, MA

**Disclosures:** Ahmed Elsaeed: None; Andrey Kravets: Employee: BostonGene; Jones Nauseef: None; Majd Al Assaad: None; Erik Tadevosyan: None; Emir Radkevich: Employee: BostonGene; Olga Kudryashova: Employee: BostonGene; Jyothi Manohar: None; Michael Sigouros: None; Vladimir Kushnarev: Employee: BostonGene; Alexander Bagaev: Employee: BostonGene corporation; Nara Shin: Employee: BostonGene; Anna Love: Employee: BostonGene Corp.; Brian Robinson: None; Andrea Sboner: None; Olivier Elemento: None; Cora Sternberg: None; Juan Miguel Mosquera: None

**Background:** Androgen receptor-independent metastatic castration-resistant prostate cancer (mCRPC) represents up to 25-30% of lethal prostate cancer. We reconstructed the transcriptomic data from our Weill Cornell Medicine (WCM) cohort of patients with mCRPC with adenocarcinoma morphology (mCRPC-Ad) and treatment-emergent neuroendocrine prostate cancer (tNEPC) to observe the tumor microenvironment (TME), genomic characteristics, and molecular diversity of samples in association with clinical outcomes. Data were combined with datasets from publicly available cohorts.

# ABSTRACTS | GENITOURINARY PATHOLOGY (INCLUDING RENAL TUMORS)

**Design:** We performed RNA-seq (n=23) and whole-exome sequencing (WES; n=36) on our cohort of 14 patients, including 3 rapid autopsies with multiple samples. In addition, we developed a meta-cohort of 358 prostate cancer samples from publicly available RNA-seq cohorts (Table 1). Unsupervised clustering was used for TME classification, and the Kassandra deconvolution algorithm (*Cancer Cell* 2022) was used to calculate cellular composition. Differential gene expression (DGE) was analyzed. The Mann-Whitney U test was used for statistical analyses.

**Results:** Five distinct TME subtypes were identified (Figure 1): immune desert neuroendocrine-like (IDN) (24.3%), immune desert basal-like (IDB) (15.6%), fibrotic (F) (20.3%), immune enriched (IE)-neutrophil enriched (IENE) (16.4%), and IE-T cell enriched (IETE) (23.4%). Expression of neuroendocrine gene signatures, basal-like signatures, T-cell fractions (CD4, CD8), and neutrophil content were higher in the IDN, IDB, IETE and IENE subtypes, respectively (P<0.001) (Figure 2A). Half of mCRPC-Ad were classified as IDB and almost all tNEPC and mixed samples were within the IDN subtype. Liver, lymph node, and bone metastases were more prevalent in IDN, IETE, and IENE, respectively. Overall survival (OS) analysis showed a trend of IDN and IENE being more aggressive than IETE, F, and IDB (p > 0.05). DGE analysis to delineate tNEPC revealed a new stem cell marker, *FOXJ1* (mean logFC = 3.725, p < 0.001), a known cell stemness gene that had not previously been described in tNEPC (Figure 2B).

Dataset	No. of Samples	mCRPC-Ad	tNEPC	Mixed
phs000909 – RNA (1) *	44	30	14	0
phs000915 – RNA (2) §	177	162	4	11
GSE147250 – RNA (3) ¶	137	111	26	0
<b>WCM samples RNA</b>	<b>23</b>	<b>17</b>	<b>6</b>	<b>0</b>
<b>Total (%)</b>	<b>381</b>	<b>320 (84%)</b>	<b>50 (13%)</b>	<b>11 (3%)</b>
<b>WCM samples DNA</b>	<b>36</b>	<b>29</b>	<b>7</b>	<b>0</b>
Site	Lymph Node	Liver	Bone	Lung
<b>Total %</b>	<b>35.9%</b>	<b>21.4%</b>	<b>18.3%</b>	<b>3.4%</b>
<b>Primary</b>				
<b>Other</b>				

**Table 1. Transcriptomic profiling analysis of mCRPC.** Description of study cohorts (top) and different metastatic sites involved (bottom).

\* (1) [https://www.ncbi.nlm.nih.gov/projects/gap/cgi-bin/study.cgi?study\\_id=phs000909.v1.p1](https://www.ncbi.nlm.nih.gov/projects/gap/cgi-bin/study.cgi?study_id=phs000909.v1.p1)

§ (2) [https://www.ncbi.nlm.nih.gov/projects/gap/cgi-bin/study.cgi?study\\_id=phs000915.v2.p2](https://www.ncbi.nlm.nih.gov/projects/gap/cgi-bin/study.cgi?study_id=phs000915.v2.p2)

¶ (3) <https://www.ncbi.nlm.nih.gov/geo/query/acc.cgi?acc=GSE147250>

Figure 1 - 734

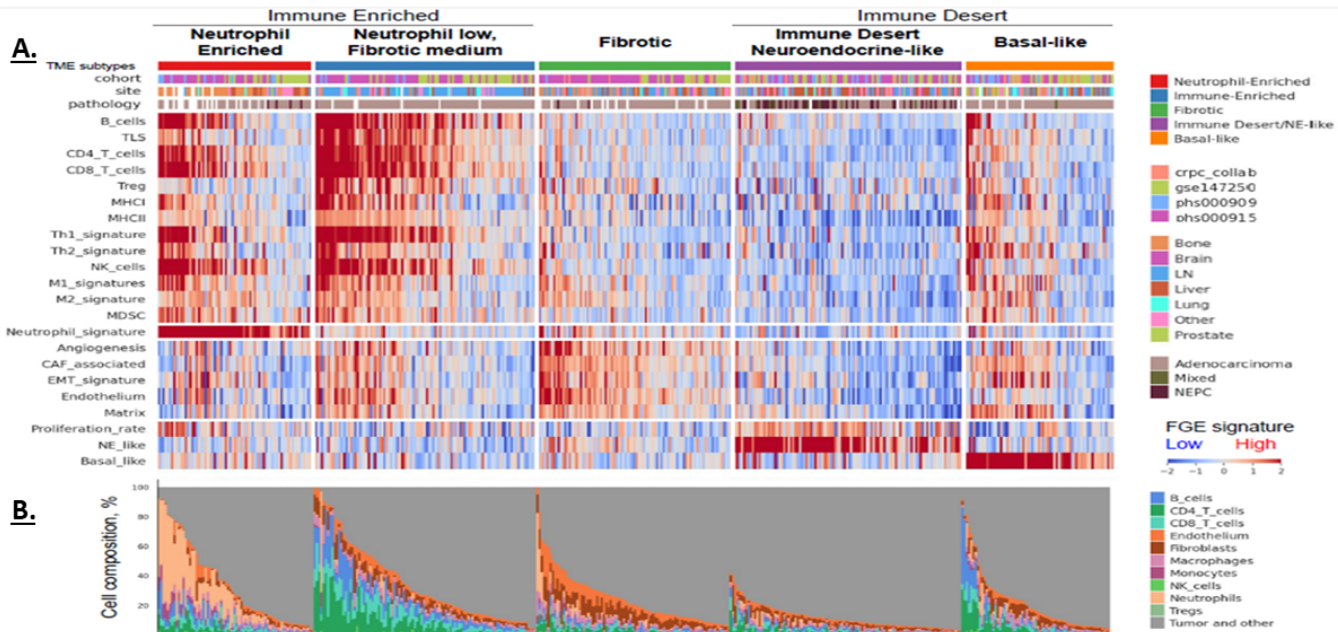


**Figure 1. Tumor microenvironment (TME) subtypes with specific signatures and cellular composition.** A. Immune desert neuroendocrine-like (IDN) shows higher neuroendocrine signatures with tNEPC. Liver is the site most enriched. B. Immune enriched (IE)-neutrophil enriched is prevalent in Bone compared to CD4/CD8 lymphocytes from the immune enriched (IE)-T cell enriched (IETE), which is prevalent in lymph node (LN).

\*Unsupervised clustering was used for TME classification. The deconvolution algorithm, Kassandra (*Cancer Cell* 2022), was used to calculate the cell composition.

Figure 2 - 734

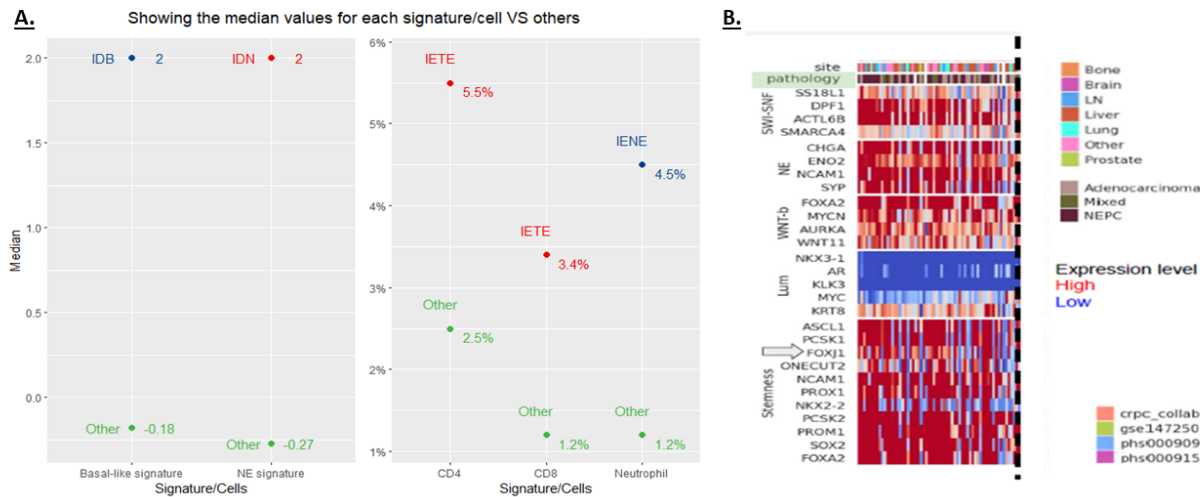


**Figure 2. Tumor microenvironment (TME) classification of prostate cancer with relevant signatures and markers.** A. Basal-like signatures medians (IDB vs. others: 2 and -0.18 respectively), Neuroendocrine signatures (IDN vs. others: 2 and -0.27 respectively), CD4 (IETE vs. Others: 5.5% and 2.5% respectively), CD8 (IETE vs. Others: 3.4% and 1.2% respectively) and Neutrophils content (IENE vs. Others: 4.5% and 1.2% respectively), P value for all <0.001. \*Mann-Whitney U test was used to assess statistical significance. B. Prevalent markers (dark red) in neuroendocrine prostate cancer, **FOXJ1** is a potential novel stem cell marker.

**Conclusions:** mCRPC has five novel TME subtypes with molecular characteristics associated with histology, sample site, and clinical annotation. We also describe **FOXJ1** as a potential novel marker of tNEPC. The subtype classification of CRPC/NEPC presents a novel molecular stratification with potential clinic-pathologic significance.

## 735 Predicting Prostate Cancer Molecular Subtype with Artificial Intelligence

Eric Erak<sup>1</sup>, Lia DePaula Oliveira<sup>1</sup>, Adrianna A Mendes<sup>2</sup>, Onur Ertunc<sup>3</sup>, Ibrahim Kulac<sup>4</sup>, Javier Baena-Del Valle<sup>5</sup>, Tracy Jones<sup>6</sup>, Jessica Hicks<sup>6</sup>, Stephanie Glavaris<sup>6</sup>, Gunes Guner<sup>7</sup>, Igor Damasceno Vidal<sup>8</sup>, Misop Han<sup>1</sup>, Mark Markowski<sup>1</sup>, Bruce Trock<sup>2</sup>, Uttara Joshi<sup>9</sup>, Chaith Kondragunta<sup>9</sup>, Nilanjan Chattopadhyay<sup>10</sup>, Saikiran Bonthu<sup>10</sup>, Nitin Singhal<sup>9</sup>, Angelo De Marzo<sup>3</sup>, Tamara Lotan<sup>6</sup>

<sup>1</sup>Johns Hopkins Hospital School of Medicine, Baltimore, MD, <sup>2</sup>Johns Hopkins Medical Institutions, Baltimore, MD, <sup>3</sup>Johns Hopkins University, Baltimore, MD, <sup>4</sup>Koç University School of Medicine, Istanbul, Turkey <sup>5</sup>Fundacion Santa Fe de Bogota University Hospital, Bogota, Colombia, <sup>6</sup>Johns Hopkins University School of Medicine, Baltimore, MD, <sup>7</sup>Hacettepe University, Ankara, Turkey, <sup>8</sup>UAB Hospital, Birmingham, AL, <sup>9</sup>AIRA Matrix Private Limited, Thane, India, <sup>10</sup>Thane, India

**Disclosures:** Eric Erak: None; Lia DePaula Oliveira: None; Adrianna A Mendes: None; Onur Ertunc: None; Ibrahim Kulac: None; Javier Baena-Del Valle: None; Tracy Jones: None; Jessica Hicks: None; Stephanie Glavaris: None; Gunes Guner: None; Igor Damasceno Vidal: None; Misop Han: None; Mark Markowski: None; Bruce Trock: None; Uttara Joshi: None; Chaith Kondragunta: None; Nilanjan Chattopadhyay: None; Saikiran Bonthu: None; Nitin Singhal: None; Angelo De Marzo: None; Tamara Lotan: None

**Background:** Unlike other genitourinary cancers, such as renal cell carcinoma, visual microscopic examination of prostate cancer has failed to reveal a reproducible association between tumor molecular subtype and morphologic features. However, deep learning-based algorithms trained on whole slide images (WSI) from large cohorts with known molecular classification may outperform the human eye and provide a cost-effective and rapid method to identify cases with clinically relevant genomic alterations. As proof of principle, we describe one such algorithm to identify prostate tumors with underlying ERG fusions and/or PTEN deletion.

**Design:** We created a Concatenated Feature Based Classification (CFBC) system based on deep learning that extracts non-linear characteristics from histopathology imaging data for improved prediction of molecular markers. The system included four stages: A) tumor identification in histopathology images; B) patch generation; C) pre-training; D) classification. The pre-training task utilized a single representative hematoxylin and eosin-stained (H&E) WSI of the dominant nodule from each of 242 tumors from a previously published Johns Hopkins radical prostatectomy cohort where ERG/PTEN status were determined by genetically validated immunohistochemistry assays. For pre-training, we applied self-supervised learning using the Barlow Twin SSL ResNeXt50 architecture. The classification task employed supervised learning using ResNet18 architecture and was performed on three Johns Hopkins validation cohorts where ERG/PTEN status were determined by previous immunohistochemistry.

**Results:** ERG algorithm performance was assessed on two radical prostatectomy cohorts, including 64 additional WSI held out from the pre-training cohort (AUC: 0.89) and 248 WSI from an independent radical prostatectomy cohort (AUC: 0.86). In addition, we tested ERG algorithm performance in 202 WSI from a needle biopsy cohort of patients undergoing radiation therapy (AUC:

0.80). PTEN algorithm performance was assessed using 64 additional WSI held out from the pre-training cohort (AUC: 0.76) and a previously published cohort of 214 WSI of Grade Group 2 needle biopsies (AUC: 0.74).

**Conclusions:** A deep learning algorithm to predict ERG/PTEN status on H&E stained WSI images from prostate carcinoma, showed excellent performance across three independent validation cohorts, including radical prostatectomy and needle biopsy tissues. Similar algorithms to predict underlying DNA repair defects may be clinically useful.

## 736 Paradoxical Detection of High-Risk HPV Genotypes in Condylomas and Low-Risk HPV Genotypes in Penile Intraepithelial Neoplasia (PeIN)

María José Fernandez-Nestosa<sup>1</sup>, Diego F Sanchez<sup>2</sup>, Sofia Canete-Portillo<sup>3</sup>, Antonio Cubilla<sup>2</sup>

<sup>1</sup>Universidad Nacional de Asunción, San Lorenzo, Paraguay, <sup>2</sup>Instituto de Patología e Investigación, Asuncion, Paraguay, <sup>3</sup>The University of Alabama at Birmingham, Birmingham, AL

**Disclosures:** María José Fernandez-Nestosa: None; Diego F Sanchez: None; Sofia Canete-Portillo: None; Antonio Cubilla: None

**Background:** High-risk HPV is considered a major etiological co-factor in penile carcinomas. About 30 to 40% of invasive carcinomas and 80 to 90% of Penile Intraepithelial Neoplasias (PeIN) are associated with high-risk genotypes of HPV. The relationship of genital condylomas and carcinoma is not well established because the majority of condylomas are associated with low-risk HPVs, not considered carcinogenic.

**Design:** Cases were selected from the files of the Instituto de Patología e Investigación. Laser Capture Microdissection (LCM)-PCR and p16 immunostaining were performed at the DDL laboratory in the Netherlands. Study cases were selected from a group of 191 lesions. Condylomas were classified as acuminatum and flat, each further subclassified in typical (common condyloma) or atypical. In the former no atypical cells were identified. In the latter atypical cells were present in the lower third of epithelial thickness.

**Results:** The majority of the lesions were from the foreskin of older patients. High-risk HPV genotypes (HPV16, 39) were identified in 14 condylomata (5 patients) as shown in Table 1. Morphological features varied from typical condylomata acuminata (3 cases), atypical condylomata acuminata (3 cases), mixed atypical flat condylomata (5 cases). Most cases were p16 positive. Low-risk HPV genotypes (HPV87, 84, 11, 44) were detected in 5 warty and basaloid PeINs from 3 patients. Most cases were p16 negative.

High- and low-risk HPV genotypes in 19 lesions.

Age	Anatomical localization	Patient ID	Pathological Classification	p16	HPV Genotype
74	Foreskin	16	Warty PeIN	Negative	87
74	Foreskin	16	Warty PeIN	Positive	84
68	Foreskin	41	Warty PeIN	Negative	11
68	Foreskin	41	Warty PeIN	Negative	11
69	Shaft	50	Basaloid PeIN	Negative	44
27	Foreskin	4	Atypical condyloma	Positive	16
Unknown	Foreskin	8	Atypical condyloma	Positive	16
Unknown	Foreskin	8	Atypical flat condyloma	Positive	16, 44, 66
Unknown	Foreskin	8	Atypical flat condyloma	Negative	16
Unknown	Foreskin	8	Atypical flat condyloma	Positive	16
Unknown	Foreskin	8	Typical condyloma	Positive	16
74	Foreskin	14	Atypical condyloma	Positive	39
74	Foreskin	14	Flat condyloma	Positive	39
74	Foreskin	14	Flat condyloma	Positive	16
74	Foreskin	14	Flat condyloma	Positive	16
39	Foreskin	55	Typical condyloma	Negative	16
39	Foreskin	55	Atypical flat condyloma	Negative	16
18	Foreskin	57	Atypical flat condyloma	Negative	16
27	Foreskin	4	Typical condyloma	Negative	11, 16

# ABSTRACTS | GENITOURINARY PATHOLOGY (INCLUDING RENAL TUMORS)

**Conclusions:** Unexpectedly, high-risk HPV genotypes were present in a set of condylomas, especially those with moderate atypia, and low-risk HPV genotypes in high-grade variants of PeIN. The findings suggest that more studies are needed to elucidate the role of condylomas in the pathogenesis of HPV driven penile carcinomas

## 737 Somatic Genomic Alteration Prevalence and Association with Tumor Grade Reclassification in Prostate Cancer Patients Undergoing Active Surveillance

Jacqueline Fontugne<sup>1</sup>, Kehao Zhu<sup>2</sup>, Wael Al Zoughbi<sup>3</sup>, Ahmed Elsaeed<sup>3</sup>, Aram Vosoughi<sup>4</sup>, Hung Tran<sup>3</sup>, Beerinder Karir<sup>5</sup>, Samaneh Motanagh<sup>6</sup>, Kyung Park<sup>7</sup>, Andrea Sboner<sup>3</sup>, Juan Miguel Mosquera<sup>3</sup>

<sup>1</sup>Institut Curie, Paris, France, <sup>2</sup>Fred Hutchinson Cancer Research Center, University of Washington, Seattle, WA, <sup>3</sup>Weill Cornell Medicine, New York, NY, <sup>4</sup>H. Lee Moffitt Cancer Center & Research Institute, Tampa, FL, <sup>5</sup>New York-Presbyterian/Weill Cornell Medical Center, New York, NY, <sup>6</sup>UPMC Magee-Womens Hospital, Pittsburgh, PA, <sup>7</sup>NYU Langone Health, New York, NY

**Disclosures:** Jacqueline Fontugne: None; Kehao Zhu: None; Wael Al Zoughbi: None; Ahmed Elsaeed: None; Aram Vosoughi: None; Hung Tran: None; Beerinder Karir: None; Samaneh Motanagh: None; Kyung Park: None; Andrea Sboner: None; Juan Miguel Mosquera: None

**Background:** Although active surveillance has emerged as a therapeutic option for low-risk prostate cancer (PCa), optimal prognostic biomarkers to select patients who may benefit from early curative treatment are lacking. Previous studies have shown an association between germline mutations, such as those in DNA repair genes (ATM, BRCA1/2), and grade reclassification. However, prevalence and clinical significance of somatic genomic alterations in large cohorts of PCa patients on active surveillance have not been reported. Our aim was to identify potential somatic genomic biomarkers of progression (grade reclassification) for patients with PCa undergoing active surveillance.

**Design:** We included patients from a large multi-institutional cohort of men with low-risk PCa on active surveillance. Tumor DNA was assessed using Oncomine Comprehensive Panel (OCP v2), a next-generation sequencing clinical assay to interrogate single nucleotide variants (SNVs) and small insertions/deletions (indels) in 99 oncogenes and tumor suppressors, copy number variations (CNVs) in 75 genes.

**Results:** Of 634 patients with available diagnostic FPPE prostate biopsy blocks, 291 had PCa with sufficient tumor DNA. Clinico-pathological characteristics of the patients are summarized in Table 1. Of 291 patients, 121 (41.6%) experienced upgrading (reclassification) at a follow-up biopsy at time of analysis. We identified 52 somatic SNVs and indels in 41 patients (14.1%). Among them, 26 likely pathogenic/pathogenic somatic alterations were found in the tumors of 23 patients (7.9%), including in ATM (n=3), BRCA1 (n=2), BRCA2 (n=1), CHEK2 (n=1), PIK3CA (n=1), TP53 (n=1), SPOP (n=4), PTEN (n=1) or RAS (n=5) genes. FGFR1 and APEX1 gene amplifications were found in 1 tumor. No significant association was identified between individual pathogenic SNVs/CNVs, including those occurring in DNA repair genes, and tumor grade reclassification (Figure 1A). Patients with genomic alterations classified as benign/likely benign/variant of uncertain significance (n=18) had shorter time to grade reclassification (Figure 1B). Whether this association reflects a biological significance remains to be elucidated.

# ABSTRACTS | GENITOURINARY PATHOLOGY (INCLUDING RENAL TUMORS)

	No mutation (N=250)	Pathogenic/Likely Pathogenic mutations (N=23)	Benign/Likely Benign/VUS mutations (N=18)	Overall (N=291)
<b>Age at diagnosis</b>				
Mean Years (SD)	63 (7.0)	63 (6.5)	64 (6.2)	63 (6.9)
<b>Race</b>				
African-American	16 (6.4%)	1 (4.3%)	1 (5.6%)	18 (6.2%)
White	223 (89.2%)	21 (91.3%)	15 (83.3%)	259 (89.0%)
Other	11 (4.4%)	1 (4.3%)	2 (11.1%)	14 (4.8%)
<b>BMI</b>				
Mean (SD)	28 (4.1)	28 (4.7)	31 (7.3)	28 (4.4)
<b>Family History of PCa</b>				
Not reported	164 (65.6%)	14 (60.9%)	11 (61.1%)	189 (64.9%)
1 or 2 degree relatives with PCa	86 (34.4%)	9 (39.1%)	7 (38.9%)	102 (35.1%)
<b>Clinical T stage</b>				
T1	227 (90.8%)	23 (100%)	16 (88.9%)	266 (91.4%)
T2a	22 (8.8%)	0 (0%)	2 (11.1%)	24 (8.2%)
T2c	1 (0.4%)	0 (0%)	0 (0%)	1 (0.3%)
<b>Gleason Grade Group</b>				
1	227 (90.8%)	20 (87.0%)	15 (83.3%)	262 (90.0%)
2	23 (9.2%)	3 (13.0%)	2 (11.1%)	28 (9.6%)
3	0 (0%)	0 (0%)	1 (5.6%)	1 (0.3%)
<b>% positive cores</b>				
Mean (SD)	16 (11)	13 (5.4)	17 (12)	16 (11)
<b>Prostate Size (cc)</b>				
Mean (SD)	46 (24)	44 (18)	36 (13)	45 (23)
<b>PSA value (ng/ml)</b>				
Mean (SD)	5.2 (3.1)	5.2 (2.5)	5.1 (2.8)	5.2 (3.0)
<b>Gleason grade reclassification</b>				
Not yet reclassified	150 (60.0%)	13 (56.5%)	7 (38.9%)	170 (58.4%)
Reclassified	100 (40.0%)	10 (43.5%)	11 (61.1%)	121 (41.6%)
<b>Adverse Pathology at Radical Prostatectomy</b>				
No	36 (14.4%)	5 (21.7%)	2 (11.1%)	43 (14.8%)
Yes	30 (12.0%)	0 (0%)	5 (27.8%)	35 (12.0%)
No RP yet	184 (73.6%)	18 (78.3%)	11 (61.1%)	213 (73.2%)
<b>Primary Treatment</b>				
Radical prostatectomy	66 (26.4%)	5 (21.7%)	7 (38.9%)	78 (26.8%)
Radiation therapy	44 (17.6%)	6 (26.1%)	6 (33.3%)	56 (19.2%)
Androgen deprivation therapy	3 (1.2%)	0 (0%)	0 (0%)	3 (1.0%)
Not yet treated	135 (54.0%)	12 (52.2%)	5 (27.8%)	152 (52.2%)
Other	2 (0.8%)	0 (0%)	0 (0%)	2 (0.7%)

Figure 1 - 737

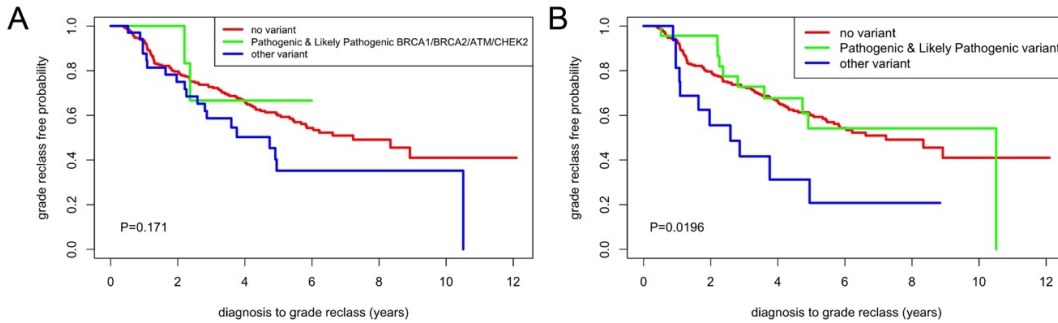


Figure 1. Kaplan-Meier curves of grade reclassification-free probability when stratifying patients according to mutational status, distinguishing patients with pathogenic mutations in BRCA1/BRCA2/ATM/CHEK2 specifically (A), or all pathogenic mutations (B).

**Conclusions:** We provide a first assessment of somatic genomic alterations in PCa in a large multi-institutional cohort of patients on active surveillance. Potentially owing to the low prevalence of pathogenic genomic alterations (7.9%), no association between pathogenic genomic alterations and grade reclassification was identified.

## 738 De Novo Large Cell Neuroendocrine Carcinoma of the Prostate: Clinicopathologic, Immunohistochemical Profile and Molecular Characterization

Alcino Gama<sup>1</sup>, Anthony Serritella<sup>1</sup>, Ruoji Zhou<sup>1</sup>, Ivan De La Riva<sup>1</sup>, Xiaoqi Lin<sup>2</sup>, Bonnie Choy<sup>1</sup>, Maha Hussain<sup>1</sup>, Ximing Yang<sup>1</sup>  
<sup>1</sup>Northwestern University Feinberg School of Medicine, Chicago, IL, <sup>2</sup>Northwestern University, Chicago, IL

**Disclosures:** Alcino Gama: None; Anthony Serritella: None; Ruoji Zhou: None; Ivan De La Riva: None; Xiaoqi Lin: None; Bonnie Choy: None; Maha Hussain: None; Ximing Yang: None

**Background:** Large cell neuroendocrine carcinoma of the prostate (LCNCAP) is a rare entity that has been mostly described in patients associated with androgen-deprivation therapy (ADT). *De novo* cases have been reported, but not well studied. We report six cases of *de novo* LCNCAP from our institution with detailed clinical, pathological analyses and molecular characterization.

**Design:** We conducted a retrospective search in our database from 2012 to 2022, and 6 cases of LCNCAP were identified. Clinical and morphologic information including age, serologic markers, histologic findings, ancillary tests, treatment, and follow-up are summarized.

**Results:** Median age at diagnosis was 65 years (60-78). None of our patients had previously received ADT. Median PSA level was 27.1 ng/mL (1.5-115). Two patients had elevated serum chromogranin. The tumors had large solid nests with focal central necrosis and large pleomorphic cells with prominent nucleoli, salt/pepper chromatin, and brisk mitotic activity (Fig 1A). Three cases (50%) had concomitant adenocarcinoma, and all cases partially retained at least one prostatic marker (NKX-31, PSA, AMACR) (Fig 1B). All three cases tested for TTF-1 were negative. The tumors were highly proliferative with a median Ki-67 of 70% (20-90) (Fig 1C). All cases tested positive for neuroendocrine markers (synaptophysin, chromogranin, NSE) (Fig 1D). Three cases were subjected to next-generation sequencing, and all were microsatellite stable. TP53 mutations (2/3), PTEN (2/3) and RB1 (2/3) losses were identified. Among six patients, one was treated with radical prostatectomy/radiation, two with radiation or radiation/chemotherapy, and three with chemotherapy only. All patients had metastatic disease at the diagnosis, the most common sites being lymph nodes (50%) and bone (50%), followed by liver (33%) and lung (33%). After a median follow-up of 15 months, 4 patients died (median survival 15 months). Two patients are alive with multisite metastasis (23 and 8 months of follow-up).

Figure 1 - 738

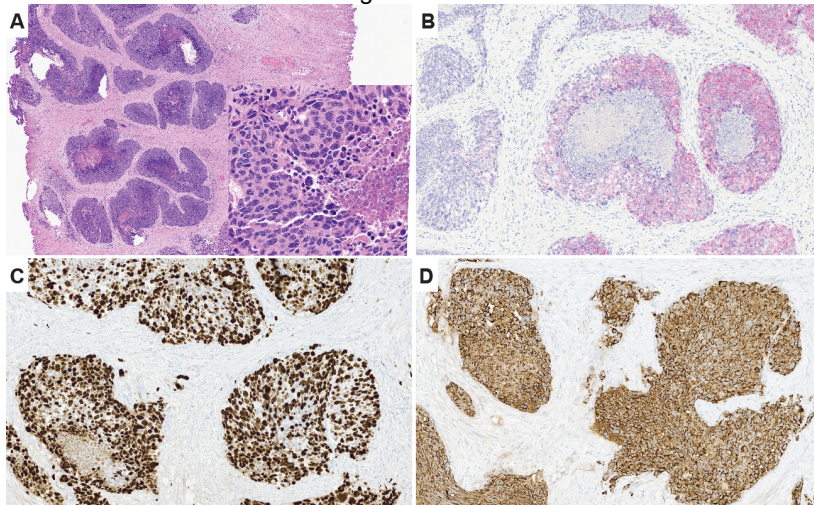


Figure 1. Histologic features and immunohistochemical profiles of large cell neuroendocrine carcinoma of the prostate (LCNCAP). Tumor composed of solid nests with central necrosis (A). Tumor cells are large and pleomorphic with salt/pepper chromatin (A insert). Tumor cells are partially positive for AMACR, negative for p63, HMWK (B) and NKX31 (not shown). Tumor cells exhibit very high Ki67 proliferative activity up to 95% (C). Tumor cells also stain positive for chromogranin (D).

**Conclusions:** LCNCAP is a morphologically defined variant of prostate cancer. At least half of our cases coexisted with Grade group 5 adenocarcinoma. LCNCAP is composed of large pleomorphic cells with partial loss of prostatic markers, diffuse positivity for neuroendocrine markers, and high Ki-67. Our cases were microsatellite stable, but we identified TP53 mutations and loss of PTEN and RB1. The prognosis is dismal despite active therapy, with 67% mortality after a median follow-up of 15 months.

## 739 Pathological, Clinical and Molecular Characterization of Large Cell Neuroendocrine Carcinoma (LCNEC) of the Urinary Tract

Jatin Gandhi<sup>1</sup>, Brendan Guercio<sup>2</sup>, Leili Mirsadraei<sup>3</sup>, Qin Zhou<sup>2</sup>, Jie-Fu Chen<sup>2</sup>, Judy Sarungbam<sup>2</sup>, Ying-Bei Chen<sup>2</sup>, Anuradha Gopalan<sup>2</sup>, S. Joseph Sirintrapun<sup>2</sup>, Samson Fine<sup>2</sup>, Marina Baine<sup>2</sup>, Natasha Rekhtman<sup>2</sup>, William Travis<sup>2</sup>, Bernard Bochner<sup>2</sup>, David Solit<sup>2</sup>, Gopa Iyer<sup>2</sup>, Hikmat Al-Ahmadie<sup>2</sup>

<sup>1</sup>Emory University Hospital, Atlanta, GA, <sup>2</sup>Memorial Sloan Kettering Cancer Center, New York, NY, <sup>3</sup>NYU Langone Health/NYU Winthrop Hospital, Mineola, NY

**Disclosures:** Jatin Gandhi: None; Brendan Guercio: None; Leili Mirsadraei: None; Qin Zhou: None; Jie-Fu Chen: None; Judy Sarungbam: None; Ying-Bei Chen: None; Anuradha Gopalan: None; S. Joseph Sirintrapun: None; Samson Fine: None; Marina Baine: None; Natasha Rekhtman: None; William Travis: None; Bernard Bochner: None; David Solit: None; Gopa Iyer: None; Hikmat Al-Ahmadie: None

**Background:** Primary LCNEC of the urinary tract is a rare and poorly characterized, in contrast to pulmonary LCNEC where it is a distinct entity. Using microscopic criteria of pulmonary LCNEC (organoid nests, rosette-like structures, trabecular growth, peripheral palisading and cells with abundant cytoplasm, vesicular chromatin, & prominent nucleoli. We report the clinical, pathological, and molecular features of a cohort of urothelial LCNEC.

**Design:** We identified 80 LCNEC cases (77 from bladder, 3 from upper urinary tract) and performed IHC for synaptophysin, chromogranin, INSM1, CD56, p53, Rb, and Ki-67. Molecular profiling by NGS was performed on 37 tumors. Clinical correlation and treatment outcomes (DFS, OS) were analyzed.

**Results:** The study included 21 pure LCNEC tumors (26%), (LCNEC group); 21 combined small cell carcinoma (SMC) and LCNEC tumors (26%), with or without urothelial or other histologic subtypes (LCNEC/SMC group); and 38 LCNEC tumors (48%) that co-existed with urothelial with/without divergent differentiation/histologic subtypes (LCNEC/UC group). LCNEC morphology was organoid/nests (n=49, 61%), trabecular (n=23;29%), sheets (n=36, 45%), palisading (n=12;15%) and rosette/glandular (n=25;31%). Prominent nucleoli were seen in 34 cases (43%). IHC showed Syn positivity in 63/71 tumors (89%), Chr in 39/66 (56%), INSM1 in 15/16 (94%) and CD56 in 39/40 (98%). Abnormal p53 expression was seen in 34/41 tumors (83%) (71% overexpression vs 12% null) and Rb loss was seen in 33/47 tumors (70%). Ki67 ranged from 20 to 100% (median 70%). LCNEC and LCNEC/SMC pts were compared to pts with bladder SMC without concurrent LCNEC and UC-NOS. LCNEC pts treated with cystectomy +/- perioperative therapy (n = 38) had shorter DFS than SMC pts (n = 95, p = 0.009) or UC NOS (n = 75, p = 0.01). Platinum-based NACT in 26 LCNEC patients was not associated with improved DFS or OS. Molecular profiling identified mutations in TP53, RB1 and TERT promoter in 34 (92%), 24 (65%) and 28 (76%) tumors, respectively. Potentially targetable alterations were seen in ERBB2, ERBB3, & PIK3CA (4 cases each,11%). TMB of LCNEC was lower than SMC (p = 0.003).

**Conclusions:** Urothelial LCNEC is rare with a wide histopathologic spectrum. LCNEC is more commonly admixed with SMC, urothelial or other histologic subtypes, but can also be pure. Among patients treated with cystectomy +/- perioperative therapy, LCNEC is associated with shorter DFS compared to those with SMC or UC NOS. Genomic profiles of LCNEC and SMC are similar.

## 740 Clinicopathologic Features and Survival Characteristics of Urothelial Carcinoma Subtypes Among Patients with Neoadjuvant Chemotherapy versus Radical Cystectomy Only

Rose George<sup>1</sup>, Asef Aziz<sup>1</sup>, Arkar Htoo<sup>1</sup>, Ebubekir Ucar<sup>1</sup>, Elif Özeller<sup>1</sup>, Svetlana Avulova<sup>1</sup>, Mahmut Akgul<sup>1</sup>

<sup>1</sup>Albany Medical Center, Albany, NY

**Disclosures:** Rose George: None; Asef Aziz: None; Arkar Htoo: None; Ebubekir Ucar: None; Elif Özeller: None; Svetlana Avulova: None; Mahmut Akgul: None

**Background:** Urothelial carcinoma (UCa) subtypes (UCaS) and their differences in biological behavior and response to neoadjuvant chemotherapy (NAC) may have important prognostic implications. Currently there are sparse and disparate evidence on the efficacy of NAC and overall survival of the UCAs.

**Design:** RC with or without NAC for UCa in between January 2015-March 2022 were selected. Clinicopathologic features, treatment, and survival data (date of surgery to date of death/last follow-up) were obtained. When applicable, changes in UCAs between biopsy and the RC specimen were noted. Squamous (Sq; Fig. 1A), glandular (Gl; Fig. 1B), micropapillary (MP; Fig. 1C), plasmacytoid (P; Fig. 1D), lymphoepithelioma-like (LEL), clear-cell (CC), nested (N; Fig. 1E), neuroendocrine (NE), sarcomatoid (Sarc), and poorly differentiated (PD; Fig. 1F) subtypes were identified. Pre- and post-treatment UCaS changes were compared between NAC+RC and RC using Pearson Chi-Square, Likelihood ratios, Fisher's exact, and post hoc Bonferroni tests. A multivariate Cox regression (treatment, pathologic staging, lymphovascular invasion, margin status, and extranodal extension) was performed to analyze survival outcomes of UCaS between NAC+RC and RC only groups. A p-value of <0.05 was considered significant.

# ABSTRACTS | GENITOURINARY PATHOLOGY (INCLUDING RENAL TUMORS)

**Results:** Table 1 summarizes the findings. Of a total of 91 cases (male:female ratio = 28/4; median age 69.1), 32 (35%) had UCaS either in their biopsies or resection, 5/32 (16%) had more than one UCaS. 15/32 (47%) patients with UCaS received NAC+RS. 16 (50%) biopsies had no UCaS, and biopsies with UCaS were as follows: 5 (16%) Sq, 2 (6%) GI, 2 (6%) MP, 2 (6%) P, 2 (6%) Sarc, 1 (3%) NE, 1 (3%), and 1 PD (3%). In RC 11 (34%) Sq, 7 (22%) MP, 6 (19%) N, 1 (3%) PI, 1 (3%) Sarc, and 1 (3%) PD UCaS were identified. 16 (50%) cases had UCaS in RC that were absent in biopsy. 16 new UCAs (9 RC only, 7 NAC+RC) were present in resection (8 Sq, 3 MP, 2 PD, 1 GI, 1 LEL, 1 N). 7/15 (47%) UCaS identified in biopsy (1 Sq, 1 GI, 1 CC, 1 MP, 1 PI, 1 PD, 1 NE) were not present in resections in cases with NAC+RC (vs. no such cases in RC only group, p=0.005). The mean overall for cases with is 17.15 months (Median 3.6, range: 0.03-83.13). Multivariate Cox regression analysis showed margin status to be most predictive of better survival outcome (Table1).

Figure 1 - 740

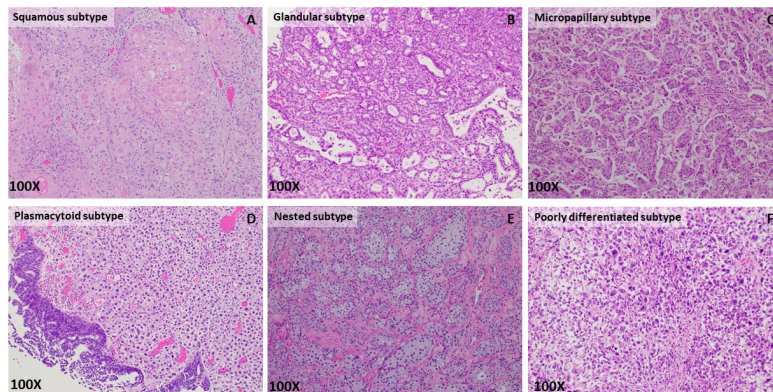


Figure 2 - 740

TABLE 1

				Total (n=32)
Age Mean (Median, range)				69.16 (70.50, 51-83)
Gender	Male			28 (87.5%)
	Female			4 (12.5%)
<b>Change in UCaS in Biopsy vs Resection</b>				
	No change in UCaS	Absent UCaS in resection (Present in Biopsy)	New UCaS resection (Absent in Biopsy)	Total
Only RC (n)	6 <sub>a</sub>	0 <sub>b</sub>	11 <sub>a, b</sub>	17
NAC & RC (n)	1 <sub>a</sub>	7 <sub>b</sub>	7 <sub>a, b</sub>	15
Total	7	7	18	32
<b>Multivariate Cox Regression for Predictors of Overall Survival in UCaS</b>				
	HR (95% CI)	Forward selection (Wald)		
NAC vs only RC	1.766 (0.741-4.209)			
Pathologic T stage	0.733 (0.484-1.111)			
Pathologic N stage	1.087 (0.644-1.836)			
LVI	3.818 (0.887-16.439)			
<b>Margins</b>	4.713 (1.356-16.378)	<b>5.489 (1.893-15.918), p = 0.002</b>		
ENE	1.689 (0.419-6.804)			

**Conclusions:** NAC+RC was associated with significant UCaS changes in biopsy versus resection, with complete absence of biopsy proven UCaS in following resection subset of cases.

## 741 Clinical Significance of Location of Perineural Invasion by Prostate Cancer Detected on Needle Core Biopsy

Benjamin Gertsen<sup>1</sup>, Yuki Teramoto<sup>2</sup>, Ying Wang<sup>1</sup>, Hiroshi Miyamoto<sup>1</sup>

<sup>1</sup>University of Rochester Medical Center, Rochester, NY, <sup>2</sup>Kyoto University Hospital, Kyoto, Japan

**Disclosures:** Benjamin Gertsen: None; Yuki Teramoto: None; Ying Wang: None; Hiroshi Miyamoto: None

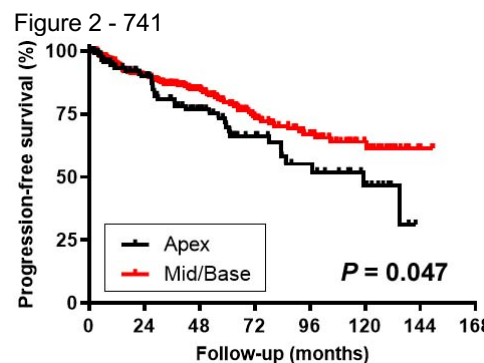
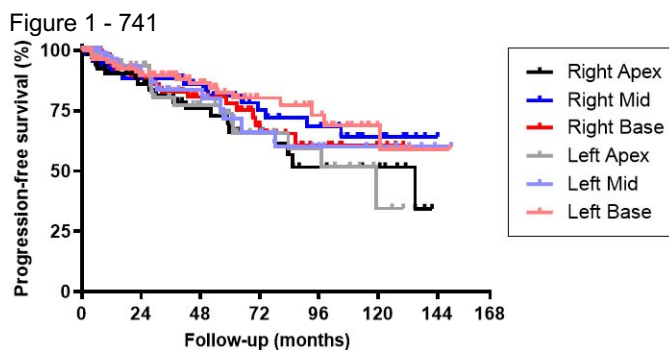
**Background:** The presence of perineural invasion (PNI) by prostate cancer, particularly in biopsy (Bx) specimen, has been associated with adverse pathologic features, including extraprostatic extension, and resultant poor clinical outcomes. However, the

# ABSTRACTS | GENITOURINARY PATHOLOGY (INCLUDING RENAL TUMORS)

impact of PNI location (e.g. apex vs. mid vs. base) on Bx remains poorly understood. We herein compare radical prostatectomy (RP) findings and long-term oncologic outcomes in prostate cancer patients with single Bx site PNI.

**Design:** We assessed consecutive patients who had undergone systematic sextant prostate Bx (*i.e.* 6 sites) followed by RP from 2009 to 2018. 434 men in our Surgical Pathology database met the inclusion criteria for PNI detected in only 1 of 6 Bx sites. Cases with PNI on targeted Bx were excluded from analysis.

**Results:** PNI was present in right apex (n=62; 14.3%), right mid (n=70; 16.1%), right base (n=89; 20.5%), left apex (n=64; 14.7%), left mid (n=58; 13.4%), and left base (n=91; 21.0%). There were no significant differences in clinicopathologic features, including age, preoperative prostate-specific antigen level, Bx findings [e.g. highest Grade Group (GG), GG at the site with PNI, total tumor length], RP findings (e.g. GG, pT, pN, surgical margin status, estimated tumor volume), and the need for adjuvant therapy before recurrence, between those exhibiting PNI on the right and left. Similarly, no significant differences in these features were seen in PNI at apex vs. mid vs. base. Kaplan-Meier analysis coupled with log-rank test revealed no significant difference in the risk of disease progression after RP in patients with PNI on the right vs. left ( $P=0.614$ ). However, PNI at the apex was associated with a significantly higher risk of progression, compared with PNI at the mid or base. In multivariate analysis with Cox regression model, apex (vs. mid or base) PNI showed significance for progression (hazard ratio 1.829, 95% confidence interval 1.183-2.827,  $P=0.007$ ).



**Conclusions:** In Bx specimens exhibiting PNI in 1 of sextant sites, PNI at the apex was independently associated with poorer prognosis, but not worse histopathologic features in RP specimens, compared with PNI at the mid or base. Pathologists may thus need to report the presence of PNI in every Bx site, which is likely to be useful for the risk stratification of prostate cancer.

## 742 Getting Ready for AI Assisted Histological Analysis of Prostate Biopsies – Baseline Analysis of Current Standard of Care in the Articulate 4ro Study

Abhisek Ghosh<sup>1</sup>, Lisa Browning<sup>2</sup>, Richard Colling<sup>1</sup>, Nasullah Alham<sup>1</sup>, Jacqueline Birks<sup>1</sup>, Andrew Protheroe<sup>2</sup>, Pelvender Gill<sup>3</sup>, Raman Begraj<sup>5</sup>, Margaret Horton<sup>5</sup>, David Snead<sup>6</sup>, Nasir Rajpoot<sup>7</sup>, Jon Oxley<sup>8</sup>, Samir Al Hyassat<sup>9</sup>, Monica Dolton<sup>1</sup>, Clare Verrill<sup>1</sup>

<sup>1</sup>Oxford University, Oxford, United Kingdom, <sup>2</sup>Oxford University Hospitals NHS Foundation Trust, Oxford, United Kingdom, <sup>3</sup>John Radcliffe Hospital, United Kingdom, <sup>4</sup>PAIGE, London, United Kingdom, <sup>5</sup>PAIGE, New York, NY, <sup>6</sup>University Hospital, Coventry, United Kingdom <sup>7</sup>University of Warwick, Warwick, United Kingdom, <sup>8</sup>North Bristol NHS Trust, Bromsgrove, United Kingdom, <sup>9</sup>Hamad Medical Corporation, Qatar

**Disclosures:** Abhisek Ghosh: None; Lisa Browning: None; Richard Colling: None; Nasullah Alham: None; Jacqueline Birks: None; Andrew Protheroe: None; Pelvender Gill: None; Raman Begraj: None; Margaret Horton: None; David Snead: None; Nasir Rajpoot: None; Jon Oxley: None; Samir Al Hyassat: None; Monica Dolton: None; Clare Verrill: None

**Background:** Approximately 1 million prostate biopsies are undertaken in the US each year representing a significant proportion of histopathology workload. With many laboratories facing insufficient staff coverage, diagnostic AI-based software is an attractive option. To justify the use of these technologies, we must first understand the landscape of current standard of care which is pathologist without AI assistance; but detailed workflow data on diagnostic practices are not routinely available.

**Design:** Articulate Pro (Artificial Intelligence for Cellular Pathology Transformation in Prostate Practice) is a prospective study of a market authorized prostate biopsy AI diagnostic assistance software with tumor detection, quantification and grading modules. To enable data collection by pathologists, an interactive browser-based study capture tool was developed using the Grails open-source web application framework (figure 1&2). Pathologists captured diagnostic and health economic data within the study capture tool alongside reporting of cases as part of standard of care to establish the baseline workflow, enabling quantitative comparison with AI assisted workflows in later phases of the study.

# ABSTRACTS | GENITOURINARY PATHOLOGY (INCLUDING RENAL TUMORS)

**Results:** 100 consecutive prostate biopsies were reported by 4 histopathologists in one academic hospital histopathology laboratory with a fully digital pathology workflow. Cases included Transrectal Ultrasound (TRUS) biopsies (n=56, mean 11.9 biopsies per case) and Local Anaesthetic Transperineal (LATP)/template systematic biopsies (n=44, mean 19.8/23.5 biopsies). The mean viewing and typing times are shown in table 1 with an overall mean time to view the digital slides per case of 32.3 min (range 8.7-101.6). Cases were also stratified by complexity with mean times for digital slide viewing into: i)One reporting pathologist with H&E alone (n=67) (24.7 min, range 8.7-64.2), ii)Further work needed (IHC and/or deeper levels) necessitating multiple reporting sessions but only one reporting pathologist (n=18) (43.2 min, range 13.1-70.1), iii)Complex cases requiring more than one pathologist (n=15) (53.6 min, range 11.8-101.6 including further opinions).

Time in minutes	Number of cases	Mean	Std. dev.
<b>Biopsy type = LATP</b>			
Total time to view WSI	41	39.83	20.63
Total time to type report	41	14.02	9.73
Total time to request extra work	41	0.91	2.09
<b>Biopsy type = TRUS</b>			
Total time to view WSI	56	25.81	15.77
Total time to type report	56	7.71	5.21
Total time to request extra work	56	0.78	2.15
<b>Biopsy type = template systematic</b>			
Total time to view WSI	3	52.02	20.53
Total time to type report	3	7.01	1.71
Total time to request extra work	3	1.42	0.84

Figure 1 - 742

Initial Timing

Enter Histology Number \*

Type of reporting session \*

Primary (H&E only)

Start Timer 00 : 00 : 00 Pause Timer Stop Timer Reset Timer

Total time view slides/case \*

When was reporting pathologist aware slides were available for viewing?

Report Now \*

Yes

Start Timer 00 : 00 : 00 Pause Timer Stop Timer Reset Timer

Total time to report \*

Additional work requested \*

Yes

Start Timer 00 : 00 : 00 Pause Timer Stop Timer Reset Timer

Length of time to request \*

Type

- Please choose -

Save

© University of Oxford 2022

Figure 2 - 742

Back to homepage

Biopsy Information

Enter Histology Number \*

Previous prostate biopsy on record?

Biose Number

Age range (decades)

Identify Type of Biopsy

Total number of pots

Identify Total number of biopsies

Comments on biopsy information

Is serum PSA available on request form

MRI PIRADS Score

Technical issues with reporting

Documentation

Confirm Laboratory

Date and time case received in laboratory?

Identify reporting pathologist

Date and time case signed out? (this field is auto populated based on timing sessions)

TAT (Days:Hours:Minutes)

Was case reported with a trainee?

Location of case reporting

Were any glass slides reviewed with the digital images?

**Conclusions:** This study provides a detailed picture of prostate biopsy reporting in Articulate Pro as the baseline for deployment of AI in one study centre, with case complexity increasing reviewing time. Histopathology workflows are complex, but this complexity must be captured to evidence the potential health economic benefits of AI assistance.

## 743 Prostatic Amyloidosis: Mass Spectrometry-Based Analysis of 150 Specimens

Sarwat Gilani<sup>1</sup>, Surendra Dasari<sup>1</sup>, Loren Herrera Hernandez<sup>1</sup>, John Cheville<sup>1</sup>, Rafael Jimenez<sup>1</sup>, Karen Rech<sup>1</sup>, Linda Dao<sup>1</sup>, Matthew Howard<sup>1</sup>, Joanna Dalland<sup>1</sup>, April Chiu<sup>1</sup>, Jason Theis<sup>1</sup>, R. Houston Thompson<sup>1</sup>, Bradley Leibovich<sup>1</sup>, R. Jeffrey Karnes<sup>1</sup>, Stephen Boorjian<sup>1</sup>, Ellen McPhail<sup>1</sup>, Sounak Gupta<sup>1</sup>

<sup>1</sup>Mayo Clinic, Rochester, MN

**Disclosures:** Sarwat Gilani: None; Surendra Dasari: None; Loren Herrera Hernandez: None; John Cheville: None; Rafael Jimenez: None; Karen Rech: None; Linda Dao: None; Matthew Howard: None; Joanna Dalland: None; April Chiu: None; Jason Theis: None; R. Houston Thompson: None; Bradley Leibovich: None; R. Jeffrey Karnes: None; Stephen Boorjian: None; Ellen McPhail: None; Sounak Gupta: None

**Background:** Prostatic amyloidosis may be a localized or a systemic process. We have reviewed a large series of prostatic amyloidosis analyzed using mass spectrometry (MS) to determine the prevalence of amyloid subtypes, and to correlate with patterns of histologic localization.

**Design:** 150 consecutive cases of prostatic amyloidosis analyzed using MS were reviewed. Pathology review was performed for 99/150 (66%) cases to correlate amyloid subtype with pattern of histologic localization. Medical chart review was performed for a subset of patients for relevant clinicopathologic features.

**Results:** The mean age at diagnosis was 69 years. Amyloid subtyping revealed systemic amyloidosis in 86/150 (57%) cases, and localized amyloidosis (semenogelin) in 64/150 (43%) cases (Table 1). Systemic amyloidosis was predominantly comprised of ATTR (n=55), followed by AL (lambda: 25; kappa: 2), and ALECT2 in rare instances (n=4). In cases with known specimen type (Table 1), 75% (51/68) of cases of systemic amyloidosis were identified on biopsy. In contrast, localized amyloidosis (semenogelin) was predominantly identified on resection specimens 27/40 (68%). Assessment of patterns of histologic localization revealed that all cases with localized amyloidosis had a subepithelial distribution (semenogelin, 39/39, 100%), as opposed to systemic amyloidosis, in which none of the cases had similar localization (0/60, 0%). Among patients with available follow-up and systemic amyloidosis, ATTR amyloidosis was identified in 10 patients. No evidence of hereditary ATTR amyloidosis was identified on ancillary molecular studies in patients that were tested (8/10). Two patients within this cohort had multiple subtypes of amyloid (semenogelin/ATTR & AL-lambda/ATTR). Of note, 7 of 17 patients had documented cardiac amyloidosis, and 5 of these patients were identified following detection of amyloid on histologic evaluation of prostate specimens (ATTR: 4; AL-lambda: 1). Clinical follow-up was available for 17 patients (mean follow-up: 57 months, range: 4-129), and 3 of 17 patients died of systemic amyloidosis-related complications. No prostate cancer-specific mortality was identified.

MS Amyloid Subtype	Cases (n=150)	Histology review (%)	Age in years (mean, range)	Specimen Type	Amyloid Localization
1. Light Chain	27/150 (18%)	17/27 (63%)	68 (49-87)	Prostatectomy: 4/27 (15%) TURP: 5/27 (19%) Biopsy: 10/27 (37%) NS: 8/27 (30%)	Subepithelial*: 0/17 (0%) Stromal and perivasculat: 9/17 (53%) Perivasculat: 6/17 (35%) Stromal: 2/17 (12%)
a) Kappa	2/150 (1%)	2/2 (100%)	58 (49-66)	Prostatectomy: 1/2 (50%) TURP: 0/2 (0%) Biopsy: 1/2 (50%) NS: 0/2 (0%)	Subepithelial*: 0/2 (0%) Stromal and perivasculat: 1/2 (50%) Perivasculat: 1/2 (50%) Stromal: 0/2 (0%)
b) Lambda	25/150 (17%)	15/25 (60%)	69 (55-87)	Prostatectomy: 3/25 (12%) TURP: 5/25 (20%) Biopsy: 9/25 (36%) NS: 8/25 (32%)	Subepithelial*: 0/15 (0%) Stromal and perivasculat: 8/15 (53%) Perivasculat: 5/15 (33%) Stromal: 2/15 (13%)
2. ATTR	55/150 (37%)	39/55 (71%)	75 (63-91)	Prostatectomy: 5/55 (9%) TURP: 3/55 (5%) Biopsy: 37/55 (67%) NS: 10/55 (18%)	Subepithelial*: 0/39 (0%) Stromal and perivasculat: 24/39 (62%) Perivasculat: 6/39 (15%) Stromal: 9/39 (23%)
3. ALECT2	4/150 (3%)	4/4 (100%)	67 (64-68)	Prostatectomy: 0/4 (0%) TURP: 0/4 (0%) Biopsy: 4/4 (100%) NS: 0/4 (0%)	Subepithelial*: 0/4 (0%) Stromal and perivasculat: 4/4 (100%) Perivasculat: 0/4 (0%) Stromal: 0/4 (0%)
4. Semenogelin	64/150 (43%)	39/64 (61%)	65 (36-88)	Prostatectomy: 26/64 (41%) TURP: 1/64 (2%) Biopsy: 13/64 (20%) NS: 24/64 (38%)	Subepithelial*: 39/39 (100%) Stromal and perivasculat: 0/39 (0%) Perivasculat: 0/39 (0%) Stromal: 0/39 (0%)

Abbreviations  
 MS: mass spectrometry; TURP: transurethral resection, prostate; NS: not specified.  
 \*Subepithelial refers to seminal vesicle/ ejaculatory duct-type epithelium.

# ABSTRACTS | GENITOURINARY PATHOLOGY (INCLUDING RENAL TUMORS)

**Conclusions:** In summary, our results confirm specific patterns of systemic amyloid localization in prostatic tissue compared to localized amyloidosis (semenogelin). Our results emphasize that diagnosis and MS-based subtyping of amyloid on histopathologic examination of prostatic specimens can have significant impact on patient management.

## 744 Large Cribriform Glands (>0.25 mm Diameter) as a Predictor of Adverse Pathology in Men with Gleason Score 3+4=7 (Grade Group 2) Prostate Cancer

Nancy Greenland<sup>1</sup>, Janet Cowan<sup>1</sup>, Peter Carroll<sup>1</sup>, Jeffry Simko<sup>1</sup>, Bradley Stohr<sup>1</sup>, Emily Chan<sup>1</sup>

<sup>1</sup>University of California, San Francisco, San Francisco, CA

**Disclosures:** Nancy Greenland: None; Janet Cowan: None; Peter Carroll: None; Jeffry Simko: None; Bradley Stohr: None; Emily Chan: None

**Background:** A recent outcome-based radical prostatectomy (RP) study defined >0.25 mm diameter to distinguish large versus small cribriform glands, with >0.25 mm diameter cribriform glands associated with worse recurrence free survival. We aim to determine whether identification of >0.25 mm cribriform glands in Gleason score 3+4=7 (Grade Group 2, GG2) patients at biopsy is associated with adverse pathology at RP.

**Design:** We identified 133 GG2 prostate cancer patients biopsy with subsequent RP (2000-2016). Tumor containing slides were re-reviewed for largest diameter cribriform gland; henceforth, large is defined as largest cribriform diameter >0.25 mm and small as <=0.25 mm. The primary outcome was adverse pathology (Gleason score 4+3=7 or greater, GG3-5; stage pT3a or greater, or pN1). The secondary outcome was recurrence free survival (RFS), defined as 2 consecutive prostate specific antigen (PSA) measurements greater than 0.02 ng/ml 7-8 weeks following RP or receipt of salvage treatment.

**Results:** Cribriform pattern was present in 53/133 (40%) patients; of these, 37/53 (70%) had small cribriform glands and 16/53 (30%) had large cribriform glands. Patients with large cribriform glands had significantly increased adverse pathology at RP compared to patients with small cribriform glands, and patients without cribriform glands (large 11/16, 69%; small 12/37, 32%; no cribriform 25/80, 31%; Chisq p-value 0.01). On multivariate analysis, largest cribriform gland was also associated with adverse pathology, independent of age at diagnosis, PSA and PSA density at diagnosis, year of diagnosis, and biopsy cores % positive (global p-value 0.0171). Large cribriform glands was also associated with increased CAPRA-S surgical risk score relative to small cribriform glands (Interquartile range: large 2.00-5.00; small 1.00-3.00; no cribriform 1.00-4.00; Kruskal-Wallis p-value 0.02). No significant differences were seen with RFS after RP.

**Conclusions:** In GG2 patients who underwent RP, large cribriform glands is associated with increased risk of adverse pathology, but not BCR, which could be due to sampling error or low power. The presence of large cribriform histology should be taken into account when considering AS for those with GG2 disease.

## 745 Morphologic Patterns Observed in Prostate Biopsy Cases with Discrepant Gleason Score and Molecular Risk Classification

Nancy Greenland<sup>1</sup>, Matthew Cooperberg<sup>1</sup>, Peter Carroll<sup>1</sup>, Janet Cowan<sup>1</sup>, Bradley Stohr<sup>1</sup>, Jeffry Simko<sup>1</sup>, Emily Chan<sup>1</sup>

<sup>1</sup>University of California, San Francisco, San Francisco, CA

**Disclosures:** Nancy Greenland: None; Matthew Cooperberg: None; Peter Carroll: None; Janet Cowan: None; Bradley Stohr: None; Jeffry Simko: None; Emily Chan: None

**Background:** Molecular-based risk classifier tests are increasingly being utilized by urologists to guide clinical decision making. The Decipher prostate biopsy test is designed to predict likelihood of high-grade disease at radical prostatectomy (RP) and risk of metastasis and mortality. The test provides a risk category of low, intermediate, or high. We investigated histologic features of biopsies in which the Grade Group (GG) and Decipher risk category were discrepant.

**Design:** We included patients who had the Decipher molecular assay performed from 2016 to 2020 and were either GG $\geq$ 3 with low Decipher risk category or were GG1 with high Decipher risk category. The biopsy slide on which Decipher testing was performed was re-reviewed for Gleason score and various histologic patterns, including types of Gleason pattern 4 and pattern 5, intraductal carcinoma (IDC), mucinous carcinoma, atrophic carcinoma, carcinoma with basal cells, carcinoma with vacuolations, ductal carcinoma, collagenous fibroplasia, and stromal reaction.

**Results:** Among 234 men who underwent RP and had Decipher testing on their biopsy specimen, there were 23 cases (10%) with discrepant molecular risk and GG, of which 15 (6%) had biopsy slides available for review. Of the 5 GG1 cases with high molecular risk, 2 were GG2 on re-review, with non-cribriform Gleason pattern 4. At least one unusual histologic pattern was seen in each of the 5 cases. These 5 cases showed carcinoma with basal cells (1), atrophic carcinoma (3), mucinous carcinoma (1), collagenous fibroplasia (1), and mild stromal reaction (1). Of these 5 patients, 4 underwent RP, and all 4 were pT2 at RP.

# ABSTRACTS | GENITOURINARY PATHOLOGY (INCLUDING RENAL TUMORS)

Of the 10 cases with low molecular risk and GG $\geq$ 3, 1 had large cribriform, 2 had small cribriform, and 1 had both large and small cribriform. One case had single cell/single file Gleason pattern 5, 1 had IDC, 1 had vacuolated carcinoma, 1 had ductal carcinoma, and 1 had mild stromal reaction. Of these 10 patients, 2 remained on active surveillance, 1 was lost to follow up, and 7 underwent RP. Of the 7 patients who underwent RP, 4 were pT3a and 3 were pT2 at RP.

**Conclusions:** Unusual histologic patterns were rarely seen in increased molecular risk relative to GG. Despite training in large data sets, molecular classifiers may be less robust in rare patterns.

## 746 Reevaluation of Sampling Protocol for Transurethral Resection of the Prostate Specimens with Incidentally Detected Prostate Cancer in the Contemporary Era

Scott Gregory<sup>1</sup>, Michael Feely<sup>1</sup>, Cathy Gonsalves<sup>2</sup>, Robert Allan<sup>3</sup>, Sara Falzarano<sup>2</sup>

<sup>1</sup>University of Florida, Gainesville, FL, <sup>2</sup>University of Florida College of Medicine, Gainesville, FL, <sup>3</sup>Tampa, FL

**Disclosures:** Scott Gregory: None; Michael Feely: None; Cathy Gonsalves: None; Robert Allan: None; Sara Falzarano: None

**Background:** The aim of this study is to evaluate optimal surgical pathology tissue sampling in TURPs from men with incidentally found T1a (less than 5% of tissue involvement) prostatic adenocarcinoma (PCA) and assess whether additional sampling has the potential to significantly affect risk assessment and follow up in the contemporary era.

**Design:** Our surgical pathology files were interrogated for all TURPs with PCA diagnosis performed at our institution between November 2016 and December 2021. Patients with previously diagnosed PCA were excluded. The remaining cases were reviewed and clinicopathological data were recorded in an IRB approved database, including age, race, PSA, presence/absence and type of symptoms, specimen weight, initial number of blocks submitted, total blocks submitted, Grade Group(GG), percent Gleason pattern 4(%GP4), presence/absence of cribriform morphology (CRM) and/or intraductal carcinoma (IDCP), % of tissue involved, number of blocks involved, first positive block ID, change in % tissue, GG, and %GP4 with added blocks, and follow up (F/U) information, when available, such as MRI (PIRADS), biopsy results, and treatment.

**Results:** Of total 502 TURPs, 57 (11%) cases fulfilled study inclusion criteria. Clinicopathological data are summarized in table 1. With an average weight of 1.1 grams of tissue per block, 91% of cancers were identified within the first 10 submitted blocks (Figure 1). Additional sampling did not change the percent of tissue involved or the final GG, nor significantly increased or decreased percentage of pattern 4. Of the 4 (9%) cases not identified within the first 10 blocks, all were GG1 and T1a.

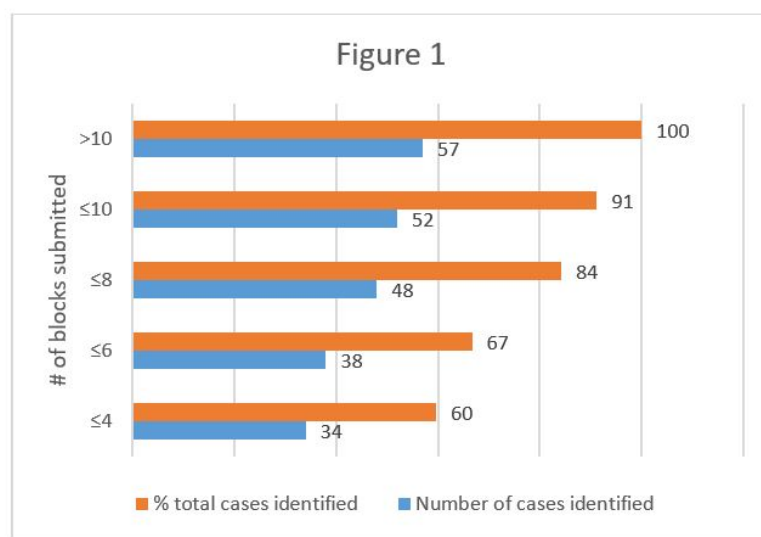
# ABSTRACTS | GENITOURINARY PATHOLOGY (INCLUDING RENAL TUMORS)

Table 1. Clinicopathological feature in 57 TURP cases with incidental PCA

Age (mean, range, years)	72 (55 – 92)
Race	N (%)
White	46 (81)
Black	6 (11)
Other	5 (9)
PSA (mean, range, ng/mL)	7.59 (0.66 – 35.67)
Lower urinary tract symptoms	N (%)
Present (obstructive)	54 (95)
Present (NOS)	3 (5)
Absent	0
Specimen weight (mean, range, grams)	20.7 (0.9 – 81.1)
Initial number of blocks (median, range)	13 (3 – 28)
Total blocks (median, range)	15 (3 – 49)
Tissue weight per block submitted (mean, range, grams)	1.1 (0.3 – 2.3)
Grade Group(GG)	N (%)
1	43 (75)
2	6 (11)
3	5 (9)
4	0
5	3 (5)
Percent pattern 4 (%GP4)	N (%)
- For GG2 cases (N=6)	1 (17)
5 or less	5 (83)
Greater than 5	1 (20)
- For GG3 cases (N=5)	4 (80)
60 or less	
greater than 60	
cirriform morphology (CRM)*	N (%)
yes	2/14 (14)
no	12/14 (86)
intraductal carcinoma (IDCP)	N (%)
yes	1 (2)
no	56 (98)
% of tissue involved (average, range, %)	7 (1 – 95)
Number of blocks involved (median, range)	3 (1 – 13)
First positive block ID	N (%)
≤4	34 (60)
≤6	38 (67)
≤8	48 (84)
≤10	52 (91)
>10	57 (100)
F/U MRI (Total = 16)	N (%)
PIRADS 1	3 (19%)
PIRADS 2	9 (56%)
PIRADS 3	0
PIRADS 4	4 (25%)
PIRADS 5	0
F/U biopsy (Total = 16)	N (%)
Positive	8 (50%)
Same GG as TURP	6 (75%)
Upgraded	2 (25%)
Negative	8 (50%)

\*Applicable in 14 cases

Figure 1 - 746



**Conclusions:** Sampling of 10 blocks of TURP chips led to identification of greater than 90% of incidental cancer at TURP with no clinically significant cancer left undetected. Moreover, additional sampling in cases with less than 5% of tissue involved by cancer did not result in any change in risk category by pathologic findings.

## 747 Molecular Characterization of Spermatocytic Tumors with Anaplasia or Sarcomatoid Change

Sounak Gupta<sup>1</sup>, Lynette Sholl<sup>2</sup>, Yiyi Yang<sup>3</sup>, Ivy Tran<sup>3</sup>, Adeboye Osunkoya<sup>4</sup>, Jennifer Gordetsky<sup>5</sup>, Kristine Cornejo<sup>6</sup>, Kvetoslava Michalova<sup>7</sup>, Fiona Maclean<sup>8</sup>, Matija Snuderl<sup>9</sup>, Michelle Hirsch<sup>10</sup>, William Anderson<sup>11</sup>, Rafael Jimenez<sup>1</sup>, John Cheville<sup>1</sup>, Peter Sadow<sup>12</sup>, Daniel Berney<sup>13</sup>, Andres Acosta<sup>11</sup>

<sup>1</sup>Mayo Clinic, Rochester, MN, <sup>2</sup>Harvard Medical School, Boston, MA, <sup>3</sup>NYU Langone Health, New York, NY, <sup>4</sup>Emory University School of Medicine, Atlanta, GA, <sup>5</sup>Vanderbilt University Medical Center, Nashville, TN, <sup>6</sup>Massachusetts General Hospital, Boston, MA, <sup>7</sup>Biopicka laborator s.r.o., Plzen, Czech Republic, <sup>8</sup>Douglass Hanly Moir Pathology, Melbourne, Australia, <sup>9</sup>New York University, New York, NY, <sup>10</sup>Brigham and Women's Hospital, Boston, MA, <sup>11</sup>Brigham and Women's Hospital, Harvard Medical School, Boston, MA, <sup>12</sup>Massachusetts General Hospital, Harvard Medical School, Boston, MA, <sup>13</sup>Queen Mary University of London, London, United Kingdom

**Disclosures:** Sounak Gupta: None; Lynette Sholl: None; Yiyi Yang: None; Ivy Tran: None; Adeboye Osunkoya: None; Jennifer Gordetsky: None; Kristine Cornejo: None; Kvetoslava Michalova: None; Fiona Maclean: None; Matija Snuderl: None; Michelle Hirsch: None; William Anderson: None; Rafael Jimenez: None; John Cheville: None; Peter Sadow: None; Daniel Berney: None; Andres Acosta: None

**Background:** Spermatocytic tumor (ST) is a testicular germ cell tumor (TGCT) that commonly affects older men. Unlike type II post-pubertal TGCTs, STs do not arise from germ cell neoplasia in situ (GCNIS) and typically lack i(12p). Recently, it has been reported that a subset of anaplastic ST harbor copy number gains involving chromosome 12; however, an in-depth molecular evaluation of ST with anaplasia and/or aggressive clinicopathologic features (ST-A) has not been undertaken.

**Design:** We evaluated 17 STs (14 ST-A, 3 conventional) using next-generation sequencing (447-gene panel) and genome-wide methylation profiling.

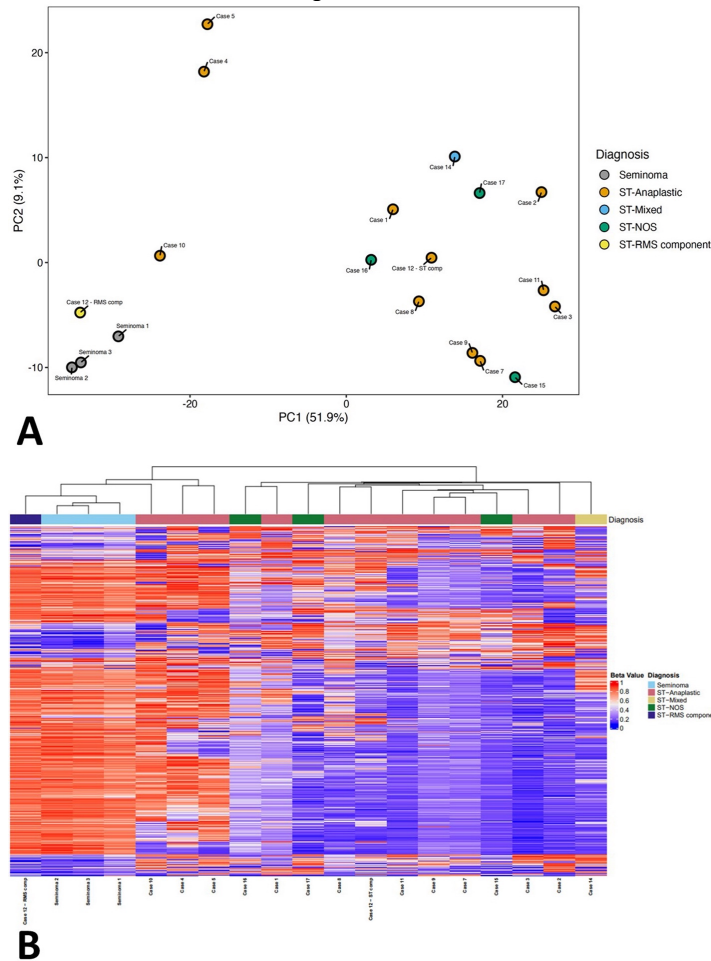
**Results:** Among 14 ST-A cases, 10 were uniformly anaplastic (with or without other aggressive features), 1 had conventional histology and lymphovascular invasion, 1 had sarcomatous transformation and 2 had a combination of conventional and anaplastic areas. DNA sequencing was successful in 15/17 cases (Table 1), demonstrating hotspot gain-of-function NRAS/HRAS/BRAF alterations in 5/15 cases (4 ST-A, 1 conventional) and loss-of-function TP53 mutations in 2/15 cases (both ST-A). One of the latter was a ST with rhabdomyosarcomatous (RMS) transformation (case 12) in which the ST and RMS components were differentially dissected and sequenced in parallel, both demonstrating a shared TP53 alteration. Copy-number gains involving chromosome 9/9p (12/15 cases) and evidence of whole-genome duplication with widespread loss-of-heterozygosity (6/15 cases, all ST-A) were significantly recurrent. A subset demonstrated copy-number losses or copy-neutral loss-of-heterozygosity of chromosome 13 (4/15 cases, all ST-A). Copy number gains involving 12/12p were identified in case 9 (by prior SNP array only) and case 10 (by sequencing and prior SNP array). Findings suggestive of 12p were also identified in a background of widespread copy number changes in the RMS component of case 12. Methylation analysis was performed to compare a subset of 15 cases (12 ST-A, 3 conventional) with 3 seminomas. Using the top 1000 differentially methylated probes, case 10 (ST-A) and the RMS component of case 12 clustered together with the seminomas, whereas most remaining anaplastic/aggressive and conventional STs comprised a separate cluster (Figure 1). Interestingly, both the RMS component of case 12 and case 6 had evidence of +12p.

Table 1 - Molecular characteristics of spermatocytic tumors

Case	Classification	Mutations	Copy number variants		
			+9/+9p	-13	Other
1	Anaplastic	NRAS	Yes	Yes	--
2	Anaplastic	--	No	Yes	--
3	Anaplastic	--	Yes	No	Widespread CNVs
4	Anaplastic	HRAS	Yes	No	--
5	Anaplastic	--	Yes	No	--
6	Anaplastic	NRAS	Yes	No	--
7	Anaplastic	--	Yes	No	WGD, +5, +14
8	Anaplastic	BRAF	Yes	No	--
9	Anaplastic + aggressive histologic features	--	Yes	No	WGD, +12 <sup>3</sup>
10	Anaplastic + aggressive histologic features	--	Yes	No	WGD, +12 <sup>4</sup>
11	ST with aggressive histologic features	--	Yes	Yes	WGD
12	ST with sarcomatous transformation (ST component)	TP53	No	No	WGD
12	ST with sarcomatous transformation (RMS component)	TP53	No	No	WGD, +12
13	ST with mixed features <sup>1</sup>	Failed	Failed	Failed	Failed
14	ST with mixed features <sup>1</sup>	TP53	Yes	No	Widespread CNVs
15	ST, NOS <sup>2</sup>	--	Yes	No (CN LOH present)	--
16	ST, NOS <sup>2</sup>	NRAS	Yes	No	--
17	ST, NOS <sup>2</sup>	Failed	Failed	Failed	Failed

Abbreviations: CN LOH = copy-neutral loss of heterozygosity, CNV = copy number variant, NOS = Not otherwise specified, RMS = Rhabdomyosarcoma, ST = Spermatocytic tumor, WGD = whole-genome duplication. <sup>1</sup>Denotes cases with a mixture of anaplastic and conventional histologic features. <sup>3</sup>Demonstrated by single nucleotide polymorphism array only. <sup>2</sup>Denotes cases with conventional clinicopathologic features. <sup>4</sup>DNA sequencing findings suggestive of gains of the short arm of chromosome 12, pending confirmation by further studies.

Figure 1 - 747



**Conclusions:** Our results suggest that a small subset of ST-A may harbor molecular features that overlap those of seminoma, including copy number gains of chromosome 12/12p.

#### 748 Rapid Examination of Non-Processed Renal Tissue by Nonlinear Microscopy: Benign Renal Parenchyma and Tumors

Yairen Guzman-Arocho<sup>1</sup>, Timothy Weber<sup>2</sup>, Leo Wu<sup>3</sup>, James Fujimoto<sup>2</sup>, Seymour Rosen<sup>1</sup>, Yue Sun<sup>1</sup>

<sup>1</sup>Beth Israel Deaconess Medical Center, Boston, MA, <sup>2</sup>Massachusetts Institute of Technology, Cambridge, MA, <sup>3</sup>Beth Israel Deaconess Medical Center, Harvard Medical School, Boston, MA

**Disclosures:** Yairen Guzman-Arocho: None; Timothy Weber: None; Leo Wu: None; James Fujimoto: None; Seymour Rosen: None; Yue Sun: None

**Background:** Nonlinear microscopy (NLM) is a laser scanning microscopy technique that generates images of fresh or fixed tissues closely resembling paraffin-embedded H&E, but without the need for fixation, embedding, microtome sectioning, or slide preparation. NLM has been successfully utilized to evaluate bone, bone marrow, lymph nodes, skin, prostate, and breast tissue. The ability of NLM to characterize kidney tumors has not been previously examined.

**Design:** Fresh or formalin-fixed tissues from kidney tumors, not required for clinical assessment, were evaluated. Tissue slices were stained for 2 minutes with acridine orange to highlight the nuclei and sulforhodamine 101 to highlight the stroma and cytoplasm, followed by a 30-second saline rinse. Real-time evaluation of the tissue was performed with NLM and subsequently compared with standard paraffin-embedded H&E histology.

**Results:** We evaluated 103 tissue samples from partial or total nephrectomies with renal cell carcinoma (RCC), including clear cell RCC (International Society of Urologic Pathologists [ISUP] low grade and high grade), papillary RCC, chromophobe RCC, clear cell papillary RCC, oncocytoma, and oncocytic renal cell neoplasms. Figure 1 shows representative NLM images of normal kidney parenchyma illustrating glomeruli, tubules, arteries, and inflammatory cells. Figure 2 shows representative NLM images of RCC.

# ABSTRACTS | GENITOURINARY PATHOLOGY (INCLUDING RENAL TUMORS)

The low-grade clear cell RCC exhibited nested groups of cells with clear cytoplasm and a delicate capillary network. In contrast, rhabdoid cells and giant multinucleated tumor cells were identified on the high-grade clear cell RCC. The papillary RCC showed basophilic cuboidal cells and foamy macrophages. The chromophobe demonstrated cells with clear cytoplasm, distinct cell membrane, perinuclear halos, nuclear grooves, and raisinoid nuclei; additionally, cells with eosinophilic cytoplasm were observed. The clear cell papillary RCC displayed a tubular and papillary pattern.

Figure 1 - 748

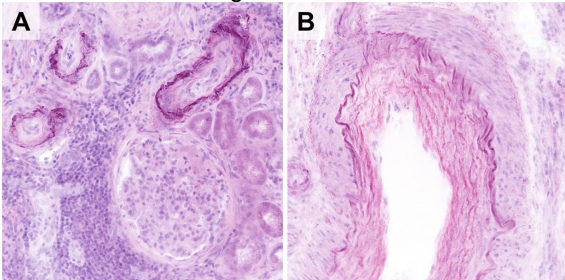


Figure 1. Benign kidney, glomerulus, tubules, small and larger arteries; and inflammation. The staining technique emphasizes vascular elastic components.

Figure 2 - 748

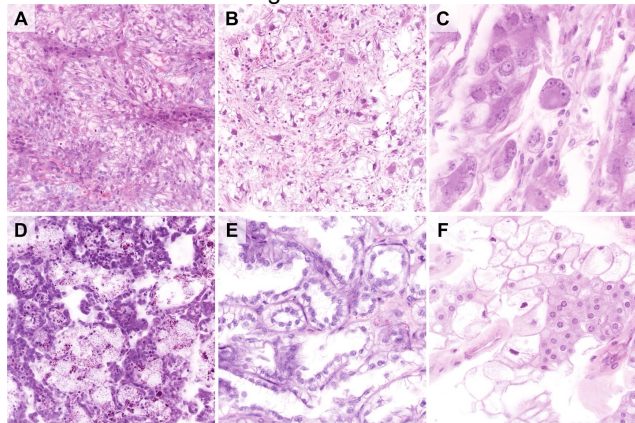


Figure 2. A. Clear cell RCC, ISUP low grade. B-C. Clear cell RCC, ISUP high grade; rhabdoid elements seen (C). D. Papillary RCC with foamy macrophages, ISUP low grade; the phagolysosomes stain distinctively. E. Clear cell papillary RCC. F. Chromophobe RCC.

**Conclusions:** NLM enables rapid assessment of kidney tissue for the presence of RCC and characterization of RCC subtypes. Possible future applications include the use of NLM to diagnose RCC, rapid adequacy assessment of targeted kidney biopsies for the presence of tumor, and collection of fresh viable tumor tissue and tumor-infiltrating lymphocytes for molecular studies.

## 749 Rapid Examination of Non-Processed Tissue by Nonlinear Microscopy: Benign Testicular Parenchyma and Tumors

Yairen Guzman-Arocho<sup>1</sup>, Timothy Weber<sup>2</sup>, James Fujimoto<sup>2</sup>, Seymour Rosen<sup>1</sup>, Yue Sun<sup>1</sup>

<sup>1</sup>Beth Israel Deaconess Medical Center, Boston, MA, <sup>2</sup>Massachusetts Institute of Technology, Cambridge, MA

**Disclosures:** Yairen Guzman-Arocho: None; Timothy Weber: None; James Fujimoto: None; Seymour Rosen: None; Yue Sun: None

**Background:** Nonlinear microscopy (NLM) is a laser scanning microscopy technique that generates real-time images and optical serial sections closely resembling paraffin-embedded H&E, but without the need for fixation, embedding, microtome sectioning, or slide preparation. NLM has been successfully utilized to evaluate bone, bone marrow, lymph nodes, skin, prostate, and breast tissue. The ability of NLM to characterize testicular parenchyma and tumors has not been previously examined.

**Design:** Testicular tissues, not required for clinical assessment, were stained for 2 minutes with acridine orange (nuclear features) and sulforhodamine 101 (stomal and cytoplasmic features) followed by a 30-second saline rinse. The tissue slices were evaluated in real-time using NLM. Subsequently, the images were compared to the standard formalin-fixed, paraffin-embedded H&E histology.

**Results:** The study included 18 samples from radical orchectomies including normal parenchyma and mixed germ cell tumors. NLM allows novel appreciation of seminiferous tubules and interstitial tissues. The normal cellular components of the seminiferous tubules can be recognized and the tunica propria constituents become distinct. Leydig cells and crystalloids of Reinke could be defined and examined by optical serial sections. Intratubular germ cell neoplasia was distinctive. The large pleiomorphic cells with prominent nuclei and nucleoli with a high mitotic count characteristic of embryonal carcinoma were easily visualized. The usual features of yolk sac carcinoma were delineated. Multinucleated syncytiotrophoblasts were seen in choriocarcinoma, confirmed by immunohistochemistry on paraffin-embedded tissue. Seminomatous tissue was characterized by cells with monomorphic large nuclei admixed with lymphocytes.

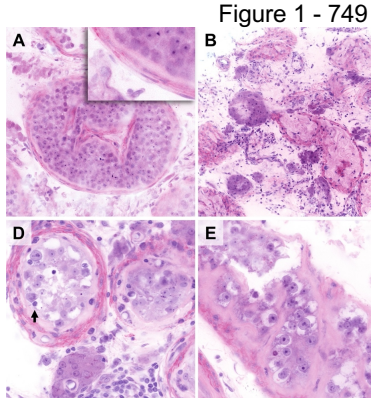


**Figure 1.** A. Normal seminiferous tubules with spermatogenesis; elastic fibers in the tunica propria are well delineated (inset). B. Atrophic and hyalinized seminiferous tubules admixed with clusters of Leydig cells. C. Leydig cells and a crystalloid of Reinke; the juxtaposition of a crystal to the cell nucleus is seen in the optical serial sections. D-F. Atrophic seminiferous tubules with germ cell neoplasia in situ; lymphocytes can be seen in adjacent interstitial spaces or focally within tubules (arrow) in D, and Sertoli cells (arrow) can be recognized in F, as well.

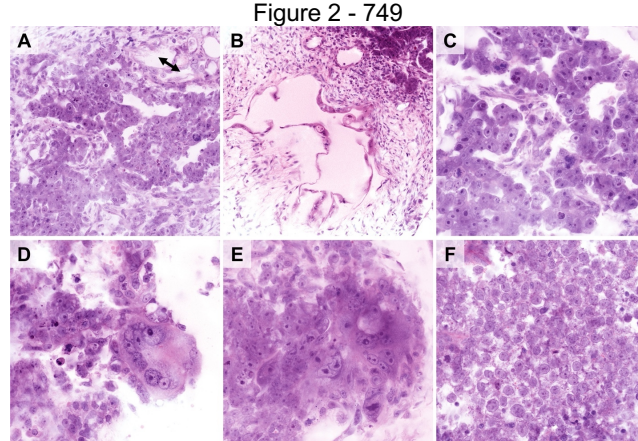


**Figure 2.** A. Embryonal carcinoma with admixed yolk sac tumor (arrows). B. Yolk sac tumor. C. Embryonal carcinoma. D-E. Choriocarcinoma (confirmed by immunohistochemistry) with distinctive syncytiotrophoblasts. F. Seminoma

**Conclusions:** NLM facilitates rapid assessment of testicular tissue and tumors. Additionally, NLM allows the novel visualization and characterization of benign testicular tissue.

## 750 Cell Quantification Using Machine Learning for Fast Relapse of High Grade Bladder Cancer Patients post-Cystectomy

Wenchao Han<sup>1</sup>, Ekaterina Olkhov-Mitsel<sup>2</sup>, Alison Cheung<sup>3</sup>, Martin Yaffe<sup>1</sup>, Michelle Downes<sup>2</sup>, Anne Martel<sup>3</sup>

<sup>1</sup>Sunnybrook Health Sciences Centre, University of Toronto, Toronto, ON, <sup>2</sup>Sunnybrook Health Sciences Centre, Toronto, ON, <sup>3</sup>Sunnybrook Research Institute, Toronto, ON

**Disclosures:** Wenchao Han: None; Ekaterina Olkhov-Mitsel: None; Alison Cheung: None; Martin Yaffe: None; Michelle Downes: None; Anne Martel: None

**Background:** After radical cystectomy, approximately 50% of patients with high-grade urothelial carcinoma (HGUC) experience recurrence, with more than 80% of them relapsing within 2 years (fast relapse) [1]. The tumor immune microenvironment is increasingly relevant for predicting response to therapy and prognostication. We investigated the relationship between fast relapse and the immune-cell count using machine learning (ML) methodology.

**Design:** From a retrospective cohort of 209 HGUC patients post-cystectomy, we created tissue microarrays of triplicate 1-mm cores. Adjacent sections were stained with Hematoxylin and Eosin (H&E) and with CD3 and CD20 antibodies. We 1) used a pretrained model (HoverNet [2]) to identify and quantify the count of tumor-infiltrating lymphocytes (TILs) on H&E images, then 2) re-trained the model with our internal immunohistochemistry (IHC) dataset of acute myeloid leukemia to identify and count the CD3+ cells on CD3 IHC images. For reference, cell counts were manually evaluated by the pathologist at the hotspot region-of-interest. Spearman correlation was used to evaluate ranking of automated counting against the manual cell counts for: 1) TIL counts from H&E vs. the sum of CD3 and CD20 manual counts on IHC (an approximation of TIL counts), 2) automated vs. manual CD3+ counts on IHC. The Mann-Whitney U-test was used to assess the patient outcome of fast relapse within 2 years with a subset of 96 cases, after removing cases having incomplete follow-up/cell count scores, and pT1 cases.

**Results:** We observed high Spearman correlations for CD3 IHC ( $R_s=0.84$ ) and H&E ( $R_s=0.80$ ) images, between manual and our ML-based automated counting technique. In the fast relapse analysis, there were significant differences in the cell counts from the automatic system between patients with fast recurrence (71) vs. not (25) with a p value of 0.006 and U value of 583.0 on CD3 IHC images, and a p value of 0.009 and U value of 603.0 on the H&E images. Significant difference was also reported using manual estimated CD3+ cell count on IHC with a p value of 0.017 and U value of 548.5.

Cell count correlation	Spearman correlation
Automatic vs. manual CD3+ cell count on IHC	0.84
Automatic TIL counts (H&E) vs. sum of CD3 + and CD20+ manual counts (IHC)	0.80

**Conclusions:** Our machine learning based methods demonstrated the feasibility of automatically quantifying CD3+ cells on IHC images and TILs on H&E-stained images. CD3+ cell counts and TIL cell counts are associated with fast relapse of HGUC patients.

## 751 Development and Clinical Outcome Evaluation of Cascaded AI Algorithm for Cancer Detection and Grading in Prostate Cancer

Stephanie Harmon<sup>1</sup>, Sushant Patkar<sup>1</sup>, Rosina Lis<sup>1</sup>, Jesse McKenney<sup>2</sup>, Maria Merino<sup>3</sup>, Denise Young<sup>4</sup>, G. Thomas Brown<sup>5</sup>, Kimberly Greenfield<sup>6</sup>, John McGeehey<sup>7</sup>, Sally Elsamanoudi<sup>4</sup>, Jiji Jiang<sup>4</sup>, Shyh-Han Tan<sup>8</sup>, Gyorgy Petrovics<sup>4</sup>, Albert Dobi<sup>9</sup>, Francisco Rentas<sup>6</sup>, Peter Pinto<sup>5</sup>, Gregory Chesnut<sup>4</sup>, Peter Choyke<sup>1</sup>, Baris Turkbey<sup>10</sup>, Isabell Sesterhenn<sup>7</sup>, Joel Moncur<sup>7</sup>

<sup>1</sup>Center for Cancer Research, National Cancer Institute, National Institutes of Health, Bethesda, MD, <sup>2</sup>Cleveland Clinic, Cleveland, OH, <sup>3</sup>National Cancer Institute, Bethesda, MD, <sup>4</sup>Center for Prostate Disease Research, Bethesda, MD, <sup>5</sup>National Institutes of Health, Bethesda, MD, <sup>6</sup>The Joint Pathology Center, Bethesda, MD, <sup>7</sup>The Joint Pathology Center, Silver Spring, MD, <sup>8</sup>Uniformed Services University of the Health Sciences, Bethesda, MD, <sup>9</sup>Center for Prostate Disease Research, USU, Bethesda, MD, <sup>10</sup>National Cancer Institute, National Institutes of Health, Bethesda, MD

**Disclosures:** Stephanie Harmon: None; Sushant Patkar: None; Rosina Lis: None; Jesse McKenney: None; Maria Merino: None; Denise Young: None; G. Thomas Brown: None; Kimberly Greenfield: None; John McGeehey: None; Sally Elsamanoudi: None; Jiji Jiang: None; Shyh-Han Tan: None; Gyorgy Petrovics: None; Albert Dobi: None; Francisco Rentas: None; Peter Pinto: None; Gregory Chesnut: None; Peter Choyke: None; Baris Turkbey: None; Isabell Sesterhenn: None; Joel Moncur: None

**Background:** While the Gleason Grading system is the primary prognostic feature in prostate cancer, its subjective nature underestimates tumor heterogeneity and suffers from poor inter-reader agreement. The objective of this work was to develop Artificial Intelligence (AI) algorithms for detection and grading of prostate cancer and investigate quantitative correlation with recurrence interval after Radical prostatectomy (RP).

**Design:** Digital pathology slides from patients previously undergoing RP at three institutions were retrospectively collected. Pathologist-defined Gleason score and recurrence-free survival (RFS) defined as time from surgery to biochemical or clinical evidence of recurrent disease was recorded, when available. Data were supplemented with publicly available PANDAS challenge set. A detection algorithm was trained using MobileNetV3 on image tiles corresponding to 0.5mmx0.5mm at 10x was trained (validation loss = 0.275629) from 6551 slides from biopsy (6210 PANDAS) and RP (69 Center1, 148 Center2, 124 Center3). Multi-label Gleason classification was trained using ResNet50 on identical size tiles using 6326 slides from biopsy (6098 PANDAS) and RP (149 Center2, 81 Center3). An additional 246 slides from 152 patients were reserved for testing cascaded detection and grading algorithms (Fig1). Kaplan-Meier and Cox-Proportional Hazard Regression were used to compare pathologist scoring to quantitative AI outputs with RFS.

**Results:** In 197 slides from Center3 in the testing set, detection performance based on individual tumors (n=144) and individual foci across all tumors (n=593), achieving 94.7% and 92.7% Sensitivity, respectively, with median 13 (range 0-50) false positives per slide. In cancer grading, artificially forcing grade heterogeneity in training patches, i.e. "cut-mix", improved generalizability to test set and the final model achieved a patch-based mean F1 score of 0.74. Of test patients with available RFS information from Center3 (Table 1), quantitative burden of AI-predicted Gleason 4 and Gleason 5 resulted in significant association to RFS (AI-Gls4 HR=1.5[1.1-2.0];p=0.004, AI-Gls5 HR=1.5[1.1-2.1];p=0.021). Unsupervised clustering of AI grading outputs resulted in improved patient RFS stratification compared to traditional scoring (Fig 2).

Clinical Feature	Summary
median time to recurrence, years	5.55 (0.15-23.5)
median f/u no recurrence, years	1.52 (0.17-11.2)
Age, years	62.06 (40-75)
Race	
Caucasian	68
African American	29
Hispanic	2
PSA, ng/ml	6.3 (0.3-29.1)
Gleason	
6	23
7	44
8	9
9	19
10	1

Figure 1 - 751

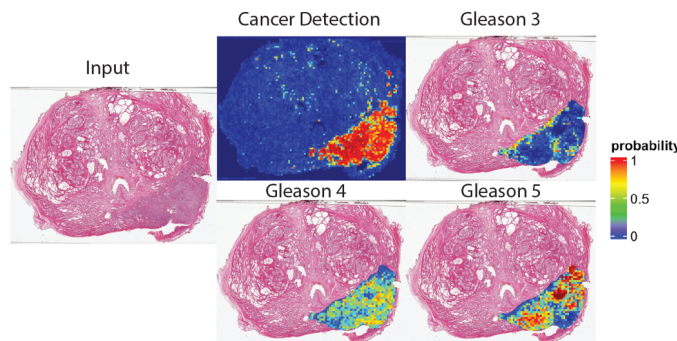


Figure 1. Depiction of AI predictions for RP case.

Figure 2 - 751

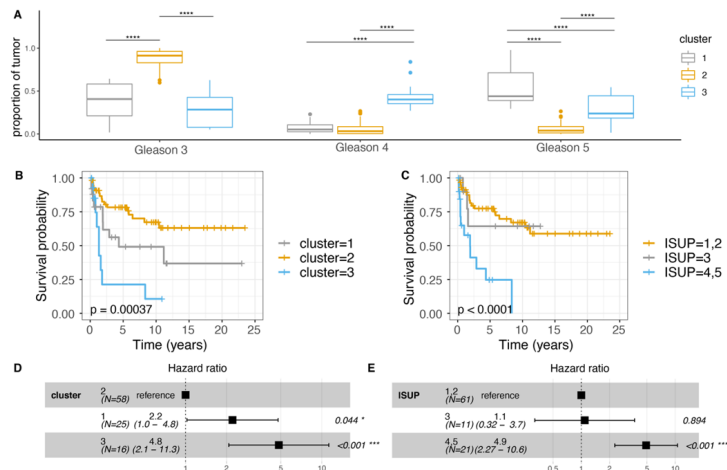


Figure 2. Unsupervised clustering resulting in low, intermediate, and high risk groups based on quantitative outputs from AI algorithm (A) and association with RFS (B); compared to traditional ISUP Gleason Grade Group categories of low (GG1-2), intermediate (GG 3), and high (GG4-5), shown in (C). Hazard ratios depicting association to RFS are shown in (D) and (E).

**Conclusions:** AI can accurately detect and grade prostate cancer, providing quantitative heterogeneity estimations of grade distribution that may improve prognostication of patients after surgery.

## 752 PAX-8 Based Machine Learning Nuclear Model Better Stratifies Nuclear Grade in Clear Cell Renal Cell Carcinoma

Lin He<sup>1</sup>, Averi Perny<sup>1</sup>, Hua Zhong<sup>1</sup>, Satwik Rajaram<sup>1</sup>, Payal Kapur<sup>1</sup>

<sup>1</sup>UT Southwestern Medical Center, Dallas, TX

**Disclosures:** Lin He: None; Averi Perny: None; Hua Zhong: None; Satwik Rajaram: None; Payal Kapur: None

**Background:** Grading of renal cell carcinoma (RCC) has been recognized as a prognostic factor for decades. Fuhrman and the current grading system adopted formally by the International Society of Urological Pathology (ISUP) and subsequently by the World Health Organization (WHO) is based upon nucleolar prominence for grades 1-3, while grade 4 requires nuclear anaplasia (including tumor giant cells, sarcomatoid differentiation and/or rhabdoid morphology). This gradings is subjective and can be challenging for non-genitourinary trained pathologists. Automated computational algorithms have been developed to grade the tumor using nuclear segmentation, but inevitably include non-neoplastic cells such as endothelial cells or lymphocytes.

**Design:** Digitalized hematoxylin and eosin (H&E) stained tissue microarrays (TMAs) sections of clear cell RCC and corresponding de-stained PAX-8 immunohistochemistry were utilized to develop the model. All cell nuclei (blue in Figure 1) were segmented from H&E slides using a convolutional neural network U-Net. Neoplastic nuclei (orange in Figure 1) were localized using PAX-8 images using the thresholding algorithm from QuPath. H&E slides and PAX-8 slides were co-localized and all nuclei were registered and classified as neoplastic or non-neoplastic. Thirty-seven morphological (8), intensity (16) and texture (13) features were extracted from 231 H&E 256x256-pixel image patches were generated. Two classifier models, random forest (RF) and support vector

# ABSTRACTS | GENITOURINARY PATHOLOGY (INCLUDING RENAL TUMORS)

machine (SVM), were applied to correlate nuclear features with the WHO/ISUP grades. Receiver operating characteristics (ROC) curves were plotted to compared WHO/ISUP grades rendered by 2 trained pathologists and the classifier models.

**Results:** Area under the curve (AUC) for the RF classifier model for each tumor grade is 0.988, 0.976, 0.988 and 0.989 respectively. AUC for SVM classifier model is lower for grade 1-3 tumor (0.960, 0.890 and 0.905 respectively) and 0.994 for grade 4 tumor (Figure 2). PAX-8 guided nuclear segmentation overall improves grade effect by excluding smaller non-neoplastic nuclei that tend to bias more on the high grade (3 & 4) tumor cells. In the RF model, nuclei morphological, intensity and texture features contribute 53.2%, 26.9% and 20.0% respectively to the final tumor grade (Table 1).

Table 1. Nuclear features and individual contribution to the WHO/ISUP RCC grades.

Nuclear Features	Histological Relevance	Grade Contributions (%)
Area	Morphology: Size	7.24
BBox_Area	Morphology: Size	7.89
Equivalent_Diameter	Morphology: Size	7.41
Eccentricity	Morphology: Shape	5.65
Major_Axis_Length	Morphology: Size	10.55
Minor_Axis_Length	Morphology: Size	5.77
Convex_Area	Morphology: Shape	6.37
Solidity	Morphology: Shape	2.27
H_Int_Mean	Intensity: Chromatin chromacity	1.38
H_Int_Median	Intensity: Chromatin chromacity	1.51
H_Int_Std	Intensity: Variation in chromatin chromacity	0.79
H_Int_MAD	Intensity: Chromatin chromacity	0.75
H_Int_Min	Intensity: Chromatin chromacity	1.20
H_Int_Max	Intensity: Chromatin chromacity	1.58
H_Int_Kurtosis	Intensity: Variation in chromatin chromacity	1.87
H_Int_Skewness	Intensity: Variation in chromatin chromacity	3.10
LabL_Int_Mean	Intensity: Chromatin chromacity	1.10
LabL_Int_Median	Intensity: Chromatin chromacity	1.20
LabL_Int_Std	Intensity: Variation in chromatin chromacity	0.84
LabL_Int_MAD	Intensity: Chromatin chromacity	0.70
LabL_Int_Min	Intensity: Chromatin chromacity	2.84
LabL_Int_Max	Intensity: Chromatin chromacity	0.75
LabL_Int_Kurtosis	Intensity: Variation in chromatin chromacity	2.18
LabL_Int_Skewness	Intensity: Variation in chromatin chromacity	5.05
Hint_Haralick_2nd_moment	Texture: Chromatin granularity	1.17
Hint_Haralick_contrast	Texture: Chromatin granularity	0.84
Hint_Haralick_correlation	Texture: Chromatin granularity	4.36
Hint_Haralick_variance	Texture: Chromatin granularity	0.58
Hint_Haralick_inv_diff_moment	Texture: Chromatin granularity	1.35
Hint_Haralick_sum_avg	Texture: Chromatin granularity	1.65
Hint_Haralick_sum_variance	Texture: Chromatin granularity	1.02
Hint_Haralick_sum_entropy	Texture: Chromatin granularity	2.06
Hint_Haralick_entropy	Texture: Chromatin granularity	1.78
Hint_Haralick_diff_var	Texture: Chromatin granularity	1.08
Hint_Haralick_diff_entropy	Texture: Chromatin granularity	1.05
Hint_Haralick_inf_corr1	Texture: Chromatin granularity	2.05
Hint_Haralick_inf_corr2	Texture: Chromatin granularity	1.02

Figure 1 - 752

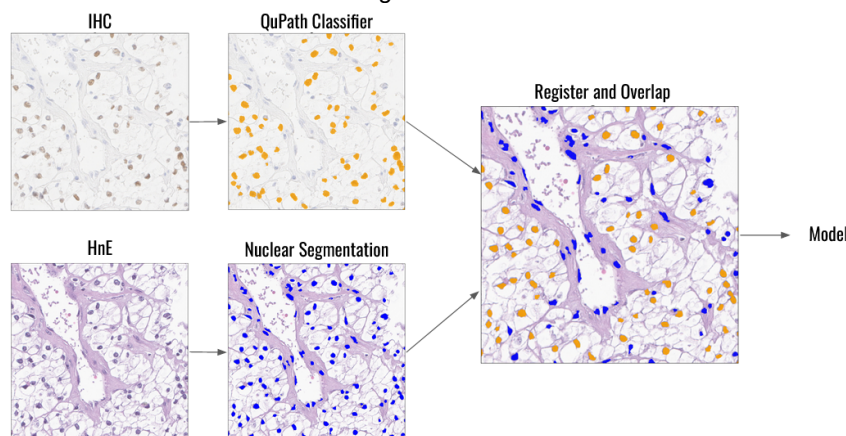
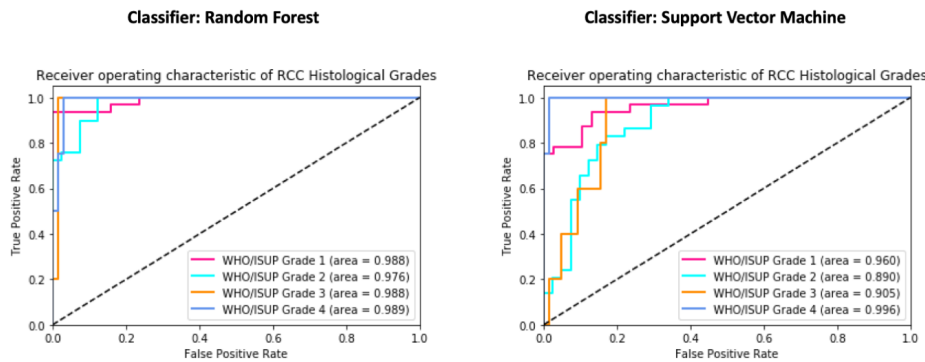


Figure 2 - 752



**Conclusions:** PAX-8 localized nuclei model is effective in distinguish RCC cells from non-neoplastic endothelial cells and lymphocytes. Random Forest model shows better performance in predicting tumor grade.

### 753 Non-ESC-RCC with Aberrant Cytokeratin 20 Expression: A Marker of Aggressiveness?

David Henriquez Ticas<sup>1</sup>, Rajen Goyal<sup>2</sup>, Maria Tretiakova<sup>1</sup>

<sup>1</sup>University of Washington, Seattle, WA, <sup>2</sup>CellNetix Pathology and Laboratories, Seattle, WA

**Disclosures:** David Henriquez Ticas: None; Rajen Goyal: None; Maria Tretiakova: None

**Background:** Cytokeratin 20 (CK20) is a structural protein predominantly expressed in epithelial cells of the gastric and intestinal mucosa. This protein is generally negative in renal cell carcinomas (RCC), except for eosinophilic solid and cystic renal cell carcinoma (ESC-RCC). Herein we report a series of non-ESC-RCC cases with CK20 expression.

**Design:** We retrospectively reviewed all RCC cases showing CK20 expression, excluding ESC-RCC cases, between 2008-2022. In addition, tissue microarrays with 259 renal tumors (133 clear cell RCC, 78 PRCC, 20 chromophobe RCC, 24 oncocytomas and 4 collecting duct carcinomas) and 14 non-neoplastic kidneys were immunostained with CK20 as a control group.

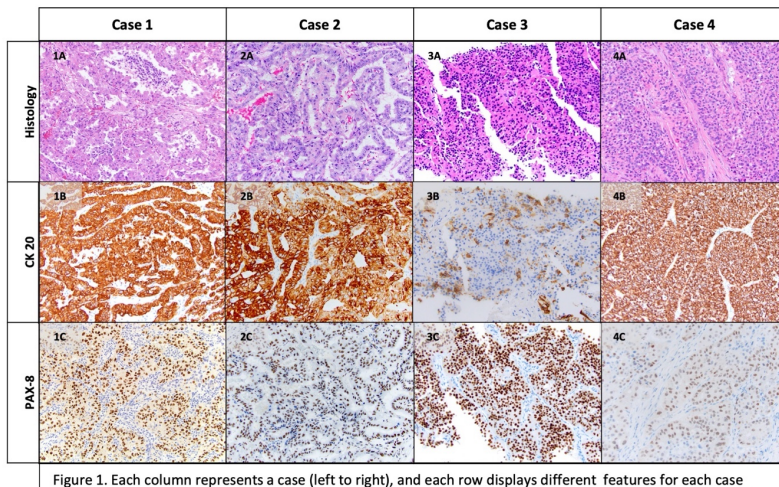
**Results:** Four CK20 positive non-ESC-RCC cases were identified; all cases are from males with a median age of 68 years (range 47-78). Three specimens are radical nephrectomies presented as advanced stage disease, and one is a lung metastasis biopsy (table). Morphologic findings were heterogenous combining solid, alveolar, tubulopapillary, or biphasic morphology with nuclear grades 3 or 4. All cases were positive for PAX8 and CK20 (figure); 3 out of 4 cases additionally expressed melanocytic markers or cathepsin K. All cases were negative for TFE3, CK7, and CAIX. Molecular and/or cytogenetics studies were available for 3 of 4 cases. Case 1 had copy number gain on chromosome 6p, including the TFEB locus, identified by chromosome genomic array testing (CGAT) and demonstrated TFEB (6p21.1) amplification, identified by fluorescence in-situ hybridization (FISH) and RNA-ISH. Case 2 had on CGAT demonstrated complex copy number alterations with allelic imbalances of chromosomes 6 and 17 harboring TFEB and KRT20 loci, but without amplification. Case 3 did not have cytogenetic studies available, however, demonstrated positive staining for 2 melanocytic markers, suspicious for a TFEB-amplified RCC phenotype. Case 4 had TFEB (6p21.1) amplification by FISH. None of other 259 renal tumors or 14 benign kidneys from tissue microarrays were positive for CK20.

	Case 1	Case 2	Case 3	Case 4
Age	47	63	78	73
Sex	M	M	M	M
Location	Right kidney	Left kidney	Lung	Left kidney
Original diagnosis	CCRCC	PRCC, type 2	Metastatic RCC, unclassified	TFEB-amplified
Final diagnosis	TFEB-amplified	TFEB-amplified like	TFEB-amplified-like	TFEB-amplified
Molecular studies	CGAT, FISH, RNA-ISH	CGAT	Pending	FISH
WHO nuclear grade	3	4	3	4
Stage AJCC 8th Ed	pT3bN2	pT3aN2	pT4	pT3aN0
Primary/metastasis	Primary, multifocal	Primary, unifocal	Metastatic	Primary, unifocal
Representative IHC stains	PAX8	+	+	+
	CAIX	-	-	n/a
	CK7	-	-	-
	CK20	+	+	+
	Melan A	-	n/a	+
	HMB45	-	n/a	+ focal
	Cathepsin K	+	n/a	n/a

# ABSTRACTS | GENITOURINARY PATHOLOGY (INCLUDING RENAL TUMORS)

Table 1. Pathologic features of selected cases. M: Male. PRCC: papillary renal cell carcinoma; CGAT: comparative genome analysis tool; FISH: fluorescence in situ hybridization; RNA-ISH: RNA in situ hybridization; IHC: immunohistochemistry.

Figure 1 - 753



**Conclusions:** Our findings highlight CK20 expression in a subset of aggressive tumors which were either molecularly proven or highly suspicious for TFEB-amplification RCC. Thus, we postulate that CK20 could serve as a potential marker for this recently described entity and may indicate a more aggressive RCC presentation.

## 754 Accuracy of Gleason Grading of Prostatic Adenocarcinoma in Community Practice

Jake Hill<sup>1</sup>, Ameer Hamza<sup>2</sup>

<sup>1</sup>The University of Kansas School of Medicine, Kansas City, KS, <sup>2</sup>University of Kansas Medical Center, Kansas City, KS

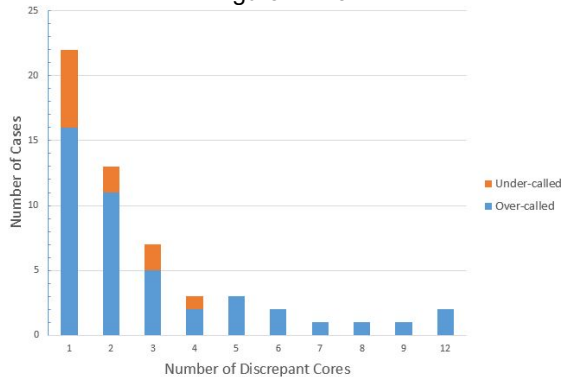
**Disclosures:** Jake Hill: None; Ameer Hamza: None

**Background:** Gleason grading in prostatic adenocarcinoma is the most important factor in disease management and prognosis. However, in the community practice setting, the grading is not always accurate. The objective of this study is to identify Gleason Grade discrepancies in prostate biopsy specimens received at our institution for a second opinion.

**Design:** Prostate biopsy specimens from outside institutions that were reviewed at our institution between July 1, 2020 and June 30, 2022 were included in this study. In total, 92 specimens were identified, and in-house and outside pathology reports were reviewed. Mischaracterization of any single core was considered a discrepancy. Discrepancies were stratified based on number of discrepant cores, incorrect benign versus malignant categorization, including high grade prostatic intraepithelial neoplasia (HGPIN), Gleason score and Grade Group discrepancies, and highest Grade Group discrepancy in an entire case.

**Results:** Of the 92 cases identified, 55 had discrepancies. The number of discrepant cores in a given case ranged from 1 to 12, summarized in Figure 1. In nine cases, at least one core was found to be discrepant based on the misclassification of the sample as benign versus malignant; in seven cases malignancy was missed and in two cases it was over-called. A difference of one Grade Group was present in 38 cases with 29 over-calls and 9 under-calls. Seventeen of these single Grade Group discrepancies were cases of Grade Group 1 versus 2. In 11 of the cases, at least one core was incorrectly identified by the outside institution as Grade Group 2, when it was Grade Group 1; in six of these cases, the outside institution under-called the Grade Group. Discrepancy by a difference of two Grade Groups was present in nine cases; eight over-calls and one under-call. Discrepancy by a difference of three Grade Groups was found in four cases, all of which were over-called. In 17 cases, at least one core was found to be discrepant based on the diagnosis of HGPIN versus benign prostate; in 16 cases HGPIN was over-called and in one it was under-called.

Figure 1 - 754



**Conclusions:** A high proportion (60%) of cases had discrepancies. These discrepancies, especially that of Grade Group 1 versus Grade Group 2, can potentially lead to over- or under-treatment. This highlights the need for further training in the diagnosis and grading of prostate adenocarcinoma in the community practice setting.

## 755 Diagnostic Discrepancies in Transurethral Resection of Bladder Tumor Specimens

Jake Hill<sup>1</sup>, Ameer Hamza<sup>2</sup>

<sup>1</sup>The University of Kansas School of Medicine, Kansas City, KS, <sup>2</sup>University of Kansas Medical Center, Kansas City, KS

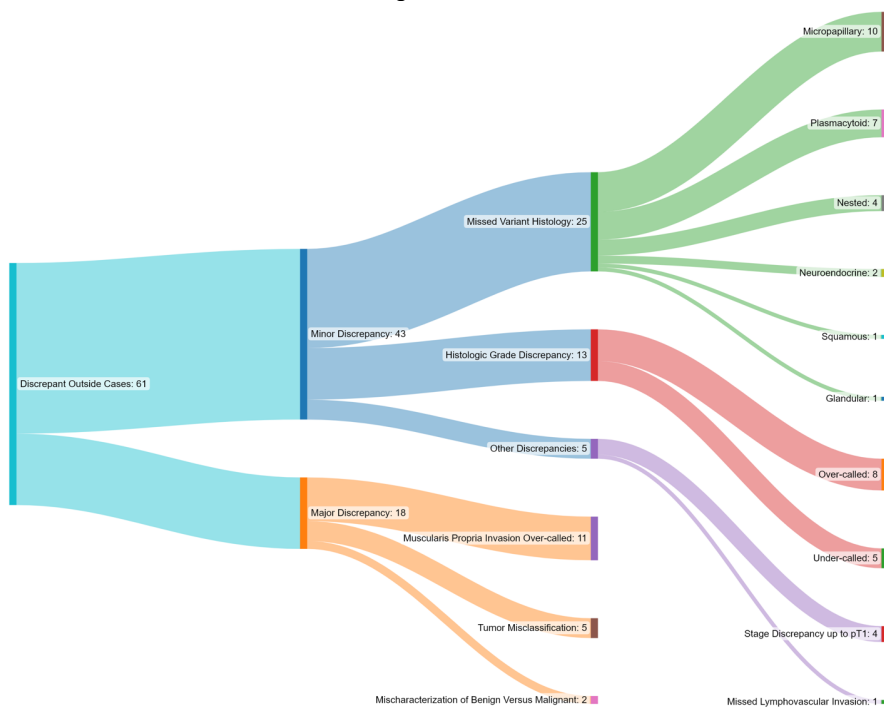
**Disclosures:** Jake Hill: None; Ameer Hamza: None

**Background:** Transurethral resection of bladder tumor is a common surgical pathology specimen. However, evaluation by non-subspecialty trained pathologists often results in diagnostic discrepancies. The objective of this study is to identify and classify discrepancies in urothelial carcinoma diagnoses made by pathologists at an academic institution versus pathologists in the community setting.

**Design:** The outside urothelial carcinoma cases reviewed at our institution between July 1, 2020 and June 30, 2022 were included in the study. A total 337 specimens were identified. Both the inhouse and outside pathology reports were reviewed. Discrepancies were classified as major or minor. Major discrepancies included change from a benign to malignant category and vice versa; over and under calling of muscle (muscularis propria) invasive disease and incorrect tumor classification. Minor discrepancies included discrepancy in tumor grade, non-recognition of variant histology and lymphovascular invasion and stage discrepancies including pTis, pTa and pT1.

**Results:** Of the 337 specimens, diagnostic discrepancies were identified in 61 (18%) specimens. Among these 43 were classified as minor and 18 as major. Major discrepancies included 11 specimens with overcalling of muscularis propria invasion; three cases of prostatic adenocarcinoma being called urothelial carcinoma; two cases of urothelial carcinoma with squamous differentiation being called squamous cell carcinoma; one case of urothelial carcinoma with small tubules being called nephrogenic adenoma; and one case of a polypoid cystitis with exuberant von Bruns nests being called high-grade urothelial carcinoma. Minor discrepancies included inability to recognize variant histology in 25 specimens. Of these 10 had micropapillary, seven had plasmacytoid, four had nested, two had neuroendocrine, one had squamous, and one had glandular differentiation. Other minor discrepancies included discrepancy of histology grade i.e., low versus high grade in 13 specimens (eight over-calls and five under-calls), staging discrepancy up to pT1 in four specimens and inability to recognize lymphovascular invasion in one specimen.

Figure 1 - 755



**Conclusions:** Over and under calling of muscle invasive disease, wrong tumor classification and inability to recognize aggressive variants of urothelial carcinoma can potentially lead to inappropriate management. Diagnostic discrepancy in a considerable proportion of a common surgical pathology specimen indicates the need for subspecialized training.

## 756 Tumor Infiltrating T-cells and Loss of Expression of SWI/SNF Genes in Varying Stages of Clear Cell Renal Cell Carcinoma

Alaa Hrizat<sup>1</sup>, Ruihe Lin, Yan Xiang<sup>2</sup>, Caleb Holtmeyer<sup>1</sup>, Kristen Koob<sup>3</sup>, Jaime Eberle-Singh<sup>4</sup>, Peter Mccue<sup>3</sup>, Haifeng Yang, Li Li<sup>1</sup>

<sup>1</sup>Thomas Jefferson University Hospital, Philadelphia, PA, <sup>2</sup>Goshen Health, Goshen, IN, <sup>3</sup>Thomas Jefferson University, Philadelphia, PA, <sup>4</sup>Sidney Kimmel Medical College, Thomas Jefferson University, Philadelphia, PA

**Disclosures:** Alaa Hrizat: None; Ruihe Lin: None; Yan Xiang: None; Caleb Holtmeyer: None; Kristen Koob: None; Jaime Eberle-Singh: None; Peter Mccue: None; Haifeng Yang: None; Li Li: None

**Background:** Patients with clear cell renal cell carcinoma (ccRCC) metastases have poor prognoses even with adjuvant therapies. Studies have shown that T-cells and macrophages are the primary tumor-infiltrating immune cells that target antigenic tumor cells in the renal tumor microenvironment. The robustness of this response could predict clinical response to immune checkpoint inhibitor treatment. Large scale gene-sequencing studies have identified several driver genes beyond VHL in ccRCC. These genes encode for subunits of the SWI/SNF remodeling complex, including PBRM1, BAP1, ARID1A, SETD2, SMARCA4 (BRG1), and SMARCA2 (BRM). We hypothesized that the loss of SWI/SNF subunit protein expression may impact tumor-infiltrating T-cells in the ccRCC microenvironment.

**Design:** A tumor tissue microarray (TMA) of 160 ccRCC cases was used in this study. 4 different areas were analyzed for each tumor. Immunohistochemistry (IHC) quantification was performed to analyze expression of PBRM1, BAP1, ARID1A, SETD2, BRG1, and BRM(p). A dual-color IHC protocol was developed for evaluation of intratumoral CD4+ and CD8+ T-cells (Fig 1). Clinical and pathologic features were obtained through electronic medical records. One-way ANOVA, paired t-test, and Pearson correlation were used for statistical analyses.

**Results:** There was a statistically significant association between ccRCC stage and expression of PBRM1, BAP1, BRM(p), BRG1, and SetD2 ( $P$  all<0.05), but not ARID1A ( $P=0.273$ ). The number of intratumoral CD4+ T-cells in stage 4 ccRCC was significantly higher than in stage 1 ( $P=0.002$ ), but no significant difference occurred for CD8+ T-cells. Interestingly, intratumoral infiltrations of both CD4+ and CD8+ T-cells were significantly increased in tumors that had loss of PBRM1 and BAP1. However, this was only observed in stage 1 vs. stage 4 tumors ( $P$  all<0.05) (Fig 2). There was no correlation between loss of expression of SWI/SNF complex proteins and T cell infiltration when stratified by stage.

# ABSTRACTS | GENITOURINARY PATHOLOGY (INCLUDING RENAL TUMORS)

Figure 1 - 756

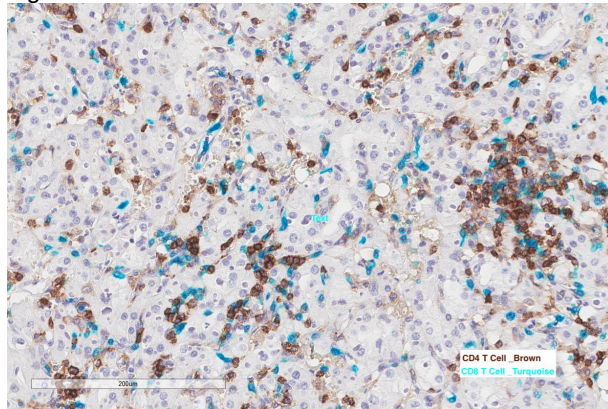
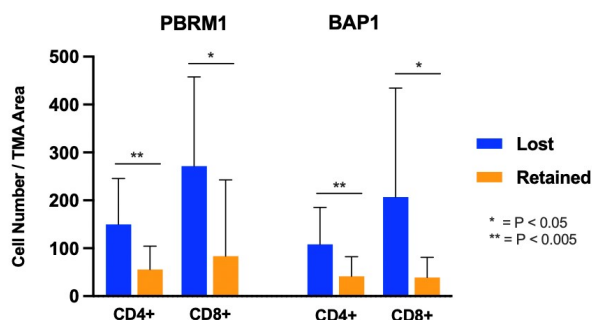


Figure 2 - 756

CD4+ and CD8+ T-Cell Infiltration in Stage 1 ccRCC



**Conclusions:** Our study demonstrated that loss expression of PBRM1, BAP1, SETD2, BRG1, and BRM(p) was significantly associated with ccRCC tumor stage. A significant increase in infiltrating CD4+ T-cells was present in more advanced stage ccRCC. CD4+ and CD8+ T-cells were significantly increased in PBRM1- and BAP1-mutated ccRCC in early stage ccRCC, indicating they may play an important role in tumor microenvironment and progression. Our results provide important information that may help predict response to immune checkpoint blockade.

## 757 Accuracy of Reporting Pathology Data for Prostate Cancer in State-Wide Cancer Registries

Sophie Huynh<sup>1</sup>, Adrianna A Mendes<sup>1</sup>, Lia DePaula Oliveira<sup>2</sup>, Kevin Ward<sup>3</sup>, Ann Hamilton<sup>4</sup>, Christopher Haiman<sup>4</sup>, David Conti<sup>4</sup>, Tamara Lotan<sup>5</sup>

<sup>1</sup>Johns Hopkins Medical Institutions, Baltimore, MD, <sup>2</sup>Johns Hopkins Hospital School of Medicine, Baltimore, MD, <sup>3</sup>Emory University, Atlanta, GA, <sup>4</sup>USC Norris Comprehensive Cancer Center, Los Angeles, CA, <sup>5</sup>Johns Hopkins University School of Medicine, Baltimore, MD

**Disclosures:** Sophie Huynh: None; Adrianna A Mendes: None; Lia DePaula Oliveira: None; Kevin Ward: None; Ann Hamilton: None; Christopher Haiman: None; David Conti: None; Tamara Lotan: None

**Background:** SEER (Surveillance, Epidemiology and End Results) cancer registry data are utilized by numerous prostate cancer epidemiologic studies, and clinical data on tumor characteristics are based on pathology reports abstracted by hospitals and reported to cancer registries. These variables include tumor grade (Gleason score) and stage which are critical for risk models developed in these analyses. However, few prior studies have evaluated the accuracy of reporting pathology data originating from multiple institutions. We leveraged the ongoing RESPOND study of prostate cancer in 1400 African-American men to examine the concordance between the pathology variables recorded in cancer registries and the original pathology report re-examined by a centralized review.

**Design:** Pathology reports from needle biopsies (n=698) and radical prostatectomies (n=697) from men diagnosed from 2010-2019 and enrolled in the RESPOND study were sent to Johns Hopkins by registries in 6 states (GA, TX, NJ, LA, CA, and MI) for central review. A pathologist at JHU re-reviewed each pathology report to extract the Gleason Grade Group and T-stage, and these data were compared to data initially reported by hospital registrars to the respective cancer registries for each patient.

**Results:** Registry tumor grade data was available for 94% (659/698) of prostate needle biopsies and 82% (571/697) of radical prostatectomy samples. Among needle biopsies with registry grade available, there was agreement between the re-review of the pathology report with the original reported variable in 91% of available cases, with  $\kappa = 0.881$ . Among radical prostatectomies with registry grade available, there was agreement with the original pathology report in 94% of cases, with  $\kappa = 0.907$ . Registry pT stage data was available for 77% (429/557) of radical prostatectomy samples, and there was concordance with the original pathology report in 98% of cases, corresponding to  $\kappa = 0.951$ .

**Conclusions:** There is high concordance between the centralized pathology report review and pathology grade and stage information originally recorded in cancer registries. Grade discordances may be due to multiple independent biopsies obtained in patients undergoing active surveillance, misinterpretation of pathology reports containing multiple needle cores, or input errors. As cancer registry data elements and grading and staging systems evolve over time, studies to examine accuracy are especially valuable given the widespread utilization of SEER data in epidemiologic studies.

**758 Cribiform and Intraductal Carcinoma of the Prostate Frequently Harbor TP53, ATM and BRCA2 Gene Mutations Among Other Homologous Recombination DNA Repair Genes**

Ekta Jain<sup>1</sup>, Shivani Sharma<sup>1</sup>, Aditi Aggarwal<sup>1</sup>, Deepika Jain<sup>2</sup>, Vipra Malik<sup>2</sup>, Sayali Shinde<sup>1</sup>, Mallika Dixit<sup>2</sup>, Samriti Arora<sup>2</sup>, Hena Singh<sup>1</sup>, Juhi Varshney<sup>1</sup>, Anandi Lobo<sup>3</sup>, Mahul Amin<sup>4</sup>, Sambit Mohanty<sup>5</sup>

<sup>1</sup>Core Diagnostics, Gurgaon, India, <sup>2</sup>Core Diagnostics, Gurugram, India, <sup>3</sup>Kapoor Centre of Urology and Pathology, Raipur, India, <sup>4</sup>The University of Tennessee Health Science Center, Memphis, TN, <sup>5</sup>Advanced Medical and Research Institute, New Delhi, India

**Disclosures:** Ekta Jain: None; Shivani Sharma: None; Aditi Aggarwal: None; Deepika Jain: None; Vipra Malik: None; Sayali Shinde: None; Mallika Dixit: None; Samriti Arora: None; Hena Singh: None; Juhi Varshney: None; Anandi Lobo: None; Mahul Amin: None; Sambit Mohanty: None

**Background:** Cribiform (CB) histology and intraductal carcinoma of prostate (IDC-P) are important morphologic correlates of prostate cancer (PC) harboring mutations in the genes involved in homologous recombination repair (HRR) pathway leading to high genomic instability. Recently, revised clinical guidelines from the NCCN have recommended genetic testing for all PC patients with an IDC-P or CB histology. Paucity of literature from the Indian perspective prompted us to correlate CB and IDC-P histology with HRR mutations and the common genes altered.

**Design:** Specimens from 78 advanced metastatic castrate resistant PC (mCRPC) patients were studied for HRR gene somatic and germline mutations referred from Uro-oncologists. The complete coding region and splice junctions of HRR pathway genes including *ATM*, *MRE11*, *BARD1*, *NBN*, *BRCA1*, *PALB2*, *BRCA2*, *PPP2R2A*, *BRIP1*, *RAD51B*, *CDK12*, *RAD54L*, *CHEK2*, *TP53*, *FANCD2*, *RAD51C* and *RAD51D* were sequenced by next generation sequencing on Illumina sequencing platform at ≥1000X mean depth and HRR mutations were analyzed for association with CB histology and IDC-P.

**Results:** HRR somatic mutation was seen in 25 of 78 patients (32.1%). The age ranged from 50 to 81 years with a mean age of 66.1. Of the positive patients, somatic testing was performed on the prostate biopsy in 20 and on the metastatic biopsy in 5 patients. Various mutations noticed were: *TP53* (n=12;48%), *ATM* (n=6;24%), *BRCA2* (n=4;16%), *PALB2* (n=3;12%), *RAD51D*, *CDK12*, and *BRIP1* (n=1 each;4%). Nine, 8 and 3 patients (80%) had both CB and IDC-P, isolated CB pattern 4 and isolated IDC-P histologies, respectively (Figure 1). The prevalence of HRR mutation was 11 (44%), 4 (16%) and 2 (8%) for Gleason score 9, 8 and 7 and grade groups 5, 4 and 3 tumors, respectively (Table 1). Genomic abnormalities detected in the tumors are described in Figure 2. None of these patients had germline genomic abnormality.

S.No	Age (Years)	Tissue for testing	Intraductal carcinoma	Cribiform pattern 4 cancer	Gleason score / Grade group	Gene symbol
1	75	Prostate	Not identified	Present (20%)	9 (5+4)/5	<i>TP53</i>
2	58	Prostate	Not identified	Present (30%)	9 (4+5)/5	<i>TP53</i>
3	59	Prostate	Not identified	Present (40%)	7 (4+3)/3	<i>ATM</i>
4	64	Prostate	Present (15%)	Present (20%)	9 (4+5)/5	<i>BRCA2</i>
5	70	Prostate	Present (25%)	Present (15%)	9 (4+5)/5	<i>TP53</i>
6	67	Prostate	Not identified	Present (35%)	9 (5+4)/5	<i>TP53</i>
7	62	Prostate	Not identified	Present (50%)	8 (4+4)/4	<i>PALB2</i>
8	65	Prostate	Present (40%)	Present (50%)	9 (4+5)/5	<i>RAD51D</i>
9	77	Prostate	Present (20%)	Present (50%)	9 (4+5)/5	<i>TP53</i> and <i>BRCA2</i>
10	77	Prostate	Present (25%)	Present (50%)	8 (4+4)/4	<i>TP53</i> and <i>ATM</i>
11	61	Prostate	Present (100%)	Not identified	NA	<i>TP53</i>
12	61	Prostate	Present (10%)	Present (30%)	7 (4+3)/3	<i>ATM</i>
13	56	Prostate	Present (80%)	Present (20%)	8 (4+4)/4	<i>CDK12</i> and <i>PALB2</i>
14	61	Prostate	Present (100%)	Not identified	NA	<i>PALB2</i>
15	64	Prostate	Present (50%)	Present (55%)	9 (4+5)/5	<i>TP53</i>
16	58	Prostate	Not identified	Present (35%)	9 (4+5)/5	<i>ATM</i>
17	71	Prostate	Not identified	Present (30%)	9 (4+5)/5	<i>ATM</i>
18	70	Prostate	Not identified	Present (35%)	9 (4+5)/5	<i>TP53</i>
19	68	Prostate	Present (25%)	Present (50%)	8 (4+4)/4	<i>BRCA2</i>
20	75	Prostate	Present (100%)	Not identified	NA	<i>BRIP1</i> and <i>ATM</i>
21	70	Para-aortic LN	NA	NA	NA (solid and CB)	<i>TP53</i>
22	75	Liver	NA	NA	NA (solid)	<i>TP53</i>
23	50	Para-aortic LN	NA	NA	NA (solid and CB)	<i>TP53</i>
24	81	Inguinal LN	NA	NA	NA (solid and CB)	<i>TP53</i>
25	57	Liver	NA	NA	NA (solid)	<i>BARD1</i>

Figure 1 - 758

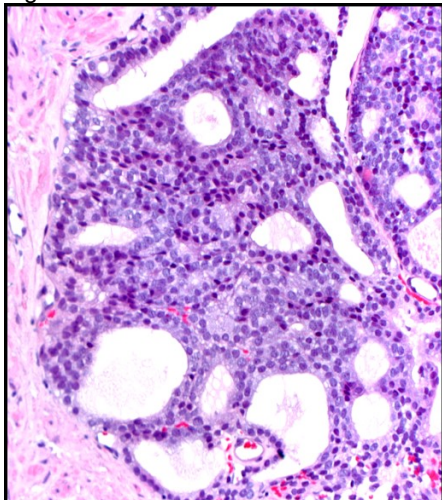
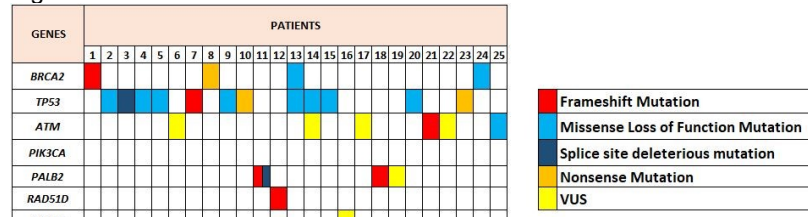


Figure 2 - 758



**Conclusions:** This is the first Indian study to highlight the relationship between CB and IDC-P histology with HRR mutation. The prevalence of HRR mutation in this study is similar to the West (32.1% versus 34%). *ATM*, *BRCA2* and *TP53* were the common mutations detected. There is a higher prevalence of HRR mutations in mCRPC with CB/IDC-P histology as compared to West (80% versus 40% from the West). The mutations were more prevalent in Group grade 5 tumors. However, further studies with large cohort of patients is warranted to substantiate our observations.

## 759 An Artificial Intelligence-based Estimation of Tumor Purity is More Reliable than Pathologists in Bladder Cancer

Jinahn Jeong<sup>1</sup>, Yeon-Mi Ryu<sup>2</sup>, Ja-Min Park<sup>2</sup>, Sun Young Yoon<sup>2</sup>, Bokyung Ahn<sup>1</sup>, Gi Hwan Kim<sup>1</sup>, Se Un Jeong<sup>3</sup>, Hyun-Jung Sung<sup>3</sup>, Yong Mee Cho<sup>1</sup>, Sang-Yeob Kim<sup>2</sup>

<sup>1</sup>Asan Medical Center, University of Ulsan College of Medicine, Songpa-gu, South Korea,

<sup>2</sup>Asan Institute for Life Sciences, Asan Medical Center, Songpa-gu, South Korea,

<sup>3</sup>Asan Medical Center, Seoul, South Korea

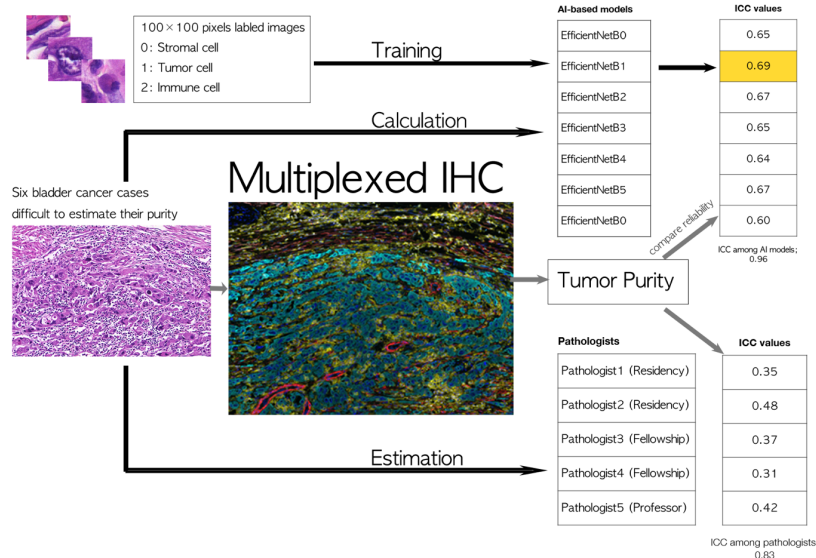
**Disclosures:** Jinahn Jeong: None; Yeon-Mi Ryu: None; Ja-Min Park: None; Sun Young Yoon: None; Bokyung Ahn: None; Gi Hwan Kim: None; Se Un Jeong: None; Hyun-Jung Sung: None; Yong Mee Cho: None; Sang-Yeob Kim: None

**Background:** The accurate assessment of tumor purity is essential for diagnostic molecular testing. The tumor purity is defined as the proportion of tumor cells in a tumor tissue, which usually consists not only tumor cells but also non-tumor cells such as stromal cells and inflammatory cells. Although manual counting by pathologists is gold-standard currently, the tumor purity estimation is tedious, time consuming process and suffers from high interobserver variability. We aimed to find an accurate and easy-to-use artificial intelligence (AI)-based method for the tumor purity assessment of bladder cancer.

**Design:** Among 245 bladder cancer cases tested for next generation sequencing in our institution, we carefully selected six cases, of which tumor purity estimation was extremely difficult due to extensive inflammatory cell infiltration, severe stromal desmoplastic reaction, sarcomatoid dedifferentiation, or divergent differentiation. A tissue-microarray construct (TMA) was generated from tumor tissues of the six cases and used for multiplexed immunohistochemistry (mIHC) with pan-cytokeratin, alpha-SMA and CD45 antibodies, which were representing tumor cells, mesenchymal cells, and lymphocytes, respectively. Based on the tumor purity assessed by the mIHC as reference value, the performance of five pathologists and seven AI-based deep learning models, EfficientNetB0 to EfficientNetB6, were examined on 34 regions of interest in the TMA tissue. Interclass correlation coefficients (ICC) was used to demonstrate the reliability to the reference value of the mIHC.

**Results:** As shown in the Figure, the pathologists showed relatively poor reliability and wide range of interobserver variability (ICC range, 0.31 – 0.48). In contrast, the EfficientNet models showed moderate reliability, among which the highest ICC was 0.69 (95% CI, 0.48, 0.83) from EfficientNet B1. The EfficientNetB1 showed 85.0% of accuracy, 85.2 % of sensitivity, 94.2% of specificity, 88.5 of F1-score, and 0.95 of area under ROC.

Figure 1 - 759



**Conclusions:** These results demonstrate that AI-based deep learning models assessed tumor purity more accurately than pathologists in extremely difficult bladder cancer cases. Therefore, the AI-based models could be a useful tool for pathologists to better estimate tumor purity in the difficult cases and conventional urothelial carcinoma cases with minor adjustment.

## 760 The Morphologic, Clinical and Molecular Spectrum of Succinate Dehydrogenase A-Deficient Renal Cell Carcinoma (SDHA RCC)

Richard Judelson<sup>1</sup>, Deepika Sirohi<sup>2</sup>, Georges Gebrael<sup>3</sup>, Michelle Hirsch<sup>4</sup>, Manju Aron<sup>5</sup>, Sambit Mohanty<sup>6</sup>, Anandi Lobo<sup>7</sup>, Shilpy Jha<sup>8</sup>, Harrison Tsai<sup>4</sup>, Shivani Kandukuri<sup>9</sup>

<sup>1</sup>LAC+USC Medical Center, Los Angeles, CA, <sup>2</sup>The University of Utah/ARUP Laboratories, Salt Lake City, UT, <sup>3</sup>Huntsman Cancer Institute, Salt Lake City, UT, <sup>4</sup>Brigham and Women's Hospital, Boston, MA, <sup>5</sup>Keck School of Medicine of USC, Los Angeles, CA, <sup>6</sup>Advanced Medical and Research Institute, New Delhi, India, <sup>7</sup>Kapoor Centre of Urology and Pathology, Raipur, India, <sup>8</sup>Advanced Medical and Research Institute, Bhubaneswar, India, <sup>9</sup>University of Southern California, Keck School of Medicine of USC, Los Angeles, CA

**Disclosures:** Richard Judelson: None; Deepika Sirohi: None; Georges Gebrael: None; Michelle Hirsch: None; Manju Aron: None; Sambit Mohanty: None; Anandi Lobo: None; Shilpy Jha: None; Harrison Tsai: None; Shivani Kandukuri: None

**Background:** Succinate dehydrogenase-deficient renal cell carcinomas (SDH RCC) are defined as RCC's with mutations in SDH subunits, and are known to have an association with hereditary paraganglioma-pheochromocytoma syndrome and gastrointestinal stromal tumors in most cases. Herein we report the distinctive features that characterize the rarely reported and seemingly higher-grade SDHA RCC via the morphologic, immunohistochemical (IHC) and molecular analysis of 5 tumors.

**Design:** Morphologic and IHC features were examined in all 5 cases, including SDHB and SDHA IHC. Molecular analysis via next-generation sequencing (NGS) was performed on 4/5 cases including 2 metastatic tissue samples.

**Results:** The findings are summarized in the Table 1.

- Five kidney tumors were identified (4 by NGS, 1 by IHC) with a patient median age of 40 years and a male predominance (4M:1F)
- Morphologic features included areas with solid growth (75%), nests (100%), papillae (100%), cysts (25%), eosinophilic/flocculent cytoplasm (100%), cytoplasmic vacuoles with inclusions (75%), and nuclear grooves (25%)
- 4/5 tumors were reported as high grade (ISUP/WHO nuclear grade 3) (the core biopsy was not graded) with desmoplastic stromal changes and a mixed inflammatory response
- The metastatic tumors showed a predominantly nested growth pattern
- All primary tumors were stained with SDHB IHC with 4/5 (80%) showing loss of expression while SDHA IHC showed loss of expression in 3/5 (60%) of cases

# ABSTRACTS | GENITOURINARY PATHOLOGY (INCLUDING RENAL TUMORS)

Case #	Age/Sex	Specimen type	High grade morphology	SHDB-like features	SDHB IHC in Primary	SDHA IHC in Primary	NGS in Primary tumor	Metastasis	NGS in Metastasis	Survival	Initial Diagnosis
1	64/M	Radical nephrectomy	Solid sheets, nests, papillary, cystic	Oncocytic cytoplasm and intracytoplasmic vacuoles	Lost	Retained	Germline mutation present SDHA R589W	Retropertitoneal lymph nodes	Variant Exon 13 p.R589W	AWD 51 months	Collecting Duct carcinoma (CDC)
2	64/M	Radical nephrectomy	Nests, papillary, cystic	Flocculent but no intracytoplasmic vacuoles	Retained	Retained	SDHA c.91C>T, p.R31*	Lung, T12 vertebrae	N/A	DOD	N/A
3	40/M	Radical nephrectomy	Solid sheets, nest, papillary	Flocculent cytoplasm and intracytoplasmic vacuoles	Lost	Lost	SDHA c.1765C>T, p.A589W	Thoracic vertebrae	SDHA c.1765C>T, p.A589W	AWD 14 months (the lost to follow up)	Renal cell carcinoma, NOS
4	31/F	Radical nephrectomy	Solid sheets, nest, papillary	Flocculent cytoplasm and intracytoplasmic vacuoles	Lost	Lost	SDHA c.1526C>G, p.S509W	None	N/A	AWD 2 months	Renal cell carcinoma with mixed papillary and CDC-like features
5	25/M	Core biopsy	No high grade morphology	Flocculent cytoplasm and intracytoplasmic vacuoles	Lost	Lost	N/A	N/A	N/A	N/A	N/A

SDH-succinate dehydrogenase; NGS-next generation sequencing; AWD-alive with disease; DOD-dead of disease

Figure 1 - 760

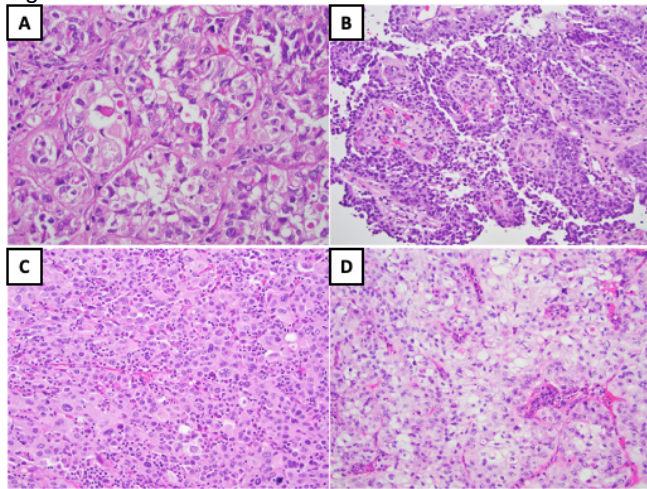


Figure 1 (H&E from Case#1): High-power nested pattern with vacuolization (A). High-power papillary pattern (B). High-power solid pattern with intracytoplasmic vacuoles (C). High-power nested pattern with clear cytoplasm and intracytoplasmic vacuoles (D).

Figure 2 - 760

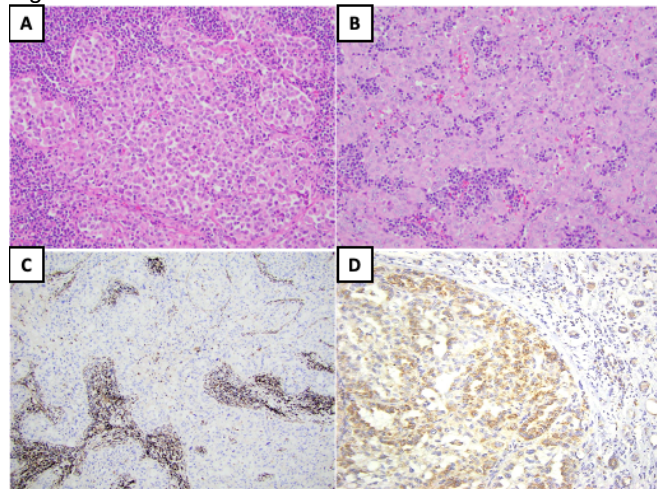


Figure 2 (H&E and IHC from Case#1): Lymph node metastasis appear nested with eosinophilic, high-grade cells (A & B). SDHB (lost) and SDHA (retained) immunostains performed on the primary renal tumor (C & D). Normal renal tissue seen in background acts as control.

**Conclusions:** The histologic spectrum of SDHA RCC ranges from classic low-grade SDH morphology to heterogeneous high grade features and brisk inflammation. SDHA RCC should be included in the differential diagnosis of RCCs with high grade features. SDHA IHC should be subsequently performed on all cases that show SDHB loss on IHC. In case #1, the SDHA IHC showed retained staining which may be explained by the presence of a dysfunctional protein and in case #2, the SDHB IHC is retained possibly due to a truncating mutation; both cases will need further evaluation. Request NGS on RCC, NOS with papillary and CDC-like morphology, especially as SHDA IHC can be retained in cases with SDHA mutation. With 2/5 (40%) patients dead of disease and one with extensive metastasis, SDHA RCC should be considered an aggressive RCC subtype. Compared to most SDHB RCC, it appears that the rare SDHA RCC is a high-grade tumor with increased risk for metastatic disease and a worse overall prognosis.

## 761 Recognition and Interpretation of Molecularly Defined RCCs Listed in the WHO-2022 Renal Tumor Classification: A Survey of Genitourinary Pathologists

Seema Kaushal<sup>1</sup>, Hena Khandakar<sup>1</sup>, Sambit Mohanty<sup>2</sup>, Sean Williamson<sup>3</sup>, Samson Fine<sup>4</sup>, Victor Reuter<sup>4</sup>, Michelle Hirsch<sup>5</sup>, Holger Moch<sup>6</sup>, Hikmat Al-Ahmadie<sup>4</sup>, Rohit Mehra<sup>7</sup>, Kiril Trpkov<sup>8</sup>, Cristina Magi-Galluzzi<sup>9</sup>, Rajal Shah<sup>10</sup>, Manju Aron<sup>11</sup>, Fiona Maclean<sup>12</sup>, Maria Picken<sup>13</sup>, Ankur Sangoi<sup>14</sup>, Rodolfo Montironi<sup>15</sup>, Antonio Lopez-Beltran<sup>16</sup>, Christopher Przybycin<sup>3</sup>, Adeboye Osunkoya<sup>17</sup>, Mahmut Akgul<sup>18</sup>, Khaleel Al-Obaidy<sup>19</sup>, Jatin Gandhi<sup>20</sup>, Lara Harik<sup>17</sup>, Katrina Collins<sup>21</sup>, Stewart Fleming<sup>22</sup>, Giovanna Giannico<sup>23</sup>, Andres Acosta<sup>24</sup>, Claudia Manini<sup>25</sup>, Fadi Brimo<sup>26</sup>, Laurence Galea<sup>27</sup>, Deepika Sirohi<sup>28</sup>, Levente Kuthi<sup>29</sup>, Steven Smith<sup>30</sup>, Ali Amin<sup>31</sup>, Priti Lal<sup>32</sup>, João Lobo<sup>33</sup>, Luca Cima<sup>34</sup>, Shivani Kandukuri<sup>35</sup>, Sangeeta Desai<sup>36</sup>, Santosh Menon<sup>37</sup>, Sandhya Sundaram<sup>38</sup>, B Vishal Rao<sup>39</sup>, Divya Midha<sup>40</sup>, Sankalp Sancheti<sup>41</sup>, Anandi Lobo<sup>42</sup>, Shilpy Jha<sup>43</sup>, Lovelesh Nigam<sup>44</sup>, Ekta Jain<sup>45</sup>, Rupanita Biswal<sup>46</sup>, Shivani Sharma<sup>45</sup>, Francisco Queipo<sup>47</sup>, Priya Rao<sup>48</sup>, Daniel Luthringer<sup>49</sup>, Anil Parwani<sup>50</sup>, Swati Satturwar<sup>51</sup>, Pheroze Tamboli<sup>48</sup>, Lisa Browning<sup>52</sup>, Nilesh Gupta<sup>19</sup>, Bonnie Balzer<sup>53</sup>, Liang Cheng<sup>31</sup>, Ramani Kumar<sup>54</sup>, Rohan Sardana<sup>55</sup>, Vipra Malik<sup>56</sup>, Samriti Arora<sup>56</sup>, Deepika Jain<sup>56</sup>, Meenakshi Swain<sup>57</sup>, Jose Lopez<sup>58</sup>, Gabriela Quiroga-Garza<sup>59</sup>, Guido Martignoni<sup>60</sup>, Gorka Muñiz Unamunzaga<sup>61</sup>, Mahul Amin<sup>62</sup>

<sup>1</sup>All India Institute of Medical Sciences, New Delhi, India, <sup>2</sup>Advanced Medical and Research Institute, New Delhi, India, <sup>3</sup>Cleveland Clinic, Cleveland, OH, <sup>4</sup>Memorial Sloan Kettering Cancer Center, New York, NY, <sup>5</sup>Brigham and Women's Hospital, Boston, MA, <sup>6</sup>University Hospital Zurich, Zürich, Switzerland, <sup>7</sup>University of Michigan, Ann Arbor, MI, <sup>8</sup>University of Calgary, Calgary, AB, <sup>9</sup>The University of Alabama at Birmingham, Birmingham, AL, <sup>10</sup>UTSouthwestern Medical Center, Dallas, TX, <sup>11</sup>Keck School of Medicine of USC, Los Angeles, CA, <sup>12</sup>Douglass Hanly Moir Pathology, Melbourne, Australia, <sup>13</sup>Loyola University Medical Center, Maywood, IL, <sup>14</sup>El Camino Hospital, Mountain View, CA, <sup>15</sup>Ancona, Italy, <sup>16</sup>Fundação Champalimaud/IPO Lisboa, Lisbon, Portugal, <sup>17</sup>Emory University School of Medicine, Atlanta, GA, <sup>18</sup>Albany Medical Center, Albany, NY, <sup>19</sup>Henry Ford Health System, Detroit, MI, <sup>20</sup>Emory University Hospital, Atlanta, GA, <sup>21</sup>Indiana University School of Medicine, Indianapolis, IN, <sup>22</sup>University of Dundee, Dundee, United Kingdom, <sup>23</sup>Vanderbilt University Medical Center, Nashville, TN, <sup>24</sup>Brigham and Women's Hospital, Harvard Medical School, Boston, MA, <sup>25</sup>University of Turin, Turin, Italy, <sup>26</sup>McGill University, Montréal, QC, <sup>27</sup>Melbourne Pathology, Australia, <sup>28</sup>The University of Utah/ARUP Laboratories, Salt Lake City, UT, <sup>29</sup>University of Szeged, Szeged, Hungary, <sup>30</sup>VCU School of Medicine, Richmond, VA, <sup>31</sup>Alpert Medical School of Brown University, Providence, RI, <sup>32</sup>University of Pennsylvania, Philadelphia, PA, <sup>33</sup>Portuguese Oncology Institute - Porto, Porto, Portugal, <sup>34</sup>Santa Chiara Hospital of Trento, <sup>35</sup>University of Southern California, Keck School of Medicine of USC, Los Angeles, CA, <sup>36</sup>Tata Memorial Centre, Mumbai, India, <sup>37</sup>Tata Memorial Hospital, Mumbai, India, <sup>38</sup>Sri Ramachandra Institute of Higher Education and Research, Chennai, India, <sup>39</sup>Basavataramak Indo-American Cancer Hospital and Research Institute, West Bengal, India, <sup>40</sup>Tata Medical Center, Kolkata, India, <sup>41</sup>Homi Bhabha Cancer Hospital, New Chandigarh, India, <sup>42</sup>Kapoor Centre of Urology and Pathology, Raipur, India, <sup>43</sup>Advanced Medical and Research Institute, Bhubaneswar, India, <sup>44</sup>KDRC-ITS, Ahmedabad, India, <sup>45</sup>Core Diagnostics, Gurgaon, India, <sup>46</sup>IMS & SUM Hospital, Bhubaneswar, India, <sup>47</sup>Complejo Hospitalario Universitario A Coruña (CHUAC), A Coruña, Galicia, Spain, <sup>48</sup>The University of Texas MD Anderson Cancer Center, Houston, TX, <sup>49</sup>Cedars-Sinai Medical Center, West Hollywood, CA, <sup>50</sup>The Ohio State University Wexner Medical Center, Columbus, OH, <sup>51</sup>The Ohio State University Wexner Medical Center/James Cancer Hospital, Columbus, OH, <sup>52</sup>Oxford University Hospitals NHS Foundation Trust, Oxford, United Kingdom, <sup>53</sup>Cedars-Sinai Medical Center, Los Angeles, CA, <sup>54</sup>Palakkad, India, <sup>55</sup>Sardana Labs, <sup>56</sup>Core Diagnostics, Gurugram, India, <sup>57</sup>Apollo Hospitals, Hyderabad, India, <sup>58</sup>Cruces University Hospital, Barakaldo, Spain, <sup>59</sup>University of Pittsburgh Medical Center, Pittsburgh, PA, <sup>60</sup>University of Verona, Ospedale Pederzoli, Peschiera del Garda, Italy, <sup>61</sup>Hospital San Jorge, Aragon, Spain, <sup>62</sup>The University of Tennessee Health Science Center, Memphis, TN

**Disclosures:** Seema Kaushal: None; Hena Khandakar: None; Sambit Mohanty: None; Sean Williamson: None; Samson Fine: None; Victor Reuter: None; Michelle Hirsch: None; Holger Moch: None; Hikmat Al-Ahmadie: None; Rohit Mehra: None; Kiril Trpkov: None; Cristina Magi-Galluzzi: None; Rajal Shah: None; Manju Aron: None; Fiona Maclean: None; Maria Picken: None; Ankur Sangoi: None; Rodolfo Montironi: None; Antonio Lopez-Beltran: None; Christopher Przybycin: None; Adeboye Osunkoya: None; Mahmut Akgul: None; Khaleel Al-Obaidy: None; Jatin Gandhi: None; Lara Harik: None; Katrina Collins: None; Stewart Fleming: None; Giovanna Giannico: None; Andres Acosta: None; Claudia Manini: None; Fadi Brimo: None; Laurence Galea: None; Deepika Sirohi: None; Levente Kuthi: None; Steven Smith: None; Ali Amin: None; Priti Lal: None; João Lobo: None; Luca Cima: None; Shivani Kandukuri: None; Sangeeta Desai: None; Santosh Menon: None; Sandhya Sundaram: None; B Vishal Rao: None; Divya Midha: None; Sankalp Sancheti: None; Anandi Lobo: None; Shilpy Jha: None; Lovelesh Nigam: None; Ekta Jain: None; Rupanita Biswal: None; Shivani Sharma: None; Francisco Queipo: None; Priya Rao: None; Daniel Luthringer: None; Anil Parwani: None; Swati Satturwar: None; Pheroze Tamboli: None; Lisa Browning: None; Nilesh Gupta: None; Bonnie Balzer: None; Liang Cheng: None; Ramani Kumar: None; Rohan Sardana: None; Vipra Malik: None; Samriti Arora: None; Deepika Jain: None; Meenakshi Swain: None; Jose Lopez: None; Gabriela Quiroga-Garza: None; Guido Martignoni: None; Gorka Muñiz Unamunzaga: None; Mahul Amin: None

**Background:** The fifth edition of the WHO classification (2022) has integrated a new category of molecularly defined renal tumors. The list includes *TFE3*-rearranged RCC, *TFEB*-rearranged RCC, *ELOC* (previously *TCEB1*)-mutated RCC, *ALK*-rearranged RCC, fumarate hydratase-deficient RCC, *SDH*-deficient RCC, and *SMARCB1*-deficient RCC. Recognition and awareness of these entities are still evolving among pathologists and clinicians.

**Design:** A survey instrument was shared among uropathologists using Survey Monkey software, and de-identified and anonymized respondent data were analyzed.

# ABSTRACTS | GENITOURINARY PATHOLOGY (INCLUDING RENAL TUMORS)

**Results:** Seventy three participants completed the survey, of which 51% (n=37) were from North America, 29% (n=21) were from Asia, and remaining were from Europe and Australia. The majority were pathologists with at least 10 years of experience (n=45; 62%), associated with a University or an academic centre (n=64; 88%), 5 of them handled >200 RCCs per month. The majority (n=52; 71%) of participants reported difficult-to-classify renal neoplasms at least 2-5 times per month and 49% (n=36) reported seeing at least 2 molecularly-defined RCCs per month. The principal reason for performing molecular work-up on RCC was a diagnostic clue or challenge by morphology / IHC. A majority (n=47; 64%) used specific IHC alone (n=30) or in conjunction with FISH for diagnosis of molecularly defined RCCs and were aware of characteristic morphology and essential diagnostic criteria. However, *ELOC* mutated RCC was not seen by one-third of respondents. Most common diagnostic techniques used were break-apart FISH probes (-for *TFE3* / *TFEB*); NGS (for *ELOC*); IHC (for FH def, SDH def, *ALK*-rearranged, and *SMARCB1*-def RCC). A third of respondents believed that SDH testing should be performed for all oncocytic tumors irrespective of tumor grade or patient age. Most were not sure if WHO / ISUP grading was preferred or not in molecularly defined RCCs. Most commonly utilized IHC panel for diagnosis of molecularly defined RCCs included KRT7, CD117, SDH-B, FH, 2-SC, *TFE3*, *TFEB*, *ALK*, Melan A, HMB45, cathepsin K, *SMARC-B1*, & *PAX8*. Only 60% had experience with cathepsin-K IHC (n=42). Papillary neoplasm with reverse polarity (n=51; 70%) was the most accepted emerging molecularly defined RCC followed by EVT (eosinophilic vacuolated tumor).

Figure 1 - 761

Figure 1: Frequency of renal neoplasms requiring molecular work-up in practice of poll respondents (n=73)

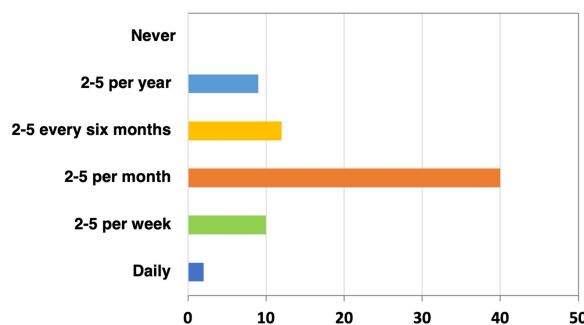
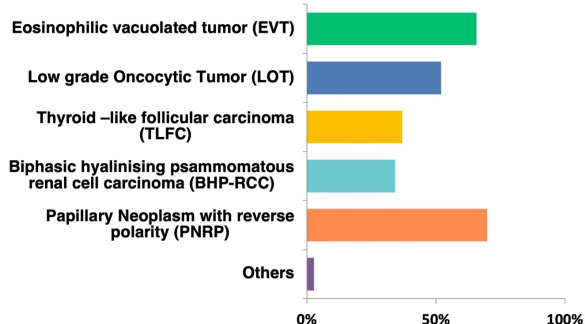


Figure 2 - 761

Figure 2: Poll results on emerging renal entities likely to be included next in the list of molecularly defined RCCs



**Conclusions:** Molecular testing is increasingly utilized, in conjunction with IHC as a surrogate for molecularly defined RCCs. Awareness and recognition of these entities are important for unequivocal genotype-phenotype correlation.

## 762 Tumor-Infiltrating Macrophages as Poor Prognostic Marker in MIBC

Florestan Koll<sup>1</sup>, Jens Köllermann<sup>2</sup>, Luis Kluth<sup>1</sup>, Séverine Banek<sup>1</sup>, Felix Chun<sup>1</sup>, Andreas Weigert<sup>3</sup>, Peter Wild<sup>2</sup>, Henning Reis<sup>2</sup>

<sup>1</sup>University Hospital Frankfurt, Frankfurt, Germany, <sup>2</sup>University Hospital Frankfurt, Dr. Senckenberg Institute of Pathology, Frankfurt, Germany, <sup>3</sup>Goethe-University Frankfurt, Frankfurt, Germany

**Disclosures:** Florestan Koll: None; Jens Köllermann: None; Luis Kluth: None; Séverine Banek: None; Felix Chun: None; Andreas Weigert: None; Peter Wild: None; Henning Reis: None

**Background:** Muscle-invasive urothelial bladder cancer (MIBC) is associated with limited response rates to systemic therapy leading to significant risk of recurrence and death. Tumor infiltrating immune cells have been described to be associates with patient's outcome and response to chemotherapy. We aimed to profile the immune cells in the tumor microenvironment (TME) to predict prognosis in MIBC and responses to adjuvant chemotherapy.

**Design:** We performed multiplex immunohistochemical (IHC) profiling and quantification of immune and stroma cells (CD3, CD4, CD8, CD163, FoxP3, PD1 and CD45, Vimentin, aSMA, PD-L1, Pancytokeratin, Ki67) in 101 patients with MIBC that received radical cystectomy. We used uni- and multivariate survival analyses to identify cell types that could predict prognosis. Samples were clustered into three K-means clusters for their Treg and macrophage infiltration: cluster 1: T-reg high, cluster 2: macrophage high, cluster 3: T-reg and macrophage low. Standardized CD68 and CD163 IHC was digitally analyzed with QuPath in an extended cohort of 141 MIBC patients.

**Results:** High rates of macrophages were associated decreased overall survival probability (OS) (HR 10.9, 95%CI 2.8-40.5; p=0.0004) and high concentration of T-reg were associated with decreased risk of death (HR 0.1, 95%CI 0.01-0.7; p=0.03) in the multivariate Cox-regression model adjusting for adjusting for adjuvant chemotherapy, tumor and lymph node stage. Cluster 1 and 2 both were rich in PD1 and PD-L1 expression on tumor and immune cells. Patients in the macrophage rich cluster (2) showed the

# ABSTRACTS | GENITOURINARY PATHOLOGY (INCLUDING RENAL TUMORS)

poorest OS with and without adjuvant chemotherapy. High levels of the macrophage marker CD163 confirmed poorer prognosis in an extended MIBC cohort

**Conclusions:** T-reg and macrophage rates in MIBC are independent predictors of prognosis and are important players in the tissue microenvironment. Standard IHC for macrophages (CD163) is feasible to predict prognosis but validation studies, especially to predict response to systemic therapies, are required.

## 763 Renal Cell Carcinoma Occurring in Patients with PTEN Hamartoma Tumor Syndrome: Clinicopathologic Study of 12 Tumors from 9 Patients

Diana Kozman<sup>1</sup>, Chia-Sui (Sunny) Kao<sup>2</sup>, Jane Nguyen<sup>1</sup>, Steven Smith<sup>3</sup>, Maria Tretiakova<sup>4</sup>, Jesse McKenney<sup>1</sup>, Reza Alaghehbandan<sup>1</sup>

<sup>1</sup>Cleveland Clinic, Cleveland, OH, <sup>2</sup>Stanford Medicine/Stanford University, Stanford, CA, <sup>3</sup>VCU School of Medicine, Richmond, VA, <sup>4</sup>University of Washington, Seattle, WA

**Disclosures:** Diana Kozman: None; Chia-Sui (Sunny) Kao: None; Jane Nguyen: None; Steven Smith: None; Maria Tretiakova: None; Jesse McKenney: None; Reza Alaghehbandan: None

**Background:** Cowden syndrome (CS) is the prototype of *PTEN* hamartoma tumor syndrome (PHTS) and is most clearly associated with cancer predisposition. While rare and not generally a defining feature, patients with CS have a risk of developing renal cell carcinoma (RCC). The aim of this study was to assess the histopathologic spectrum and clinical behavior of renal tumors in patients with PHTS.

**Design:** A multi-institutional collaborative study was conducted to obtain clinical and pathologic data on renal tumors arising in patients with PHTS, either diagnosed by germline mutational analysis or clinical criteria. Histologic sections of the renal tumors were re-reviewed to classify tumors under current WHO criteria.

**Results:** Twelve renal tumors from 9 patients, 6 confirmed germline *PTEN* mutation and 3 clinically diagnosed as CS, were identified. One patient had 3 metachronous tumors, and one had 2. There were 4 males and 5 females, with mean age of 41.8 years old (range 7-64 years old). The mean tumor size was 4.4 cm (range 0.5-10.2 cm). All 12 tumors were RCCs: 5 were classic chromophobe RCCs, 4 papillary RCCs, and 3 unclassified RCCs. Eleven of 12 tumors had available staging data (one was received fragmented): 7 (59%) pT1a, 2 pT1b (17%), 1 (8%) pT2a, 1 (8%) pT2b, and 1 (8%) pT3a. ISUP/WHO histologic grade was applicable in 7 (54%) tumors: 3 (43%) G1, 1 (14%) G2, 2 (28%) G3, and 1 (14%) G4. The grade 4 tumor was a pT1b unclassified RCC with rhabdoid differentiation. Three of 12 (one clear cell and two papillary RCCs) showed marked intratumoral and peritumoral lymphoplasmacytic infiltrate. The average follow-up time was 67.8 months (13-172 months): 5 patients had no evidence of disease, 2 were lost to follow up, 1 died of other cause/disease, and 1 patient had metastatic RCC to the lung (unclassified RCC with rhabdoid differentiation).

**Conclusions:** Renal tumors associated with PHTS represent a heterogeneous group of RCCs with classic chromophobe RCC being the most common, followed by papillary RCC. In contrast to other hereditary renal neoplasia syndromes, morphologic features do not allow for identifying PHTS-associated neoplasia with any degree of specificity in the absence of clinical setting and/or prior history. The majority of PHTS-associated RCCs demonstrate a favorable clinical behavior. RCCs with unclassifiable morphology or renal tumor multifocality in young patients should raise suspicion for hereditary associated syndromes, and prompt appropriate genetic counseling.

## 764 Co-inactivation of TP53 and RB1 is Necessary, but Not Sufficient for Small Cell Carcinoma Bladder (SCCB) Transformation from High Grade Urothelial carcinoma (HGUC)

Deepika Kumar<sup>1</sup>, Juan Silva Campos<sup>2</sup>, Jeremy Mao<sup>3</sup>, Arnaud Augert<sup>1</sup>, Tong Sun<sup>1</sup>, Peter Humphrey<sup>1</sup>, Minghao Zhong<sup>1</sup>

<sup>1</sup>Yale School of Medicine, New Haven, CT, <sup>2</sup>Yale New Haven Hospital, New Haven, CT, <sup>3</sup>Yale Pathology Labs, New Haven, CT

**Disclosures:** Deepika Kumar: None; Juan Silva Campos: None; Jeremy Mao: None; Arnaud Augert: None; Tong Sun: None; Peter Humphrey: None; Minghao Zhong: None

**Background:** Extensive studies, including next generation sequencing, have established that *TP53* and *RB1* co-inactivation is a hallmark of small cell lung carcinoma (SCLC). This result has been translated to pathology practice: IHC stains for *TP53*, *RB1* and *P16* are helpful supplemental diagnostic markers of SCLC. Small cell carcinoma of the bladder (SCCB), the most common extra-pulmonary small cell carcinoma, presents with identical morphology and immunohistochemical profile as SCLC. In contrast with SCLC, SCCB usually accompanies high grade urothelial carcinoma (HGUC), metachronically or synchronically. In the current study, we investigated *TP53* and *RB1* status in SCCB and its associated urothelial carcinoma by IHC staining.

# ABSTRACTS | GENITOURINARY PATHOLOGY (INCLUDING RENAL TUMORS)

**Design:** We collected 20 consecutive SCCB cases from our institute between 2018 to 2022. The prior or concurrent HGUC for the SCCB cases were also included in this study. IHC stains for TP53, RB1 and P16 were performed on these SCCB and HGUC specimens. The mutation profile of *TP53* and *RB1* in HGUC was evaluated via cBioPortal database.

**Results:** Among these 20 SCCB cases, 8 had prior or concurrent HGUC. We found that all 20 SCCB cases presented with a non-wild type pattern for TP53 (either null or mutant pattern), complete RB1 protein loss, and diffuse and strongly positive P16 staining. All 8 prior or concurrent HGUC cases, except one (87.5%) showed concordant results with the corresponding SCCB. The remaining one HGUC showed mutant TP53 pattern, reduced (but intact) RB1 expression, and negative P16 (focal and weak pattern). Among 2769 urothelial carcinoma samples from the cBioPortal database, we identified 164 samples (5.9%) with co-inactivation of *TP53* and *RB1*.

**Conclusions:** In summary, our data demonstrates that SCCB shares similar genetic features with SCLC: co-inactivation of *TP53* and *RB1*. Interestingly, the urothelial carcinomas associated with SCCB also exhibited the same genetic features in majority of the cases (87.5%). In contrast, only 5.9% UC have the same genetic changes. This result indicates that other genetic and/or epigenetic alterations, in addition to co-inactivation of *TP53* and *RB1*, are required for the progression of HGUC to small cell carcinoma bladder.

## 765 Searching for “Borderline” Neuroendocrine Morphology in High Grade Prostatic Adenocarcinoma

Jung Woo Kwon<sup>1</sup>, Gladell Paner<sup>2</sup>

<sup>1</sup>University of Chicago Medical Center, Chicago, IL, <sup>2</sup>University of Chicago, Chicago, IL

**Disclosures:** Jung Woo Kwon: None; Gladell Paner: None

**Background:** Prostatic adenocarcinoma has the potential to undergo neuroendocrine (NE) differentiation either in post-treatment or de novo settings. NE carcinomas (NEC), including small cell and large cell carcinomas, have poor prognosis and usually do not respond to hormonal therapy. Molecular evidence suggests that NEC arises via transdifferentiation from pre-existing usual prostatic adenocarcinoma. However, borderline phenotype that is in the midst of NE transdifferentiation has not been identified or studied. Herein, we attempt to identify non-typical NE cells that have immunophenotypic NE expression in high grade prostatic adenocarcinoma.

**Design:** As baseline, 20 cases (8 RPs, 8 prostate biopsies, and 4 TURPs) of frank prostatic NECs were examined for areas with non-typical NE morphologies. 8 cases had areas of non-typical NE morphologies with positive synaptophysin expression adjacent to the frank NEC (Figures 1 [H&E] and 2 [synaptophysin]). Subsequently, 63 cases (43 RPs, 15 prostate biopsies, and 5 TURPs) of grade group 5 prostatic adenocarcinoma with no frank NE features were retrospectively searched for areas with similar morphologies, and immunohistochemically stained with synaptophysin.

**Results:** In 63 cases of grade group 5 prostatic adenocarcinoma with no frank NE features, 25 (40%) contained foci with somewhat similar morphologies to non-typical NE morphologies seen adjacent to the frank prostatic NECs. These foci were subsequently stained with synaptophysin, and in 10 (16%) cases, positive synaptophysin expression was demonstrated (Table 1). These foci with non-typical NE morphologies usually had dense nuclear crowding. The nuclei usually showed prominent nucleoli in the background of granular chromatin. The tumor cells had ample cytoplasm, and often formed fused or cribriform gland patterns. Synaptophysin expression was typically patchy in these areas.

	N		
Total number of screened GG5 PCa with no frank NE features	63		
GG5 PCa with non-typical NE morphology after screening	25/63 (40%)		
GG5 PCa without non-typical NE morphology after screening	38/63 (60%)		
	N	vs. total # of screened cases	vs. total # of screened cases with non-typical NE morphology
GG5 PCa with non-typical NE morphology & SYP(+)	10	10/63 (16%)	10/25 (40%)
GG5 PCa with non-typical NE morphology but SYP(-)	15	15/63 (24%)	15/25 (60%)

**Table 1: Distribution of the screened cases of grade group 5 prostatic adenocarcinoma with no frank NE features based on the presence of non-typical NE morphology and its respective SYP IHC expression**

Figure 1 - 765

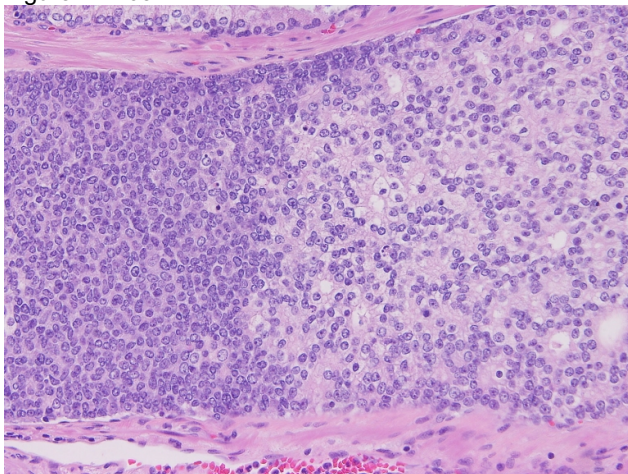
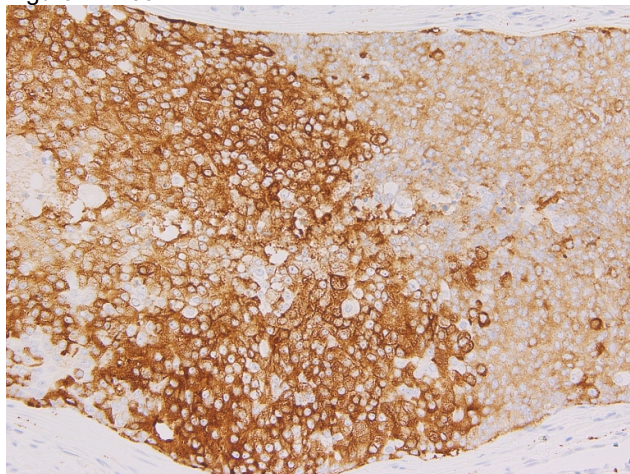


Figure 2 - 765



**Conclusions:** Non-typical NE morphologies with NE marker expression can be seen in grade group 5 prostatic adenocarcinoma. These morphologies overlap with the non-typical NE morphologies seen adjacent to frank prostatic NEC. These morphologies may represent the elusive "borderline" NE morphology depicting prostatic adenocarcinoma in the midst of NE transdifferentiation. Additional studies are underway to further characterize this "borderline" NE morphology and investigate its clinical relevance.

## 766 Tumor-Infiltrating Lymphocytes and Tertiary Lymphoid Structures in Renal Cell Carcinoma Predict Clinical Outcome

Israa Laklouk<sup>1</sup>, Rong Hu<sup>2</sup>, Andrew Wentland<sup>1</sup>, Meghan Lubner<sup>1</sup>, Wei Huang<sup>1</sup>, E Jason Abel<sup>1</sup>, Daniel Shapiro<sup>1</sup>

<sup>1</sup>University of Wisconsin-Madison, Madison, WI, <sup>2</sup>University of Wisconsin School of Medicine and Public Health, Madison, WI

**Disclosures:** Israa Laklouk: None; Rong Hu: None; Andrew Wentland: None; Meghan Lubner: None; Wei Huang: None; E Jason Abel: None; Daniel Shapiro: None

**Background:** The prognostic value of tumor-infiltrating lymphocytes (TIL) and tertiary lymphoid structures (TLS) in localized renal cell carcinoma (RCC) is unclear. This study investigated the prognostic impact of tumor-infiltrating lymphocytes (TIL) and tertiary lymphoid structures (TLSs) on the recurrence and survival of patients with surgically treated RCC.

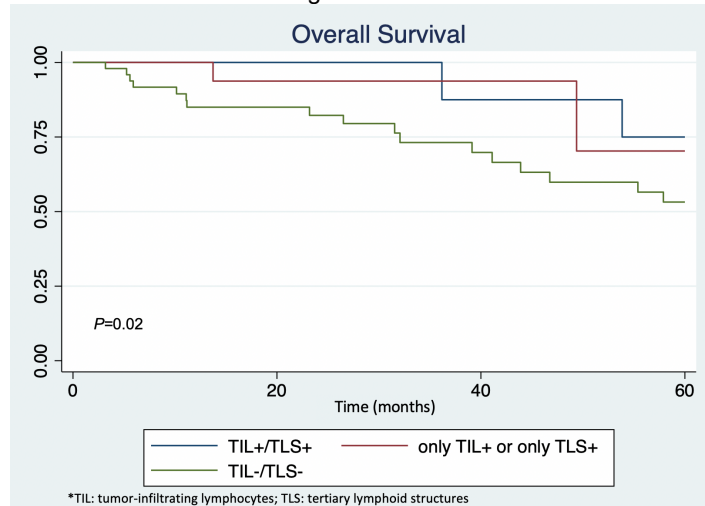
**Design:** A total of 88 patients with  $\geq 7\text{cm}$  pT3N0M0 RCC underwent complete surgical resection at a single institution with median follow-up 31 months (IQR 15-62). TIL presence (minimal, moderate, heavy) and TLS maturation (aggregate, primary follicle, secondary follicle) was graded using brightfield H&E slides according to previously published criteria. We categorized tumors into three groups: heavy inflammation with mature TLS (TIL+/TLS+, N=18), either heavy inflammation or mature TLS (TIL+ or TLS+, N=20), and neither heavy inflammation nor mature TLS (TIL-/TLS-, N=50). The prognostic impact of TIL and TLS on survival were analyzed using multivariable Cox regression adjusting for prognostic factors (sarcomatoid, rhabdoid, nuclear grade, and tumor size). Multivariable logistic regression evaluated these factors for associations with early ( $\leq 12$  months) recurrence.

**Results:** Most tumors (90%) were clear cell with median tumor size 9.5 cm (Table 1). Heavy presence of TILs was observed in 41%. TLS were seen in 76%, of which 23% were mature. Presence of mature TLS was associated with reduced odds of early recurrence [OR 0.19 (95% CI 0.04-0.97)  $P=0.04$ ] and presence of heavy TIL was associated with improved OS [HR 0.27 (95% 0.09-0.82)  $P=0.02$ ]. Tumors categorized as TIL-/TLS- were associated with a significantly worse OS [HR 3.6 (95% CI 1.2-11),  $P=0.02$ ] compared to tumors that had heavy TILs or mature TLS [figure 1.]

# ABSTRACTS | GENITOURINARY PATHOLOGY (INCLUDING RENAL TUMORS)

Variable	N=88
Median age, years (IQR)	62 (55-68)
Female gender, no. (%)	23 (26)
Median pathologic size, cm (IQR)	9.5 (8-12)
Subtype	
Clear cell	79 (90)
Papillary	5 (6)
Chromophobe	2 (2)
Other	2 (2)
Sarcomatoid, no. (%)	7 (8)
Rhabdoid features, no. (%)	22 (25)
Grade no. (%)	
1-2	17 (19)
3-4	69 (78)
Not graded	2 (2)
Renal vein invasion, no. (%)	55 (63)
Renal sinus/perinephric fat invasion, no. (%)	82 (93)
Inflammation (TIL) degree, no. (%)	
Minimal	30 (34)
Moderate	22 (25)
Heavy	36 (41)
TLS present, no. (%)	67 (76)
Aggregates only	13 (15)
Primary follicles	34 (39)
Secondary follicles	20 (23)

Figure 1 - 766



**Conclusions:** TILs and mature TLS are independently associated with improved survival and decreased rate of early recurrence for high-risk localized RCC tumors. Further studies should validate these potential low-cost biomarkers.

## 767 Immunohistochemistry for GPNMB in the Differential Diagnosis of Renal Cell Tumors with Clear Cell Morphology

Huili Li<sup>1</sup>, Pedram Argani<sup>1</sup>, Tamara Lotan<sup>2</sup>, Victor Reuter<sup>3</sup>, Andres Matoso<sup>4</sup>

<sup>1</sup>Johns Hopkins Hospital, Baltimore, MD, <sup>2</sup>Johns Hopkins University School of Medicine, Baltimore, MD, <sup>3</sup>Memorial Sloan Kettering Cancer Center, New York, NY, <sup>4</sup>Johns Hopkins Medical Institutions, Baltimore, MD

**Disclosures:** Huili Li: None; Pedram Argani: None; Tamara Lotan: None; Victor Reuter: None; Andres Matoso: None

**Background:** Renal cell tumor with clear cell morphology encompasses different tumor entities with various genetic alterations and prognoses, such as conventional clear cell renal cell carcinoma (CCRCC), clear cell papillary renal cell tumor (CCPRCT), ELOC/TCEB1 mutated RCC, RCC with leiomyomatous stroma (TSC associated RCC). Besides high morphologic similarity, a subset of these tumors is also known to be diffusely positive CAIX and CK7 by immunohistochemistry. We have previously demonstrated diffusely strong GPNMB (glycoprotein nonmetastatic B) expression in TFE3/TFEB RCC and in TSC/mTOR alteration-associated renal tumors including eosinophilic solid and cystic renal cell carcinoma, low grade oncocytic tumor, and angiomyolipomas, while only focally weakly positive or negative in CCRCC and CCPRCT. In this study, we evaluated the utility of

# ABSTRACTS | GENITOURINARY PATHOLOGY (INCLUDING RENAL TUMORS)

GPNMB immunostain in renal tumors with clear cell morphology that are also diffusely positive for CK7 and CAIX (CCPRCT, ELOC mutated RCC, and RCC with leiomyomatous stroma).

**Design:** Immunohistochemical stains of CAIX, CK7 and CK903 and GPNMB were performed on whole sections of CCPRCT (n=7), molecularly confirmed ELOC mutated RCC (n=4), and RCC with leiomyomatous stroma (n=3 with one molecularly confirmed TSC mutant).

**Results:** GPNMB immunostain was strong and diffusely positive in all three RCC with leiomyomatous stroma, weakly focally positive in (one of seven; 14%) of CCPRCT, and negative in ELOC mutated RCC. CK903 immunostain is variably positive in most of CCPRCT (five of seven; 71%) and RCC with leiomyomatous stroma, but negative in all ELOC mutated RCC. CAIX and CK7 immunostain were diffusely positive in all tested cases, except for one ELOC mutated RCC, which was negative for CK7.

**Conclusions:** Our study demonstrated that positive CK903 and/or GPNMB immunostain in tumors with clear cell morphology and diffusely positive CK7 and CAIX immunostain excludes ELOC mutated RCC. Since both ELOC mutated RCC and TSC-associated RCC with leiomyomatous stroma are morphologically very similar, positive GPNMB immunostain could confirm TSC-associated tumor and exclude ELOC mutated RCC avoiding costly molecular testing. These findings should be confirmed with a larger cohort of cases.

## 768 Targeted Biopsy with Systemic Biopsy Improves Cancer Detection in Prostate Cancer Screenings

Peizi Li<sup>1</sup>, Pu Ni<sup>2</sup>, Faruk Kombak<sup>1</sup>, Emily Wolters<sup>1</sup>, George Haines<sup>1</sup>, Qiusheng Si<sup>1</sup>

<sup>1</sup>Icahn School of Medicine at Mount Sinai, New York, NY, <sup>2</sup>Icahn School of Medicine at Mount Sinai St Luke's-Roosevelt Hospital Center, New York, NY

**Disclosures:** Peizi Li: None; Pu Ni: None; Faruk Kombak: None; Emily Wolters: None; George Haines: None; Qiusheng Si: None

**Background:** Magnetic resonance imaging (MRI)/ultrasound targeted biopsy has been used together with the 12-core systematic biopsy for prostate cancer screenings in the past few years. However, the efficacy of targeted biopsy compared to systematic biopsy as well as its clinical-histological correlation has only been assessed by limited studies and is further investigated in this study.

**Design:** We collected 960 cases with targeted and systematic prostate biopsies from 04/2019 to 04/2022. We compared cancer detection rates between targeted and systematic prostate biopsies in different grade groups. The correlations between the size of prostate lesions, PSA level, and PI-RADS scale using these two biopsy methods were also analyzed.

**Results:** Among the 960 men who underwent targeted biopsy with systematic biopsy, prostatic adenocarcinoma was diagnosed in 652 (67.9%) cases. 489 (50.9%) cases were diagnosed by targeted biopsy and 576 (60.0%) cases were diagnosed by systematic biopsy (Table 1). In the 384 negative cases diagnosed by systemic biopsy, targeted biopsy identified cancer in 76 (19.8%) cases. Systemic biopsy was able to detect 163 cancer cases that were missed by targeted biopsy. Systematic biopsy detected more grade group 1 cancer compared to targeted biopsy. However, as the grade went higher, the differences between the cancer detection rates of targeted biopsy and systemic biopsy became negligible. Targeted biopsy upgraded the grade group (Figure 1) categorized by systemic biopsy (20.1%, 10.2%, 5.3%, and 5.7% in Grade Groups 1, 2, 3, and 4, respectively, Table 1). Targeted biopsy was more likely to detect cancer in larger lesions (13.17mm VS 11.41mm, p=0.0056) and higher PI-RADS scales (4.19 VS 3.68, p<0.0001). The cancers detected by targeted biopsy also had higher PSA levels (10.38ng/ml VS 6.39ng/ml, p=0.0026) (Figure 2).

		Target biopsy							
		Negative	Grade 1	Grade 2	Grade 3	Grade 4	Grade 5	Total	
Systematic biopsy	No cancer	308	36	25	9	4	2	384	
	Grade 1	106	81	42	4	1	0	234	
	Grade 2	37	37	76	12	3	2	167	
	Grade 3	11	9	26	26	3	1	76	
	Grade 4	7	6	4	27	22	4	70	
	Grade 5	2	0	4	5	5	13	29	
	Total	471	169	177	83	38	22	960	
		Target biopsy							
Systematic biopsy	No cancer	80.21%	9.37%	6.51%	2.34%	1.04%	0.52%	384	
	Grade 1	45.29%	34.62%	17.95%	1.71%	0.43%	0.00%	234	
	Grade 2	22.15%	22.15%	45.51%	7.19%	1.79%	1.19%	167	
	Grade 3	14.47%	11.84%	34.21%	34.21%	3.95%	1.32%	76	
	Grade 4	10.00%	8.57%	5.71%	38.57%	31.43%	5.71%	70	
	Grade 5	6.89%	0.00%	13.79%	17.24%	17.24%	44.83%	29	

# ABSTRACTS | GENITOURINARY PATHOLOGY (INCLUDING RENAL TUMORS)

Table 1. Gleason grade groups of each case identified by targeted biopsy were compared with systematic biopsy. Data in blue indicated concordance between targeted and systematic biopsy. Data in green showed that targeted biopsy detected new tumors or upgraded the grade groups compared to systematic biopsy. Data in yellow indicated that targeted biopsy downgraded the grade groups compared to the systematic biopsy.

Figure 1 - 768

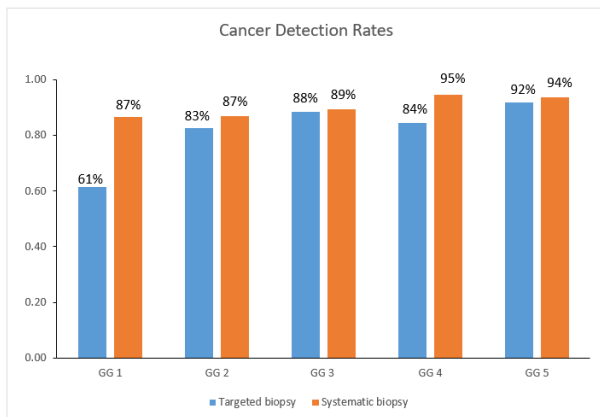


Figure 1. Cancer Detection rates in targeted biopsy compared with systematic biopsy in different grade groups (GG).

Figure 2 - 768

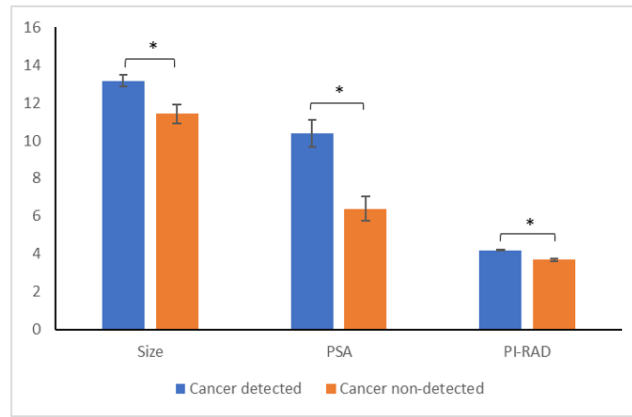


Figure 2. Lesion size, PSA level, and PI-RADS scale comparison in target-detected cancer group and target missed/systematic detected cancer group.

**Conclusions:** Targeted biopsy with systematic biopsy improved cancer detection rate compared with systemic biopsy alone. Targeted biopsy is not sensitive to grade group 1 cancer but is as sensitive as systemic biopsy in detecting higher-grade cancers. Targeted biopsy is more effective at detecting cancers when the patients have larger lesions, higher PI-RADS scales, and higher PSA levels.

## 769 Multi-Center Study Shows a Beneficial Effect of Adding Cribriform/Intraductal Status to CAPRA and NCCN Prediction Algorithms in Prostatic Adenocarcinoma

Kristen Liu<sup>1</sup>, Yan Hong (Shirley) Yu<sup>2</sup>, Katherine Lajkosz<sup>3</sup>, Theodorus Van Der Kwast<sup>4</sup>, Michelle Downes<sup>5</sup>, Kenneth Iczkowski<sup>1</sup>

<sup>1</sup>Medical College of Wisconsin, Milwaukee, WI, <sup>2</sup>University of Toronto, Toronto, ON, <sup>3</sup>Princess Margaret Cancer Centre, Toronto, ON, <sup>4</sup>University Health Network, Toronto, ON, <sup>5</sup>Sunnybrook Health Sciences Centre, Toronto, ON

**Disclosures:** Kristen Liu: None; Yan Hong (Shirley) Yu: None; Katherine Lajkosz: None; Theodorus Van Der Kwast: None; Michelle Downes: None; Kenneth Iczkowski: None

**Background:** Dozens of studies have proven the adverse effect of cribriform (C) or intraductal (IDC) patterns of prostate cancer (PC) [PMID:28820750]. Recent evidence suggested adding C/IDC may significantly enhance the predictive power of the UCSF-CAPRA and NCCN patient risk stratification nomograms [PMID:35676330], but its generalizability was uncertain.

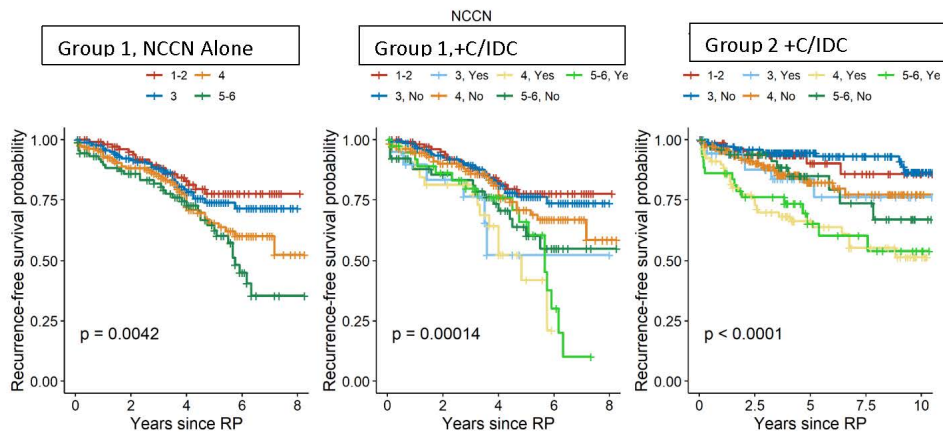
**Design:** We chose to focus on biopsy findings since that is the clinical decision point. Patient cohorts from 2 different countries (n=537 and n=612) were assessed for C/IDC presence in their biopsy. Biopsy CAPRA scores were grouped as 0-2, 3-5, and 6-10. NCCN scores were grouped as very low/low, favorable intermediate, unfavorable intermediate, and high/very high. All men underwent radical prostatectomy. Biochemical recurrence (BCR) was defined as a PSA >0.1 and Event-free survival (EFS) was defined as survival without nodal positivity /metastasis. Counted data were analyzed by chi-square or Fisher exact test; measured data by Kruskal-Wallis test. ANOVA was used to evaluate whether +/- C/IDC made a difference in model performance. The with/without C/IDC for lowest scores of CAPRA and NCCN were merged into 1 group due to small numbers.

**Results:** Group 1 tended to have lower Gleason, CAPRA, and NCCN scores and less C/IDC than Group 2 (all p<0.001). The median follow-up was 4.0 years for Group 1 and 4.4 years for Group 2. For BCR-free survival with CAPRA, the addition of C/IDC status increased the c-index from 0.60 to 0.61, p=0.0871 in Group 1, and 0.66 to 0.71, p=0.0038 in Group 2. With NCCN, the addition of C/IDC increased the c-index from 0.57 to 0.60, p=0.0126 in Group 1, and from 0.62 to 0.68, p<0.001 in Group 2 (Table 1). For EFS with CAPRA, the addition of C/IDC increased the c-index 0.60 to 0.63, p=0.03 in Group 1, and from 0.62 to 0.68, p=0.0038 for Group 2. With NCCN (Figure 1), the addition of C/IDC increased the c-index from 0.59 to 0.61, p=0.1396 for Group 1, but could not be evaluated in Group 2 due to insufficient number of events.

	<b>Group 1</b>		<b>Group 2</b>	
<b>BCR-Free:</b>				
CAPRA	0.60→0.61	p=0.09	0.66→0.71	<b>p=0.004</b>
NCCN	0.57→0.60	<b>p=0.01</b>	0.62→0.68	<b>p&lt;0.001</b>
<b>Event-Free:</b>				
CAPRA	0.60→0.63	<b>p=0.03</b>	0.62→0.68	<b>p=0.003</b>
NCCN	0.59→0.61	p=0.14	Too few events	

Table 1. Increase in the c-Index enabled by including C/IDC status

Figure 1 - 769



**Conclusions:** For both BCR and EFS, CAPRA discriminated better than NCCN did before adding C/IDC. For BCR, in both groups, adding C/IDC helped split the intermediate group of CAPRA. The effect was stronger in Group 1 than Group 2. There was more group separation in NCCN with Group 2 than Group 1. For EFS, the CAPRA 6-10 subset was split by adding C/IDC. NCCN 4 and 5-6 were split, again with stronger effect in Group 2. Findings affirm the practical value of including C/IDC status in biopsy reporting.

## 770 Prevalence of Peripheral Basal Cells in Variably Sized Neoplastic Cribriform and Comedonecrosis Prostatic Lesions

Shuman Liu<sup>1</sup>, Miriam Velazquez<sup>1</sup>, Ryan Xiao<sup>2</sup>, Brian Ma<sup>3</sup>, Guang-Qian Xiao<sup>4</sup>

<sup>1</sup>Keck Hospital of USC, LAC+USC Medical Center, Los Angeles, CA, <sup>2</sup>Pasadena, CA, <sup>3</sup>LAC+USC Medical Center, Los Angeles, CA, <sup>4</sup>Keck School of Medicine of USC, Los Angeles, CA

**Disclosures:** Shuman Liu: None; Miriam Velazquez: None; Ryan Xiao: None; Brian Ma: None; Guang-Qian Xiao: None

**Background:** Since the pre-immunohistochemistry (IHC) era, it has been assumed that classic neoplastic/malignant cribriform and comedonecrosis (comedo) prostatic lesions are stroma invasive prostatic carcinoma (PC) and graded as Gleason 4 and 5, respectively. Compared to non-cribriform pattern 4 PC, cribriform PC has recently been shown to have a more aggressive behavior, and cribriform morphology has been recommended to be included in the pathology report. No study has been done to evaluate the prevalence of peripheral basal cells (BCs) in these neoplastic patterns.

**Design:** Classic neoplastic/malignant cribriform lesion is defined as cribriform glands lined with cytologic malignant cells spanning the lumen. In this study, cribriform was divided by size into small ( $\leq$ normal gland size), medium (1-3 times normal gland size) and large cribriform ( $\geq$ 3 times normal gland size). Cases accessioned in the past 3 years at our hospital, contained at least 20% cribriform/comedo of tumor volume with or without glomeruloid pattern and with triple antibody PIN cocktail IHC performed, were reviewed for the presence of peripheral BCs. A total of 48 such cases (38 prostatectomies, 10 biopsies) were retrieved.

**Results:** 38 cases contained small cribriforms, 39 contained medium-sized cribriforms, 23 contained large cribriforms and 18 had comedo. The number and % of cribriform/comedo cases with BCs only, no BCs at all, or mixtures of both with BCs and without BCs are summarized in Table 1. The locations of these lesions were variable. All 8 cases of glomeruloid PCa were absent of BCs.

# ABSTRACTS | GENITOURINARY PATHOLOGY (INCLUDING RENAL TUMORS)

	Small-sized cribriform (n=38)			Medium-sized cribriform (n=39)			Large-sized- cribriform (n=23)			Comedonecrosis (n=18)			Glomeruloid pattern (n=8)	
Total cases n= 48	Cases with BC only	Cases with no BC only	Cases with both BC & no BC	Cases with BC only	Cases with no BC only	Cases with both BC & no BC	Cases with BC only	Cases with no BC only	Cases with both BC & no BC	Cases with BC only	Cases with no BC only	Cases with both BC & no BC	Cases with BC only	Cases with no BC only
# and % of cases	2 (5%)	12 (32%)	24 (63%)	19 (49%)	3 (7%)	17 (44%)	9 (39%)	6 (26%)	8 (35%)	13 (72%)	0 (0%)	5 (28%)	0 (0%)	8 (100%)
Location	Varyably in PZ or C/TZ or mixed													

BC: Basal cells. PZ: peripheral zone, C/TZ: Central/transition zone

Figure 1 - 770

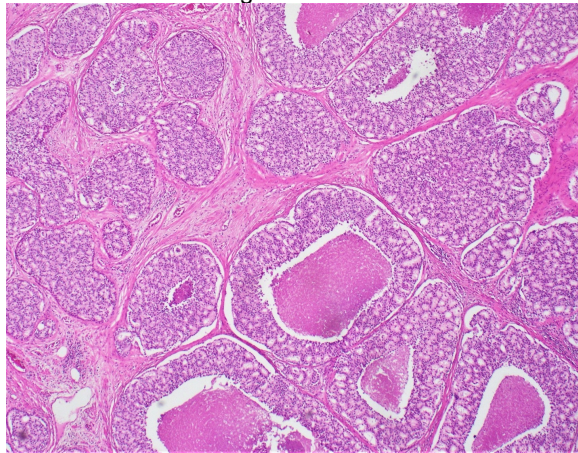
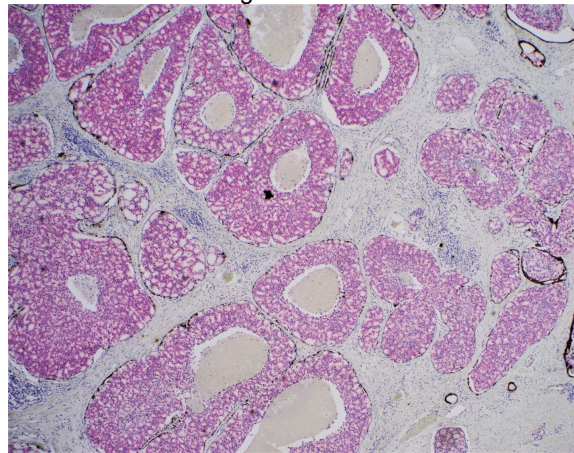


Figure 2 - 770



**Conclusions:** The study showed the neoplastic/malignant cribriform/comedo lesions oftentimes contained BCs and, strictly speaking, were not stroma invasive PC. Small cribriforms were more likely to be invasive. Comedo lesions mostly contained peripheral BCs and none of the cases showed pure stroma invasive comedo only (i.e., complete absence of basal cells in all the comedo), though they could represent either the precursor lesions of PC or intraductal carcinoma. The findings may infer that small and large cribriforms and comedo be derived/progressed from the medium-sized cribriforms, and, overtime, some may eventually lose their BCs. There seems to be no location difference in the distribution of variably sized cribriforms and comedo lesions. Glomeruloid pattern was always absent of BCs, stroma invasive and located in the peripheral zone. This suggests that glomeruloid PC may not be related to cribriform lesions.

## 771 SS18-SSX Expression And Clinicopathologic Profiles In a Contemporary Cohort of Primary Paratesticular Synovial Sarcoma: A Series of Eight Patients

Anandi Lobo<sup>1</sup>, Sayali Shinde<sup>2</sup>, Deepika Jain<sup>2</sup>, Shilpy Jha<sup>3</sup>, Mahmut Akgul<sup>4</sup>, Manas Baisakh<sup>5</sup>, Indranil Chakrabarti<sup>6</sup>, Seema Kaushal<sup>7</sup>, Subhasini Naik<sup>8</sup>, Niharika Pattnaik<sup>3</sup>, Abhishek Satapathy<sup>9</sup>, Sean Williamson<sup>10</sup>, Anil Parwani<sup>11</sup>, Mahul Amin<sup>12</sup>, Sambit Mohanty<sup>13</sup>

<sup>1</sup>Kapoor Centre of Urology and Pathology, Raipur, India, <sup>2</sup>Core Diagnostics, Gurgaon, India, <sup>3</sup>Advanced Medical and Research Institute, Bhubaneswar, India, <sup>4</sup>Albany Medical Center, Albany, NY, <sup>5</sup>Prolife Diagnostics, Bhubaneswar, India, <sup>6</sup>All India Institute of Medical Sciences, Kalyani, India, <sup>7</sup>All India Institute of Medical Sciences, New Delhi, India, <sup>8</sup>Prolife Diagnostics and Apollo Hospitals, Bhubaneswar, India, <sup>9</sup>AMRI Hospital, Bhubaneswar, India, <sup>10</sup>Cleveland Clinic, Cleveland, OH, <sup>11</sup>The Ohio State University Wexner Medical Center, Columbus, OH, <sup>12</sup>The University of Tennessee Health Science Center, Memphis, TN, <sup>13</sup>Advanced Medical and Research Institute, New Delhi, India

**Disclosures:** Anandi Lobo: None; Sayali Shinde: None; Deepika Jain: None; Shilpy Jha: None; Mahmut Akgul: None; Manas Baisakh: None; Indranil Chakrabarti: None; Seema Kaushal: None; Subhasini Naik: None; Niharika Pattnaik: None; Abhishek Satapathy: None; Sean Williamson: None; Anil Parwani: None; Mahul Amin: None; Sambit Mohanty: None

**Background:** Genitourinary sarcomas comprise less than 2.7% of all sarcomas. Synovial sarcoma (SS) is an extremely rare genitourinary malignant mesenchymal neoplasm with variable epithelial differentiation and a specific SS18::SSX 1/2 gene fusion. The paratesticular location of this neoplasm, is even more rare with only a single case reported in literature till date. Paratesticular region contains various structures, including the epididymis, tunical layers, spermatic cord, and the surrounding supportive fat, muscular, and ligamentous tissues. Patients usually have a poor outcome, with metastases to the lung and/or other sites. Herein, we describe the clinicopathologic and molecular findings of paratesticular SS in the largest case series to date and to the best of our knowledge, the only series to use novel SS18-SSX antibody for immunohistochemistry (IHC).

# ABSTRACTS | GENITOURINARY PATHOLOGY (INCLUDING RENAL TUMORS)

**Design:** Paratesticular SS cases were identified from the anatomic pathology files of the collaborating institutions. Clinicopathologic, IHC, molecular, treatment, and follow-up data were analysed.

**Results:** There were 8 patients, ranging from 15 years to 47 years (median 31 years) in age. The tumor size ranged from 4.0 cm to 15.0 cm. Grossly, the tumors were solid and homogeneous tan-white, (n=8); with spindle cell morphology (Figure 1). SS18-SSX IHC was positive in all tumors (diffuse, n=5; multifocal, n=2; focal, n=1). All tumors harbored SS18::SSX1 gene rearrangement (Figure 2). All 8 tumors exhibited TLE1 immunoreactivity. Other positive immunostains included were CD99 (n=8/8) and BCL2 (n =7/7). NKX2.2, BCOR, and STAT6 immunostains were negative in 7/7 tumors. Surgical radical orchiectomy resections with high ligation of the spermatic cord were done for all. Metastases to liver, lymph nodes, brain, and lung (n=1); liver and lungs (n=1); liver (n=1) was identified. Adjuvant chemotherapy history was available in 6/8 patients. Follow-up was available for 6 patients (range: 5 months to 24 months), 2 patients died of disease, and 4 patients are alive with no recurrence or metastasis.

Figure 1 - 771

Age/ Gend er	Laterality	Size (cm); testic ular involv ement	Cell type	Mitoses (2.5 sq. mm)	Necrosis (%)	LVI	Pathologi c stage	SS18- SSX IHC	TLE1 IHC	SS18 % of Break- apart FISH signals	Adjuvant Chemothe rapy	Follow up duration (months )	Metastasis at the last follow-up	Vital Status
23M	Right	15; No	Spindl e	23	Yes, 30%	Yes	pT <sub>2b</sub>	Diffuse; 80%	Diffuse; 75%	70%	Yes	6	Yes; liver	Alive
15M	Left	8; No	Spindl e	16	No	No	pT <sub>1</sub>	Diffuse; 90%	Diffuse; 90%	29%	Yes	11	None	Alive
25M	Left	10; No	Spindl e	10	No	No	pT <sub>3</sub>	Multifo cal; 60%	Diffuse; 90%	45%	Yes	5	Liver, lung, lymph nodes, and brain	Died
47M	Left	4; No	Spindl e	18	Yes, 20%	No	pT <sub>2a</sub>	Diffuse; 80%	Diffuse; 80%	85%	Unknown	Lost to follow up	Lost to follow up	Lost to follow up
33M	Left	7.5; Yes	Spindl e	20	Yes, 40%	Yes	pT <sub>3</sub>	Diffuse; 80%	Multifoc al; 50%	35%	Yes	13	Liver and lungs	Died
17M	Right	5; No	Spindl e	31	No	No	pT <sub>2b</sub>	Multifo cal; 70%	Diffuse; 75%	60%	Yes	24	Yes; lungs	Alive
29M	Left	11; No	Spindl e	20	Yes, 50%	Yes	pT <sub>1</sub>	Diffuse; 90%	Diffuse; 90%	50%	Unknown	Lost to follow up	Lost to follow up	Lost to follow up
41M	Right	9.5; No	Spindl e	11	Yes, 50%	No	pT <sub>2a</sub>	Focal; 40%	Diffuse; 80%	38%	Yes	5	None	Alive

Figure 2 - 771

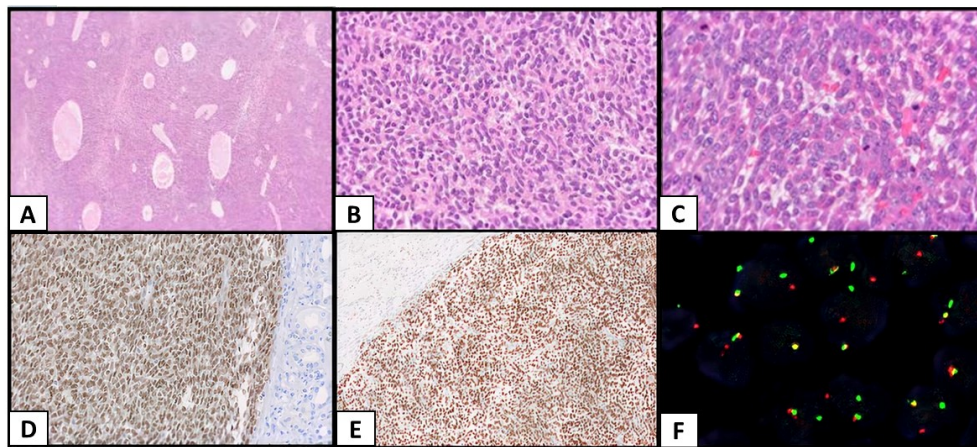


Figure 2. Primary Paratesticular Synovial Sarcoma A. Low power view of H&E-stained section showing a hypercellular spindle cell tumor with thin-walled vessels of rounded, elongated, and oval lumens; B. High power view of H&E-stained section showing plump, spindle cells with mild nuclear atypia and minimal to moderate cytoplasm; C. H&E-stained section of the tumor showing multiple mitotic figures. D. SS18-SSX IHC showing diffuse, strong nuclear staining of the tumor cells and negative staining of the adjacent uninvolved renal parenchyma; E. TLE1 IHC showing diffuse, strong nuclear staining of the tumor cells and negative staining of the adjacent uninvolved renal parenchyma; F. FISH showing red/orange and green signals with more than 2 signal diameters apart and isolated red/orange signal indicating SS18 gene rearrangement.

**Conclusions:** 1. Paratesticular SS is an extremely rare sarcoma of the paratestis with few reported contemporary case series; tumors have a poor prognosis with metastasis. 2. Patients with multiorgan metastasis have a more aggressive course and died due to disease. 3. SS18-SSX IHC shows excellent concordance with the FISH results, therefore may reliably be used as a molecular surrogate for paratesticular SS, particularly in a resource-limited setting.

## 772 Morphologic Review of the Cancer Genome Atlas Papillary Renal Cell Carcinoma Dataset

Taryme Lopez Diaz<sup>1</sup>, Dibson Gondim<sup>1</sup>

<sup>1</sup>University of Louisville, Louisville, KY

**Disclosures:** Taryme Lopez Diaz: None; Dibson Gondim: None

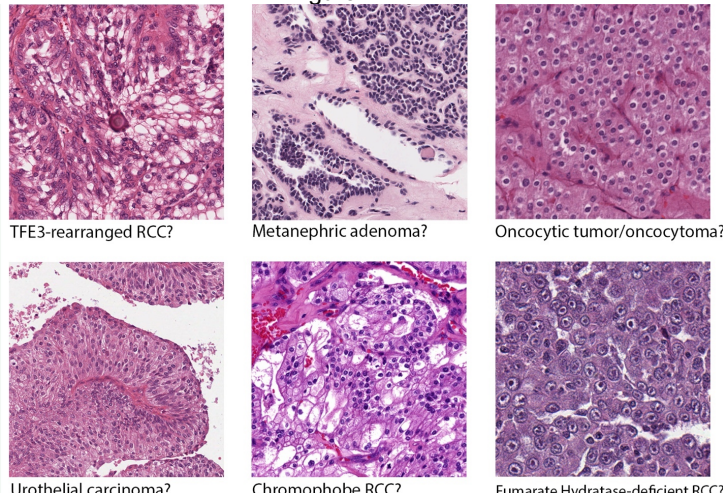
**Background:** Artificial intelligence (AI) is slowly but steadily being incorporated in the pathology practice. This was fueled by adoption of deep learning-based techniques, graphic processing units, and large-scale datasets. While the size of the datasets is extremely important, data accuracy is also essential. There is widespread use of whole slide images (WSI) from the Cancer Genome Atlas (TCGA) repository to build and/or assess the accuracy of AI-based models. We hypothesized the presence of potential diagnostic misclassifications in one of the TCGA's datasets. We conducted a morphologic review of the papillary renal cell carcinoma (RCC) dataset with documentation of microscopic findings, histology artifacts and identification of debatable diagnoses.

**Design:** All WSIs from permanent slides (300) of the papillary RCC dataset from the TCGA portal (<https://portal.gdc.cancer.gov/repository>) were reviewed by two pathologists. The following variables were documented: diagnosis, morphology consistency, architecture(s), percentage of solid areas, cytoplasm color and amount, necrosis, presence of foamy histiocytes within tumor stalks, hemosiderin inclusions, intratumoral blood, intratubular mucin, calcifications, non-tumoral elements in WSIs, and types of artifacts.

**Results:** 16/300 WSIs were found to have potential diagnostic discrepancies – TFE3-rearranged RCC (1 WSI), papillary renal neoplasm with reverse polarity (4), metanephric adenoma (3), chromophobe RCC (2), urothelial carcinoma (2), fumarate hydratase-deficient RCC (3), and an oncocytic tumor/oncocytoma (1). See Figure 1 for examples. Other significant findings were WSIs with no tumor (1), necrosis in >99% of tissue (3), tumor in less than 1% of tissue (1), WSIs of immunostains only (3). See Table for summary of morphologic findings and artifacts.

Microscopic Findings/Artifacts	Number of WSIs
Papillary Architecture	218
Papillary & Solid Architecture	50
Cytoplasm, Eosinophilic	199
Cytoplasm, Basophilic	47
Cytoplasm, Clear	3
Cytoplasm, Mixed	40
Foamy Histiocytes within Stalks	172
Hemosiderin Inclusions	104
Intratubular Mucin	24
Tumor Only	193
Calcifications	29
Artifacts	38

Figure 1 - 772



Examples of potential misclassified cases in the TCGA papillary renal cell carcinoma (RCC) dataset.  
Exclusion of cases with questionable diagnosis or additional work-up should be considered.

**Conclusions:** Multiple WSIs with questionable diagnosis were found. Raising awareness about these WSIs would give researchers the opportunity to exclude them from some types of AI-model creation/data analysis workflows. Publication of morphologic findings and artifacts would enable subgroup analysis on the WSI-level. Dataset data accuracy is paramount for AI development. Therefore, morphologic review of public open-source datasets could minimize introduction of systemic errors in the literature.

## 773 Characterization of L1 Cell Adhesion Molecule (L1CAM), a Nephronal Principal cell Marker, as a Diagnostic and Lineage Specific Marker for Nephrogenic Adenoma

Rahul Mannan<sup>1</sup>, Anya Chinnaiyan<sup>2</sup>, Xiaoming (Mindy) Wang<sup>2</sup>, Yuping Zhang<sup>3</sup>, Sylvia Zelenka-Wang<sup>3</sup>, Lisa McMurry<sup>3</sup>, Xuhong Cao<sup>2</sup>, Fengyun Su<sup>2</sup>, Rui Wang<sup>2</sup>, Saravana Dhanasekaran<sup>2</sup>, Arul Chinnaiyan<sup>2</sup>, Rohit Mehra<sup>2</sup>

<sup>1</sup>Michigan Medicine, University of Michigan, Ann Arbor, MI, <sup>2</sup>University of Michigan, Ann Arbor, MI, <sup>3</sup>Michigan Center for Translational Pathology, Ann Arbor, MI

**Disclosures:** Rahul Mannan: None; Anya Chinnaiyan: None; Xiaoming (Mindy) Wang: None; Yuping Zhang: None; Sylvia Zelenka-Wang: None; Lisa McMurry: None; Xuhong Cao: None; Fengyun Su: None; Rui Wang: None; Saravana Dhanasekaran: None; Arul Chinnaiyan: None; Rohit Mehra: None

**Background:** Nephrogenic adenoma (NA) is a benign proliferative lesion seen in the urinary bladder and other genitourinary sites. Its varied morphology (papillary, tubular, and signet ring cell) frequently causes diagnostic dilemmas in histology as both urothelial and prostatic carcinoma are the differential diagnoses. The literature cites renal tubular epithelial cell origin for NA despite its predominant lower genitourinary tract localization. The current diagnostic immunohistochemical (IHC) biomarkers: PAX-2, PAX-8, and GATA3 used contextually neither address the lineage specificity nor describe the specific cell(s) of origin for NA. Hence refining biomarkers for NA is an unmet clinical need that we explore in this study.

**Design:** Our recent single-cell sequencing study (PMID: 34099557) nominated lineage-specific markers for renal distal tubular (DCT) epithelial cells including L1CAM -for principal cells and, FOXI1/LINC01187- for intercalated cells of the kidney. To characterize the exact cellular lineage for NA, we performed a comprehensive evaluation of these markers. GATA3 was also interrogated since it is known to be enriched in DCT and collecting duct epithelium. A specialized tissue cohort comprising 12 NA, 10 benign urothelial, 5 benign prostates, 5 prostatic, and 2 urothelial carcinomas was interrogated for L1CAM, GATA3, and FOXI1 IHC and LINC01187 RNA in situ hybridization.

**Results:** L1CAM was positive in all (12/12; 100%) NA with uniform diffuse strong to moderate membranous expression (average product score=203.6; and a range of 140 to 268), devoid of any intra-lesional heterogeneity. (Table-1 and Figure-1) Additionally, L1CAM showed no expression in either benign or malignant urothelial/prostatic samples. GATA3 expression was patchy and focal and seen in 7/12 (58.3%) NA cases and was expressed in 100% benign and malignant urothelium and prostate tissues (basal cells). Interestingly, the other predominant DCT intercalated cell-specific markers, FOXI1 and LINC01187, were found to be negative.

Table-1 Clinicopathological details of Nephrogenic Adenoma Cases

Case No.	Morphology	Age	Gender	Site	L1CAM Score
1	Papillary	48	M	Urinary Bladder	225
2	Tubular	64	M	Urinary Bladder	152
3	Papillary and tubular	78	M	Urinary Bladder	253
4	Papillary	61	F	Urinary Bladder	215
5	Tubular	66	M	Urethra	250
6	Papillary	69	M	Urinary bladder	180
7	Papillary tubular	63	M	Prostate	165
8	Papillary	48	M	Urinary Bladder	140
9	Tubular	76	M	Urinary Bladder	140
10	Tubular	66	F	Urethra	268
11	Tubular	62	M	Urinary Bladder	255
12	Papillary and tubular	53	F	Urinary Bladder	150

Figure 1 - 773

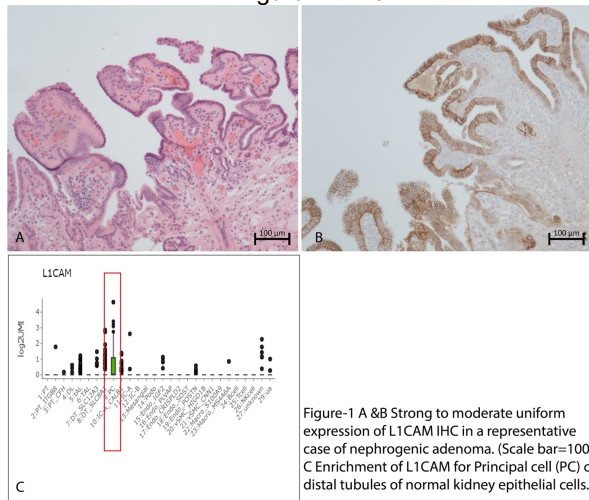


Figure-1 A & B Strong to moderate uniform expression of L1CAM IHC in a representative case of nephrogenic adenoma. (Scale bar=100um).  
C Enrichment of L1CAM for Principal cell (PC) of distal tubules of normal kidney epithelial cells.

**Conclusions:** L1CAM, a marker for principal cells of the DCT, was uniformly expressed in NA, and negative in other relevant tissues (including prostatic and urothelial adenocarcinoma). The absence of intercalated cell markers (FOXI1/LINC01187) in NA provides additional evidence that the principal cells of DCT (and not intercalated cells) are a putative cell of origin for NA. Based on these findings, we demonstrate L1CAM as a potential diagnostic and lineage-specific biomarker for NA.

#### 774 ABCC2 as a Prognostic Biomarker in Papillary Renal Cell Carcinoma: A Large, Multi-institutional Study of 254 Cases

Mehdi Masoomian<sup>1</sup>, Vincent Francis Castillo<sup>2</sup>, Kiril Trpkov<sup>3</sup>, Michelle Downes<sup>4</sup>, Fadi Brimo<sup>5</sup>, Theodorus Van Der Kwast<sup>6</sup>, Abraam Zakhary<sup>2</sup>, Fabio Rotondo<sup>7</sup>, Wondwossen Kidanewold<sup>7</sup>, Gina Saad<sup>8</sup>, Vy-nhan nguyen<sup>1</sup>, Catherine Streutker<sup>7</sup>, Corwyn Rowsell<sup>9</sup>, Rola Saleeb<sup>2</sup>

<sup>1</sup>University of Toronto, Toronto, ON, <sup>2</sup>St. Michael's Hospital/University of Toronto, Toronto, ON, <sup>3</sup>University of Calgary, Calgary, AB, <sup>4</sup>Sunnybrook Health Sciences Centre, Toronto, ON, <sup>5</sup>McGill University, Montréal, QC, <sup>6</sup>University Health Network, Toronto, ON, <sup>7</sup>Unity Health Toronto, Toronto, ON, <sup>8</sup>St. George's University, West Indies, Grenada, <sup>9</sup>St. Michael's Hospital, Toronto, ON

**Disclosures:** Mehdi Masoomian: None; Vincent Francis Castillo: None; Kiril Trpkov: None; Michelle Downes: None; Fadi Brimo: None; Theodorus Van Der Kwast: None; Abraam Zakhary: None; Fabio Rotondo: None; Wondwossen Kidanewold: None; Gina Saad: None; Vy-nhan nguyen: None; Catherine Streutker: None; Corwyn Rowsell: None; Rola Saleeb: None

**Background:** Subtyping of papillary renal cell carcinoma (PRCC) is not recommended in the 2022 WHO classification. Currently, WHO/ISUP nuclear grade is the only prognostic marker for PRCC. ABCC2 is a transporter protein that localizes to the apical cell membranes of the proximal renal tubules. ABCC2 expression by immunohistochemistry (IHC) has been shown to significantly predict outcome in PRCC (*Hum. Pathol.* 2022; 120: 57-70). In this study, we assess the prognostic significance of ABCC2 IHC staining patterns with correlation to the ABCC2 in situ transcript levels in a large multi-institutional PRCC cohort, and with focus on tumors of small size (pT1a; ≤4 cm).

**Design:** A cohort comprising 254 PRCCs was collected from 6 institutions, along with corresponding clinicopathologic data. TMAs were constructed for 211 cases, and 43 cases were evaluated as whole slides. PRCC cases were stained for ABCC2 by IHC, and the results were stratified into: negative, cytoplasmic, brush border (BB) <50%, and BB ≥50%. RNA in-situ hybridization (ISH) for ABCC2 was performed in 65 cases. ISH slides were assessed quantitatively using the HALO™ software system. Statistical analysis was performed using GraphPad and SPSS software.

**Results:** The distribution of ABCC2 IHC patterns was as follows: 77 (30%) negative, 72 (28%) cytoplasmic, 63 (25%) BB <50%, and 42 (17%) BB ≥50% (Figure 1). ABCC2 BB staining was associated with a significant increase in the RNA transcript levels, as compared to the negative/cytoplasmic group ( $p=0.0337$ ). Higher ABCC2 expression (IHC BB patterns) was associated with worse disease free survival (DFS) on univariate analysis ( $p=0.0002$ ) (Figure 2). Conversely, WHO/ISUP grade did not show a significant association with DFS ( $p=0.309$ ) on univariate analysis. ABCC2 BB staining was also useful in stratifying the DFS in pT1a (≤4 cm) cases,  $n=120$  ( $p=0.0002$ ), while WHO/ISUP grade was not ( $p=0.324$ ). Cox regression analysis adjusted for age, stage, grade and tumor size showed that only ABCC2 IHC patterns ( $p=0.003$ ) and stage ( $p<0.001$ ) had a DFS prognostic significance.

Figure 1 - 774

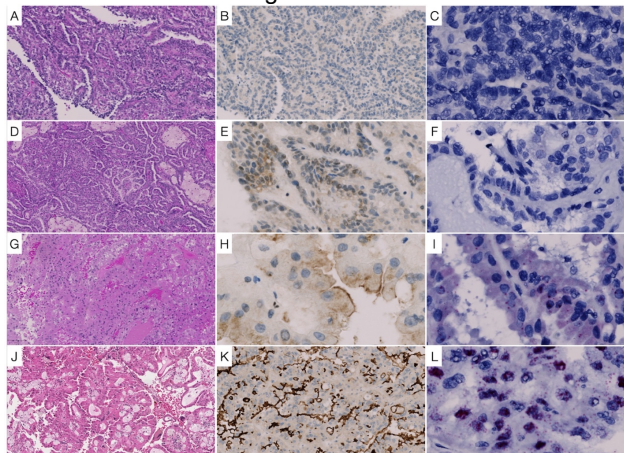


Figure 1: Representative microscopic images of the following: A-C) PRCC with negative ABCC2 staining with corresponding RNA-ISH; D-F) PRCC with cytoplasmic staining with corresponding RNA-ISH; G-H) PRCC with brush border <50% staining with corresponding RNA-ISH; I-L) PRCC with brush border ≥50% staining with corresponding RNA-ISH

Figure 2 - 774

### DFS of ABCC2 IHC Staining Patterns n = 254

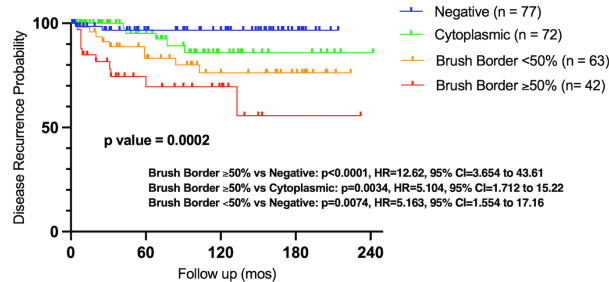


Figure 1: Univariate disease-free survival analysis of ABCC2 IHC staining patterns using log-rank test

**Conclusions:** ABCC2 BB expression by IHC in PRCC correlates with significantly higher gene expression. ABCC2 was also significant in predicting survival outcomes for PRCC on both univariate and multivariate analysis, and provided better prognostic stratification than the WHO/ISUP grade. Importantly, ABCC2 was useful for prognostic separation of small PRCC tumors ( $\leq 4$  cm), which may guide active surveillance decisions in that group.

## 775 The Importance of Recognizing Somatic FH-Deficient Renal Cell Carcinoma

Maria Merino<sup>1</sup>, Christopher Ricketts<sup>2</sup>, W Linehan<sup>3</sup>, Ramaprasad Srinivasan<sup>3</sup>

<sup>1</sup>National Cancer Institute, Bethesda, MD, <sup>2</sup>Center for Cancer Research, National Cancer Institute, MD, <sup>3</sup>National Institutes of Health, Bethesda, MD

**Disclosures:** Maria Merino: None; Christopher Ricketts: None; W Linehan: None; Ramaprasad Srinivasan: None

**Background:** Hereditary leiomyomatosis and renal cell cancer (HLRCC) is a hereditary cancer syndrome where affected individuals are predisposed to the development of leiomyomas in skin and uterus and aggressive forms of kidney cancer. Affected individuals harbor germline pathogenic mutations of the fumarate hydratase(FH) gene and tumors demonstrate loss of function of FH. Somatic FH-deficient RCC with somatic mutational inactivation of FH is not well recognized or described, which may lead to misdiagnosis that have great impact in the treatment of the patients. Herein, we report the clinical, morphological, and genetic findings of 7 patients with Somatic FH-deficient RCC

**Design:** All patients had metastatic RCC disease when accepted on an IRB approved UOB/NCI protocol. Patients (4 males, 3 females) ranged in age from 27 to 77 and all denied family history of RCC, skin lesions or uterine leiomyomas. Clinical, morphological evaluation, IHC for FH and 2SC and Germline genetic testing was performed in all cases.

**Results:** The tumors varied in size (4-10cm). The predominant morphologic pattern of the RCCs was extensive tubular formation with small tubules lined by cells with eosinophilic cytoplasm and the characteristic nuclear features of HLRCC (large prominent nucleous with orangophilic nucleoli and perinucleolar halos). Other tumors showed papillary formation and in two cases a cystic

# ABSTRACTS | GENITOURINARY PATHOLOGY (INCLUDING RENAL TUMORS)

component was also present. The IHC staining for FH was negative confirming the non functional FH protein and 2SC was diffusely and strongly positive. However, none of the patients gave clinical history consistent with HLRCC. Germline genetic testing was negative in all patients, but each tumor demonstrated pathogenic somatic mutations/alterations of FH, including point mutation, homozygous deletion of 1q43, multiple break points on chromosome 1, and loss of heterozygosity.

**Conclusions:** Pathologists need to be aware that Somatic FH-deficient RCC that lack FH germline mutation can occur and have an aggressive behavior. Affected patients deny clinical features or family history usually associated with HLRCC syndrome. Morphology and IHC are the key tools in highlighting this potential diagnosis. Any high grade tumor with morphologic features similar to HLRCC and negative FH staining should raise suspicion and patients should be evaluated for both germline and somatic FH mutation to ensure proper diagnosis and that patients receive the correct targeted therapy for these highly malignant tumors.

## 776 A Retrospective Study of Patients with Advanced Urothelial Carcinoma Treated with Immunotherapy with Molecular and Imaging Mass Cytometry Insights

Jeremy Miyauchi<sup>1</sup>, Ahmed Elsaeed<sup>1</sup>, Hiranmayi Ravichandran<sup>2</sup>, Andre Rendeiro<sup>1</sup>, Hussein Alnajar<sup>3</sup>, Michael Sigouros<sup>1</sup>, Jyothi Manohar<sup>1</sup>, Andrea Sboner<sup>1</sup>, Olivier Elemento<sup>1</sup>, Juan Miguel Mosquera<sup>1</sup>

<sup>1</sup>Weill Cornell Medicine, New York, NY, <sup>2</sup>New York-Presbyterian/Weill Cornell Medical Center, New York, NJ, <sup>3</sup>NorthShore University HealthSystem, Evanston, IL

**Disclosures:** Jeremy Miyauchi: None; Ahmed Elsaeed: None; Hiranmayi Ravichandran: None; Andre Rendeiro: None; Hussein Alnajar: None; Michael Sigouros: None; Jyothi Manohar: None; Andrea Sboner: None; Olivier Elemento: None; Juan Miguel Mosquera: None

**Background:** Bladder cancer accounts for more than 80,000 new cancer diagnoses and 17,000 deaths per year in the United States. Muscle invasive cancer portends a poor prognosis with high morbidity and mortality. In patients with metastatic disease, particularly those who cannot tolerate chemotherapy, immunotherapy is an approved and sometimes highly successful treatment option. However, certain patients have little to no therapeutic response and ongoing work is necessary to understand why.

**Design:** A retrospective search of patients with advanced stage or metastatic bladder cancer was performed in our case database from 2012 to 2019. A retrospective chart and cBioPortal review was performed and 43 cases with sufficient clinical follow up were identified and reviewed. For two cases, imaging mass cytometry was performed to characterize immune cell populations in the tumors.

**Results:** Of the 43 cases identified, 33 had molecular analysis of their tumors performed with 17 having whole exome sequencing. 22 patients had long term progression free survival. Furthermore, 22 patients were identified that had documented treatment with immunotherapy targeting either PD-1, PDL-1, or CTLA-4. Of this cohort, 8 of 22 of these patients had sustained response to immunotherapy without radiological or pathologic evidence of recurrence. One of these cases had a PDL-1 CPS score <1 although demonstrated mismatch repair deficiency. There was no significant difference between patients who responded to therapy and those who did not in terms of sex, age, history of tobacco use, stage, positive nodal status, positive margins, or angiolympathic invasion at resection. A significant difference was seen in that the patients who responded to immunotherapy had not received neoadjuvant chemotherapy ( $p=0.0419$ ). No significant differences in mutations associated with better patient outcomes were seen although 3 of 3 patients with FGFR3 mutations had poor outcomes. Imaging mass cytometry revealed an inflamed phenotype in one of the patients with sustained immunotherapy response.

Figure 1 - 776

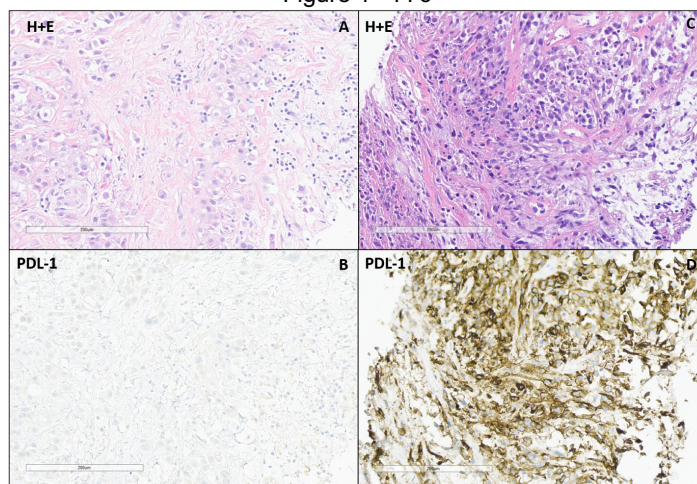
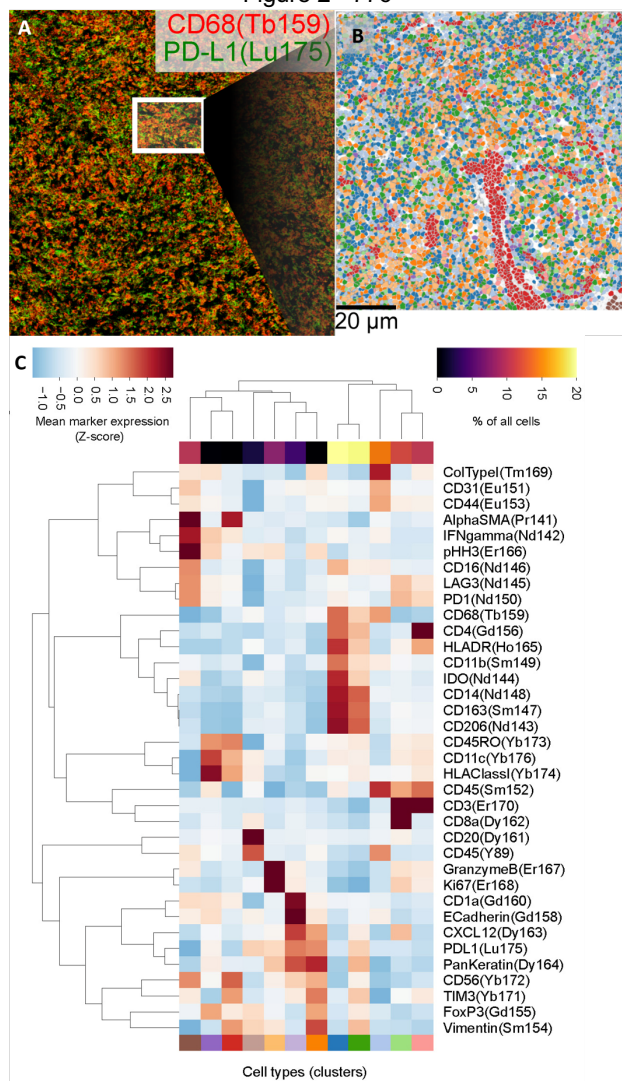


Figure 2 - 776



**Conclusions:** While no significant differences in genomic phenotypes seem to be associated with outcome in sustained response to immunotherapy from these data, imaging mass cytometry may demonstrate clues to tumor microenvironmental differences which predict therapeutic response. Further work is required to elucidate which patients will have the best therapeutic response to immunotherapy in order to provide them with the most successful personalized care.

## 777 Comprehensive Molecular Profiling of a Series of Unclassified Low Grade Oncocytic Renal Epithelial Neoplasms (ULGOREN)

Sambit Mohanty<sup>1</sup>, Tiffany Lee<sup>2</sup>, Aditi Aggarwal<sup>3</sup>, Sean Williamson<sup>4</sup>, Manju Aron<sup>5</sup>, Anil Parwani<sup>6</sup>, Seema Kaushal<sup>7</sup>, Liang Cheng<sup>8</sup>, Katherine Scribner<sup>9</sup>, Shivani Kandukuri<sup>10</sup>

<sup>1</sup>Advanced Medical and Research Institute, New Delhi, India, <sup>2</sup>University of Southern California, Keck School of Medicine of USC, LAC+USC Medical Center, Los Angeles, CA, <sup>3</sup>Core Diagnostics, Gurgaon, India, <sup>4</sup>Cleveland Clinic, Cleveland, OH, <sup>5</sup>Keck School of Medicine of USC, Los Angeles, CA, <sup>6</sup>The Ohio State University Wexner Medical Center, Columbus, OH, <sup>7</sup>All India Institute of Medical Sciences, New Delhi, India, <sup>8</sup>Alpert Medical School of Brown University, Providence, RI, <sup>9</sup>LAC+USC Medical Center/Keck Medicine of USC, Los Angeles, CA, <sup>10</sup>University of Southern California, Keck School of Medicine of USC, Los Angeles, CA

**Disclosures:** Sambit Mohanty: None; Tiffany Lee: None; Aditi Aggarwal: None; Sean Williamson: None; Manju Aron: None; Anil Parwani: None; Seema Kaushal: None; Liang Cheng: None; Katherine Scribner: None; Shivani Kandukuri: None

**Background:** ULGOREN of the kidney are a challenging subset of tumors. Despite the emergence of newer entities there is a group of oncocytic renal tumors that ultimately remain unclassified.

# ABSTRACTS | GENITOURINARY PATHOLOGY (INCLUDING RENAL TUMORS)

**Design:** This multi-institutional study aims to investigate ULGOREN. Along with evaluation of histologic features, immunostains (IHC) Keratin 7, Keratin 20, CD 117, SDHB, FH/2SC, ALK-1, GATA3 and MIB-1 were performed to exclude an oncocytoma, chromophobe RCC (ChRCC), eosinophilic solid and cystic RCC (ESC RCC), low grade oncocytic tumors (LOT), SDH-deficient RCC (SDH RCC), low grade FH-deficient RCC (FHD RCC) and ALK-1 rearranged RCC (ALK RCC). Molecular evaluation using a targeted NGS-based panel to detect small nucleotide variants/substitutions, small indels (insertions and/or deletions), and copy number variations in 324 cancer associated genes (including genes involved in PI3K/AKT/MTOR pathway) was performed on the Illumina® HiSeq 4000 platform. Molecular analysis was performed on fourteen tumors.

**Results:** The results are in table 1. There were fourteen patients ranging from 35-68 yrs in age. A majority of the tumors showed no capsule with a well circumscribed architecture. The mixed histologic features consisted of compact and nested (LOT-like), microcystic, tubular, trabeculated, sheets of tumor cells with ChRCC-like areas, as well as areas with fibromyxoid stroma that are oncocytoma-like. The nuclear grades were ISUP/WHO 2 (*n*=11) and 3 (*n*=3). The Keratin 7 and CD117 staining patterns are summarized in the table. MIB-1 index was low (2-5%). No necrosis, rhabdoid or sarcomatoid features were present. All other IHC (SDHB+ FH+/2SC- ALK1- Keratin 20-GATA3+/-) did not support other entities. Therefore, this subset was termed as ULGOREN. Genomic analyses revealed alterations in the TSC/MTOR pathway. Mutations were as follows: *TSC2* (6), *PIK3CA* (4), *MTOR* (3), *FOX1*(3), *TSC1* (2), *PTEN*(1) and *NF2*(1). The types of mutations were nonsense, missense, splice acceptor, splice donor, frameshift and synonymous.

**Table 1. Clinical, histomorphological, immunohistochemical and molecular features of Unclassified Low Grade Oncocytic Renal Epithelial Neoplasms (ULGOREN).**

Patient #	Histopathologic features WHO/ISUP nuclear grade	CK 7	CD117	Stage	Follow up	Gene Symbol	Variant annotation (cDNA)	Variant annotation (p.)	Pathogenic role	Variant type	Molecular consequence	VAF
1	Unencapsulated and well-circumscribed; Mixed oncocytoma and LOT histology; ISUP/WHO grade 3 nuclei	Strong, focal (upto <5%)	Weak, focal (10%)	pT1b	Alive with NED 48 months	<i>TSC2</i>	c.358A>T	p.Arg120Ter	Pathogenic	Single nucleotide variant	Nonsense	25%
						<i>PIK3CA</i>	c.241G>A	p.Glu81Lys	Pathogenic	Single nucleotide variant	Missense	14%
2	Unencapsulated and well-circumscribed; Mixed oncocytoma and LOT histology; ISUP/WHO grade 3 nuclei	Strong, focal (upto 5%)	Weak, focal (10%)	pT1a	Alive with NED 6 months	<i>PIK3CA</i>	c.248T>C	p.Phe83Ser	Pathogenic	Single nucleotide variant	Missense	50.80%
3	Unencapsulated and well-circumscribed; Predominantly oncocytoma-like IHC and morphology of ChRCC; ISUP/WHO grade 2 nuclei; Renal vein involvement was present	Negative	Weak, focal (20%)	pT3a	LTF	<i>mTOR</i>	c.7500T>G	p.Ile2500Met	Likely pathogenic	Single nucleotide variant	Missense	40%
						<i>TSC1</i>	c.2866C>T	p.Gln992ThrfsTer17	Pathogenic	Single nucleotide variant	Nonsense	23%
4	Unencapsulated and poorly circumscribed; Mixed oncocytoma and LOT histology and degenerative atypia; ISUP/WHO grade 2 nuclei	Strong, focal (upto 5-10%)	Weak, focal (20%)	pT1a	Alive with NED 7 months	<i>TSC2</i>	c.1717-1G>C	p.Arg1174GlyfsTer17	VUS	Single nucleotide variant	Splice acceptor	61%
						<i>FOX1</i>	c.1112A>C	p.Tyr371Ser	VUS	Single nucleotide variant	Missense	29%
5	Unencapsulated and roughly well circumscribed; Mixed ChRCC and oncocytoma with acinar or pseudo-glandular features with rare foci of degenerative atypia; ISUP/WHO grade 2 nuclei	Strong, focal (upto 5-10%)	Weak, focal (upto 5%)	pT1a	Alive with NED 6 months	<i>MTOR</i>	c.3352A>G	p.Ile1118Val	Benign/Likely benign	Single nucleotide variant	Missense	47.20%
						<i>TSC2</i>	c.2972dup	p.Gln992fs	Pathogenic	Duplication	Frameshift	23.50%
6	Unencapsulated and well-circumscribed; Mixed oncocytoma and LOT histology; ISUP/WHO grade 2 nuclei	Strong, focal (upto 5-10%)	Negative	pT1a	Alive with NED 60 months	<i>TSC2</i>	c.3520del	p.Arg1174fs	Pathogenic	Deletion	Frameshift	41.70%
7	Unencapsulated and well-circumscribed; Predominantly like LOT with a few foci of ChRCC-like perineurial clearing, however, nuclear envelope is smooth; ISUP/WHO grade 2 nuclei	Negative	Negative	pT1b	Alive with NED 7 months	<i>FOX1</i>	c.92A>G	p.Tyr31Cys	Likely Pathogenic	Single nucleotide variant	Missense	21.90%
8	Unencapsulated and well-circumscribed; like oncocytoma on a core biopsy but did not stain like one either on the biopsy or on the resection; ISUP/WHO grade 2 nuclei	Negative	Weak, focal (upto 5-10%)	pT1a	LTF	<i>TSC2</i>	c.358A>T	p.Arg120Ter	Pathogenic	Single nucleotide variant	Nonsense	48%
						<i>MTOR</i>	c.5930C>A	p.Thr1977Lys	Pathogenic	Single nucleotide variant	Missense	57%
9	Unencapsulated and well-circumscribed; LOT-like sheet and compact nested architecture with many foci and wrinkling of the nuclear membrane associated with perinuclear clearing; ISUP/WHO grade 2 nuclei	Negative	Negative	pT1a	Alive with NED 43 months	<i>PIK3CA</i>	c.2758A>G	p.Asn920Asp	Likely Pathogenic	Single nucleotide variant	Missense	20%
10	Unencapsulated and well-circumscribed; appeared exactly like classical LOT, but did not stain like one; ISUP/WHO grade 2 nuclei	Negative	Negative	pT1a	LTF	<i>TSC1</i>	c.363+2_363+5d <del>el</del>	p.?	Likely pathogenic	Deletion	Splice donor	
11	Biopsy had oncocytoma-like feature; Resection revealed mass that was unencapsulated and well-circumscribed; had mixed areas: oncocytoma-like, compact nest of LOT, Ch RCC-like nuclear change; ISUP/WHO grade 2 nuclei; ISUP/WHO grade 2 nuclei; renal sinus fat is involved;	Strong, focal (upto 5-10%)	Negative	pT3a	Alive with NED 19 months	<i>FOX1</i>	c.468C>T	p.Asn156=	Likely benign	Single nucleotide variant	Synonymous	45%
12	Unencapsulated and well-circumscribed; Focal papillary area admixed with solid sheets; rare compressed tubules; subtle nuclear vacuolization; ChRCC-like areas were prominent; ISUP/WHO grade 3 nuclei	Strong, focal (upto 5-10%)	Weak, focal (<5%)	pT2	Alive with NED 22 months	<i>TSC2</i>	c.226-2A>G	p.?	Pathogenic	Single nucleotide variant	Splice acceptor	43.70%
						<i>PTEN</i>	c.898del	p.Ile300SerfsTer7	Likely pathogenic	Deletion	Frameshift	
13	Unencapsulated and well-circumscribed; Hybrid features of Oncocytoma and ChRCC but did not appear like a LOT; ISUP/WHO grade 2 nuclei	Negative	Negative	pT1a	LTF	<i>PIK3CA</i>	c.241G>A	p.Glu81Lys	Pathogenic	Single nucleotide variant	Missense	65.80%
14	Unencapsulated and well-circumscribed; Appeared like classical LOT, but did not stain like one; ISUP/WHO grade 2 nuclei	Negative	Weak, focal (<5%)	pT1a	LTF	<i>NF2</i>	c.1387G>A	p.Glu463Lys	Likely benign/Uncertain significance	Single nucleotide variant	Missense	34%

Ch RCC: Chromophobe RCC; NED: No evidence of disease; LTF: Lost to follow up

Figure 1 - 777

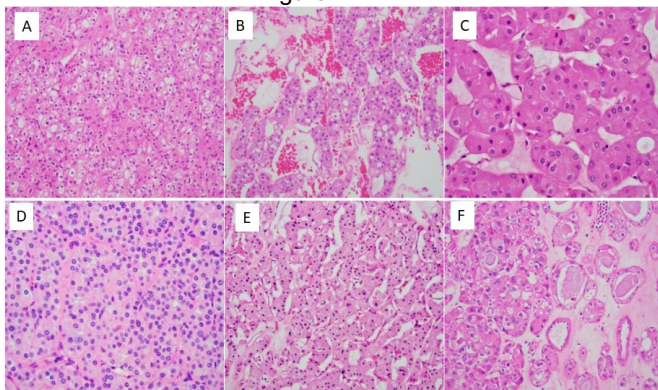


Figure 1. A. LOT-like areas. B. Nests of tumor cells separated by fibromyxoid stroma. C. Tumor cells in a trabeculated pattern with hemorrhage. D. Compact nests of tumor cells. E. Eosinophilic tumor cells with slit-like space. F. Nests and tubules of tumor cells separate by a fibromyxoid stroma.

Figure 2 - 777

GENES	PATIENTS													
	1	2	3	4	5	6	7	8	9	10	11	12	13	14
TSC1														
TSC2														
MTOR														
PIK3CA														
NF2														
FOXI1														
PTEN														

Frameshift Mutation
Non-Frameshift Mutation
Missense Gain of Function Mutation
Missense Loss of Function Mutation
Splice site deleterious mutation
Nonsense Mutation
VUS
Conflicting (Benign/VUS)
Likely Benign/Benign

**Conclusions:** ULGOREN harbors frequent alterations in the TSC/MTOR pathway, thus expanding the morphologic spectrum of low grade oncocytic neoplasms to include such tumors with heterogenous histomorphology without diffuse Keratin 7 staining. It is critical to perform Keratin 7 and CD117 among other immunostains listed above. Given the commonality of involvement of TSC/MTOR pathway in LOT's as well as ULGOREN as described above, the morphologic spectrum of LOT could be expanded to include such tumors.

## 778 ELOC-Mutated Renal Cell Carcinoma: A Comprehensive Clinicopathologic and Molecular Characterization in a Series of Eleven Patients

Sambit Mohanty<sup>1</sup>, Anandi Lobo<sup>2</sup>, Shilpy Jha<sup>3</sup>, Aditi Aggarwal<sup>4</sup>, Divyangi Paralkar<sup>5</sup>, Divya Midha<sup>6</sup>, Seema Kaushal<sup>7</sup>, Deepika Jain<sup>8</sup>, Mahmut Akgul<sup>9</sup>, Manas Baisakh<sup>10</sup>, Niharika Pattnaik<sup>3</sup>, Sourav Mishra<sup>3</sup>, Sean Williamson<sup>11</sup>, Anil Parwani<sup>12</sup>, Sunil Jaiswal<sup>13</sup>, Mahul Amin<sup>14</sup>

<sup>1</sup>Advanced Medical and Research Institute, New Delhi, India, <sup>2</sup>Kapoor Centre of Urology and Pathology, Raipur, India, <sup>3</sup>Advanced Medical and Research Institute, Bhubaneswar, India, <sup>4</sup>Core Diagnostics, Gurgaon, India, <sup>5</sup>University of Southern California, Keck School of Medicine of USC, Los Angeles, CA, <sup>6</sup>Tata Medical Center, Kolkata, India, <sup>7</sup>All India Institute of Medical Sciences, New Delhi, India, <sup>8</sup>Core Diagnostics, Gurugram, India, <sup>9</sup>Albany Medical Center, Albany, NY, <sup>10</sup>Prolife Diagnostics, Bhubaneswar, India, <sup>11</sup>Cleveland Clinic, Cleveland, OH, <sup>12</sup>The Ohio State University Wexner Medical Center, Columbus, OH, <sup>13</sup>Apollo Hospitals, Bhubaneswar, India, <sup>14</sup>The University of Tennessee Health Science Center, Memphis, TN

**Disclosures:** Sambit Mohanty: None; Anandi Lobo: None; Shilpy Jha: None; Aditi Aggarwal: None; Divyangi Paralkar: None; Divya Midha: None; Seema Kaushal: None; Deepika Jain: None; Mahmut Akgul: None; Manas Baisakh: None; Niharika Pattnaik: None; Sourav Mishra: None; Sean Williamson: None; Anil Parwani: None; Sunil Jaiswal: None; Mahul Amin: None

**Background:** ELOC (formerly TCEB1)-mutated renal cell carcinoma (ELOC-RCC) is a recently renamed molecularly defined RCC that harbors mutation in the elongin C(ELOC) gene at 8q21.11. These tumors are characterized by a nodular appearing low-grade clear cell neoplasm arranged in nests and tubules with prominent thick transecting smooth muscle and fibrous stroma and a distinct molecular signature.

**Design:** Because of the rarity of this tumor, we performed a multi-institutional study to comprehend the overarching clinicopathologic, immunohistochemical (IHC), and molecular features of 11 patients with ELOC-mutated RCC (defined by morphological features and somatic ELOC mutation).

**Results:** The patients' age ranged from 31-54 years (mean=41 years) with M:F::1:1.8. All patients presented with a solitary renal mass. None had family history or features of tuberous sclerosis(TS). All patients had pT1 disease(size range=1-3.8cm). The tumors showed classical gross and microscopy of ELOC-RCC. Other changes included focal papillae(2), lymphoplasmacytic infiltrate(1), foamy histiocytes and siderophages(2), collapsed acini(4). The non-neoplastic renal parenchyma lacked any features of TS. The tumors were CK7+(11)/CA9+(11)/PAX8+(11)/CD10+(11)/CAM5.2+(7)/AMACR+(3)/TFE3-/CathepsinK-/SDHB+/FH+/HMB45-/Ki-67(1-7%). Desmin immunoreactivity in the smooth muscle component was observed (Figure 1). The table 1 and figure 2 show the somatic genomic alterations in the 11 patients. Germline testing in 5 patients did not reveal any genomic alteration. All patients were alive and without disease progression after a mean follow-up of 11.8 months (range=3-49 months).

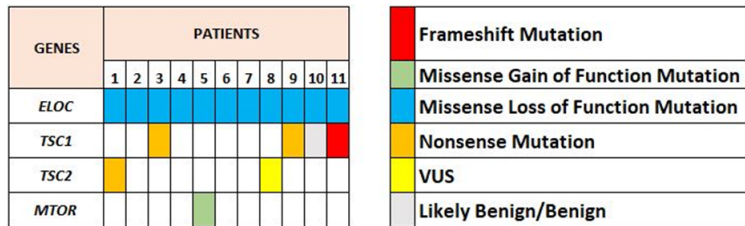


Figure 1 - 778

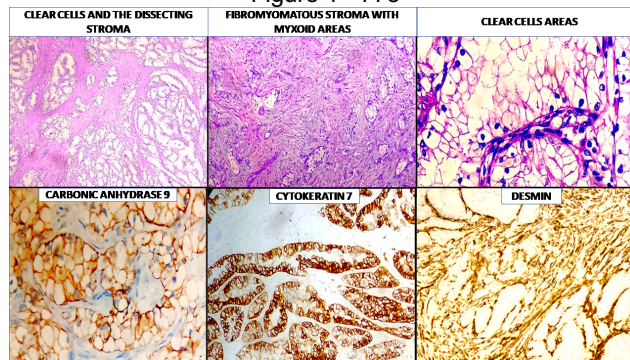


Figure 2 - 778

Patient #	Gene Symbol	Gene Name	Transcript ID	Variant annota	Variant annota	Pathogenic role	Variant type	Molecular consequence	VAF
1	<i>ELOC</i>	Elongin C	NM_005648.4	p.Tyr79Phe	c.236A>T	Likely pathogenic	Single nucleotide variant	Missense	36%
2	<i>ELOC</i>	Elongin C	NM_005648.4	p.Arg120Ter	c.356A>T	Pathogenic	Single nucleotide variant	Nonsense	25%
3	<i>ELOC</i>	Elongin C	NM_005648.4	p.Tyr79Ser	c.236A>C	Likely pathogenic	Single nucleotide variant	Missense	44%
	<i>TSC1</i>	Tuberous sclerosis 1	NM_00368.5	p.Glu87Ter	c.262G>T	Pathogenic	Single nucleotide variant	Missense	21.00%
4	<i>ELOC</i>	Elongin C	NM_005648.4	p.Tyr79Phe	c.236A>T	Likely pathogenic	Single nucleotide variant	Missense	41.00%
5	<i>ELOC</i>	Elongin C	NM_005648.4	p.Tyr79Asn	c.235T>A	Likely pathogenic	Single nucleotide variant	Missense	18.00%
	<i>MTOR</i>	Mammalian target of rapamycin	NM_004958.4	p.Ile250Phe	c.7498A>T	Likely pathogenic	Single nucleotide variant	Missense	23%
6	<i>ELOC</i>	Elongin C	NM_005648.4	p.Tyr79Cys	c.236A>G	Pathogenic	Single nucleotide variant	Missense	48.00%
7	<i>ELOC</i>	Elongin C	NM_005648.4	p.Tyr79Phe	c.236A>T	Likely pathogenic	Single nucleotide variant	Missense	62%
8	<i>ELOC</i>	Elongin C	NM_005648.4	p.Tyr79Phe	c.236A>T	Likely pathogenic	Single nucleotide variant	Missense	29%
	<i>TSC2</i>	Tuberous sclerosis 2	NM_000548.5	p?	c.1717-1G>C	VUS	Single nucleotide variant	Splice acceptor	37%
9	<i>ELOC</i>	Elongin C	NM_005648.4	p.Tyr79Phe	c.236A>T	Likely pathogenic	Single nucleotide variant	Missense	38.00%
	<i>TSC1</i>	Tuberous sclerosis 1	NM_00368.5	p.Glu485Ter	c.1453G>T	Pathogenic	Single nucleotide variant	Nonsense	29.00%
10	<i>ELOC</i>	Elongin C	NM_005648.4	p.Tyr79Cys	c.236A>G	Pathogenic	Single nucleotide variant	Missense	20.00%
	<i>TSC1</i>	Tuberous sclerosis 1	NM_00368.5	p.Thr300=	c.900A>G	Likely benign	Single nucleotide variant	Synonymous	31.00%
11	<i>ELOC</i>	Elongin C	NM_005648.4	p.Tyr79Phe	c.236A>T	Likely pathogenic	Single nucleotide variant	Missense	45%
	<i>TSC1</i>	Tuberous sclerosis 1	NM_00368.5	p.Glu478Lysfs	Ter53	c.1431_1434del	Pathogenic	Deletion	Frameshift
									31%

**Conclusions:** *ELOC*-mutated RCC is a distinct subtype of RCC with morphologic, immunohistochemical, and molecular characteristics distinct from clear cell RCC and clear cell papillary tumors as these tumors frequently harbors mutations in the *ELOC* gene and demonstrate recurrent mutations involving the *TSC/MTOR* pathway. Also, RCC with fibromyomatous stroma harboring *TSC/MTOR* alteration and/or *ELOC* mutation could be grouped together because of their overlapping morphology and CK7 positivity, despite the differing molecular alterations.

## 779 Expanding the Histomorphologic, Clinical and Molecular Spectrum of Low Grade Fumarate Hydratase Deficient Renal Cell Carcinoma (FHD RCC) in the Largest Reported Case Series of Six Renal Oncocytic Tumors

Sambit Mohanty<sup>1</sup>, Manju Aron<sup>2</sup>, Sean Williamson<sup>3</sup>, Shilpy Jha<sup>4</sup>, Anandi Lobo<sup>5</sup>, Mahmut Akgul<sup>6</sup>, Sepideh Madahian<sup>7</sup>, Shivani Kandukuri<sup>8</sup>

<sup>1</sup>Advanced Medical and Research Institute, New Delhi, India, <sup>2</sup>Keck School of Medicine of USC, Los Angeles, CA, <sup>3</sup>Cleveland Clinic, Cleveland, OH, <sup>4</sup>Advanced Medical and Research Institute, Bhubaneswar, India, <sup>5</sup>Kapoor Centre of Urology and Pathology, Raipur, India, <sup>6</sup>Albany Medical Center, Albany, NY, <sup>7</sup>LAC+USC Medical Center, CA, <sup>8</sup>University of Southern California, Keck School of Medicine of USC, Los Angeles, CA

**Disclosures:** Sambit Mohanty: None; Manju Aron: None; Sean Williamson: None; Shilpy Jha: None; Anandi Lobo: None; Mahmut Akgul: None; Sepideh Madahian: None; Shivani Kandukuri: None

**Background:** Fumarate hydratase-deficient renal cell carcinoma (FHD RCC) represents a distinct morphologically characteristic high grade, aggressive neoplasm. Low- grade FHD RCC has also been described associated with and independent of hereditary leiomyomatosis-renal cell carcinoma (HLRCC) syndrome.

# ABSTRACTS | GENITOURINARY PATHOLOGY (INCLUDING RENAL TUMORS)

**Design:** This multi-institutional study aims to investigate unclassifiable low grade oncocytic tumors to identify low grade FHD RCC. Along with evaluation of histologic features, immunostains (IHC) Keratin 7, Keratin 20, CD 117, SDHB, FH/2SC, ALK-1, GATA3 and MIB-1 were performed. Molecular evaluation using targeted NGS-based panel to detect small nucleotide variants/substitutions, small indels (insertions and/or deletions), and copy number variations in 324 cancer associated genes (including genes involved in *FH* and *PI3K/AKT/MTOR* pathway) on Illumina® HiSeq 4000 platform. Six tumors were identified on which molecular analysis was performed.

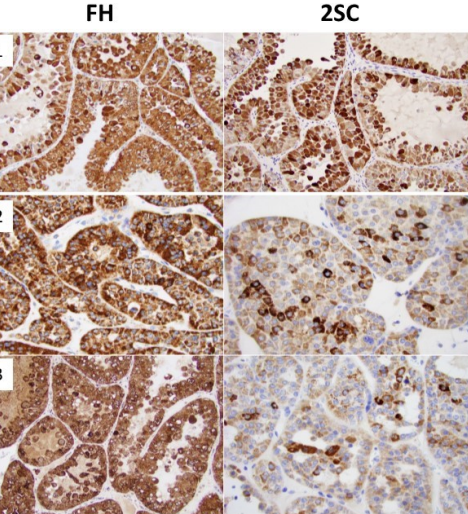
**Results:** The results are in table 1. The mixed histologic features (see image 1.) ranged from solid nests, to microcystic, papillary, tubules and trabeculae with sheets of tumor cells some with Chromophobe RCC-like areas and areas with fibromyxoid stroma that are oncocyтома-like and some are Low grade oncocytic tumor-like. The nuclear grades were ISUP/WHO 2 (n=5) and 3 (n=1). The Keratin 7 is positive in 5/6 cases and ranges from focal to diffuse. The FH/2SC staining patterns are summarized in image 2. MIB-1 index was low (2-8%). No necrosis, rhabdoid, sarcomatoid features were present. Most of the other IHC (SDHB+ ALK1- Keratin 20- GATA3+/CD117+/-) appear to be inconsistent and unreliable. The FH is retained in 4 of 6 cases, of which 3 had diffuse and one had patchy weak-moderate staining (comprising 60% of tumor cells). The 2SC is diffuse with moderate intensity in all cases. Mutation in the *FH* gene were identified in all cases. The types of mutations included were nonsense, missense, frameshift and synonymous.

**Table 1. Clinical, histomorphological, immunohistochemical and molecular features of low grade *Fumarate Hydratase deficient* renal cell carcinoma of the kidney.**

Patient #	AGE/GENDER	HISTOLOGY	STAGE	FOLLOW UP	IMMUNOHISTOCHEMISTRY				Gene Symbol	Gene Name	Variant annotation (p.)	Variant annotation (cDNA)	Pathogenic role	Variant type	Molecular consequence	VAF	
					CK 7	FH	2SC	MIB-1									
1	52 M	Unencapsulated and partially circumscribed; compact tubules/follicles and in a uniform, sieve-like pattern with broad intersecting bands of fibrosis present focally WHO/ISUP grade 2 nuclei	pT1a	Alive NED month	12	Diffuse positivity	Retained	Positive	<5%	<i>FH</i>	Fumarate hydratase	p.Ile487=	c.1461C>A	Single nucleotide variant	Likely benign	Synonymous	11.80%
2	66 M	Unencapsulated and well circumscribed; mixed morphology oncocytic cells with abundant eosinophilic cytoplasm packed with back to back tubules some areas that are chRCC-like; WHO/ISUP grade 2 nuclei	pT1a	Alive NED month	3	Focal positive	Retained	Positive	<5%	<i>FH</i>	Fumarate hydratase	p.Trp500Ter	c.1499G>A	Single nucleotide variant	Pathogenic	Nonsense	15.20%
3	58 M	Unencapsulated and well circumscribed; overlapping oncocyтома and chRCC-like areas with readily identifiable intranuclear cytoplasmic inclusions; WHO/ISUP grade 2 nuclei	pT1a	Alive NED months	12	Focal positive	Retained	Positive	<5%	<i>FH</i>	Fumarate hydratase	p.Thr481=	c.1443C>T	Single nucleotide variant	Likely benign	Synonymous	40.30%
4	41F	Unencapsulated and partially circumscribed; LOT-like histology with focal papillary areas; WHO/ISUP grade 2 nuclei	pT3a	Alive NED months	9	Negative	Lost	Positive	8%	<i>FH</i>	Fumarate hydratase	p.Tyr465Cys	c.1394A>G	Single nucleotide variant	Pathogenic/Likely pathogenic	Missense	29.40%
5	63M	Unencapsulated and partially circumscribed;oncocytic-like histology; WHO/ISUP grade 2 nuclei	pT1a	Alive NED months	37	Focal positive	Lost	Positive	2%	<i>FH</i>	Fumarate hydratase	p.Ala458fs	c.1370_1371insTCAC	Insertion	Pathogenic	Frameshift	35.20%
6	38 M	Unencapsulated and partially circumscribed;hybrid features between an ESC and papillary type 2 RCC; WHO/ISUP grade 3 nuclei	pT1a	LTf		Focal positive	Retained	Positive	<5%	<i>FH</i>	Fumarate hydratase	p.Leu482Phe	c.1446A>C	Single nucleotide variant	Pathogenic	Missense	19%

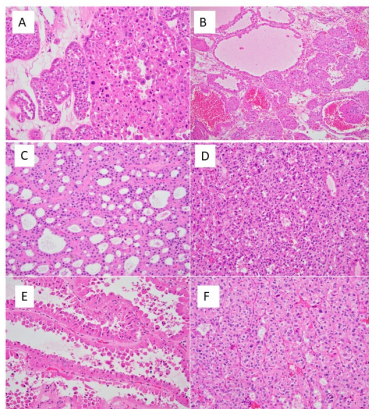
chRCC: Chromophobe RCC, NED: No evidence of disease, LTF: Lost to follow up

Figure 2 - 779



Images 1, 2 & 3. These are images of retained FH in 3 cases and the corresponding 2SC in those cases. FH appears to be strongly positive while 2SC is variably retained.

Figure 1 - 779



- A. Nests of tumor cells with oncoblast-like features
- B. Tumor with solid nests with cystic areas
- C. Tumor cells with cribriform or sieve-like areas
- D. Areas of tumor with compressed tubules
- E. Tumor cells showing papillary areas lined by plump eosinophilic cells
- F. Areas of tumor that are LOT-like

**Conclusions:** 1. Low grade FHD RCC is a heterogeneous group of tumors. 2. Interestingly, a synonymous mutation (case # 1 and 3) could lead to a defect in the FH protein folding and function without altering the encoded amino acid while a nonsense mutation (case # 2) could lead to the protein that is incomplete and shorter than the usual. These may likely explain the retention of FH staining in these cases. 3. It is critical that FH and 2SC be performed in conjunction. In equivocal cases, NGS may be needed to arrive at the right diagnosis.

## 780 Transcriptome Analysis of Primary Prostate Tumor Foci and Corresponding Lymph Node Metastases Identifies Pathways Associated with Metastatic Disease

Carlos Moreno<sup>1</sup>, Cynthia Winham<sup>2</sup>, Emma Klein<sup>1</sup>, Yijian Huang<sup>1</sup>, David Schuster<sup>1</sup>, Martin G. Sanda<sup>2</sup>, Adeboye Osunkoya<sup>2</sup>

<sup>1</sup>Emory University, Atlanta, GA, <sup>2</sup>Emory University School of Medicine, Atlanta, GA

**Disclosures:** Carlos Moreno: None; Cynthia Winham: None; Emma Klein: None; Yijian Huang: None; David Schuster: None; Martin G. Sanda: None; Adeboye Osunkoya: None

**Background:** Prostate cancer (PCa) is a highly heterogeneous disease, and mortality is mainly due to metastases. However, the molecular underpinnings that lead to the initial steps of metastasis have not been well characterized. We performed transcriptome analysis of primary prostate tumor foci and corresponding lymph node metastases (LNM).

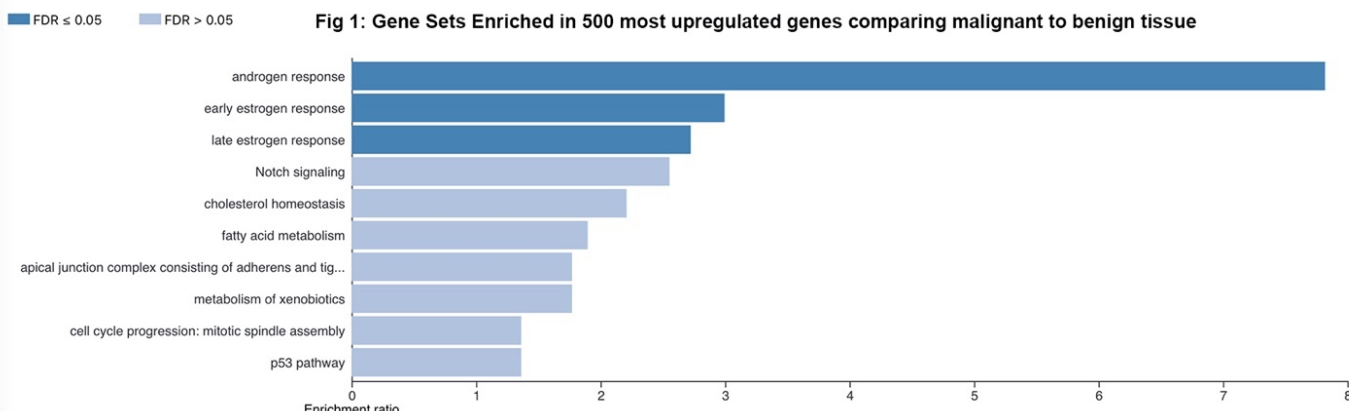
**Design:** Primary tumor foci (PTF) and LNM from 40 patients with high-risk PCa were analyzed by RNAseq. Two or more PTF and all available LNM greater than 0.4cm were subjected to sequencing. Of these 40 patients, 17 (42.5%) had LNM and 23 (57.5%) had benign LNs. A total of 155 tissue samples (97 PTF, 39 benign LNs, and 19 LNM) were sequenced and mapped to the human transcriptome with STAR mapper after QC trimming and removal of adapter sequences using TrimGalore. Differentially expressed genes between PTF, LNM, and benign LNs were identified using DESeq2, and gene set enrichment analysis was performed using WebGestalt.

**Results:** A median of 57 million paired-end reads were obtained per sample, with a median of 10 million total readcounts per sample across the transcriptome, and 39,021 transcripts were detected in at least 5% of samples. Comparing PTF to LNM, 6203 transcripts were differentially expressed ( $p\text{-adj} < 0.01$ ). PTF were enriched relative to LNM in gene sets associated with Wnt signaling, hormone signaling, Hippo signaling, KRAS signaling, and the epithelial to mesenchymal transition. Comparing PTF from metastatic patients to non-metastatic patients, 1265 transcripts were differentially expressed ( $p\text{-adj} < 0.01$ ). PTF from metastatic patients were enriched in gene sets associated with cell cycle progression, oxidative phosphorylation, ER stress, fatty acid metabolism, and DNA repair. LNM gene sets were enriched in endoplasmic reticulum (ER) stress and oxidative phosphorylation. The top 500 upregulated genes in malignant tissues were significantly enriched in genes related to androgen and estrogen signaling as expected. We also identified a set of 193 genes whose expression was significantly increased in primary tumor over benign LNs and in LNM over primary tumors. This gene set was significantly enriched in genes related to oxidative phosphorylation and included oncogenes such as PIK3CB, NCOA2, and SCHLAP1.

Table 1: Gene Sets Enriched in Genes with expression higher in LNM than PTF and higher in PTF than benign LNs

Gene Set	Description	FDR
hsa01100	Metabolic pathways	4.46E-07
HALLMARK_OXIDATIVE_PHOSPHORYLATION	oxidative phosphorylation and citric acid cycle	6.57E-07
hsa00190	Oxidative phosphorylation	1.98E-05
hsa00280	Valine, leucine and isoleucine degradation	6.51E-03
GO:1902600	proton transmembrane transport	7.73E-03
GO:0033108	mitochondrial respiratory chain complex assembly	7.77E-03
GO:0006081	cellular aldehyde metabolic process	1.15E-02
GO:0140053	mitochondrial gene expression	1.43E-02
GO:0006520	cellular amino acid metabolic process	1.56E-02
GO:0006414	translational elongation	2.08E-02
GO:0006091	generation of precursor metabolites and energy	2.36E-02
GO:0044282	small molecule catabolic process	3.45E-02
hsa00071	Fatty acid degradation	4.14E-02
GO:0009123	nucleoside monophosphate metabolic process	4.19E-02

Figure 1 - 780



# ABSTRACTS | GENITOURINARY PATHOLOGY (INCLUDING RENAL TUMORS)

**Conclusions:** Signaling pathways associated with ER stress, oxidative phosphorylation, fatty acid metabolism, and cell cycle progression are prominent in LNM of aggressive PCa. *PIK3CB*, *NCOA2*, and *SCHLAP1* expression are significantly increased in LNM.

## 781 Examining the Landscape of Concurrent Upper Tract and Lower Tract Urothelial Carcinoma Using Spatial Transcriptomic Analysis

Shreyas Naidu<sup>1</sup>, Elizabeth Davaro<sup>1</sup>, Facundo Davaro<sup>1</sup>, Xuefeng Wang<sup>1</sup>, Gustavo Borjas<sup>1</sup>, Kyle Rose<sup>1</sup>, Carlos Moran-Segura<sup>1</sup>, Vaibhav Chumbalkar<sup>2</sup>, Li Roger<sup>1</sup>, Aram Vosoughi<sup>1</sup>

<sup>1</sup>H. Lee Moffitt Cancer Center & Research Institute, Tampa, FL, <sup>2</sup>H. Lee Moffitt Cancer Center & Research Institute, University of South Florida, Tampa, FL

**Disclosures:** Shreyas Naidu: None; Elizabeth Davaro: None; Facundo Davaro: None; Xuefeng Wang: None; Gustavo Borjas: None; Kyle Rose: None; Carlos Moran-Segura: None; Vaibhav Chumbalkar: None; Li Roger: None; Aram Vosoughi: None

**Background:** Despite histologic similarities between upper-tract urothelial carcinoma (UTUC) and urothelial carcinoma of the bladder (UCB), there are differences in the clonal types, mutations, and the immune landscape between these tumors. Patients with concomitant UTUC and UCB present a unique platform to examine these differences. In this study, we performed multiplex spatial profiling of RNA on tumor samples from patients with concomitant UTUC and UCB to include tumor and tumor environment heterogeneity in the evaluation of the tumors using the GeoMx™ Digital Spatial Profiling platform.

**Design:** Three patients with concomitant high grade non-invasive UTUC and UCB were identified. Six FFPE samples from cystectomy and nephroureterectomy for the three patients were identified. A pathologist selected 18 regions of interest (ROIs), including tumor, tumor-stroma interface, and stroma area on each specimen. Multiplex IHC was performed on each sample with stains for DNA, Pan-CK, CD20 (B cells), and CD45 (immunocytes). The GeoMx™ Digital Spatial Profiling platform was used to sequence the RNA from the ROIs on each FFPE slide. Chi-squared analysis was performed.

**Results:** Multiplex IHC images demonstrated the increased infiltration of CD20 and CD45 immune cells in the UCB in compared to UTUC tumors; however, the proportion of inflammatory cells component (i.e. T-cells, B-cells, plasma cells, T-regulatory cells, macrophages) are similar in different ROIs within each tumor and in UCB and UTUC tumors in each patient and even in samples from same sites among all patients. From the 11000+ genes identified through GeoMx analysis, we identified the variable expression among UTUC and UCB samples. Notably, UNC5B, a gene that codes for a netrin receptor that is correlated with bladder cancer recurrence, was highly expressed in UCB. Additionally, UTUCs showed higher expression of histone regulatory genes (H1-3, H2BC5, H2BC8), which may lead to tumorigenesis and progression to muscle-invasive UC.

Figure 1 - 781

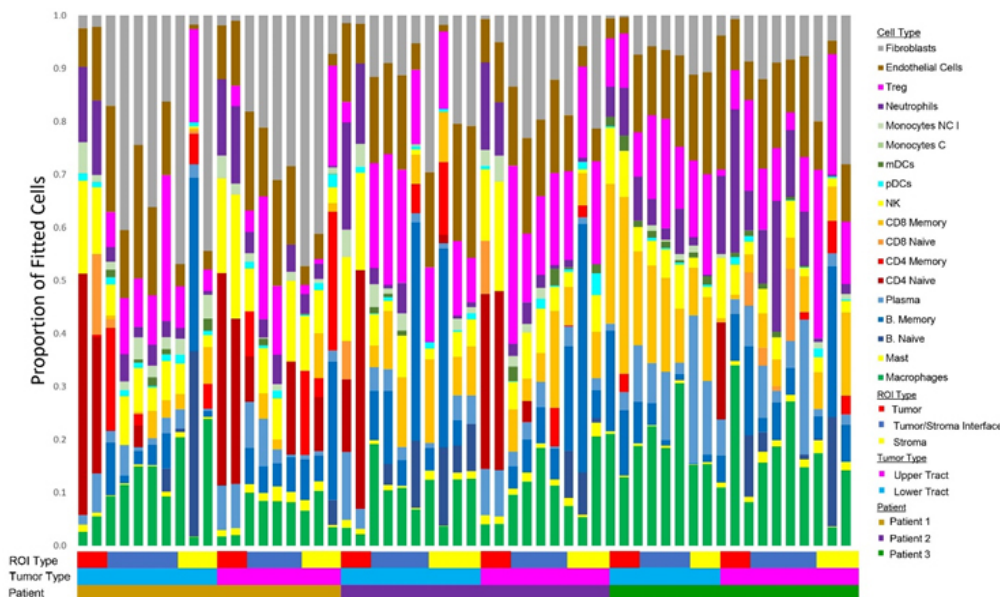
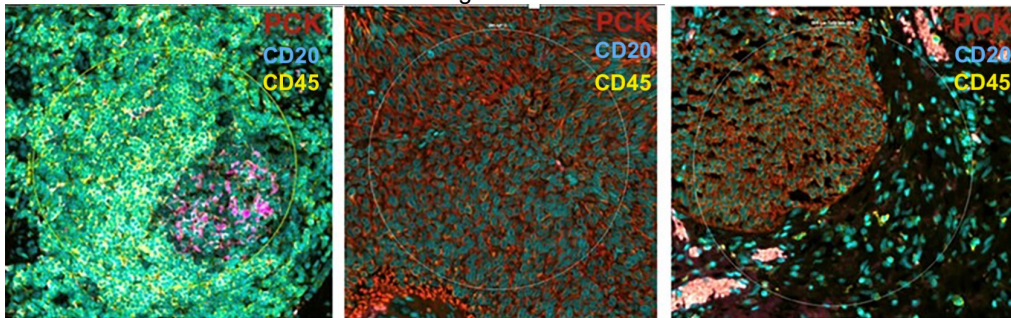


Figure 1: Distribution of Immune Cell Types across ROIs

Figure 2 - 781



**Conclusions:** UTUC demonstrates lower immune cells infiltration, consistent with previous UTUC studies; however, the proportion of inflammatory cells component is similar in different foci of the tumor and in concomitant UCB and UTUC tumors in each patient and even among all tumor samples from the same site. UNC5B, which has been associated with tumor recurrence, is highly expressed in UCB. UTUC patients showed higher expression of histone regulatory genes.

## 782 Genomic Landscape of Upper Tract Urothelial Carcinoma and its Histologic Subtypes

Behtash Nezami<sup>1</sup>, Mohammed Alghamdi<sup>2</sup>, Andrew Katims<sup>1</sup>, Jie-Fu Chen<sup>1</sup>, Judy Sarungbam<sup>1</sup>, S. Joseph Sirintrapun<sup>1</sup>, Anuradha Gopalan<sup>1</sup>, Ying-Bei Chen<sup>1</sup>, Samson Fine<sup>1</sup>, Gopa Iyer<sup>1</sup>, David Solit<sup>1</sup>, Jonathan Coleman<sup>1</sup>, Hikmat Al-Ahmadie<sup>1</sup>  
<sup>1</sup>Memorial Sloan Kettering Cancer Center, New York, NY, <sup>2</sup>Hospital of the University of Pennsylvania, Philadelphia, PA

**Disclosures:** Behtash Nezami: None; Mohammed Alghamdi: None; Andrew Katims: None; Jie-Fu Chen: None; Judy Sarungbam: None; S. Joseph Sirintrapun: None; Anuradha Gopalan: None; Ying-Bei Chen: None; Samson Fine: None; Gopa Iyer: None; David Solit: None; Jonathan Coleman: None; Hikmat Al-Ahmadie: None

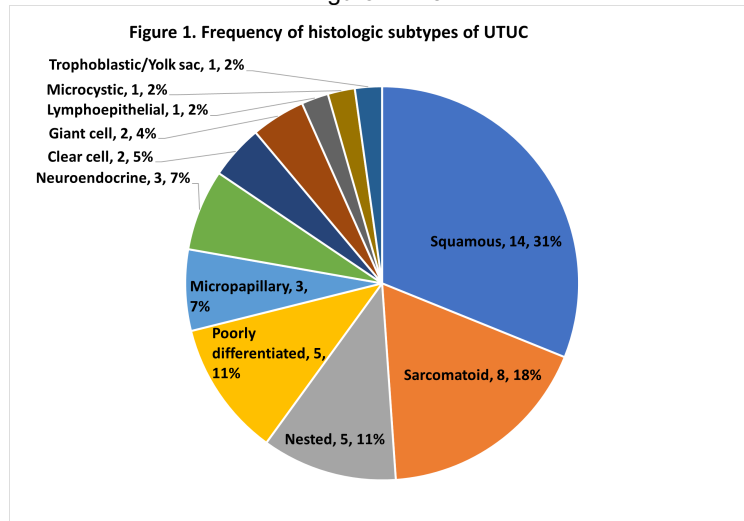
**Background:** Urothelial carcinoma of the upper urinary tract (UTUC) exhibits notable differences in the prevalence of common genomic alterations compared to urothelial carcinoma of the bladder (UCB). Similar to UCB, histologic subtypes of UTUC are associated with more advanced stage and poor survival. However, data is limited regarding the spectrum of genomic alterations and their association with morphologic subtypes.

**Design:** Retrospective review was performed of nephroureterectomy specimens for UTUC with available molecular testing using next generation sequencing (NGS) between 2015 and 2022. H&E slides of the region sampled for molecular testing was reviewed for histologic features in the non-invasive (grade and configuration) and invasive components (histologic subtype). Mutational profiles for 26 genes commonly altered in urothelial carcinoma were correlated with histologic findings.

**Results:** The study included 173 patients, 102 males and 71 females, with (mean ± SD) age of 67±10.9 years at the time of sequencing. Five-year overall survival was 32.6%. The cohort was divided into 5 subgroups (Table 1) as follows: noninvasive (low grade, high grade, and high grade with a low-grade background), and invasive (UC, NOS only and with histologic subtype). Invasive UTUC was present in 124 cases (71%), of which 89 (72%) had pure UC, NOS. Histologic subtypes were present in 35 (28%) tumors, the most frequent of which were squamous (n=14, 40%) and sarcomatoid (n=7, 20%). PIK3CA, CDKN2A, FGFR3, and BRAF mutations were more frequent in squamous compared to UC, NOS or sarcomatoid tumors. Within cases containing a non-invasive component (n=141), bulky papillary morphology (reported to be associated with FGFR3 alterations) were enriched in FGFR1, FGFR2, FGFR3, HRAS or KRAS alterations (78%, 35/45), while only 46% (44/96) without this morphology harbored these alterations. A non-invasive flat component was present in 31 patients, and papillary in 104. FGFR3 and PIK3CA were present more frequently in papillary tumors (42% and 23% respectively, vs. 3% and 3% in flat tumors). TP53 was present more frequently in flat tumors (52% vs. 24% in the papillary tumors).

Table 1. Breakdown of the 5 groups in the study		No. of specimens (n, %)
Non-invasive (n = 49)		
Low grade		9, 18%
High grade		31, 63%
High in low		9, 18%
Invasive (n = 124)	(32 pure invasive, 92 with non-invasive)	
NOS only		89, 72%
Variant histology		35, 28%

Figure 1 - 782



**Conclusions:** Histologic subtypes are present in 28% of invasive UTUCs in this cohort. Histologic subtypes are associated with differences in genomic alterations in UTUC. Non-invasive UTUC with bulky papillary morphology is enriched for *FGFR1*, *FGFR2*, *FGFR3*, *HRAS* or *KRAS* alterations. *TP53* mutations are more common in flat precursor lesions.

## 783 Pathologic Findings in Patients on Active Surveillance for Prostatic Adenocarcinoma: Comparison Between Caucasian and African American Patients

Thi Nguyen<sup>1</sup>, Dattatraya Patil<sup>1</sup>, Adeboye Osunkoya<sup>1</sup>

<sup>1</sup>Emory University School of Medicine, Atlanta, GA

**Disclosures:** Thi Nguyen: None; Dattatraya Patil: None; Adeboye Osunkoya: None

**Background:** Active surveillance for prostate cancer (PCa) in patients who meet the criteria has become widely accepted across the United States (US), though the appropriateness of this approach for African American (AA) patients has not been well characterized in the pathology literature. The aim of this study was to compare the differences in pathologic findings between AA and Caucasian American (CA) patients who underwent active surveillance for PCa at a major academic institution in the US.

**Design:** A search was made through our urology database for consented subjects with self-reported race as AA or CA with biopsy-proven PCa diagnosed between 2008 and 2021 who underwent active surveillance with at least 1 repeat biopsy. We examined the differences in the pathological findings and other clinicopathological features, including follow-up.

**Results:** One hundred and ten patients were included in the study. Twenty-seven (25%) were AA and eighty-three (75%) were CA. Mean patient age was 62 years (range: 40-103 years). The mean duration of follow-up was 22 months (range: 6-113 months). Among the CA patients, 79 (95%) had Gleason score 3+3=6 (Grade group 1), and 4 (5%) had Gleason score 3+4=7 (Grade group 2) on the initial biopsy. The mean number of positive cores was 2. Perineural invasion was present in 7 patients (8%). In the AA patient cohort, 26 (96%) had Gleason score 3+3=6 (Grade group 1) and 1 (4%) had Gleason score 3+4=7 (Grade group 2). The mean number of positive cores was 2.2. Perineural invasion was present in 4 patients (15%). All patients had at least one repeat biopsy (range: 1 - 3), with 1 repeat biopsy in 91 patients (69 CA, 22 AA), 2 repeat biopsies in 14 patients (10 CA, 4 AA), and 3 repeat biopsies in 5 patients (4 CA, 1 AA). The rate of higher Gleason scores (Grade groups) identified on subsequent biopsies was 33/83 (40%) for CA patients versus 8/27 (30%) for AA patients ( $p=0.34$ ). Of the patients with upgraded Gleason scores (Grade groups), 16 had newly identified perineural invasion, 13 of whom were CA, and 3 were AA.

**Conclusions:** In our study, AA patients on active surveillance for PCa were not at increased risk for higher Gleason scores (Grade groups) or other adverse pathology findings at subsequent repeat needle core biopsies compared to CA patients. The results of this study may play a critical role in counseling and risk stratification of AA patients with PCa who are eligible for active surveillance.

**784 Prostatic Adenocarcinoma with Cribriform Morphology and Mucin Extravasation: Correlation with Adverse Features at Radical Prostatectomy**Sarah Ni Mhaolcatha<sup>1</sup>, Susan Prendeville<sup>2</sup><sup>1</sup>Cork University Hospital, Cork, Saint Kitts and Nevis, <sup>2</sup>University Health Network, University of Toronto, Toronto, ON**Disclosures:** Sarah Ni Mhaolcatha: None; Susan Prendeville: None

**Background:** Cribriform carcinoma (CC) is recognised as an adverse prognostic parameter in prostate carcinoma (PCa). Despite recent consensus definitions of CC, PCa with cribriform architecture and mucin extravasation has been identified as a challenging area with limited studies assessing the prognostic significance of this pattern. This study evaluated the frequency and pathologic correlates of mucinous cribriform pattern (MCP) at radical prostatectomy (RP).

**Design:** A series of completely embedded RPs (n=488) were reviewed for the presence of MCP and CC. MCP was defined as tumours with cribriform epithelial proliferation associated with intraglandular or extraglandular mucin as the only CC component (absence of non-mucinous CC or intraductal carcinoma). Cases with non-mucinous CC were identified as a comparison group. Findings were correlated with serum PSA, grade group and pathologic stage at RP.

**Results:** Results are summarised in table 1. MCP was identified in 19/488 (4%) cases while CC was identified in 158/488 cases (32%). MCP showed predominantly intraglandular mucin with 1 case containing abundant extraglandular mucin pools. The overwhelming majority of MCP were GG2 (18/19, 95%) with no cases >GG3 in this series. Among GG2 cases, the rate of non organ-confined disease was significantly greater in the CC group compared to the MCP group (p value <0.001). Of those undergoing lymph node dissection (LND), lymph node metastasis was identified in 7% of CC tumours and 0% of MCP tumours.

GG and serum PSA		
GG	MCP (n=19)	CC (n=158)
GG1	-	-
GG2	18 (95%)	75 (47%)
GG3	1 (5%)	63 (40%)
GG4	0	12 (8%)
GG5	0	8 (5%)
Median PSA (range)	6.09 (5 - 11)	7.2 (1.2 - 45)
Pathologic findings in GG2 cases		
pT stage	MCP (n=18)	CC (n=75)
pT2	17 (95%)	30 (40%)
≥ pT3	1 (5%)	45 (60%)
pN stage (of cases with LND)	MCP (n=10)	CC (n=31)
pN1	0	7 (23%)
pN0	10 (100%)	24 (77%)

**Conclusions:** MCP is an uncommon morphologic pattern at RP and was not associated with adverse features in our series when compared with non-mucinous CC. These findings support excluding MCP when reporting cribriform carcinoma as an adverse prognostic marker. Further study assessing biopsy findings and correlating with clinical outcome is underway and evaluation in larger cohorts may help to further refine the prognostic significance of this morphologic growth pattern.

# ABSTRACTS | GENITOURINARY PATHOLOGY (INCLUDING RENAL TUMORS)

## 785 Metastatic Solid Tumors of the Penis: A Clinicopathologic Evaluation of 109 Cases from an International Collaboration

Luiz Nova-Camacho<sup>1</sup>, Andres Acosta<sup>2</sup>, Sean Williamson<sup>3</sup>, João Lobo<sup>4</sup>, Susan Prendeville<sup>5</sup>, Katrina Collins<sup>6</sup>, Liang Cheng<sup>7</sup>, Maria Delia Perez Montiel<sup>8</sup>, Michael Hwang<sup>9</sup>, Fiona Maclean<sup>10</sup>, Manju Aron<sup>11</sup>, Isabel Alvarado-Cabrero<sup>12</sup>, Inés de Torres<sup>13</sup>, Mahmut Akgul<sup>14</sup>, María García Martos<sup>15</sup>, Manuel Manrique-Celada<sup>1</sup>, Ankur Sangi<sup>16</sup>, Howard Wu<sup>6</sup>, Laurence Galea<sup>17</sup>, Antonio Polonia<sup>18</sup>, Angela Chou<sup>19</sup>, Francisco Queipo<sup>20</sup>, Felix Contreras<sup>21</sup>, Ângelo Rodrigues<sup>4</sup>, Asli Yilmaz<sup>22</sup>, Nicole Zalles<sup>3</sup>, Kiril Trpkov<sup>23</sup>, Maria Rosaria Raspollini<sup>24</sup>, Thomas Ulbright<sup>6</sup>, Angel Panizo<sup>25</sup>

<sup>1</sup>Hospital Universitario Donostia - Osakidetza, Donostia, Spain, <sup>2</sup>Brigham and Women's Hospital, Harvard Medical School, Boston, MA, <sup>3</sup>Cleveland Clinic, Cleveland, OH, <sup>4</sup>Portuguese Oncology Institute - Porto, Porto, Portugal, <sup>5</sup>University Health Network, University of Toronto, Toronto, ON, <sup>6</sup>Indiana University School of Medicine, Indianapolis, IN, <sup>7</sup>Alpert Medical School of Brown University, Providence, RI, <sup>8</sup>Instituto Nacional de Cancerología, Mexico City, Mexico, <sup>9</sup>Indiana University Health, Indianapolis, IN, <sup>10</sup>Douglass Hanly Moir Pathology, Melbourne, Australia, <sup>11</sup>Keck School of Medicine of USC, Los Angeles, CA, <sup>12</sup>Mexican Oncology Hospital SXII, IMSS, Mexico City, Mexico, <sup>13</sup>Vall d'Hebron Campus and Autonomous University of Barcelona (UAB), Barcelona, Spain, <sup>14</sup>Albany Medical Center, Albany, NY, <sup>15</sup>University Gregorio Marañón Hospital, Madrid, Spain, <sup>16</sup>El Camino Hospital, Mountain View, CA, <sup>17</sup>Melbourne Pathology, Australia, <sup>18</sup>Institute of Molecular Pathology and Immunology (IPATIMUP)/Instituto de Investigação e Inovação em Saúde (i3S), Porto, Portugal, <sup>19</sup>Royal North Shore Hospital, Sydney, Australia, <sup>20</sup>Complejo Hospitalario Universitario A Coruña (CHUAC), A Coruña, Galicia, Spain, <sup>21</sup>Clínica Unión Médica, Santiago, Dominican Republic, <sup>22</sup>Alberta Precision Laboratories, University of Calgary, Calgary, AB, <sup>23</sup>University of Calgary, Calgary, AB, <sup>24</sup>University Hospital Careggi, Firenze, Italy, <sup>25</sup>Complejo Hospitalario de Navarra, Pamplona, Spain

**Disclosures:** Luiz Nova-Camacho: None; Andres Acosta: None; Sean Williamson: None; João Lobo: None; Susan Prendeville: None; Katrina Collins: None; Liang Cheng: None; Maria Delia Perez Montiel: None; Michael Hwang: None; Fiona Maclean: None; Manju Aron: None; Isabel Alvarado-Cabrero: None; Inés de Torres: None; Mahmut Akgul: None; María García Martos: None; Manuel Manrique-Celada: None; Ankur Sangi: None; Howard Wu: None; Laurence Galea: None; Antonio Polonia: None; Angela Chou: None; Francisco Queipo: None; Felix Contreras: None; Ângelo Rodrigues: None; Asli Yilmaz: None; Nicole Zalles: None; Kiril Trpkov: None; Maria Rosaria Raspollini: None; Thomas Ulbright: None; Angel Panizo: None

**Background:** Metastases to the penis are rare, and their clinicopathologic spectrum remains incompletely described.

**Design:** In this multi-institutional study, we compiled a series of 109 patients to investigate the histologic and clinical features of solid malignancies that secondarily involve the penis.

**Results:** The mean patient age at diagnosis was 71 years (range 7-94 years). 95/109 (87%) patients had clinically manifest disease most commonly presenting with a penile nodule/mass (48/95; 51%), pain (14/95; 15%), and hematuria (11/95; 12%); 1/109 (1%) patients was diagnosed incidentally, while 13/109 (12%) patients had no available data. A history of prior cancer was identified in 92/104 (89%) patients, whereas in 12/104 (12%) patients, penile metastases were the initial clinical presentation. Diagnosis was made mainly on biopsy (82/109; 75%) or penectomy (either partial or total) (21/109; 19%) specimens (Fig. 1). In four patients (4/109; 4%), the diagnosis was made by fine-needle aspiration. The most common penile locations were the glans (45/98; 41%) and corpora cavernosa (39/98; 36%). Carcinoma (101/109; 93%) was the most common primary histology, followed by malignant melanoma (3/109; 3%), sarcoma (2/109; 2%), teratoma (1/109; 1%), myeloma (1/109; 1%), and yolk sac tumor (1/109; 1%). Most primary carcinomas originated in the genitourinary (76/109; 70%) and gastrointestinal (20/109; 18%) tracts. The most common genitourinary primaries included prostate (38/109; 35%) and bladder (27/109; 25%), while colorectal (18/109; 17%) was the most common gastrointestinal primary (Fig. 2). Data on metastasis to other organs were available for 78/109 (72%) patients and 50/78 (64%) patients had additional (i.e., non-penile) metastases. Outcome data were available for 87/109 (80%) patients, and 59 (68%) died during the follow-up period.

Figure 1 - 785

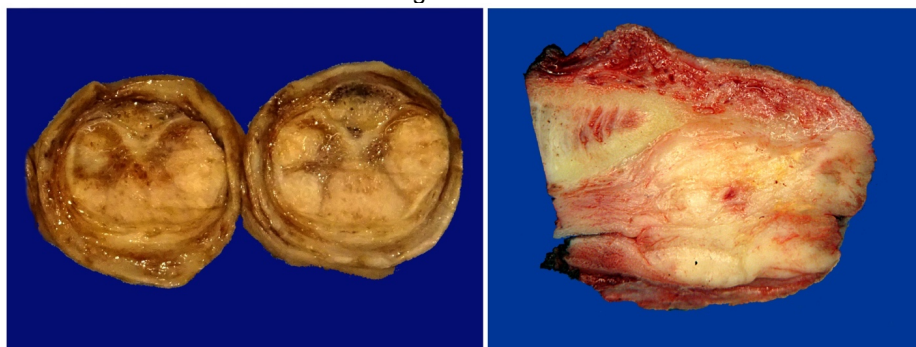
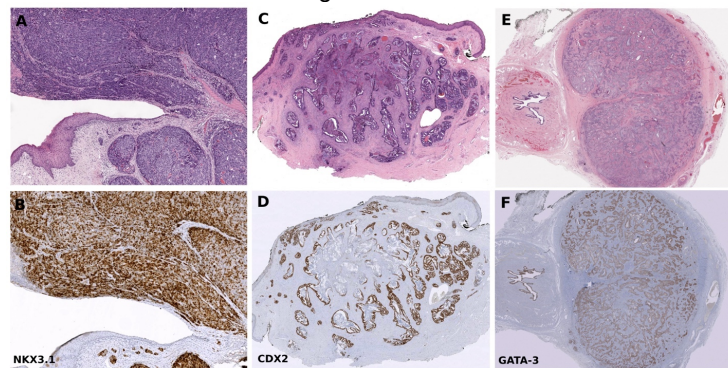


Figure 2 - 785



**Conclusions:** This largest series compiled to date on this topic demonstrates that: 1.) most secondary solid tumors of the penis originate in the genitourinary and gastrointestinal tracts; 2.) they are typically clinically manifest; and 3.) they portend poor clinical outcomes.

## 786 Secondary Solid Tumors of the Testis: A Clinicopathologic Evaluation of 158 Cases from an International Collaboration

Luiz Nova-Camacho<sup>1</sup>, Andres Acosta<sup>2</sup>, Katrina Collins<sup>3</sup>, Thomas Ulbright<sup>3</sup>, Liang Cheng<sup>4</sup>, Muhammad Idrees<sup>3</sup>, Sean Williamson<sup>5</sup>, João Lobo<sup>6</sup>, Maria Delia Perez Montiel<sup>7</sup>, Fiona Maclean<sup>8</sup>, Isabel Alvarado-Cabrero<sup>9</sup>, Kiril Trpkov<sup>10</sup>, Susan Prendeville<sup>11</sup>, Inés de Torres<sup>12</sup>, Michael Hwang<sup>13</sup>, Hector Mesa Corrales<sup>3</sup>, Mahmut Akgul<sup>14</sup>, María Garcia Martos<sup>15</sup>, Ankur Sangi<sup>16</sup>, Priti Lal<sup>17</sup>, Angela Chou<sup>18</sup>, Kammerer-Jacquet Solene-Florence, Allaume Pierre<sup>19</sup>, Nathalie Rioux-Leclercq<sup>20</sup>, Francisco Queipo<sup>21</sup>, Gorka Muñiz Unamunzaga<sup>22</sup>, Felix Contreras<sup>23</sup>, Ângelo Rodrigues<sup>6</sup>, Lauren Schwartz<sup>24</sup>, Matthew Palmer<sup>17</sup>, Irune Ruiz Díaz<sup>1</sup>, Norge Vergara<sup>25</sup>, Asli Yilmaz<sup>26</sup>, Virginie Verkarre<sup>27</sup>, Theau Tilmant<sup>28</sup>, Aurélien Morini<sup>29</sup>, Nicole Zalles<sup>5</sup>, Manju Aron<sup>30</sup>, Sara Wobker<sup>31</sup>, Maria Rosaria Raspollini<sup>32</sup>, Christopher Fletcher<sup>33</sup>, Angel Panizo<sup>34</sup>

<sup>1</sup>Hospital Universitario Donostia - Osakidetza, Donostia, Spain, <sup>2</sup>Brigham and Women's Hospital, Harvard Medical School, Boston, MA, <sup>3</sup>Indiana University School of Medicine, Indianapolis, IN, <sup>4</sup>Alpert Medical School of Brown University, Providence, RI, <sup>5</sup>Cleveland Clinic, Cleveland, OH, <sup>6</sup>Portuguese Oncology Institute - Porto, Porto, Portugal, <sup>7</sup>Instituto Nacional de Cancerología, Mexico City, Mexico, <sup>8</sup>Douglass Hanly Moir Pathology, Melbourne, Australia, <sup>9</sup>Mexican Oncology Hospital SXXI, IMSS, Mexico City, Mexico, <sup>10</sup>University of Calgary, Calgary, AB, <sup>11</sup>University Health Network, University of Toronto, Toronto, ON, <sup>12</sup>Vall d'Hebron Campus and Autonomous University of Barcelona (UAB), Barcelona, Spain, <sup>13</sup>Indiana University Health, Indianapolis, IN, <sup>14</sup>Albany Medical Center, Albany, NY, <sup>15</sup>University Gregorio Marañón Hospital, Madrid, Spain, <sup>16</sup>El Camino Hospital, Mountain View, CA, <sup>17</sup>University of Pennsylvania, Philadelphia, PA, <sup>18</sup>Royal North Shore Hospital, Sydney, Australia, <sup>19</sup>Rennes, France, <sup>20</sup>Rennes University Hospital, Rennes, France, <sup>21</sup>Complejo Hospitalario Universitario A Coruña (CHUAC), A Coruña, Galicia, Spain, <sup>22</sup>Hospital San Jorge, Huesca, Spain, <sup>23</sup>Clínica Unión Médica, Santiago, Dominican Republic, <sup>24</sup>Perelman School of Medicine at the University of Pennsylvania, Philadelphia, PA, <sup>25</sup>Hospital of the University of Pennsylvania, Philadelphia, PA, <sup>26</sup>Alberta Precision Laboratories, University of Calgary, Calgary, AB, <sup>27</sup>APHP. Hôpital Européen Georges Pompidou; Paris, INSERM UMR970, Université Paris-Cité, Paris, France, <sup>28</sup>Hôpital Européen Georges Pompidou, Paris, France, <sup>29</sup>Grand Hôpital de l'Est Francilien, Créteil, France, <sup>30</sup>Keck School of Medicine of USC, Los Angeles, CA, <sup>31</sup>The University of North Carolina at Chapel Hill, Chapel Hill, NC, <sup>32</sup>University Hospital Careggi, Firenze, Italy, <sup>33</sup>Brigham and Women's Hospital, Boston, MA, <sup>34</sup>Complejo Hospitalario de Navarra, Pamplona, Spain

**Disclosures:** Luiz Nova-Camacho: None; Andres Acosta: None; Katrina Collins: None; Thomas Ulbright: None; Liang Cheng: None; Muhammad Idrees: None; Sean Williamson: None; João Lobo: None; Maria Delia Perez Montiel: None; Fiona Maclean: None; Isabel Alvarado-Cabrero: None; Kiril Trpkov: None; Susan Prendeville: None; Inés de Torres: None; Michael Hwang: None; Hector Mesa Corrales: None; Mahmut Akgul: None; María Garcia Martos: None; Ankur Sangi: None; Priti Lal: None; Angela Chou: None; Kammerer-Jacquet Solene-Florence: None; Allaume Pierre: None; Nathalie Rioux-Leclercq: None; Francisco Queipo: None; Gorka Muñiz Unamunzaga: None; Felix Contreras: None; Ângelo Rodrigues: None; Lauren Schwartz: None; Matthew Palmer: None; Irune Ruiz Díaz: None; Norge Vergara: None; Asli Yilmaz: None; Virginie Verkarre: None; Theau Tilmant: None; Aurélien Morini: None; Nicole Zalles: None; Manju Aron: None; Sara Wobker: None; Maria Rosaria Raspollini: None; Christopher Fletcher: None; Angel Panizo: None

**Background:** Secondary solid malignancies of the testis are rare and their clinicopathologic spectrum remains incompletely understood.

**Design:** In this multi-institutional study, we evaluated a series of 158 patients who had secondary solid testicular tumors, to characterize their clinical and pathologic features.

# ABSTRACTS | GENITOURINARY PATHOLOGY (INCLUDING RENAL TUMORS)

**Results:** The mean patient age at diagnosis was 64 years (range 12-93 years). Available history of prior cancer was present in 123/141 (87%) patients, whereas in 18/141 (13%) patients, testicular involvement was the initial manifestation. Most patients (127/144; 88%) had clinically manifest disease, with either testicular mass/nodule (89/127; 70%) and/or pain (13/127; 10%) as the most common findings. In 17/144 (12%) patients, the testicular involvement was discovered incidentally on surgical specimens or imaging studies. The diagnosis was made mainly on orchectomy specimens (150/158; 95%) (Fig. 1). Different types of carcinomas (144/158; 91%), including adenocarcinomas (72/158; 46%), were the most common histologies (Fig. 2). Most primary neoplasms originated in the genitourinary (93/149; 62%), gastrointestinal (27/149; 18%), and respiratory (13/149; 9%) tracts. The most common primary sites were prostate (51/149; 34%), kidney (29/149; 20%), colorectal (13/149; 9%), and lung (12/149; 8%). Intratubular growth was identified in 13/124 (11%) cases and paratesticular involvement in 84/152 (55%) cases. The mechanism of testicular involvement was metastasis in 154/157 (98%) cases, unclear in 2/157 (1%) cases, and direct spread in 1/157 (1%) cases; in one case, there was no data available. 78/101 (77%) patients had concurrent or prior extratesticular metastases. In patients with available follow-up data (110/158; 70%), 53% (58/110) died of disease.

Figure 1 - 786

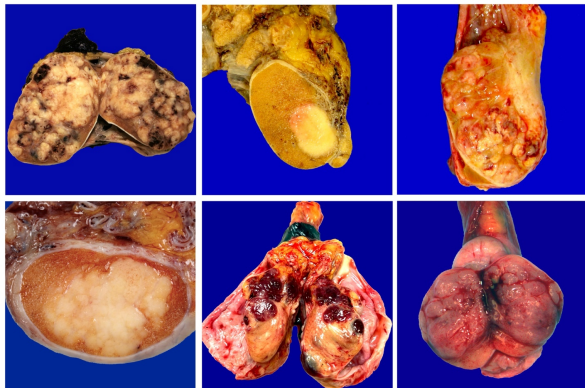
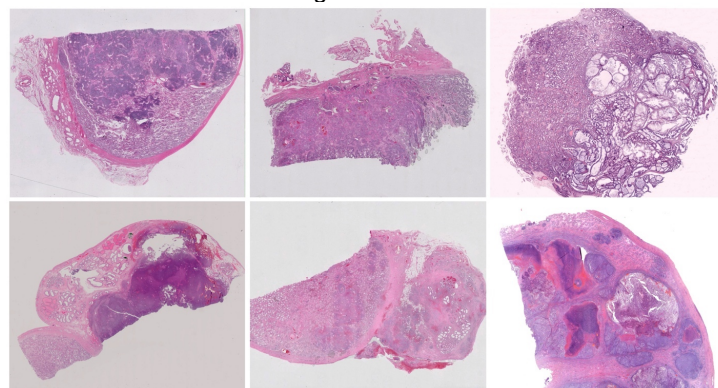


Figure 2 - 786



**Conclusions:** In conclusion, in this largest series compiled to date on this topic, we demonstrate that most secondary solid tumors of the testis represent metastatic spread from genitourinary, digestive, or respiratory primaries and often occur in the context of widespread disease.

## 787 Clinical Significance of Perineural Invasion Encircled Completely Vs. Incompletely by Prostate Cancer on Needle Core Biopsy

Julum Nwanze<sup>1</sup>, Yuki Teramoto<sup>2</sup>, Ying Wang<sup>1</sup>, Hiroshi Miyamoto<sup>1</sup>

<sup>1</sup>University of Rochester Medical Center, Rochester, NY, <sup>2</sup>Kyoto University Hospital, Kyoto, Japan

**Disclosures:** Julum Nwanze: None; Yuki Teramoto: None; Ying Wang: None; Hiroshi Miyamoto: None

**Background:** The presence of perineural invasion (PNI) by prostate cancer, particularly in biopsy specimens, is well known to be a strong indicator of aggressive disease, such as extraprostatic extension, and resultant poor prognosis. However, it remains unclear if the pattern of PNI has a clinical impact. In the present study, we compared radical prostatectomy findings and long-term oncologic outcomes to identify any differences between biopsies with PNI encircled completely vs. incompletely by cancer.

**Design:** We assessed consecutive patients with PNI on systematic sextant biopsy who had subsequently undergone radical prostatectomy at our institution from 2009 to 2016. A total of 125 men in our surgical pathology database met the inclusion criteria for PNI detected only in one focus in the entire biopsy specimen after excluding cases undergoing neoadjuvant therapy prior to prostatectomy and those where the histology slides had been unavailable for review.

**Results:** 57 (46%) cases showed completely encircled PNI, whereas 68 (54%) were non-encircled PNI. Between the two cohorts, there were no significant differences in clinicopathologic features, including preoperative prostate-specific antigen level, the number of cancer-positive biopsy site, tumor grade on biopsy or prostatectomy, pT or pN category, surgical margin status, estimated tumor volume, and the need for adjuvant therapy immediately after prostatectomy (see Table). Kaplan-Meier analysis coupled with log-rank test revealed no significant difference in the risk of postoperative disease progression in patients with encircled PNI vs. non-encircled PNI detected on biopsy (Figure 1). When the non-encircled cases were further divided into four groups [i.e. <25% encircled (n=12; 18%); ≥25%/<50% encircled (n=18; 26%); ≥50%/<75% encircled (n=10; 15%); and ≥75%/<100% encircled (n=28; 41%)], no significant differences in progression-free survival were seen (Figure 2).

	Non-encircled (n=68)	Encircled (n=57)	P
<b>Age (mean, year)</b>	61.8	63.1	0.278
<b>PSA (mean, ng/mL)</b>	8.64	7.84	0.559
<b>Bx cancer-positive sites</b>			0.719
1	4 (6%)	4 (7%)	
2	16 (24%)	12 (21%)	
3	22 (32%)	22 (39%)	
4	16 (24%)	9 (16%)	
5	7 (10%)	7 (12%)	
6	8 (12%)	3 (5%)	
<b>Bx Grade Group (highest)</b>			0.425
1	8 (12%)	6 (11%)	
2	37 (54%)	28 (49%)	
3	13 (19%)	12 (21%)	
4	9 (13%)	7 (12%)	
5	1 (1%)	4 (7%)	
<b>RP Grade Group</b>			0.827
1	1 (1%)	1 (2%)	
2	43 (63%)	31 (54%)	
3	15 (22%)	15 (26%)	
4	5 (7%)	4 (7%)	
5	4 (6%)	6 (11%)	
<b>pT</b>			0.634
2	32 (47%)	22 (39%)	
3a	29 (43%)	28 (49%)	
3b	7 (10%)	7 (12%)	
<b>pN</b>			1.000 <sup>a</sup>
0	60 (88%)	53 (93%)	
1	4 (6%)	4 (7%)	
X	4 (6%)	0 (0%)	
<b>Surgical margin</b>			0.632
Negative	58 (85%)	46 (81%)	
Positive	10 (15%)	11 (19%)	
<b>Tumor volume (mean, cc)</b>	8.9	8.7	0.840
<b>Adjuvant therapy<sup>b</sup></b>			0.632
Not performed	57 (84%)	50 (88%)	
Performed	11 (16%)	7 (12%)	

<sup>a</sup> pN0 vs pN1; <sup>b</sup> Adjuvant therapy before recurrence

Figure 1 - 787

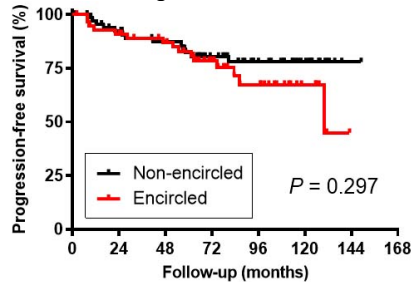
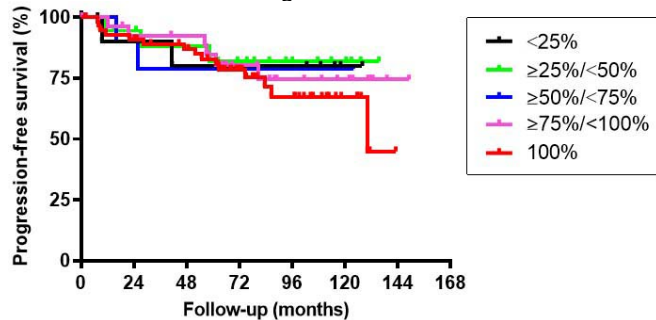


Figure 2 - 787



# ABSTRACTS | GENITOURINARY PATHOLOGY (INCLUDING RENAL TUMORS)

**Conclusions:** In biopsy specimens exhibiting PNI at only one focus, encircled vs. non-encircled PNI appears to show little clinical significance. PNI on prostate biopsy may thus need to be similarly taken into consideration irrespective of the pattern of nerve involvement.

## 788 Clinical Significance of the PI-RADS Score in Men with Prostate Cancer Undergoing Radical Prostatectomy

Julum Nwanze<sup>1</sup>, Yuki Teramoto<sup>2</sup>, Ying Wang<sup>1</sup>, Hiroshi Miyamoto<sup>1</sup>

<sup>1</sup>University of Rochester Medical Center, Rochester, NY, <sup>2</sup>Kyoto University Hospital, Kyoto, Japan

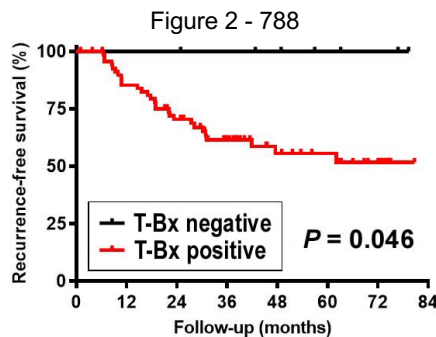
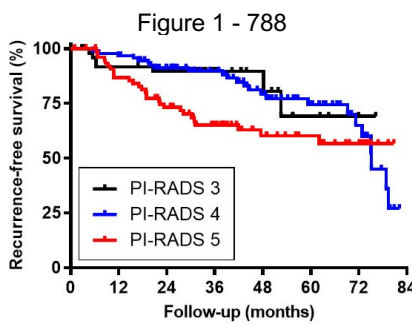
**Disclosures:** Julum Nwanze: None; Yuki Teramoto: None; Ying Wang: None; Hiroshi Miyamoto: None

**Background:** MRI-targeted biopsy (T-Bx) for which the PI-RADS score is useful has been shown to more accurately detect clinically significant prostate cancer. However, the clinical significance of prostate cancer detection on T-Bx, in conjunction with PI-RADS, needs to be further investigated. In the present study, we compared radical prostatectomy (RP) findings and oncologic outcomes in patients with prostate cancer detected on sextant biopsy (S-Bx) and/or T-Bx.

**Design:** We assessed consecutive patients who had undergone T-Bx in addition to systematic S-Bx (6 parts, ≥12 cores), followed by RP at our institution. Within our Surgical Pathology database, we identified a total of 222 men who met the inclusion criteria for prostatic adenocarcinoma on S-Bx and/or T-Bx. Cases undergoing neoadjuvant therapy prior to RP were excluded from analysis.

**Results:** Prostate cancer was detected on S-Bx only (n=32; 14%), T-Bx only (n=40; 18%), or both S-Bx and T-Bx (B-Bx: n=150; 68%), while these patients showed PI-RADS 3 (n=47; 21%), 4 (n=90; 41%), or 5 (n=85; 38%) lesion. Meanwhile, T-Bx detected cancer in 36 (77%) of PI-RADS 3 cases, 76 (84%) of PI-RADS 4 cases, and 78 (92%) of PI-RADS 5 cases. Compared with PI-RADS 3 lesion, PI-RADS 4 lesion was associated with significantly higher tumor grade on biopsy or RP. Similarly, some of RP findings (i.e. Grade Group, pT, estimated tumor volume) were significantly worse in cases with PI-RADS 5 lesion than in those with PI-RADS 3 lesion. There were no significant differences in any of clinicopathologic features examined, except age, between PI-RADS 4 vs. 5 lesions. Kaplan-Meier analysis coupled with log-rank test revealed significantly higher risks of biochemical recurrence after RP in patients with PI-RADS 5 lesion than in those with PI-RADS 3 ( $P=0.027$ ), 4 ( $P=0.040$ ), or 3 or 4 ( $P=0.016$ ) lesion. Additionally, compared to cases with no cancer, cancer detection on T-Bx (i.e. T-Bx + B-Bx cases) was associated with a significantly higher risk of recurrence in patients with PI-RADS 5 lesion ( $P=0.046$ ), but not in those with PI-RADS 3 ( $P=0.254$ ) or 4 ( $P=0.085$ ) lesion.

	PI-RADS 3	PI-RADS 4	PI-RADS 5	P (3 vs 4)	P (3 vs 5)	P (4 vs 5)
<b>N</b>	47	90	85			
<b>Age (mean, year)</b>	65.6	64.5	66.2	0.327	0.523	0.044
<b>PSA (mean, ng/mL)</b>	8.69	8.57	10.44	0.908	0.158	0.081
<b>Cancer detection on Bx</b>				0.472	0.037	0.080
S-Bx only	11 (23%)	14 (16%)	7 (8%)			
T-Bx only	7 (15%)	12 (13%)	21 (25%)			
Both S-Bx and T-Bx	29 (62%)	64 (71%)	57 (67%)			
<b>Bx Grade Group (highest)</b>				0.030	0.084	0.256
1	10 (21%)	9 (10%)	7 (8%)			
2	22 (47%)	38 (42%)	40 (47%)			
3	9 (19%)	26 (29%)	16 (19%)			
4	2 (4%)	15 (17%)	15 (18%)			
5	4 (9%)	2 (2%)	7 (8%)			
<b>RP Grade Group</b>				0.016	0.013	0.144
1	3 (6%)	0 (0%)	0 (0%)			
2	29 (62%)	44 (49%)	43 (51%)			
3	12 (26%)	39 (43%)	26 (31%)			
4	0 (0%)	1 (1%)	3 (4%)			
5	3 (6%)	6 (7%)	12 (14%)			
<b>pT stage</b>				0.642	0.043	0.137
2/2+	29 (62%)	50 (56%)	35 (41%)			
3a	16 (34%)	37 (41%)	47 (55%)			
3b	2 (4%)	3 (3%)	3 (4%)			
<b>pN stage</b>				0.554 <sup>a</sup>	0.094 <sup>a</sup>	0.094 <sup>a</sup>
0	43 (91%)	85 (94%)	76 (89%)			
1	0 (0%)	2 (2%)	7 (8%)			
X	4 (9%)	3 (3%)	2 (2%)			
<b>Surgical margin</b>				0.472	0.051	0.157
Negative	41 (87%)	73 (81%)	61 (72%)			



**Conclusions:** PI-RADS 5 lesions are associated with adverse pathology in RP specimens, such as higher tumor grade, stage, and volume, as well as poorer prognosis following RP. Moreover, the failure of cancer detection on T-Bx of PI-RADS 5 lesion, but not PI-RADS 3 or 4 lesion, may particularly indicate favorable outcomes.

### 789 Correlation of CDKN2A Status with MTAP: Association with Molecular Subtype and Clinical Outcomes of Muscle Invasive Urothelial Carcinoma

Alexander Oberc<sup>1</sup>, Ekaterina Olkhov-Mitsel<sup>2</sup>, Elzbieta Slodkowska<sup>3</sup>, Kenneth Craddock<sup>3</sup>, Michelle Downes<sup>2</sup>

<sup>1</sup>University of Toronto, Toronto, ON, <sup>2</sup>Sunnybrook Health Sciences Centre, Toronto, ON, <sup>3</sup>Sunnybrook Health Sciences Centre, University of Toronto, Toronto, ON

**Disclosures:** Alexander Oberc: None; Ekaterina Olkhov-Mitsel: None; Elzbieta Slodkowska: None; Kenneth Craddock: None; Michelle Downes: None

**Background:** CDKN2A deletions are adverse features in non-muscle invasive bladder cancers however their impact and associations in the muscle invasive (MIBC) setting are still being investigated. Methylthioadenosine phosphorylase (MTAP), which also resides on chromosome 9p21, is reported as a reproducible surrogate immunohistochemistry (IHC) test for CDKN2A fluorescent in situ hybridization (FISH) in mesothelioma but such correlation in MIBC has not been described. We assessed CDKN2A and MTAP correlation in a MIBC cystectomy cohort and explored their relationship to FGFR3 mutations, molecular subtypes, and outcomes.

**Design:** A tissue micro-array of 302 high grade urothelial MIBC was created and assessed for CDKN2A status: normal, polysomy, homozygous (HOM-Del), heterozygous deletion (HET-Del) using DAKO probes and MTAP IHC (Abnova, clone 2G4). IHC was interpreted as negative when carcinoma completely lacked MTAP expression with appropriate internal controls. Results were compared with a subset of cases with known FGFR3 mutation status by next generation sequencing. Molecular subtype was defined as basal, luminal-URO and luminal-GU using CK5/6, GATA3, and p16 IHC. Relapse free (RFS) and overall survival (OS) were assessed. Statistical analysis was completed using SPSS.

**Results:** 281/302 cases (pT2=46, T3=151, T4=84) were assessable by FISH and all IHC markers (basal=53, URO=119, GU=100, negative=9). CDKN2A was deleted in 130/281 (46%) with MTAP loss in 80/281 (28%),  $p < 0.001$  (Table 1). Cases with MTAP loss were highly concordant with all CDKN2A deletions (PPV 92.5%, sensitivity=57%, specificity=96%) with improved sensitivity for HOM-Del (sensitivity=85%, specificity= 95%). CDKN2A status did not correlate with stage or nodal metastases. CDKN2A deletions were most frequent in luminal-URO (70% cases) and lowest in luminal-GU (17%) subtypes with 51% in basal subtype,  $p < 0.001$ . In a subset of cases assessed for FGFR3 mutations ( $n=47$  cases), CDKN2A deletions were seen in 6/7 FGFR3 mutated and 12/40 wild-type cases,  $p=0.0091$ . In luminal-URO, CDKN2A deletions or polysomy reduced RFS ( $p=0.080$ ) but not OS.

	Total	CDKN2A FISH		$\chi^2$ P-Value
	N=281	No deletion	Deletion	
<b>Stage</b>				
pt2	46	26 (56.5)	20 (43.5)	0.406
pt3	151	85 (56.3)	66 (43.7)	
pt4	84	40 (47.6)	44 (52.4)	
<b>Node</b>				
N0	168	95 (56.5)	73 (43.5)	0.249
N1	113	56 (49.6)	57 (50.4)	
<b>Molecular Subtypes</b>				
Basal	53	26 (49.1)	27 (50.9)	<0.001
Luminal - Uro	119	36 (30.3)	83 (69.7)	
Luminal - GU	100	83 (83)	17 (17)	
DN	9	6 (66.7)	3 (33.3)	
<b>MTAP status</b>				
Loss	80	6 (7.5)	74 (92.5)	<0.001
Retained	201	145 (72.1)	56 (27.9)	

**Conclusions:** *CDKN2A* deletions are frequent in MIBC, predominantly within the luminal-URO group where they impact RFS. MTAP staining shows high sensitivity and specificity for HOM-Del in *CDKN2A*. There is a strong correlation of *CDKN2A* deletions with *FGFR3* mutations as previously found in the non-muscle invasive setting.

## 790 Deep Learning Identifies FGFR Alterations from H&E Whole Slide Images in Bladder Cancer

Josh Och<sup>1</sup>, Boleslaw Osinski<sup>1</sup>, Kshitij Ingale<sup>1</sup>, Caleb Willis<sup>1</sup>, Rohan Joshi<sup>1</sup>, Nike Beaubier<sup>2</sup>, Martin Stumpe<sup>1</sup>  
<sup>1</sup>Tempus Labs, Chicago, IL, <sup>2</sup>Tempus, Chicago, IL

**Disclosures:** Josh Och: None; Boleslaw Osinski: None; Kshitij Ingale: None; Caleb Willis: None; Rohan Joshi: None; Nike Beaubier: None; Martin Stumpe: None

**Background:** Several targeted therapies for FGFR alterations in bladder cancer are either currently in clinical trials or already FDA-approved. FGFR alterations—including activating single nucleotide variants (SNVs) and fusions—are common in bladder cancer and detectable via next-generation sequencing of DNA and RNA. The ability to rapidly screen patients based on routine pathology would help prioritize patients for full NGS workup. Here, we developed a model using H&E whole slide images (WSIs) to predict FGFR alterations using real-world data.

**Design:** WSIs and ground truth labels pertaining to FGFR mutational status (obtained by DNA- and RNA-seq) were collected from primary and metastatic bladder cancer specimens (N=3,706, Table 1). Positive labels were defined as those harboring a pathogenic SNV or fusion of FGFR, as confirmed by a molecular pathologist (n=214 FGFR3, n=10 other FGFR genes). A holdout set (20% of data) was reserved for future validation purposes and not assessed further. Model development was performed on the remaining set of data as follows: i) a custom attention-based convolutional neural network with ResNet-18 backbone was trained to predict FGFR alteration from each WSI in the training set (60%), ii) hyperparameters were selected using an optimization set (20%) and iii) performance was reported on an evaluation set of data (20%). Training, optimization, and evaluation was performed in 5-fold cross-validation (CV). Cohorts were stratified to maintain a similar distribution of tissue site and scanner types across each fold.

**Results:** In 5-fold CV, the FGFR model achieved a mean receiver operating characteristic area under curve (ROC-AUC) of 0.79 (95% CI 0.72 - 0.87, Figure 1). The ROC-AUC was 0.82 (95% CI 0.77 - 0.87) for WSIs within the bladder and 0.76 (95% CI 0.69 - 0.83) for non-bladder, non-lymph node WSIs (Figure 2). The ROC-AUC was 0.80 (95% CI 0.72 - 0.88) for Philips UFS WSIs and 0.78 (95% CI 0.68 - 0.87) for Leica GT450 WSIs. The ROC-AUC when considering only FGFR3 mutated alterations was 0.79 (95% CI 0.72 - 0.87), and for FGFR1 / FGFR2 alterations was 0.81 (95% CI 0.69 - 0.94).

Table 1. Characteristics of the full cohort (N=3,706). A chi-square test was performed for each characteristic to determine association with the target label.				
Characteristic	Value	FGFR negative	FGFR positive	p-value
<b>Tissue site</b>	Bladder	1981	119	0.00448
	Lymph Node	309	9	
	Other	1192	96	
<b>Procedure Type</b>	Biopsy (unspecified)	752	42	0.72
	Needle Biopsy	529	39	
	Resection	2112	139	
	Excisional/Incisional Biopsy	89	4	
<b>Scanner Type</b>	Leica GT450	1792	145	3.64e-6
	Philips UFS	1690	79	

Figure 1 - 790

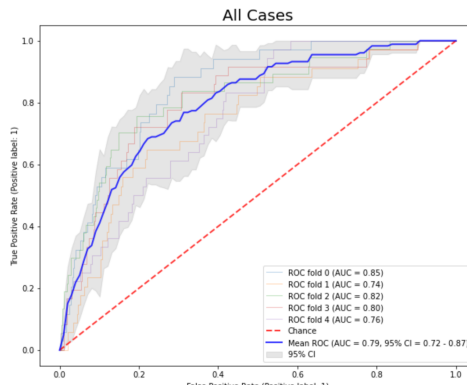
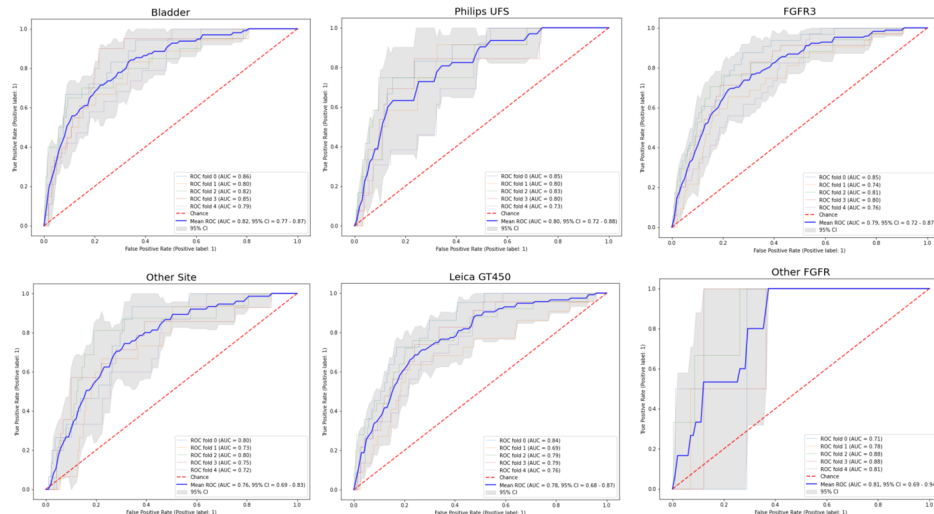


Figure 2 - 790



**Conclusions:** This work demonstrates the ability to predict FGFR SNVs and fusions in bladder cancer using a deep learning model trained on H&E WSIs. Performance was similar across tissue sites, scanner types, and genes within the FGFR family. We anticipate that this model could be used to rapidly identify patients enriched for FGFR alterations, who could then be prioritized for NGS screening.

## 791 Cribiform Growth is Associated with Higher Risk of Biochemical Recurrence After Radical Prostatectomies with Grade Group 5 Prostate Cancer

Jihane Oufattolle<sup>1</sup>, Andres Acosta<sup>2</sup>, Tanujit Dey<sup>1</sup>

<sup>1</sup>Brigham and Women's Hospital, Boston, MA, <sup>2</sup>Brigham and Women's Hospital, Harvard Medical School, Boston, MA

**Disclosures:** Jihane Oufattolle: None; Andres Acosta: None; Tanujit Dey: None

**Background:** Gleason pattern 5 (GP5) is heterogeneous, comprising single cells, files of single cells, solid masses/sheets and cribiform growth with comedonecrosis. Recent studies have suggested that cribiform carcinoma with comedonecrosis and large solid masses (comedo/solid) are associated with worse outcomes, but data on the prognostic significance of these sub-patterns in the context of Grade Group 5 (GG5) disease is limited. The goal of this study was to evaluate the prognostic significance of solid/comedo in radical prostatectomies (RP) with GG5 Prostate cancer (PCa).

**Design:** We identified all in-house RP with GG5 PCa and excluded cases with limited archival material, history of neoadjuvant ADT, prior radiation, and those in which GG5 could not be confirmed after re-review of slides. All slides were reviewed for each case to determine GP5 sub-patterns. Cases with any amount of comedo/solid were considered comedo/solid+. Other variables obtained by review of slides and medical records included: cribriform carcinoma/intraductal carcinoma without comedonecrosis (CC/IDC), T stage, N stage, margin status, lymphovascular invasion, PSA and biochemical recurrence (BCR).

**Results:** One-hundred and thirty (130) patients with a median age of 65 years and median pre-operative PSA values of 8 ng/mL were included in the analysis. Fifty-six (56, 43%) were comedo/solid+ and 74 (57%) were comedo/solid-. Among comedo/solid+, 48 (86%) were also CC/IDC+. Among comedo/solid-, 34 (46%) were also CC/IDC+. On multivariable regression analysis, comedo/solid- was associated with a lower risk of BCR (OR=0.45, 95% CI=0.21, 0.96,  $p=0.039$ ) only when CC/IDC status was excluded from the model. When CC/IDC status was included, CC/IDC+ was the only variable significantly associated with higher rates of BCR (OR=4.22, 95% CI=1.77, 11.0,  $p=0.002$ ). Interestingly, pT stage, margin status and PSA values were not associated with outcomes in this series of RP with GG5 PCa. The number of cases with pTN1 stage was too small to analyze in a multivariable model.

# ABSTRACTS | GENITOURINARY PATHOLOGY (INCLUDING RENAL TUMORS)

Table 1- Comparison of Grade Group 5 radical prostatectomies with and without large solid growth and comedonecrosis			
	Comedo/Solid+	Comedo/Solid-	
<b>Age</b>			
Median (range)	65 (50,77)	65 (43,79)	
<b>PSA</b>			
Median (range)	8 (1,42)	8 (2,43)	
<b>Stage</b>			
pT2	9 (16%)	18 (24%)	
pT3a	27 (48%)	35 (47%)	
pT3b	20 (36%)	21 (28%)	
<b>Cribiform/intraductal carcinoma</b>			
Present	48 (86%)	34 (46%)	
Absent	8 (14%)	40 (54%)	
<b>Lymphovascular invasion</b>			
Present	25 (45%)	20 (27%)	
Absent	31 (55%)	54 (73%)	
<b>Surgical margin status</b>			
Positive	26 (46%)	27 (36%)	
Negative	30 (54%)	47 (64%)	
<b>Multivariable analysis</b>			
<b>Characteristic</b>	<b>OR<sup>1</sup></b>	<b>95% CI<sup>1</sup></b>	<b>p-value</b>
<b>Age</b>	0.99	0.93, 1.05	0.654
<b>GP5</b>			
Comedo/Solid+	—	—	
Comedo/Solid-	0.69	0.30, 1.58	0.376
<b>Cribiform</b>			
0	—	—	
1	3.63	1.43, 9.96	<b>0.009</b>
<b>T Stage</b>			
2	—	—	
3a	2.00	0.64, 6.84	0.244
3b	1.66	0.47, 6.24	0.441
<b>Margin</b>			
<b>Negative</b>	—	—	
<b>Positive</b>	0.57	0.24, 1.30	0.189
<b>LVI</b>			
No	—	—	
Yes	1.47	0.64, 3.41	0.364
<b>PSA</b>	1.03	0.98, 1.09	0.239

<sup>1</sup>OR = Odds Ratio, CI = Confidence Interval

**Conclusions:** The results of this study suggest that large solid growth and comedonecrosis is highly associated with CC/IDC in RPs with GG5 PCa. In this context, the presence of CC/IDC seems to be an important independent predictor of BCR. Additional studies with a larger number of CC/IDC- cases are needed to determine if large solid growth and comedonecrosis have independent prognostic value in RPs with GG5 PCa.

## 792 Fibrous Epithelial Cellular Component in Renal Oncocytomas: A Morphological and Immunohistochemical Study of a Challenging Diagnostic Finding

Angel Panizo<sup>1</sup>, Luiz Nova-Camacho<sup>2</sup>, Francisco Queipo<sup>3</sup>, Gregorio Aisa<sup>1</sup>, Guillermo Garcia Diego<sup>4</sup>, María Garcia Martos<sup>4</sup>

<sup>1</sup>Complejo Hospitalario de Navarra, Pamplona, Spain, <sup>2</sup>Hospital Universitario Donostia - Osakidetza, Donostia, Spain, <sup>3</sup>Complejo Hospitalario Universitario A Coruña (CHUAC), A Coruña, Galicia, Spain, <sup>4</sup>University Gregorio Marañon Hospital, Madrid, Spain

**Disclosures:** Angel Panizo: None; Luiz Nova-Camacho: None; Francisco Queipo: None; Gregorio Aisa: None; Guillermo Garcia Diego: None; María Garcia Martos: None

**Background:** Renal oncocytoma (RO) is a benign neoplasm, which may show potentially problematic and worrisome microscopic features. Fibrous epithelial cellular component (FECC) refers to entrapped epithelial cells with cytoplasmic clearing (ccRCC-like foci) within the fibrous stroma/scar. FECC has been previously reported although not to date studied in detail. The aim of our study has been to characterize the morphology and its IHC profile.

**Design:** We retrospectively evaluated cases of RO with scar, collected from four tertiary academic centers. Cases with fibrous stroma/scar containing FECC were selected and examined for architectural patterns, cytological features, and IHC (CK7, CD117, vimentin, CA-IX, AMACR/P504S, cyclin-D1, and CK34bE12) in comparison to the surrounding oncocytoma.

# ABSTRACTS | GENITOURINARY PATHOLOGY (INCLUDING RENAL TUMORS)

**Results:** Three hundred sixty one ROs were retrieved, and 114 cases (31.6%) showed a gross or microscopic central scar. Seventy-eight cases containing a scar with FECC were finally evaluated. In 25 ROs, the FECC was so abundant that it showed a tumor-like morphology or tumor-in-tumor collision. Six architectural patterns were recognized: tubular, trabecular-solid, microcystic, nephrogenic adenoma-like, angiomyomatoid-like, and mixed. The FECC was located immediately adjacent to the oncocytoma component (32.1%), in the central portion of the scar (15.4%) or diffusely (52.6%). Cytologically, four cell types were identified in the FECC, all of them with cleared (ccRCC-like) or eosinophilic cytoplasm: flat-elongated, cuboidal, hobnail, and vacuolated-signet ring-like. In most FECC (88.5%), the nuclei were “higher grade” than oncocytes or atypical/reactive with nucleolus. The IHC study showed positivity for CK7 (100%), vimentin (100%), CA-IX (85.7%), AMACR (100%), and negativity for CD117 and cyclin D1 in the FECC. The RO showed an inverse IHC pattern to FECC.

	FECC	Oncocytoma
Predominant Architecture		
Tubular	47 (60.3%)	
Trabecular-solid	8 (10.3%)	
Microcystic	5 (6.4%)	
Nephrogenic adenoma-like	12 (15.4%)	
Angiomyomatoid	6 (7.7%)	
Predominant Cytology		
Flat-elongated	36 (46.2%)	
Cuboidal	36 (46.2%)	
Hobnail	4 (5.1%)	
Vacuolated-signet ring-like	2 (2.6%)	
Cytoplasm		
Cleared	49 (62.8%)	
Cleared+eosinophilic	29 (37.2%)	
Nucleus		
“Higher grade”	69 (88.5%)	
Oncocyte-like	9 (11.5%)	
Mucinous basophilic secretion		
Present	18 (23.1%)	
Absent	60 (76.9%)	
IHC CK7		
Positive	66/66 (100%)	0/73 (0%)
Negative	0/66 (0%)	73/73 (100%)
IHC CD117		
Positive	0/63 (0%)	65/65 (100%)
Negative	63/63 (100%)	0/65 (0%)
IHC Vimentin		
Positive	54/54 (100%)	0/54 (0%)
Negative	0/54 (0%)	54/54 (100%)
IHC CA-IX		
Positive	6/7 (85.7%)	0/7 (0%)
Negative	1/7 (14.3%)	7/7 (100%)
IHC AMACR/P504S		
Positive	10/10 (100%)	0/10 (0%)
Negative	0/10 (0%)	10/10 (100%)
IHC Cyclin D1		
Positive	0/4 (0%)	4/4 (100%)
Negative	4/4 (100%)	0/4 (0%)

Figure 1 - 792

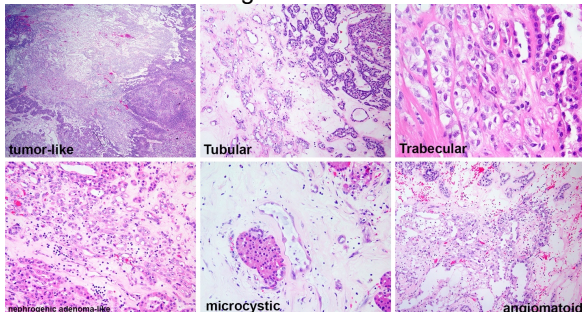
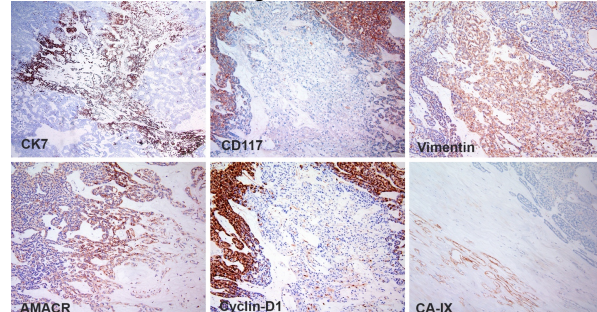


Figure 2 - 792



**Conclusions:** FECC is a relatively unusual finding, which in our series appeared in 21.6% of all ROs. FECC can show widely variable architectural and cytological patterns. It is important to know and keep FECC in mind, when evaluating an oncocytic tumor, since it may pose diagnostic problems, especially in needle core biopsies. Its IHC profile is the inverse of the RO. This raises questions about its origin: trapped normal renal tubular component with reactive changes vs. changes in tumor cells in a fibrotic “hostile” hypoxic microenvironment.

**793 Methylation Profiling and Machine Learning Identify and Classify Clinically Relevant Types of Renal Neoplasms**

Antonios Papanicolau-Sengos<sup>1</sup>, Omkar Singh<sup>2</sup>, Rohit Gupta<sup>3</sup>, Yu Liu<sup>4</sup>, Kyung Park<sup>5</sup>, Jonathan Antonios Papanicolau-Sengos<sup>1</sup>, Omkar Singh<sup>2</sup>, Rohit Gupta<sup>3</sup>, Yu Liu<sup>4</sup>, Kyung Park<sup>5</sup>, Jonathan Serrano<sup>6</sup>, Jasper Wu<sup>7</sup>, Jairo Barreto<sup>3</sup>, Zied Abdullaev<sup>8</sup>, Rust Turakulov<sup>8</sup>, Fang-Ming Deng<sup>9</sup>, Maria Merino<sup>10</sup>, Maria Tretiakova<sup>11</sup>, Jeffry Simko<sup>7</sup>, Bradley Stohr<sup>7</sup>, Emily Chan<sup>7</sup>, Drew Pratt<sup>1</sup>, Matija Snuderl<sup>6</sup>, David Solomon<sup>7</sup>, Kenneth Aldape<sup>8</sup>

<sup>1</sup>Center for Cancer Research, National Cancer Institute, Bethesda, MD, <sup>2</sup>Center for Cancer Research, National Cancer Institute, National Institutes of Health, Bethesda, MD, <sup>3</sup>University of California San Francisco, San Francisco, CA, <sup>4</sup>National Cancer Institute, Laboratory of Pathology, Bethesda, MD, <sup>5</sup>NYU Langone Health, New York, NY, <sup>6</sup>New York University, New York, NY, <sup>7</sup>University of California, San Francisco, San Francisco, CA, <sup>8</sup>National Institutes of Health, Bethesda, MD, <sup>9</sup>New York University Medical Center, New York, NY, <sup>10</sup>National Cancer Institute, Bethesda, MD, <sup>11</sup>University of Washington, Seattle, WA

**Disclosures:** Antonios Papanicolau-Sengos: None; Omkar Singh: None; Rohit Gupta: None; Yu Liu: None; Kyung Park: None; Jonathan Serrano: None; Jasper Wu: None; Jairo Barreto: None; Zied Abdullaev: None; Rust Turakulov: None; Fang-Ming Deng: None; Maria Merino: None; Maria Tretiakova: None; Jeffry Simko: None; Bradley Stohr: None; Emily Chan: None; Drew Pratt: None; Matija Snuderl: None; David Solomon: None; Kenneth Aldape: None

**Background:** DNA methylation is an early and stable event in cell differentiation and tumorigenesis. Measurement of genome-wide methylation signatures by Illumina arrays is feasible in FFPE clinical samples and has well demonstrated utility in brain and mesenchymal neoplasm classification.

**Design:** We profiled FFPE samples of renal neoplasms on Illumina methylation arrays and obtained methylation data from publicly available sources. Machine learning applications were used to characterize distinct methylation groups and identify relationships with known clinicopathologic parameters.

**Results:** We analyzed DNA methylation data (450k and 850k) of 1626 kidney and urothelial neoplasms and normal kidney controls. Of these, 226 were newly profiled and the remaining 1400 samples were obtained from publicly available datasets. Using unsupervised dimensionality reduction, we identified 20 groups comprising cortex, medulla, and 18 neoplasm classes (1 urothelial group and 17 classes of kidney neoplasms) (Figure 1). Several histologically defined tumor entities resolved into distinct epigenetic subclasses including prognostically favorable (Cluster 1) and unfavorable (Cluster 2) classes of both clear cell RCC (ccRCC) and papillary RCC (pRCC) (Figure 2). pRCC Cluster 2 tumors (unfavorable prognosis) often had both *SETD2* and *PBRM1* mutations. A distinct class of *VHL*-wild-type clear cell papillary RCC (ccpRCC) without chromosome 3p loss was also identified. Tumors with a histologic diagnosis of chromophobe RCC (ChRCC) resolved into 3 classes: a major ChRCC class enriched in *TP53* mutations, an MTOR pathway mutation enriched class, and a smaller class of eosinophilic renal tumors with benign clinical course. Additional groups included FH-deficient RCC, *FLCN*-mutant hybrid oncocytic tumor, *KRAS*-mutant papillary renal neoplasm with reverse polarity, *BRAF*-mutant metanephric adenoma, angiomyolipoma, Wilms tumor, malignant rhabdoid tumor, and clear cell sarcoma of the kidney. A support vector machine (SVM)-based classifier was developed using a reference set of 1268 samples and applied to a validation set (n=358), showing that 353 samples (99%) were correctly assigned to one of the 20 classes (Table).

	Correctly classified	Misclassified
ccRCC Cluster 1	94	0
ccRCC Cluster 2	8	1
pRCC Cluster 1	48	0
pRCC Cluster 2	4	1
Clear cell papillary RCC	6	0
Major ChRCC	10	0
ChRCC MTOR enriched	2	0
Eosinophilic renal tumor	3	0
Oncocytoma	5	0
Reverse polarity	1	0
FH-deficient	10	1
FLCN-mutant hybrid	4	0
Malignant rhabdoid tumor	21	1
Urothelial	87	0
Clear cell sarcoma of kidney	3	0
Wilms	36	0
Metanephric adenoma	1	0
Renal angiomyolipoma	3	0
Cortex	4	1
Medulla	3	0

Figure 1 - 793

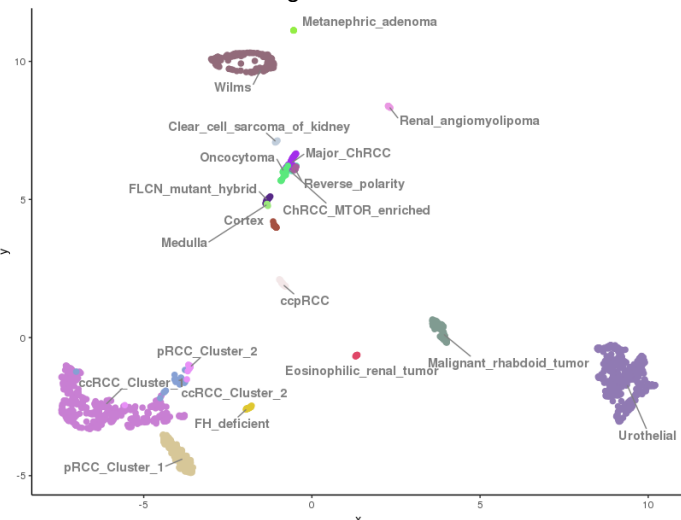
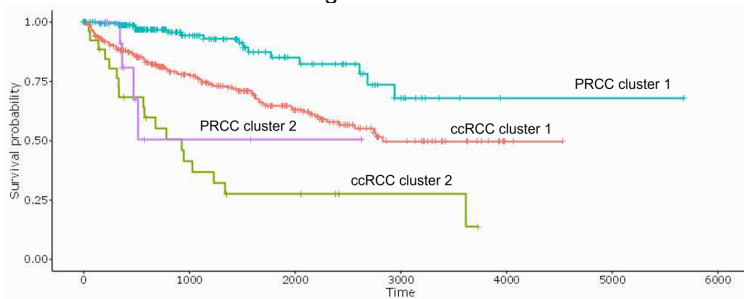


Figure 2 - 793



**Conclusions:** We used DNA methylation profiling to identify novel renal neoplasm molecular classes and achieved robust classification of these clinicopathologically distinct classes. Future work will expand the number and diagnostic utility of kidney tumor methylation classes.

## 794 Genomic Alterations of Mexican Patients with Bladder Cancer

Maria Delia Perez Montiel<sup>1</sup>, Dennis Cerrato Izaguirre<sup>1</sup>, Carlo Cortes<sup>1</sup>, José Díaz-Chávez<sup>1</sup>, Miguel Angel Jimenez<sup>1</sup>, Anna Scavuzzo<sup>1</sup>, Alicia Orozco<sup>1</sup>, Andrea Ramirez<sup>1</sup>, Jairo Rubio<sup>1</sup>, Yessenia Sanchez Perez<sup>1</sup>, Luis Herrera<sup>2</sup>, David Cantu de Leon<sup>1</sup>, Diddier Prada<sup>1</sup>

<sup>1</sup>Instituto Nacional de Cancerología, Mexico City, Mexico, <sup>2</sup>Mexico City, Mexico

**Disclosures:** Maria Delia Perez Montiel: None; Dennis Cerrato Izaguirre: None; Carlo Cortes: None; José Díaz-Chávez: None; Miguel Angel Jimenez: None; Anna Scavuzzo: None; Alicia Orozco: None; Andrea Ramirez: None; Jairo Rubio: None; Yessenia Sanchez Perez: None; Luis Herrera: None; David Cantu de Leon: None; Diddier Prada: None

**Background:** Bladder urothelial carcinoma (BUC) is the most common neoplasm of the urinary tract. Muscle invasive bladder carcinoma (MIBUC) is the most aggressive BUC and is characterized by genomic instability and a high mutational rate. Genomic data has led to a better molecular classification of BUC, but this data is elusive in Hispanic patients. Thus, we aim to identify the somatic variants and copy number variations (CNV) of Mexican patients with BUC assessing for a potential relationship with the MIBUC.

**Design:** We conducted a retrospective, cross-sectional study using data from 37 patients. Genomic DNA was isolated from formalin-fixed, paraffin-embedded BC tissues obtained from the National Cancer Institute – Mexico pathology department for each patient. DNA was sequenced and mapped against the reference genome hg19. High confidence variants were identified by two or more variant callers (Mutect2, Strelka2, and Lancet). CNVs were identified with Facets. Mutations and CNV events frequency were contrasted with the MIBC phenotype using Fisher's exact test.

**Results:** A total of 37 patients with a mean age at diagnosis of 62.49 years (Standard Deviation [SD]: 11.41 years) and a greater proportion of male patients (70.73%) were included. MIBUC was identified in 45.95% (n=17) of the cases and displayed a poorer overall survival compared to patients with non-MIBUC ( $p=0.001$ ). A total of 15,770 somatic variants were identified, from which 601

were considered driver mutations. *KMT2C* (32%), *CDC27* (27%), *ARID1A* (24%), *KMT2D* (22%), and *MUC16* (22%) were the Top-5 genes more mutated. Chromosomes 20, 19, and 8 were affected almost entirely by CNV gains, whereas chromosomes 9, 10, 17, 21, and 22 were affected mainly by CNV losses. The cytobands 5q31.3 (94.59%), 1p36.21 (91.89%), and 19q13.42 (81.08%) were the most frequently affected. When comparing the mutations landscape, patients with MIBUC tended to present frequent mutations in *KMT2CD* ( $p=0.06$ ) and focal amplifications in 11p15.5 ( $p=0.06$ ), whereas patients with non-MIBUC tend to have more *BRCA1* ( $p=0.07$ ), *CTNNND1* ( $p=0.07$ ) and *STPAN1* ( $p=0.07$ ) and focal deletions in chr7q11.23 ( $p=0.005$ ).

**Conclusions:** Mexican patients with MIBUC showed a high frequency of *KMT2CD* mutation and focal amplification of 11p15.5. To our knowledge, this is the first genomic evaluation of BUC in a Hispanic cohort. Further research is needed to confirm the high mutation frequency of *KMT2D* in Hispanic patients and to assess its potential as a prognostic biomarker.

## 795 Characterizing the Genomic Landscape of Micropapillary Variant of Urothelial Carcinoma of the Bladder Harboring Activating Extra-Cellular Mutations of the ERBB2 Gene

Jessica Posada<sup>1</sup>, Evgeny Yakirevich<sup>2</sup>, Jeffrey Ross<sup>3</sup>, Liang Cheng<sup>4</sup>

<sup>1</sup>Brown University Lifespan Academic Medical Center, Providence, RI, <sup>2</sup>Rhode Island Hospital, Providence, RI, <sup>3</sup>SUNY Upstate Medical University, Syracuse, NY, <sup>4</sup>Alpert Medical School of Brown University, Providence, RI

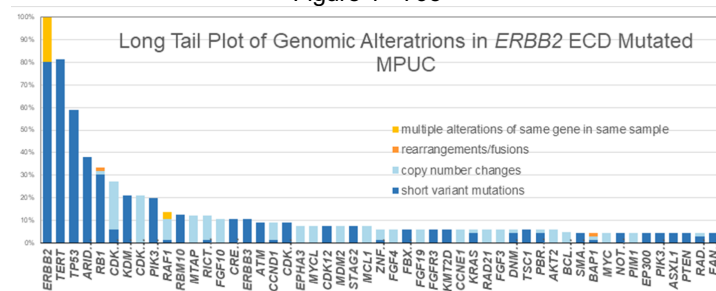
**Disclosures:** Jessica Posada: None; Evgeny Yakirevich: None; Jeffrey Ross: None; Liang Cheng: None

**Background:** Micropapillary variant of urothelial carcinoma of the bladder (MPUC) is a rare and aggressive histological variant of bladder cancer and has been associated with a poor prognosis. A high frequency of MPUC contain activating mutations in the extracellular domain (ECD) of *ERBB2*. We sought to further characterize *ERBB2* ECD-mutated tumors to identify additional genomic alterations (GA) that have been associated with tumor progression, therapeutic response and treatment resistance.

**Design:** DNA was extracted from 219 cases of formalin-fixed paraffin-embedded sections from *ERBB2* ECD-mutated bladder tumors. We used comprehensive genomic profiling (CGP) to evaluate the frequencies of GA. Sequencing was performed using hybridization-captured, adaptor ligation-based libraries to a mean coverage depth of  $>500\times$  for 315 cancer-related genes. Tumor mutational burden (TMB) was determined on up to 1.1 Mbp of sequenced DNA and microsatellite instability (MSI) was determined on 114 loci.

**Results:** We identified 219 cases of urothelial bladder cancer with *ERBB2* ECD mutations, 63 (28.7%) of which were MPUC. The median age of patients was 74 and 71 for MPUC and non-MPUC, respectively. Male sex was predominant in both cohorts (87% in MPUC and 81% in non-MPUC). Analysis of co-mutated genes revealed that *TERT*, *TP53*, and *ARID1A* were the most common co-altered genes in *ERBB2*-mutant MPUC (82.5%, 58.3%, and 39.7%) and did not differ significantly from *ERBB2*-mutant non-MPUC (86.5%, 51.9%, and 35.3%). The main genomic differences between *ERBB2* ECD-mutated MPUC versus non-MPUC were in frequencies of *KMT2D*, *RB1* and *MTAP* mutations. *KMT2D* and *RB1* are tumor suppressor genes. *KMT2D* frequency was significantly decreased in *ERBB2* ECD-mutated MPUC (6.4%) versus non-MPUC tumors (27.6%) ( $p=0.02$ ). *RB1* mutations were higher in *ERBB2* ECD-mutated MPUC (33.3%) than non-MPUC (17.3%). Lastly, *MTAP* is an arginine metabolism gene and is an emerging biomarker for new synthetic lethality based anti-cancer drugs (PRMT5 and MTA2 inhibitors). *MTAP* loss was lower in *ERBB2* ECD-mutated MPUC (11.1%) compared to non-MPUC (26.9%).

Figure 1 - 795



**Conclusions:** Characterizing the genomic landscape of urothelial carcinoma is an important tool to identify possible diagnostic and prognostic biomarkers that drive tumor progression and dictate treatment response. This study identified *KMT2D*, *RB1* and *MTAP* as potential important genomic driver co-mutations that differ between *ERBB2* ECD-mutated MPUC versus non-MPUC tumors.

## 796 The Impact of a Second Opinion Review of Prostatic Specimen Reports by a Subspecialist Genitourinary Pathologist: The Experience of a Brazilian Cancer Center

João Henrique Quintão<sup>1</sup>, Gabriel Oliveira<sup>1</sup>, Warley Nunes<sup>1</sup>, Stephania Bezerra<sup>1</sup>

<sup>1</sup>A.C.Camargo Cancer Center, São Paulo, Brazil

**Disclosures:** João Henrique Quintão: None; Gabriel Oliveira: None; Warley Nunes: None; Stephania Bezerra: None

**Background:** Middle-income countries face challenging health care and educational systems. Regarding the training of the pathologists, the reduced offer of fellowship programs leads to a small number of subspecialist pathologists. Correct pathological evaluation of prostatic specimens is crucial for patient prognostic assessment and therapeutic planning. This study aims to compare original prostatic cancer reports with subspecialist second-opinion reviews and determine the concordance rate in a tertiary Brazilian cancer center.

**Design:** Reviewed reports of prostatic specimens were searched in our institution pathology database between April 2017 and August 2022. The cases were referred for second opinion or reviewed routinely by trained genitourinary pathologists before initiation of the treatment. Our study included reviewed reports of biopsy, transurethral resections of the prostate (TURP) and radical prostatectomies (RP). Diagnostic agreement after review was evaluated for the following variables: diagnosis of prostatic adenocarcinoma (PA), Gleason score (GS) and ISUP grading group (GG). Kappa coefficient ( $\kappa$ ) was performed to establish diagnostic concordance.

**Results:** In the period of study, 729 cases of 725 patients were reviewed, including 678 biopsies, 33 RP and 18 TURP. 708 cases (97.1%) showed diagnosis agreement ( $\kappa=0.797$ ;  $p<0.001$ ) in which 662 cases agreed on the diagnosis of PA. Among PA cases, GS concordance was observed in 408 cases (61.6%) and disagreement in 254 (38.4%) ( $\kappa=0.496$ ;  $p<0.001$ ). Among all cases with GS disagreement, there was an upgrade in 155 cases (61.0%), downgrade in 75 cases (29.5%) and maintenance of GG in 24 cases (9.5%) ( $\kappa=0.537$ ;  $p<0.001$ ). Specifically in biopsy and TURP cases, in which the change of GG can potentially define surgical indication, there was GS disagreement in 243 cases (38.5%) ( $\kappa=0.488$ ;  $p<0.001$ ), with an upgrade, downgrade, and maintenance of GG in 59.3%, 30.8% and 9.9%, respectively ( $\kappa=0.532$ ;  $p<0.001$ ). Among all cases, there was diagnostic discordance in 21 cases (2.9%) after review, one case with change in the diagnosis from benign to PA and from PA to benign in 8 cases.

**Conclusions:** Accurate pathological diagnosis is crucial for defining the best therapeutic approach for patients. Thus, the relevant rate of diagnostic disagreement regarding GS and GG in prostatic samples found in our study endorses the significant role of pathologic report review by a subspecialist genitourinary pathologist.

## 797 Augmentation of Prostatic Tissue Sampling for Molecular Analysis Using Nonlinear Microscopy

Daniel Ram<sup>1</sup>, Timothy Weber<sup>2</sup>, Lisha Wang<sup>1</sup>, James Fujimoto<sup>2</sup>, Seymour Rosen<sup>3</sup>, Yue Sun<sup>3</sup>

<sup>1</sup>Beth Israel Deaconess Medical Center, Harvard Medical School, Boston, MA, <sup>2</sup>Massachusetts Institute of Technology, Cambridge, MA, <sup>3</sup>Beth Israel Deaconess Medical Center, Boston, MA

**Disclosures:** Daniel Ram: None; Timothy Weber: None; Lisha Wang: None; James Fujimoto: None; Seymour Rosen: None; Yue Sun: None

**Background:** Molecular analysis has been useful in translational studies of prostatic tissues, but is hampered by the availability and quality of appropriate tissues, i.e. tumor recognition in radical prostatectomies. Nonlinear microscopy (NLM) is a laser microscopy technique that can rapidly image tissue without requiring sectioning. It can recognize prostate carcinoma in both fresh and fixed tissue with high sensitivity and specificity. NLM produces high resolution images that resemble H&E histology by using a scanned, short-pulsed laser to excite exogenous fluorescence only at the laser focus. NLM does not interfere with subsequent tissue processing or immunohistochemical analysis. In this study we obtained fresh tissues from prostatectomies of patients enrolled in a NIH funded project (NIH 5R01CA249151-02) designed to examine prostate tissue margins and putatively reduce neurovascular bundle sacrifice.

**Design:** Fresh tissue specimens were stained in acridine orange and sulforhodamine 101 solution for 2 min and rinsed for 30-second in saline. Areas of cancer and tumor infiltrating lymphocytes (TILs) were identified by NLM. Collected fresh tissues were mechanically disrupted and filtered through a nylon mesh screen. Single cell suspensions were centrifuged at 500 x g for 5 min and the cell pellet was washed before staining. Collected single cell suspensions were processed for TILs functional assays and isolation of TIL-specific RNA, DNA and proteins.

**Results:** NK cells and T cells were identified by first gating on lymphocytes and then gating on CD45+ and amine negative viable cells that were either NK cells (CD14-CD20-CD3-CD159A+) or T cells (CD14-CD20-CD3+CD159A-). Prostate cancer and benign prostatic hyperplasia (BPH) tissue along with sorted NK cells and CD8+ T cells from these tissues were sequenced using third generation sequencing (TGS) direct RNA sequencing (Nanopore). NK cells and CD8+ T cells were also assessed for activation state and general phenotypes in addition to more functional properties using multiparametric flow cytometry panels. Preliminary

# ABSTRACTS | GENITOURINARY PATHOLOGY (INCLUDING RENAL TUMORS)

TGS approaches have also generated 5-20 long RNA sequence reads per gene, on average, with associated epitranscriptional modification of RNA bases.

Table I. Representative 30 parameter (28 colors plus FSC/SSC) phenotypic panel for tissue leukocyte phenotyping.

BUV395	BV421	DAPI(450)	BUV496	BV510	BB515	BUV563
CD127	CD40L	Live/Dead	CCR7	CXCR3	Ki67	HLA-DR
BV570	PE/BYG584	BUV615	BV605	PE CF594	BB660	BUV661
CD16	CD25	CD14	PD-1	Granzyme B	CD57	FOXP3
PE Cy5	APC	BV650	BV711	BB700	PE Cy5.5	BUV737
NKG2A	$\alpha$ 4 $\beta$ 7	CD4	CCR4	NKG2C	CD45RA	CD28
A700	BV750	PE Cy7	BB790	APC Cy7	BV786	BUV805
CD3	NKG2D	NKp46	CD56	CD8	CD20	CD95

Figure 1 - 797

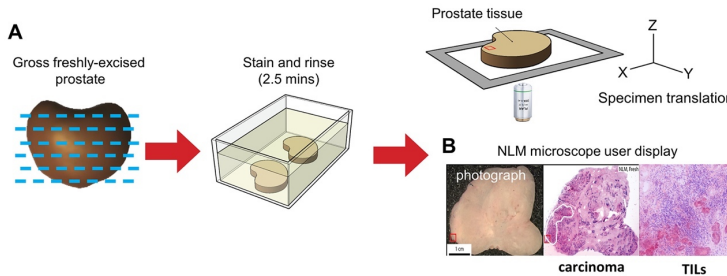


Figure 1. A. Schematic showing NLM imaging procedure. B. Carcinoma and TILs can be identified by NLM of fresh radical prostatectomy specimen.

Figure 2 - 797

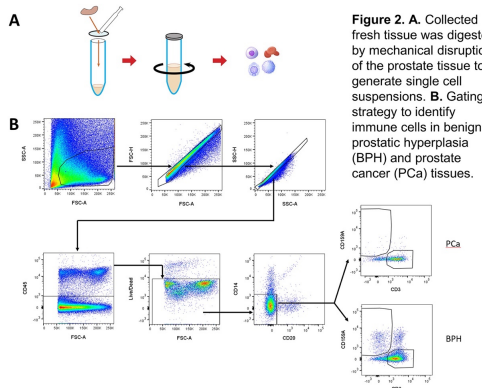


Figure 2. A. Collected fresh tissue was digested by mechanical disruption of the prostate tissue to generate single cell suspensions. B. Gating strategy to identify immune cells in benign prostatic hyperplasia (BPH) and prostate cancer (PCa) tissues.

**Conclusions:** We report initial data using NLM for fresh prostatic tissue sampling. This method enables researchers to collect fresh tumor tissue and TILs from radical prostatectomy specimens enhancing specimen quality, while preserving surgical margins and diagnostic tissue.

## 798 Extent of Primary Gleason Pattern 4 Carcinoma Predicts Adverse Outcome Independent of Secondary Pattern 3 or 5 in Prostatic Needle Core Biopsies

Pranav Renavikar<sup>1</sup>, Subodh Lele<sup>1</sup>

<sup>1</sup>University of Nebraska Medical Center, Omaha, NE

**Disclosures:** Pranav Renavikar: None; Subodh Lele: None

**Background:** Gleason score and grade group of prostate adenocarcinoma on needle core biopsies help in risk stratification and prognosis. Higher grade groups typically demonstrate increased risk of biochemical recurrence and advanced (metastatic) disease. Within one grade group, the percentage of cores involved by tumor is directly related to increased risk of aggressive disease. Recent studies have shown that volume of Gleason pattern 4 in radical prostatectomies has the most influence on pre- and post-operative serum prostate specific antigen (PSA) as well as disease progression. Our aim was to predict the clinical behavior based on prostate biopsy assessment of limited versus extensive Gleason pattern 4 carcinoma compared across separate grade groups and secondary patterns. To our knowledge, such a study has not been previously published.

**Design:** Our institutional pathology database was searched for prostate carcinoma cases which had Gleason score 4+3=7 and higher on biopsy. Cases were classified into Gleason score 4+5=9 with less than 50% cores involved (limited pattern 4) and Gleason score 4+3=7 with more than 50% cores involved (extensive pattern 4). Cases with any additional cores showing differing Gleason scores were excluded. Follow-up information like radical prostatectomy findings, treatment modalities provided and percentage of cases with biochemical recurrence was obtained.

**Results:** A total of 972 prostate biopsies (2015-2018) with Gleason score 4+3=7 and higher were reviewed. More than 95% of the cases had been diagnosed and graded by one of the authors. All cases had received clinical interventions like radical prostatectomy, androgen deprivation, radiation therapy or combination modalities. 23 cases had Gleason score 4+5=9 with less than 50% cores involved. 4 of 23 cases (17%) had biochemical recurrence (mean recurrence free survival = 15 months). 7 cases had Gleason score 4+3=7 with more than 50% cores involved. 3 of 7 cases (43%) had biochemical recurrence (mean recurrence free survival = 27 months).

# ABSTRACTS | GENITOURINARY PATHOLOGY (INCLUDING RENAL TUMORS)

**Conclusions:** Extent of involvement by primary Gleason pattern 4 carcinoma on prostate biopsies predicts adverse outcome independent of secondary pattern 3 or 5.

## 799 Mutations of NOTCH Genes as an Alternative Mechanism to Activate mTOR pathway in Low-grade Oncocytic Tumor (LOT) of the Kidney

Costantino Ricci<sup>1</sup>, Maria Sirolli<sup>1</sup>, Francesca Ambrosi<sup>2</sup>, Tania Franceschini<sup>3</sup>, Francesca Giunchi<sup>3</sup>, Federico Bianchi<sup>3</sup>, Riccardo Schiavina<sup>1</sup>, Francesco Massari<sup>1</sup>, Veronica Mollica<sup>1</sup>, Michelangelo Fiorentino<sup>2</sup>, Thais Maloberti<sup>4</sup>, Giovanni Tallini<sup>5</sup>, Dario de Biase<sup>5</sup>

<sup>1</sup>S.Orsola-Malpighi Hospital, University of Bologna, Bologna, Italy, <sup>2</sup>Maggiore Hospital, University of Bologna, Bologna, Italy, <sup>3</sup>S.Orsola-Malpighi Hospital, Bologna, Italy, <sup>4</sup>Alma Mater Studiorum-University of Bologna, Bologna, Italy, <sup>5</sup>University of Bologna School of Medicine, Bologna, Italy

**Disclosures:** Costantino Ricci: None; Maria Sirolli: None; Francesca Ambrosi: None; Tania Franceschini: None; Francesca Giunchi: None; Federico Bianchi: None; Riccardo Schiavina: None; Francesco Massari: None; Veronica Mollica: None; Michelangelo Fiorentino: None; Thais Maloberti: None; Giovanni Tallini: None; Dario de Biase: None

**Background:** Low-grade oncocytic tumor (LOT) of the kidney is a recently described entity, characterized by an oncocytoma-like morphology, a distinct immunohistochemical profile (CK7+, CD117-), and gene mutations (TSC1/2, MTOR) resulting in a constitutive mTORC1 complex activation. Herein, we analyzed a case series of LOT to verify whether, in addition to the mutations directly affecting the mTOR pathway, other genes could be involved in the activation of the mTORC1 complex through alternative mechanisms.

**Design:** We retrospectively collected 9 cases of LOT diagnosed at our two Institutions between January 1st 2019-May 1st 2022; all cases were reviewed and confirmed by two uropathologists, also adopting a large immunohistochemical (PAX8, CD117, CK7, AMACR, CK20, Ki67, FH, SHDB, Cathepsin-K). Subsequently, each case was tested with two laboratory-developed NGS panels targeting a total of 19 tumor-associated genes (for a total of 888 amplicons), including the genes involved in the pathogenesis of RCC and mTOR pathway.

**Results:** The mean age at diagnosis was 66.1 years (range: 50-79 years), with 5 (55.6%) males and 4 (44.4%) females, respectively. No patients had a history of tuberous sclerosis, with the majority of the lesions (77.8%) located in the right kidney. All cases showed the characteristic histological (no capsule; solid/nested/tubular-reticular growth; a central area with "boats in a bay" aspect; rare lymphocytic clusters; oncocytic cells without "raisinoid" nuclei; no necrosis, pleomorphism and mitoses) and immunohistochemical (CK7+, CD117-) features of LOT. In one case the extracted DNA did not pass the quality control. *MTOR* mutations were found in 4 (50%) cases (p.Ala2420Val, p.Ser2215Tyr, p.Leu2427Gln, p.Ser2215Phe), with 1 (12.5%) case showing *NOTCH1* (p.Glu515Lys) and *NOTCH4* (p.Asp272Gly) mutations; 3 (37.5%) cases did not show mutations. No mutations in *TSC1/2* were found in our cases, contrary to what was previously reported.

**Conclusions:** Our data confirm the main role of the mTOR pathway in the pathogenesis of LOT, mostly due to *MTOR* rather than *TSC1/TSC2* mutations. Besides, our study suggests that activating mutations of *NOTCH* genes (proved to be associated with an exaggerated and constitutive activation of the mTOR pathway in neoplastic cell lines, solid tumors, and leukemias) could be involved in the pathogenesis of a subgroup of LOT through a non-canonical activation of mTORC1 complex, not directly involving mTOR pathway genes and so not detected by the commonly used NGS panels.

## 800 Homologous Recombination Deficiency is Detectable from H&E Whole Slide Images in Real World Prostate Needle Core Biopsies

Abbas Rizvi<sup>1</sup>, Kunal Nagpal<sup>1</sup>, Rohan Joshi<sup>1</sup>, Geoffrey Schau<sup>1</sup>, Rachel Baits<sup>1</sup>, Yoni Muller<sup>1</sup>, Martin Stumpe<sup>1</sup>, Nike Beaubier<sup>2</sup>  
<sup>1</sup>Tempus Labs, Chicago, IL, <sup>2</sup>Tempus, Chicago, IL

**Disclosures:** Abbas Rizvi: None; Kunal Nagpal: None; Rohan Joshi: None; Geoffrey Schau: None; Rachel Baits: None; Yoni Muller: None; Martin Stumpe: None; Nike Beaubier: None

**Background:** Homologous recombination deficiency (HRD) is an increasingly important molecular phenotype given the development of targeted treatments for HRD positive tumors. While HRD is routinely assessed in breast and ovarian cancer, prostate cancer patients with homologous recombination repair (HRR) gene loss may also benefit from targeted therapy. Here, we applied weakly supervised deep learning to predict HRD status from hematoxylin and eosin (H&E) stained whole-slide images (WSIs) in prostate cancer as a potential screening assay for confirmatory sequencing.

**Design:** Real world prostate cancer tumor biopsy and resection specimens were collected; each sample additionally included: 1) clinical characteristics, 2) molecular profiles via DNA/RNA sequencing, and 3) digitized WSI data. The ground truth HRD status for each WSI was generated from an analytically validated commercial assay that relies on RNA expression. Attention-based multiple-instance-learning networks were trained to predict HRD status from WSIs. All WSIs (N=3210, HRD+ 8.1%) were split into training

# ABSTRACTS | GENITOURINARY PATHOLOGY (INCLUDING RENAL TUMORS)

(N=2038, HRD+ 7.8%), tuning (N=455, HRD+ 9.8%), and test sets (N=332, HRD+ 8.4%). The test set consisted of needle core biopsies scanned on Leica GT450, while the training/tuning sets included biopsies and resections scanned on Leica GT450 or Philips UFS instruments.

**Results:** The cohort skewed towards high Gleason scores (GS) and these high GS samples had a higher prevalence of HRD (Table 1). Predicting HRD from WSI resulted in an area under receiving operating characteristic (AUROC) of 0.73 [0.64-0.82 95% CI] on the test set (Figure 1A). At 70% sensitivity, the predictor had a 21.3% PPV across all samples compared to an underlying prevalence of 8.4%. In additional analysis, we found that the model is able to effectively stratify patients with BRCA double hit mutations (AUROC: 0.77 [0.68-0.84 95% CI], Figure 1B). Performance remained robust in GS7-8 (AUROC 0.81, PPV 23.5% at 70% sensitivity) and GS9-10 (AUROC 0.68, PPV 16.7% at 70% sensitivity). Visualization of high attention HRD+/HRD- tiles suggest the model relies on dense tumor regions in making its predictions (Figure 2).

Characteristic	N	Cohort Characteristics					
		HRD+ Train (N=165)	HRD+ Tune (N=46)	HRD+ Test (N=29)	HRD- Train (N=1909)	HRD- Tune (N=418)	HRD- Test (N=313)
Procedure Type	2719						
Biopsy		32 (20%)	3 (7.0%)	0 (0%)	260 (15%)	70 (18%)	0 (0%)
Core needle biopsy		62 (39%)	15 (35%)	29 (100%)	717 (40%)	109 (28%)	313 (100%)
Excisional biopsy		2 (1.3%)	0 (0%)	0 (0%)	9 (0.5%)	3 (0.8%)	0 (0%)
Surgical resection		61 (39%)	25 (58%)	0 (0%)	806 (45%)	203 (53%)	0 (0%)
Gleason Score	2112						
6		2 (1.7%)	0 (0%)	0 (0%)	37 (2.7%)	10 (3.2%)	3 (1.1%)
7		8 (6.8%)	3 (8.8%)	1 (4.2%)	298 (22%)	76 (24%)	34 (13%)
8		13 (11%)	4 (12%)	6 (25%)	245 (18%)	63 (20%)	56 (21%)
9		72 (62%)	22 (65%)	11 (46%)	671 (50%)	144 (45%)	145 (55%)
10		22 (19%)	5 (15%)	6 (25%)	104 (7.7%)	24 (7.6%)	27 (10%)

Figure 1 - 800

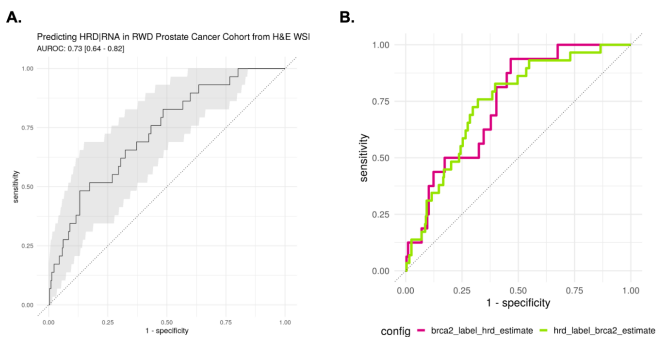


Figure 1. (A) ROC for HRD predictor evaluated on test set. (B) ROC for models trained on BRCA2 double hit labels, and tested against HRD labels (red) and trained on HRD labels while tested against BRCA2 double hit labels resulted in AUCs of 0.69 and 0.77 respectively.

Figure 2 - 800

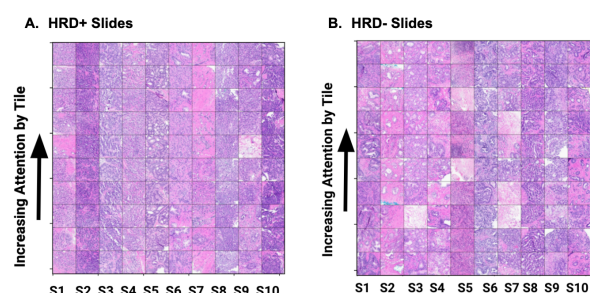


Figure 2. Highest attention tiles from randomly WSIs predicted as HRD+ and HRD- respectively. Both (A) and (B) primarily highlight dense tumor areas. (A) HRD+ shows mainly sheets, nests and single cells comprising Gleason pattern 5 areas (B) HRD- also shows a plurality of Gleason pattern 5 areas with glandular and fused gland pattern 3 and 4 areas.

**Conclusions:** An imaging-based model effectively predicts HRD status and BRCA double-hit mutations from routine H&E images. This low-cost and rapid detection capability could help to prioritize tissue for confirmatory molecular testing and better identify populations that may benefit from existing therapy or clinical trial enrollment eligibility.

## 801 DNA Methylation Landscapes of Prostate Cancer Brain Metastasis Are Shaped by Early Driver Genetic Alterations

Antonio Rodriguez<sup>1</sup>, John Gallon<sup>2</sup>, Mark Rubin<sup>3</sup>, Salvatore Piscuoglio<sup>4</sup>

<sup>1</sup>Institute of Pathology, University of Bern, Liebefeld, Switzerland, <sup>2</sup>University of Basel and University Hospital Basel, Department of Biomedicine, Basel, Switzerland, <sup>3</sup>University of Bern, Bern, Switzerland, <sup>4</sup>University of Basel, Basel, Switzerland

**Disclosures:** Antonio Rodriguez: None; John Gallon: None; Mark Rubin: None; Salvatore Piscuoglio: None

**Background:** Epigenetic dysregulation is a feature of primary prostate cancer, and distinct DNA methylation profiles are associated with the mutually exclusive SPOP mutant or TMPRSS2-ERG fusion genetic backgrounds. Metastases from primary

# ABSTRACTS | GENITOURINARY PATHOLOGY (INCLUDING RENAL TUMORS)

prostate cancers to rare locations, such as the brain, are becoming more common due to longer life expectancy thanks to improved treatments and a deep molecular understanding of these is lacking.

**Design:** Our cohort includes samples from 42 patients with PCBMs and 17/42 patients with available paired primary tumor, collected from Pathology Departments across Switzerland and from the Department of Pathology, Emory University, Atlanta, USA. We collected archived FFPE tissue from CNS (brain/spinal cord) and meningeal metastases as well from available paired primary tumors. Multi-region sampling permitted evaluation of intra-tumoural epigenetic heterogeneity at the primary (56 samples) and metastatic sites (96 samples). All 155 selected areas underwent DNA methylation analysis, and were integrated with whole exome sequencing and targeted-RNA-seq data, produced in an already published manuscript by our group.

**Results:** We performed unsupervised hierarchical consensus clustering using the top 1% most variably methylated CpG sites across the metastatic samples. This separated the *TMPRSS2-ERG* fused samples from the non-fused samples, which included those with *SPOP* mutations. We calculated the mean methylation change of the *SPOP* mutant, or *TMPRSS2-ERG* fusion PCBMs samples, compared to normal prostate tissue, and observed the previously reported hypermethylator phenotype in the *SPOP* mutant samples (Fig. 1). The variably methylated CpG sites were predominantly CpG island-associated. *SPOP* mutant metastases showed hypermethylation in comparison to metastases lacking mutation. To understand what processes might drive the detected hypermethylation, we performed gene set enrichment analysis using the CpG-level DM data. When examining the methylation changes specifically associated with either the *TMPRSS2-ERG* fusion or *SPOP* mutant backgrounds, in comparison to the other metastases, PRC2-associated pathways were enriched in the *SPOP* mutant metastases. RNA-seq data showed a significant increase in EZH2 expression, a component of PRC2, in the metastases compared to primaries (Fig. 2).

Figure 1 - 801

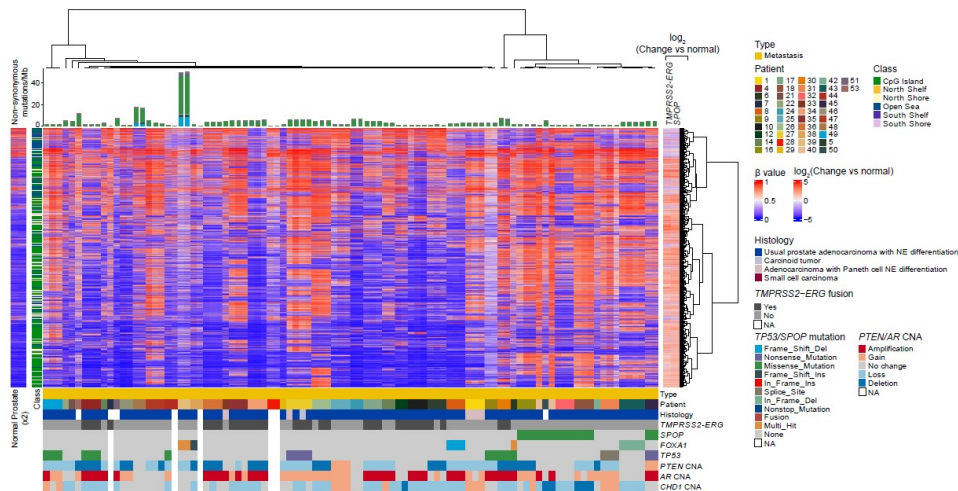
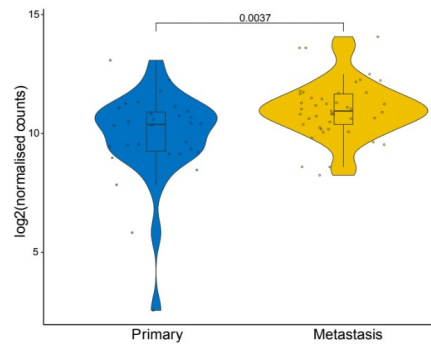


Figure 2 - 801



**Conclusions:** We found aberrant methylation in PCBMs is associated with mutational background, PRC2 complex activity and upregulation of *EZH2*, an effect that is particularly pronounced in *SPOP* mutant PCBMs.

## 802 Gene Mutations in Urothelial Carcinoma of the Upper Urinary Tract: An Analysis of 55 Cases by Next-Generation Sequencing

Prih Rohra<sup>1</sup>, Ahmed Shehabeldin<sup>1</sup>, Kingsley Ebare<sup>2</sup>, Varsha Nair<sup>1</sup>, Jianping Zhao<sup>1</sup>, Bogdan Czerniak<sup>1</sup>, Charles Guo<sup>1</sup>

<sup>1</sup>The University of Texas MD Anderson Cancer Center, Houston, TX, <sup>2</sup>Indiana University, Indianapolis, IN

**Disclosures:** Prih Rohra: None; Ahmed Shehabeldin: None; Kingsley Ebare: None; Varsha Nair: None; Jianping Zhao: None; Bogdan Czerniak: None; Charles Guo: None

**Background:** Urothelial carcinoma (UC) of the upper urinary tract (UUT) is a rare malignancy that demonstrates similar histologic features to those of urinary bladder UC. However, UUTUC may be a genetically different disease from bladder UC. Recent studies have revealed that bladder UC can be divided into different molecular subtypes which are associated with distinct biological behaviors. Herein we analyzed the gene mutational profile of UUTUC in correlation with its clinical and pathological features.

**Design:** We searched our pathology files from 2014-2016 and identified 54 patients with UUTUC who underwent Next-Generation-Sequencing (NGS) on formalin-fixed paraffin-embedded tissue specimens. Pathologic features were reviewed, and clinicopathologic parameters were collected from patient records.

**Results:** The patients included 33 males and 21 females with a mean age of 67 years (range, 41-90 years). The primary tumors were located at the renal pelvis (30), ureter (10), or both (14). All tumors were high-grade UC, and 18 tumors showed divergent differentiation, squamous (5), micropapillary (3), sarcomatoid (2), small cell carcinoma (2), and others (6). NGS tests were performed on 43 primary tumors and 11 metastatic tumors. Mutations were detected in 50 cases, and the most common mutations were TP53 (23), followed by PIK3CA (11), FGFR3 (10), TSC1 (6), ERBB2(5), KIT (5), ATM (5), TERT-P (4), ERG (4), and APC (4). TP53 mutations were more common in male patients (Table 1). Renal pelvis UC had higher rates of PIK3CA and FGFR3 mutations than ureteral UC. ERBB2 and ATM mutations were more frequent in UC with divergent differentiation. Twenty-eight patients died of disease in a mean time of 31 months (range 1-107 months). While TP53 mutations were associated with high-stage UC and a shorter survival time (mean 27 months), FGFR3 mutations were associated with low-stage UC with a longer survival time (mean 43 months).

Table 1 Gene Mutations and Clinicopathological Features in UUTUC

Gene Mutations	Sex		Tumor Location			Histology		Clinical Stage*	
	Female	Male	Pelvis	Ureter	Both	Pure UC	Subtype UC	Low	High
TP53	13%	28%	15%	15%	11%	42%	44%	36%	60%
FGFR3	11%	7%	11%	0	7%	17%	22%	43%	13%
PIK3CA	11%	7%	11%	2%	6%	22%	17%	21%	27%
TSC1	6%	6%	6%	0	6%	11%	11%	7%	17%
ATM	2%	7%	6%	2%	2%	6%	17%	7%	13%
ERBB2	0	9%	6%	0	4%	3%	22%	7%	13%
KIT	4%	4%	4%	2%	2%	8%	11%	7%	13%
APC	0	7%	2%	0	6%	8%	6%	21%	3%
EGFR	0	6%	6%	0	0	6%	11%	0%	13%
TERT-P	6%	2%	2%	4%	2%	3%	17%	0%	13%

\*Clinical stage: low - stage I-III; high - stage IV.

**Conclusions:** UTTUC demonstrates frequent gene mutations, which may underlie the development of this rare disease. Our results suggest that gene mutations may be associated with distinct pathologic and clinical features, which may be useful in the targeted therapy of UTTUC.

## 803 Complementary Pilot Analysis of Tumor Microenvironment and Nuclei in Recurrent vs. Non-Recurrent Low-Grade Noninvasive Bladder Cancer Using Pathologic Review and Artificial Intelligence

Kyle Rose<sup>1</sup>, Ekin Tiu<sup>2</sup>, Viswesh Krishna<sup>2</sup>, Heather Huelster<sup>1</sup>, Gustavo Borjas<sup>1</sup>, Shreyas Naidu<sup>1</sup>, Elizabeth Davaro<sup>1</sup>, Philippe Spiess<sup>1</sup>, Damir Vrabac<sup>2</sup>, Hriday Bhambhani<sup>3</sup>, Wade Sexton<sup>1</sup>, Anirudh Joshi<sup>2</sup>, Li Roger<sup>1</sup>, Aram Vosoughi<sup>1</sup>

<sup>1</sup>H. Lee Moffitt Cancer Center & Research Institute, Tampa, FL, <sup>2</sup>Palo Alto, CA, <sup>3</sup>New York-Presbyterian/Weill Cornell Medical Center, New York, NY

**Disclosures:** Kyle Rose: None; Ekin Tiu: None; Viswesh Krishna: None; Heather Huelster: None; Gustavo Borjas: None; Shreyas Naidu: None; Elizabeth Davaro: None; Philippe Spiess: None; Damir Vrabac: None; Hriday Bhambhani: None; Wade Sexton: None; Anirudh Joshi: None; Li Roger: None; Aram Vosoughi: None

**Background:** Low-grade noninvasive urothelial carcinoma (LGUCa) of the bladder exhibits a heterogeneous clinical course following initial diagnosis. Identification of clinical variables associated with tumor recurrence may help to risk stratify patients and develop personalized surveillance protocols. We aimed to utilize a complementary histological investigation along with artificial intelligence (AI) to predict LGUCa tumor recurrence.

**Design:** Patients with LGUCa from 2015-2019 with at least 3 years of clinical follow up were enrolled in the study. Tumors were stratified by downstream recurrences (Non-Recurrent: NR: vs. Recurrent: R). A genitourinary pathologist reviewed H&E stained slides, noting cytologic and architectural atypia, including inverted growth pattern and percentage of non-tumor cell component. Histologic features in R vs. NR tumors were analyzed using Fisher's Exact Test. To construct a morphological signature for recurrence risk stratification, a deep learning algorithm was used to extract quantitative features from segmented nuclei on high-resolution digitized whole slide images. These features were then correlated to recurrence free survival (RFS) utilizing a multivariable Cox proportional hazards (CPH) model and recurrence risk stratification was examined using Kaplan-Meier analysis and log-rank test.

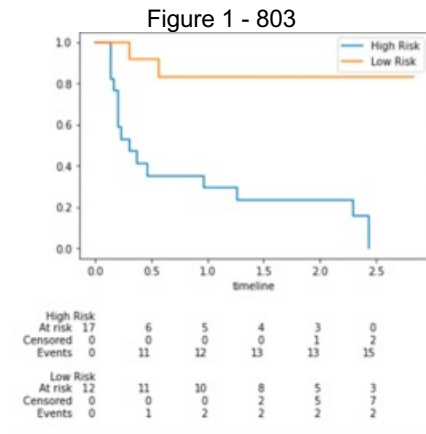
**Results:** Twenty-nine LGUCa from 29 patients were identified, of which 17 (59%) had subsequent recurrence. The median (IQR) follow up was 59 months, and the median (IQR) number of recurrences following initial diagnosis was 4 in the R cohort. R tumors exhibited a higher frequency of inverted growth pattern (45% vs. 11%, p=0.04) and higher median stroma percentage (50% vs. 20%, p<0.01). The AI derived morphological signature was predictive of recurrence with an AUROC of 0.81. Kaplan-Meier analysis demonstrated the model was able to risk stratify the cohort with a statistically significant hazard ratio of 5.43 [95% CI 1.1, 26.76] (p=0.02) for prediction of high and low risk of recurrence. Patients in the high risk group had a 87.5% recurrence rate while those in the low risk group had a 28.5% recurrence rate.

Table 1. Clinicopathologic Data and Pathologic Analysis of Tumor Microenvironment in Patients with Non-Recurrent vs. Recurrent Low-Grade Noninvasive Bladder Cancer			
	Non-recurrent LGTa n= 12	Recurrent LGTa n= 17	p-value
<b>Demographics</b>			
Age (years)*	67.0 (63.5-72.5)	68.0 (60.0-75.0)	0.97
Gender	3	5	
Female	8	12	0.22
Male			
Smoking History	2	5	
Yes	9	4	0.20
No			
Tumor Size (mm)*	12.0 (11.0-30.5)	14.0 (12.0-19.0)	0.53
No. Recurrences*	4 (2-10)	NA	
Months to Recurrence	9.0 (6.0-17.0)	NA	
Follow up (months)*	71.0 (48.0-77.5)	54.0 (49.0-62.0)	0.86
<b>Tumor Microenvironment Analysis<sup>§</sup></b>	n=9	n=11	
Focal Cytologic and Architectural Atypia Suggestive of HGT	2	3	0.97
Inverted Growth Pattern	1	5	0.04
Papillary Fusion	8	7	0.99
Squamous Morphologic Features	0	0	0.99
Muscularis Propria Present	4	5	0.60
Median Stroma %	20%	50%	<0.01

\*Continuous variables are presented as median values with interquartile range in parentheses

<sup>§</sup>Tumor Microenvironment Analysis was performed on tumors with adequate tissue and surrounding stroma

HGT=High Grade Tumor



**Figure 1.** Kaplan Meier of Recurrence Free Survival for patients categorized in the High and Low risk of recurrence.

**Conclusions:** Utilizing a complimentary approach with histologic analysis and AI, we were able to identify critical differences between R and NR LGUC bladder tumors. These hypothesis-generating findings will guide future studies to identify tumors that are at high risk for recurrence, thereby allowing for surveillance protocol tailoring and improved patient stratification.

#### **804 Inter-Observer Variability Amongst Expert Pathologists in Assessment of Percent Tumor Cell PD-L1 Expression in Real World Urothelial Carcinoma Samples**

Josef Rueschoff<sup>1</sup>, Bharat Jasani<sup>1</sup>, Sunil Badve<sup>2</sup>, Nathalie Rioux-Leclercq<sup>3</sup>, Federico Rojo<sup>4</sup>, Maurizio Martini<sup>5</sup>, Liang Cheng<sup>6</sup>, Maria Tretiakova<sup>7</sup>, Catherine Mitchell<sup>8</sup>, Robert Anders<sup>9</sup>, James Pratt<sup>10</sup>, Maria Karasarides<sup>10</sup>, George Kumar<sup>11</sup>, Arndt Hartmann<sup>12</sup>

<sup>1</sup>Discovery Life Sciences Biomarker Services GmbH, Kassel, Germany, <sup>2</sup>Emory University, Atlanta, GA, <sup>3</sup>Rennes University Hospital, Rennes, France, <sup>4</sup>Hospital Universitario Fundación Jiménez Díaz, Madrid, Spain, <sup>5</sup>Università degli Studi di Messina, Messina, Italy, <sup>6</sup>Alpert Medical School of Brown University, Providence, RI, <sup>7</sup>University of Washington, Seattle, WA, <sup>8</sup>Peter MacCallum Cancer Centre, Melbourne, Australia, <sup>9</sup>Johns Hopkins University, Baltimore, MD, <sup>10</sup>Bristol Myers Squibb, Princeton, NJ, <sup>11</sup>Bristol Myers Squibb, Lawrenceville, NJ, <sup>12</sup>Institut für Pathologie, Erlangen, Germany

**Disclosures:** Josef Rueschoff: None; Bharat Jasani: None; Sunil Badve: None; Nathalie Rioux-Leclercq: None; Federico Rojo: None; Maurizio Martini: None; Liang Cheng: None; Maria Tretiakova: None; Catherine Mitchell: None; Robert Anders: None; James Pratt: None; Maria Karasarides: None; George Kumar: None; Arndt Hartmann: None

**Background:** Demonstration of programmed death ligand-1 (PD-L1) expression has become a prerequisite for decision-making around immune checkpoint therapy in a variety of tumors. Assessment of PD-L1 expression by percent tumor cell positivity (%TC) using IHC 28-8 pharmDx correlates with enhanced response from nivolumab in urothelial cancer. The quality of PD-L1 scoring and potential routes for optimization were investigated in an international study using diagnostic urothelial cancer samples covering the whole range of PD-L1 scores.

**Design:** Tissue sections from 50 advanced pre-treatment urothelial carcinomas were preselected by three pathologists from 132 specimens according to their PD-L1 score distribution, with most cases (80%) being close to the FDA approved cut-off of  $\geq 1\%$ TC expression using 28-8 and 22C3 assays centrally performed (CellCarta). Whole slide images were scanned at 40x magnification (3DHISTECH) and uploaded into the PathoTrainer platform (CellCarta). Ten pathologists across the world performed PD-L1 scoring prior and after 2 hours of online training at TC  $\geq 1\%$  cutoff. Scoring agreement was assessed using the intraclass correlation coefficient (ICC). Key challenges of scoring were identified by using mean absolute deviation (MAD) analysis.

**Results:** Incident rate of samples  $\geq 1\%$  TC was generally in the 20-30% range for 8 of the 10 pathologists with only slightly lower scores for 22C3 as compared to 28-8. Training did not change positivity rate significantly. Interobserver variability for %TC expression was low with good agreement between pathologists both pre- (ICC range 0.80-0.88) and post-(ICC range 0.75-0.86) training by both assays. Review of PD-L1 expression in slides exhibiting high variability (MAD>10) revealed some challenges. Accordingly, faint membrane staining raises difficulty of scoring at the 1% cut off, particularly in tumors with optically prominent cell borders. In high score tumors discrepancy is mostly due to strong cytoplasmic staining obscuring the membrane related reaction.

**Conclusions:** Inter-observer agreement of %TC expression scoring in bladder cancer was at an acceptable level between pathologists regardless of training or assay. Routes of improvement include PD-L1 training addressing challenges specific for low and high-score tumors. In addition, use of artificial or augmented intelligence may also contribute to the standardization of PD-L1 %TC expression analysis to accurately identify patients likely to benefit from immune checkpoint inhibitor therapy.

## 805 Lymph Node Findings in Patients with Prostatic Adenocarcinoma and Seminal Vesicle Invasion

Faisal Saeed<sup>1</sup>, Adeboye Osunkoya<sup>2</sup>

<sup>1</sup>Emory University Hospital, Atlanta, GA, <sup>2</sup>Emory University School of Medicine, Atlanta, GA

**Disclosures:** Faisal Saeed: None; Adeboye Osunkoya: None

**Background:** Prostatic adenocarcinoma (PCa) with seminal vesicle invasion (SVI) is frequently associated with high grade and high-volume disease, tumor recurrence, and poor prognosis. In this study we analyzed the lymph node (LN) findings in patients with PCa and SVI on radical prostatectomy (RP).

**Design:** A search was made through our urologic pathology files for patients who had RP and LN dissection demonstrating PCa with SVI. The number of LNs involved, laterality of LN involvement, size of metastatic foci, extranodal extension (ENE), Gleason scores/Grade groups, presence of Gleason pattern 5, and laterality of SVI were documented and analyzed in all patients.

**Results:** A total of 224 patients were included in the study. The mean patient age was 62 years (range: 42-79 years). Patients were stratified into 2 cohorts; 1] PCa Grade group 2 with no tertiary pattern 5 (24/224 patients, 11%) and 2] PCa Grade group 2 with tertiary pattern 5 and Grade group 3 or higher (200/224 patients, 89%). LN metastasis was present in 100/224 (44.6%) patients. Three of 24 (12.5%) patients in cohort 1 had LN metastasis whereas 97/200 (48.5%) patients in cohort 2 had LN metastasis. The mean number of positive LNs was 4 (range: 1-42) and the mean size of the metastatic foci was 1.0 cm (range: 0.1-4.3 cm). ENE was present in 57/100 (57%). Forty-eight of the 100 (48%) patients with LN metastasis had unilateral SVI, 25/48 (52.1%) patients had LN metastasis ipsilateral to the SVI, whereas only 3/48 (6.2%) patients had LN metastasis contralateral to the SVI. The remaining 20/48 (41.7%) patients had bilateral LN metastasis. Of the 52 patients with bilateral SVI, 32 (62%) had bilateral lymph node metastasis and 20 (38%) had unilateral LN metastasis.

**Conclusions:** Patients with SVI and PCa Grade group 3 or higher and those with Grade group 2 associated with tertiary pattern 5 have a higher risk of LN metastasis compared to those with SVI invasion and PCa Grade group 2 with no tertiary pattern 5 ( $p=0.000802$ ). Patients with bilateral SVI are more likely to have bilateral LN metastasis ( $p=0.046903$ ), and patients with unilateral SVI have a higher likelihood of ipsilateral LN metastasis ( $p=<0.00001$ ). These findings are important for risk stratification, and may also guide post-operative lymph node sampling strategies for patients who initially have radical prostatectomy without lymph node dissection.

## 806 Cribiform Morphology in Prostate Biopsy Specimens Revisited: A Study on the Prognostic Significance of Intraductal Carcinoma Vs. Invasive Cribiform Carcinoma

Manduwa Saka<sup>1</sup>, Yuki Teramoto<sup>1</sup>, Sachiko Minamiguchi<sup>1</sup>, Hiroshi Miyamoto<sup>2</sup>, Hironori Haga<sup>1</sup>

<sup>1</sup>Kyoto University Hospital, Kyoto, Japan, <sup>2</sup>University of Rochester Medical Center, Rochester, NY

**Disclosures:** Manduwa Saka: None; Yuki Teramoto: None; Sachiko Minamiguchi: None; Hiroshi Miyamoto: None; Hironori Haga: None

**Background:** Cribiform morphology (CM) in prostate biopsy and radical prostatectomy specimens is known to be associated with adverse clinical outcomes. CM can be present in invasive cribiform carcinoma (ICC) as well as intraductal carcinoma (IDC). Although they are pathologically distinct entities, the prognostic value of each component has not been studied in detail. In this study, we evaluated the prognostic heterogeneity of prostate cancers presenting with CM in pretreatment biopsies, using comprehensive immunostaining to rigorously distinguish between ICC and IDC.

**Design:** We surveyed consecutive patients who had undergone prostate biopsy at our institution from 2017-2021 and identified 370 cases of Grade Group 2-5 cancer from the pathology database. We then performed immunohistochemical staining with p63/AMACR cocktail antibodies on all cores in each case, and two urologic pathologists independently reviewed and evaluated the presence of ICC and/or IDC.

**Results:** We classified the patient cohort into four groups: G1 [ICC-/IDC-; n=239], G2 [ICC+/IDC-; n=66], G3 [ICC-/IDC+; n=34], G4 [ICC+/IDC+; n=31]. Patients with CM had significantly longer tumors and higher Grade Groups. In Kaplan-Meier analysis by log-rank test, both disease-specific survival (DSS) and progression-free survival after prostatectomy were in the order G1>G2>G3>G4, with a significant difference in DSS between G1 and G2-G4 ( $P<0.001$ ), but not between G2 and G3 ( $P=0.088$ ) or G3 and G4 ( $P=0.978$ ). Multivariate analysis with Cox regression model (G1 as a reference) showed significance for DSS in G3 (hazard ratio 6.250,  $P=0.003$ ) and G4 (hazard ratio 14.940,  $P<0.001$ ) with IDC, but not in G2 with ICC alone (hazard ratio 3.317,  $P=0.059$ ).

# ABSTRACTS | GENITOURINARY PATHOLOGY (INCLUDING RENAL TUMORS)

	G1 ICC-/IDC-	G2 ICC+/IDC-	G3 ICC-/IDC+	G4 ICC+/IDC+	P (G1 vs G2)	P (G1 vs G3)	P (G2 vs G3)	P (G2 vs G4)	P (G3 vs G4)
n	239	66	34	31					
Age (mean $\pm$ SD, year)	71.68 $\pm$ 7.12	73.44 $\pm$ 6.78	73.09 $\pm$ 7.89	75.74 $\pm$ 7.46	0.074	0.289	0.817	0.161	0.197
PSA (median, ng/mL)	8.30	19.45	16.70	59.00	<0.001	<0.001	0.608	0.118	0.170
Biopsy Grade Group					<0.001	<0.001	<0.001	0.171	0.005
Grade Group 2	81 (33.9%)	0 ( 0.0%)	2 ( 5.9%)	1 ( 3.2%)					
Grade Group 3	47 (19.7%)	13 (19.7%)	6 (17.6%)	2 ( 6.5%)					
Grade Group 4	48 (20.1%)	28 (42.4%)	3 ( 8.8%)	14 (45.2%)					
Grade Group 5	63 (26.4%)	25 (37.9%)	23 (67.6%)	14 (45.2%)					
Tumor length (mean $\pm$ SD, mm)	25.5 $\pm$ 24.8	44.9 $\pm$ 31.7	47.2 $\pm$ 40.9	38.3 $\pm$ 27.5	<0.001	<0.001	0.754	0.369	0.307
Cribiform glands (mean $\pm$ SD, %)	-	0.28 $\pm$ 0.20	0.18 $\pm$ 0.11	0.33 $\pm$ 0.28	-	-	0.087	0.070	0.016

Figure 1 - 806

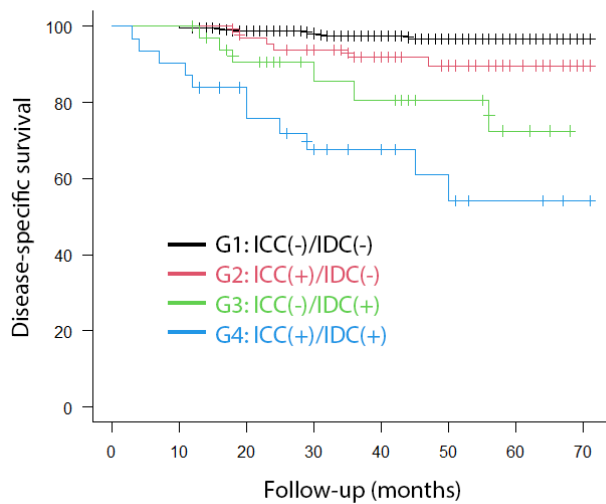
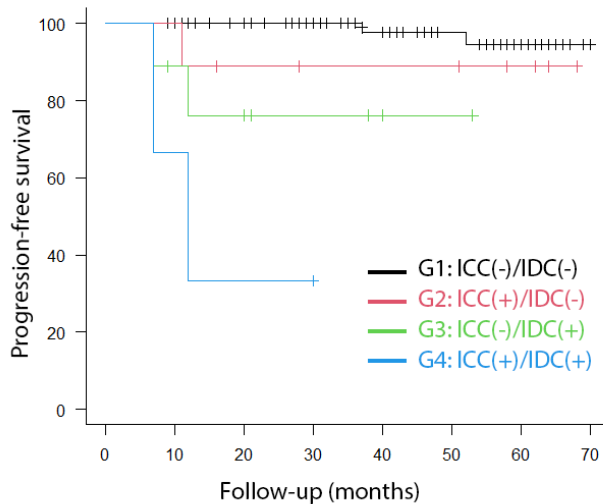


Figure 2 - 806



**Conclusions:** Despite the limitation of the relatively short follow-up period, our results suggest that evaluating biopsy specimens, along with for the presence of IDC when CM is present may be useful for better risk stratification.

## 807 Elucidating Molecular Signatures and Mutational Patterns In Eosinophilic Solid Cystic Renal Cell Carcinoma: A Multicentric Study

Sankalp Sancheti<sup>1</sup>, Aditi Aggarwal<sup>2</sup>, Deepika Jain<sup>3</sup>, Shilpy Jha<sup>4</sup>, Seema Kaushal<sup>5</sup>, Anandi Lobo<sup>6</sup>, B Vishal Rao<sup>7</sup>, Mahmut Akgul<sup>8</sup>, Manas Baisakh<sup>9</sup>, Indranil Chakrabarti<sup>10</sup>, Niharika Pattnaik<sup>4</sup>, Sourav Mishra<sup>4</sup>, Sean Williamson<sup>11</sup>, Anil Parwani<sup>12</sup>, Liang Cheng<sup>13</sup>, Sambit Mohanty<sup>14</sup>

<sup>1</sup>Homi Bhabha Cancer Hospital, New Chandigarh, India, <sup>2</sup>Core Diagnostics, Gurgaon, India, <sup>3</sup>Core Diagnostics, Gurugram, India, <sup>4</sup>Advanced Medical and Research Institute, Bhubaneswar, India, <sup>5</sup>All India Institute of Medical Sciences, New Delhi, India, <sup>6</sup>Kapoor Centre of Urology and Pathology, Raipur, India, <sup>7</sup>Basavataram Indo-American Cancer Hospital and Research Institute, West Bengal, India, <sup>8</sup>Albany Medical Center, Albany, NY, <sup>9</sup>Prolife Diagnostics, Bhubaneswar, India, <sup>10</sup>All India Institute of Medical Sciences, Kalyani, India, <sup>11</sup>Cleveland Clinic, Cleveland, OH, <sup>12</sup>The Ohio State University Wexner Medical Center, Columbus, OH, <sup>13</sup>Alpert Medical School of Brown University, Providence, RI, <sup>14</sup>Advanced Medical and Research Institute, New Delhi, India

**Disclosures:** Sankalp Sancheti: None; Aditi Aggarwal: None; Deepika Jain: None; Shilpy Jha: None; Seema Kaushal: None; Anandi Lobo: None; B Vishal Rao: None; Mahmut Akgul: None; Manas Baisakh: None; Indranil Chakrabarti: None; Niharika Pattnaik: None; Sourav Mishra: None; Sean Williamson: None; Anil Parwani: None; Liang Cheng: None; Sambit Mohanty: None

**Background:** Eosinophilic solid and cystic renal cell carcinoma (ESC RCC) has been recently described as a unique and indolent renal neoplasm, with or without tuberous sclerosis complex (TSC). The morphologic variation and molecular profile of this relatively novel neoplasm is still evolving. To address this, we sought to elucidate the somatic and germline genomic alterations in a contemporary cohort of ESC RCC from various institutions.

# ABSTRACTS | GENITOURINARY PATHOLOGY (INCLUDING RENAL TUMORS)

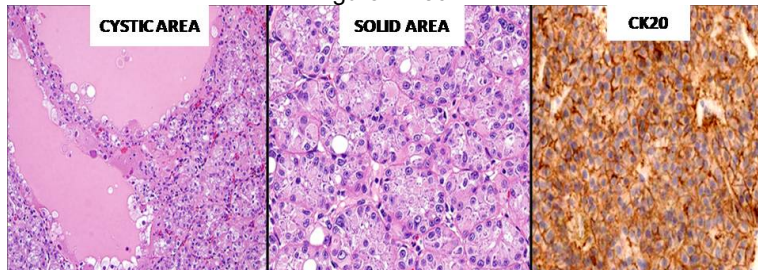
**Design:** Because of the rarity of this tumor, we performed a multi-institutional collaboration to comprehend the overarching clinical, gross, microscopic, and immunohistochemical profile of 13 ESC RCC from multiple institutions. Genomics was done using targeted next generation sequencing to detect small nucleotide variants/substitutions, small indels (insertions and/or deletions) and copy number variations in 324 cancer-associated genes. The panel was based on Illumina® Hi Seq 4000 platform.

**Results:** The results are illustrated in figures 1 and 2. There was a female preponderance (F:M=2.3:1) and the patients' age ranged from 11 to 60 years with a median of 27 years. None of the patients had clinical features of TSC. Three patients had a history of a prior neoplasm (pilocytic astrocytoma, papillary thyroid carcinoma, and low-grade urothelial carcinoma). All the patients had unifocal renal tumors. Twelve patients were of stage pT1 (pT1a=6; pT1b=6) and one patient had stage pT2a. Classical histology of ESC RCC was observed in all tumors. The tumors exhibited PAX8+/CK20+/CD10+ with variable Cathepsin K and AMACR staining; Ki-67 indices were low; SDHB and FH were retained. Ten patients on follow up were alive without evidence of disease progression or metastasis (3-34 months). All the 13 tumors harbored somatic genomic alterations (Figure 1 and 2). Germline testing in 6 patients was negative.

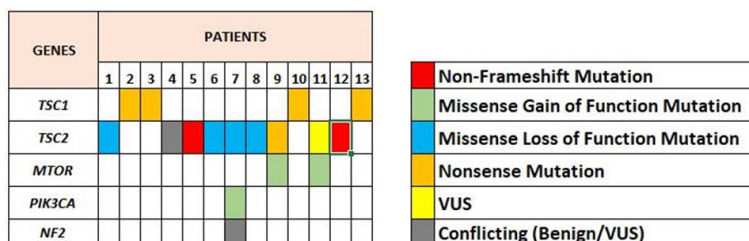
Figure 1 - 807

Case # and Gene Symbol	Transcript ID	Variant annotation (p.)	Variant annotation (cDNA)	Pathogenic role	Variant type	Molecular consequence
#1 TSC2	NM_000548.5	p.Arg1713His	c.5138G>A	Pathogenic	Single nucleotide variant	Missense
#2 TSC1	NM_000368.4	p.Leu612	c.1835T>A	Likely pathogenic	Single nucleotide variant	Missense
#3 TSC1	NM_000368.4	p.Glu876Ter	c.2626G>T	Pathogenic	Single nucleotide variant	Nonsense
#4 TSC2	NM_000548.5	p.Val534Leu	c.1600G>T	Benign/Uncertain significance	Single nucleotide variant	Missense
#5 TSC2	NM_000548.5	p.Tyr407_Arg413del	c.1220_1240del	Pathogenic	Deletion	Deletion
#6 TSC2	NM_000548.5	p.Arg1713His	c.5138G>A	Pathogenic	Single nucleotide variant	Missense
#7 TSC2	NM_000548.5	p.Met11le	c.3G>T	Likely pathogenic	Single nucleotide variant	Missense
#7 PIK3CA	NM_006218.4	p.Glu545Lys	c.1633G>A	Pathogenic/Likely pathogenic	Single nucleotide variant	Missense
#7 NF2	NM_000268.4	p.Glu463Lys	c.1387G>A	Likely benign/Uncertain significance	Single nucleotide variant	Missense
#8 TSC2	NM_000548.5	p.Arg1743Gln	c.5228G>A	Likely pathogenic	Single nucleotide variant	Missense
#9 mTOR	NM_004958.4	p.Cys1483Phe	c.4448G>T	Pathogenic	Single nucleotide variant	Missense
#9 TSC2	NM_000548.5	p.Arg120Ter	c.358A>T	Pathogenic	Single nucleotide variant	Nonsense
#10 TSC1	NM_000368.4	p.Glu876Ter	c.2626G>T	Pathogenic	Single nucleotide variant	Nonsense
#11 TSC2	NM_000548.5	—	c.1717-1G>C	Uncertain significance	Single nucleotide variant	Splice acceptor
#11 mTOR	NM_004958.4	p.Ile2500Phe	c.7498A>T	Likely pathogenic	Single nucleotide variant	Missense
#12 TSC2	NM_000548.5	p.Tyr407_Arg413del	c.1220_1240del	Pathogenic	Deletion	Deletion
#13 TSC1	NM_000368.4	p.Glu876Ter	c.2626G>T	Pathogenic	Single nucleotide variant	Nonsense

Figure 2 - 807



MUTATIONAL PROFILE OF EOSINOPHILIC SOLID AND CYSTIC RENAL CELL CARCINOMA



# ABSTRACTS | GENITOURINARY PATHOLOGY (INCLUDING RENAL TUMORS)

**Conclusions:** ESC RCC appears to be a unique keratin 20 positive renal neoplasm with a female preponderance having an indolent clinical course and harbors characteristic *TSC1/2* gene mutation. They appear histologically identical to a subset of renal neoplasms seen in *TSC* patients, but in this study they were found in a sporadic setting. The molecular signature of ESC RCC in our study identified a distinct oncogenic *PI3K/AKT/mTOR* pathway activation in three patients.

## 808 The pT1 Subclassifications Predict Progression-Free Survival in En Bloc Resection of Bladder Tumor Specimen

Shun Sato<sup>1</sup>, Takafumi Yanagisawa<sup>1</sup>, Jun Miki<sup>1</sup>, Hajime Onuma<sup>1</sup>, Takahiro Kimura<sup>1</sup>, Masayuki Shimoda<sup>1</sup>, Hiroyuki Takahashi<sup>1</sup>

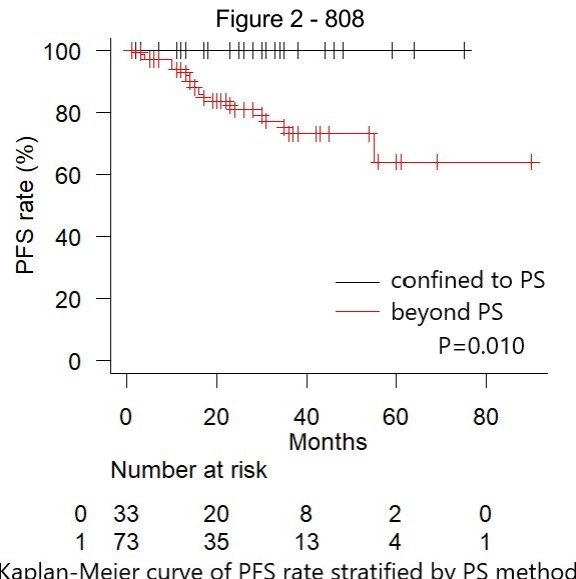
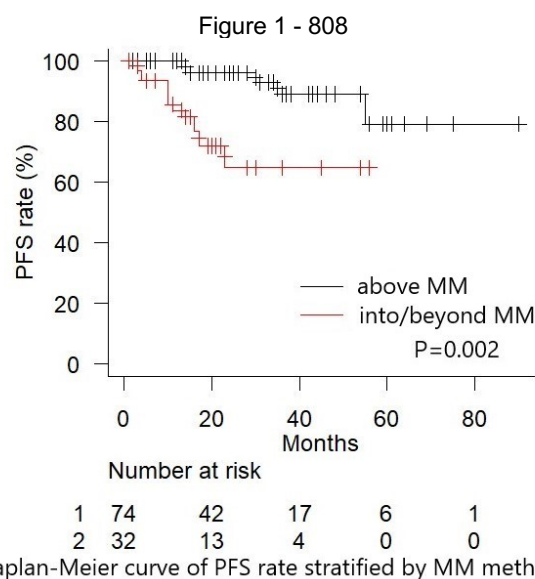
<sup>1</sup>The Jikei University School of Medicine, Minato-ku, Japan

**Disclosures:** Shun Sato: None; Takafumi Yanagisawa: None; Jun Miki: None; Hajime Onuma: None; Takahiro Kimura: None; Masayuki Shimoda: None; Hiroyuki Takahashi: None

**Background:** The pT1 subclassification has been shown to be a prognosticator for T1 bladder cancer (BCa), although it is often challenging owing to fragmentation and cauterization in conventional transurethral resection of bladder tumor (cTURBT) specimen. En bloc resection of bladder tumor (ERBT) is a relatively novel method in which BCa is resected in en bloc manner with surrounding bladder tissue. The ERBT has been known as better diagnostic feasibility and accuracy in pT1 subclassification compared to cTURBT. Here, we examined prognostic value of pT1 subclassification in ERBT specimen.

**Design:** A total of 106 T1 BCa patients who underwent ERBT from 2013 to 2021 was adopted. The pT1 substages were assigned by three different subclassification methods: muscularis mucosae (MM) method dividing cases into tumors with invasion above and into/beyond MM; depth of invasion (DOI) method dividing cases into tumor with single invasive focus of DOI <0.5mm and others; papillary stalk (PS) method dividing cases into tumors with invasion confined to and beyond PS. Inter-group difference of progression- (PFS) and recurrence- (RFS) free survival rate were analyzed by log-rank test. Then, prognostic value of clinicopathological factors for progression/recurrence were analyzed by univariate/multivariate Cox proportional hazard regression analysis.

**Results:** The pT1 substage was evaluable in all cases. Tumors with invasion into/beyond MM and those beyond PS were associated with worse PFS ( $P=0.002$  and 0.010, respectively; Figure 1 and 2). Notably, cases with invasion confined to PS did not presented progression during 23 months of median follow-up period. Difference was not shown between two substages of DOI method. In the multivariate analysis, only MM method was an independent prognosticator of progression ( $P=0.033$ ). All three different pT1 subclassification methods did not predict recurrence.



**Conclusions:** The pT1 subclassification by MM method was shown to be a strong prognosticator of disease progression in the ERBT specimen. The PS method which can detect better prognostic group is another candidate for clinical application. The ERBT with accurate pT1 subclassification for T1 BCa patients will contribute to appropriate postoperative planning.

## 809 Current Gross Examination and Reporting Practices for Post-Neoadjuvant Chemotherapy Cystectomy Specimens – Is It Time for a Standardized Approach?

Katherine Saunders<sup>1</sup>, Nicola Gerken<sup>1</sup>, Francesca Khani<sup>2</sup>, Sean Williamson<sup>3</sup>, Sara Wobker<sup>1</sup>

<sup>1</sup>The University of North Carolina at Chapel Hill, Chapel Hill, NC <sup>2</sup>Weill Cornell Medicine, New York, NY, <sup>3</sup>Cleveland Clinic, Cleveland, OH

**Disclosures:** Katherine Saunders: None; Nicola Gerken: None; Francesca Khani: None; Sean Williamson: None; Sara Wobker: None

**Background:** Neoadjuvant chemotherapy (NAC) is currently recommended for muscle-invasive bladder cancer and may result in absence of gross tumor. Presently, gross examination and reporting protocols do not include standard guidance on the approach to these post-NAC specimens.

**Design:** A Qualtrics survey to evaluate gross examination and reporting practices for post-NAC cystectomy specimens was disseminated via email and Twitter. Only US pathologists and Pathologists' Assistants (PAs) responses were included in the final results. The survey interrogated demographics, practice settings, approach to gross examination, block selection, and reporting practices.

**Results:** The survey received 46 responses (13 PAs, 27 pathologists, 6 Other) with broad representation by geographic location, with most pathologists having urologic pathology fellowship training (63%). Based on respondents' experience, identifying gross tumor occurs less frequently than tumor bed/ulcer (39% vs. 69%). Lack of identification of any gross lesions was estimated to occur in 31% of cases. Grossing practices were relatively consistent in cases with residual gross tumor or gross tumor bed, with agreement that gross tumor should be submitted 1 block/centimeter (64%) and tumor bed should be submitted entirely (97%). However, grossing practices appeared more varied when no gross lesions are identified (Figure 1). It was uncommon (21%) for final staging to be determined based on random sections. Pathologists reported microscopic pathologic complete response (ypT0) in 48% of cases, and for these, most pathologists selected yes or maybe (83%) when asked if they request and submit additional sections of bladder. Overall, most responders definitely or maybe support a standardized grossing (88%) and reporting (96%) protocol.

Figure 1 - 809

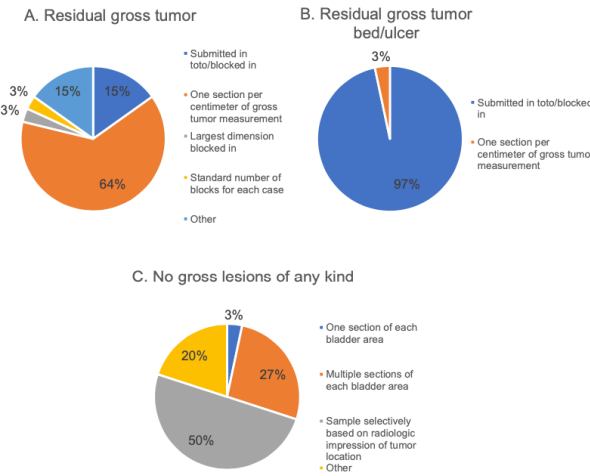


Figure 1: Grossing practices in post-NAC cystectomy specimens with A) residual gross tumor, B) gross tumor bed/ulcer, and C) no gross lesions of any kind

**Conclusions:** With the increased use of NAC, lack of any gross lesion occurs in approximately 1/3<sup>rd</sup> of cystectomies post-treatment. The most consistent grossing practices in post-NAC specimens were seen when gross tumor or tumor bed were present, but less consistency was seen when no gross lesion was identified. Lack of standardization can lead to inconsistent grossing techniques and uncertainty regarding best practices for cases with no gross lesion or presumed pathologic complete response. Standardization of grossing and reporting protocols should be considered for post-NAC cases, with guidance for sampling when no gross lesion is present, while also focusing on conservative submission of blocks when unlikely to change stage.

## 810 Somatic Tumor Testing in Prostate Cancer: Experience of a Tertiary Care Center Including Reflex Pathologist-driven Testing of Non-metastatic Tumors at Primary Diagnosis

Shamini Selvarajah<sup>1</sup>, Shervin Ansari<sup>1</sup>, Shifaa Alqaqa<sup>2</sup>, Harpreet Kaur<sup>1</sup>, Tracy Stockley<sup>1</sup>, Katherine Lajkosz<sup>3</sup>, Theodorus Van der Kwast<sup>4</sup>, Carol Cheung<sup>5</sup>, Susan Prendeville<sup>4</sup>

<sup>1</sup>Genome Diagnostics University Health Network, Toronto, ON, <sup>2</sup>Laboratory Medicine Program, Departments of Anatomical Pathology, University Health Network and University of Toronto, Toronto, ON, <sup>3</sup>Princess Margaret Cancer Centre, Toronto, ON, <sup>4</sup>University Health Network, University of Toronto, Toronto, ON, <sup>5</sup>Laboratory Medicine Program, Toronto General Hospital/University Health Network, Toronto, ON

**Disclosures:** Shamini Selvarajah: None; Shervin Ansari: None; Shifaa Alqaqa: None; Harpreet Kaur: None; Tracy Stockley: None; Katherine Lajkosz: None; Theodorus Van der Kwast: None; Carol Cheung: None; Susan Prendeville: None

**Background:** Somatic tumor testing in prostate cancer (PCa) can guide treatment options by identifying clinically actionable variants, including acquired variants not detected by germline testing alone. While testing is most often initiated in the metastatic setting, there is currently limited data on the yield and value of routine testing outside of this context. This study describes the first year experience of somatic PCa testing at a tertiary center, including pathologist-driven reflex testing of non-metastatic tumors at primary diagnosis.

**Design:** For our reflex pathway, all primary tumors with Grade Groups (GG)  $\geq 3$  and GG2 tumors with cribriform/intraductal morphology were tested. Non-reflex cases included institutional historical cases with clinical progression and referrals. Specimens meeting criteria were sequenced with a custom enrichment hybrid capture NGS panel (Illumina platform). Variant calls were generated using a custom bioinformatics pipeline, and for those meeting quality thresholds, the AMP/ASCO/CAP standards and guidelines were used for variant interpretation. Pathology characteristics and genetic results were collated.

**Results:** To date, 280 cases have been tested, comprising prostate biopsies (64%), radical prostatectomies (25%), metastatic biopsies (8%) and TURPs (3%). Tumors with GG5 (31%) and GG3 (29%) were the predominant groups, followed by GG2 (24%) and GG4 (15%). Approximately a third of patients had at least one Tier I, II or III variant. Of these 28% were Tier I/II (actionable/potentially actionable) variants, of which 82% were detected in *ATM* (31%), *BRCA1* (11%) or *BRCA2* (40%). Only 10% of Tier I/II were detected in the MMR genes (mostly *MSH2* and *MSH6*). Copy number loss was detected in 40% of cases, of which half were in *BRCA2*. Tier I/II variants were most frequently detected in GG5 tumors (48%), followed by GG3 (28%), GG2 (12%) and GG4 (8%). Among 171 in-house reflex tests performed on hormone naïve primaries, 25% contained a variant. Overall, 5% of this unique subgroup contained a Tier I/II variant - GG2 (4%), GG3 (2%), GG4 (5%) and GG5 (7%).

**Conclusions:** Our findings confirm the utility of somatic tumor testing to detect variants of clinical significance in PCa. Of interest, reflex testing on hormone naïve primary non-metastatic PCa identified variants in 25% of the cases, including a subset of intermediate risk cases with potentially actionable variants requiring follow-up germline testing. Further analysis on a larger cohort of cases is ongoing.

## 811 Primitive Soft Tissue Neoplasms of the Penis: Our Thirty-Years Experience

Sascia Pietro Servillo<sup>1</sup>, Giancarlo Pruner<sup>1</sup>, Nicola Nicolai<sup>1</sup>, Maurizio Colecchia<sup>2</sup>

<sup>1</sup>Fondazione IRCCS Istituto Nazionale Tumori Milano, Milan, Italy, <sup>2</sup>University Vita-Salute San Raffaele, Milan, Italy

**Disclosures:** Sascia Pietro Servillo: None; Giancarlo Pruner: None; Nicola Nicolai: None; Maurizio Colecchia: None

**Background:** Primitive urogenital sarcomas are rare tumors, accounting for less than 5% of all sarcomas. They occur in the para testis, kidney, bladder, and prostate. Penile sarcomas are exceptionally rare, usually described in case-reports or small case series. To date, only one comprehensive study including 46 cases was published in 1970. Here we describe a series of 18 primitive penile sarcomas collected in the last thirty years at our institution.

**Design:** Consecutive primitive penile neoplasms diagnosed from 1990 to 2020 were identified in the Pathology archive. All cases were reviewed by two experienced pathologists and adjunctive immunohistochemical and molecular analyses were performed when paraffin blocks were available. Clinico-pathological data were collected and updated including disease-free and overall survival data.

**Results:** Among 1150 penile neoplasms, we found 18 (1,5%) penile soft tissue tumors. Four were hemangiomas. Following the revision, the diagnoses of the malignant neoplasms were as follows: Kaposi sarcoma (4 cases), epithelioid angiosarcoma (1), "proximal-type" epithelioid sarcomas (3), myogenic sarcomas (2), dedifferentiated liposarcoma (1), low-grade fibromyxoid sarcoma (1), and synovial sarcoma (1). One more case previously diagnosed as epithelioid hemangioendothelioma is currently under further investigation (the alternative diagnosis is epithelioid hemangioma). Most (10) of these cases were internal, while 4 were received for second opinion. The age range was 20-89 years. Clinical data were retrieved for the 10 inpatients: 2 patients underwent radical penectomy, 1 partial penectomy, 4 local excisions, and 3 patients only received chemotherapy and radiotherapy. The follow-up

# ABSTRACTS | GENITOURINARY PATHOLOGY (INCLUDING RENAL TUMORS)

range was 7-217 months (updated to January 2022): 3 patients died for the disease, 2 were alive without disease, 2 were alive with disease, 1 died for other causes, and 2 were lost to follow-up.

Clinical data and histological diagnosis of 10 primitive sarcomas of the penis. DOD: dead of disease; DWD: dead with disease; AWD: alive with disease; DFS: disease free survival; LFU: lost to follow-up.									
Pt	Age	Location	Dimension (cm)	Diagnosis	Therapy	Follow-up	Outcome	Previous neoplasms	
1	20	root	6	"proximal-type" epithelioid sarcoma	CT + RT	7	DOD	none	
2	24	root	4	"proximal-type" epithelioid sarcoma	CT + RT	88	DOD	none	
3	39	root	2	epithelioid hemangioendothelioma/epithelioid hemangioma	local excision	217	LFU	none	
4	47	glans and foreskin	>10	myogenic sarcoma	radical penectomy	52	DOD	fibroblastic osteosarcoma of the leg	
5	59	foreskin	N/A	"proximal-type" epithelioid sarcoma	local excision	8	LFU	Hodgkin lymphoma	
6	63	glans	4	myogenic sarcoma	partial penectomy	36	DFS	carcinoma in situ of the glans	
7	69	glans and shaft	0,8	epithelioid angiosarcoma	CT + radical penectomy	125	DFS	none	
8	71	glans	0,8	Kaposi sarcoma	local excision	96	AWD	none	
9	77	glans and foreskin	N/A	Kaposi sarcoma	local excision + CT + RT	161	DWD	Hodgkin lymphoma, prostate adenocarcinoma	
10	89	root	4	dedifferentiated liposarcoma	RT	12	AWD	none	

Figure 1 - 811

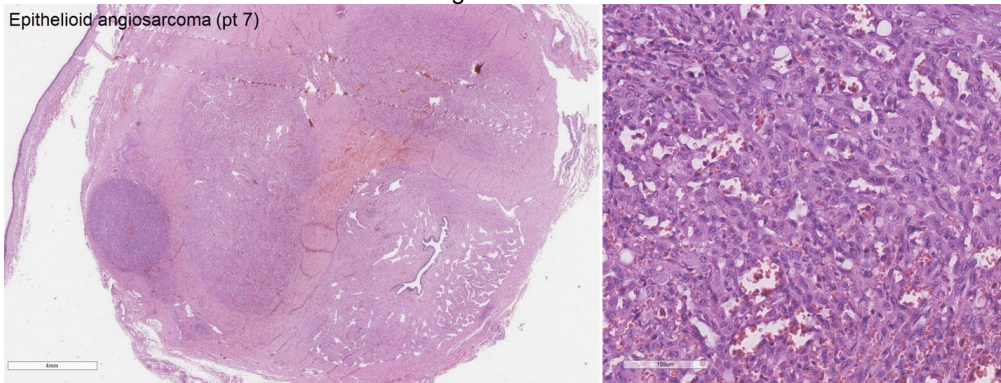
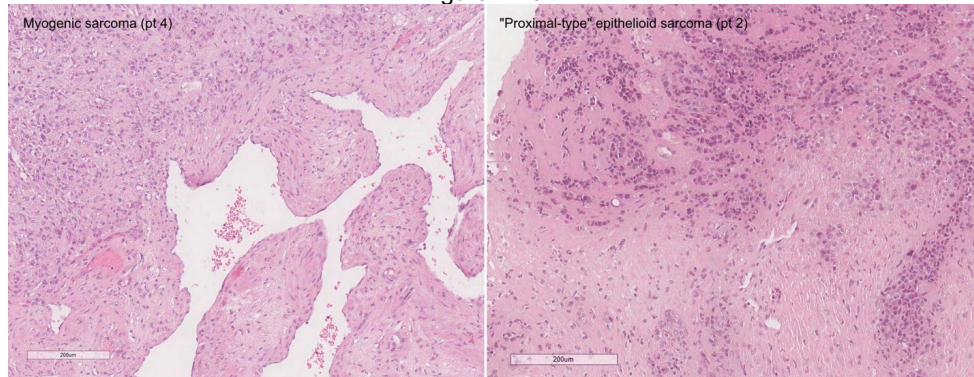


Figure 2 - 811



**Conclusions:** Penile soft tissue neoplasms affect all ages. They are often misdiagnosed both clinically (an induration mimicking Peyronie's disease) and histologically (granulomatous appearance in epithelioid sarcomas mimicking chronic inflammation, epithelioid morphology resembling a carcinoma). The absence of intraepithelial penile neoplasia, a true primitivity in the penis, and the presence of urinary symptoms are clues for the diagnosis. Most cases are vascular neoplasms and epithelioid sarcomas, in line with the previous observations. Here we describe the first case of penile dedifferentiated liposarcoma.

## 812 Review of the Clinicopathological Correlation and Survival Data of Genitourinary Liposarcoma

Nada Shaker<sup>1</sup>, Nuha Shaker<sup>2</sup>, Swati Satturwar<sup>1</sup>, Anil Parwani<sup>3</sup>

<sup>1</sup>The Ohio State University Wexner Medical Center/James Cancer Hospital, Columbus, OH, <sup>2</sup>University of Kentucky, Lexington, KY, <sup>3</sup>The Ohio State University Wexner Medical Center, Columbus, OH

**Disclosures:** Nada Shaker: None; Nuha Shaker: None; Swati Satturwar: None; Anil Parwani: None

**Background:** Genitourinary sarcomas (GUSs) are rarely encountered in the genitourinary tract and account for less than 1% of all malignant neoplasms. Among GUSs, liposarcoma is a major contributor to mesenchymal lesions in this anatomic location. We aim to analyze the burden of liposarcoma among GUSs and evaluate their overall survival.

**Design:** Data of 61 patients were queried over a period of seven years (2015-2022) from The Ohio State University Wexner Medical Center to identify cases of primary GU liposarcomas. Pathology reports from patients with liposarcoma were extracted and data on tumor characteristics were collected.

**Results:** A total of 61 cases of GUSs were identified, out of which, 28/61 (45%) liposarcoma cases were retrieved. Liposarcoma preferentially involves the testicular region 25/28 (89%) followed by the kidney 3/28 (10%). The testicular region included specimens from: 10/28 (35%) scrotum, 6/28 (21%) para-testicular, 4/28 (14%) spermatic cord, 3/28 (10%) para-testicular and testicular, and 2/28 (7%). The tumor size range was 2.8 – 30.6 cm. The median follow-up time, available for 20 patients, was 31.5 months with a mean of 66.1 months. Well-differentiated (WDL) 9/28 (32%) and de-differentiated liposarcomas (DDL) 19/28 (67%) were the only histologic types in the genitourinary tract. No LVI or PNI was noted. Regional lymph node involvement was identified in one case of DDL of the scrotum. Local recurrence was noted in 14/28 (50%) of cases. Recurrence was not restricted to cases with positive margins. Distant metastases to the adrenal, lung, skin, and ureter were observed in 4/28 (14%) of patients. Remarkably, the scrotum was the origin of 3/4 (75%) of the metastasis. At the time of the last review, 5/28 (17%) patients were deceased, three of whom had either metastasis or recurrence 3/5 (60%). DDL was the prominent diagnosis in all deceased patients. The mean overall survival was 23.8 months.

Table 1 summarize the clinicopathological records of 28 patients diagnosed with genitourinary liposarcoma

PT #	SIZE (CM)	LCN.	TYPE	STG.	MG.	GRADE	LVT	PNT	RECURR.	MET.	MFU (MO.)	OS (MO.)	D/A	
1	9	SPC	WDL	pT2NX	NA		N	N	NA	NA	27	NA	A	
2	2 x 3.5	PTST	WDL	NA	-		N	N	+	N	18	NA	A	
3	9.5	SCR	Liposarcoma	pT2Nx	-	1	N	N	+	N	104	NA	A	
4	K	PTST		pT1Nx	-	1	N	N	N	N	25	NA	A	
5	3.2	PTST		DDL	pT1Nx	-	3	N	NA	+++	N	21	NA	A
6	3	PTST		DDL	pT1Nx	-	N	NA	N	N	120	NA	A	
7	9.6	PTST		DDL	pT2Nx	-	N	NA	N	N	0	0	D	
8	9	TST	DDL	pT2Nx	-	2	N	NA	N	N	1	NA	A	
	+	SPC												
9	4.6	SCR	DDL	NA	NA	2	NA	NA	+ (Multi.)	N	225	NA	A	
10	8.9	SCR	DDL	pT2bpN0	NA	3	NA	NA		Skin	16	16	D	
11	11	SPC	DDL	NA	NA		NA	NA	+		88	88	D	
12	14	TST	DDL	NA	NA	2	NA	NA	+	N	48	NA	A	
	+	SPC												
13	2.8	SCR	WDL	NA	+	NA	NA	NA	++++	Lung after 4 years	132	NA	A	
14	9	SCR	DDL	NA	+	NA	NA	NA	+		156	NA	A	
15	4	SPC	DDL	NA	+	2/3	N	N						
16	9.0	T	DDL	pT2 Nx	N	2	N	N	N	N	12	NA	A	
17	5.1	K	DDL	pT2	NA	1	N	N	N	N	1	NA	A	
18	SCR	DDL	LYMPHNODE	+ (Multi.)	NA	NA	NA	NA			3	3	D	
19	8.6	SCR	DDL w/ myoid diff		+	1			+	N	12	NA	A	
20	7.6	SCR				3			+					
21	9.0	T/SP ERM ATIC COR D		WDL	pT2 NX	NA	1	N	N	N	36	NA	A	
22	9.5	T	WDL	NA	N	NA	NA	NA	+ (after 7 yrs.)	N	120	NA	A	
23	30.6	K	DDL	pT4 NX	+	3	N	NA	+	Adrenal	24	NA	A	
24	3.5	ParaT	DDL	pT1 Nx	N	3	N	NA	+ (After 7 yrs.)	N	110	NA	A	
25	SCR	DDL		NA	NA	3	NA	NA		Ureter	12	12	D	
26	4	Spermatic cord	DDL	NA	+	NA	NA	NA	N	N	10	10	A	
27	9.8	SCR	WDL	NA	N	NA	NA	NA	+	NA	NA	NA	A	
28	3.5	PenT	WDL	NA	N				+ (after 7 yrs.)	N	120	NA	A	

**Conclusions:** Liposarcoma of the genitourinary tract is most frequently encountered within the testicular region. Noteworthy, DDL is the most frequently identified in the testicular region and is associated with an unfavorable prognosis and overall survival.

## 813 The Diagnosis of Extraprostatic Extension on Prostate Biopsy Correlates with a Higher Pathologic Stage at Radical Prostatectomy

Khalid Shittu<sup>1</sup>, Oudai Hassan<sup>1</sup>, Nilesh Gupta<sup>1</sup>, Khaleel Al-Obaidy<sup>1</sup>

<sup>1</sup>Henry Ford Health System, Detroit, MI

**Disclosures:** Khalid Shittu: None; Oudai Hassan: None; Nilesh Gupta: None; Khaleel Al-Obaidy: None

**Background:** The detection of adenocarcinoma extending into the adipose tissue signifies extraprostatic tumour extension and therefore pT3a stage category. However, the presence of intraprostatic adipose tissue, albeit rare, had put some reluctance on such diagnosis and subsequently staging on needle biopsy specimens. In the present study, we aimed at evaluating cases of prostatic adenocarcinoma diagnosed with extraprostatic extension (i.e. extension into adipose tissue) and comparing the pathologic stage category (T) to that of the resection specimen from the same patient.

**Design:** The pathology electronic archive from department of Pathology at our institution was searched for needle core biopsies with a diagnosis of extraprostatic extension (i.e. extension into adipose tissue) between 2015 and 2022. All cases with such diagnosis were retrieved and cases with subsequent prostatectomy were included. Our system utilizes a subspecialty sign out system and cases were signed out by urologic pathologists.

**Results:** One-fifty-eight (158) needle core biopsy cases with the diagnosis of extraprostatic extension (i.e. extension into adipose tissue) were identified in our electronic databases. Of these, 38 cases had subsequent radical prostatectomy in our system within 6 months of the EPE diagnosis. The grade group of these cases were 2 (n=8; 21%), 3 (n=13; 34%) and 5 (n=17; 45%). All 38 cases diagnosed with EPE on biopsy were found to have EPE on resection (concordant rate is 100%). Of these, the pathologic stage category pT3a in 12 cases (32%), pT3b in 14 cases (63%) and pT4 in 2 cases (invading adjacent organs on resection; 5%). Additionally, of the remaining 120 cases without follow-up prostatectomy, 6 patients had biopsy confirmed metastases to the liver (2), brain (1), spinal cord (1), lymph node (1) and bone (1).

**Conclusions:** Our findings signifies the importance of diagnosing extraprostatic extension in needle core biopsies. Interestingly, most of the cases (68%) had a higher pT stage category on follow-up resections, and 6 cases had documented metastasis.

## 814 Dysregulation of Genetic Pathways in Histological Growth Patterns of Clear Cell Renal Cell Carcinomas

Deepika Sirohi<sup>1</sup>, Yeonjung Jo<sup>2</sup>, Beatrice Knudsen<sup>1</sup>

<sup>1</sup>The University of Utah/ARUP Laboratories, Salt Lake City, UT, <sup>2</sup>Huntsman Cancer Institute, Salt Lake City, UT

**Disclosures:** Deepika Sirohi: None; Yeonjung Jo: None; Beatrice Knudsen: None

**Background:** We previously demonstrated that histological growth patterns (HGP) can be used to grade clear cell renal cell carcinoma (CCRCC) as accurately as WHO/ISUP nuclear grade and that HGP are predictive of disease outcomes. Herein, we investigate genomic pathway dysregulation related to HGPs in the cancer genome atlas (TCGA) database.

**Design:** We analyzed cases from the TCGA CCRCC cohort (n=416) that correspond to established diagnostic criteria of combined morphological and molecular data for ccRCC. Digital slides were separated into 3 HGP grade groups (HGP-GG) based on HGP subtype and nuclear grade as: HGP-GG1: small nests, expansile nests, nests with high nuclear to cytoplasmic ratio; HGP-GG2: tubular and/or papillary, HGP-GG 3: sarcomatoid, rhabdoid, low grade spindled (LGS), fused nests (FN) and pleomorphic tumor giant cells. RNA expression data in c-Bioportal were used to identify dysregulated pathways in each case. Chi square test was used to determine the significance of frequencies of dysregulated pathways between pairwise groups of HGP-GGs. Univariate and multivariate analysis using the Cox proportional hazard model was used to determine whether dysregulated pathways are predictive of overall survival (OS) across all cases and within specific HGP-GGs.

**Results:** *PI3K* pathway was dysregulated in HGP-GG 3 compared to HGP-GG 2 (adjusted p-value 0.002). Across all cases, *RTK-RAS-PI3K* pathway ( $HR=0.68$ ,  $p=0.034$ ) and *NOTCH* signaling pathway ( $HR=0.53$ ,  $p=0.003$ ) dysregulation were associated with longer OS. This result was most significant in HGP-GG2 tumors. In tumors with sarcomatoid and rhabdoid features, alterations in apoptotic and Hippo pathways were associated with longer OS ( $HR=0.05$ ,  $p=0.06$  each), while activation of *TGFB* pathway predicted shorter OS ( $HR=11.8$ ,  $p=0.02$ ). In tumors with FN and LGS HGPs, dysregulated *BRCA2* signaling was predictive of shorter OS ( $HR=13.73$ ,  $p=0.02$ ). Finally, dysregulated *WNT* signaling showed a trend towards shorter OS in HGP-GG2 ( $HR=0.55$ ,  $p=0.07$ ).

**Conclusions:** HGP-based grade groups of CCRCC express dysregulated pathways that are predictive of OS. We confirmed the expected dysregulation of the *TGFB* pathway in tumors with mesenchymal differentiation and phenotypes of sarcomatoid and rhabdoid HGPs. Data reveals additional associations between molecular alterations leading to pathway dysregulation and morphologic characteristics of HGPs.

## 815 Overexpression of UBE2C Correlates to Immune Infiltration and Poor Prognosis: A Potential Prognostic Biomarker and Promoting Therapeutic Target for Papillary Renal Cell Carcinoma

Qingyang Sun<sup>1</sup>, Yao Fu<sup>2</sup>, Xiangshan Fan<sup>3</sup>

<sup>1</sup>Nanjing Drum Tower Hospital Clinical College of Nanjing Medical University, Nanjing, China, <sup>2</sup>Affiliated Drum Tower Hospital Nanjing University Medical School, Nanjing, China, <sup>3</sup>Nanjing Drum Tower Hospital, Nanjing, China

**Disclosures:** Qingyang Sun: None; Yao Fu: None; Xiangshan Fan: None

**Background:** *UBE2C* is a protein coding gene and its protein product involves the modification of proteins with ubiquitin, an important cellular mechanism for targeting abnormal or short-lived proteins for degradation. Contributions to tumor pathogenesis of overexpression by *UBE2C* have been discovered in several cancers, such as lung cancer, breast cancer. However, the correlation of *UBE2C* and papillary renal cell carcinoma (PRCC) remains unclear. In this study, we tend to identify the underlying impact of *UBE2C* expression on PRCC.

**Design:** Using public databases, we analyzed the gene expression status of *UBE2C* and explored the relevance of its expression level to patients prognosis. And we performed *UBE2C* immunohistochemical(IHC) staining on tumor tissues of PRCC cases in our department to further its overexpression in PRCC. We continued gene oncology and gene set enrichment analysis(GSEA) to identify potential biological functions of *UBE2C*. Finally, we explored whether expression level correlates to immune infiltration status and corresponding miRNA level. Finally, given the risks we identified above, we designed a prognosis model to predict outcomes of patients suffering from PRCC.

**Results:** Expression level of *UBE2C* was much higher in tumor tissues than in normal ones, and even in tumor samples, its expression level in higher stages exceeded that in lower stages, while higher expression level appeared worse patients prognosis in PRCC as well. We further validated *UBE2C* overexpression in PRCC cases in our department by IHC staining, with tumor samples displaying stronger IHC staining. GSEA results revealed *UBE2C* involved in chromosome organization, mitotic cell cycle, mitotic cell cycle process, negative regulation of transcription by RNA polymerase II and nerve system process. *UBE2C* high-expression expression group, on contract to low-expression group, tended to show higher immune infiltration reactions and higher IDO1 expression level. Then, high-expression group of *UBE2C* in our study showed high corresponding upstream miRNAs level. When came to the prognosis model we constructed, it could efficiently predict patients overall survivals of different expression groups under situations of >2years, >3years and >5years.

Clinical features		Total(282)	Percentage(%)
Gender			
	male	206	73.0
	female	76	27.0
Age			
	>=60	150	53.2
	<60	132	46.8
T stage			
	T1	192	67.7
	T2	32	11.3
	T3	57	20.2
	T4	2	1.0
N stage			
	N0	49	17.4
	N1	27	9.6
M stage			
	M0	93	33.0
	M1	9	3.2
TNM stage			
	I	197	70.0
	II	32	11.2
	III	42	14.8
	IV	11	4.0
OS status			
	Alive	240	85.1
	Dead	44	14.9
UBE2C expression level			
	High	141	50
	Low	141	50

Figure 1 - 815

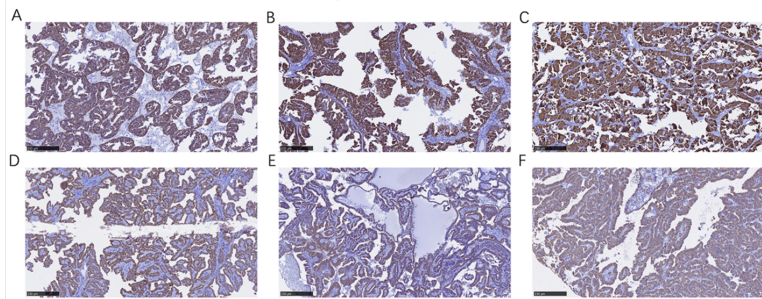


Figure1. Immunohistochemical staining of UBE2C (A-E), all six PRCC tumor tissues show mediate to strong UBE2C staining.

Figure 2 - 815

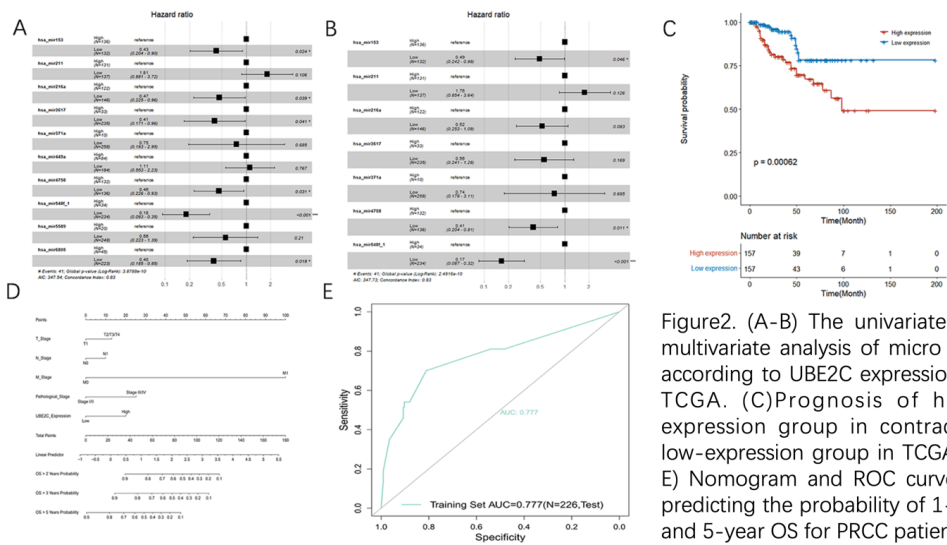


Figure2. (A-B) The univariate and multivariate analysis of micro RNA according to UBE2C expressions in TCGA. (C) Prognosis of high-expression group in contrast to low-expression group in TCGA.(D-E) Nomogram and ROC curve for predicting the probability of 1-, 3-, and 5-year OS for PRCC patients.

**Conclusions:** In this study, we revealed overexpression of *UBE2C* in PRCC correlation to patients' prognosis as well as immune infiltration, suggesting *UBE2C* playing a role as a potential biomarker in PRCC and providing additional alterations for clinical treatments.

## 816 Classification of Renal Oncocytic Tumors Using 2022 WHO Criteria

Jerasit Surinrspanont<sup>1</sup>, Khalid Algarrahi<sup>2</sup>, Elizabeth Genega<sup>3</sup>, Ming Zhou<sup>4</sup>

<sup>1</sup>Tufts Medical Center, Boston, MA, <sup>2</sup>Massachusetts General Hospital, Boston, MA, <sup>3</sup>Emory School of Medicine, Atlanta, GA, <sup>4</sup>Tufts University School of Medicine, Boston, MA

**Disclosures:** Jerasit Surinrspanont: None; Khalid Algarrahi: None; Elizabeth Genega: None; Ming Zhou: None

**Background:** The classification of renal oncocytic tumors has undergone significant revision in recent years with more precise diagnostic criteria and discovery of novel and emerging entities, which is reflective of the clinical behavior and genetics. Using the 2022 World Health Organization (WHO) Classification of Urinary and Male Genital Tumors, this study attempts to reclassify "pink" renal tumors and determine the impact of the new classification system.

**Design:** Fifty-six renal neoplasms with the diagnoses of renal oncocytoma (RO), chromophobe renal cell carcinoma (ChRCC), oncocytic renal tumor, NOS (OT NOS), and unclassified RCC with "oncocytic features" from 50 patients, between 2010 and 2020, were retrieved from the surgical pathology file at the authors' institution. H&E and immunohistochemical (IHC) slides were reviewed; additional IHC stains were performed if alternative diagnoses were considered. The IHC panel for working up oncocytic tumors included CK7, CK20, vimentin, CD117, Cathepsin K, SDHB, and FH. The final diagnoses were made based on morphology and IHC profiles.

**Results:** Twenty tumors were reclassified (20/56 = 36%): 6 RO were reclassified as OT NOS; 6 ChRCC were reclassified as unclassified RCC (2), suspicious for TSC/MTOR-mutated RCC (1), and low grade oncocytic tumor (LOT) (3); 6 OT NOS were

# ABSTRACTS | GENITOURINARY PATHOLOGY (INCLUDING RENAL TUMORS)

reclassified as RO (2), ChRCC (1), eosinophilic vacuolated tumor (EVT) (1), suspicious for TSC/MTOR-mutated RCC (1), and eosinophilic solid cystic RCC (ESC RCC) (1); and 2 unclassified RCC from the same patient were reclassified as ESC RCC. Eleven cases remained unclassified: OT NOS (9) and unclassified RCC (2). During a median follow up time of 78.7 months (range: 16.2-147.7 months), most patients had no evidence of disease (44/50 = 88%); 2 were alive with disease (2/50 = 4%): ChRCC and OT NOS; 1 patient died of other causes (1/50 = 2%); and 3 patients were lost to follow up (3/50 = 6%).

Pre-Workup Diagnoses	Post-Workup Diagnoses					Total
	RO	ChRCC	OT NOS	Other		
RO	16	-	6	-	22	
ChRCC	-	17	-	Unclassified RCC 2*, Suspicious for TSC/MTOR-mutated RCC 1**, LOT 3	23	
OT NOS	2	1 (eosinophilic subtype)	3	EVT 1, Suspicious for TSC/MTOR-mutated RCC 1, ESC RCC 1	9	
Unclassified RCC	-	-	-	ESC RCC 2	2	
Total	18	18	9	11	56	
Outcome	NED: 11/14 (79%) DOO: 1/14 (7%) LFU: 2/14 (14%)	NED: 16/18 (89%) AWD: 1/18 (5.5%) LFU: 1/18 (5.5%)	NED: 7/8 (88%) AWD: 1/8 (12%)	NED: 10/10 (100%)	NED: 44/50 (88%) AWD: 2/50 (4%) DOO: 1/50 (2%) LFU: 3/50 (6%)	

\*One of the patients with unclassified RCC has MUTYH likely pathogenic variant c.934-2A>G. (monoallelic); she also has colon cancer, melanoma, and desmoid fibromatosis.

\*\*One patient with suspected TSC/MTOR-mutated RCC has a history of developmental delay, mental retardation, and seizure (no documented tuberous sclerosis complex in electronic medical record); his father also has RCC.

RO, renal oncocytoma; ChRCC, chromophobe renal cell carcinoma; OT NOS, oncocytic tumor NOS; RCC, renal cell carcinoma; LOT, low grade oncocytic tumor; EVT, eosinophilic vacuolated tumor; ESC RCC, eosinophilic solid cystic renal cell carcinoma; NED, no evidence of disease; LFU, lost to follow up; AWD, alive with disease; DOO, died of other causes

**Conclusions:** This study showed that the 2022 WHO criteria have a significant impact on the classification of renal oncocytic tumors. Some of the previously unclassifiable oncocytic renal tumors can now be diagnosed as specific entities. It is important to recognize these tumors as many of them have indolent or benign behavior, and some of them may occur in genetic syndrome. A significant proportion of tumors would require additional tests to be further classified. This study also shows that a panel of IHC stains can aid the classification of oncocytic tumors in routine clinical practice.

## 817 BAP1 is the Most Common Disrupted Gene in VHL Mutation-negative Advanced Clearcell Renal Cell Carcinoma

Kotaro Takeda<sup>1</sup>, Gabriela Quiroga-Garza<sup>2</sup>, Sheldon Bastacky<sup>2</sup>, Rajiv Dhir<sup>1</sup>

<sup>1</sup>University of Pittsburgh Medical Center Presbyterian Shadyside, Pittsburgh, PA, <sup>2</sup>University of Pittsburgh Medical Center, Pittsburgh, PA

**Disclosures:** Kotaro Takeda: None; Gabriela Quiroga-Garza: None; Sheldon Bastacky: None; Rajiv Dhir: None

**Background:** Clear cell renal cell carcinoma (ccRCC) is the most common renal malignant neoplasm in adults, and advanced stage of ccRCC is associated with poor prognosis. Approximately 90% of ccRCC is caused by VHL gene abnormalities such as gene mutation, 3p loss and hypermethylation, which leads to uncontrolled activation of hypoxia-inducible factors (HIF) and a number of HIF targets including vascular endothelial growth factors (VEGF) and carbonic anhydrase IX (CAIX). However, approximately 10% of ccRCC cases do not have VHL gene abnormalities, thus VHL independent oncogenic mechanism must be involved.

**Design:** We retrospectively reviewed morphologically diagnosed ccRCC with advanced pathological stage (pT3 or greater) between January 2021 and July 2022, and analyzed VHL gene mutation status and additional 161 commonly mutated genes in cancer by targeted next generation sequencing (Oncomine testing). To prove whether HIF pathway is indeed activated, immunohistochemical analysis for CAIX was performed and only diffuse box-like membranous staining pattern is considered to be positive. Tumor size, nuclear grade (WHO/ISUP), lymphovascular invasion, presence of sarcomatoid and rhabdoid features were also analyzed.

**Results:** We identified 68 cases of advanced ccRCC. The diagnosis was confirmed by histological morphology and positive immunoreactivity for CAIX. Among these cases, 60 cases (88%) were found to have VHL mutations, and 8 cases (12%) were negative for VHL gene mutations. The Oncomine analysis for these 8 cases revealed that BRCA1-associated protein 1 (BAP1) gene abnormality was identified in 4 cases (50%); one case of BAP1 p.T111Pfs\*2, three cases of BAP1 copy number loss. Other

# ABSTRACTS | GENITOURINARY PATHOLOGY (INCLUDING RENAL TUMORS)

gene abnormalities include ARID1A, SETD2, PTEN, TERT and p53. In contrast, BAP1 abnormality was found in 26.6 % of VHL mutation-positive ccRCC. As shown in Table, The VHL mutation-negative ccRCC tends to have milder features compared to VHL mutation-positive ccRCC, such example includes nuclear grade, sarcomatoid/rhabdoid features and the average tumor size.

clear cell RCC (>pT3)	VHL mutation Negative	VHL mutation Positive
Case #	8	60
BAP1 abnormal	4 (50%)	16 (26.6 %)
Tumor size	6.2 cm	7.6 cm
Sarcomatoid/Rhabdoid	3 (37.5%)	38 (63.3%)
Nuclear grade 3/4	6 (75%)	54 (90%)
Vascular invasion	5 (62.5%)	34 (56.6%)

**Conclusions:** We identified BAP1 gene is the most common abnormality in VHL mutation-negative ccRCC. BAP1 loss has been reported to alter cell metabolism toward anaerobic glycolysis and allow cancer cells to survive in hypoxic conditions (often called Warburg effect). Our data suggest BAP1 alteration may be another route to activate HIF pathway in the context of no VHL abnormality in ccRCC. Further molecular analysis is warranted.

## 818 Impact of Grading Small Tumor Volumes with Gleason Pattern 4, with an Emphasis on Global Biopsy Scoring

Ingrid Tam<sup>1</sup>, Andres Acosta<sup>2</sup>, Michelle Hirsch<sup>3</sup>, Karan Vats<sup>1</sup>, Nicholas Baniak<sup>4</sup>

<sup>1</sup>University of Saskatchewan, Saskatoon, SK, <sup>2</sup>Brigham and Women's Hospital, Harvard Medical School, Boston, MA, <sup>3</sup>Brigham and Women's Hospital, Boston, MA, <sup>4</sup>University of Saskatchewan, Saskatchewan Health Authority, Saskatoon, SK

**Disclosures:** Ingrid Tam: None; Andres Acosta: None; Michelle Hirsch: None; Karan Vats: None; Nicholas Baniak: None

**Background:** The Gleason Score/Grade Group (GS/GrGr) is an important factor in therapeutic decision making for prostatic adenocarcinoma (PCa). However, in core biopsies (CBx) with limited tumor volumes, grading small areas of PCa is difficult; this is especially challenging with small tumor foci containing Gleason pattern 4 (GP4), which may lead to erroneous upgrading of cases. The terminology 'small GP4' was introduced by the BWH group in 2019, with cores being diagnosed as "small focus of PCa, not amenable to precise Gleason grading; however, GP4 is present". Reports have been conflicting on the impact of grading small foci of PCa in terms of correlation with grading radical prostatectomies (RP). The aim of this study was to evaluate the significance of grading small tumor volumes containing GP4, particularly in the context of global CBx scoring.

**Design:** We retrospectively reviewed 503 matched prostate CBx and RP specimens between 2014 and 2022. Only cases with at least 12 cores were included. For each CBx, the number of positive cores, the maximum percent of core involved, the highest GrGr, and global GrGr was recorded. Cores with less than 1mm of tumor or less than 10% involvement containing GP4 were designated as small GP4 (SmGP4); any core with GrGr5 was excluded.

**Results:** We identified 42 CBx cases (8.3%) with SmGP4 in one of the cores. In 20 cases (3.9%), SmGP4 corresponded to the core with the highest grade in the case. If grading according to the relative volume of GP4, 14 (70%) would have been over-graded compared to the final grade in the RP, 4 (20%) would have been concordant, and 2 (10%) would have been under-graded. SmGP4 was the only focus of PCa in only 4 cases (0.8%), affecting both the highest and global GrGr. In the remaining 16 CBx cases, assigning a GS/GrGr rather than a designation of SmGP4 did not change the global GrGr. Of the 4 cases where the global GrGr would be changed, 2 (50%) would be over-graded compared to the RP, 1 (25%) would have been concordant, and 1 (25%) would have been under-graded. As a small comparison group, in CBx cases with only 1 positive core and a tumor volume between 10 and 20%, only 1/9 (11%) were over-graded compared to the RP, while 8/9 (89%) were concordant.

**Conclusions:** Grading small foci of PCa containing GP4 has a minimal impact on the global GS/GrGr, but more often changes the highest GS/GrGr. When considering a highest-grade approach on CBx, these cases should be diagnosed descriptively, ex. SmGP4, rather than being assigned a GS/GrGr.

## 819 High Risk-HPV Status & Outcomes for Penile Squamous Cell Carcinoma: A Single Institution Experience

Burak Tekin<sup>1</sup>, Antonio Cubilla<sup>2</sup>, John Cheville<sup>1</sup>, Surendra Dasari<sup>1</sup>, Loren Herrera Hernandez<sup>1</sup>, Rafael Jimenez<sup>1</sup>, R. Houston Thompson<sup>1</sup>, Bradley Leibovich<sup>1</sup>, R. Jeffrey Karnes<sup>1</sup>, Stephen Boorjian<sup>1</sup>, Lance Paglialoro<sup>1</sup>, Lori Erickson<sup>1</sup>, Ruifeng (Ray) Guo<sup>1</sup>, Sounak Gupta<sup>1</sup>

<sup>1</sup>Mayo Clinic, Rochester, MN, <sup>2</sup>Instituto de Patologia e Investigacion, Asuncion, Paraguay

**Disclosures:** Burak Tekin: None; Antonio Cubilla: None; John Cheville: None; Surendra Dasari: None; Loren Herrera Hernandez: None; Rafael Jimenez: None; R. Houston Thompson: None; Bradley Leibovich: None; R. Jeffrey Karnes: None; Stephen Boorjian: None; Lance Paglialoro: None; Lori Erickson: None; Ruifeng (Ray) Guo: None; Sounak Gupta: None

# ABSTRACTS | GENITOURINARY PATHOLOGY (INCLUDING RENAL TUMORS)

**Background:** Patient outcomes for squamous cell carcinoma (SCC) based on high-risk Human Papilloma Virus (HPV) positivity at sites such as the head and neck are relatively well defined. However, limited data have been reported for penile SCC. Herein, therefore, we aimed to study the prevalence of high-risk HPV positivity in patients with penile SCC and to evaluate relevant clinicopathologic features including tumor morphology, pathologic stage, and outcomes based on HPV status.

**Design:** A single institutional pathology archive was interrogated for patients who underwent a partial or total penectomy for SCC between 2000 and 2021. Clinicopathologic variables were evaluated by chart review and corresponding H&E-stained slides were evaluated by 4 pathologists blinded to the original diagnosis and HPV status. High-risk HPV positivity was established based on a combination of histology, P16 immunohistochemistry (IHC), DNA *in situ* hybridization (ISH, low and high-risk genotypes), and/or RNA ISH (E6/7 transcripts in high risk genotypes). In addition, IHC (22c3 clone) was performed to determine PD-L1 status in invasive tumors.

**Results:** The clinicopathologic features of 120 consecutive patients treated with penectomy are outlined in Table 1. Histologic evaluation had a sensitivity of approximately 97% (115/119) in correctly predicting HPV status when compared to ancillary testing (IHC/ISH). PD-L1 IHC was performed in 106 cases and showed a mean combined positivity score (CPS) of 7.9 (0 – 90), and a mean h-score of 12 (0 – 220). Follow-up was available for 102 patients with  $\geq$ pT1 tumors. Our results show that compared to patients with high-risk HPV-positive tumors, those with HPV-negative tumors had an older age at penectomy, larger tumor size, and higher PD-L1 CPS (mean values listed; age at penectomy: 70.2 vs 64.4 years; size: 3.7 vs 2.8 cm; CPS: 9 vs 3.3; p<.05). However, no significant differences in outcome based on HPV status were identified when patients were stratified based on pathologic stage. Finally, 8 patients had grossly multifocal lesions and had an aggressive clinical course (cancer-specific mortality in 4/8 patients).

Table 1. Clinicopathologic features.

Clinicopathologic feature	Subcategories	Number of cases (percentage), or mean (range)			
Age at penectomy (years, n=120)		68.5 (34 – 92)			
Type of penectomy (n=120)	Partial Total	89 (74%) 31 (26%)			
Positive margin (PeIN and/or invasive tumor, n=120)		7 (6%)			
Tumor focality (n=120)	Unifocal Multifocal	112 (93%) 8 (7%)			
Tumor site (n=120)	Glans Glans + another site Shaft Foreskin Penile urethra Not otherwise specified Coronal sulcus	84 (70%) 14 (12%) 6 (5%) 6 (5%) 6 (5%) 3 (3%) 1 (1%)			
Tumor size at penectomy (cm, n=120)		3.39 (0.3 – 13)			
HPV status - IHC: p16 - DNA ISH: low risk (6, 11) & high risk (16, 18, 31, 33, and 55) - RNA ISH: E6/E7 transcripts in high-risk genotypes	Negative Positive, low-risk genotype Positive, high-risk genotype Not tested	82 (68%) 1 (1%) 36 (30%) 1 (1%)			
HPV-independent morphologic subtypes (n=82, 68%)	Usual type Verrucous carcinoma Papillary, not otherwise specified Pseudohyperplastic Mixed (usual and verrucous)	71 (59%) 6 (5%) 3 (3%) 1 (1%) 1 (1%)			
HPV-associated morphologic subtypes (n=38, 32%)	Basaloid Warty-basaloid Medullary Warty Warty with condylomatous and papillary features Mixed	17 (14%) 4 (3%) 3 (3%) 1 (1%) 1 (1%) 12 (10%)			
Follow-up for $\geq$ pT1 tumors (n = 102)					
Stage	Differentiation* (well, moderate, poor)	Mean follow-up (months)	Without local recurrence or metastasis	Local recurrence and/or metastasis during follow-up	Outcome (DOD)
pT1 (HPV-, n=17)	W: 9/17 (53%), M: 7/17 (41%), P: 1/17 (6%)	61	16/17 (94%)	1/17 (6%)	1/17 (6%)
pT1 (HPV+, n=11)	N/A	62	8/11 (73%)	3/11 (27%)	0/11 (0%)
pT1 (All, n=28)	N/A	62	24/28 (86%)	4/28 (14%)	1/28 (4%)
pT2 (HPV-, n=27)	W: 5/27 (19%), M: 15/27 (56%), P: 7/27 (26%)	43	16/27 (59%)	11/27 (41%)	6/27 (22%)
pT2 (HPV+, n=9)	N/A	73	4/9 (44%)	5/9 (56%)	1/9 (11%)
pT2 (All, n=36)	N/A	51	20/36 (56%)	16/36 (44%)	7/36 (19%)
pT3/4 (HPV-, n=25)	W: 3/25 (12%), M: 16/25 (64%), P: 6/25 (24%)	30	10/25 (40%)	15/25 (60%)	6/25 (24%)
pT3/4 (HPV+, n=13)	N/A	67	8/13 (62%)	5/13 (38%)	3/13 (23%)
pT3/4 (All, n=38)	N/A	43	18/38 (47%)	20/38 (53%)	9/38 (24%)

\*Differentiation assessed for non-HPV tumors only (M: moderately differentiated; P: poorly differentiated; W: well differentiated). DOD: Dead of disease; HPV: Human papilloma virus; IHC: immunohistochemistry; ISH: *in situ* hybridization; N/A: Not applicable; PeIN: penile intraepithelial neoplasia.

**Conclusions:** Our results suggest that reproducible morphologic features can accurately predict HPV status with a sensitivity of approximately 97%. Multifocal disease was identified in a small subset of patients and correlated with aggressive disease.

# ABSTRACTS | GENITOURINARY PATHOLOGY (INCLUDING RENAL TUMORS)

Approximately a third of all cases were HPV-positive, and HPV status was not a prognostic indicator in patients with >=pT2 disease.

## 820 Clinical Significance of Focal or Nonfocal Extraprostatic Extension, Microscopic Bladder Neck Invasion, and Unilateral or Bilateral Seminal Vesicle Invasion in Men with Prostate Cancer Undergoing Radical Prostatectomy: A Proposal for a New pT3 Subclassification

Yuki Teramoto<sup>1</sup>, Numbereye Numbere<sup>2</sup>, Ying Wang<sup>2</sup>, Hiroshi Miyamoto<sup>2</sup>

<sup>1</sup>Kyoto University Hospital, Kyoto, Japan, <sup>2</sup>University of Rochester Medical Center, Rochester, NY

**Disclosures:** Yuki Teramoto: None; Numbereye Numbere: None; Ying Wang: None; Hiroshi Miyamoto: None

**Background:** The presence of extraprostatic extension (EPE), including bladder neck and seminal vesicle invasion, does not uniformly indicate poor clinical outcomes in men with prostate cancer. Accordingly, further risk stratification of the current pT3 disease is required. Indeed, we have recently demonstrated the prognostic significance of either nonfocal/established EPE (E-EPE) or microscopic bladder neck invasion (mBNI) vs. both, the absence vs. presence of the current pT3a lesions in the current pT3b disease, and unilateral (Uni) vs. bilateral (Bil) seminal vesicle invasion (SVI), as well as comparable prognosis between focal EPE (F-EPE) only vs. mBNI only. The present study aims to further determine the clinical impact of these pT3 lesions (*i.e.* F-EPE, E-EPE, mBNI, Uni-SVI, Bil-SVI) and their combinations in radical prostatectomy (RP) cases.

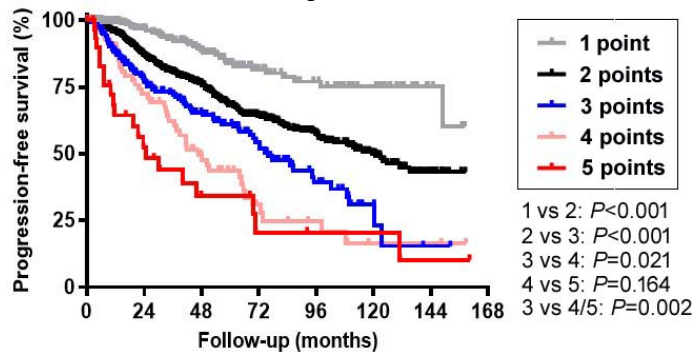
**Design:** We assessed consecutive 1,223 patients who had undergone RP without neoadjuvant therapy at our institution from 2009 to 2018. Based on our previous findings, the following points were given (1 point to F-EPE, mBNI, or Uni-SVI; 2 points to E-EPE or Bil-SVI) and summed up in each case.

**Results:** The cases had 1 point (n=258, 21.1%; P1), 2 points (n=666, 54.5%; P2), 3 points (n=189, 15.5%; P3), 4 points (n=78, 6.4%; P4), and 5 points (n=32, 2.6%; P5). Kaplan-Meier analysis revealed that the prognosis was worse in the following order: P1, P2, P3, P4, and P5, and that the differences in progression-free survival (PFS) between any two groups, except P4 vs. P5, were statistically significant. When P4 and P5 were combined, significant differences in PFS were also seen in subgroups of patients, such as those with pN0 disease and those without adjuvant therapy immediately after RP. When RP findings (*e.g.* tumor grade, lymph node metastasis, surgical margin, estimated tumor volume) were compared, significant differences were observed in all except surgical margin status in P1 vs. P2 patients. In multivariate analysis with Cox regression model (P1 as a reference), P2 (HR=1.939,  $P<0.001$ ), P3 (HR=2.569,  $P<0.001$ ), and P4/P5 (HR=3.615,  $P<0.001$ ) showed significance for progression.

	1 point	2 points	3 points	4 or 5 points	<i>P</i> (1 vs 2)	<i>P</i> (2 vs 3)	<i>P</i> (3 vs 4/5)
<b>N</b>	258	666	189	110			
<b>Age (mean, year)</b>	63.6	63.9	63.3	64.1	0.565	0.548	0.481
<b>PSA (mean, ng/mL)</b>	7.11	8.42	16.08	15.11	<0.001	<0.001	0.729
<b>Grade Group</b>					<0.001	<0.001	<0.001
1	5 (2%)	0 (0%)	0 (0%)	0 (0%)			
2	167 (65%)	296 (44%)	50 (26%)	8 (7%)			
3	66 (26%)	228 (34%)	83 (44%)	41 (37%)			
4	10 (4%)	43 (6%)	10 (5%)	10 (9%)			
5	10 (4%)	99 (15%)	46 (24%)	51 (46%)			
<b>pN</b>					0.047 <sup>a</sup>	<0.001 <sup>a</sup>	<0.001 <sup>a</sup>
0	216 (84%)	542 (81%)	144 (76%)	56 (51%)			
1	17 (7%)	74 (11%)	40 (21%)	53 (48%)			
X	25 (10%)	50 (8%)	5 (3%)	1 (1%)			
<b>Surgical margin</b>					0.371	<0.001	0.001
Negative	208 (81%)	519 (78%)	112 (59%)	44 (40%)			
Positive	50 (19%)	147 (22%)	77 (41%)	66 (60%)			
<b>Tumor volume (mean, cc)</b>	10.1	13.1	20.1	34.3	<0.001	<0.001	<0.001
<b>Adjuvant therapy<sup>b</sup></b>					0.018	<0.001	0.013
Not performed	231 (90%)	555 (83%)	119 (63%)	53 (48%)			
Performed	27 (10%)	111 (17%)	70 (37%)	57 (52%)			

<sup>a</sup> pN0 vs. pN1; <sup>b</sup> Adjuvant therapy before recurrence

Figure 1 - 820



**Conclusions:** We believe these data provide a logical rationale for a novel subclassification, pT3a (1 point), pT3b (2 points), pT3c (3 points), and pT3d (4 or 5 points), which more accurately stratifies the prognosis of pT3 prostate cancer. Further studies, ideally prospectively designed, are warranted to validate our results.

## 821 Morphologic Features of Prostate Cancer with TMPRSS2-ERG Gene Fusion Detected by Immunohistochemistry

Wei Tian<sup>1</sup>, Ji Yoon Yoon<sup>1</sup>, Karen Shore<sup>2</sup>, Anuradha Singhal<sup>1</sup>, Franto Francis<sup>1</sup>

<sup>1</sup>Inform Diagnostics, Irving, TX, <sup>2</sup>UT Southwestern Medical Center, Dallas, TX

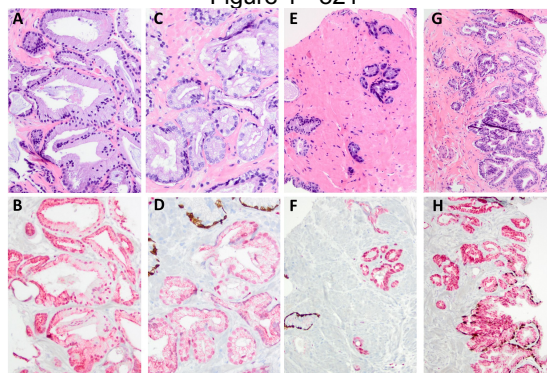
**Disclosures:** Wei Tian: None; Ji Yoon Yoon: None; Karen Shore: None; Anuradha Singhal: None; Franto Francis: None

**Background:** TMPRSS2-ERG gene fusion is the most common genetic rearrangement in prostatic adenocarcinomas (PCa), with a reported rate of about 50%. ERG nuclear expression detected by immunohistochemistry (IHC) is considered a surrogate for TMPRSS2-ERG fusion. The multiplex antibody panel PIN4ERG (p63/CK903, AMACR, and ERG) is a useful cocktail for PCa diagnosis and is routinely used in our high-volume urologic pathology practice. This study aimed to identify if certain morphologic features of PCa were associated with ERG protein expression.

**Design:** We assessed prostate biopsy cases with cancer diagnoses and available PIN4ERG IHC signed out by three urologic pathologists from April 2021 to August 2022. The IHCs were performed based on diagnostic necessity. Cancer morphology, Gleason Score/Grade Group, association with intraductal carcinoma (IDC-P), patient age, and PSA were collected. Histology was reviewed in consensus conferences. We defined five morphologic categories in this study: 1. Conventional/NOS morphology; 2. Marked amphophilic cytoplasm and hyperchromatic chromatin; 3. Abundant foamy or flocculent cytoplasm with basally located nuclei; 4. PIN-associated; 5 Atrophic features.

**Results:** The study included 237 ERG-positive (41 heterogeneous expression) and 247 ERG-negative cases. PCa with ERG protein expression were diagnosed at a younger age than the ERG-negative group: mean 65.7 (range 34-83) vs 67.2 (range 47-90) ( $P=0.039$ ). PSA and Grade group distribution showed no significant differences between the two groups ( $p=0.128$  and 0.058, respectively). Three morphologic features were associated with ERG protein expression: abundant foamy (Fig A-B, H&E, PIN4ERG IHC)/flocculent cytoplasm (Fig C-D) (49 cases, 20.6%), marked amphophilic cytoplasm (33, 13.9%) (Fig E-F), and PIN- associated (38, 16%) (Fig G-H), all with  $p < 0.001$ . 10% of PCas with ERG protein expression were associated with IDC-P, significantly higher than in the ERG-negative group (2%,  $p=0.0001$ ).

Figure 1 - 821



# ABSTRACTS | GENITOURINARY PATHOLOGY (INCLUDING RENAL TUMORS)

**Conclusions:** Our study is the largest cohort to date to identify morphologic features in PCa associated with ERG protein expression. We found that certain morphologic features have a higher propensity to show nuclear ERG expression, including abundant foamy/flocculent cytoplasm, marked amphophilic cytoplasm, and PIN-associated cancer. ERG-positive PCa were also more frequently associated with IDC-P. Our study may provide valuable information for pathologists when making diagnoses and considering additional ERG FISH or IHC testing.

## 822 Neuroendocrine Carcinoma of the Urinary Bladder (UB-NEC): Clinico-Pathological Boundaries of a Rare Entity and Immunohistochemical markers for Diagnosis and Prognosis

Silvia Uccella<sup>1</sup>, Giacomo Pini<sup>2</sup>, Roberta Maragliano<sup>5</sup>, Stefano La Rosa<sup>2</sup>, Carlo Patriarca<sup>3</sup>, Maurizio Colecchia<sup>4</sup>

<sup>1</sup>Humanitas Cancer Center, Rozzano, Italy, <sup>2</sup>University of Insubria, Varese, Italy, <sup>3</sup>Como, Italy, <sup>4</sup>University Vita-Salute San Raffaele, Milan, Italy, <sup>5</sup>Varese, Italy

**Disclosures:** Silvia Uccella: None; Giacomo Pini: None; Roberta Maragliano: None; Stefano La Rosa: None; Carlo Patriarca: None; Maurizio Colecchia: None

**Background:** Neuroendocrine carcinoma of the urinary bladder is a rare and aggressive cancer. The correct diagnosis of this entity and its separation from poorly differentiated urothelial carcinoma are a challenge for practicing pathologist and have important implication in patients' management and prognosis. The latest WHO classifications of urinary tract tumors, and of endocrine and neuroendocrine tumors provide updated diagnostic criteria that must be validated on clinical series.

**Design:** The files of four different Italian Institution were searched for "neuroendocrine neoplasms" or "neoplasms with neuroendocrine differentiation" of the urinary bladder diagnosed between 2010 and 2020. 78 cases with available histopathological material were reviewed by expert uropathologists and endocrine pathologist and only 52 carcinomas with convincing small cell or large cell neuroendocrine morphology and immunohistochemical expression of at least two general neuroendocrine markers (among chromogranin A, synaptophysin, and INSM1) were defined as UB-NEC and included in the study. Data on clinical presentation, therapy and follow-up were collected and an extensive immunohistochemical study was performed, including transcription factors (CDX2, TTF1, SATB2, GATA3, p63), cytokeratins (CK 7, 19, 20), key cancer genes protein products (p53, Rb, p16), and PDL1.

**Results:** Patients with UB-NEC were mostly elderly men and more than 50% had a smoking history. Large cell morphology was far less frequent than small cell (5 out of 52). 28 of 52 UB-NECs were mixed neuroendocrine/non-neuroendocrine neoplasms (MiNEN), with a morphologically evident non-neuroendocrine component. The sensitivity and specificity of INSM1 were overlapping with those of synaptophysin. The comparison between the two components of MiNENs highlighted that GATA3 and p63 were consistently absent in NEC, as well as CK20, whereas abnormal expression of p53, Rb, and p16 was mostly observed in NEC. SATB2 was frequently expressed in NEC. PDL1 expression was present in NECs, although to a lesser extent than in non-NEC. The survival analysis showed a worse outcome for patients with pure NEC, compared with MiNENs. Neoadjuvant chemotherapy resulted in prolonged survival.

**Conclusions:** Our study demonstrates that the employment of strict morphological and immunohistochemical diagnostic criteria identifies UB-NEC as a defined entities, with distinct prognosis and provides clues for differential diagnosis of difficult cases as well as for predicting response to therapy.

## 823 Clinical, Pathological, and Immunohistochemical Features of Biphasic Squamoid Alveolar Renal Cell Carcinoma: A Review of 219 Papillary Renal Cell Carcinomas

Andrea Val-Carreres Castellote<sup>1</sup>, Saúl De Burgos González<sup>1</sup>, Irune Ruiz Díaz<sup>1</sup>, Ander Ezkurra-Altuna<sup>1</sup>, María Carrillo Cobarro<sup>1</sup>, Manuel Manrique-Celada<sup>1</sup>, Luiz Nova-Camacho<sup>1</sup>

<sup>1</sup>Hospital Universitario Donostia - Osakidetza, Donostia, Spain

**Disclosures:** Andrea Val-Carreres Castellote: None; Saúl De Burgos González: None; Irune Ruiz Díaz: None; Ander Ezkurra-Altuna: None; María Carrillo Cobarro: None; Manuel Manrique-Celada: None; Luiz Nova-Camacho: None

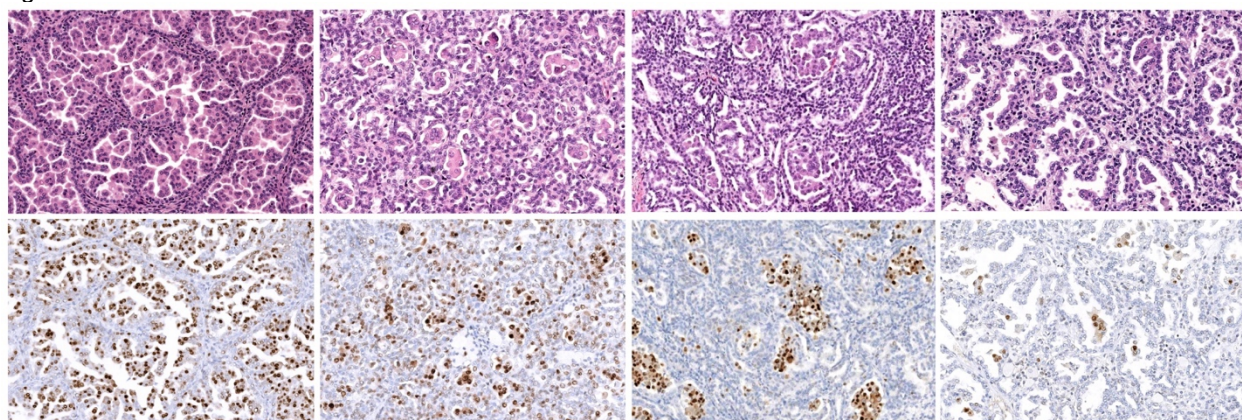
**Background:** In the 5<sup>th</sup> edition of the WHO classification of renal tumors, recently described tumor entities and/or subtypes have been added. One of these is the biphasic squamoid alveolar renal cell carcinoma (BSARCC). This tumor is characterized by the presence of two cell populations: large squamoid cells with different growth patterns, and small cells with a papillary/alveolar architecture. To date there have been around 65 cases of BSARCC reported.

**Design:** We carried out a retrospective study of 1771 renal tumors from the files of our hospital from 2000 to 2021. From 219 previously diagnosed papillary renal cell carcinomas (PRCC), we selected those that showed at least areas with a morphology consistent with BSARCC. The clinical and pathologic data were reviewed in detail, and the expression of PAX-8, CK7, CK20, EMA, CD10, AMACR, vimentin, e-cadherin, CAIX, Cyclin D1 and ki67 by immunohistochemistry (IHC) was evaluated in both small and large cells using paraffin-embedded tissue.

# ABSTRACTS | GENITOURINARY PATHOLOGY (INCLUDING RENAL TUMORS)

**Results:** We found nine cases consistent with BSARCC. The median patient age was 62 years. Three patients were females and six were males. Four patients had end-stage renal disease. No recurrence, metastasis, or tumor-related death occurred in a mean follow-up period of 76 months. None of the patients had a family history of RCC. Seven patients underwent a partial nephrectomy. Tumor size ranged from 1.5 to 6 cm. Three of the patients had multiple tumors. Grossly, most of the tumors were homogenous, soft, and well-demarcated; and five (5/9; 55%) cases had a fibrous capsule. All cases were pT1. The squamous area-extend varied between 10 to 95% of the tumor. Emperipoleisis was present in all cases. The large cells showed a higher ISUP/WHO histologic grade than the small cells. Four (4/9; 44%) cases showed psammomatous calcifications, and foamy histiocytes were present in all cases. None of the cases had either a sarcomatoid component or tumor necrosis. Both cell populations revealed diffuse expression of PAX-8, CK7, EMA, and AMACR by IHC. Cyclin D1 was positive only in the large cells (Fig. 1). Additionally, we found a papillary adenoma that showed the same morphology as this tumor.

Figure 1 - 823



**Conclusions:** BSARCC represented 4.1% (9/219 cases) of PRCC and 0.50% (9/1771) of all renal tumors during the 22-year period in our series. BSARCC shows two cell populations with different morphologies and immunophenotypes. All the patients in our study exhibited an indolent clinical course in a mean follow-up period of 76 months.

## 824 Artificial intelligence (AI) prediction on prostate biopsy images is an effective diagnostic time saving tool

Jennifer Vazzano<sup>1</sup>, Kun Hu<sup>2</sup>, Dorota Johansson<sup>3</sup>, Kristian Euren<sup>4</sup>, Ming Zhou<sup>5</sup>, Anil Parwani<sup>1</sup>

<sup>1</sup>The Ohio State University Wexner Medical Center, Columbus, OH, <sup>2</sup>Tufts Medical Center, Boston, MA, <sup>3</sup>Stockholm, Sweden, <sup>4</sup>Contextvision AB, Stockholm, Sweden, <sup>5</sup>Tufts University School of Medicine, Boston, MA

**Disclosures:** Jennifer Vazzano: None; Kun Hu: None; Dorota Johansson: None; Kristian Euren: None; Ming Zhou: None; Anil Parwani: None

**Background:** Artificial intelligence (AI) can be used to facilitate diagnosis and reporting of prostate cancer. In this study, the impact of AI on the diagnostic efficiency (time spent establishing diagnosis) was evaluated.

**Design:** 484 prostate biopsies (236 non-cancer; 248 cancer) were selected retrospectively from Boston and Ohio. Reference diagnosis was performed by senior pathologists. The resident pathologists performed diagnosis without AI in a cross over manner (Boston resident diagnosed WSIs from Ohio and vice versa). After 4 weeks, the AI was applied to predict suspicious cancer areas and the residents repeated diagnoses in a blinded manner. Time to establish diagnoses was recorded.

**Results:** Time for diagnosis was  $3.65 \pm 1.75$  minutes for Boston images and  $2.67 \pm 0.59$  minutes for Ohio images. The time decreased with AI predictions ( $2.50 \pm 1.75$  minutes for Boston images,  $1.65 \pm 0.63$  minutes for Ohio images,  $p < .00001$ ). The time decrease is  $\sim 1$  minute irrespective of slide type (benign or cancer). The largest time decrease (1.63 minutes/image) is seen for images where the resident was least confident initially; while the time decrease for images where the resident was confident was significantly lower (0.91 minute/image,  $p < .00001$ ). The time is decreased for majority of WSIs (Figures 1 and 2). The time decrease is achieved without drop in performance (sensitivity and specificity).

Figure 1 - 824

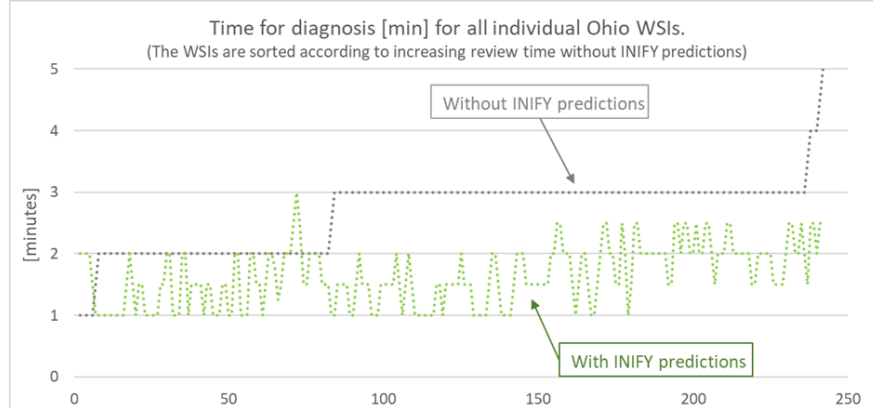
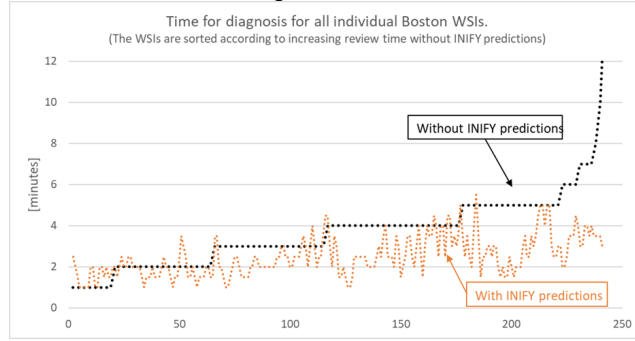


Figure 2 - 824



**Conclusions:** With AI predictions, resident pathologists diagnosed WSIs significantly faster than without AI, without loss of performance. The time saving is likely facilitated by AI predictions and learning to effectively use the system.

## 825 Results on Follow-Up Transurethral Resection of Bladder Tumor (TURBT) in cases Ambiguous for Muscularis Propria Invasion (AMPMUS), our Institutional Experience

Alyssa Vitale<sup>1</sup>, Oluwayomi Oyedele<sup>2</sup>, Khaleel Al-Obaidy<sup>2</sup>, Nilesh Gupta<sup>2</sup>, Oudai Hassan<sup>2</sup>

<sup>1</sup>Henry Ford Hospital, Detroit, MI, <sup>2</sup>Henry Ford Health System, Detroit, MI

**Disclosures:** Alyssa Vitale: None; Oluwayomi Oyedele: None; Khaleel Al-Obaidy: None; Nilesh Gupta: None; Oudai Hassan: None

**Background:** Evaluation of muscularis propria (MP) invasion in TURBT maybe challenging. In this study we report on the findings in follow up TURBT in cases that were diagnosed as ambiguous for muscularis propria invasion at our institution.

**Design:** All consecutive in-house TURBTs with the diagnosis of ambiguous for MP invasion from 2015 to 2022 were included. AMPMUS was defined as: either extensive carcinoma displaying small muscle bundles where it is hard to decide if those muscle bundles represent muscularis mucosae or MP (pattern 1) or invasive carcinoma sitting adjacent to thick muscle bundles (pattern 2). No case with small cell carcinoma or prior therapy were included. All cases were double reviewed by specialized urologic pathologists.

**Results:** Thirty cases were included. 19 (63%) cases with pattern 1 AMPMUS and 11 (37%) cases with pattern 2 AMPMUS. Median patient age was 75 (53-92). The median number of follow up TURBT was 1 (1-6). The median period before the first follow up TURBT was 2 months (1-9). Of the 19 cases with pattern 1 AMPMUS 10 had follow TURBT, two went directly to cystectomy while seven patients had no follow up at our institution. Of the 10 cases with follow up TURBT 5 (50%) showed MP invasion, 1 (10%) showed Ta/T1 disease and 4 (40%) were negative on follow up. Of the two patients who went directly to cystectomy, one had muscle invasive disease on cystectomy and the other patient had no residual invasive carcinoma and only urothelial carcinoma in situ. Of the 11 patients with pattern 2 AMPMUS, 10 had follow TURBT and one went directly to cystectomy. Of the 10 patients with follow up TURBT, 4 (40%) had muscle invasive disease, 5 (50%) had Ta/T1 disease and 1 (10%) was still AMPMUS. The patient who went directly to cystectomy showed invasion into perivesical adipose tissue. No significant difference is seen between pattern 1 and pattern 2 AMPMUS.

**Conclusions:** Although most patients with the diagnosis of non-muscle invasive high-grade urothelial carcinoma undergo a follow up TURBT within 12 weeks. 7 (23%) of the 30 patients in our cohort did not get a follow up TURBT. Of the 23 AMPMUS patients

# ABSTRACTS | GENITOURINARY PATHOLOGY (INCLUDING RENAL TUMORS)

who had follow-up at our institution, 11 (48%) had T2 disease or higher on first follow up. Our findings support that these patients with the diagnosis of urothelial carcinoma ambiguous for muscularis propria invasion are at high risk of having advanced pathologic stage and emphasize the importance of immediate follow up TURBT to appropriately stage these patients.

## 826 Determination of Exosomal Cargo Profile (microRNA) in Urine can be used as Biomarker in the Diagnosis or Recurrences of Renal Cell Carcinoma.

Beatriz Walter Rodriguez<sup>1</sup>, Cathy Vocke<sup>1</sup>, Juan Pineda-Reyes<sup>1</sup>, W Linehan<sup>2</sup>, Maria Merino<sup>3</sup>

<sup>1</sup>National Cancer Institute, National Institutes of Health, Bethesda, MD, <sup>2</sup>National Institutes of Health, Bethesda, MD, <sup>3</sup>National Cancer Institute, Bethesda, MD

**Disclosures:** Beatriz Walter Rodriguez: None; Cathy Vocke: None; Juan Pineda-Reyes: None; W Linehan: None; Maria Merino: None

**Background:** Renal cell carcinoma (RCC) comprises 3% of all malignant tumors. More than 61,000 new cases and 15,000 deaths are due to RCC in the US. It is frequently diagnosed in advance stage, thus the need for markers for early detection. MicroRNAs (miRNAs) are small non-coding RNAs responsible for gene regulation at a post-transcriptional level. Exosomes present in biofluids, including urine, act as a transporting system for miRNAs. Recently, studies of urine have gained interest as a liquid biopsy because its easy sampling. Therefore, miRNA profile in the urinary exosomes of patients with RCC could serve as non-invasive biomarkers for initial detection and follow up.

**Design:** A total of 31 cell-free urines (CFU) from patients with Von-Hippel-Lindau associated clear cell RCC (VHL-ccRCC) and the available FFPE tumor samples were collected previous patient's consent from the Urologic Oncology Branch Clinic, at the NIH. Samples from healthy human donors were also included for comparison. After centrifugation, CFU were prepared for Exosome RNA Purification. The presence of exosomes was confirmed by Exo-Check Exosome Antibody Array (SBI) and Western Blots (abcam, exosome panel). RNA's were then analysed by Next-Generation Sequencing. Clinico-pathological information was also evaluated.

**Results:** Between 112 and 336 unique known miRNAs per sample were identified. Unsupervised hierarchical clustering based on miRNA expression showed two major clusters. The first group of cases showed highly expressed miRNAs contrasting with the second cluster that grouped mostly with the non-tumor samples and had downregulated miRNAs. Most upregulated miRNAs were miR200b-5p, 320b, 107 and 152-5p and the downregulated ones were miR291-5p, 342-5p, 378a-5p and 24-2-5p (fold change 2.3 and -2.3). When we compared our results with miRNAs already known to be dysregulated in VHL-ccRCC (miR30c, 182-5p, 92a, 210, 17-5p, 224, 28-5p 204 and 155); all of them with miR21 were also altered in a similar fashion.

**Conclusions:** Our results show that most of the differentially expressed miRNAs have downstream target genes with important roles in the pathogenesis of RCC that are involved in pathways related to Hypoxia and Epithelial-Mesenchymal Transition (EMT). These results also demonstrate the potential use of exosomal microRNAs as non-invasive biomarkers for diagnosis, detection of tumor recurrence or progression, and possibly the evaluation of treatment response.

## 827 Metabolomic Features of Human Prostate Cancers that are Visible or Invisible by Multiparametric Magnetic Resonance Imaging

Bangchen Wang<sup>1</sup>, Rohith Arcot<sup>2</sup>, Xue Jiang<sup>1</sup>, Jerry Fu<sup>3</sup>, Rajan Gupta<sup>1</sup>, Thomas Polascik<sup>1</sup>, Xia Gao<sup>4</sup>, Jiaoti Huang<sup>3</sup>

<sup>1</sup>Duke University Medical Center, Durham, NC, <sup>2</sup>Ochsner Health System, New Orleans, LA, <sup>3</sup>Duke University, Durham, NC, <sup>4</sup>Baylor College of Medicine, Houston, TX

**Disclosures:** Bangchen Wang: None; Rohith Arcot: None; Xue Jiang: None; Jerry Fu: None; Rajan Gupta: None; Thomas Polascik: None; Xia Gao: None; Jiaoti Huang: None

**Background:** Multiparametric magnetic resonance imaging (mpMRI) is currently the most sensitive and specific imaging technique for the detection of prostate cancer. However, approximately 20% of clinically significant prostate cancers are invisible by mpMRI. We hypothesize that the metabolomic profiles of prostate cancers determine their visibility on mpMRI.

**Design:** By comparing mpMRI images with whole mount pathology analysis of prostatectomy specimens, we identified 12 patients each with both MRI-visible and MRI-invisible tumors in the prostate. Tissue cores were obtained from formalin-fixed paraffin-embedded (FFPE) prostatectomy tissue from areas of benign prostate glands, MRI-visible tumors, and MRI-invisible tumors. Polar metabolites were extracted and analyzed by ultra-high performance liquid chromatography–mass spectrometry (UHPLC-MS).

**Results:** Characteristics of MRI-visible versus MRI-invisible tumors are included in Table 1. Compared to MRI-visible tumors, the MRI-invisible tumors are generally smaller in size and lower in Gleason grade. MRI-visible and MRI-invisible tumors show significant differences in the levels of 42 out of 300 metabolites. Enrichment analysis identified potential metabolic pathways that

# ABSTRACTS | GENITOURINARY PATHOLOGY (INCLUDING RENAL TUMORS)

differ between MRI-visible and MRI-invisible tumors (Figure 1). Specifically, the polyamine levels are significantly lower in MRI-visible tumors but comparable between benign prostate and MRI-invisible tumors (Figure 2).

**Table 1.** Characteristics of MRI-visible and MRI-invisible tumors; p value is calculated for tumor size by student's t test; p values for Gleason grade and T stage are calculated by Fisher's exact test. GG, Gleason grade.

	Visible Tumor	Invisible Tumor	p value
Tumor size (cm) (mean ± SEM)	2.4 ± 0.2	1.6 ± 0.2	0.012
Gleason grade (N)	GG2	6	0.059
	GG3	5	
	GG4	0	
	GG5	1	
T stage (N)	T2	8	0.640
	T3a	4	

Figure 1 - 827

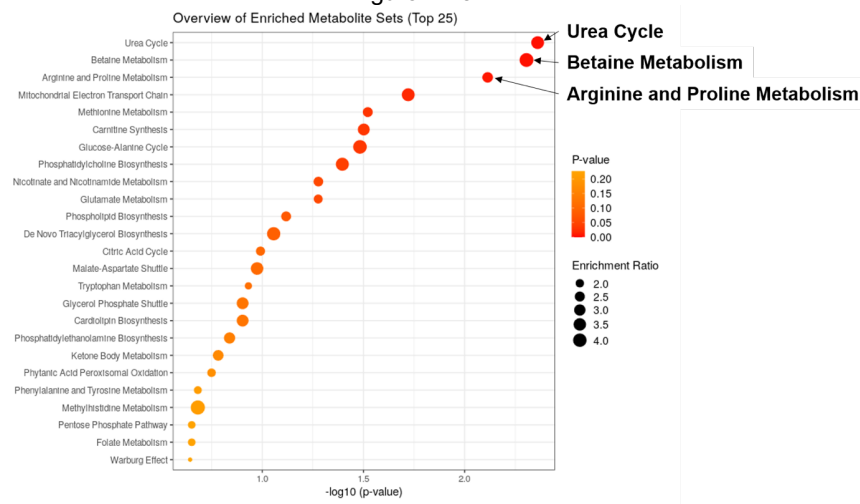


Figure 1. Enrichment analysis of MRI-visible and MRI-invisible tumors.

Figure 2 - 827  
Polyamine Levels

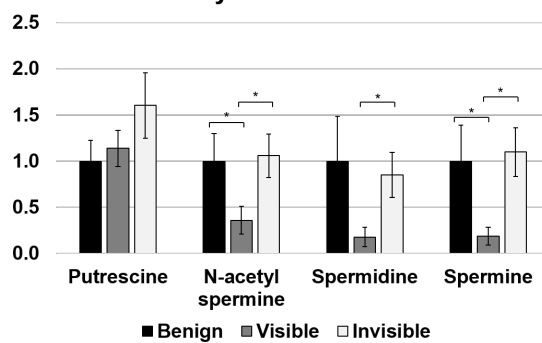


Figure 2. Polyamine levels of benign prostate glands, MRI-visible tumors, and MRI-invisible tumors.  $p < 0.05$  by student's t test. Y-axis: relative MS intensity.

**Conclusions:** Our results demonstrate the distinct metabolomic profiles of MRI-visible and MRI-invisible prostate cancers. MRI-invisible tumors are not detected by mpMRI possibly because of their metabolomic similarity to benign prostate glands, while certain metabolic features (e.g., lower polyamine levels) may be the molecular basis of tumor detection by mpMRI. We conclude that further metabolomic studies of prostate cancer tissue could provide novel insights to improve the sensitivity and specificity of radiologic detection of prostate cancer.

## 828 Biomarker Characterization of Hybrid Oncocytic Tumor in Birt-Hogg-Dubé Syndrome

Xiaoming (Mindy) Wang<sup>1</sup>, Rahul Mannan<sup>2</sup>, Yuping Zhang<sup>3</sup>, Anya Chinnaiyan<sup>1</sup>, Roshni Rangaswamy<sup>4</sup>, Seema Chugh<sup>1</sup>, Fengyun Su<sup>1</sup>, Xuhong Cao<sup>1</sup>, Rui Wang<sup>1</sup>, Stephanie Skala<sup>1</sup>, Maria Picken<sup>5</sup>, Khaled Hafez<sup>1</sup>, Ulka Vaishampayan<sup>1</sup>, Jesse McKenney<sup>6</sup>, Maria Tretiakova<sup>7</sup>, Reza Alaghehbandan<sup>6</sup>, Pedram Argani<sup>8</sup>, Arul Chinnaiyan<sup>1</sup>, Saravana Dhanasekaran<sup>1</sup>, Rohit Mehra<sup>1</sup>

<sup>1</sup>University of Michigan, Ann Arbor, MI, <sup>2</sup>Michigan Medicine, University of Michigan, Ann Arbor, MI, <sup>3</sup>Michigan Center for Translational Pathology, Ann Arbor, MI, <sup>4</sup>Michigan Center for Translational Pathology, Ypsilanti, MI, <sup>5</sup>Loyola University Medical Center, Maywood, IL, <sup>6</sup>Cleveland Clinic, Cleveland, OH, <sup>7</sup>University of Washington, Seattle, WA, <sup>8</sup>Johns Hopkins Hospital, Baltimore, MD

**Disclosures:** Xiaoming (Mindy) Wang: None; Rahul Mannan: None; Yuping Zhang: None; Anya Chinnaiyan: None; Roshni Rangaswamy: None; Seema Chugh: None; Fengyun Su: None; Xuhong Cao: None; Rui Wang: None; Stephanie Skala: None; Maria Picken: None; Khaled Hafez: None; Ulka Vaishampayan: None; Jesse McKenney: None; Maria Tretiakova: None; Reza Alaghehbandan: None; Pedram Argani: None; Arul Chinnaiyan: None; Saravana Dhanasekaran: None; Rohit Mehra: None

**Background:** Birt-Hogg-Dubé (BHD) syndrome is an inherited genetic disorder associated with an increased risk of kidney lesions, including cysts and renal tumors called hybrid oncocytic tumor (HOT).<sup>1</sup> HOT are usually low-grade tumors, displaying a mixture of neoplastic cells with histologic features of chromophobe renal cell carcinoma (chRCC) and renal oncocytoma (RO). The development of HOT specific biomarker would improve the diagnostic accuracy, facilitate disease management, and assist familial genetic monitoring.

**Design:** We analyzed RNA sequencing (RNAseq) data from HOT and matched benign kidney tissue to identify lineage markers expressed in HOT. In parallel, we utilized single cell RNAseq data from benign kidney tubular epithelial cell types to train a random forest model to nominate putative cell of origin for HOT, chRCC, and RO.<sup>2</sup> We simultaneously characterized the expression pattern of candidate biomarkers using immunohistochemistry (IHC) and RNA in situ hybridization (RNA-ISH) in 16 HOT tumors obtained from 10 genetically confirmed BHD patients and further validated the top candidate biomarker specificity in various common and uncommon renal tumors.

**Results:** We identified candidate biomarkers highly expressed in HOT, including *L1CAM*, *FOXI1*, and long non-coding RNA *LINC01187*. *L1CAM* is known to be expressed in the principal cells of distal nephron, while *FOXI1* and *LINC01187* are expressed in the intercalated cells of benign kidney.<sup>3</sup> *L1CAM*, *FOXI1*, and *LINC01187* are expressed in a unique “checkered” pattern in HOT, where *L1CAM* (a principal cell marker) staining pattern showed mutual exclusivity with *FOXI1/LINC01187* (intercalated cell markers), among the two morphologically distinct cellular populations of HOT (Figure 1). Overall, 15/16 (93.8%) HOT tumors showed checkered *L1CAM* expression pattern and 1/16 (6.2%) HOT tumor cases showed focal/low expression of *L1CAM*. *L1CAM* expression was negative in 16/20 (80%) chRCC and patchy or focal in the other 4 chRCC cases. *L1CAM* expression was also negative in 5/5 RO cases.

Figure 1 - 828

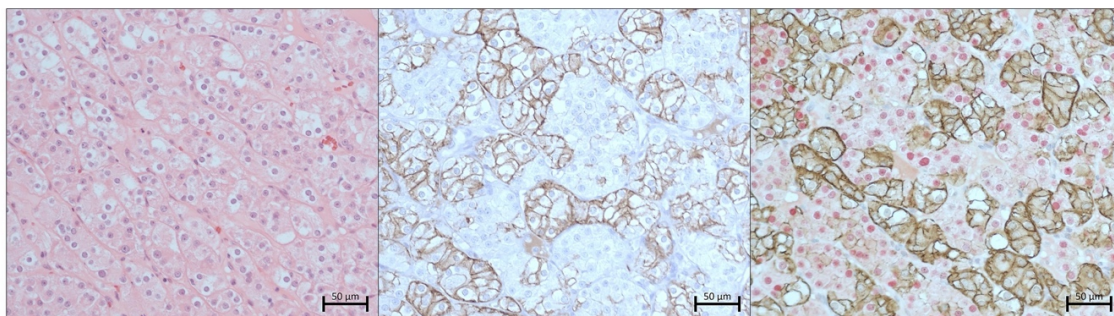


Figure 1. “Checkered” pattern of L1CAM expression and mutual exclusive expression of L1CAM and FOXI1 in HOT. **(A)** Hematoxylin and Eosin stain. **(B)** L1CAM immunohistochemistry. **(C)** L1CAM (brown) and FOXI1 (red) dual immunohistochemistry.

**Conclusions:** L1CAM protein is expressed in a unique “checkered” pattern in BHD associated HOT tumors. L1CAM expression shows mutual exclusivity to FOXI1/*LINC01187* expression, which collectively captures the two unique tumor epithelial populations that co-exist in BHD associated HOT tumors, and helps distinguish HOT from chRCC and RO. These markers will inform future studies on the evolution and interaction between the two transcriptionally distinct tumor epithelial populations in HOT.

# ABSTRACTS | GENITOURINARY PATHOLOGY (INCLUDING RENAL TUMORS)

## 829 MiTF Family Altered Renal Cell Carcinoma: An 8-year Review of 781 Clinical TFE3/TFEB FISH Assays Performed at a Tertiary Institution (2014-2022)

Xiaoming (Mindy) Wang<sup>1</sup>, Hong Xiao<sup>1</sup>, Lina Shao<sup>1</sup>, Liron Pantanowitz<sup>1</sup>, Rahul Mannan<sup>2</sup>, Stephanie Skala<sup>1</sup>, Jeffrey Myers<sup>3</sup>, Arul Chinnaiyan<sup>1</sup>, Bryan Betz<sup>1</sup>, Noah Brown<sup>1</sup>, Rohit Mehra<sup>1</sup>

<sup>1</sup>University of Michigan, Ann Arbor, MI, <sup>2</sup>Michigan Medicine, University of Michigan, Ann Arbor, MI, <sup>3</sup>Michigan Medicine, Ann Arbor, MI

**Disclosures:** Xiaoming (Mindy) Wang: None; Hong Xiao: None; Lina Shao: None; Liron Pantanowitz: None; Rahul Mannan: None; Stephanie Skala: None; Jeffrey Myers: None; Arul Chinnaiyan: None; Bryan Betz: None; Noah Brown: None; Rohit Mehra: None

**Background:** MiTF family altered renal cell carcinoma (MiTF-RCC) demonstrates a wide morphologic spectrum and can histologically resemble common RCC subtypes, posing a diagnostic challenge. MiTF-RCC are known to harbor recurrent chromosomal rearrangements involving the MiTF family of transcription factors, *TFE3* and *TFEB*. Clinical fluorescence *in situ* hybridization (FISH) assays for detection of *TFE3* and *TFEB* gene aberrations have been performed at our institution since 2014.

**Design:** Interphase FISH was performed using commercial dual-color break-apart probes specific to the *TFE3* locus at Xp11.2 (*TFE3* FISH) and *TFEB* locus at 6p21 (*TFEB* FISH) employing previously established methodologies (PMID: 28840857). We reviewed clinical *TFE3*/*TFEB* FISH assays performed during 2014-2022 and summarized test results.

**Results:** *TFE3* FISH was performed on 424 tumor cases suspicious for *TFE3* rearrangement associated renal cell carcinoma. 62 of these 424 cases (15%) tested positive for *TFE3* translocation. Age for positive cases ranged from 14 to 86 years (average 47 years), including 40 females, 21 males, and 1 patient without gender information. One of the positive cases also showed high copy number gain of the *TFE3* locus in > 50% cells. *TFEB* FISH was performed on 357 tumor cases. 28 of these cases (8%) tested positive for *TFEB* rearrangement (including translocation and amplification). Patients with any *TFEB* rearrangement ranged in age from 19 to 77 years (average 59 years), including 15 females and 13 males. *TFEB* amplification interpretation has been included in our *TFEB* FISH test reports since 2017. Since then, 18 cases were diagnosed with *TFEB* amplification, while 5 cases were consistent with *TFEB* translocation. Patients with *TFEB* translocation ranged in age from 19 to 62 years (average 41 years), including 3 females and 6 males. Patients with *TFEB* amplification ranged in age from 55 to 77 years (average 67 years), including 9 females and 9 males. Between 2014-2017, 1 patient (68-year female) had a complex gene fusion, amplification, or partial tandem duplication of *TFEB*, and 5 cases had copy number gain in a subset of tumor cells. *TFE3* and *TFEB* rearrangements were never detected in the same patient.

Table 1. Summary of in house *TFE3*/*TFEB* FISH test results in 2014-2022.

Type of <i>TFE3</i> / <i>TFEB</i> rearrangement	Average age (range) /years	Gender		No. of positive cases		
		No. male patients	No. female patients	2014-2022	2014-2016	2017-2022
<i>TFE3</i> translocation	47 (14-86)	21	40	62 (15%)	20	42
<i>TFEB</i> translocation	41 (19-62)	6	3	9 (3%)	4	5
<i>TFEB</i> amplification	67 (55-77)	9	9	18 (5%)	0	18
Atypical <i>TFEB</i> FISH	68	0	1	1 (0.3%)	1	NA
Cases with subset of tumor cells with low or mid copy number gain at <i>TFEB</i> locus	58 (32-69)	3	2	5 (1.4%)	0	5

**Conclusions:** Clinical *TFE3*/*TFEB* FISH assays successfully identified those rare MiTF-RCC with *TFE3* and *TFEB* rearrangements. *TFE3* and *TFEB* translocations tend to occur in relatively younger patients. *TFEB* amplifications occur more frequently than *TFEB* translocations in renal tumors and manifest largely in older patients.

## 830 Cribiform Morphology in Conventional Prostatic Adenocarcinoma Vs. Intraductal Carcinoma of the Prostate: Their Clinical Significance May Not Be Comparable

Ying Wang<sup>1</sup>, Yuki Teramoto<sup>2</sup>, Hiroshi Miyamoto<sup>1</sup>

<sup>1</sup>University of Rochester Medical Center, Rochester, NY, <sup>2</sup>Kyoto University Hospital, Kyoto, Japan

**Disclosures:** Ying Wang: None; Yuki Teramoto: None; Hiroshi Miyamoto: None

**Background:** Intraductal carcinoma of the prostate (IDC) in most of which cribriform morphology (CM) is present is a distinct entity of aggressive prostate cancer. Meanwhile, assigning a Gleason grade to IDC associated with conventional prostatic adenocarcinoma (CPA) remains controversial. In particular, the clinical impact of CM seen in CPA vs. IDC needs to be further

# ABSTRACTS | GENITOURINARY PATHOLOGY (INCLUDING RENAL TUMORS)

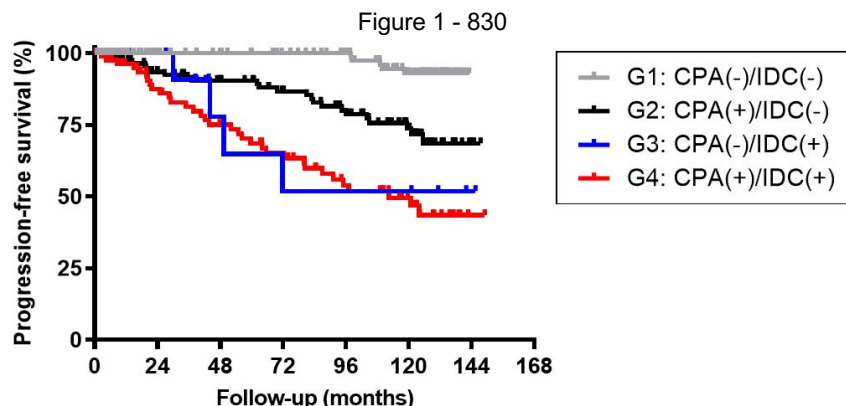
investigated. We herein compared radical prostatectomy (RP) findings and long-term oncologic outcomes in patients with CPA and/or IDC exhibiting CM.

**Design:** We studied consecutive patients who had undergone RP at our institution from 2010-2011. Within our Surgical Pathology database, we identified a total of 426 cases with Grade Group (GG) 2-4 CPA with or without IDC after excluding cases showing any Gleason grade 5 pattern (including minor tertiary 5 and comedonecrosis within IDC) or undergoing neoadjuvant therapy prior to RP, as well as those where the histology slides had been unavailable for review.

**Results:** We divided our patient cohort into 4 groups: G1) no CM [CPA(-)/IDC(-): n=174, 41%]; G2) CM only in CPA [CPA(+)/IDC(-): n=142, 33%]; G3) CM only in IDC [CPA(-)/IDC(+): n=16, 4%]; and G4) CM in both CPA and IDC [CPA(+)/IDC(+): n=94, 22%]. Compared with G2 patients, G4 was associated with significantly worse clinicopathological features, including higher GG, higher pT/pN category, larger estimated tumor volume, and the need for adjuvant therapy immediately after RP. Similarly, G4 patients showed significantly higher GG and larger tumor volume than G3 patients. There were no significant differences in these features between G2 and G3 patients. Kaplan-Meier analysis coupled with log-rank test revealed significantly higher risks of disease progression after RP in G2 than in G1 ( $P<0.001$ ) as well as in G4 than in G2 ( $P<0.001$ ), while there were no significant differences in progression-free survival between G2 vs. G3 ( $P=0.267$ ) and G3 vs. G4 ( $P=0.611$ ). In multivariate analysis with Cox regression model (G1 as a reference), G2 (hazard ratio 4.264,  $P=0.004$ ), G3 (hazard ratio 4.957,  $P=0.003$ ), and G4 (hazard ratio 12.35,  $P<0.001$ ) showed significance for progression.

	G1: CPA(-) /IDC(-) (n=174)	G2: CPA(+)/IDC(-) (n=142)	G3: CPA(-) /IDC(+) (n=16)	G4: CPA(+)/IDC(+) (n=94)	P (G2 vs G3)	P (G2 vs G4)	P (G3 vs G4)
<b>PSA (mean, ng/mL)</b>	5.83	7.01	5.23	7.28	0.096	0.692	0.183
<b>Grade Group</b>					0.279	<0.001	0.002
2	161 (93%)	95 (67%)	14 (88%)	38 (40%)			
3	13 (7%)	38 (27%)	2 (13%)	41 (44%)			
4	0 (0%)	9 (6%)	0 (0%)	15 (16%)			
<b>pT stage</b>					0.632	<0.001	0.120
2/2+	134 (77%)	90 (63%)	9 (56%)	29 (31%)			
3a	39 (22%)	51 (36%)	7 (44%)	56 (60%)			
3b	1 (1%)	1 (1%)	0 (0%)	9 (10%)			
<b>pN stage</b>					0.211 <sup>a</sup>	0.006 <sup>a</sup>	1.000 <sup>a</sup>
0	136 (78%)	111 (78%)	13 (81%)	79 (84%)			
1	1 (1%)	1 (1%)	1 (6%)	8 (9%)			
X	37 (21%)	30 (21%)	2 (13%)	7 (7%)			
<b>Surgical margin</b>					0.695	0.688	1.000
Negative	163 (94%)	124 (87%)	15 (94%)	82 (87%)			
Positive	11 (6%)	18 (13%)	1 (6%)	12 (13%)			
<b>Tumor volume (mean, cc)</b>	4.7	5.9	4.8	8.6	0.375	<0.001	0.030
<b>Adjuvant therapy<sup>b</sup></b>					1.000	0.023	0.208
Not performed	171 (98%)	136 (96%)	16 (100%)	82 (87%)			
Performed	3 (2%)	6 (4%)	0 (0%)	12 (13%)			

<sup>a</sup> pN0 vs. pN1; <sup>b</sup> Adjuvant therapy before recurrence



**Conclusions:** Compared with CPA(+)/IDC(-), CPA(+)/IDC(+) was found to be associated with not only adverse histopathologic features in RP specimens but also poorer prognosis, while the prognosis of CPA(-)/IDC(+) vs. CPA(+)/IDC(+) was similar. These findings suggest that the clinical significance of CM in CPA vs. IDC is not comparable.

## 831 Cytologic Assessment of Supernatants of Formalin Solution Following Histological Assessment of Transurethral Resection Specimens: Potential Detection of Denuded Urothelial Cancer Cells

Ying Wang<sup>1</sup>, John Plavnick<sup>1</sup>, Donna Russell<sup>1</sup>, Jerome Jean-Gilles<sup>2</sup>, Hiroshi Miyamoto<sup>1</sup>

<sup>1</sup>University of Rochester Medical Center, Rochester, NY, <sup>2</sup>University of Rochester, Rochester, NY

**Disclosures:** Ying Wang: None; John Plavnick: None; Donna Russell: None; Jerome Jean-Gilles: None; Hiroshi Miyamoto: None

**Background:** Urothelial denudation is often seen in transurethral biopsy specimens even where no definitive cancer is identified. Importantly, it may reflect cases of carcinoma in situ or otherwise high-grade cancer in which the neoplastic cells have shed as a result of discohesion. The present study aims to determine if denuded cells remain in the supernatants of formalin solution after submission of transurethral resection specimens for histological assessment.

**Design:** Formalin supernatants were collected from the containers of transurethral resection/biopsy specimens after the entire tissue (mostly with filtration) was submitted for histological examination. The cell block (n=43) was prepared from the centrifuged supernatant, while the ThinPrep smear (n=37) was prepared by the T2000 ThinPrep processor (Hologic).

**Results:** In the cell blocks from cases showing urothelial carcinoma in situ (n=7), non-invasive high-grade papillary urothelial carcinoma (n=14), invasive high-grade papillary/non-papillary urothelial carcinoma (n=7), or denuded urothelial mucosa with no definitive cancer (n=15), urothelial cells were detected in only 2 (5%) specimens (1 case of pTa tumor and 1 case of invasive tumor). We then used the ThinPrep method (see Table). Overall, the smear was satisfactory for evaluation in 34 (92%) of 37 cases. In all 13 cases with pTis disease (including those suspicious for but not diagnostic of carcinoma in situ), high-grade urothelial carcinoma cells (see Figure 1), cells suspicious for high-grade urothelial carcinoma, and/or atypical urothelial cells were detected. Similarly, in 13 (87%) of 15 cases with pTa or pT1 disease, denuded urothelial cells were detected. More interestingly, atypical urothelial cells (n=2; see Figure 2) or benign-appearing urothelial cells (n=6) were present in the supernatants from cases showing urothelial denudation (without definitive cancer), and only 1 (11%) case was unsatisfactory.

	HGUC	SHGUC	AUC	NHGUC	Unsat
pTis <sup>a</sup>	6 (46%)	3 (23%)	4 (31%)	0 (0%)	0 (0%)
pTa or pT1 <sup>b</sup>	7 (47%)	3 (20%)	1 (7%)	2 (13%)	2 (13%)
Denuded <sup>c</sup>	0 (0%)	0 (0%)	2 (22%)	6 (67%)	1 (11%)

HGUC, High-grade urothelial carcinoma; SHGUC, Suspicious for high-grade urothelial carcinoma; AUC, Atypical urothelial cells; NHGUC, Negative for high-grade urothelial carcinoma; Unsat, Nondiagnostic/ unsatisfactory

<sup>a</sup> Includes cases suspicious for but not diagnostic of carcinoma in situ; <sup>b</sup> All high-grade; <sup>c</sup> No definitive cancer in the specimen

Figure 1 - 831

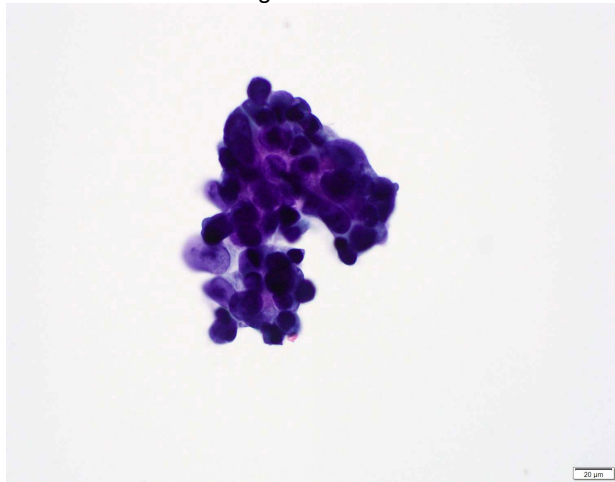
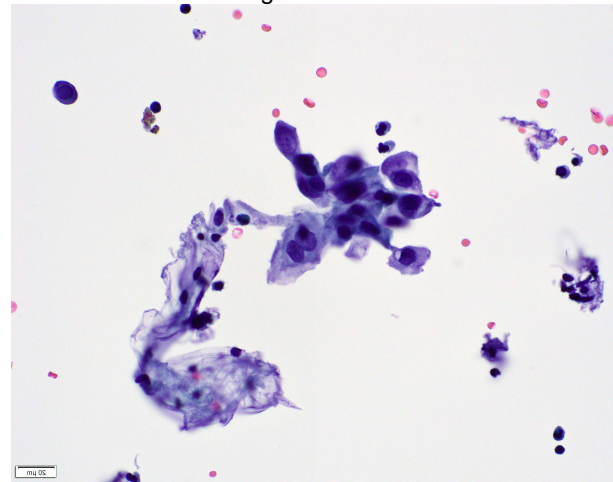


Figure 2 - 831



**Conclusions:** The present results suggest that cytologic examination of the ThinPrep smear from the supernatants of formalin solution following histological examination of transurethral resection specimens is useful for assessing denuded cells. In particular, this technique can be applied to non-neoplastic or indeterminate cases showing extensive urothelial denudation to detect possible malignant cells.

## 832 Examination of Non-Processed Bladder Tissue by Nonlinear Microscopy

Timothy Weber<sup>1</sup>, Yairen Guzman-Arocho<sup>2</sup>, Leo Wu<sup>3</sup>, Jason Zhang<sup>1</sup>, James Fujimoto<sup>1</sup>, Boris Gershman<sup>2</sup>, Seymour Rosen<sup>2</sup>, Yue Sun<sup>2</sup>

<sup>1</sup>Massachusetts Institute of Technology, Cambridge, MA, <sup>2</sup>Beth Israel Deaconess Medical Center, Boston, MA, <sup>3</sup>Beth Israel Deaconess Medical Center, Harvard Medical School, Boston, MA

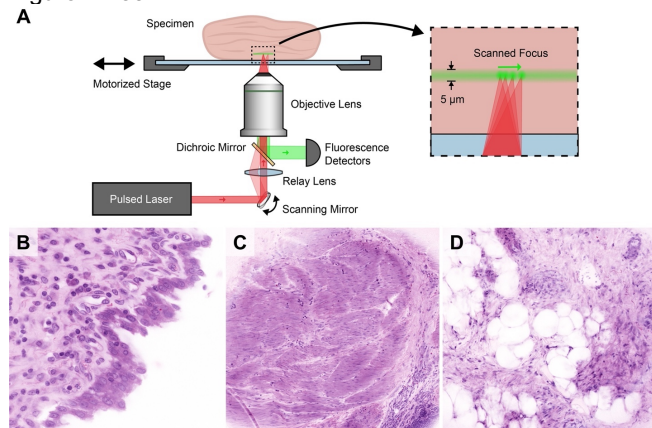
**Disclosures:** Timothy Weber: None; Yairen Guzman-Arocho: None; Leo Wu: None; Jason Zhang: None; James Fujimoto: None; Boris Gershman: None; Seymour Rosen: None; Yue Sun: None

**Background:** Nonlinear microscopy (NLM) is a laser scanning microscopy technique that generates real-time images and optical serial sections closely resembling formalin-fixed, paraffin-embedded H&E without the need for fixation, embedding, microtome sectioning, or slide preparation. Both fresh and fixed tissues can be imaged. NLM has been successfully utilized to evaluate bone, bone marrow, lymph nodes, skin, prostate, and breast tissue. Herein, we evaluated the ability of NLM to characterize benign bladder tissue and bladder tumors.

**Design:** Discarded (not required for clinical assessment) unsectioned bladder tissue was stained for 2 minutes with fluorescent dyes consisting of acridine orange (nuclear staining) and sulforhodamine 101 (stromal/cytoplasmic staining), followed by a 30-second rinse in saline. The tissue specimens were evaluated in real-time using NLM (Fig. 1A) and subsequently compared with standard paraffin-embedded H&E histology.

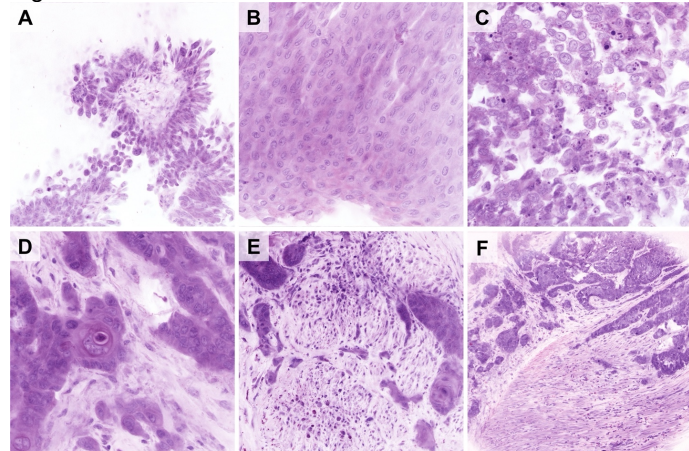
**Results:** This study included 36 tissue samples from radical cystectomies with known urothelial carcinoma (low and high grade). Representative NLM images of bladder tissue are shown in Figures 1 and 2. The background bladder tissue was well characterized, including the presence of benign urothelial epithelium, muscularis propria, and fibroadipose tissue. The characteristic features of low-grade tumors were observed, including papillary structures. High-grade tumors showed nuclear pleomorphism, brisk mitotic count, apoptosis, and focal squamous differentiation. Additionally, muscularis propria invasion was visualized.

Figure 1 - 832



**Figure 1.** A. Cross-sectional NLM system diagram. A pulsed laser beam is rapidly scanned through the sample exciting a sheet of fluorescence at the focal plane (right). Fluorescence is collected through the objective, separated from the laser path, detected with photomultipliers, and recolored to resemble H&E contrast. B-D. Benign urothelial mucosa in B; the lamina propria contains chronic inflammatory cells. Muscularis propria is well seen in C. Fibroadipose tissue (D) is easily imaged without distortion.

Figure 2 - 832



**Figure 2.** A, B. Papillary urothelial carcinoma, low-grade. In A, a discrete papillary frond is seen with associated umbrella cells. The low-grade nature of the urothelium is seen in B. High-grade urothelial carcinoma is seen in C with focal squamous differentiation in D. Invasion of the muscularis propria is apparent (E, F).

**Conclusions:** We demonstrate the capability of NLM for the evaluation of benign bladder tissue and bladder tumors. Possible future applications of NLM include: intraoperative confirmation of the presence of muscularis propria in transurethral resections of bladder tumors (TURBT), rapid confirmation of diagnostic tissue in urinary tract biopsies, and collection of fresh tissue for research from TURBT procedures while preserving the adequate specimens for staging and diagnosis.

# ABSTRACTS | GENITOURINARY PATHOLOGY (INCLUDING RENAL TUMORS)

## 833 Molecular Characterization of TFE3 rearranged Renal Cell Carcinoma: A Study of Twenty-one Cases

Shuanzeng Wei<sup>1</sup>, Harris Krause<sup>2</sup>, Daniel Geynisman<sup>1</sup>, Andrew Elliott<sup>2</sup>, Jun Yin<sup>3</sup>, Pedro Barata<sup>4</sup>, Elisabeth Heath<sup>5</sup>, Alex Farrell<sup>3</sup>, Chadi Nabhan<sup>3</sup>, Rouba Ali-Fehmi<sup>6</sup>, Rana McKay<sup>7</sup>

<sup>1</sup>Fox Chase Cancer Center, Philadelphia, PA, <sup>2</sup>Caris Life Sciences, Irving, TX, <sup>3</sup>Caris Life Sciences, Phoenix, AZ, <sup>4</sup>Tulane Medical School, New Orleans, LA, <sup>5</sup>Karmanos Cancer Institute, Detroit, MI, <sup>6</sup>Wayne State University, Detroit, MI, <sup>7</sup>UC San Diego Health, La Jolla, CA

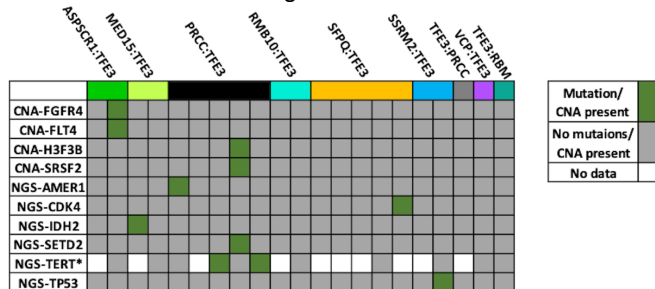
**Disclosures:** Shuanzeng Wei: None; Harris Krause: Employee: Caris Life Sciences; Daniel Geynisman: Advisory Board Member: Merck; Consultant: BMS; Andrew Elliott: Employee: Caris Life Sciences; Jun Yin: Employee: Caris Life Sciences; Pedro Barata: Consultant: BMS; Pfizer; Elisabeth Heath: None; Alex Farrell: Employee: Caris Life Sciences; Chadi Nabhan: Employee: Caris; Rouba Ali-Fehmi: None; Rana McKay: Consultant: BMS; Merck; Pfizer;

**Background:** Background: Renal cell carcinoma (RCC) is comprised of distinct histological subtypes, the most common of which are clear cell (ccRCC), papillary (pRCC) and chromophobe RCC. The recently renamed “TFE3 rearranged RCC” (2022 WHO classification) is rare subtype of RCC belonging to the MiT family translocation RCCs, harboring TFE3 translocations with various gene fusion partners. These rearrangements have a unique morphology and immunophenotype. To further elucidate the molecular alterations in TFE3 rearranged RCC, we characterized the genomic, transcriptional, and immune landscapes in comparison to ccRCC and type II pRCC.

**Design:** Design: Next-generation sequencing of RNA (whole transcriptome) and DNA (592-gene panel or whole exome) for TFE3 rearranged RCC (N=21), type II pRCC (N=22) and ccRCC samples (N=391) was performed on formalin-fixed paraffin-embedded tumor samples using the NextSeq platform (Illumina, Inc., San Diego, CA). PD-L1 expression was tested by IHC (SP142; Positive (+): ?2+, ?%5). Immune cell fractions of the tumor microenvironment (TME) were estimated with RNA deconvolution using quanTilseq. Differentially regulated pathways were assessed by gene set enrichment analysis. X2 and Kruskal-Wallis tests were used, and p-values were adjusted for multiple comparisons (Benjamini-Hochberg).

**Results:** Results: RCC patients with TFE3 fusions were significantly younger and more frequently female (47.0 years (y), 71.4% female) as compared to pRCC (70 y, 28.6%; p<0.05) and ccRCC (62 y, 27.6%; p<0.05). A total of 14 unique fusion partners were observed, including a novel fusion with SRRM2. Co-alteration rates in TFE3 fusion-positive RCC (Figure 1) were comparable to pRCC, while ccRCC exhibited significantly higher mutation rates of VHL (0% TFE3 RCC, 4.8% pRCC, 78.8% ccRCC; p<0.05) and PBRM1 (0% TFE3 RCC, 4.8% pRCC, 49.5% ccRCC; p<0.05). TME analysis revealed that TFE3 fusions were associated with significantly less M1 macrophages (0.8%) as compared to pRCC (1.4%) and ccRCC (2.7%) (p<0.05), suggesting a cold immune microenvironment. However, TFE3 fusion-positive tumors were more commonly PDL1+ (TFE3 50%, pRCC 19.0%, ccRCC 12.2%; p<0.05).

Figure 1 - 833



**Conclusions:** Conclusions: TFE3 rearranged RCC has different molecular alterations compared to cRCC and pRCC. Despite it having a relatively cold TME compared to pRCC and ccRCC, increased PDL1+ rates in TFE3 translocation RCC suggest a potential benefit from immune checkpoint inhibitor therapy and warrants further investigation in this rare RCC subtype.

## 834 Primitive Glandular Yolk Sac Tumor: A Morphologic Mimic of Embryonic-type Neuroectodermal Tumor, with Immunohistochemical Analysis

Rumeal Whaley<sup>1</sup>, Thomas Ulbright<sup>2</sup>

<sup>1</sup>Mayo Clinic, Rochester, MN, <sup>2</sup>Indiana University School of Medicine, Indianapolis, IN

**Disclosures:** Rumeal Whaley: None; Thomas Ulbright: None

**Background:** Yolk sac tumor (YST) is often associated with embryonic-type neuroectodermal elements (ENE) in germ cell neoplasia in situ-derived mixed germ cell tumors of the testis. The primitive endodermal-type glands of YST mimic tubules of ENE (Fig. 1), potentially leading to an overestimation of the size of ENE and misinterpretation as embryonic-type neuroectodermal tumor

# ABSTRACTS | GENITOURINARY PATHOLOGY (INCLUDING RENAL TUMORS)

(ENT) based on the WHO guideline of >5 mm diameter. A diagnosis of ENT in the testis may lead to retroperitoneal lymphadenectomy even in clinical stage I patients and in post-chemotherapy resections indicates a poor prognosis.

**Design:** We identified cases of YST (n=19) and with ENE (n=17) that were often admixed and showed morphologic overlap. Immunohistochemical studies with antibodies directed against villin, CDX2, glyican 3, AFP, synaptophysin, INSM1, CD56, GFAP, S100 protein, neurofilament, PHOX2B, cytokeratin AE1/AE3, and SALL4 were performed on 4 µm sections on a Dako automated platform with appropriate controls.

**Results:** The results are summarized in the table. ENE often admixed with YST glands that resembled tubules of ENE (Fig 1). Positivity for villin (Fig. 2), CDX2 and AFP were specific for YST in the differential with ENE, with villin having the best sensitivity (91%), followed by AFP (81%) and CDX2 (78%). Villin showed more diffuse expression (45%) than the others (AFP – 21%; CDX2 - 0%). Glycan 3 was not helpful because of frequent (64%) positivity in ENE. GFAP, synaptophysin (Fig. 2) and PHOX2B were specific for ENE, with respective sensitivities of 90%, 88%, and 40%, but were often focal/patchy, with GFAP commonly occurring at the periphery of ENE. The other markers either lacked specificity or sensitivity to be considered routinely helpful, although strong and diffuse CD56 expression favored ENE over YST.

Antigen	YST positivity (%)	YST positivity>50% (%)	ENE positivity (%)	ENE positivity>50% (%)
Villin	10/11 (91)	5/11 (45)	0/10 (0)	0/10 (0)
CDX2	7/9 (78)	0/9 (0)	0/12 (0)	0/12 (0)
GPC3	18/19 (95)	2/13* (15)	9/14 (64)	1/13* (8)
AFP	13/16 (81)	3/14* (21)	0/11 (0)	0/11 (0)
Synapto	0/15 (0)	0/15 (0)	15/17 (88)	3/16* (19)
INSM1	2/10 (20)	0/10 (0)	11/12 (92)	1/12 (8)
CD56	6/12 (50)	1/12 (8)	14/14 (100)	8/12 (67)
GFAP	0/9 (0)	0/9 (0)	9/10 (90)	1/10 (10)
S100	2/10 (20)	0/10 (0)	9/11 (82)	0/11 (0)
NF	0/8 (0)	0/8 (0)	0/8 (0)	0/8 (0)
PHOX2B	0/9 (0)	0/9 (0)	4/10 (40%)	0/10 (0)
CK AE1/AE3	9/9 ((100)	9/9 (100)	10/10 (100)	4/10 (40)
SALL4	12/12 (100)	10/11* (91)	8/12 (67)	5/12 (42)

\*In some cases the extent of positivity could not be determined because outside slides had been returned.

Figure 1 - 834

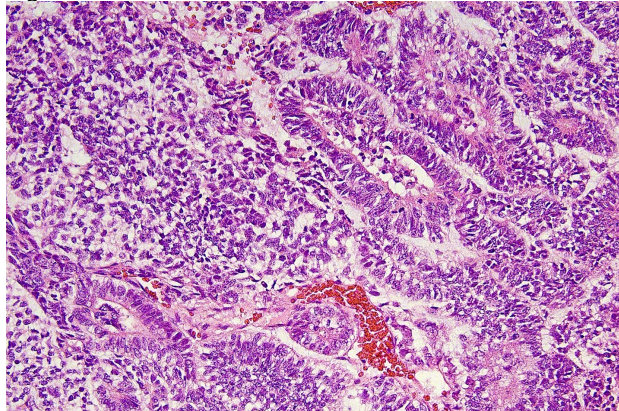
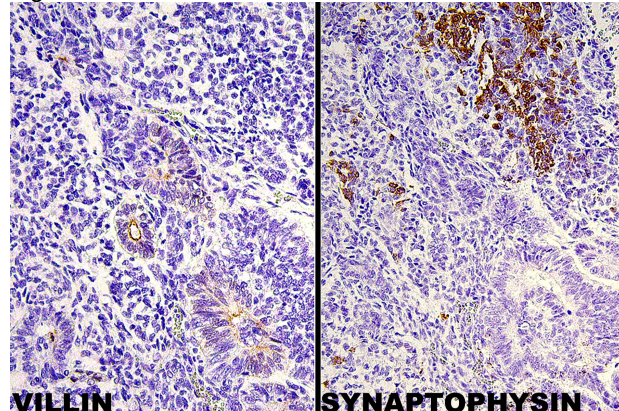


Figure 2 - 834



**Conclusions:** Primitive endodermal-type YST glands often admix with and mimic the tubules that are common as a feature of ENE. The optimal immunohistochemical panel for distinguishing these components is villin, AFP, synaptophysin and GFAP.

## 835 Current Practices in Prostate Pathology Reporting: Results From A Survey of Genitourinary Pathologists

Sean Williamson<sup>1</sup>, Reza Alaghebandan<sup>1</sup>, Ali Amin<sup>2</sup>, Mahul Amin<sup>3</sup>, Manju Aron<sup>4</sup>, Fadi Brimo<sup>5</sup>, Emily Chan<sup>6</sup>, Liang Cheng<sup>2</sup>, Maurizio Colecchia<sup>7</sup>, Jasreman Dhillon<sup>8</sup>, Michelle Downes<sup>9</sup>, Andrew Evans<sup>10</sup>, Lara Harik<sup>11</sup>, Oudai Hassan<sup>12</sup>, Aiman Haider<sup>13</sup>, Peter Humphrey<sup>14</sup>, Shilpy Jha<sup>15</sup>, Shivani Kandukuri<sup>16</sup>, Chia-Sui (Sunny) Kao<sup>17</sup>, Seema Kaushal<sup>18</sup>, Francesca Khani<sup>19</sup>, Oleksandr Kryvenko<sup>20</sup>, Charlotte Kweldam<sup>21</sup>, Priti Lal<sup>22</sup>, Anandi Lobo<sup>23</sup>, Fiona Maclean<sup>24</sup>, Cristina Magi-Galluzzi<sup>25</sup>, Rohit Mehra<sup>26</sup>, Santosh Menon<sup>27</sup>, Hiroshi Miyamoto<sup>28</sup>, Sambit Mohanty<sup>29</sup>, Rodolfo Montironi<sup>30</sup>, Gabriella Nesi<sup>31</sup>, George Netto<sup>25</sup>, Jane Nguyen<sup>1</sup>, Maya Nourieh<sup>32</sup>, Adeboye Osunkoya<sup>11</sup>, Gladell Paner<sup>33</sup>, Ankur Sangi<sup>34</sup>, Rajal Shah<sup>35</sup>, John Srigley<sup>36</sup>, Maria Tretiakova<sup>37</sup>, Patricia Troncoso<sup>38</sup>, Kiril Trpkov<sup>39</sup>, Theodorus Van Der Kwast<sup>40</sup>, Miao Zhang<sup>38</sup>, Debra Zynger<sup>41</sup>, Giovanna Giannico<sup>42</sup>

<sup>1</sup>Cleveland Clinic, Cleveland, OH, <sup>2</sup>Alpert Medical School of Brown University, Providence, RI, <sup>3</sup>The University of Tennessee Health Science Center, Memphis, TN, <sup>4</sup>Keck School of Medicine of USC, Los Angeles, CA, <sup>5</sup>McGill University, Montréal, QC, <sup>6</sup>University of California, San Francisco, San Francisco, CA, <sup>7</sup>University Vita-Salute San Raffaele, Milan, Italy, <sup>8</sup>H. Lee Moffitt Cancer Center & Research Institute, Tampa, FL, <sup>9</sup>Sunnybrook Health Sciences Centre, Toronto, ON, <sup>10</sup>Mackenzie Health Richmond Hill Hospital, Richmond Hill, ON, <sup>11</sup>Emory University School of Medicine, Atlanta, GA, <sup>12</sup>Henry Ford Health System, Detroit, MI, <sup>13</sup>University College London Hospitals NHS Foundation Trust, London, United Kingdom, <sup>14</sup>Yale School of Medicine, New Haven, CT, <sup>15</sup>Advanced Medical and Research Institute, Bhubaneswar, India, <sup>16</sup>University of Southern California, Keck School of Medicine of USC, Los Angeles, CA, <sup>17</sup>Stanford Medicine/Stanford University, Stanford, CA, <sup>18</sup>All India Institute of Medical Sciences, New Delhi, India, <sup>19</sup>Weill Cornell Medicine, New York, NY, <sup>20</sup>University of Miami Miller School of Medicine, Miami, FL, <sup>21</sup>Maasstad Hospital, Rotterdam, Netherlands, <sup>22</sup>University of Pennsylvania, Philadelphia, PA, <sup>23</sup>Kapoor Centre of Urology and Pathology, Raipur, India, <sup>24</sup>Douglass Hanly Moir Pathology, Melbourne, Australia, <sup>25</sup>The University of Alabama at Birmingham, Birmingham, AL, <sup>26</sup>University of Michigan, Ann Arbor, MI, <sup>27</sup>Tata Memorial Hospital, Mumbai, India, <sup>28</sup>University of Rochester Medical Center, Rochester, NY, <sup>29</sup>Advanced Medical and Research Institute, New Delhi, India, <sup>30</sup>Ancona, Italy, <sup>31</sup>University of Florence, Florence, Italy, <sup>32</sup>Institut Curie, Saint-Cloud, France, <sup>33</sup>University of Chicago, Chicago, IL, <sup>34</sup>El Camino Hospital, Mountain View, CA, <sup>35</sup>UTSouthwestern Medical Center, Dallas, TX, <sup>36</sup>Trillium Health Partners, Credit Valley Hospital, Montréal, ON, <sup>37</sup>University of Washington, Seattle, WA, <sup>38</sup>The University of Texas MD Anderson Cancer Center, Houston, TX, <sup>39</sup>University of Calgary, Calgary, AB, <sup>40</sup>University Health Network, Toronto, ON, <sup>41</sup>The Ohio State University Wexner Medical Center, Columbus, OH, <sup>42</sup>Vanderbilt University Medical Center, Nashville, TN

**Disclosures:** Sean Williamson: None; Reza Alaghebandan: None; Ali Amin: None; Mahul Amin: None; Manju Aron: None; Fadi Brimo: None; Emily Chan: None; Liang Cheng: None; Maurizio Colecchia: None; Jasreman Dhillon: None; Michelle Downes: None; Andrew Evans: None; Lara Harik: None; Oudai Hassan: None; Aiman Haider: None; Peter Humphrey: None; Shilpy Jha: None; Shivani Kandukuri: None; Chia-Sui (Sunny) Kao: None; Seema Kaushal: None; Francesca Khani: None; Oleksandr Kryvenko: None; Charlotte Kweldam: None; Priti Lal: None; Anandi Lobo: None; Fiona Maclean: None; Cristina Magi-Galluzzi: None; Rohit Mehra: None; Santosh Menon: None; Hiroshi Miyamoto: None; Sambit Mohanty: None; Rodolfo Montironi: None; Gabriella Nesi: None; George Netto: None; Jane Nguyen: None; Maya Nourieh: None; Adeboye Osunkoya: None; Gladell Paner: None; Ankur Sangi: None; Rajal Shah: None; John Srigley: None; Maria Tretiakova: None; Patricia Troncoso: None; Kiril Trpkov: None; Theodorus Van Der Kwast: None; Miao Zhang: None; Debra Zynger: None; Giovanna Giannico: None

**Background:** Consensus recommendations on grading and reporting of prostatic adenocarcinoma have been published by the International Society of Urological Pathology and the Genitourinary Pathology Society. Although the societies' position papers are in overall agreement, a few differences remain on important issues. Resulting practice standards among genitourinary pathologists have not been evaluated.

**Design:** This cross-sectional study was conducted using a web-based survey querying grading and reporting practices of genitourinary pathologists. Data were collected and managed using REDCap (Research Electronic Data Capture). De-identified respondent data were scored as a percentage.

**Results:** The response rate was 83% (61 of 73). For biopsies, tumor measurement would include (69%) or subtract (31%) intervening benign glands. Both Gleason score and Grade Groups are reported by 93% of participants. Most participants (98%) report percent pattern 4 (PP4) but reporting decreases to 62% if higher grades are present. In systematic biopsies, cores with different grades contained in the same jar are graded globally (74%) vs. per core (26%), and volume estimated globally (44%) vs. per core (56%). In targeted biopsies, multiple cores in the same jar are graded globally (87%) vs. per core (13%), and volume estimated globally (61%) vs. per core (39%). Cribriform morphology (CRIB) is reported by 84% of participants but CRIB size is reported by 23%. Basal cell markers (BCM)s are used by 92% for differentiating isolated intraductal vs. invasive CRIB (?IDC) and by 84% for ?IDC associated with Grade Group 1 (GG1) cancer. However, only 15% would use BCMs for ?IDC associated with  $\geq$ GG2. IDC, isolated, associated with GG1 or with  $\geq$ GG2 is not graded by 90%, 72%, and 59% of participants, respectively. In radical prostatectomies, 97% of participants report PP4, but 57% would report if overall grade  $>$ GG3. GG1 with  $<$  5% pattern 4 is graded as GG2 by 72%. A  $<$ 5% cut-off for tertiary ("minor") pattern is used by 84%, and 87% report  $>$ 5% pattern 4 or 5 as secondary pattern. Grading is assigned based on the dominant nodule for 71%. CRIB is reported by 87%. Small and large CRIB is discriminated by 18%. For ?IDC associated with GG1, 72% use BCMs. However, 21% would perform BCMs for ?IDC associated with  $\geq$ GG2. IDC, isolated, associated with GG1 or with  $\geq$ GG2 is not graded by 90%, 72%, and 57% of participants, respectively.

# ABSTRACTS | GENITOURINARY PATHOLOGY (INCLUDING RENAL TUMORS)

**Conclusions:** There is substantial agreement in grading and reporting patterns in this predominantly academic cohort of genitourinary pathologists.

## 836 Can Glomerular Involvement in Renal Pelvic Urothelial Carcinoma Be Used to Redefine pT3 to Improve Correlation with Survival?

Megan Wong<sup>1</sup>, Douglas Wu<sup>1</sup>, Cheryl Lee<sup>2</sup>, Debra Zynger<sup>3</sup>

<sup>1</sup>The Ohio State University Medical Center, Columbus, OH, <sup>2</sup>The Ohio State University, Columbus, OH, <sup>3</sup>The Ohio State University Wexner Medical Center, Columbus, OH

**Disclosures:** Megan Wong: None; Douglas Wu: None; Cheryl Lee: None; Debra Zynger: None

**Background:** pT categorization from the American Joint Committee on Cancer is an important pathologic factor for prognostication and clinical decision-making in renal pelvic urothelial carcinoma. Defined as tumor invading the renal parenchyma and/or peripelvic fat, renal pelvic pT3 is the largest pT category with notable survival heterogeneity. Using glomeruli as a boundary, this study sought to compare survival of renal pelvic pT3 tumors based on the extent of renal parenchyma invasion and determine whether redefining pT2 and pT3 improves pT correlation with survival.

**Design:** Primary renal pelvic urothelial carcinoma was identified by review of nephroureterectomies performed at our institution from 2010-2019. Patients with prior or concurrent higher pT bladder or ureter tumors and those treated with neoadjuvant chemotherapy were excluded. Slide review was completed. Cases (n=145) were stratified by pT, pN, lymphovascular invasion, and invasion of the renal medulla (adjacent to renal collecting ducts and/or tubules) versus invasion of the peripelvic fat and/or renal cortex (adjacent to or beyond at least one glomerulus). Overall survival was compared using Kaplan Meier survival curves and Cox regression multivariate analysis.

**Results:** pT3 was the most populous category (41.4%) and pT2 was the least numerous (5.5%). pT2 and pT3 tumors had similar 5-year overall survival, with multivariate analysis demonstrating overlap of hazard ratios for pT2 [HR=2.20, 95% CI (0.70-6.95)] and pT3 [HR=3.15, 95% CI (1.63-6.09)], concordant with survival curve analysis. pT3 tumors invading the peripelvic fat and/or renal cortex had a 3.25-fold worse prognosis than those with only renal medulla invasion. Furthermore, pT2 and pT3 tumors with only renal medulla invasion had similar overall survival, whereas pT3 tumors with peripelvic fat and/or renal cortex invasion had a worse prognosis ( $p=0.00036$ ). Notably, moving pT3 tumors with only renal medulla invasion to pT2 reduced overlap between survival curves and hazard ratios for pT2 [HR=1.93, 95% CI (0.93-4.02)] and pT3 [HR=6.15, 95% CI (2.92-12.96)].

Figure 1 - 836

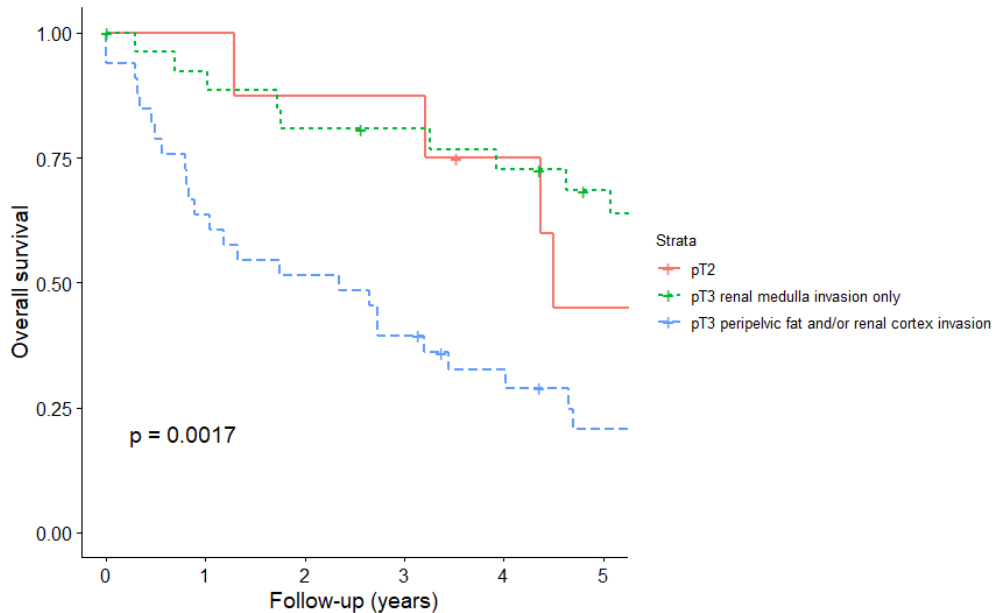
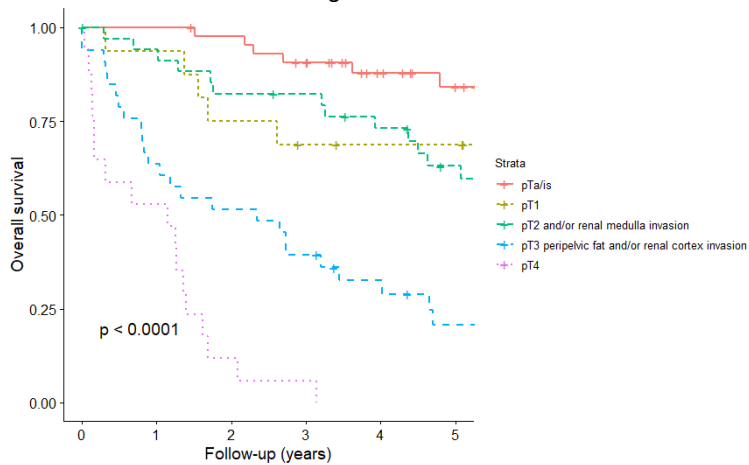


Figure 2 - 836



**Conclusions:** Modifying pT2 to include pT3 tumors with only renal medulla invasion and restricting pT3 to peripelvic fat and/or renal cortex invasion improves pT correlation with survival. Thus, we recommend using glomeruli as a landmark to stratify renal parenchyma invasion as they are easily identifiable, and our proposed modifications improve prognostic accuracy of pT classification.

### 837 Pathologic Response and Histologic Features of Cytoreductive Nephrectomy (CN) Following Immunotherapy (IO) for Patients with Metastatic Renal Cell Carcinoma (RCC)

Chih-Ying Wu<sup>1</sup>, Stephen Reese<sup>1</sup>, Hikmat Al-Ahmadie<sup>1</sup>, Samson Fine<sup>1</sup>, Anuradha Gopalan<sup>1</sup>, Judy Sarungbam<sup>1</sup>, S. Joseph Sirintrapun<sup>1</sup>, Ritesh Kotecha<sup>1</sup>, Martin Voss<sup>1</sup>, Jonathan Coleman<sup>1</sup>, Paul Russo<sup>1</sup>, Robert Motzer<sup>1</sup>, A. Hakimi<sup>1</sup>, Ying-Bei Chen<sup>1</sup>  
<sup>1</sup>Memorial Sloan Kettering Cancer Center, New York, NY

**Disclosures:** Chih-Ying Wu: None; Stephen Reese: None; Hikmat Al-Ahmadie: None; Samson Fine: None; Anuradha Gopalan: None; Judy Sarungbam: None; S. Joseph Sirintrapun: None; Ritesh Kotecha: None; Martin Voss: None; Jonathan Coleman: None; Paul Russo: None; Robert Motzer: None; A. Hakimi: None; Ying-Bei Chen: None

**Background:** IO, given alone or in combination with targeted agents, has become a mainstay for patients with metastatic RCC, either as the first line or later in the treatment course. Patients with de novo metastatic disease and favorable systemic responses to IO may be offered a CN. This population is under-characterized and the prognostic value of pathologic response assessment in this setting is unclear. Our study aims to assess pathologic response in CN following IO and identify histologic features that can help inform management.

**Design:** We conducted a retrospective study of 33 pts who underwent CN following systemic IO for metastatic RCC. Paired pre-treatment biopsies and post-IO CNs were reviewed. We evaluated %RVT [residual viable tumor area/total tumor bed area (including regression tumor bed)], necrosis, fibrosis, and additional immune-related features [tumor-infiltrating lymphocytes (TILs), lymphoid aggregates, immune cell populations by IHC, etc.]. Pathologic response was categorized based on %RVT: complete response (CR) 0%, near-CR (nCR)  $\leq 10\%$ ,  $10\% <$  partial response (PR)  $\leq 90\%$ , no response (NR)  $> 90\%$ . Kaplan-Meier method and log-rank test were used to compare the progression-free survival (PFS) and overall survival (OS) between groups. Median follow-up time was calculated using reverse Kaplan-Meier method.

**Results:** Median age at diagnosis was 61y (39-76), and 91% were male. All pts had metastatic disease at presentation and 30 (91%) had clear cell RCC. IO received before CN included ipilimumab+nivolumab(58%), combination VEGF+IO (27%), sequential VEGF and IO monotherapy (12%), and interferon (3%). At CN, pathologic CR and nCR were observed in 6 (18%) and 4 (12%), respectively (combined in Table). 18 (55%) pts had PR with a broad %RVT range (20-90%), and 5 (15%) pts were NR. Pts who demonstrated CR/nCR had a longer PFS compared to those with a PR or NR [92.4mo. vs. 5.1(PR) vs. 10.3(NR),  $p < 0.01$ ]. OS varied by the pathologic response group, but differences were not significant (Figure 1). %RVT within the PR group did not correlate with outcomes. Increased TILs (primarily T cells) were observed in the RVT of most nCR and PR cases. Further characterization of tumor immune milieu is ongoing.

# ABSTRACTS | GENITOURINARY PATHOLOGY (INCLUDING RENAL TUMORS)

**Table. Clinicopathologic Features and Outcome by Pathologic Response**

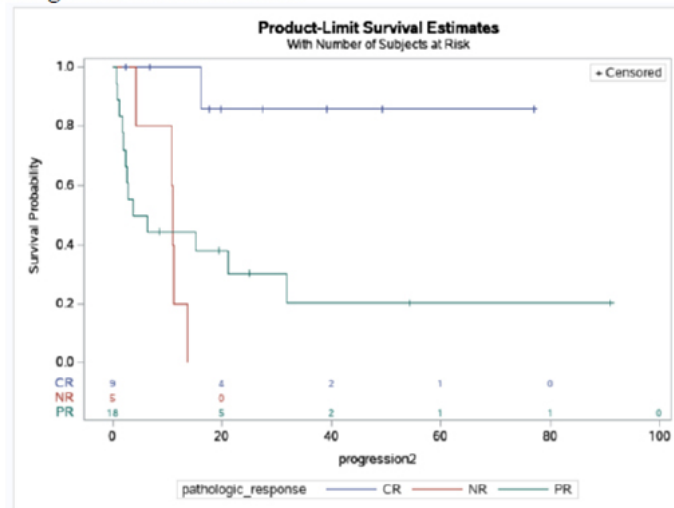
	pCR and near-pCR (N=10) (0≤%RVT≤10%)	pPR (N=18) (10%<%RVT≤90%)	pNR (N=5) (%RVT>90%)
<b>Demographic</b>			
Age	60.9 (50-71)	56.8 (39-76)	58.6 (50-66)
Gender (F:M)	0:10	3:15	0:5
BMI	34.4	24.6	27.7
KPS	84.3	78	88
<b>Radiologic Assessment [mean (range)] (cm)</b>			
Pre-Treatment tumor size	8.8 (5-14.7)	10 (4.9-15.6)	7.2 (1.3-13.5)
Post-Treatment tumor size	5.1 (1.8-9.1)	9.5 (3-20.5)	6.6 (1.6-14)
Reduced size	3.7 (0.7-8.4)	0.5 (-4.9-7.6)	0.6 (-0.5-3.8)
<b>Tumor Characteristics at CN [Median (Interquartile range)]</b>			
RVF (%)	0 (0-4)	67.5 (52.5-80)	95 (95-95)
Necrosis (%)	22.5 (6.25-50.75)	10 (5-25)	1 (0-5)
Fibrosis (%)	77.5 (46.25-90)	15 (10-30)	0 (0-6.5)
Rhabdoid	0	8 (44%)	2 (40%)
Sarcomatoid	1 (10%)	6 (33%)	1 (20%)
<b>Clinical Outcomes</b>			
Median Follow-up (months)	23.6 (2.4-49.2)	40.2 (25-54.2)	41.9 (19.9-NR)
Progression-Free survival (PFS)	92.4 (16.2-NR)	5.1 (2.0-31.8)	10.3 (4.2-NR)
Overall-Survival (OS)	188.7 (NR-NR)	45.2 (10.4-NR)	33.1 (25.6-NR)

BMI: Body mass index; KPS: Karnofsky Performance Status

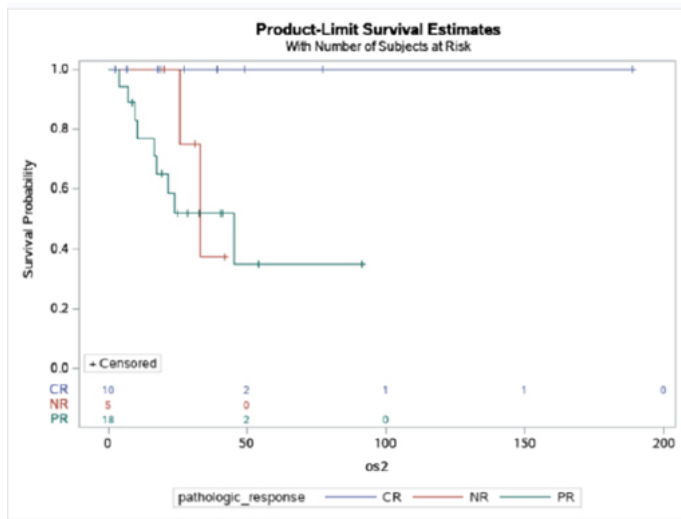
Figure 1 - 837

**Figure 1:** Progression-Free and Overall Survival, by Pathologic Response

### Progression-Free Survival



### Overall Survival



**Conclusions:** Patients demonstrating pathologic CR/nCR in CN following IO therapy had significantly longer PFS compared to patients with PR or NR and may serve as an important prognostic marker. Patients with PR had variable clinical outcomes and additional biomarkers beyond %RVT should be investigated.

### 838 Is the Stratification of Positive Lymph Nodes into pN1 and pN2 for Renal Pelvic and Ureter Carcinoma Prognostically Significant?

Douglas Wu<sup>1</sup>, Megan Wong<sup>1</sup>, Cheryl Lee<sup>2</sup>, Debra Zynger<sup>3</sup>

<sup>1</sup>The Ohio State University Medical Center, Columbus, OH, <sup>2</sup>The Ohio State University, Columbus, OH, <sup>3</sup>The Ohio State University Wexner Medical Center, Columbus, OH

**Disclosures:** Douglas Wu: None; Megan Wong: None; Cheryl Lee: None; Debra Zynger: None

**Background:** The 6<sup>th</sup> edition of the American Joint Committee on Cancer had 3 categories for positive lymph nodes (pN1-3) in upper urinary tract carcinoma. pN3 was subsequently removed, with the 7<sup>th</sup> and 8<sup>th</sup> editions defining pN1 as 1 lymph node with tumor deposit 2 cm or metastases in multiple lymph nodes. The aim of this study was to assess if the current pN categories impact overall survival in renal pelvis and ureter tumors.

# ABSTRACTS | GENITOURINARY PATHOLOGY (INCLUDING RENAL TUMORS)

**Design:** Patients who underwent nephroureterectomy with lymphadenectomy at our institution between 2010-2019 for primary upper urinary tract carcinoma were identified through review of pathology reports. Patients with prior or concurrent higher pT bladder tumors, neoadjuvant chemotherapy, and those without lymphadenectomy were excluded from additional analysis. Slide review was completed. Cases were stratified by pN, size of largest positive lymph node deposit, number of positive lymph nodes, and extranodal extension. Overall survival was compared using Kaplan Meier survival models.

**Results:** 152 patients had a nephroureterectomy with lymph nodes resected (mean 11.7 nodes, range 1-43; pN0 80.3%, pN1 7.2%, pN2 12.5%). 82 (53.9%) patients were deceased at last review [pN0, 56 (45.9%); pN1-2, 26 (86.7%)]. There was no difference in survival between pN1 and pN2 ( $p=0.24$ , Fig. 1) with 5-year survivals (95% confidence interval) of pN0, 63.1% (54.9-72.5%); pN1, 9.3% (3.7-30.2%); and pN2, 14.8% (7.8-35.6%). Analysis of the 2 current pN classification criteria, metastatic deposit size threshold of 2 cm ( $p=0.79$ ) and number of positive lymph nodes ( $p=0.24$ ), both showed no significant differences in survival. Extranodal extension did not correlate with survival ( $p=0.29$ ). As such, pN1 and pN2 were grouped together (pN+) based on any tumor presence in the lymph node(s). pN+ patients had worse survival than pN0 ( $p<0.0001$ , Fig. 2) with a 5-year survival of 11.2% (4.1-30.4%).

Figure 1 - 838

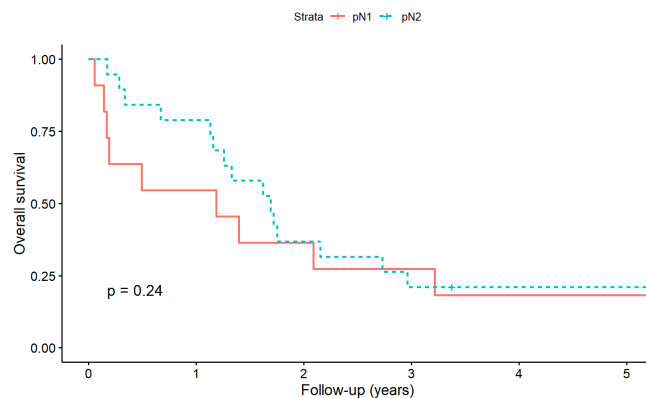
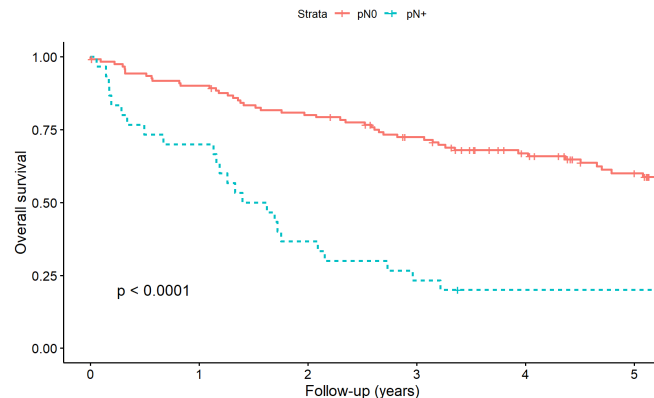


Figure 2 - 838



**Conclusions:** The current stratification of upper urinary tract carcinoma into pN1 and pN2 categories does not provide prognostic information, and both yield a stage IV classification, regardless of pT or pM category. Therefore, we recommend further simplification of the pN classification into 1 category for regional lymph node metastasis, irrespective of positive lymph node deposit size or number of positive lymph nodes.

## 839 Gleason Grade Group Concordance Between Systematic Template Combining Magnetic Resonance Imaging Fusion Targeted Biopsy and Radical Prostatectomy Specimens: A Comparison of Transperineal and Transrectal Approaches

Shulin Wu<sup>1</sup>, Adam Feldman<sup>1</sup>, Michelle Kim<sup>1</sup>, Sharron Lin<sup>1</sup>, Kristine Cornejo<sup>1</sup>, Mukesh Harisinghani<sup>1</sup>, Douglas Dahl<sup>1</sup>, Chin-Lee Wu<sup>1</sup>

<sup>1</sup>Massachusetts General Hospital, Boston, MA

**Disclosures:** Shulin Wu: None; Adam Feldman: None; Michelle Kim: None; Sharron Lin: None; Kristine Cornejo: None; Mukesh Harisinghani: None; Douglas Dahl: None; Chin-Lee Wu: None

**Background:** Both transperineal (TP) and transrectal (TR) multiparametric magnetic resonance imaging (MRI)-targeted biopsy (TBx) has shown to detect more clinically significant (cs) prostate cancer (PCa) than standard template biopsies (SBx). TP biopsy technique is becoming more favored since the lower risk of complications. Current data supports the inclusion of both TBx and SBx in obtaining an optimal csPCa detection rate for both approaches. However, the accuracy of each biopsy technique for predicting PCa Gleason Grade Group (GG) following radical prostatectomy (RP) remains under investigation. Our aim was to evaluate the accuracy of SBx and TBx by both TP and TR approaches in predicting GG at RP.

**Design:** We identified 310 PCa patients who underwent RP following TP TBx (3-core) and SBx (20-core) ( $n=105$ ) or TR TBx (4-core) and concomitant SBx (12-core) ( $n=205$ ) from September 2019 to February 2021. All patients had one or more lesions that were identified on prior prostate mpMRI. csPCa was defined as GG2 or greater.

**Results:** Overall, the TP combined Bx showed a similar csPCa detection rate as the TR approach (81.0% vs 76.1%). When comparing TBx with SBx in all patients, TBx showed a similar overall PCa to SBx (91.9% vs 91.4%), but demonstrated a significantly higher csPCa detection than SBx (70.2% vs 63.9%,  $p<0.001$ ). Compared with RP, TP combined Bx showed a better GG concordance than TR approach but did not reach a statistical significance (63.8% vs 57.1%). Furthermore, TP combined Bx

# ABSTRACTS | GENITOURINARY PATHOLOGY (INCLUDING RENAL TUMORS)

showed a similar upgrading rate (21.9% vs 22.9%) but significantly lower downgrading rate (10.5% vs 20.0%, p=0.034) than the TR approach. TP TBx showed a similar concordance as TP SBx (all p>0.05). TR TBx however showed a significantly higher concordance than TR SBx (52.2% vs 41.5%, p=0.002). Kappa coefficient of TP combined Bx was highest ( $k=0.48$ ) followed by TR combined Bx ( $k=0.39$ ), TP TBx ( $k=0.36$ ), TR TBx ( $k=0.35$ ), TP SBx ( $k=0.34$ ) and TR SBx ( $k=0.26$ ). Of 69 cases with combined clinically insignificant PCa diagnosis, 38 (55.1%) were diagnosed as csPCa. Univariate logistic regression analysis did not reveal any clinical factors for predicting final pathological upgrade except a trend that TR showed a 2.8-fold than TP approach to have a final upgrade (p=0.065).

**Conclusions:** The combined effect of SBx plus TBx led to a better pathological concordance rate and less upgrading from biopsy to RP. With more SBx cores, TP combined Bx showed the best performance.

## 840 Prostatic Urethral Polyps and Ectopic Urethral Polyps: A Case Series

Yubo Wu<sup>1</sup>, Jonathan Epstein<sup>1</sup>

<sup>1</sup>Johns Hopkins Medical Institutions, Baltimore, MD

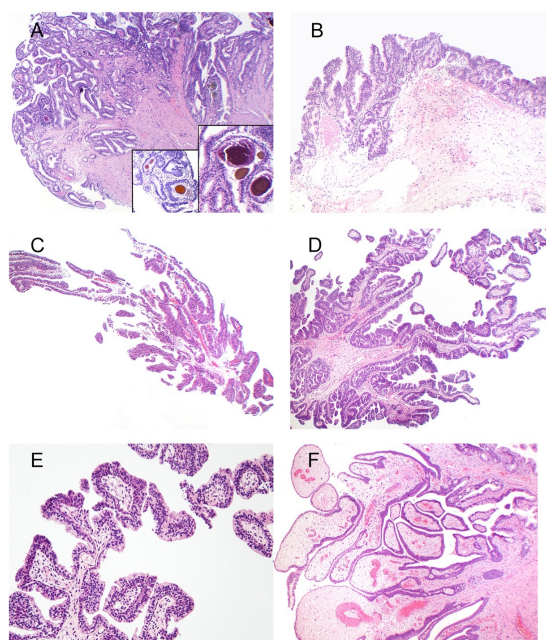
**Disclosures:** Yubo Wu: None; Jonathan Epstein: None

**Background:** Prostatic urethral polyps and ectopic prostatic polyps are rare, benign entities. This entity has been previously described in the literature in limited case series and thus remains poorly characterized.

**Design:** 57 cases (4 in-house; 53 consults) with these diagnoses were found in our Surgical Pathology files from 2012-2022. Of these, slides were available for review in 34 cases.

**Results:** The age range at presentation was 21 to 85 years. Polyps were located throughout the urothelial tract – prostatic urethra (n=30), bladder (n=20), bulbomembranous urethra (n=4), penile urethra (n=1), and indeterminate (n=2). Gross size ranged from 0.1 cm to 1.3 cm in greatest dimension with a median size of 0.3 cm. Architecturally, they were either broad-based (Figures 1A-B) or narrow-based (Fig. 1C) polypoid lesions surfaced by prostatic epithelium, urothelium, or a mixture of both. Surface morphologies included flat (Fig. 1B right) or villoglandular (Fig. 1D) or mixed. Villoglandular pattern mimicked papillary prostatic ductal adenocarcinoma, yet were lined by benign prostatic epithelium or urothelium or both (Fig. 1E). One case demonstrated severe edema mimicking polypoid cystitis (Fig. 1F). The presence of tightly-packed prostatic glands was variable, from none to florid and either were immediately beneath the surface (Fig. 1B) or filled up the underlying stroma (Fig. 1A), the latter mimicking prostatic adenocarcinoma. Verumontanum-type corpora amylacea were noted in several polyps, appearing in orange, green, blue, and dark purple colors (Fig. 1A). 4 cases had neoplastic lesions comingling with the polyps including: 1 benign inverted urothelial papilloma, 3 prostatic adenocarcinomas [prostatic urethra (2), membranous urethra (1)]; and 1 intraductal prostatic adenocarcinoma (prostatic urethra).

Figure 1 - 840



# ABSTRACTS | GENITOURINARY PATHOLOGY (INCLUDING RENAL TUMORS)

**Conclusions:** Our case series is the largest to date and demonstrates that prostatic urethral polyps and ectopic prostatic polyps have a wide range of morphological findings and can occur in a wide age range. Exceedingly rarely, they may arise in the urethra distal to the prostate. Lesions can mimic both acinar and ductal prostatic adenocarcinoma and in a minority of these cases give rise to prostatic adenocarcinoma.

## 841 Are There Differences in Outcome in Patients with Seminal Vesicle Invasion? Association of Seminal Vesicle Invasion with Extraprostatic Extension and Other Pathologic Variables Leading to Adverse Outcome

Zhengfan Xu<sup>1</sup>, Khaleel Al-Obaidy<sup>2</sup>, Nilesh Gupta<sup>2</sup>, Oudai Hassan<sup>2</sup>

<sup>1</sup>Henry Ford Hospital, Detroit, MI, <sup>2</sup>Henry Ford Health System, Detroit, MI

**Disclosures:** Zhengfan Xu: None; Khaleel Al-Obaidy: None; Nilesh Gupta: None; Oudai Hassan: None

**Background:** Extraprostatic extension of prostatic adenocarcinoma (PCa) is divided into pT3a, extraprostatic extension without SVI and pT3b; Seminal vesicle invasion (SVI) with or without extraprostatic extension. In this study we correlate SVI with other pathologic variables such as presence of extra prostatic extension (EPE) elsewhere, prognostic Grade Group (GG), percentage of gland involved by tumor (VOL) and location of dominant nodule (DN).

**Design:** All consecutive patients with SVI who underwent radical prostatectomy (RP) at our institution between 2009-2015 were included. All cases were reviewed by a urologic pathologist. Statistical analysis was done using cox proportional hazard for prognostic factors in multivariate setting. Adverse outcome was defined as biochemical recurrence (BCR), systemic recurrence or death from disease.

**Results:** 293 patients were included. Median age was 63 (45-83). Median follow up period was 84 months (6-153). Median percentage of prostate gland involvement was 25% (2-95). 42 (14.3%) patients had SVI only without EPE while 22 (7.5%) had SVI with focal EPE and 229 (78.2) had SVI with established EPE. Of the 42 patients with SVI only, 32 patients (76.2%) are alive with no recurrence, 7 (16.7%) showed biochemical recurrence (BCR) or recurrence in bone or lymph nodes, 2 (4.7%) died from disease and 1 (2.4%) died from other reasons. Of the 22 patients with SVI with focal EPE, 20 patients (91%) are alive with no recurrence, 1 (4.5%) show BCR or recurrence in bone or lymph nodes, and 1 (4.5%) died from other reasons. Of the 229 patients with SVI and established EPE, 176 patients (75.1%) are alive with no recurrence, 29 (12.7%) showed BCR or recurrence in bone or lymph nodes, 6 (2.6%) died from disease and 22 (9.6%) died from other reasons. Multivariate analysis showed that the presence of focal or nonfocal EPE in patients with SVI was not significantly associated with adverse outcome. None of the other pathologic variables was significant by multivariate analysis.

**Conclusions:** The majority of prostate cancer patients with SVI are alive and without disease after long follow up. The presence of EPE (focal or nonfocal) in patients with SVI does not appear to be associated with adverse outcome when compared with patients with Seminal vesicle invasion without EPE.

## 842 Large Cell Calcifying Sertoli Cell Tumors: Molecular Correlates of Aggressive Behavior

Sanhong Yu<sup>1</sup>, Lynette Sholl<sup>2</sup>, Thomas Ulbright<sup>3</sup>, Katrina Collins<sup>3</sup>, Maurizio Colecchia<sup>4</sup>, Pilar Gonzalez-Peramato<sup>5</sup>, Kvetoslava Michalova<sup>6</sup>, Jennifer Gordetsky<sup>7</sup>, Kristine Cornejo<sup>8</sup>, Chia-Sui (Sunny) Kao<sup>9</sup>, Sara Wobker<sup>10</sup>, Sara Vargas<sup>11</sup>, Fiona Maclean<sup>12</sup>, Muhammad Idrees<sup>3</sup>, William Anderson<sup>1</sup>, Christopher Fletcher<sup>13</sup>, Andres Acosta<sup>1</sup>

<sup>1</sup>Brigham and Women's Hospital, Harvard Medical School, Boston, MA, <sup>2</sup>Harvard Medical School, Boston, MA, <sup>3</sup>Indiana University School of Medicine, Indianapolis, IN, <sup>4</sup>University Vita-Salute San Raffaele, Milan, Italy, <sup>5</sup>La Paz Hospital, Autonoma University of Madrid, Madrid, Spain, <sup>6</sup>Biopticka laborator s.r.o., Plzen, Czech Republic, <sup>7</sup>Vanderbilt University Medical Center, Nashville, TN, <sup>8</sup>Massachusetts General Hospital, Boston, MA, <sup>9</sup>Stanford Medicine/Stanford University, Stanford, CA, <sup>10</sup>The University of North Carolina at Chapel Hill, Chapel Hill, NC, <sup>11</sup>Boston Children's Hospital, Harvard Medical School, Boston, MA, <sup>12</sup>Douglass Hanly Moir Pathology, Melbourne, Australia, <sup>13</sup>Brigham and Women's Hospital, Boston, MA

**Disclosures:** Sanhong Yu: None; Lynette Sholl: None; Thomas Ulbright: None; Katrina Collins: None; Maurizio Colecchia: None; Pilar Gonzalez-Peramato: None; Kvetoslava Michalova: None; Jennifer Gordetsky: None; Kristine Cornejo: None; Chia-Sui (Sunny) Kao: None; Sara Wobker: None; Sara Vargas: None; Fiona Maclean: None; Muhammad Idrees: None; William Anderson: None; Christopher Fletcher: None; Andres Acosta: None

**Background:** Large cell calcifying Sertoli tumor (LCCSCT) is a type of testicular sex cord-stromal tumor (TSCST) that often occurs sporadically (~60-70%) or in the context of Carney complex (~30-40%); rare examples are associated with other syndromes. A subset of LCCSCT is clinically malignant and the molecular mechanisms that drive such aggressive behavior remain unknown.

**Design:** We analyzed 20 LCCSCT (12 benign, 8 malignant) using PRKAR1A immunohistochemistry and next-generation sequencing (447-gene panel). Malignant cases were defined by the presence of metastases.

# ABSTRACTS | GENITOURINARY PATHOLOGY (INCLUDING RENAL TUMORS)

**Results:** Malignant LCCSCTs were associated with older age (median 32.5 vs. 16 years) and larger tumor size (median 3.3 vs. 1.5 cm). All tumors except one (case 20, Table 1) demonstrated loss of PRKAR1A expression. Among 14 cases sequenced to date (8 benign, 6 malignant), 4 failed QA metrics and had uninterpretable results (2 benign, 2 malignant). All cases with interpretable results harbored pathogenic single nucleotide variants of PRKAR1A (Table 1). Evidence of loss-of heterozygosity (LOH) of PRKAR1A was present in malignant LCCSCTs, but not in benign LCCSCTs. The mechanisms of LOH included mutation + copy number loss (case 15) and 2 concurrent mutations (case 14). In 2 malignant LCCSCTs (cases 13 and 18), pathogenic PRKAR1A variants were present at variant allele frequencies > 70%, but sequencing quality precluded a definitive evaluation of LOH. Co-mutation of BRCA2 (with LOH, case 15), homozygous deletion of CDKN2A/CDKN2B and arm-level or chromosome-level copy number changes were only seen in malignant LCCSCT. Analysis of consecutive metastases in case 15 (interval: 3 years) showed "stable" genomic alterations. Of note, studies have demonstrated that haploinsufficiency of PRKAR1A is tumorigenic in humans and mice, and the neoplasms that arise in this context often lack evidence of PRKAR1A LOH.

**Table 1 - Molecular finding in benign and malignant Large cell calcifying Sertoli cell tumors**

CASE	Age	Size (cm)	Classification	PRKAR1A Expression*	Metastases	SNVs	CNVs
1	25	1.5	Benign	loss	No	***	***
2**	21	0.6	Benign	loss	No	PRKAR1A p.Y246Rfs*10	--
	16	5.1	Benign	loss	No	Failed-uninterpretable	Failed-uninterpretable
4	12	0.6	Benign	loss	No	***	***
5	19	3	Benign	loss	No	PRKAR1A p.R97*	--
6	19	3.2	Benign	loss	No	***	***
7	18	1.5	Benign	loss	No	PRKAR1A c.891+2T>A	--
8	16	0.8	Benign	loss	No	PRKAR1A p.N144Kfs*2	---
9	15	1.4	Benign	loss	No	Failed-uninterpretable	Failed-uninterpretable
10	6	1.1	Benign	loss	No	PRKAR1A p.R97Tfs*7	--
11	14	2.5	Benign	loss	No	***	***
12		0.7	Benign	loss	No	Failed-uninterpretable	Failed-uninterpretable
13**	37	2.7	Malignant	loss	Yes (RPLN)	PRKAR1A p.L30Cfs*99 (VAF 78%)	+7, +8, -12p, +19q, 2DEL CDKN2A/CDKN2B,
14	30	2.0	Malignant	loss	Yes (RPLN)	PRKAR1A p.R146Kfs*2, PRKAR1A c.549+1del	+7, +8, -9p
15/1	35	2.5	Malignant	loss	Yes (RPLN, lung)	PRKAR1A c.709-2A>G, BRCA2 c.8332-3C>G, BRCA2 p.Q2870*	-4,-6, +8, -17, -16q, 1DEL PRKAR1A
15/2						PRKAR1A c.709-2A>G, BRCA2 c.8332-3C>G, BRCA2 p.Q2870*	-3p, -4, -6, +8, -16q, -17, 1DEL PRKAR1A
16	29	3.0	Malignant	loss	Yes (RPLN, bone, visceral)	***	***
17	36	15.0	Malignant	loss	Yes (RPLN)	***	***
18**	51	4.3	Malignant	loss	Yes (RPLN, bone)	PRKAR1A p.Q37* (VAF 71%)	--
19	24	3.5	Malignant	loss	Yes (LN)	Failed-uninterpretable	Failed-uninterpretable
20	28	6	Malignant	Retained	Lung, bone, and lymph nodes	Failed-uninterpretable	Failed-uninterpretable

Abbreviations: 1 DEL = heterozygous deletion, 2 DEL = deep/homozygous deletion, cm = centimeters, CNV = copy number variant, LN = lymph nodes, RPLN = retroperitoneal lymph nodes, SNV = single nucleotide variant. \*Assessed by immunohistochemistry. \*\*Denotes cases that failed QA metrics but still had interpretable sequencing results for the annotated variants. \*\*\*Denotes cases with pending sequencing results.

**Conclusions:** The present study suggests that, in LCCSCT, PRKAR1A LOH is associated with malignancy. The consistent loss of PRKAR1A expression observed in LCCSCT with both haploinsufficiency and LOH suggests that this gene might influence oncogenic processes that drive aggressive behavior at a pre-translational level or, alternatively, that immunohistochemistry is insufficiently sensitive to distinguish between reduced and ablated protein expression. The results of this study suggest that assessment of the genomic alterations present in LCCSCT might be helpful to identify a subset of tumors with malignant potential.

## 843 Decision Curve Analysis on the Addition of Cribriform Pattern 4 and Intraductal Prostatic Carcinoma to NCCN and CAPRA Patient Stratification

Yan Hong (Shirley) Yu<sup>1</sup>, Kristen Liu<sup>2</sup>, Katherine Lajkosz<sup>3</sup>, Theodorus Van Der Kwast<sup>4</sup>, Kenneth Iczkowski<sup>2</sup>, Michelle Downes<sup>5</sup>

<sup>1</sup>University of Toronto, Toronto, ON, <sup>2</sup>Medical College of Wisconsin, Milwaukee, WI, <sup>3</sup>Princess Margaret Cancer Centre, Toronto, ON, <sup>4</sup>University Health Network, Toronto, ON, <sup>5</sup>Sunnybrook Health Sciences Centre, Toronto, ON

**Disclosures:** Yan Hong (Shirley) Yu: None; Kristen Liu: None; Katherine Lajkosz: None; Theodorus Van Der Kwast: None; Kenneth Iczkowski: None; Michelle Downes: None

**Background:** The National Comprehensive Cancer Network (NCCN) and Cancer of the Prostate Risk Assessment (CAPRA) scores are pretreatment risk stratification tools which use biopsy data to guide patient management. We have previously shown that the CAPRA outperforms NCCN in patient stratification, and the addition of cribriform architecture pattern 4 (CC) and intraductal carcinoma (IDC) improves outcome stratification particularly for patients in CAPRA intermediate and NCCN unfavorable intermediate categories. In this study, we performed decision curve analysis (DCA) to determine clinical net benefit derived from the addition of CC/IDC to the NCCN and CAPRA tools.

**Design:** Multi-centre retrospective cohorts of matched biopsy-prostatectomy cases (2010-2017) were reviewed for the presence or absence of CC/IDC. Clinicopathological and follow up data were retrieved. The NCCN CAPRA scores were tabulated and categorized as follows: NCCN scores 1-2 = very low/low risk, 3 = favorable intermediate, 4 = unfavorable intermediate, 5-6 = high/very high risk; CAPRA scores 0-2 = low risk, 3-5 = intermediate risk, 6-10 = high risk. Clinical outcome variables were biochemical (BCR) and metastases/death of prostate cancer (event free survival-EFS) after prostatectomy. DCA was calculated to evaluate the models stratified by the presence of CC/IDC.

**Results:** The full cohort (n= 1149, three centres) had mean age 63 years and mean follow up of 4.9 (range 0-10.8) years. CC/IDC was present in 252/1149 (22%) biopsies. For biopsy grade groups: 20% were GG1, 51% GG2, 16% GG3, 7% GG4, and 6% GG5. BCR was present in 229 (20%) patients and there were 113 (10%) events. For BCR (Figure 1) and EFS (Figure 2) models for each separate center and the full cohort, DCA shows improved net benefit in most threshold probabilities with the addition of CC/IDC to NCCN and CAPRA risk assessment tools.

Figure 1 - 843

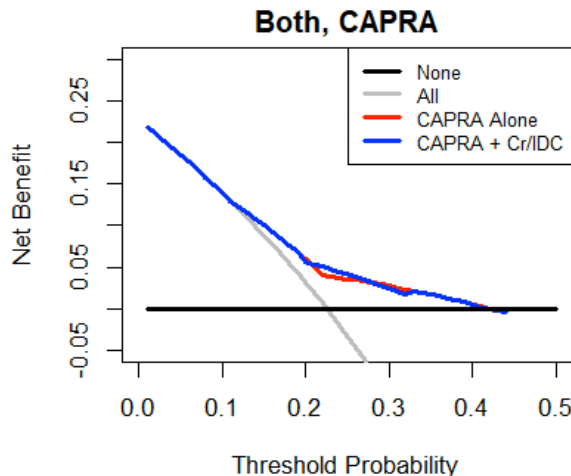
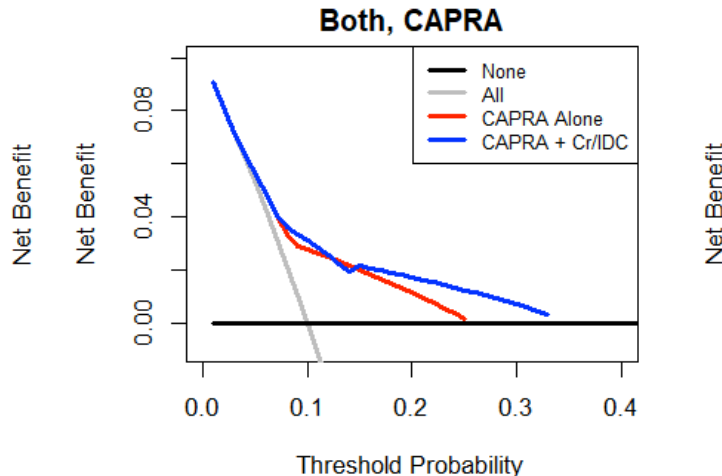


Figure 2 - 843



**Conclusions:** DCA analysis shows addition of CC/IDC improves the prognostic performance of NCCN and CAPRA patient stratification. Our study underscores the importance of including these histomorphologic features as part of pretreatment tools.

## 844 Further Morphologic and Immunohistochemical Characterization of *TFEB* Amplified Renal Cell Carcinoma: A Series of 12 Tumors

Nicole Zalles<sup>1</sup>, Sean Williamson<sup>1</sup>, Rohit Mehra<sup>2</sup>, Jesse McKenney<sup>1</sup>, Jane Nguyen<sup>1</sup>

<sup>1</sup>Cleveland Clinic, Cleveland, OH, <sup>2</sup>University of Michigan, Ann Arbor, MI

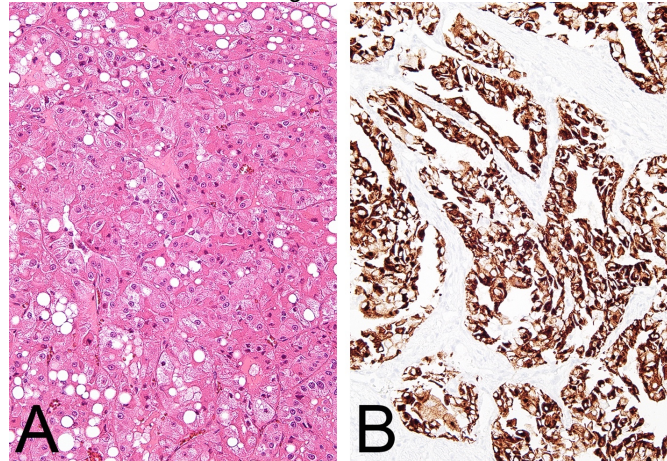
**Disclosures:** Nicole Zalles: None; Sean Williamson: None; Rohit Mehra: None; Jesse McKenney: None; Jane Nguyen: None

**Background:** *TFEB* amplified renal cell carcinoma (RCC) is a recently described entity that exhibits various morphologic patterns of high grade RCC, with a characteristic amplification of chromosome 6p21.2. We aimed to further characterize both histological and immunohistochemical features of these tumors, to aid in their identification.

**Design:** We searched our archives retrospectively to identify cases of *TFEB*-amplified RCC. Clinical and imaging features, immunohistochemical findings and histological features were reviewed. Morphologic features assessed included papillary architecture, eosinophilic or clear cytoplasm, necrosis, nucleoli, and rhabdoid and/or sarcomatoid morphology.

**Results:** We identified 12 RCCs with *TFEB* gain, of which 9 were reported by FISH as having unequivocal amplification, and 3 had increased copies below the cutoff of >10 defining amplification. Of note 1 tumor exhibited increased copies of both *TFE3* and *TFEB*. A majority demonstrated papillary or pseudo-papillary architecture (9/12), prominent nucleoli (11/12) and eosinophilic cytoplasm (10/12). Clear cytoplasm was present in 9. Most tumors showed an infiltrative growth pattern (9/12). Cytoplasmic vacuoles were florid in one tumor (Figure 1A) and two had chromophobe-like cells. Using immunohistochemistry, positivity was less frequent than previously reported for melan-A (1/11) and cathepsin K (2/12). Keratin 7 was positive in 4/11 and keratin 20 in 5/10 (Figure 1B). There was patchy staining for 2SC in 6/9, although not diffuse nuclear and cytoplasmic, and FH was normal / retained (10/10). All tumors tested were positive for alpha-methylacyl-CoA racemase (AMACR, 9/9). CA9 focal or patchy labeling was present in 4/10. More than half (7/11 with stage data) were at least pT3a, and 2 had lymph nodes involved at presentation.

Figure 1 - 844



**Conclusions:** In this novel series of RCC with *TFEB* amplification, the most consistent morphological patterns shared across a majority of the tumors included papillary or pseudo-papillary architecture, eosinophilic cytoplasm, an infiltrative growth pattern and prominent nucleoli, although a clear cell or chromophobe-like patterns were present in a minority. Florid cytoplasmic vacuoles were noted in one. Novel findings include relatively common keratin 20 positivity, overlapping with eosinophilic solid and cystic RCC and a lesser rate of melanocytic markers / cathepsin K than previously described.

## 845 Influence of Race on Pathological Radical Prostatectomy Outcomes

Guannan Zhang<sup>1</sup>, Oleksii Iakymenko<sup>2</sup>, Amr Abulaban<sup>3</sup>, Laurence Briski<sup>4</sup>, Ivan Nemov<sup>5</sup>, Merce Jorda<sup>5</sup>, Oleksandr Kryvenko<sup>5</sup>

<sup>1</sup>Jackson Memorial Hospital/ University of Miami Hospital, Miami, FL, <sup>2</sup>Albert Einstein College of Medicine, Montefiore Medical Center, Bronx, NY, <sup>3</sup>University of Miami Miller School of Medicine/Jackson Health System, Miami, FL, <sup>4</sup>University of Miami Health System, Miami, FL, <sup>5</sup>University of Miami Miller School of Medicine, Miami, FL

**Disclosures:** Guannan Zhang: None; Oleksii Iakymenko: None; Amr Abulaban: None; Laurence Briski: None; Ivan Nemov: None; Merce Jorda: None; Oleksandr Kryvenko: None

**Background:** Several publications have suggested that Black men with clinically localized prostate cancer have worse pathological radical prostatectomy (RP) findings than White men. This study evaluates whether race is an independent predictor of the pathologic outcomes at RP after controlling for other risk factors associated with locally advanced disease in a tri-ethnic population.

# ABSTRACTS | GENITOURINARY PATHOLOGY (INCLUDING RENAL TUMORS)

**Design:** We studied 2,528 men (529 Black, 1,046 White Hispanics, and 953 White non-Hispanics) who had RP at a single institution. All cases were re-reviewed. Using a multivariate COX regression model, the independent predictive value of race as a clinical prognostic factor was analyzed and controlled for patient age, PSA density, tumor volume, Grade Group, and tumor location.

**Results:** In univariable analysis, Black men were younger than Hispanics and non-Hispanics (60.6 vs 62.5 vs 64.1 y, p<0.001), had higher PSA density (0.26 vs 0.22 vs 0.2, p<0.01), and had BMI in between two other ethnicities (28.2 vs 28.5 vs 27.9, p=0.003). There was no significant difference between Black, White Hispanic, and White non-Hispanic men in age, PSA density, tumor volume, prostate weight, Grade Group, surgical margin status, stage or presence of lymph node metastasis at RP. Higher pathological T stage and lymph node metastasis correlated with higher Grade Group, higher tumor volume, higher PSA density, and posterior tumor location. In multivariable analysis, Grade Group, age, PSA density, tumor volume, and posterior tumor location directly correlated with advanced local stage. Black ethnicity inversely correlated with advanced local stage compared to White Hispanic and White non-Hispanics (OR: 0.71; p=0.025).

**Conclusions:** We demonstrate that in our region population, race may have an independent influence on behavior of prostate cancer as shown by RP findings in this study. With other variables being the same, Black men tend to have a better pathologic outcome than white Hispanics and white non-Hispanics at RP which contrasts with the prior reports. Both socioeconomic and genealogical (e.g., African or Caribbean origin) reasons can possibly contribute to different findings. A separate on-going study will examine disease progression in these populations.

## 846 Predicting NF1 Expression in Renal Tubules and Kidney Cancer Subtypes using Nuclear Hematoxylin Features

Wei Zhang<sup>1</sup>, Deepika Sirohi<sup>2</sup>, Mei Kho<sup>1</sup>, Beatrice Knudsen<sup>2</sup>

<sup>1</sup>The University of Utah, Salt Lake City, UT, <sup>2</sup>The University of Utah/ARUP Laboratories, Salt Lake City, UT

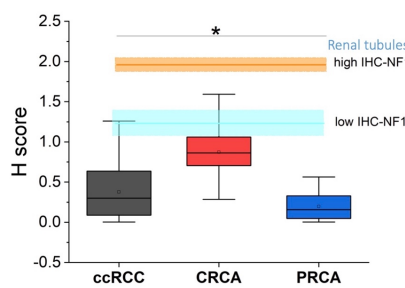
**Disclosures:** Wei Zhang: None; Deepika Sirohi: None; Mei Kho: None; Beatrice Knudsen: None

**Background:** Neurofibromin 1 (NF1) is a tumor suppressor protein that negatively regulates the RAS/MAPK pathway. In the nucleus, genetic modifiers that intersect with NF1 loss determine NF1-associated tumor formation and severity. We hypothesized that nuclear hematoxylin features are associated with loss of NF1 and IHC staining intensity of NF1 in single cells.

**Design:** The study cohort includes 97 cases of 50 clear cell carcinomas (ccRCC), 30 chromophobe carcinoma (CRCA) and 17 papillary carcinomas (PRCA). 6 cores from each case were displayed on a tissue microarray (TMA) and stained by IHC with a validated NF1 antibody. Image analysis using the open-source QuPath software included cell classification and segmentation of nuclei within renal tubules. H-scores of NF1 intensity were calculated in benign and cancer cores (IHC-NF1). Nuclear hematoxylin features (n=33) of renal tubular epithelial cells were used to train machine learning (ML) algorithms (linear regression, decision tree, random forest and XGBoost) to predict NF1 expression levels (ML-NF1) in single cells from renal tubules and from kidney cancers.

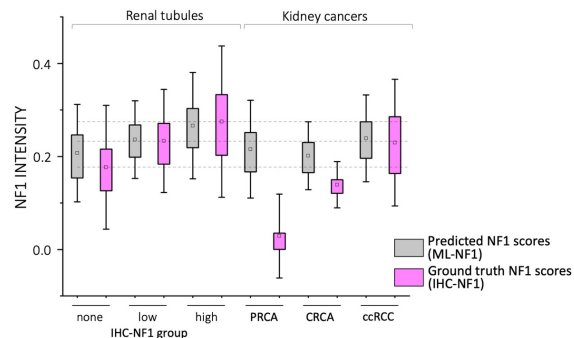
**Results:** Three subgroups of tubules were identified with high, low and absent IHC-NF1 expression. The average IHC-NF1 expression in all kidney cancer subtypes was below that of low-level NF1 tubules (Fig 1). PRCA had the lowest IHC-NF1 expression, followed by ccRCC and CRCA. To train ML models that predict NF1 expression in single cells, benign tissues were separated into training, validation and test groups at the case level, regardless of cancer type. Renal tubules were outlined to extract nuclear hematoxylin features defined by QuPath. Trained XGBoost and Random Forest (RF) models outperformed linear regression and decision tree models using IHC-NF1 scores as ground truth ( $R^2_{XGBoost}=0.53$ ). Comparing IHC-NF1 and ML-NF1 scores revealed good concordance for subgroups of tubules. ML-NF1 scores in kidney cancers were below those of renal tubules, however, the difference of average ML-NF1 scores between kidney cancer subtypes was lower than the difference of IHC-NF1 scores (Fig 2).

Figure 1 - 846



**Figure 1: IHC-NF1 expression in kidney cancer subtypes.** H scores of cancer subtypes are compared to H-scores of high- and LOW-NF1 renal tubules. \*p-values of all pairwise comparisons, including cancer subtypes versus low IHC-NF1 tubules <0.01

Figure 2 - 846



**Figure 2: Comparison of ground truth and predicted NF1 staining levels.** The XGBoost model is used to generate ML-NF1 intensity scores. Dashed lines indicate the average expression of IHC-NF1 in high NF1 expressing renal tubules, low NF1 expressing renal tubules and in renal tubules negative for NF1 expression.

**Conclusions:** Loss of NF1 expression in three subtypes types of kidney cancer suggests a role of NF1 in kidney cancer tumorigenesis. NF1 expression levels in renal tubules and kidney cancers can be predicted using nuclear features, providing novel insights into an association between nuclear morphology and cytoplasmic NF1 expression.

## 847 Diagnostic Discordance of Upper Urinary Tract Urothelial Carcinoma between Biopsy and Nephroureterectomy Specimens: A Tertiary Cancer Center Experience

Jianping Zhao<sup>1</sup>, Bogdan Czerniak<sup>1</sup>, Charles Guo<sup>1</sup>

<sup>1</sup>The University of Texas MD Anderson Cancer Center, Houston, TX

**Disclosures:** Jianping Zhao: None; Bogdan Czerniak: None; Charles Guo: None

**Background:** Upper urinary tract urothelial carcinoma (UUTUC) arises from the renal pelvis and ureter. It is challenging to provide an accurate diagnosis of UUTUC on a small biopsy specimen due to technical difficulty of obtaining sufficient tissue at these locations. Here we evaluated the diagnostic discordance of UUTUC between matched biopsy and nephroureterectomy specimens at our institution and studied possible causes of the discordance.

**Design:** We searched our pathology file and found 100 patients with UUTUC who underwent retrograde biopsy and nephroureterectomy at our institution from 2014 to 2018. Eight patients showed only urothelial carcinoma in situ or no residual tumor in the nephroureterectomy specimens after neoadjuvant treatment, and they were excluded from the study. H&E slides from biopsy and nephroureterectomy specimens were reviewed for pathologic analysis. Medical records were reviewed for clinical and demographic data.

**Results:** The patients included 64 men and 28 women with a mean age of 69 (range 47-93) years old. The tumors were located at the ureter (26 cases) or renal pelvis (66 cases). 22 patients (24%) showed low-grade UC on biopsy specimens but high-grade UC on the matched nephroureterectomy specimens. The size of biopsy specimens (based on the greatest dimension) in the discordant group (mean 0.6 cm, range 0.1-2 cm) was significantly smaller than that in the concordant group (mean 0.9 cm, range 0.2-3.2 cm) ( $p<0.05$ ), and the minimum specimen size in the concordant group was 0.2 cm. 24 patients (26%) had noninvasive UC on biopsy specimens but invasive UC on the matched nephroureterectomy specimens. Although the size of biopsy specimens did not show a significant effect on the discordance of stromal invasion ( $p>0.2$ ), the tumor size in the discordant group (mean 3.9 cm, range 1.3-7.6 cm) was significantly larger than that in the concordant group (mean 2.9 cm, range 0.4-5 cm) ( $p<0.05$ ). The discordances of tumor grade and stromal invasion were not significantly associated with the tumor location.

**Conclusions:** Our study demonstrates the diagnostic challenges of UUTUC on small biopsy specimens. The size of biopsy specimen and tumor size are two significant factors that contribute to the diagnostic discordance between matched biopsy and nephroureterectomy specimens. To reduce the diagnostic discordance, a minimal size of 0.2 cm may be required for upper urinary tract biopsy specimens.

**848 Mutational Landscape of Plasmacytoid Urothelial Carcinoma of the Urinary Bladder: An Analysis of 51 cases by Next Generation Sequencing**
Lan Zheng<sup>1</sup>, Hui Chen<sup>1</sup>, Jianping Zhao<sup>1</sup>, Bogdan Czerniak<sup>1</sup>, Sinchita Roy-Chowdhuri<sup>1</sup>, Charles Guo<sup>1</sup><sup>1</sup>The University of Texas MD Anderson Cancer Center, Houston, TX

**Disclosures:** Lan Zheng: None; Hui Chen: None; Jianping Zhao: None; Bogdan Czerniak: None; Sinchita Roy-Chowdhuri: None; Charles Guo: None

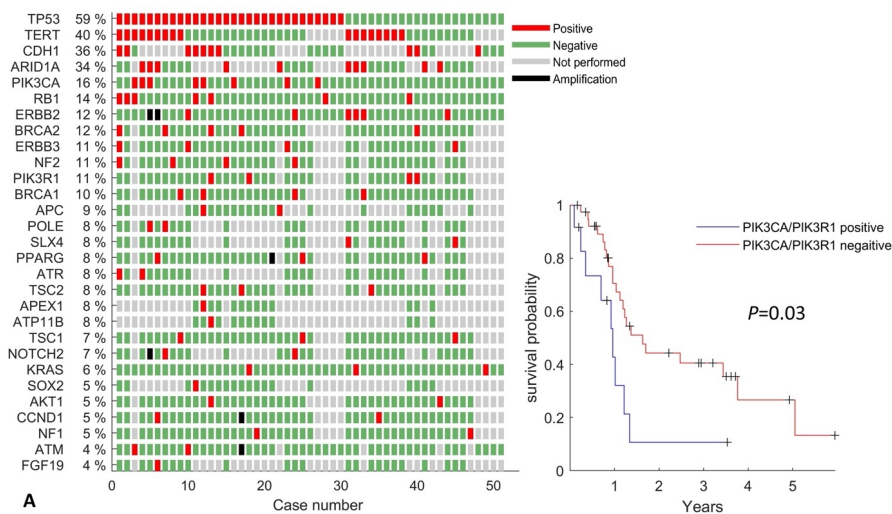
**Background:** Plasmacytoid urothelial carcinoma (PUC) is a distinct subtype of bladder cancer that demonstrates an aggressive clinical behavior. Recent studies have revealed that PUC is enriched with somatic mutations of the CDH1 gene, leading to the frequent loss of E-cadherin expression. However, the mutational profile of PUC remains to be studied. We aim to analyze the mutational profile of PUC in correlation to its pathological and clinical features.

**Design:** We searched our pathology files from 2010 to 2020 and identified 51 patients with PUC of the urinary bladder who had next-generation sequencing (NGS) tests. The molecular analysis included gene mutations, copy number variations (CNV), and gene fusions. Histologic slides were reviewed for pathological analysis. Clinical data were collected from the medical records. Survival analysis was performed using Kaplan-Meier method and compared with the log-rank test.

**Results:** The patients included 43 men and 8 women, with a median age of 64 years (range, 41-91 years) (Table 1). PUC component accounted for a mean of 47% of bladder tumor specimen (range, 5-100%). Other UC subtype components were coincidentally present in 11 cases. NGS tests demonstrated distinct somatic gene mutations in all PUC, and the most common gene mutations were *TP53* (56%), followed by *TERT* (39%), *CDH1* (35%), and *ARID1A* (32%) (Fig. 1A). CNV data were available for 34 patients, and 13 showed CNV in *ERBB2* (2), *CCND1*(2), *CCNE1*(2), and other genes (7). No gene fusion was present in any patients (0/12). The median follow-up time was 19 months (range, 1-72 months). Individual gene mutations did not show any significant effect on the clinical outcome, but gene mutations in the mTOR pathway (*PICK3CA* or *PIK3R1* mutations) were associated with significantly worse prognosis ( $p<0.05$ ). (Fig. 1B).

	Number
<b>Sex</b>	
Male	43
Female	8
<b>Tumor Stage</b>	
1	2
2	15
3	12
4	22
<b>Other subtype components</b>	
Micropapillary	3
Small cell	1
Nested	1
Sarcomatoid	5
Giant cell	1
<b>Outcome</b>	
Alive	20
Dead	31
<b>NGS types</b>	
50-gene panel	8
70-gene panel	4
134-gene panel	13
146-gene panel	20
409-gene panel	1
610-gene panel	5

Figure 1 - 848



**Conclusions:** PUC demonstrates distinct somatic gene mutations in oncogenes and tumor suppressor genes, which may underlie its aggressive behavior. A subset of plasmacytoid UC also shows distinct CNV in several oncogenes. Furthermore, gene mutations in the mTOR pathway are associated with poor outcome, indicating a potential therapeutic value of mTOR inhibitors in PUC.

#### 849 AKR1B10 is a New Sensitive and Specific Marker for Fumarate Hydratase-Deficient Renal Cell Carcinoma

Linmao Zheng<sup>1</sup>, Xingming Zhang<sup>1</sup>, Xiuyi Pan<sup>1</sup>, Qiao Zhou<sup>1</sup>, Hao Zeng<sup>1</sup>, Ni Chen<sup>1</sup>  
<sup>1</sup>West China Hospital, Sichuan University, Chengdu, China

**Disclosures:** Linmao Zheng: None; Xingming Zhang: None; Xiuyi Pan: None; Qiao Zhou: None; Hao Zeng: None; Ni Chen: None

**Background:** Fumarate hydratase-deficient renal cell carcinoma (FH-RCC) is a rare subtype of renal cancer caused by *FH* gene mutations. *FH* negativity and S-2-succinocysteine (2SC) positivity on immunohistochemistry can be used to screen for FH-RCC, but insufficient. *FH* mutation could promote aldo-keto reductase family 1 member B10 (AKR1B10) expression. We compared AKR1B10, 2SC, and FH as diagnostic biomarkers for FH-RCC.

**Design:** We retrospectively reviewed data on 544 RCC cases treated at our hospital from 2012 to 2022. We included 58 genetically confirmed FH-RCCs, 83 genetically confirmed TFE3 translocation RCCs (TFE3-tRCC), 188 clear cell RCCs (ccRCC), 128 chromophobe RCCs (chRCC), and 97 papillary RCCs (pRCC).

**Results:** *FH* gene variants were detected in 58 FH-RCC cases. Among them, 24 patients had germline *FH* mutations, 27 patients had somatic *FH* mutations, and seven patients had germline and somatic mutations. All FH-RCC tumors demonstrated diffuse and strong staining for AKR1B10 (Fig 1). In contrast, 26.5% of TFE3-tRCCs and 21.6% of pRCCs were positive for AKR1B10 (Fig 2). All ccRCC and chRCC cases were negative for AKR1B10. Thus, AKR1B10 had 100% sensitivity and 91.4% specificity for FH-RCC. All genetically confirmed FH-RCCs were 2SC positive; among them, 45 (77.6%) cases were positive in both the nucleus and cytoplasm, and 13 (22.4%) cases were positive only in the cytoplasm (Fig 1). Among other RCCs, 2SC positivity was found in 26.8% of pRCCs, 15.7% of TFE3-tRCCs, 3.2% of ccRCCs and 6.25% of chRCCs, all of which were cytoplasmic positivity (Fig 2). 2SC showed 100% sensitivity and 88.9% specificity. Of the 58 FH-RCCs, FH was negative in 49 cases, partly positive in 8 cases, and completely positive in 1 case (Fig 1). Other RCCs were negative for FH. FH was 100% specific, but 84.3% sensitive. The receiver operating characteristic (ROC) curve analysis showed AKR1B10 performed best, with an area under the ROC curve (AUC) of 0.957, followed by 2SC (0.943) and FH (0.922). For the combined markers, AKR1B10+/2SC+ showed the best diagnostic performance, with an AUC of 0.980. The others showed equal AUCs of 0.922.

**Figure 1 - 849**

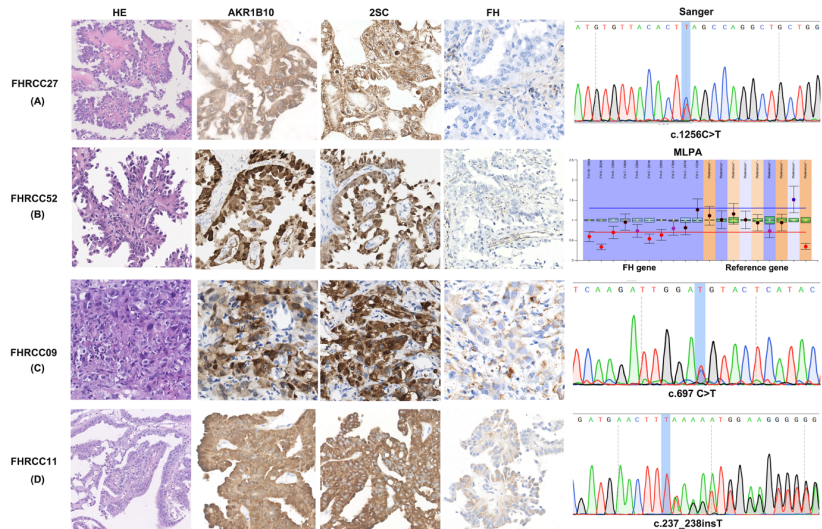
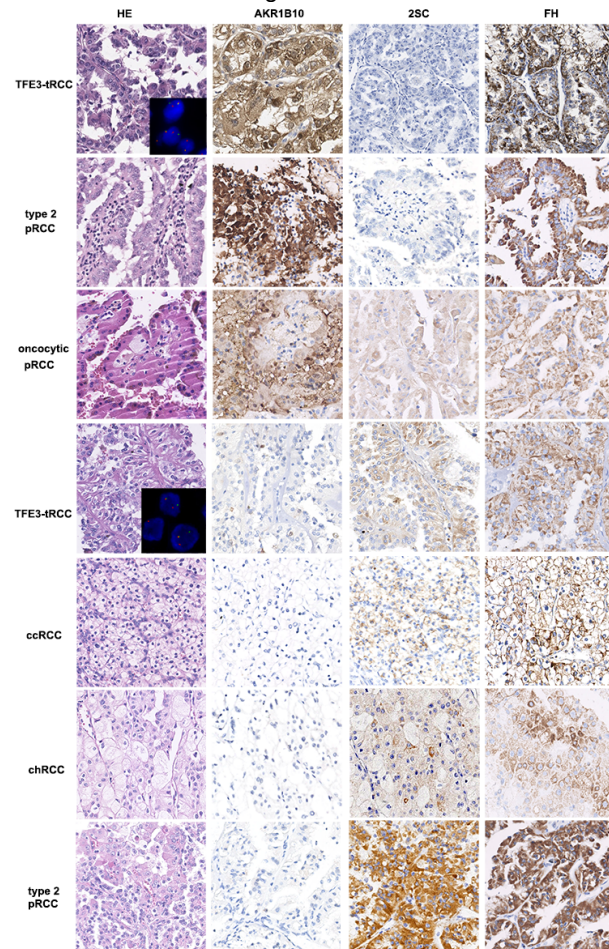


**Figure 2 - 849**



**Conclusions:** AKR1B10 served as a highly sensitive and specific diagnostic biomarker and combining with 2SC is useful to screen for FH-RCC. AKR1B10+/2SC+/FH- cases can be diagnosed as FH-RCC without molecular testing. Patients with AKR1B10+/2SC+/FH+ should be referred for FH genetic tests after excluding TFE3-tRCC and oncocytic pRCC.

## 850 Should Grade Group 1 Prostate Cancer Be Reclassified as “Non-cancer”? A Pathology Community Perspective

Ming Zhou<sup>1</sup>, Ali Amin<sup>2</sup>, Priya Rao<sup>3</sup>, Farshid Siadat<sup>4</sup>, Rajal Shah<sup>5</sup>

<sup>1</sup>Tufts University School of Medicine, Boston, MA, <sup>2</sup>Alpert Medical School of Brown University, Providence, RI, <sup>3</sup>The University of Texas MD Anderson Cancer Center, Houston, TX, <sup>4</sup>University of Calgary, Calgary, AB, <sup>5</sup>UTSouthwestern Medical Center, Dallas, TX

**Disclosures:** Ming Zhou: None; Ali Amin: None; Priya Rao: None; Farshid Siadat: None; Rajal Shah: None

**Background:** Overdiagnosis and overtreatment of Grade Group (GG) 1 prostate cancer remains a significant health care problem despite of its improved risk assessment and uptake in conservative management. Removing the cancer label from these non-lethal cancers has been proposed as an expedient way to reduce potential physical, psychological and financial harm to patients. Recently there have been an renewed effort from our clinical colleagues to implement such a name change. Such a nomenclatural change necessitates a multidisciplinary team effort by clinicians and pathologists. Genitourinary Pathology Society (GUPS) recently conducted a survey of its members, gauging their awareness of this controversy and their position on whether GG 1 prostate cancer should be reclassified.

**Design:** Full active members of GUPS with voting privilege (n=338) were invited to participate in the survey by completing a Google form containing 9 questions (<https://www.gupathsociety.org/GG1-questionnaire/>). The first 6 questions queried respondents' position on removing the cancer label from GG 1 prostate cancer, the specimen type (biopsy vs radical prostatectomy) and reasons for which they supported or opposed such a change. The last 3 questions concerned respondents' demographics, training, and working experiences.

**Results:** 240 (71.0%) members completed the full survey. Most respondents (196, 81.7%) opposed removing the cancer label from GG 1 cancer, 33 (13.8%) supported a change in nomenclature, while 11 (4.6%) responded that they were uncertain. Of those who supported the reclassification, 17 (51.5%) supported the change for radical prostatectomy only, 4 (12.1%) for biopsy only, and 12 (36.4%) for both biopsy and radical prostatectomy. The reasons for and against as well as the potential consequence of such a name change are listed in the Table.

Respondents who opposed a name change for GG 1 cancer selected the following reasons (respondents could choose more than one):
a. Current biopsy techniques may not adequately sample cancer and may miss high-grade cancer (82%) b. Grade alone does not dictate the biology of GG 1 prostate cancer (63%) c. Poor interobserver reproducibility in the grading of prostate cancer, especially for certain sub-patterns of Gleason 4 and 5 (62%) d. Lack of robust biomarkers for detection of unsampled high-grade prostate cancer (61%)
Conversely, respondents who supported a name change selected the following reasons (respondents could choose more than one):
a. Removing the cancer label would lead to fewer cancer diagnoses, treatments, treatment-related side effects, reduction in psychological and financial burden related to cancer diagnosis and treatment (49%) b. There are precedents in cancers of other organs including bladder, thyroid and soft tissue for which cancer label is removed due to their excellent prognosis and management implications (43%) c. GG 1 cancer behaves clinically like precancer rather than cancer (33%) d. Contemporary detection and management of GG 1 cancer reflects a precancer rather than cancer (28%)
Respondents that opposed a change in nomenclature were concerned about potential consequences, including:
a. Overgrading of 3+3=6 to 3+4=7 (GG2) by pathologists to avoid potential litigation (74%) b. Significant modifications in diagnosis, grading, and reporting practices of prostate cancer (72%) c. Health care disparities in many parts of the world would create significant challenges in adopting new recommendations (57%) d. Overutilization of genomic testing and biomarkers in the work up of such cases (47%)

**Conclusions:** Majority of pathologists opposed to removing the cancer label from GG prostate cancer. This survey results highlight the gap between pathologists and clinicians in whether GG1 prostate cancer should be labeled as “non-cancer” and calls for continued debates and conversations between pathologists and clinicians, and further studies on the biology, diagnostic reproducibility, and ideal management of GG 1 prostate cancer in order to make a more evidence-based decision for patients.

## 851 Digital Analysis of Smooth Muscle Bundles in Lamina Propria and Muscularis Propria of the Bladder and its Clinical Implication.

Ruoji Zhou<sup>1</sup>, Alcino Gama<sup>1</sup>, Bonnie Choy<sup>1</sup>, Xiaoqi Lin<sup>2</sup>, Joshua Meeks<sup>1</sup>, Ashely Ross<sup>1</sup>, Ximing Yang<sup>1</sup>

<sup>1</sup>Northwestern University Feinberg School of Medicine, Chicago, IL, <sup>2</sup>Northwestern University, Chicago, IL

**Disclosures:** Ruoji Zhou: None; Alcino Gama: None; Bonnie Choy: None; Xiaoqi Lin: None; Joshua Meeks: None; Ashely Ross: None; Ximing Yang: None

**Background:** Muscularis propria (MP) invasion of bladder cancer is a strong indicator of radical cystectomy. However, distinguishing smooth muscle of MP from that of lamina propria (LP) can be difficult because the descriptions of “thin and wispy” being LP and “large and thick” being MP are vague and subjective. We conducted quantitative measurement of smooth muscle bundles in LP and MP using digital analysis. Furthermore, we evaluated Smoothelin immunostaining in differentiate smooth muscles in LP from MP.

**Design:** A total of 14 whole slide images (13 H&E and 1 Smoothelin-immunostains) containing full thickness of bladder wall were generated using an Aperio GT 450 digital slide scanner (Leica). Aperio eSlide Manager (Leica) was used for measurement of thickness of H&E stained or Smoothelin-stained smooth muscle bundles.

**Results:** Total 366 foci of HE stained smooth muscle bundles were measured based on morphology and location, including 195 foci of LP and 171 foci of MP. The average thickness of smooth muscle is 37.5 µm (range, 8.1-128.2) in LP, and 290.0 µm (range, 70.2-994.8) in MP. Vast majority (97.4%, 190/195) of the measured muscle bundles in LP were less than or equal to 100µm while 95.9% (164/171) of the measured MP were greater than 100 µm. There was overlap between the thickness of muscle in LP and MP ranging from 50 µm to 150 µm (5/195 bundles in LP, 7/171 bundles in MP). All LP muscle bundles measured were less than 150 µm, while only 19 measured MP muscle bundles were smaller than 150 µm, and the small bundles in MP could be due to incomplete sectioning. The positive Smoothelin staining were categorized into three intensity groups: weak (1+), intermediate (2+) and strong (3+). The average thickness is 39.6 µm (range 12.1-105.9) in smooth muscles stained 1+, 85.1 µm (range, 12.1-105.9) in 2+ staining, and 227.1 µm (range, 60.2-676.4) in 3+ staining. 99.5% (194/195) of smooth muscle staining weakly positive was less than 100 µm; while 92.0% (161/175) of the smooth muscle stained strongly positive is more than 100 µm.

Table. Measurements of smooth muscle bundles in muscularis propria (MP) and lamina propria (LP)					
	Lamina propria	Muscularis propria		Lamina propria	Muscularis propria
≤ 100 µm	190	7	≤ 200 µm	195	19
> 100 µm	5	164	> 200 µm	0	152
Total	195	171		195	171
<b>100 µm as cut off for identifying MP</b>		<b>150 µm as cut off for identifying MP</b>			
Sensitivity	95.9%		100.0%		
Specificity	97.4%		88.9%		

**Conclusions:** Measurement of bladder smooth muscle bundles provides a benchmark to differentiate the LP from MP for better cancer staging. Using 100 µm as a cutoff, the specificity for MP is 97.4% and sensitivity is 95.9%. While using 150 µm cutoff, the specificity is 100% and sensitivity is 88.9% (152/171) (Table). In the uncertain cases, strong Smoothelin immunoreactivity (2+ and 3+) can be helpful to further distinguish MP from LP.

## 852 Surrogate Immune Marker Analysis for Simplified Molecular Classification in Upper Tract Urothelial Carcinoma

Annette Zimpfer<sup>1</sup>, Said Kdimati<sup>2</sup>, Andrea Löwl<sup>2</sup>, Anne-Sophie Becker<sup>2</sup>, Nadine Gaisa<sup>3</sup>, Desiree-Louise Dräger<sup>1</sup>, Oliver Hakenberg<sup>1</sup>, Andreas Erbersdobler<sup>1</sup>, Björn Schneider<sup>1</sup>

<sup>1</sup>Rostock University Medical Center, Rostock, Germany, <sup>2</sup>Institute of Pathology, Rostock University Medical Center, Rostock, Germany, <sup>3</sup>RWTH Aachen University, Aachen, Germany

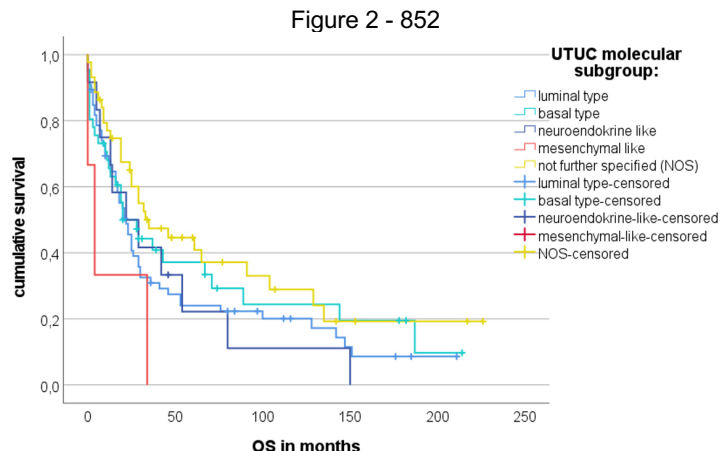
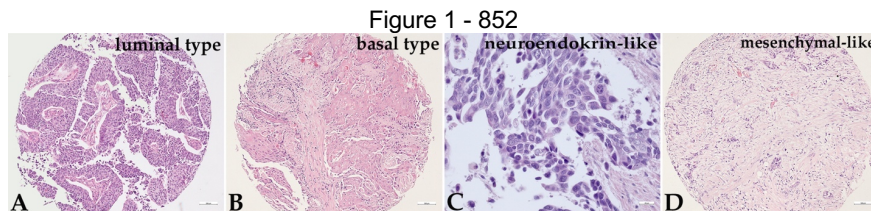
**Disclosures:** Annette Zimpfer: None; Said Kdimati: None; Andrea Löwl: None; Anne-Sophie Becker: None; Nadine Gaisa: None; Desiree-Louise Dräger: None; Oliver Hakenberg: None; Andreas Erbersdobler: None; Björn Schneider: None

**Background:** Upper tract urothelial carcinomas (UTUCs) occur in about 5-10% of all UCs and are frequently discovered at a high-stage disease. Adjuvant treatment options are rare. Similar to that for breast carcinoma, a recently published consensus classification divided muscle-invasive UCs of the urinary bladder (UCB) into different molecular groups, including luminal, basal, neuroendocrine(NE)-like, and mesenchymal(MES)-like type. A surrogate immune marker panel was previously proposed for the simplified molecular classification of muscle-invasive UCB. Since new treatment options may arise from the molecular classification of UC, the classification of UTUC into luminal, basal, and non-luminal-non-basal subtypes in particular would be important, but data in the upper urinary tract are sparse. Our aim was to perform a simplified molecular classification of UTUCs according to the consensus classification for muscle-invasive UCB and to correlate it with several known molecular changes such as microsatellite instability (MSI) status.

# ABSTRACTS | GENITOURINARY PATHOLOGY (INCLUDING RENAL TUMORS)

**Design:** In a tissue microarray-based approach, immunohistochemical analyses were performed on 186 invasive UTUCs. Except for CD56 and synaptophysin, which were considered positive when expressed >2% in tumor cells, the immunoreactive score (Remmele-Stegner score) was applied to evaluate FOXA1, CK20, GATA3, CK5/6, and CD44v. Morphologic features including the presence of a distinct mesenchymal stroma were determined on full tissue sections and considered for classification. For correlation analyses, the results of previous subgroup analyses on *ERBB2* amplification, MSI, and *FGFR3* mutation status were included. Survival analyses evaluated the prognostic value of the molecular subgroups.

**Results:** UTUC were classified as follows: 74 luminal, 44 basal, 14 NE-like, and three cases as MES-like subtype (Fig. 1A-D). A subgroup classification was not achievable in 46 UTUCs. Nine/20 UTUC with *ERBB2* amplification were luminal-type. Seven, 5, and 10 UTUCs harboring MSI were assigned to the luminal, basal, and non-luminal-non-basal type, respectively. Comparing to UTUC of no special type, the patients with UTUC classified as MES-like showed a significant shorter overall survival (OS)( $p=0.028$ ; log-rank test; Fig. 2).



**Conclusions:** The majority of UTUCs can be classified into molecular groups using a surrogate immune marker panel in combination with morphological features. This categorization could serve to optimize individualized adjuvant treatment decisions.

## 853 Molecular Diversity of Testicular Embryonic-Type Neuroectodermal Tumors (ENT; former PNET) Arising from Germ Cell Tumors

Yang Zong<sup>1</sup>, Alexandra Drakaki<sup>1</sup>, Douglas Lin<sup>2</sup>, Huihui Ye<sup>3</sup>

<sup>1</sup>David Geffen School of Medicine at UCLA, Los Angeles, CA, <sup>2</sup>Foundation Medicine, Inc., Cambridge, MA, <sup>3</sup>University of California, Los Angeles, Los Angeles, CA

**Disclosures:** Yang Zong: None; Alexandra Drakaki: None; Douglas Lin: None; Huihui Ye: None

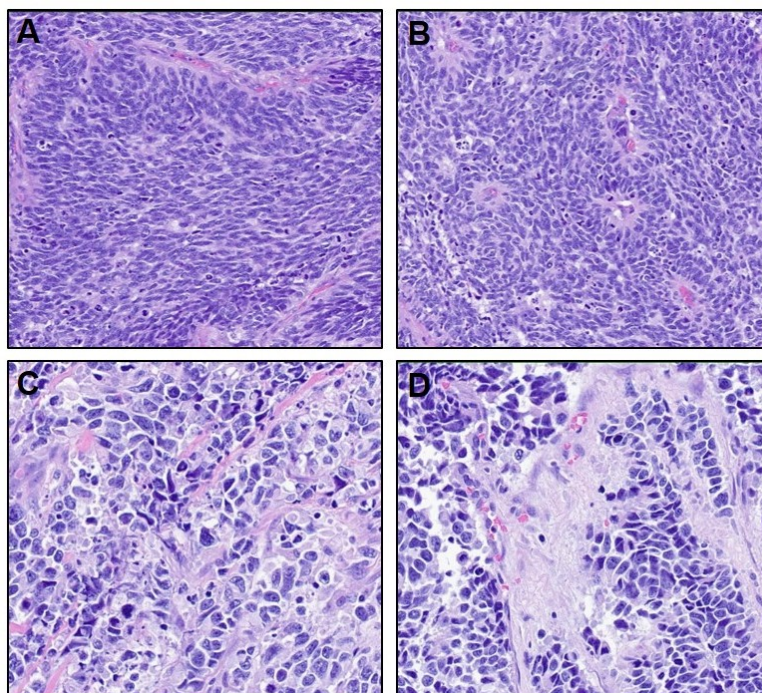
**Background:** Testicular PNET arising from germ cell tumors (GCT) is a rare type of somatic transformation in GCT with poor prognosis and limited therapeutic options, particularly when patients develop disease recurrence or metastasis. Knowledge of key events driving this transformation is limited to the paucity of comprehensive genomic data. We sought to characterize the genomic features of these rare tumors to potentially aid in molecular classification and treatment.

**Design:** A retrospective database search of a CLIA- and CAP-certified reference molecular laboratory (Foundation Medicine, Inc.) was performed for PNETs arising from testicular germ cell tumors that had previously undergone NGS-based comprehensive genomic profiling (CGP) during the course of clinical care. Clinicopathological and genomic data was centrally re-reviewed.

# ABSTRACTS | GENITOURINARY PATHOLOGY (INCLUDING RENAL TUMORS)

**Results:** Here we report the molecular features of 12 advanced testicular PNETs of GTC origin. Patient age ranged from 24 to 49 years, with a mean and median of 36 and 38 years. CGP was performed in 1 primary tumor and 11 metastases, whose submitting diagnoses were testicular PNET or ENT with or without an associated classical GCT component. All tumors harbored gain of chromosome 12p, often with *KRAS*, *CCND2* and *KMD5A* co-amplification, supporting a germ cell origin, and all were negative for *EWSR1* fusions. The tumors were microsatellite stable and exhibited low tumor mutational burden. 3 tumors (25%) exhibited *MYCN* or *MYC* amplification with co-occurring inactivation of the p53 pathway via either *TP53* mutations or *MDM2* amplification in 2 tumors. 3 additional tumors (25%) had activation of the PI3K pathway via *PIK3CA* and *PIK3CG* mutations or *PIK3C2B* amplification; one tumor with co-occurring *CDK4* amplification. Fusions or rearrangements were detected in 3 tumors (25%), such as an internal truncating *ATRX* rearrangement with no partner, as well as novel *BRD4-MAU2* and *BCOR-CLIP2* fusions. The 2 cases with *BRD4* and *BCOR* fusions were reminiscent of the emerging CNS embryonal tumor (CNS-PNET) entities that are defined by molecular alterations, such as CNS HGNET-BCOR (PMID: 26919435).

Figure 1 - 853



**Conclusions:** PNETs arising from GCT are molecularly heterogeneous; however, a subset may be stratified by alterations in 1) *MYCN/MYC/TP53/MDM2*, 2) PIK3 pathways or 3) fusions that overlap with molecularly defined CNS-PNETs entities. Additional studies examining the prognostic and therapeutic implications of our findings are warranted.